OCS Study
BOEM 2014-650

Investigations of Chemosynthetic Communities on the Lower Continental Slope of the Gulf of Mexico

Volume I: Final Report

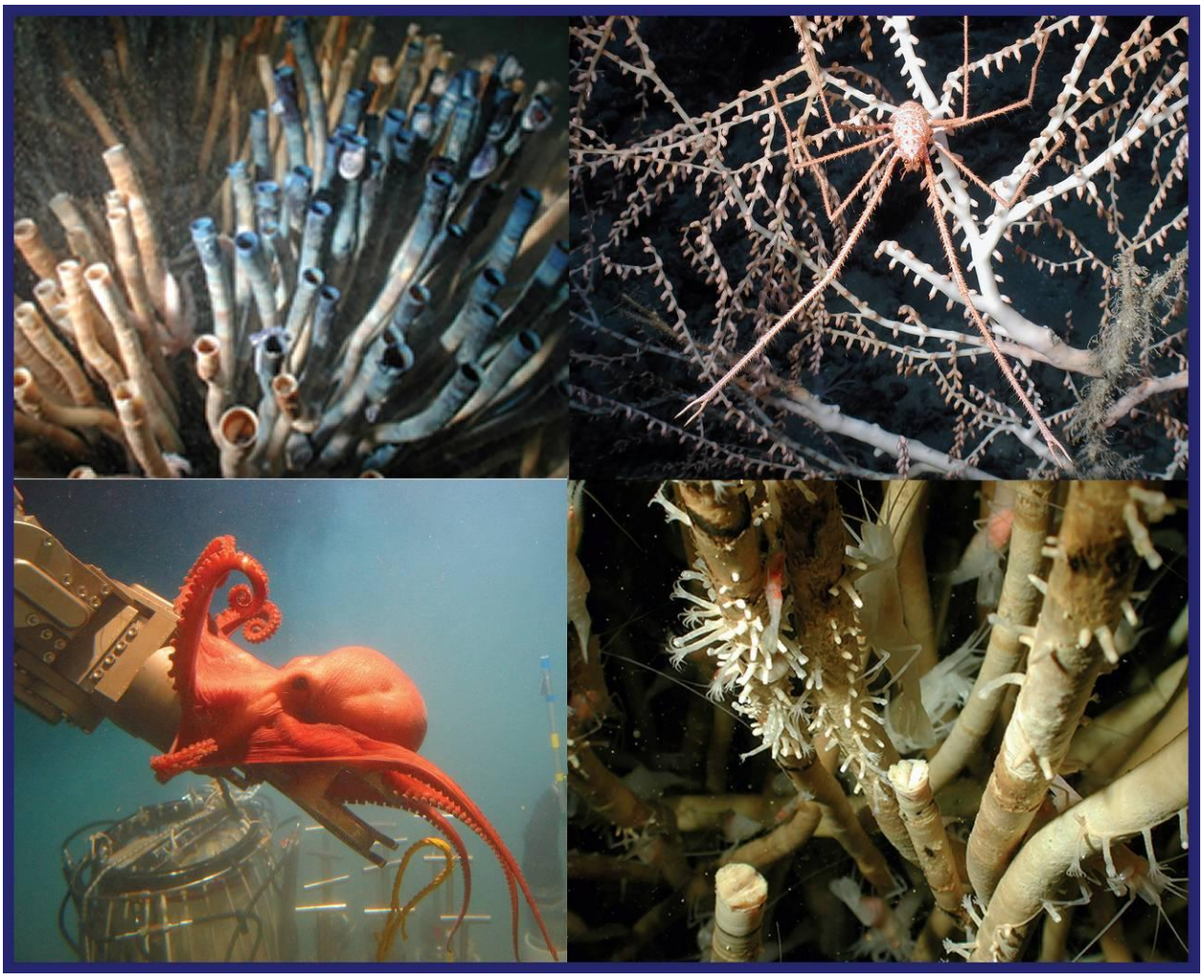

U.S. Department of the Interior
Bureau of Ocean Energy Management
Gulf of Mexico OCS Region

BOEM
Bureau of Ocean Energy Management

OCS Study
BOEM 2014-650

Investigations of Chemosynthetic Communities on the Lower Continental Slope of the Gulf of Mexico

Volume I: Final Report

Authors:

James M. Brooks
Charles Fisher
Erik Cordes
Harry Roberts
Bernie Bernard
Ian MacDonald
Robert Carney
Samantha Joye
Gary Wolff
Elizabeth Goehring
Peter Girguis
Monika Bright

Prepared under BOEM Contract
M05PC00018
by
TDI-Brooks International Inc.
14391 South Dowling
College Station, TX 77845

Published by
U.S. Department of the Interior
Bureau of Ocean Energy Management
Gulf of Mexico OCS Region

New Orleans, Louisianna
July 2014

DISCLAIMER

This report was prepared under contract between the Bureau of Ocean Energy Management (BOEM) and TDI-Brooks International Inc. (TDI-BI). This report has been technically reviewed and it has been approved for publication. Approval does not signify that the contents necessarily reflect the views and policies of BOEM, nor does mention of trade names or commercial products constitute endorsement or recommendation for use. It is, however, exempt from review and compliance with BOEM editorial standards.

REPORT AVAILABILITY

This report is available on CD from the Bureau of Ocean Energy Management, Gulf of Mexico OCS Region, for $15.00, and free of charge as a pdf file downloaded from the BOEM Web site. Copies can also be viewed at selected Federal Depository Libraries. The addresses are listed below.

To order a CD, use the Gulf of Mexico OCS Region contact information below and reference OCS Study BOEM 2014-650. To download a pdf copy, use the Environmental Studies Program Information System (ESPIS) and search on the study report number. In the near future, you will also be able to get this report also from the National Technical Information Service.

U.S. Department of the Interior
Bureau of Ocean Energy Management
Gulf of Mexico OCS Region
Public Information Office (MS GM 355A)
1201 Elmwood Park Blvd.
New Orleans, Louisiana 70123-2394
Phone: (504) 736-2519, 1-800-200-GULF
Fax: (504) 736-2620

U.S. Department of Commerce
National Technical Information Service
5301 Shawnee Rd.
Springfield, Virginia 22312
Phone: (703) 605-6000, 1-800-553-6847
Fax: (703) 605-6900
Web site: http://www.ntis.gov/

CITATION

Brooks, J.M., C. Fisher, H. Roberts, B. Bernard, I. McDonald, R. Carney, S. Joye, E. Cordes, G. Wolff, E. Goehring. 2014. Investigations of chemosynthetic communities on the lower continental slope of the Gulf of Mexico: Volume I: Final report. U.S. Dept. of the Interior, Bureau of Ocean Energy Management, Gulf of Mexico OCS Region, New Orleans, LA. OCS Study BOEM 2014-650. 560 pp.

COVER ART

Photographs from chemosynthetic communities visited during the program.

CONTENTS

LIST OF FIGURES

LIST OF TABLES

ACRONYMS LIST

AC	Alaminos Canyon
AFDW	ahs-free dry weight
ANME	anaerobic methane oxidizers (Also called anaerobic methanotroph)
ANOSIM	analysis of similarity
AMO	anaerobic methane oxidation, sometimes called anaerobic oxidation of methane (Also abbreviated AOM, anaerobic oxidation of methane)
ANOVA	Analysis of Variance
AODC	Acridine Orange-Direct Count
ASF	Alaska Satellite Facility
AT	Atwater Valley
AUV	Autonomous Underwater Vehicle [
BOEM	Bureau of Ocean Energy Management
bm	Bushmaster
bp	base pair
C	celsius
CARD-FISH	Catalyzed Auto-Reporter Deposition Fluorescence *in situ* Hybridization
CHEMO III	Investigations of Chemosynthetic Communities on the Lower Continental Slope of the Gulf of Mexico
C.I.	contour interval
cm	centimeter
C:N	carbon to nitrogen (ratio)
COI	cytochrome c oxidase (Also abbreviated CO1)
COM	combustible organic matter
CTD	conductance, temperature and depth (a sensor)
CRP	Central Reference Point
CytB	Cytochrome B
DCCC	Deep Chemosynthetic Community Characterization
DCS	Drift Camera System
DCR2	Deep Chemosynthetic Reconnaissance II Cruise
DGPS	differential global positioning system
DIC	dissolved inorganic carbon
DOC	dissolved oxygen carbon
dpm	disintegrations per minute
DSR	Deep Sea Research
DSV	deep submergible vehicle
EDT	Eastern Daylight Time
EPR	East Pacific Rise
FLEXE	From Local to EXtreme Environment
GB	Garden Banks
GC	Green Canyon
GIS	geographic information system
GLOBE	Global Learning and Observations to Benefit the Environment

GMT	Greenwich Mean Time
GoM	Gulf of Mexico
HOV	Human-occupied vehicle
hrs	hours
IC	inconsistency coefficient
ILV	input layer vector
ind.	Individual
ISMS	In Situ Mass Spectrometer
IRMS	Isotope Radio Mass Spectrometer
KC	Keathley Canyon
km	kilometer
LBL	long baseline
m	meter
M	mole
MC	Mississippi Canyon
MDS	multidimensional scaling
ML	maximum likelihood
mL	milliliter
mm	millimeter
mmol	millimole
mM	milimolar
MMS	Minerals Management Service
MP	maximum parsimony
mp	mussel pot
MPEG	Moving Picture Experts Group
MPI	Max Planck Institute
MRU	Motion Reference Unit
NASA	National Aeronautics and Space Administration
NCBI	National Center for Biotechnology Information
ND4	NADH dehydrogenase subunit 4
NIST	National Institute of Standards and Technology
NJ	neighbor joining
nM	nanomolar
nMDS	non-metric multi-dimensional scaling
NOAA	National Oceanic and Atmospheric Administration
OCS	Outer Continental Shelf
OSO	oil slick origin
PCA	principal component analysis
PCR	polymerase chain reaction
PDB	Pee Dee Belemnite
pH	negative log of the hydrogen ion concentration, a measure of acidity or alkalinity
POC	particulate organic carbon
POM	particulate organic matter
PON	particulate organic nitrogen Also called PN)
Recon	reconnaissance cruise

Cruise	
rDNA	ribosomal DNA
ROV	remotely operated vehicle
R/V	research vessel
SAR	synthetic aperture radar
SBM	standard beam mode
SBS	seafloor bright spots
SEAS	Student Experiments At Sea
SEM	scanning electron microscope
SIMPER	similarity percentage
SR	sulfate reduction
SRB	sulfate-reducing bacteria
TCNNA	Textural Classifier Neural Network Algorithm
TIFF	tagged image file format
UTC	coordinated universal time
UTM	universal transverse Mercator
USBL	ultra-short baseline (a type of transponder)
VV	Virtual Van
WGS 84	World Geodetic System 1984
WHOI	Woods Hole Oceanographic Institute
WR	Walker Ridge
XRD	X-ray diffraction
3-D	three-dimensional
µCi	microcurie
µL	microliter
µm	micrometer
µM	micromolar
%OC	percent organic carbon

1. OVERVIEW

This document is TDI-Brooks International's final report for contract number: 1435-01-05-39187, issued by the U.S. Department of the Interior, Bureau of Ocean Energy Management (BOEM) "Investigations of Chemosynthetic Communities on the Lower Continental Slope of the Gulf of Mexico" (CHEMO III). The information in this report is a compilation of laboratory studies and three cruises.

The reconnaissance cruise (Recon cruise) was conducted on the TDI-Brooks research vessel (R/V) *Gyre* from 11 to 25 March 2006 and was the initial cruise conducted for this contract. The cruise was completed in two week-long legs with an interim port call in Venice, Louisiana. Leg I (11–18 March) was dedicated to drift camera work to survey the sea-bed at selected sites. Leg II (19–25 March) involved both drift camera and trawling/box core work efforts. The cruise mobilized and embarked from Freeport, Texas (TX). The objective was to provide timely input for the site selection process for the subsequent *Alvin* expedition (May 2006).

The Deep Chemosynthetic Community Characterization Cruise (DCCC) was conducted on the Woods Hole Oceanographic Institute (WHOI) R/V *Atlantis* and the *Alvin* Deep Submergence Vehicle (DSV) from 7 May–2 June 2006, and was the second cruise conducted for this contract. The cruise mobilized and embarked from Key West, Florida (FL), and de-mobilized at Galveston, TX.

In February 2007, sampling sites were mapped in great detail using the C&C Technologies Autonomous Underwater Vehicle (AUV), in preparation for intensive sampling planned for the 2007 field season. The AUV is equipped with instrumentation for collecting high-resolution multibeam bathymetry, chirp sonar subbottom profiles, and side-scan sonar swaths. AUV data sets for AT (Atwater Valley) 340, GC (Green Canyon) 852, WR (Walker Ridge) 269, and AC (Alaminos Canyon) 601 were acquired.

The Deep Chemosynthetic Reconnaissance II Cruise (DCR2) was conducted on the National Oceanographic and Atmospheric Administration (NOAA) Ship research vessel *Ronald H. Brown* and with the remotely-operated vessel (ROV) *Jason II* from 4 June–6 July 2007, and was the fourth cruise conducted for this contract. The cruise mobilized and embarked from Panama City, FL, and de-mobilized at Galveston, TX.

Post-cruise reports were completed for all cruises and were submitted to BOEM. The data from the cruises was up-loaded to a site located on the TDI-Brooks International website. All program researchers have password-protected access to these data. This report compiles detailed information regarding operational procedures, stations occupied, sampling activity, site descriptions, results and interpretations of laboratory and field studies, and a summary and synthesis of all work.

2. BACKGROUND

The largest oil reserves in the continental United States are found in the Gulf of Mexico (GoM). The Bureau of Ocean Energy Management (, formerly the Minerals Management Service [MMS]) is responsible for overseeing the responsible extraction of these natural resources. By the early 1980s, energy companies had developed the technology to explore and extract oil and gas in waters up to 1,000 meters (m) deep.

During the mid- to late 1980s, MMS contracted with the Geochemical and Environmental Research Group at Texas A&M University to collect animals from areas of the deep sea floor associated with active oil and gas seeps. The original expectations of both the MMS and the scientists involved were that few animals would be found associated with these "toxic" sea floor environments, and that perhaps the few that were found would be unhealthy, at best. However, when the trawls came to the surface over Bush Hill, a site that became one of the best-studied seep sites in the world, they were so full of animals that the nets could be brought on board only with the help of an extra crane. The animals were not the usual fauna of the deep GoM. The nets were full of giant tube worms and mussels, which had only recently been discovered at deep-sea hydrothermal vents in the Pacific Ocean. Since that time similar (but different) cold-seep and hydrothermal-vent communities have been discovered in many different geological settings in the world's oceans.

Over the last 20 years, these animals and communities have been studied at moderate depths in the GoM, along with the geology, geochemistry, and microbiology that allows them to flourish. As a result, the hydrocarbon seep communities in less than 1,000 m water depth on the Upper Louisiana Slope of the GoM, are the most intensively studied and most understood of any deep-sea cold-seep communities in the world. The basic biology of the dominant animals, their life histories, and the biodiversity and biogeography of the seep and coral communities on the Upper Louisiana Slope is now understood. The successional processes that led to the eventual development of coral communities on carbonates created during periods of active hydrocarbon seepage is understood. Also discovered are some amazing communities, such as the ice worms that inhabit methane ice and the mussels that ring the Brine Pool NR-1.

Meanwhile, energy companies have continued to develop the technology to extract oil and gas from deeper and deeper water and now have the capability to drill oil wells in all water depths in the GoM outer continental slope. Although several GoM hydrocarbon seep sites at depths greater than 1,000 m have been visited by scientists, only a single site has been the focus of more than a few exploratory dives. This site, at 2,200 m in Alaminos Canyon, has lush communities of tube worms and mussels that are reminiscent of the shallower sites that are well known. However, the underlying geology and almost all of the species present are different. Preliminary studies indicate that the structure of the communities associated with the tube worms and mussels is also quite different. The normal "background" fauna are different at this depth, and different patterns of interaction between these animals and the seep-specific animals are expected. Not only is the ecology of this deep community not understood, at this point the types of communities that exist at depths between 1,000 and 2,200 m are not known. Advances in this understanding and knowledge are the goal of this contract.

3. PURPOSE AND PREPARATION

The primary purpose of this research is to discover and characterize the sea floor communities that live in association with hydrocarbon seepage and on hard ground in the deep GoM. The sites studied are in areas energy companies will soon drill for oil and gas.

Preparation for this program began in the fall of 2005, when Harry Roberts began to study a variety of types of information that would help discover new hydrocarbon seep and hard-ground communities in the deep GoM. Information was gathered from thousands of cores collected by the TDI-Brooks International, Inc. group, satellite images of persistent oil slicks on the surface of the Gulf, and extensive collections of geophysical data and maps of the sea floor that were made available for this project by the Minerals Management Service. Fourteen sites with a high potential to host lush chemosynthetic and/or deep-water coral communities were chosen for investigation in early 2006.

In March of 2006, the first cruise of this program, the Recon Cruise, began on the TDI-Brooks R/V *Gyre*. Thousands of pictures of the sea floor were taken at locations identified by Roberts and his team. These pictures provided the first look at the dive sites we were to dive on for the *Alvin* mission. Images from a few sites revealed little except a muddy sea floor. At most of the sites there was strong evidence of seepage, and at least scattered occurrence of the types of animals expected at seep sites. In one case there were abundant corals, and at a few, large communities of seep animals were present in the original survey images.

Based on the Recon Cruise Report, the images of the sea floor, previous knowledge of the geophysics and geochemistry of the sites, and a desire to explore over a wide depth and geographic range, the cruise and dives for the Deep Chemosynthetic Community Characterization (DCCC) expedition were planned and completed.

The Deep Chemosynthetic Community Characterization Cruise was conducted on the WHOI research vessel R/V *Atlantis* and the *Alvin* DSV from 7 May–2 June 2006, and was the second cruise conducted for this contract.

In February 2007, selected sampling sites were mapped in great detail using the C&C Technologies AUV in preparation for intensive sampling planned for the 2007 field season.

The (DCR2 was conducted on the NOAA Ship research vessel *Ronald H. Brown* and the ROV *Jason II* from 4 June–6 July 2007, and was the final cruise conducted for this contract. During this cruise several of the key sites for process-oriented studies were revisited and five additional sites were explored. The cruise mobilized and embarked from Panama City, FL, and de-mobilized at Galveston, TX.

Extensive laboratory studies were conducted with samples collected during the two Recon Cruise s with submersible assets.

4. IN SITU METHODS AND SAMPLING PROCEDURES

4.1. Navigation

Precise navigation was obtained from an ultra-short baseline (USBL) transponder calibrated with the ship's differential global positioning system (DGPS). The TDI-Brooks field group uses this system for taking piston and box cores at preset locations and is routinely able to do so within a 5 m radius of the target. TDI-Brooks has developed a system and technique for navigating a deployed tool weighing at least 400 kg over a precise location in X, Y, and Z in water depths to 3,000 m, to sample from that specified target.

In order to achieve the positioning and navigation requirements for a cruise, the field effort was equipped with a C-Nav DGPS system with a Simrad HRP-410 USBL transceiver and Simrad MST-342 3,000 m beacons. The USBL transducer head can lock onto a beacon with a ±15 degree cone of coverage, thus increasing resolution versus a wide coverage cone. When the head receives in the narrow beam range the geometry increases the noise immunity from four db to 15 db, effectively increasing the noise rejection by a factor of 16.

The HPR-410 USBL system was interfaced to a VSS DMS05 Motion Reference Unit (MRU), which is also interfaced to the WinFrog navigation system such that real time position of the transponder is displayed on the monitors for the navigator, the helmsman, and the winchman. National Marine Electronics Association output of heading from the vessel gyro and the DGPS were interfaced via RS-232 directly to the navigation computer as well as to the computer dedicated to USBL control. The transponder positions were processed and managed in real-time using Kongsberg Acoustic Positioning Operating System software. This arrangement provides an independent check on the WinFrog offsets and datum conversions. A schematic of this USBL system is shown in Figure 4-1.

This system was used for the drift camera cruise and again for the *Jason II* cruise. The *Alvin* cruise used WHOI transponder arrays. Using a combination of recognizable features and physical markers placed on the sea floor the process of calibrating our navigational data with these known navigational fixes enabled us to verify the positional accuracy. Offsets that were initially on the scale of 10's of meters (m) were reduced to several m which resulted in accuracy of several m across cruises. The use of calibrated offsets between the *Alvin* and *Jason II* cruises facilitated the reoccupation of stations without difficulty. Accuracy on the scale of m with these physical markers and the consistency between all of the extant navigation data sets will also facilitate reoccupation of all mosaic and long term study sites in future years.

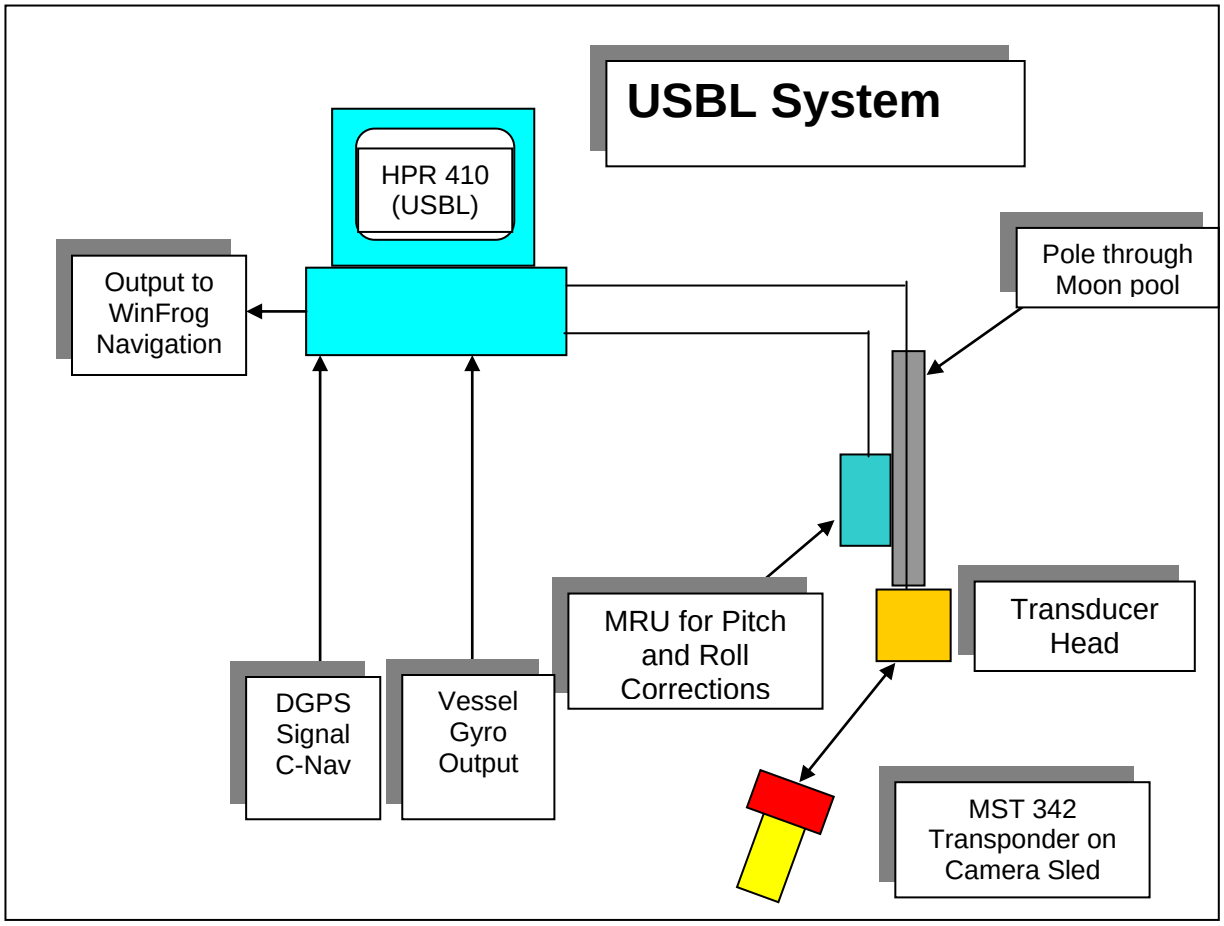

Figure 4-1. Kongsberg HPR-410 system and WinFrog data logger collected detailed position information for the vessel.

The standard operation procedure used to survey sites of interest was to locate a target area or areas based on the proprietary geophysical data provided by BOEM. The bathymetric contours of the site and the targeted area were drawn as the background on the navigation computer monitor. The on-going track of the photoplatform was visually monitored and evaluated during the deployment period.

4.2. Imaging

4.2.1. Seafloor Imaging

During the first cruise, the basic objective was to visually confirm the presence of a significant community of chemosynthetic or hard bottom fauna at the potential sites and to locate these communities as precisely as possible on the seafloor. The tool used for imaging the seafloor was the Drift Camera System (DCS). This combines a 3.2 mega-pixel Nikon digital camera with strobe illumination. The DCS was deployed on a frame lowered from the surface ship and held 2-5 m above the bottom based on feedback from a SeaBird conductivity, temperature and depth (CTD) instrument with an altimeter. A rendered drawing of the camera system and the

configuration used during the Photo Recon Cruise is shown in Figure 4-2. Lead weights were attached to the DCS to bring its weight, in air, to 400+ kg.

A 28 kHz depthfinder was used throughout the cruise. In previous efforts, this type of sensor has detected gas plumes in the water column associated with seeps. On this cruise, the high-resolution depth finder was not available until the second leg. Although some possible gas plumes were noted, the heavy seas experienced throughout the cruise precluded consistent sensing of gas plumes. Consequently, the water column imaging was not collected. Heavy seas also hampered the ability to observe natural oil slicks generated by oil and gas arriving at the surface. One active slick was observed at 27.371°N and 90.573°W.

During the second cruise (DCCC) the project used two major types of digital photographic images. Down-looking images were taken with a digital camera mounted behind the *Alvin* equipment basket and operated by a timer so that a picture was taken every 10 seconds. By merging the time each picture was taken with *Alvin*'s navigation records, an accurate record of the location of each picture could be compiled. Although image quality was generally excellent or good, it was sometimes compromised by disturbed sediment or because the submarine was too far off the bottom to view the bottom. Additionally, when the submarine was at rest on the bottom the repeated images of a small area of seafloor were of no value. The complete set of down-camera images was screened to remove unusable images. The screened subset was termed and labeled "bottom in view" images. A second set of digital images was taken using a macro-camera positioned by the *Alvin* manipulator. These images show details of animals or geology at selected locations.

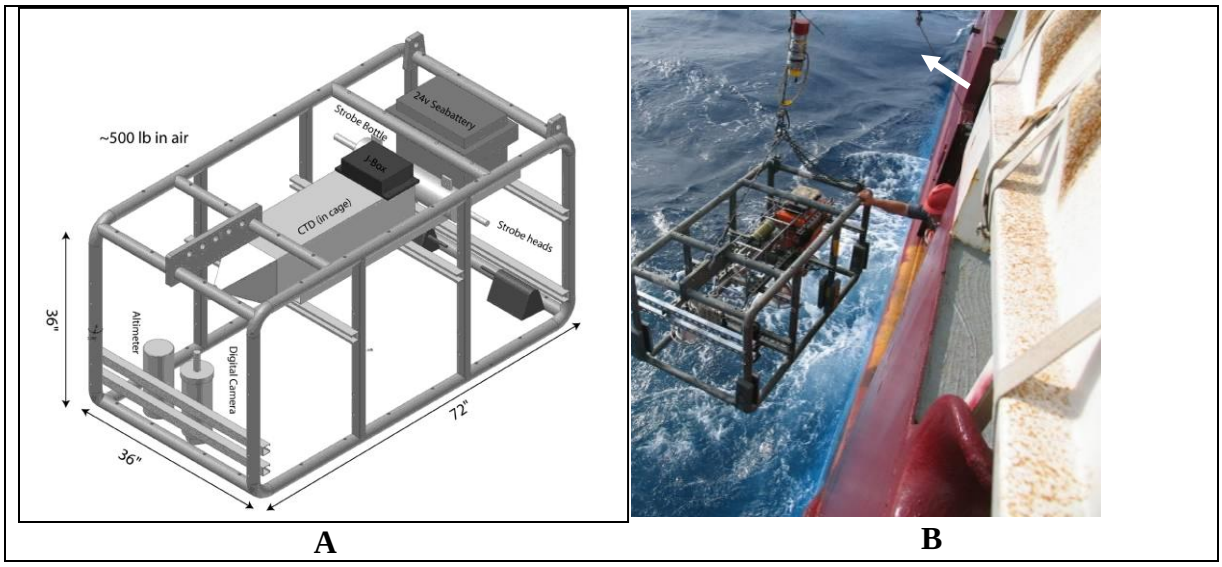

Figure 4-2. (A) Rendering of the drift camera system with components labeled. (B) DCS being deployed from *Gyre* during the survey cruise.

4.2.2. Time-Lapse Camera

This task requires developing a system for short- and long-term photographic sampling in the seep environment. The proposed methodology called for use of a digital camera controlled by a

time-lapse switch and mounted on a rotary platform. A prototype of this camera was deployed during the May 2006 *Alvin* cruise for two short intervals to test the equipment, lighting, and battery. The deployments proved somewhat problematic, but were ultimately successful and a rotary time-lapse system was left at the GC852 site for recovery during the 2007 cruise.

During the intervening time, MacDonald and his students worked to improve the design of the deployment-recovery system for the rotary time-lapse camera and to refine other aspects of this instrument. The present version of the rotary time-lapse camera is shown in Figure 4-3. Improvements on the design are:

- Glass housing was redesigned to permit deployment at all study sites.
- Compact battery housing was designed to facilitate deployment and recovery.
- Autonomous recovery platform was designed and successfully tested.
- Two rotary time-lapse systems have been acquired for use with the program.

In addition to work on the time-lapse camera, MacDonald's macro and survey digital camera systems were refurbished and checked in preparation of the 2007 cruise. Likewise, the CTD used during the March 2006 Recon Cruise was re-calibrated and checked for possible future use.

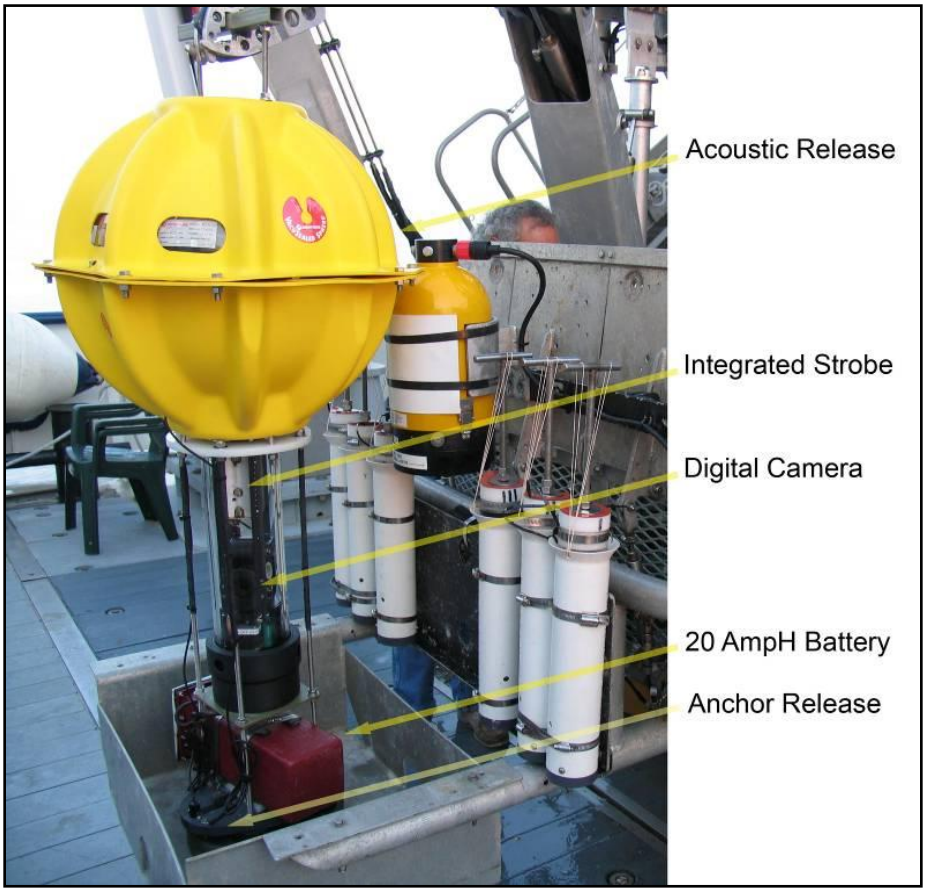

Figure 4-3. Rotary time-lapse camera and recovery platform.

4.2.3. Photo-transect Survey Field Methods

The photo-transecting survey used a methodology designed for time-efficient implementation during extended ROV operations at project study sites (Figure 4-4A). The goal was an objective characterization of habitats and fauna associated with hydrocarbon seepage within an area that contained stations where more intensive sampling and collections were concentrated. Survey design consisted of first designating a rectangular region encompassing the study sites. Size and orientation of these regions varied according to the bathymetry and locations of known features. The largest survey rectangle (AT340.3) measured 450x300 m, the smallest (Mississippi Canyon (MC) 462) measured 200x200 m. When the borders of survey rectangle were established, spreadsheet routine was used to designate a series of 10 randomly distributed center-points within the rectangle and then to extend equidistant endpoints away from the centers, thereby generating a set of ten photo-transects. The orientation of these lines was chosen at random, but was the same for all ten transects. The routine plotted the transect distribution on a preliminary graph each time a set was generated. Potential transect arrays were rejected if the lines were not more or less evenly-distributed across the entire rectangle or if the orientation of the lines with respect to the topography would pose operational problems for the ROV. Each line was assigned a number, and in a final randomization step an altitude between 3.0 and 5.0 m. The coordinates of the endpoints were then translated into the ROV's operational coordinate system (geographic latitude and longitude) and handed off to the ROV crew. The system allowed for rapid turn-around between designating a study area and completing a sampling plan. Figure 4-4B shows the sampling plans for the photo-surveys at AT340.

The imaging system used for the photo-transects included a Scorpio deep sea housing and a Nikon 990 camera that took digital images measuring 2048x1536 pixels and had a lens set at wide angle (approximately equivalent to 28 mm). Illumination was provided by two 300 watt sec strobes synchronized with the camera. Parallel lasers with a separation of 28 centimeters (cm) provided a constant visible scale in the images (Figure 4-5). Camera control was available at the ROV controls during photo collection to adjust iris and focal length settings. The camera shutter was fired by an automatic release function with an adjustable interval. Images were recorded in the camera and were not available for review until the ROV was recovered after a lowering.

During photo-surveys, the ROV pilot would choose a sequence through the transects that minimized travel time. Having one fixed orientation for the transects greatly increased travel efficiency. The supervising scientist would record the start and end times for each transect and would initiate the automatic shutter release function at the start of each line. Intervals between photographs were adjusted to eliminate overlap (and double counting of subjects). Because the area covered by each photograph changed with altitude, the ROV traveled at different speeds, and different altitudes were used on each transect, the interval was typically adjusted for each transect. Typically the interval was between 10 and 20 s. Additional entries were taken by the watch keeper on the Virtual Van (VV) log to record noteworthy animals or other features. Figure 4-4B) shows the realized survey executed from the AT340.2 and AT340.3 plans described above.

After recovery, the individual image files were downloaded to shipboard computers and time-stamped with a routine that renamed the files with the date and time of collection. The location

of each image was estimated by matching the collection time with the ROV navigation file, which recorded an ROV fix every second. Additional data such as depth and altitude were also extracted from the ROV files.

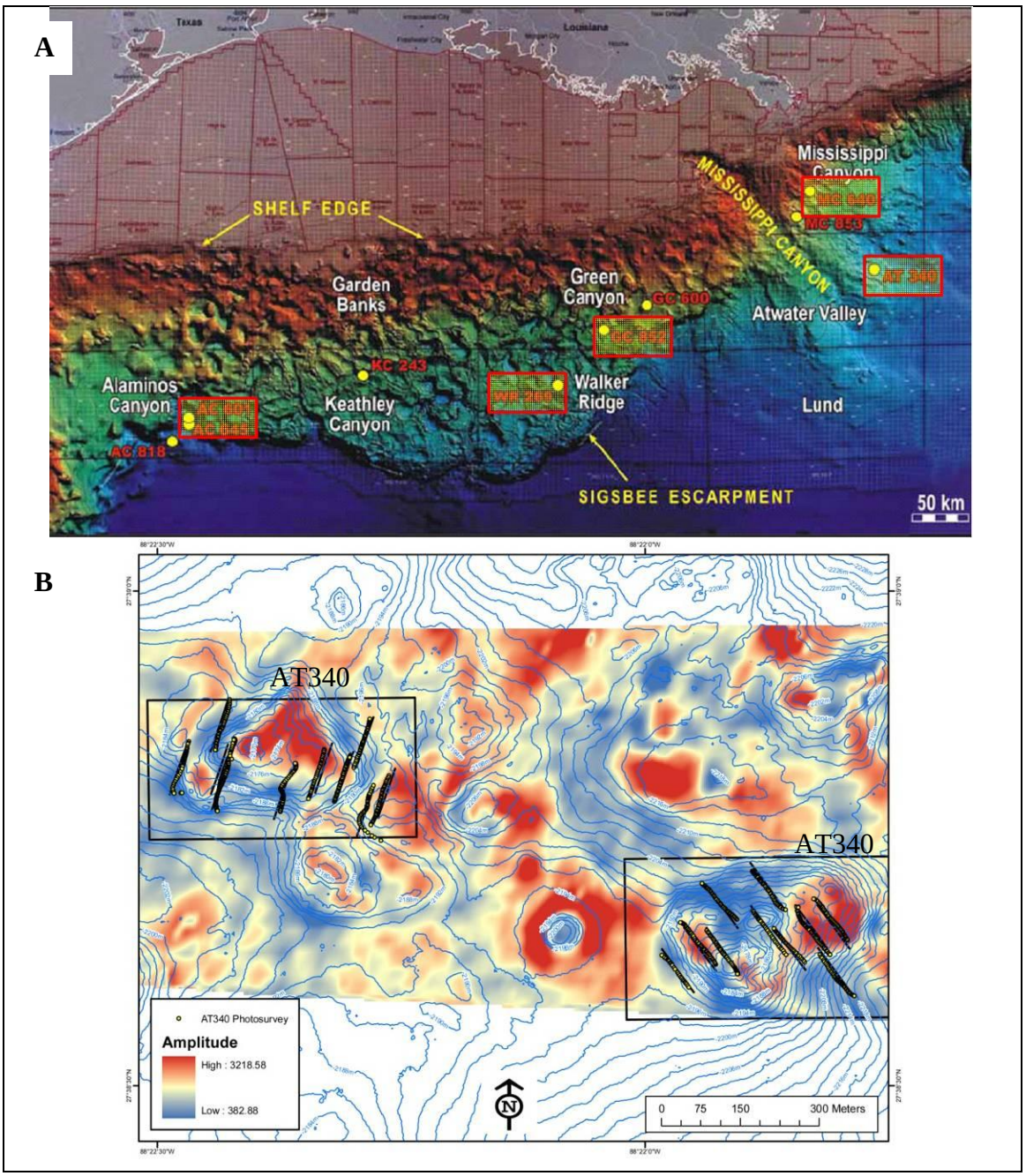

Figure 4-4. Photographic survey as completed (A) during *Jason* ***II*** 2007 expedition and (B) details of surveys AT340.2 and AT340.3 collected in lowerings 276 and 277, June 2007.

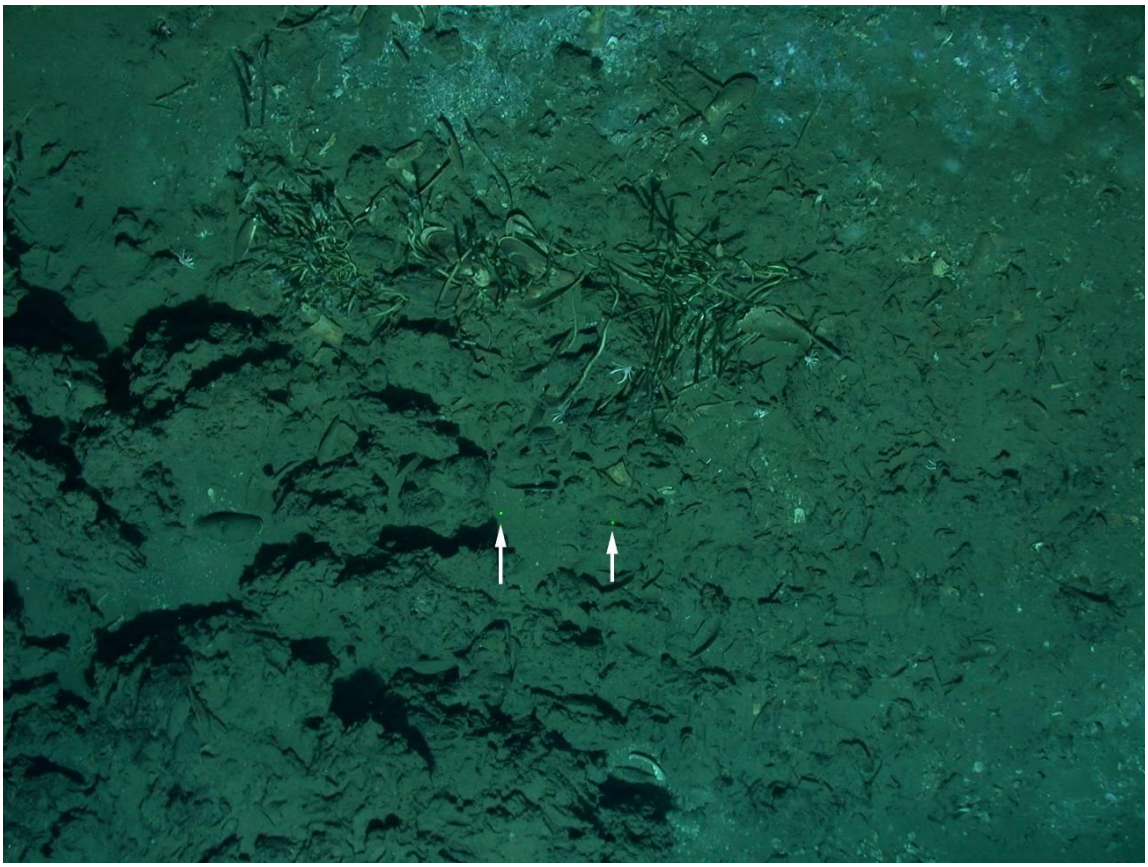

Figure 4-5. Example image from photographic survey of AT340.3 site.

4.3. Faunal Collections

4.3.1. Mussel Community Sampling

The mussel pot collection devices were modified from a design of Cindy Van Dover's (Van Dover et al., 2002) and consist of a 'pot' made of 1/8" thick rolled aluminum with an interior diameter of 26 cm and a height of 29 cm. The inside is lined with a Kevlar bag that is closed by rotating a handle on the top of the pot that cinches the bag closed using a draw-string. This can be done with a single manipulator capable of 360° rotation by using a hydraulic ram on the manipulator and an anti-rotation bar on the pot. When the bag is cinched shut, a 10 cm high aluminum ring can be released that marks the collection location and allows photographic documentation of the collection scar (and therefore quantification of megafauna missed on uneven hard substrates).

One of the most challenging aspects of the community sampling during the DCCC cruise was the presence of extremely large (up to 25 cm in length) mussels that had a tendency to foul the opening of the mussel pots. To overcome this problem, a 63 μm mesh nytex liner (similar to the liner of the Bushmaster) was fitted to the inside of a coarse-mesh net (the "scoop") and used to sample a number of mussel beds. The manipulator of the submersible dragged the scoop through the mussel bed then placed the entire scoop into a biobox and closed the lid. In planning for the

2007 field season, scientists compared the samples obtained by each method to determine if the two methods sampled similar communities from the same habitats. There were 8 scoop samples taken at 6 sites and 12 mussel pots taken at 8 sites in 2006. Scoop samples contained an average of 9.0 species and 243 individuals per sample, while mussel pots contained an average of 7.2 species and 79 individuals per sample, and the scoop sampled species at a greater rate per sample. Statistical analyses were carried out on relative abundance data (proportion of individuals in each species) because not all scoop samples were lined with the finer mesh in 2006 and not all mussel individuals were measured in all scoop samples. Even with these differences in methodology, the relative abundance of species was not significantly different between the two sampling devices (analysis of similarity (ANOSIM), Global R = 0.055, P = 0.237). A multidimensional scaling (MDS) ordination confirmed this result, where similarity among mussel communities was more highly governed by site than by collection method. These results indicate that the scoop samples are a sufficient sampling method for determination of species richness and diversity indices for the mussel beds encountered, particularly for the mussel beds composed of large *B. brooksi* individuals. Therefore, these two sampling devices were both used as appropriate and the data combined in the subsequent analyses.

4.3.2. Tubeworm Community Sampling

Sampling of tube worm aggregations was generally carried out using the Bushmaster Jr. collection device (Bergquist et al., 2003a). This device is a net that is suspended and held open by a framework of flexible ribs, with a "drawstring" stainless steel cable that can be hydraulically actuated to close the net completely. The inside of the net is lined with a 63 micrometer (µm) nylon mesh and retains all fauna above that size. The open diameter of the Bushmaster Jr. is 0.7 m. In some cases, the need for multiple samples from different stained aggregations during a single dive necessitated collections of stained tube worms using the manipulator of *Jason II* and recovery in the bioboxes. These collections were not used in the community analyses, but were used for both growth rate analyses and for the analyses of vestimentiferan stable isotope content.

4.3.3. Opportunistic Faunal Sampling

Other samples of fauna of interest were obtained opportunistically using the manipulators, non-lined collection nets, or pushcores. This included larger mobile fauna around seeps not normally collected with the quantitative community collection devices, larger mobile vagrant fauna including crustaceans, holothuroids, and other echinoderms, monoliferan and frenulid siboglinid tube worms, and infaunal meiofauna.

4.4. Trawling

A 40-ft, semi-balloon trawl was used during the Recon Cruise. It was towed at least 5 km from detailed study sites to obtain a large number of background species for isotopic characterization. The trawling was conducted during day and night operations on the R/V *Gyre*.

All trawl samples on the DCCC cruise were taken with an eight foot Agassiz-type beam trawl that was lowered and recovered at 50 m/min as tension allowed. Towing speed was 1–2 knots over ground. The purpose of sampling was to obtain specimens for trophic analysis within 5 km of seep sites.

Trawling was concentrated at study sites AT340, GC825, and AC818. Sampling at GC825 proved problematic due to strong currents. Adequate material was obtained at all three sites.

4.5. Box Coring

A 30 cm x 30 cm box core was used during the Recon Cruise to sample background benthic infauna at 1 km and 5 km from detailed study sites. Due to tissue requirements of isotope analysis, larger macrofauna were sought and samples processed through a 0.5-mm screen.

4.6. Shipboard Sample Processing and Identification

Samples from the Bushmaster and mussel pots were placed in containers lined with 63 µm mesh on the front of the submersible while the mussel scoops were twisted closed and placed into a biobox. Upon retrieval of the submersible, the sampling gear were labeled and transferred to designated bins for immediate processing. Tube worms and mussels were rinsed and removed. Large macrofauna was removed. The remaining material was sieved and all fauna retained on a 1 mm sieve was added to the macrofauna collection. Subsamples of the material passing through the 1mm sieve and retained on a 32 µm sieve were taken for meiofauna studies. Macrofauna and megafauna were identified and sorted to the lowest possible taxonomic level, counted, weighed on board using a motion-compensated shipboard balance, and subsampled for genetic and stable isotope analyses. Unresolved species were sent to taxonomic experts for final identification or confirmation of ship-board identifications. Anders Waren identified all gastropods, Sabine Stohr identified all ophiuroids, S. Hourdez identified all polychaetes, and Martha Nizinski identified galatheid crustaceans.

All foundation species were identified and measured on board ship and surface areas were calculated as a cone frustrum for vestimentiferans following Bergquist et al. (2003a) and as a cone for mussels following Cordes et al. (2007b). Faunal abundances in each collection were standardized to densities using foundation species surface area.

4.7. Microbiology and Biogeochemistry

4.7.1. Water Column Biogeochemistry

4.7.1.1. Sample Collection and Analysis: DCCC Cruise

At the intensively sampled stations, during the DCCC cruise, water samples were collected at 20 depths between the surface and about 3 m above the sediment column using a rosette package. The rosette package consisted of:

1) 20 (10 liter go-flo trace-metal) clean water sampling bottles,
2) SBE9+ CTD (dual SBE3T/SBE4C sensor system plus extra SBE3T temp, SBE4C conductivity, and SBE43 oxygen sensor),
3) Benthos-Datasonics PSA-916 altimeter;
4) 100x gain Wetlabs C-Star transmissometer, and
5) 660 nanometer wavelength, 25 cm pathlength Wetlabs ECO-AFL chlorophyll fluorometer.

Physical data from sensors 1 through 4 were collected during descent and ascent. The go-flo bottles were remotely triggered at select depths during assent of the rosette except for the second cast at AC601, where bottles were tripped on the descent as well as on the ascent.

Once on deck, the go-flo bottles were opened carefully to collect samples for subsequent quantification of concentrations of dissolved oxygen, dissolved methane, inorganic nutrients (ammonium, nitrate+nitrite, phosphate, and silicate) and dissolved organic carbon (DOC). Oxygen concentrations were determined with a high-sensitivity galvanic oxygen sensor in a closed circulation cell. To quantify dissolved methane concentrations, sonication/vacuum extraction was used to isolate methane and quantify its concentration using gas chromatography (Suess et al., 1999). Nutrient (NO_3^-, PO_4^{3-}, and SiO_2) concentrations were determined using automated flow-injection on a Lachat QuickChem 8000. Ammonium (NH_4^+) concentrations were measured using the phenol hypochlorite method (Solarazano 1969). DOC was determined using a Shimadzu TOC 5000 (Sharp et al., 1993). Rates of aerobic methane oxidation were measured by incubating triplicate live and dead (mercury-killed) samples in the presence of isotope-tagged methane ($^{14}CH_4$) (Joye et al., 1999) for 48 hours (hrs). Unreacted $^{14}CH_4$ tracer was removed by purging samples with water-saturated CH_4 and the oxidation product, $H^{14}CO_3^-$, was quantified by liquid scintillation counting (Joye et al., 1999).

4.7.1.2. Sample Collection and Analysis: Jason II Cruise

Water samples were collected using Niskin bottles fired from the *Jason II* at GC697, AT340, GC852, Garden Banks (GB) 647, AC645 and AC601.

Once on deck, the Niskin bottles were opened carefully to collect samples for subsequent quantification of concentrations of dissolved oxygen, dissolved methane, inorganic nutrients (ammonium, nitrate+nitrite, phosphate, and silicate) and DOC. Oxygen concentrations were determined with a high-sensitivity galvanic oxygen sensor in a closed circulation cell. To quantify dissolved methane concentrations, headspace extraction followed by gas chromatography was employed. Nutrient (NO_3^-, PO_4^{3-}, and SiO_2) concentrations were determined using automated flow-injection on a Lachat QuickChem 8000. NH_4^+ concentrations were measured using the phenol hypochlorite method (Solarazano 1969). DOC was determined using a Shimadzu TOC 5000 (Sharp et al., 1993). Rates of aerobic methane oxidation were measured by incubating triplicate live and dead (Hg-killed) samples in the presence of $^{14}CH_4$ (Joye et al., 1999) for 48 hrs. Unreacted $^{14}CH_4$ tracer was removed by purging samples with water-saturated methane (CH_4) and the oxidation product, $H^{14}CO_3^-$, was quantified by liquid scintillation counting (Joye et al., 1999). Nitrification rates were determined by measuring the increase in nitrate concentration over time.

4.7.1.3. Sample Inventory: DCCC Cruise

Seven CTD casts at three stations (two at AT340, three at GC852, and two at AC601; Table 4-1) generated 148 samples for oxygen, methane, nutrient and DOC concentration analyses. Six rate samples each were generated for 100 of these water samples, yielding 600 additional samples.

Table 4-1

Summary of Water Column Sampling Program--DCCC Cruise

Date	Site	CTD Cast #	Go-flo bottles tripped
5/15/06	AT340	1	23
5/17/06	AT340	2	20
5/20/06	GC852	3	18
5/22/06	GC852	4	20
5/22/06	GC852	5	21
5/29/06	AC601	6	23
5/31/06	AC601	7	23

4.7.1.4. Sample Inventory: Jason II Cruise

Six sets of water samples were collected, generating 18 samples for oxygen, methane, nutrient and DOC concentration analyses. Six to ten rate samples were generated each water sample, yielding 100 additional samples (Table 4-2).

Table 4-2

Summary of Water Column Sampling Program: *Jason II* Cruise

Date	Site	CTD Cast #
6/16/07	GB697	J2-274
6/21/07	AT340	J2-277
6/23/07	GC852	J2-278
6/26/07	GB647	J2-280
6/28/07	GC645	J2-281
7/2/07	AC601	J2-283

4.7.2. Sediment Biogeochemistry

4.7.2.1. Sample Collection and Analysis: DCCC Cruise

Sediment push cores (~8 cm inside diameter) were collected into polycarbonate core liner by positioning the core liner over an appropriate site with the *Alvin*'s manipulator arm (Appendix 1). Up to 12 cores were collected on each of the coring dives (14 of the 24 dives were coring

dives; see Table 4-3 and Table 4-4). For each set of cores, one core was used to generate pore water and solid phase geochemical data; one to two cores were used for rate assays to determine rates of sulfate reduction, methane oxidation and methanogenesis; and one to two sets of cores were sectioned to collect microbiology samples (see Microbiology section). For each geochemistry core, 11 different subsamples were collected from 4 to 11 depth intervals. A total of 254 depth intervals were sampled in the 27 geochemistry cores, generating 2,794 individual geochemistry samples.

Thirty-eight cores were used for determination of rates of microbial activity (Table 4-4). About 380 depth intervals were sampled, generating 3,000 individual samples (~1,200 sulfate reduction rate samples, 1,200 methane oxidation rate samples, and 600 methanogenesis rate samples).

Some degassing of methane-laden cores occurred during return to the surface and this was particularly notable at the deepest sites (e.g., AC601). Once the submersible was secure in the hanger, cores (or brine samples) were transferred immediately to the 4 ºC environmental room. Geochemistry cores were sectioned under anaerobic conditions and sub-samples were collected at 2 cm depth intervals for determination of concentrations of the following components: pH, salinity, dissolved gases, dissolved and particulate carbon and sulfur species, dissolved nutrients, metals, and redox metabolites (e.g., hydrogen sulfide and dissolved inorganic carbon (DIC)). Salinity was determined using a hand-held refractometer. Measurements of pH were done on board ship using an Accumet high precision electrometer that was calibrated with National Bureau of Standards (pH 4, 7 and 10).

Concentrations of C_1 to C_5 hydrocarbons were determined on a sediment sub-sample via headspace extraction (done on board the ship) and gas concentration was quantified using gas chromatography (Joye et al., 2004). Concentrations of dissolved hydrogen in the sediment porewater were determined following sediment incubations (~10 days) using a reduction gas analyzer (Orcutt et al., 2005). Sediment porosity was determined as weight loss after drying (Joye et al., 2004). Concentrations of DIC in the pore water were determined using a high sensitivity infrared gas analyzer.

Concentrations of hydrogen sulfide were determined colorimetrically (Cline 1969). Concentrations of anions (sulfate, chloride, iodide, and bromide) and cations (sodium, potassium, calcium, magnesium and barium) were determined using ion chromatography (Joye et al., 2004). Concentrations of Fe^{2+} and Mn^{2+} were analyzed colorimetrically using the ferrozine and formaldoxime methods, respectively (Stookey 1970; Armstrong et al., 1979). Concentrations of volatile fatty acids (i.e., formate, glycolate, acetate, proprionate, butyrate, lactate, and succinate) were determined following derivitization using high-performance liquid chromatography HPLC (Albert and Martens 1997). Concentrations of DOC were determined with a Shimadzu TOC 5000 (Sharp et al., 1993). Nutrient concentrations (nitrate+nitrite, phosphate, silicate) were determined using a lachat autoanalyzer (Joye et al., 2004) and concentrations of ammonium were determined using the phenol hypochlorite technique (Solarazano 1969). Concentrations of solid phase, organic and inorganic, carbon, nitrogen and sulfur were determined using standard methods on a ThermoFinnigan Flash Elemental Analyzer. Concentrations of methane were determined on board the ship. Nutrient concentrations were determined the week after the cruise.

Two to three cores from each set of cores collected were sub-sampled to determine rates of microbial metabolic activity. Rates of sulfate reduction (SR) and the anaerobic methane oxidation (AMO) were determined for all core sets. For SR and AMO rate measurements, six plexiglass sub-cores (2.54-cm inside diameter x 30 cm long) were collected from a core by manual insertion. Three sub-cores were used for SR rate assays while the other three were used for AMO rate assays. The overlying water phase was maintained during sub-coring and the ends of each tube were sealed with black rubber stoppers. Radiotracer (either $^{35}S\text{-}SO_4^{2-}$ or $^{14}CH_4$ dissolved in filter-sterilized (0.1 µm filtered) seawater) was added to pre-drilled, silicone filled holes at 0.5 cm intervals down the length of the core (Joye et al., 2004; Orcutt et al., 2005). For AMO, 100 µL of dissolved $^{14}CH_4$ tracer (about 60,000 dpm) was injected into each silicone-filled port. Cores were incubated for 12 to 24 hrs at bottom water temperature. Following incubation, cores were extruded and sub-samples were collected at 1 cm intervals and immediately transferred to a 50 (milliliter) mL plastic centrifuge tube containing 2 mL of 2M NaOH (which served to arrest biological activity and fix $^{14}C\text{-}CO_2$ and $^{14}C\text{-}HCO_3^-$). Each vial was sealed, vortexed to mix the sample and base, and immediately frozen. Time zero samples were fixed immediately after tracer injection. The specific activity of the tracer ($^{14}CH_4$) was determined by injecting 100 µL directly into scintillation cocktail (Scintiverse BD) followed by liquid scintillation counting. The accumulation of ^{14}C product ($^{14}CO_2$) was determined by acid digestion following the method of Joye et al. (1999). The AMO rate was calculated using a standard equation (Orcutt et al., 2005).

For SR rate measurements, 100 µL of tracer containing about 2 microCurie (µCi) of $Na_2{}^{35}SO_4$ was added to each port. Cores were incubated and sectioned as described above. Each sediment section was transferred to a 50 mL centrifuge tube containing 10 mL of 20% zinc acetate to halt microbial activity and fix $H_2{}^{35}S$ as $Zn^{35}S$. The accumulation of $H_2{}^{35}S$ product was recovered in a one-step hot chromous acid digestion. The activity of ZnS and sulfate fractions was determined by scintillation counting. The SR rate was calculated using a standard equation (Orcutt et al., 2005).

4.7.2.2. Sample Collection and Analysis: Jason II Cruise

Sediment push cores were collected into polycarbonate core liner by positioning the core liner over an appropriate site with the *Jason* II's manipulator arm. Up to 12 cores were collected per dive. A total of 193 cores were attempted. Of those, 42 cores failed to retrieve sediment or lost sediment during return to the ship; eleven were used by biologists; 7 were used by geologists. Of the remaining 130, the deepest cores (80 in all) were sampled for biogeochemistry and microbiology.

4.7.2.3. Sample Inventory: Jason II Cruise

Sediment cores were collected from 10 sites:

1. AT340: 48 cores (8 biology; 2 geology; 16 geochemestry/microbiology; 8 failed)
2. MC462: 9cores (3 geochemistry/microbiology; 4 failed)
3. GC415: 9 cores (3 geochemistry/microbiology; 6 failed)
4. GC852: 23 cores (15 geochemistry/microbiology; 1 geology; 1 failed)
5. GB697: 8 cores (3 geochemistry/microbiology; 2 failed)
6. WR269/270: 13 cores (8 geochemistry/microbiology; 1 failed)

7. GB647: 8 cores (3 geochemistry/microbiology; 4 failed)
8. AC645: 8 cores (4 geochemistry/microbiology)
9. AC601: 41 cores (18 geochemistry/microbiology; 14 failed)
10. AC818: 26 cores (16 geochemistry/microbiology; 2 failed)

Four replicate cores were processed for each habitat. We attempted to sample 4 to 5 key habitats (Brines, Urchins, Microbial Mats, Pogonophorans and/or an off-site Control) at each site (if the habitat was present at the site; see Table 4-4). Sediment from twenty-five cores was stored anaerobically for subsequent laboratory experiments. The other cores were too short to work with and/or disturbed and were discarded. Pore water samples, solid phase samples, samples for rate assays (sulfate reduction, methane oxidation and methanogenesis) and microbiology samples were collected from each replicate core. Table 4-4 summarizes the samples collected and analyzed during the *Jason II* cruise. For each geochemistry core, 15 different subsamples were collected from 4 depth intervals. A total of 345 depth intervals were sampled in the 68 geochemistry cores, generating approximately 5,300 individual geochemistry samples. For rate assays, triplicate samples for SR and anaerobic methane oxidation (AMO) were collected from each core and 4 depths per core were sampled (except at WR269 where 6 depths per core were sampled) generating a total of about 4,200 samples for SR and AMO rates.

Once the *Jason II* was secured on deck, cores (and/or water samples) were transferred immediately to the 4 ºC environmental room. Geochemistry cores were sectioned under anaerobic conditions and sub-samples were collected at 2 cm depth intervals for determination of concentrations of the following components: pH, salinity, dissolved gases, dissolved and particulate carbon and sulfur species, dissolved nutrients, metals, and redox metabolites (e.g., hydrogen sulfide and DIC). Salinity was determined using a hand-held refractometer. Measurements of pH were done on board ship using an Accumet high precision electrometer that was calibrated with National Bureau of Standards. (pH 4, 7 and 10).

Concentrations of C_1 to C_5 hydrocarbons were determined on a sediment sub-sample via headspace extraction (done on board the ship) and gas concentration was quantified using gas chromatography (Joye et al., 2004). Concentrations of dissolved hydrogen in the sediment porewater were determined following sediment incubations (~10 days) using a reduction gas analyzer (Orcutt et al., 2005). Sediment porosity was determined as weight loss after drying (Joye et al., 2004). Concentrations of DIC in the pore water were determined using a high sensitivity infrared gas analyzer.

Concentrations of hydrogen sulfide were determined colorimetrically (Cline 1969). Concentrations of anions (sulfate, chloride, iodide, and bromide) and cations (sodium, potassium, calcium, magnesium and barium) were determined using ion chromatography (Joye et al., 2004). Concentrations of Fe^{2+} and Mn^{2+} were analyzed colorimetrically using the ferrozine and formaldoxime methods, respectively (Stookey 1970, Armstrong et al., 1979). Concentrations of volatile fatty acids (i.e., formate, glycolate, acetate, proprionate, butyrate, lactate, and succinate) were determined following derivitization using high-performance liquid chromatography (Albert and Martens 1997). Concentrations of DOC were determined with a Shimadzu TOC 5000 (Sharp et al., 1993). Nutrient concentrations (nitrate+nitrite, phosphate, silicate) were determined using a LACHAT autoanalyzer (Joye et al., 2004) and concentrations of ammonium were determined

using the phenol hypochlorite technique (Solarazano 1969). Concentrations of solid phase, organic and inorganic, carbon, nitrogen and sulfur were determined using standard methods on a ThermoFinnigan Flash Elemental Analyzer. Concentrations of methane were determined on board the ship. Nutrient concentrations were determined the week after the cruise.

Eight sub-samples from each geochemistry core were used to determine rates of microbial metabolic activity. Rates of SR and AMO were determined for all core sets. For SR and AMO rate measurements, 5-cc sub-cores were collected from each depth interval by manual insertion. Four sub-samples (3 live, 1 control) were used for SR rate assays while the other four (three live, one control) were used for AMO rate assays. Radiotracer (either $^{35}S\text{-}SO_4^{2-}$ or $^{14}CH_4$ dissolved in filter-sterilized (0.1 µm filtered) seawater) was added to pre-drilled, silicone filled holes at 0.5 cm intervals down the length of the core (Joye et al., 2004, Orcutt et al., 2005). For AMO, 100 microliter (µL) of dissolved $^{14}CH_4$ tracer (about 200,000 disintegrations per minute (dpm) was injected into each sample. Cores were incubated for 12 to 24 hrs at bottom water temperature. Following incubation, cores were extruded and sub-samples were collected at 1 cm intervals and immediately transferred to a 50 mL plastic centrifuge tube containing 2 mL of 2M NaOH (which served to arrest biological activity and fix $^{14}C\text{-}CO_2$ and $^{14}C\text{-}HCO_3^-$). Each vial was sealed, vortexed to mix the sample and base, and immediately frozen. Time zero samples were fixed immediately after tracer injection. The specific activity of the tracer ($^{14}CH_4$) was determined by injecting 100 µL directly into scintillation cocktail (Scintiverse BD) followed by liquid scintillation counting. The accumulation of ^{14}C product ($^{14}CO_2$) was determined by acid digestion following the method of Joye et al. (1999). The AMO rate was calculated using a standard equation (Orcutt et al., 2005).

For SR rate measurements, 100 µL of tracer containing about 2 µCi of $Na_2{}^{35}SO_4$ (about 5,000,000 dpm) was added to each sample. Cores were incubated and sectioned as described above. Each sediment section was transferred to a 50 mL centrifuge tube containing 10 mL of 20% zinc acetate to halt microbial activity and fix $H_2{}^{35}S$ as $Zn^{35}S$. The accumulation of $H_2{}^{35}S$ product was recovered in a one-step hot chromous acid digestion. The activity of ZnS and sulfate fractions was determined by scintillation counting. The SR rate was calculated using a standard equation (Orcutt et al., 2005).

4.7.2.4. Sample Inventory: DCCC Cruise

Twenty-seven sets (a "set" is used here to denote four to six replicate cores) of sediment cores were collected from nine sites (Table 4-3):

1. AT340: five sets of cores;
2. GC600: four sets of cores;
3. GC852: four sets of cores;
4. MC853: two sets of cores;
5. MC640: three sets of cores;
6. WR269/270: one set of cores;
7. AC818: two sets of cores;
8. AC645: two set of cores ,
9. AC601: six sets of cores.

Table 4-3

Summary of Samples Used for Geochemistry: *Alvin* Cruise

Site	Dive	Core Designation	Depth of Sediment (cm)
1. AT340	4173	R1	14
2. AT340	4173	Y1	20
3. GC600	4174	Y2	20
4. GC600	4174	R4	12
5. GC852	4177	R1	22
6. MC853	4178	R4	20
7. MC853	4178	Y2	16
8. AT340	4181	R3	10
9. MC640	4182	R2	18
10. MC640	4182	Y4	16
11. MC640	4182	Y3	6
12. AT340	4183	Y2	22
13. AT340	4183	R2	18
14. GC600	4184	Y6	16
15. GC600	4184	R2	14
16. GC852	4189	Y1	12
17. GC852	4189	R3	12
18. GC852	4189	Y6	16
19. WR269/270	4191	Y5	20
20. AC818	4192	R5	18
21. AC818	4192	Y3	20
22. AC601	4193	Brine fluid	Brine fluid
23. AC601	4193	Y1	20
24. AC601	4193	R2	22
25. AC601	4193	Y6	20
26. AC645	4194	Y6	20
27. AC601	4196	Y5	20
28. AC601	4196	R5	18
29. AC601	4196	Brine Fluid	Brine fluid

Table 4-4

Summary of Samples Used for Microbial Rate Assays

Site	Dive	Core Designation
1. AT340	4173	Y4
2. AT340	4173	R4
3. GC600	4174	R4
4. GC600	4174	R1
5. GC852	4177	R5
6. GC852	4177	R6
7. MC853	4178	Y4
8. MC853	4178	Y5
9. MC853	4178	R1
10. MC853	4178	R6
11. AT340	4181	R3
12. AT340	4181	R4
13. MC640	4182	Y5
14. MC640	4182	R3
15. MC640	4182	R4
16. AT340	4183	Y1
17. AT340	4183	R4
18. AT340	4183	R5
19. GC600	4184	Y1
20. GC600	4184	Y3
21. GC600	4184	Y5
22. GC852	4189	R2
23. GC852	4189	Y5
24. WR269/270	4191	R2
25. WR269/270	4191	R3
26. AC818	4192	R6
27. AC818	4192	Y5
28. AC601	4193	Y5
29. AC601	4193	Y2
30. AC601	4193	R6
31. AC645	4194	Y2
32. AC645	4194	Y5
33. AC601	4196	R1
34. AC601	4196	R2
35. AC601	4196	R4
36. AC601	4196	Y1
37. AC601	4196	Y2
38. AC601	4196	Y3

4.7.3. Microbiology and Molecular Biology

4.7.3.1. Sample Collection, Inventory, and Discussion: DCCC Cruise

During the cruise, two types of microbiology samples were collected: water column and sediment. While shipboard, the microbiology samples were fixed for subsequent analysis at the University of Georgia, Athens, Georgia, and the Max Planck Institute (MPI), Bremen, Germany. A summary of the microbiology sample inventory, shipboard preparations, and methods in progress at shore-based facilities, and a discussion of how these procedures contribute to the goals of the CHEMO III program follows.

Approximately 125 water column microbiology samples were collected during seven CTD casts at three different sites. A majority of the water column samples were acquired during night-time CTD operations. Some additional samples were obtained from Niskins mounted on the DSV *Alvin*. Water column microbiology samples were from Niskin bottles, which were sampled immediately after the rosette was secured on the deck. A 10 mL sub-sample was fixed with a 4% formaldehyde solution for 30 minutes and then frozen at -20 ºC. All water column samples were analyzed using epifluorescence microscopy to determine microbial abundance (via Acridine Orange-Direct Count, AODC) and to determine the abundance of methanotrophs (via Fluorescence *in situ* Hybridization, FISH).

Approximately 140 microbiology sediment samples were collected during 23 dives at a diverse group of sites (e.g., brines, mussel beds, clam beds, oil seeps, bacterial mats) (Table 4-5). Molecular sediment samples were collected and fixed for a variety of molecular analyses: AODC, Catalyzed Auto-Reporter Deposition Fluorescence *in situ* Hybridization (CARD-FISH), deoxyribonucleic acid (DNA) extraction and sequencing, and biomarker analysis. Sediment samples were collected from cores in 2 cm intervals for each of these analyses. At each depth, one cm^3 of sediment was fixed in 4%formaldehyde in filter-sterilized (0.1 µm filtered) Sargasso seawater. The fixed portion was then split for AODC and CARD-FISH. The CARD-FISH split was stored in an ethanol/phosphate buffer at -20 ºC. From each two cm interval, 20–30 grams of wet sediment were stored at -20ºC for DNA extraction. The remainder of the two cm intervals was collected for biomarker analysis. At approximately six sites, live mud was collected and stored under an argon atmosphere at 4 ºC for subsequent laboratory enrichment experiments.

Because one of the major themes of the program is to investigate the biogeography and ecology of the lower continental slope, microbiology methods that allow quantification of microbial abundance as well as the determination of individual microbial (type) distributions (i.e., how many microbes and which microbes are there) were selected. The two cm intervals from which all microbiology samples were collected are paired directly with geochemical and rate samples described in Sediment Biogeochemistry. The ability to link all these data is pivotal to revealing what microbes are doing in their environment.

For a general determination of total microbial abundance in sediment, epifluorescence microscopy (AO-DC, Hobbie et al., 1977) was used. Since this is a non-specific method (i.e., the dye illuminates all cells indiscriminately) and the interest is to describe microbial community structure and associations, CARD-FISH will be used to identify specific groups of bacteria and archaea (e.g. specific sulfate reducing bacteria and methane oxidizing archaea) and visualize

their associations (Amann et al., 1990). In CARD-FISH, probes are used to selectively illuminate microbial cells based on functional genes or 16S rDNA (ribosomal deoxyribonucleic acid) for that specific cell type. CARD-FISH will be used to determine the abundance of the anaerobic methane oxidiers (ANME) and sulfate reducing bacteria (SRB) consortium (Boetius et al., 2003, Orcutt et al., 2005).

Table 4-5

Inventory of Sediment Microbiology Samples

Dive #	Core ID	# Depths	FISH	DNA	AODC	Biomarker
1. 4173	R5	13	x	x	x	x
2. 4173	Y2	11	x	x	x	x
3. 4174	Y4	4	x	x	x	x
4. 4174	R5	10	x	x	x	x
5. 4177	R2	5	x	x	x	x
6. 4178	Y4	9	x	x	x	x
7. 4178	R2	6	x	x	x	x
8. 4183	Y6	3	x	x	x	x
9. 4184	Y1	7	x	x	x	x
10. 4189	R1	4	x	x	x	x
11. 4191	Y4	10	x	x	x	x
12. 4192	Y4	10	x	x	x	x
13. 4192	R4	5	x	x	x	x
14. 4193	R1	12	x	x	x	x
15. 4193	R5	8	x	x	x	x
15. 4193	Y5	9	x	x	x	x
16. 4194	Y3	6	x	x	x	x
17. 4196	Y6	5	x	x	x	x
18. 4196	R1	5	x	x	x	x

The final method used to investigate sediment microbial abundance and identity at the lower continental slope is an analysis of biomarkers. Each microbe has a specific lipid membrane make-up (i.e., glycerol fatty acid esters, isoprenoid glycerol ether, or isoprenoid hydrocarbons). Much like humans, the biomarker composition of a sample offers a microbial "fingerprint." The biomarker method quantifies specific lipids to determine which microbes are present and thereby their relative abundance. This method also helps determine the abundance and occurrence of the ANME/SRB consortia, and which ANME archaeans (ANME-1, ANME-2, and ANME-3) and SRB are responsible for the consortia (Niemann, et al., 2005).

"Live mud" was used for manipulating constituent microbes to gain an understanding of their limitations, genetic makeup, and activities in the environment. Preliminary analysis of geochemical samples shows that along the lower continental slope sulfide concentrations are, at some sites, extremely high. One of the potential uses of live mud would therefore be to test the tolerance of *in situ* microorganisms to high sulfide concentrations. Sulfide inhibits the activity of

microbes, including SRB that produce sulfide. Locally, the sulfide concentrations can greatly impact the ecology at the respective sites.

4.7.3.2. Sample Collection, Inventory, and Discussion: Jason II Cruise

During the cruise, microbiology samples were collected from each core/depth where geochemistry samples were collected. While shipboard, the microbiology samples were fixed for subsequent analysis at UGA.

Approximately 300 microbiology sediment samples were collected (e.g., brines, oil seeps, bacterial mats, pogonophorans and controls). Molecular sediment samples were collected and fixed for a variety of molecular analyses: AODC, CARD-FISH, DNA extraction and sequencing, and biomarker analysis. Sediment samples were collected from cores in 2 cm intervals for each of these analyses. At each depth, one cm^3 of sediment was fixed in 4% formaldehyde in filter-sterilized (0.1 µm filtered) Sargasso seawater. The fixed portion was then split for AODC and CARD-FISH. The CARD-FISH split was stored in an ethanol/phosphate buffer at -20 ºC. From each two cm interval, 20–30 grams of wet sediment were stored at -20ºC for DNA extraction. The remainder of the two cm intervals was collected for biomarker analysis. At approximately six sites, live mud was collected and stored under an argon atmosphere at 4 ºC for subsequent laboratory enrichment experiments.

Because one of the major themes of the program is to investigate the biogeography and ecology of the lower continental slope, microbiology methods that allow quantification of microbial abundance as well as the determination of individual microbial (type) distributions (i.e., how many microbes and which microbes are there) were selected. The ability to link all these data is pivotal to revealing what microbes are doing in their environment.

For a general determination of total microbial abundance in sediment, epifluorescence microscopy (AO-DC, Hobbie et al., 1977) was used. Since this is a non-specific method (*i.e.*, the dye illuminates all cells indiscriminately) and the interest is to describe microbial community structure and associations, CARD-FISH will be used to identify specific groups of bacteria and archaea (e.g., specific sulfate reducing bacteria and methane oxidizing archaea) and visualize their associations (Amann et al., 1990). In CARD-FISH, probes are used to selectively illuminate microbial cells based on functional genes or 16S rDNA for that specific cell type. CARD-FISH will be used to determine the abundance of the anaerobic methane oxidiers (ANME) and SRB consortium (Boetius et al., 2003, Orcutt et al., 2005).

Live mud was used for manipulating constituent microbes to gain an understanding of their limitations, genetic makeup, and activities in the environment.

5. *IN SITU* CHEMICAL SENSORS

5.1. Overview of Systems Tested

There is a paucity of sensors that are effective for making robust chemical measurements relevant to chemosynthetic communities *in situ*. In the context of this program, we attempted to employ several different sensor technologies to measure sulfide and methane *in situ*. The first sensor system used in 2006 (provided through collaborations with MPI) did not provide useful data because of serious noise problems due to electrical interference with the submersible *ALVIN*. In 2007, we tested three additional sensor technologies. A solid-state sensor for methane quantification was purchased and tested on numerous dives. There was an apparent (and variable) pressure/temperature effect detected during ascent and descent, but more importantly it was not reliable in the seep environment. The records were not consistent with the deployment locations and variable baseline shifts during dives could not be explained from submersible activities. Other investigators have suggested that it is neither quantitative nor sensitive after the first exposure to methane in situ. A small infrared-based system was also deployed in 2007. After several runs, it was apparent that methane quantification was not possible as there was significant interference from another co-occurring volatile (likely sulfide).

The third sensor system tested was an In Situ Mass Spectrometer (ISMS) developed by Dr. Peter Girguis of Harvard. This system was deployed in two different pressure housings over the course of the 2007 expedition using newly developed sampling wands for the first time. By the end of the cruise the system was performing very reliably, and we were able to collect a variety of valuable data throughout the 2007 expedition.

All ISMS data has now been compiled and sorted preliminary analyses are complete. In addition, the support provided by the BOEM has enabled significant advances in this instrument, moving it from a technology readiness level of 5 (technology demonstration) to a technology readiness level of 9 (operational system, with ongoing optimization for efficiency and cost).

5.2. Results from the *In Situ* Mass Spectrometer

The ISMS was deployed on seven dives, during which time it was used to scan a variety of environments including mussel beds, tube worm clumps, brine pools and gas hydrates. Most often, the ISMS was used to look at fine scale variations in sulfide and methane in and around megafaunal communities. The ISMS was used to collect data from approximately 105 discrete locales on the seafloor (see Appendix 2). While sampling, the ISMS acquired 25 scans from each locale, for a total of 2,625 scans.

The ISMS is the first mass spectrometer to ever acquire data on dissolved volatiles from depths greater than 1,000 m, and remains the only mass spectrometer capable of directed sampling via its pumped inlet system. This enabled the ISMS user to sample fluid volumes at rates as low as 3 mLs per minute, which is essential for sampling seep fluids without excessive dilution by overlying bottom water. As this was the first deepwater ISMS deployment, there were issues that arose and hindered both our deployment and sampling efforts. With respect to the data acquisition, the presence of mineral oil inside the vacuum chamber led to a series of peaks that coincided with one of the three sulfide peaks. This made observing changes in sulfide in real time quite challenging. However, final data clean-up employed well-established signal to noise filtering methods, enabling us to remove the oil signature from 85% of the acquired data.

Prior to publishing these data, we completed an extensive series of calibrations that allowed us to empirically validate the efficacy of the instrument's accuracy (in determining concentration) and precision (in repeatability). During lab experiments, relative changes in signal intensity were proportional to changes in the permeation of gas through the membrane (either due to changes in permeate concentration or changes in the permeability coefficient). We, and others, have observed that changes in hydrostatic pressure can have an influence on permeation of gases through membrane materials, in particular polydimethylsiloxane interpreted to be caused by compression of the membrane pore space through which analyte gas passes (Bell et al., 2007). A change in the relationship between dissolved gas concentration and signal intensity was observed during large changes in hydrostatic pressure. To account for this response, we conducted calibrations using methane dissolved in seawater over a range of in situ pressures and used these results to develop an empirical correction as previously described (Bell et al., 2007).

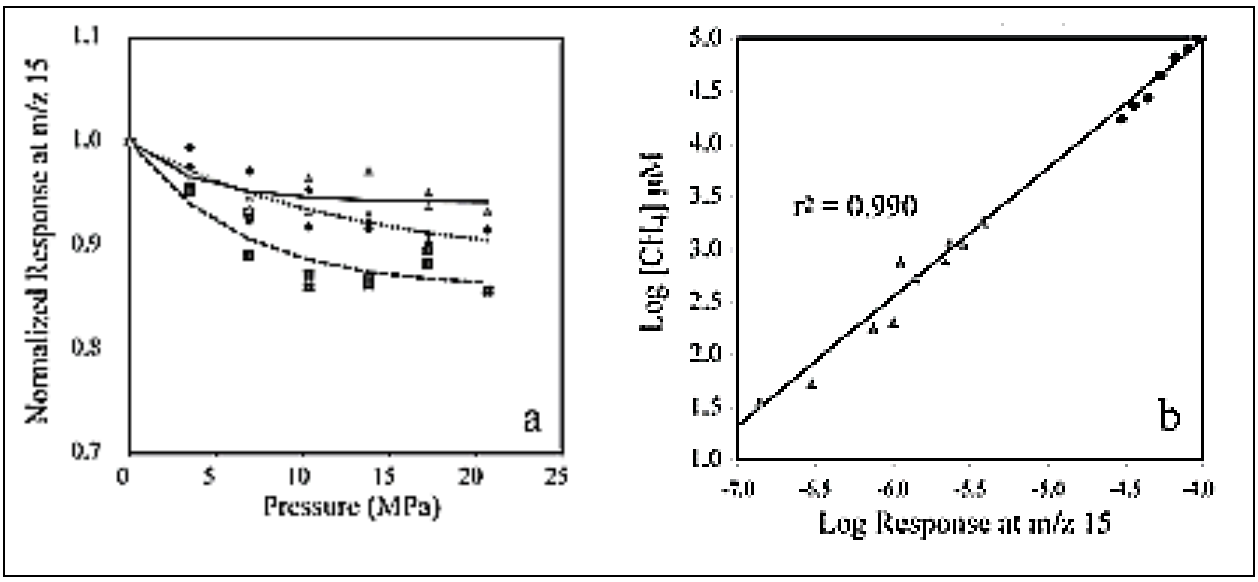

Figure 5-2. (A) Normalized response at mass to charge ratio (m/z) 15 over a range of hydrostatic pressure for three example fluid temperatures and concentrations, 10˚C 1160 millimolar (mmol) CH_4 (grey squares), 2˚C 800 mmol CH_4 (black triangles) and 14˚C 180 mmol CH_4 (grey triangles). Responses to pressure were experimentally fit under a wide range of temperatures and concentrations (as in Bell et al., 2007) with values of b' ranging between 0.02 to 0.24 and values of k ranging between 0.84 to 0.94. (B) The response of m/z 15 (corrected for pressure effects) was linearly proportional to methane concentrations as measured independently by gas chromatography (grey triangles) and as calculated after Duan et al., 2006 during high pressure calibration measurements (black circles).

While this approach corrects for implicit changes in membrane behavior, it should be noted that the ISMS dataset presented here is comprised entirely of fluids sampled at a relatively constant depth (~2330 m) thus the temperature and as such effects due to differential pressure or temperature among the samples collected were negligible. Based on benchtop calibrations, the accuracy of the ISMS methane concentrations in the configuration described here was ± 10%.

This is primarily due to the correction required for the pressure effects on the polydimethysiloxane membrane and the use of a small-scale pumping system (accuracy has since been improved to ± 2% through the use of pressure-treated membranes and higher flow pumping systems). Notably, however, the precision of the ISMS measurements is much better than this and, based on benchtop calibrations, is within ±1%.

Our ability to re-create the high pressures and chemical conditions found in situ has enabled us to produce a robust calibration series that is applicable to all future deployments. These calibrations have been incorporated into a sophisticated spreadsheet, that may be used by other users to determine concentrations directly from their mass spectra (to date, the ISMS has been used by groups from Harvard, Naval Research Lab, MPI, MARUM Center for Marine Environmental Sciences, and the Roscoff Institute in France.

Data collected during the 2007 *Jason II* cruise and our subsequent laboratory work will lead to the publication of at least two papers. The first, a manuscript on methane flux from brine pools has been published in the special edition of Deep Sea Research II coordinated by Dr. Harry Roberts (Roberts and Boland, 2010).

In brief, for this manuscript we used the ISMS to measure methane concentrations in a GoM brine pool (lease block 601) located at a depth of over 2300 m. Concentrations of up to 33 miliMoles (mmol) methane were observed within the brine pool, while concentrations in the water directly above were three orders of magnitude lower. These direct measurements enable the first accurate estimates of the diffusive flux from a brine pool, calculated to be 1.1 ± 0.2 mole m-2 yr-1. Integrated rate measurements of aerobic methane oxidation in the water column overlying the brine pool were ~320 microMoles (μmol) m 2 yr-1, accounting at most for just 0.03% of the diffusive methane flux from the brine pool. Calculated rates of anaerobic methane oxidation were 600 to 1200 μM yr-1, one to two orders of magnitude higher than previously published values of AMO in anoxic fluids (see Figure 5-3). These findings suggest that brine pools are enormous point sources of methane in the deep sea, and may, in aggregate, have a pronounced impact on the global marine methane cycle.

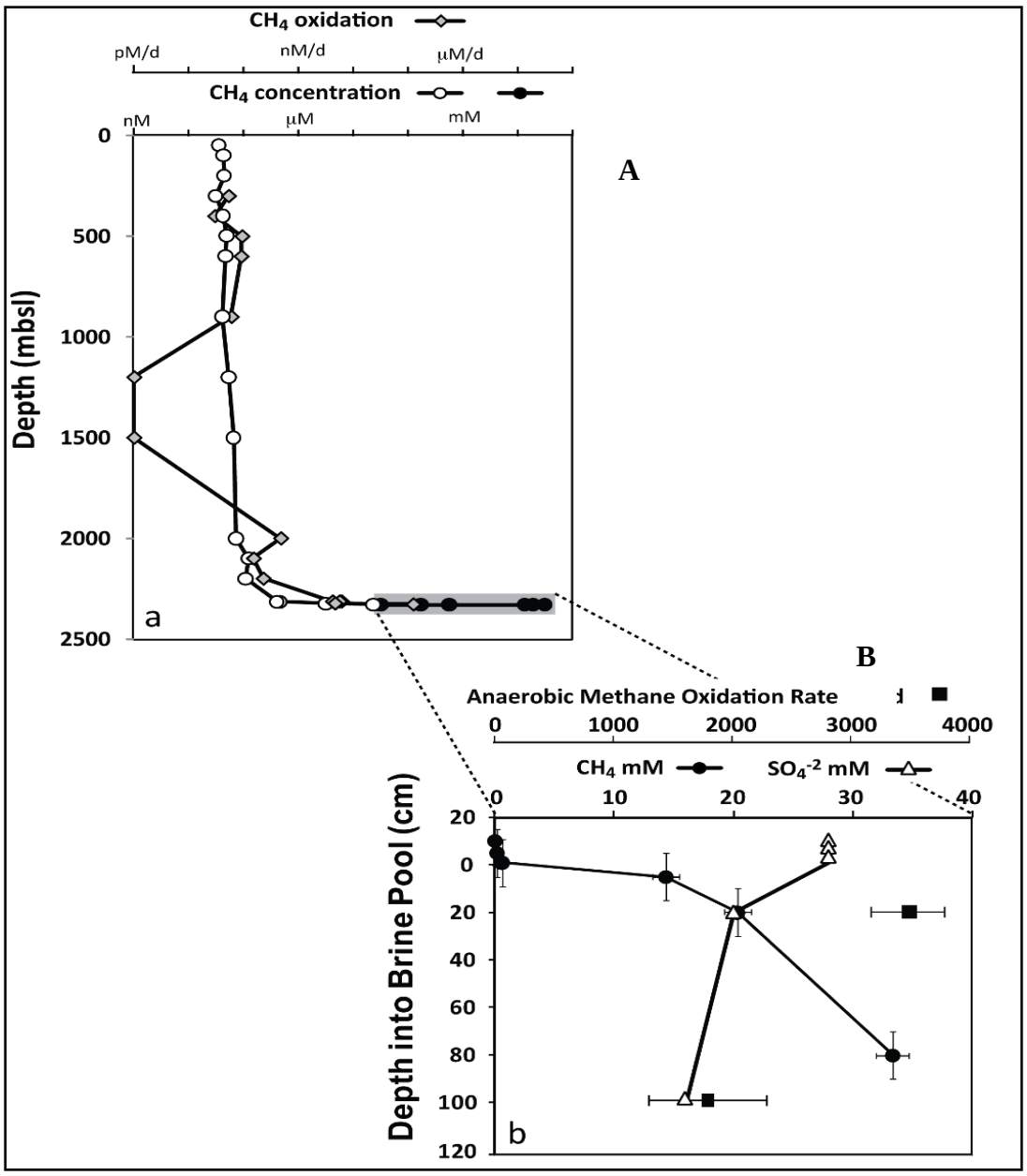

Figure 5-3. (A) Depth profile (in meters below sea level) of methane concentration and methane oxidation rates in the water column above brine pool AC601. Note log scale. Open circles are concentration measurements made from Niskin bottle samples, while black circles are those made *in situ* using the ISMS. (B) Close-up of seawater/brine pool interface and profile into the brine fluid. Note the linear scale in contrast to panel a. Measured rates of anaerobic methane oxidation (AMO) at two depths within the brine pool are shown. Note that these, when corrected for in situ CH4 concentrations, these rates are 30–45 times higher. Sulfate concentrations are depleted in the brine, consistent with its role in AMO.

Our second manuscript will be focused on the distribution of higher alkanes in the GoM and their relation to the microbial and megafaunal communities found therein. This paper is being

prepared, in collaboration with Dr. Mandy Joye, for submission to Geophysical Research Letters. In recent years, integrative biogeochemical studies focused on anaerobic methane oxidation (or AMO), have revealed much about the microbes that mediate this process. Recent work has shown that SR rates are decoupled from those of AMO indicating a coupling of SR to the oxidation of other hydrocarbons (Joye et al., 2004). The precise nature and extent of this as well as the influence on AMO is unconstrained, but it is possible that C2-C5 hydrocarbon degradation is a significant process that co-occurs with and influences AMO (Joye et al., 2004). This could have global implications because AMO is considered responsible for consuming the majority of methane in anoxic marine sediments and plays a major role in the cycling of methane, preventing its escape into the atmosphere. It is plausible that C2-C5 oxidation could contribute to the production of methane, thereby supporting AMO or it could compete with AMO for the use of sulfate as an oxidant via consortial interactions. To date, the anaerobic oxidation of C2-C5 hydrocarbons has been inferred from stable carbon isotope data to occur in the Gulf of Cadiz as well the northern slope of the GoM (e.g., Sassen et al., 2004). However, while the degradation of heavier hydrocarbons has been extensively studied and numerous reviews on the subject exist (Van Hamme et al., 2003 and references therein), C2-C5 hydrocarbon degradation has largely been overlooked.

The northern slope of the GoM is an ideal site to study the cycling of non-methane hydrocarbons (C2-C5) as the area is associated with significant alkane "seepage" from the dissolution of structure II and structure H gas hydrates (Sassen and MacDonald, 1997). In light of the aforementioned geochemical and microbiological observations, it is evident that a thorough investigation of C2-C5 hydrocarbon oxidizing organisms and their interactions with each other, as well as the surrounding microbial community, is required to understand their role in global geochemical cycles. During the 2007 *Jason II* cruise, we collected an extensive dataset on the distribution of C2-C5 alkanes in the GoM, and have begun synthesizing these data for publication. Briefly, we have observed that the distribution of alkanes inversely correlates to sulfate concentrations, again suggesting a linkage between alkane oxidation and sulfate reduction. This paper will focus on quantifying those relationships, to better understand the interplay between these short chain alkanes, and their influence on the marine carbon and sulfur cycles. Table 5-1 is representative data on methane and ethane concentrations in and near to the brine lake in AC-601. Propane and butane were also quantified, though not shown here.

Table 5-1

Summary of Concentrations for Methane and Ethane from Sites 81 through 94

Site	Description	Study Object	CH4 (µM)	Ethane (µM)
83	Background above brine pool	Brine Pool	9.85	.433
85	1 cm above seds - on the shore of brine pool	Brine Pool	77.06	13.8
86	Inside brine pool	Brine Pool	3682.81	170.7
88	20 cm depth into brine pool	Brine Pool	6644.37	273.7
89	50 cm depth into brine pool	Brine Pool	33792.08	667.5
90	Urchin core hole - Marshall - Core #6 Red	Brine Pool	60.27	5.78
91	Background Scan - mussels	Mussels	3.19	N/A
92	Into mussel pot scar	Mussels	2.98	6.06
93	Between 2 mussels	Mussels	89.29	9.248
94	Depression near Brine Pool	Brine Pool	56.56	2.312

5.3. Concluding Remarks

Despite the fact that Dr. Girguis' laboratory and the ISMS were brought into the program very shortly before our last field expedition, we were able to demonstrate that the ISMS is capable of quantifying the key biologically relevant seep volatiles (methane, carbon dioxide, hydrogen sulfide, hydrogen, oxygen, among others) simultaneously, and in a manner of minutes. As already mentioned, the BOEM support raised this instrument to a TLR of 9, and current efforts are aimed at increasing sensitivity, reducing power usage, and improving the user interface. To date, we have improved sensitivity to methane and other volatiles by two orders of magnitude, and have reduced power consumption by 20%. The instrument is also being re-packaged into a small lighter housing, which will reduce its weight and size by 30%. It is our objective to make this instrument readily available to the broader community (including those participating in BOEM projects). In particular, we are moving towards automating the system so it can be deployed independent of an ROV or a human occupied vehicle (HOV). This effort is being supported in part by the National Aeronautics and Space Administration (NASA).

6. COMMENTS ON SITE SELECTION

Over two decades, research has been conducted across the northern Gulf of Mexico's continental slope using seismic data, coring, ROVs, and manned submersible dives to study the impacts of fluid-gas expulsion on the geology and biology of the modern seafloor. These investigations have been made primarily in water depths of 1,000 m or shallower, but over the last five years projects have been fielded to put emphasis on the middle and lower continental slope. Finding sites of fluid-gas expulsion where deepwater corals and/or chemosynthetic communities may exist is a difficult task when the enormous area of the northern GoM is considered. However, because the GoM is a productive oil and gas province, most of the slope is now covered with high quality, industry-acquired three-dimensional (3-D)-seismic data. These datasets currently consist of 192 3-D-seismic surveys acquired over 76,000 mi^2 (196,850 km^2) which amounts to about 98% of the slope area from the Texas-Louisiana border to the DeSoto Canyon. More data are being acquired each year and some areas of the slope are represented by multiple survey datasets. The data are held proprietary by BOEM in their New Orleans, Louisiana office, where they are used for regulatory purposes in oil and gas lease evaluations. Because the research project described in this document is partially funded by BOEM, the 3-D-seismic data are available for project support, but may not be published without the consent of the owner company(s).

Research conducted in the early 1990s demonstrated that the strength or amplitude of the seafloor reflector and its plan-view pattern as derived from 3-D-seismic data are powerful methodologies for making informed interpretations of surface geology and benthic habitat characteristics. Sheriff (2002) defines amplitude as "the maximum departure of a wave from its average value." Reflection is defined as the energy or wave from a seismic source that has been reflected (returned) from an acoustic impedance contrast (reflector) or series of contrasts within the earth. The objective of most reflection seismic work is to determine the locations and altitudes of reflectors from measurements of the travel time of primary reflections and to infer geologic structure and stratigraphy from these relationships. In the study reported here, interpretation of subsurface geology is certainly important for determining location and characteristics of hydrocarbon migration pathways to the modern seafloor. Conditions at the sediment-water interface, however, are critical to determining settings that are likely to support diverse and well-populated communities of chemosynthetic organisms and provide hard substrates suitable for support of deepwater coral communities. These hard substrates form as nodular masses in sediment, sheet-like hardgrounds, and mounds of various sizes. They are the by-products of microbial oxidation of hydrocarbons at or near the seafloor of seepage sites.

These hard bottom areas clearly result in seafloor reflectivity (SBS), easily identified on 3-D-seismic data. Appraisals of surface reflectivity (amplitude) from regional 3-D-seismic data sets indicated that the continental slope of the northern GoM is punctuated with thousands of SBS. Most of them are related to seeps and more active vents. There are, however, a few exceptions, such as recently deposited sand-rich slope fans. Also, at the shelf edge, biogenic carbonate veneers on shelf edge knolls are highly reflective, but by far the greatest number of SBS sites across the slope is related to the fluid-gas expulsion process. Seafloor response to the expulsion process is qualitatively related to delivery rate of hydrocarbons, formation fluids, and sometimes

fluidized sediment. Patterns of seafloor reflectivity are clues to the delivery rate and seafloor responses.

The methodology of using seafloor reflectivity from 3-D-seismic data as a tool for identifying and further evaluating potential sites for the occurrence of deepwater coral communities, *Lophelia* and other genera, has been very successful. Using this methodology in conjunction with reconnaissance level drift camera work has been enormously successful in finding scientifically productive sites. Information from these procedures focuses researchers on where to dive and so saves project resources.

7. REMOTE SENSING EVALUATION OF CHEMOSYNTHETIC COMMUNITIES AND GEOPHYSICAL ANOMALY SITES WITH USE OF SATELLITE SAR

7.1. Introduction

Remote sensing detection of natural hydrocarbon seeps in the ocean is of interest to the scientific community and the oil and gas industry. From a biological perspective, seeps often associated with chemosynthetic communities in the deep sea (Fisher, 1990; MacDonald et al., 2003), so existence of these communities may be detected on the basis of remote sensing data. From the geological point of view, seeps can be associated with geophysical features that are indicative of potential energy reserves, including gas hydrates (Roberts and Carney, 1997a; Sassen et al., 2001).

Satellite SAR (synthetic aperture radar) images have proven to be a reliable tool for localizing natural seepage of hydrocarbons (Espedal and Wahl, 1999; Garcia-Pineda et al., 2008; Pellon de Miranda et al., 2004). In addition, SAR provides a means for quantifying seepage at a basin-wide scale and for assessing the temporal variability in discharge (MacDonald et al., 1996; Mitchell et al., 1999). However, active oil seeps that can be detected with SAR probably represent a subset of the total array of geophysical features generated by hydrocarbon migration on the continental slope (Frye, 2008). Additional work is needed to determine the relationship between oil seeps visible on the sea surface, the geology of the underlying formations, and the biological response of the deep-sea benthos to hydrocarbon enrichment.

7.1.1. Seeps Detected by Remote Sensing

Seeps known from the upper slope occur where focused sources of gas or liquid hydrocarbons migrate from deep structures into unconsolidated sediment near the seafloor (Roberts and Carney, 1997b). Focused flow is sometimes accompanied with mud volcanism and discharge of brines and cognate fluids (MacDonald et al., 2002; Roberts, 2006). Biological interactions consume a substantial portion of seeping hydrocarbons (Fisher, 1990). Formation of gas hydrate also reduces sediment porosity and flux (Roberts and Carney, 1997b). However, where flow exceeds equilibrium consumption and hydrate formation rates, a fraction of gas and oil escapes into the water column from discrete vents within a larger seep site (Brooks et al., 1990). One question for the current study is whether the model of seepage developed on the upper slope would apply to depths beyond 1000 m. This line of inquiry extends to the remote sensing signature of deep-water seeps.

Hydrocarbons detected in remote sensing begin as material that was vented at the seafloor and rises to the surface. Gas is released to the water column as small (1–10 mm) bubbles (Leifer and MacDonald, 2003). Oil coats the walls of the bubbles or rises as gassy droplets. During vertical transit through the water column streams of oil bubbles may be laterally deflected by currents (MacDonald et al., 2002). However the cross-section of bubble streams does not expand substantially between the seafloor and the sea surface. A significant part of oil and gas at natural seeps is consumed and mixed through the water column (Leifer and MacDonald, 2003). Oil that reaches the surface forms a thin layer (~0.1μm) of surfactant particles, called an oil slick, that

drifts along a curvilinear path determined by wind and surface currents; the persistence of oil slicks is strongly influenced by wind strength and sea state (MacDonald et al., 2002).

Oil slicks produce distinctive remote sensing signatures detectable by SAR satellites. When small (~10 cm) surface wavelets are dampened by viscoelastic properties of an oil slick or any other surfactant, energy from the SAR spacecraft is reflected away from the sensor, reducing radar backscatter and producing a dark area on the image (Figure 7-1). From previous investigations, it is known that expressions of oil slicks can range in width from 60 to several hundred m and can exhibit lengths of several kilometers (km) (Garcia-Pineda et al., 2008). As described in several studies (De Beukelaer et al., 2003; Espedal and Wahl, 1999; Fortuny-Guasch, 2003; Pellon de Miranda et al., 2004), oil slicks from natural hydrocarbon seeps are best detected by SAR satellites within in a wind range from 2 to 8 m/s and in an angle of incidence range from 20 to 45 degrees.

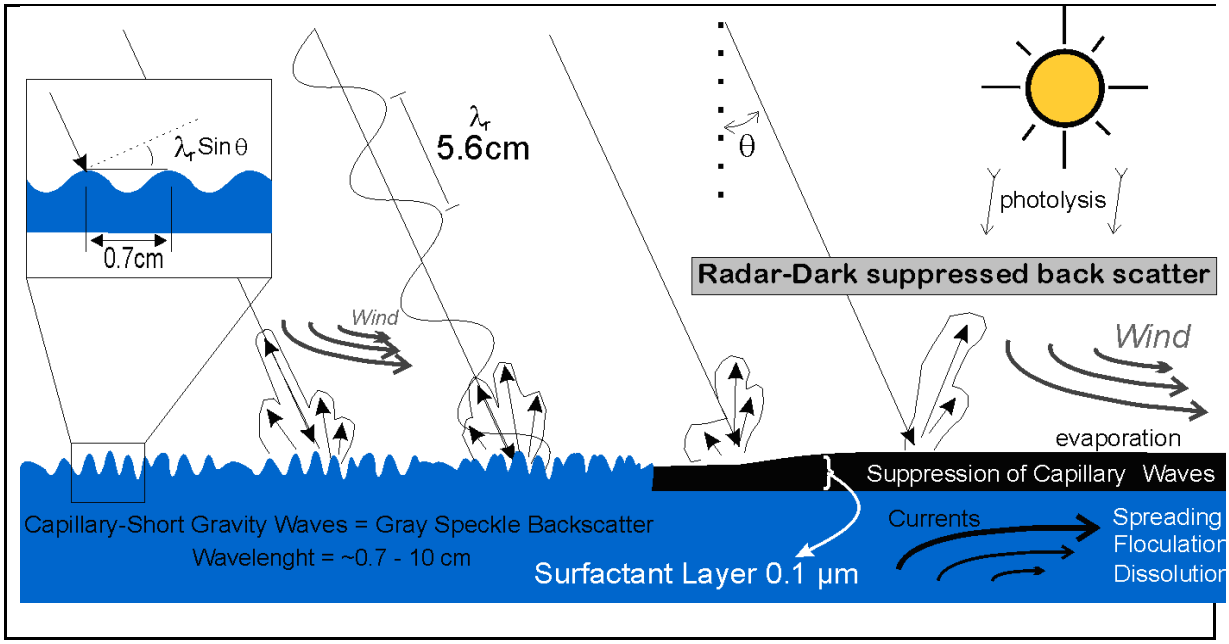

Figure 7-1. Schematic showing how layers of floating oil (surfactant) create a radar-dark signature on the sea surface.

Starting from when SAR became available in 1991 (with the Earth Resource Satellite-1), SAR satellite platforms have increasingly been used to monitor ocean surfactants (surface-active-agent). Currently, 12 radar satellites remain operational, with more than 70 different combinations of SAR image products between spatial resolution, polarization and incidence angles (Garcia-Pineda et al., 2009). In previous investigations, it was found that the Standard Beam Mode (SBM) 1, 2, and 3, from RADARSAT-1 to have the optimal balance between spatial scales and coverage to study fine scale ocean features like oil slicks from natural hydrocarbon seeps (Garcia-Pineda et al., 2008). RADARSAT-1 SBM images cover square areas of 100 by 100 km with a resolution of 25 m per pixel.

7.1.2. Geophysical Data Considered

Geophysical records from the GoM show abundant seep formations including reservoirs, faults, and migration conduits found in seismic profiles, as well as hard grounds and mud flows identified in surface amplitude maps (Roberts, 2006). These geophysical data are also important remote sensing indicators of active seeps, gas hydrate deposits, and chemosynthetic communities (Frye, 2008). Seeps and mud volcanoes undergo distinct activity phases over geologic time and may eventually become dormant or extinct as active sources (MacDonald and Peccini, 2009). It is likely therefore that seeps active today represent a small fraction of the total array of seeps found in the geologic record. Comparing active seeps with the geological record could shed light on the proportion of active to extinct seeps.

Repeated imaging of oil slicks in the same region has been widely interpreted as a robust indicator of an active seep on the seafloor (Alpers and Espedal, 2004; De Beukelaer et al., 2003; Kornacki et al., 1994; MacDonald et al., 1996). Reviewing an extensive archive of SAR images, which covers a large marine basin over a decadal time scale, makes it possible to examine fine scale features of the seep process. Ground truth of satellite data with geophysical records and seafloor observations from submersibles provide verification of image interpretation.

This study compared SAR images (collected covering the GoM from 1994 to 2008) with geophysical data archived by BOEM-GoM-OCS (Frye, 2008) within the broad region that contains the study sites for the CHEMO III study (Figure 7-2). Study sites were initially selected based on geophysical characteristics interpreted from seafloor reflectivity, underlying seismic structure (e.g., migration paths), and their topography. Characteristics of these geophysical sites have been described elsewhere (Roberts, 2006). Dive sites have likewise been described in greater detail in this report and parallel investigations (Roberts et al., 2007). The goal of this section is to present a characterization of natural oil discharge as detected in SAR images over these sites and in the region. The results examined the following questions: 1) how the utility of satellite SAR for basin-wide assessment of hydrocarbon flux into the ocean and atmosphere is affected by the spatial scales of seep geophysical features and individual vents as well as 2) investigating how winds and currents influence SAR signals created by natural oil and gas seeps.

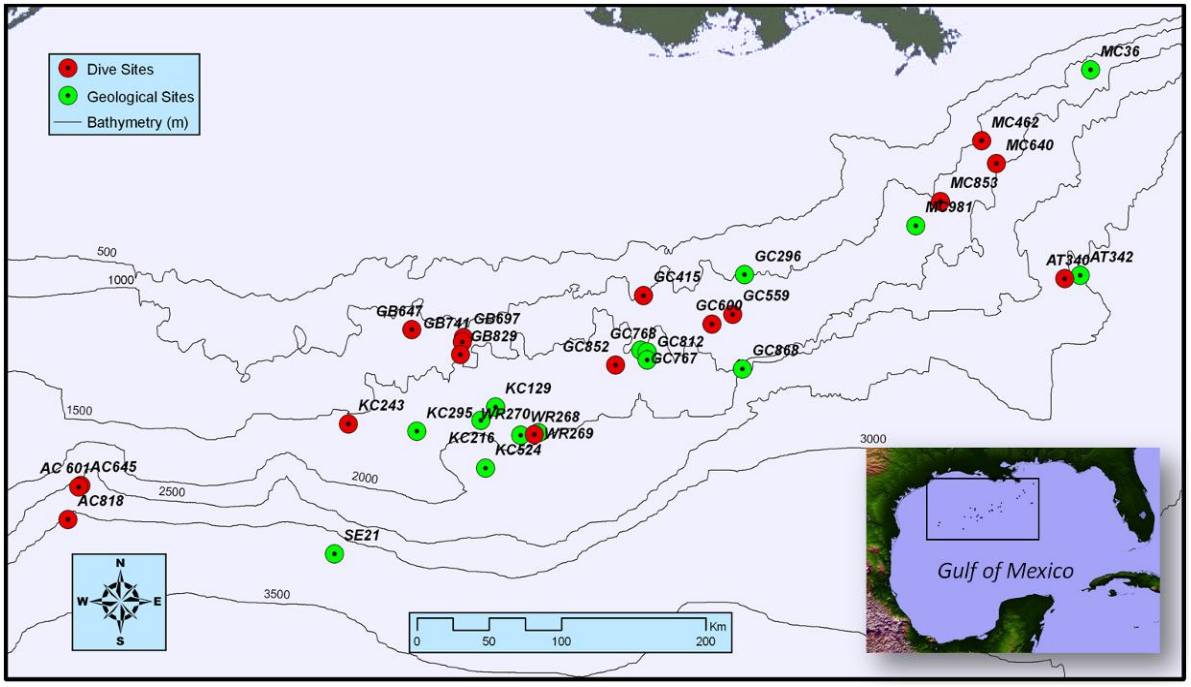

Figure 7-2. Study area and sites located on the OCS in the Northern GoM, investigated by satellite and geologic remote sensing.
Dive sites were investigated during the submersible dives in 2006 and 2007.

7.2. Materials and Methods

7.2.1. SAR Image Acquisition and Pre-processing

Satellite images used in this study were provided through a data-sharing agreement with NASA and The Alaska Satellite Facility (ASF). The images included collections made on request over the area of interest and archived images requested for other users. A series of 64 SBM SAR images were collected by RADARSAT-1, while the R/V *Atlantis* was at sea (during May, June and July 2006) conducting in situ observations of the geophysical anomalies with the human-occupied submersible *Alvin*. In 2007, 128 SBM SAR images were acquired by RADARSAT-1 while some of the sites were investigated with the R/V *Ronald Brown* using the ROV *Jason II*.

Data collected by RADARSAT-1 during both research expeditions were obtained along orbital paths that covered the individual sampling sites. Navigation records from research and vessels which could be detected as SAR targets in some of the RADARSAT-1 images were used to confirm the georectification of the images. In addition to 192 SBM SAR images taken during the 2006 and 2007 field operations, a set of 387 images (76 ScanSAR Wide, 68 ScanSAR Narrow, and 243 SBM) covering the extent of the study area was obtained from NASA-ASF from an archive of more than 30,000 images which span over 18 years of observations. The total effort analyzed 579 images covering the study sites a minimum of 16 times per unit area, and up to 89 times at those sites where intense seepage was detected or where geophysical or submersible

observations were focused (Figure 7-3). Maximum repeat coverage for any portion of the northern GoM region was exceeded 100 times.

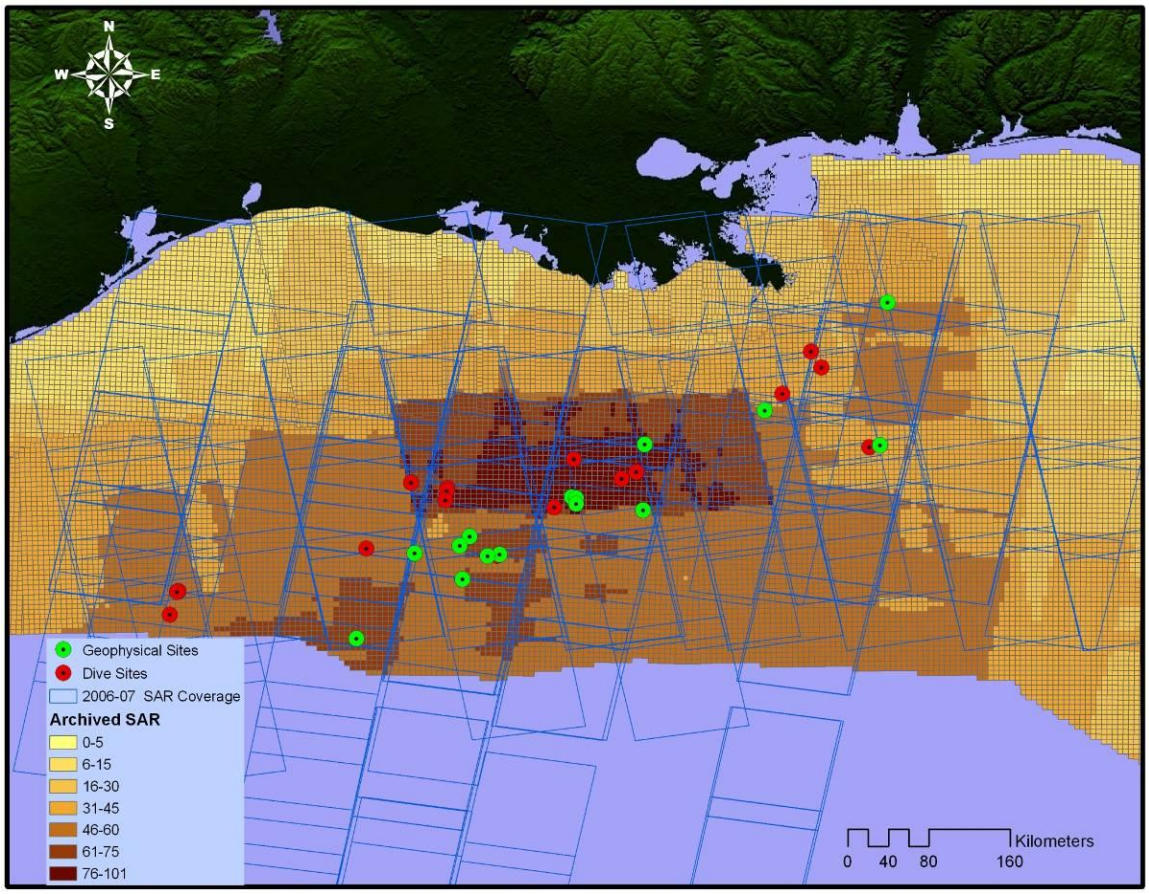

Figure 7-3. Repeated coverage of the northern GoM with SAR is shown as a shaded grid, corresponding to increasing frequency of collection (387 total) in 5x5 km lease blocks.
Images (192 total) collected during the 2006 and 2007 field efforts are shown with image outlines.

Analysis and interpretation of SAR images required a series of processing steps. After converting analog SAR signals from the RADARSAT-1 spacecraft into binary SAR signal data, Alaska Satellite Facility Data Center provided the SAR data in CEOS level one SKY telemetry format (Gens and Logan, 2003). Converter tool software provided by the Alaska Satellite Facility was then used to construct GeoTIFF (tagged image file format) images from the raw binary SAR data. GeoTIFF format has georeferencing information embedded, and depending on the spatial extent of each image, Universal Transverse Mercator (UTM) north zones 15 and 16 were used to project all SAR images from offshore Texas to offshore Florida.

7.2.2. Image Processing

The first step to detect seep features in SAR imagery is to consider the size of features under analysis and the SAR spatial resolution. Different resolutions are used to segment even the narrowest oil slicks, neighborhood texture controls in regions of 25 x 25 pixels (for SAR data in the range of 12.5 m resolution), 13 x 13 pixels (for SAR data in the range of 25 m resolution) or 7 x 7 pixels (for SAR data in the range of 50 m resolution). In these parameters, oil slicks can be as thin as 6 pixels wide equivalent to 75m in a RADARSAT-1 standard beam mode, or can be as thin as 3 pixels wide in a RADARSAT-1 ScanSAR Narrow beam mode, also equivalent to 75m.

The goal of image processing is to segment the original SAR scene into a binary image so that each pixel is classified as "oil" or "clean sea." The first processing step was to construct an Input Layer Vector (ILV) of conditions for each pixel in the image. The input layer vector contains data and conditions ordered as follows: 1) energy backscattered to the satellite, represented by the 8 bit pixel value, 2) radar incidence angle, 3) wind conditions (when available), 4) pixel neighborhood descriptors, and 5) convolution of a series of texton filters over a squared regular neighborhood centered on the pixel (Figure 7-4).

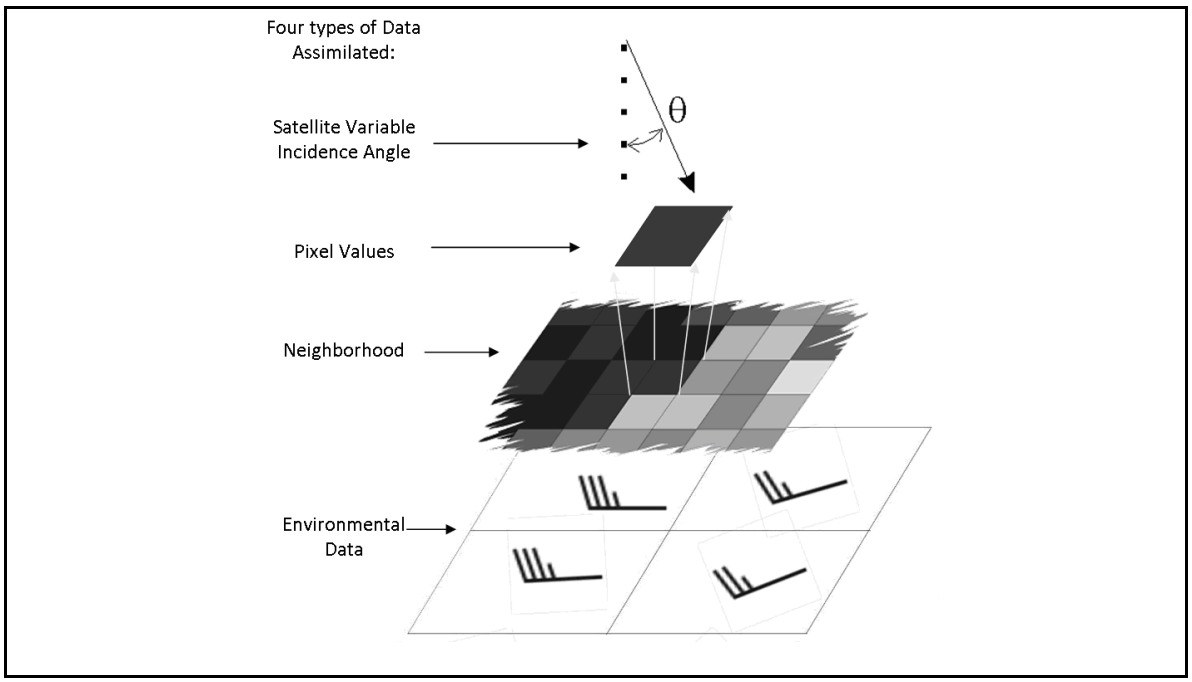

Figure 7-4. Schematic showing components of the Input Layer Vector (ILV) for each pixel in the SAR images analyzed.

To standardize the comparison between a pixel and its neighborhood, the statistical properties of each neighborhood were analyzed using texture descriptors (Gonzalez et al., 2004); i.e., mean, standard deviation, smoothness, third moment, uniformity, and entropy. These values are included with the ILV. This analysis is important because the texture of SAR images varies within different regions of an image, depending on radar incidence angle and sea state. The next level of analysis is to test for features using the Leung-Malik Filter Bank , which comprises 48

multi-scale, multi-orientated filters for edge, bars and point detections (Leung and Malik, 2001). For the purpose of oil slick detection, only used edge and bar detectors were used (the first 36 filters of the 48 element Leung-Malik Filter Bank set). Figure 7-5 shows schematically how the filters were applied to the ILV and the pixel neighborhoods.

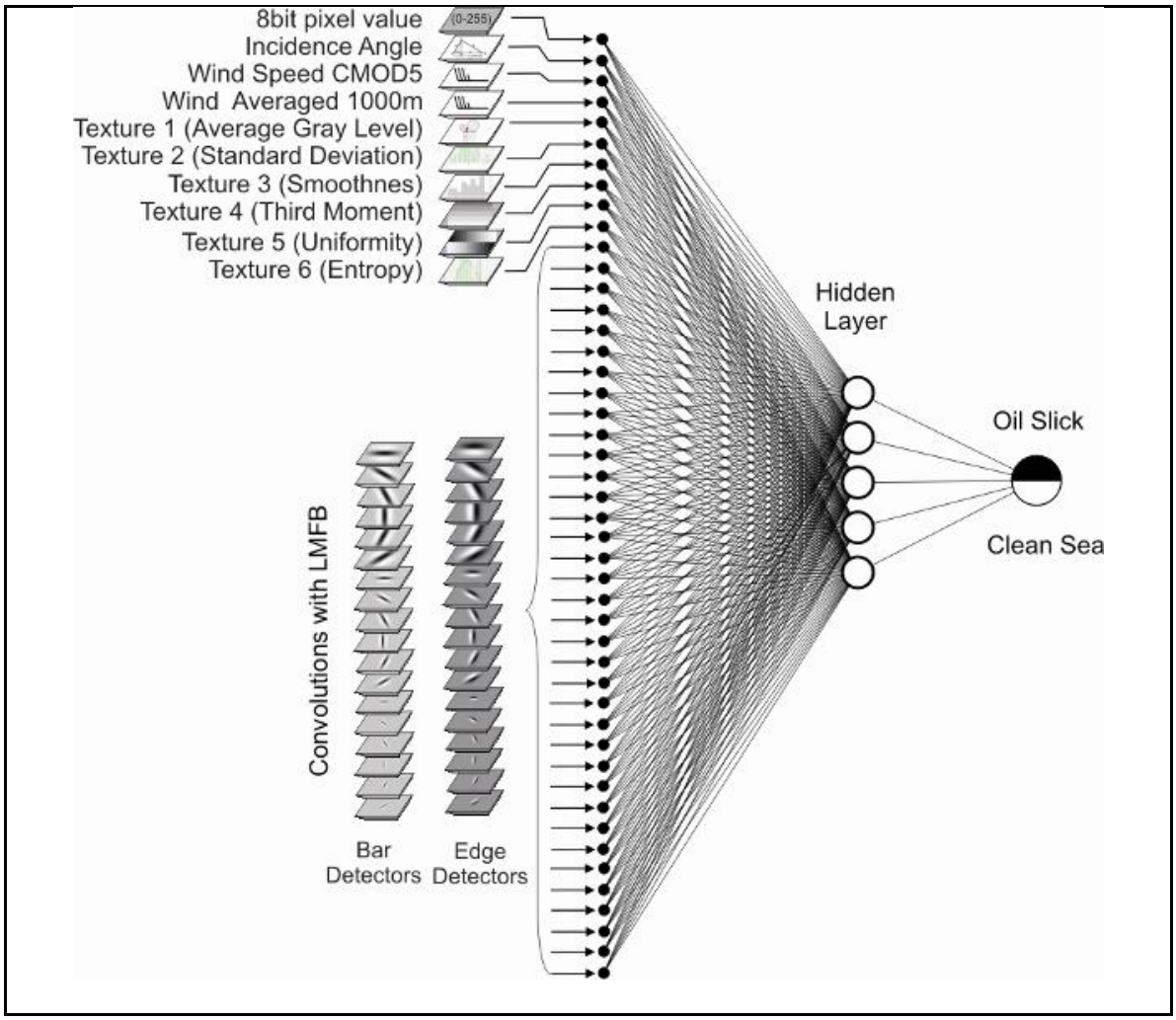

Figure 7-5. Image processing steps applied to segmenting SAR images to show oils slicks.
The ILV (upper left) evaluates pixels individually and as neighborhoods with incorporation of environmental data. The image filters (lower left) rate the response level of each pixel to standard shapes. The neural network algorithm interpolates these data to segment the image (right side).

Environmental data, e.g. wind intensity, were obtained from various sources and resolutions. To match data spatially, input values for these variables were computed based on the closest linear interpolation from direct satellite measurements and model outputs.

After initial processing, a Textural Classifier Neural Network Algorithm (TCNNA) was used to identify floating oil-layers in a semi-supervised operation (Garcia-Pineda et al., 2009). The TCNNA employs a combination of edges and bar detection filters that are a subset of the Leung Malik Filter Banks (Leung and Malik, 2001). It also merges descriptors of texture (Gonzalez et al., 2004), collection information (i.e. incidence angle, resolution), and environmental data (wind speed). These variables form an input vector for each pixel that is processed with a feed-forward neural network. The TCNNA is conditioned on a training set in which SAR features of interest (i.e. floating oil) have been previously identified by an operator. The TCNNA segments the images into target and non-target pixels; it operates in a range of environmental and sensor conditions. Automated segmentations are more rapid and precise than human interpretation. Minor post-processing supervision is required to check the TCNNA outputs, which are easily stored and manipulated in geographic information system (GIS) software. Using the TCNNA, oil slicks were detected and processed in 207 SAR images from the total archive of 579 (Figure 7-3).

7.2.3. Mapping and Clustering Process

Using the TCNNA, the total area covered by each slick detected in each image was computed, and an Oil Slick Origin (OSO) was selected as single points within detected oil slicks (Figure 7-6). The OSO points were identified based on the shape of floating oil layers, following characteristics described in previous work (De Beukelaer et al., 2003; MacDonald et al., 1996), i.e. origins tend to be wider and more distinct ends of curvilinear features, which narrow and attenuate with increasing distance from the point where fresh oil reaches the sea surface. Regional distribution of seep features was examined using geographic information system (GIS) tools. A GIS layer, including environmental and sensor descriptors, was constructed for each of the 207 images that contained oil.

We analyzed the tendency of OSO points to cluster within each individual image to determine characteristic spatial scales. A Hierarchical Cluster Tree based on pair-wise distances between OSO points was constructed for each image. In such a tree, points close together get grouped in a cluster. Depending on the definition of "close," different clusters may emerge. We used the idea of maximal distance within a cluster for grouping. The reasoning is that in an individual satellite image, OSO points that originate from the same sources on the ocean floor will be emcompassed by a radius characteristic of seep formation geology. The clustering starts by grouping the closest two points together and then regarding this group of two points as a new point and repeating the process.

Each clustering step involves a distance matrix that contains all the distances between the current set of points. With each step the distance matrix shrinks by one row and one column. The art in clustering is to decide at what distance things should not be in the same cluster. We opted to use the Inconsistency Coefficient (IC), also called "factor of inconsistency," (Jain and Dubes, 1988; Zahn, 1971) to decide on the maximal distances within a cluster. Other authors use the index of clumping (Ripley, 2005) to decide on cutoffs, but the results are equivalent. The inconsistency coefficient for a grouping of two "points" or sub-clusters into a new cluster is similar to a z-

score. It uses the mean distance between all the original unclustered points in both sub-clusters and the standard deviation of all those distances.

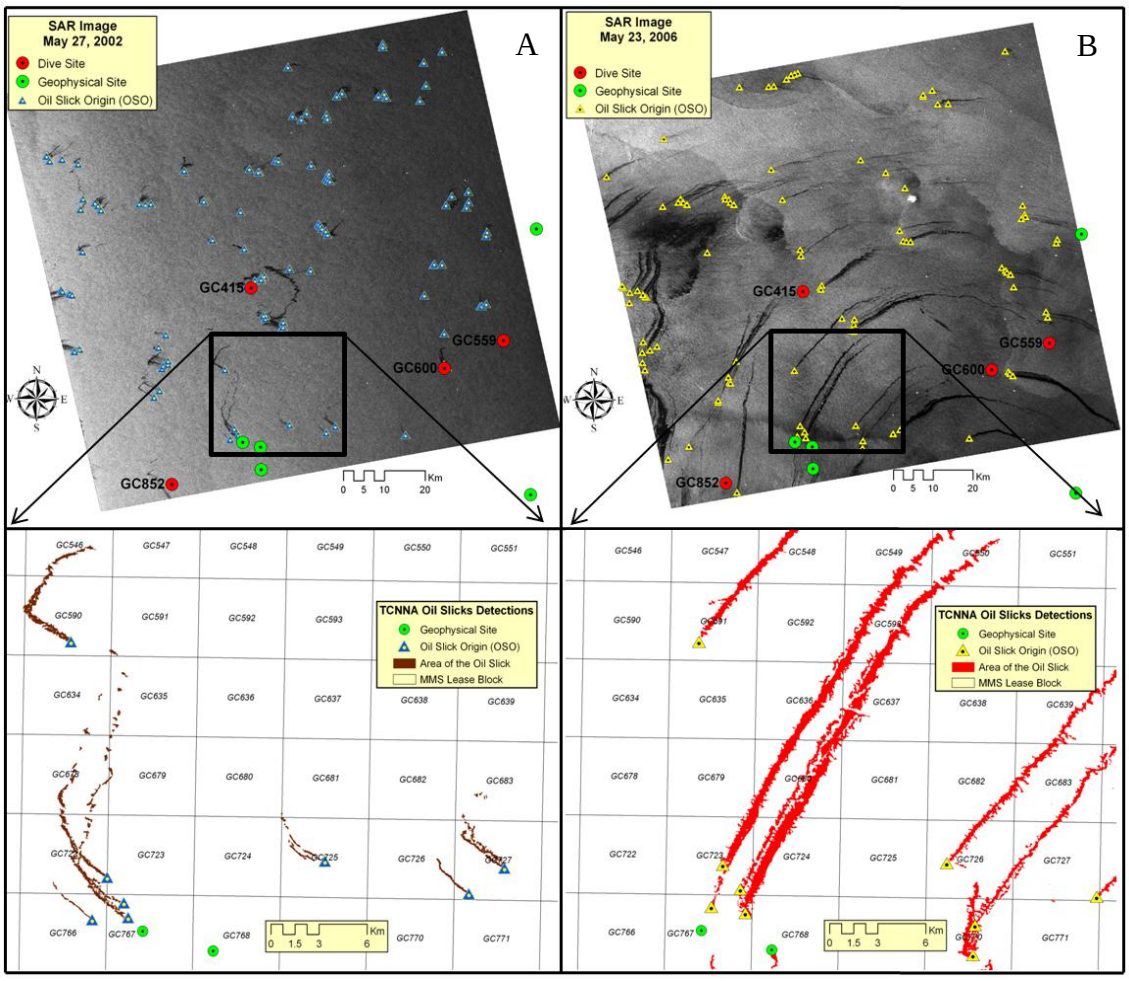

Figure 7-6. SAR images covering several geophysical and dive sites. (A) Scene collected on May 27, 2002. Detail shows binary segmentation of oil and non-oil areas over GC767 and GC768 geophysical sites. Prevailing winds produced a northwesterly drift for surface slicks. (B) Identical coverage on May 23 2006. Oil slicks were larger and showed northeasterly drift on this date.

The distance between the two sub-clusters (as defined here, the maximum distance between any two elements of the sub-clusters) is normalized by subtracting the mean of all distances and dividing the result by the standard deviation of all the sub-clusters. A small inconsistency value means that the distance between the two sub-clusters combined into a new cluster is similar to distances encountered in previous clustering steps, or, said differently, that there is no large jump in distances by combining the sub-clusters. If the inconsistency index exceeds one, things should not be clustered together. But even if the index is less than one, the inconsistency index is not a sufficient method for deciding on cluster size. The process also looked for a jump in maximal

distances within a cluster to decide at which maximal distance at which to stop clustering. Background info on hierarchical clustering can be found in (Deonier et al., 2005; Ripley, 2005). After determination of clustering radii for individual images, the centroids of OSO clusters were assumed to be estimates for the location of active seep formations for the conditions occurring at each image collection time. When centroid locations are compared among multiple images covering the same region, a second scale of clustering was determined by repeating the pair-wise distance comparison for centroids.

7.3. Results

7.3.1. Association of Oil Slicks with Geophysical Anomalies

The occurrence of oil slicks associated with geophysical anomalies and dive sites (Figure 7-2) are summarized in Table 7-1. Oil slicks were detected at 20 of the 32 sites, however in 4 sites there was only one slick detected. At 16 sites, slicks were detected in multiple SAR images. The four most active sites have over 20 slick detections. However in all cases, there is a consistent association between oil slicks and the geophysical signatures of seep formations. (e.g., Figure 7-6). Consistent with earlier observations (MacDonald et al., 2003) a single seep formation can include several active vents. Analysis of the distribution of OSO points provides details on the spatial scale of formation and the clustering of active vents. This pattern is repeated in the sites described in Table 7-1.

Figure 7-6 shows clusters of two to five OSO points detected in two SAR images with identical spatial coverage. Water depth below the areas shown ranges from 150 m on the north side to 1800 m on the south side. These two images were collected 4 years apart by RADARSAT-1 using the SBM. Differences in wind conditions and sea surface height were identified in these two scenes at the moment of each synoptic image. Figure 7-6A had an average wind speed of 4 m s-1, while the average wind speed in Figure 7-6B was 5 m s-1. Sea surface height records indicates that the curvilinear signatures detected in Figure 7-3B are influenced by the presence of a warm core eddy. The curved shape of oil slicks was influenced by geostrophic currents, produced by the slope of the sea level anomalies generated by the eddy. Figure 7-6A and Figure 7-6B show different orientations and sizes of oil slicks signatures due to particular oceanographic and meteorological conditions, however, the numbers of OSO points detected in both cases are similar. In Figure 7-6A, 108 OSO points were detected in an area of 100 x 100 km. In Figure 7-6B, 99 OSO points were scattered in the identical area. Comparing patterns of OSO points, it was apparent that there was an offset of 4 km between OSO points arising from the same formation, depending on the deflection of the oil bubbles rising through the water column. With this analysis, the number of OSOs appears to be related to environmental conditions.

Examples of OSO points detected over the GC767/768 site in Figure 7-7 illustrate the general relationship between OSOs, active vents and the scale of the seep formations. There is a degree of variability in the size, drift direction, and apparent location for OSO points that probably originate from the same individual seep formation. For example, Figure 7-7 shows details of three SAR images collected in 1997, 2002, and 2006, respectively. The same distinctive pattern of four OSO points is evident in all three images despite the 10-year collection interval. The four

active vents are related to the same geophysical anomaly. These observations were further confirmed by dive operations in 2007 during which drops of oil were seen escaping from the sea floor amid a congregation of chemosynthetic tube worms.

Table 7-1

Results of Oil Slick Detection in SAR Images over Target Sites Selected on the Basis of Geophysical Characteristics (descriptions are sorted by depth)

SITE Name	Latitude	Longitude	Depth (m)	Active	Number of Archived SAR Images	Number of Images with Oil Slicks	All Slicks Sources Observed	Maximum slicks per image	Minimum slicks per image	Largest slick area	Maximum Deflection from Centroid	Calculated Deflection Offset (Radius)
MC36	28.93417	-88.2047	935	No	6	1	1	1	1	0.36	n/a	1950
MC462 *	28.49667	-88.8839	982	Int.	19	2	2	1	1	0	n/a	2008
GC415 *	27.5422	-90.9903	985	Per.	87	25	58	8	1	17.963	2361	2012
GC296	27.67139	-90.3611	994	Int.	80	2	2	1	1	0.41	n/a	2023
GB647 *	27.33139	-92.435	1000	Per.	82	22	65	11	3	15.852	1909	2031
MC853 *	28.12333	-89.1397	1082	Per.	22	8	12	3	1	8.62	1545	2132
GC600 *	27.36639	-90.5642	1248.8	Per.	74	31	65	4	1	26.07	2742	2338
GB697 *	27.28361	-92.1128	1300	No	78	1	1	1	1	3.9	n/a	2401
GC559 *	27.42666	-90.4341	1300	No	73	0	0	0	0	0	n/a	2401
MC981	27.97389	-89.295	1300.3	Per.	28	5	5	1	1	5.7	1807	2401
GB741 *	27.257	-92.12	1400	Int.	81	3	4	3	1	5.11	n/a	2525
MC640 *	28.35583	-88.7931	1414.9	No	21	0	0	0	0	0	n/a	2543
GC852 *	27.1125	-91.1642	1448.4	Int.	73	8	11	2	1	9.954	1639	2584
GB829 *	27.1775	-92.1303	1500	Int.	81	2	3	1	1	6.8	3210	2648
GC767	27.20444	-91.0083	1585.9	Per.	80	27	67	5	1	34.27	2816	2754
KC243 *	26.75028	-92.8292	1610	Int.	67	3	3	1	1	1.36	n/a	2784
GC768	27.19361	-90.9689	1619.1	No	83	0	0	0	0	0	n/a	2795
KC129	26.85472	-91.9131	1691.6	Int.	44	5	12	4	1	0.25	3012	2885
KC216	26.77194	-92.0033	1753.8	Int.	46	2	2	1	1	9.54	n/a	2961
KC524	26.47667	-91.9758	1771.8	Per.	57	12	12	1	1	2.68	3592	2984
GC812	27.14472	-90.9675	1802	No	82	0	0	0	0	0	n/a	3021
GC868	27.09	-90.3744	1811.1	No	53	0	0	0	0	0	n/a	3032
KC295	26.70444	-92.4033	1814.2	Int.	80	14	14	2	1	17.19	3412	3036
WR270	26.69722	-91.6475	1924.5	No	56	0	0	0	0	0	n/a	3172
WR269 *	26.68444	-91.6714	1925.4	No	49	0	0	0	0	0	n/a	3173
WR268	26.68028	-91.7558	2055.6	No	54	0	0	0	0	0	n/a	3334
AC645 *	26.37139	-94.4969	2226	No	55	0	0	0	0	0	n/a	3544
AT340 *	27.64639	-88.3658	2242.1	No	26	1	1	1	1	5.58	n/a	3564
AC601 *	26.3625	-94.5103	2366	No	55	0	0	0	0	0	n/a	3717
AT342	27.66667	-88.2697	2405.2	No	27	0	0	0	0	0	n/a	3766
AC818 *	26.16139	-94.5767	2875	No	62	0	0	0	0	0	n/a	4346
SE21	25.94889	-92.9178	2891.9	No	68	1	1	1	1	3.07	n/a	4366

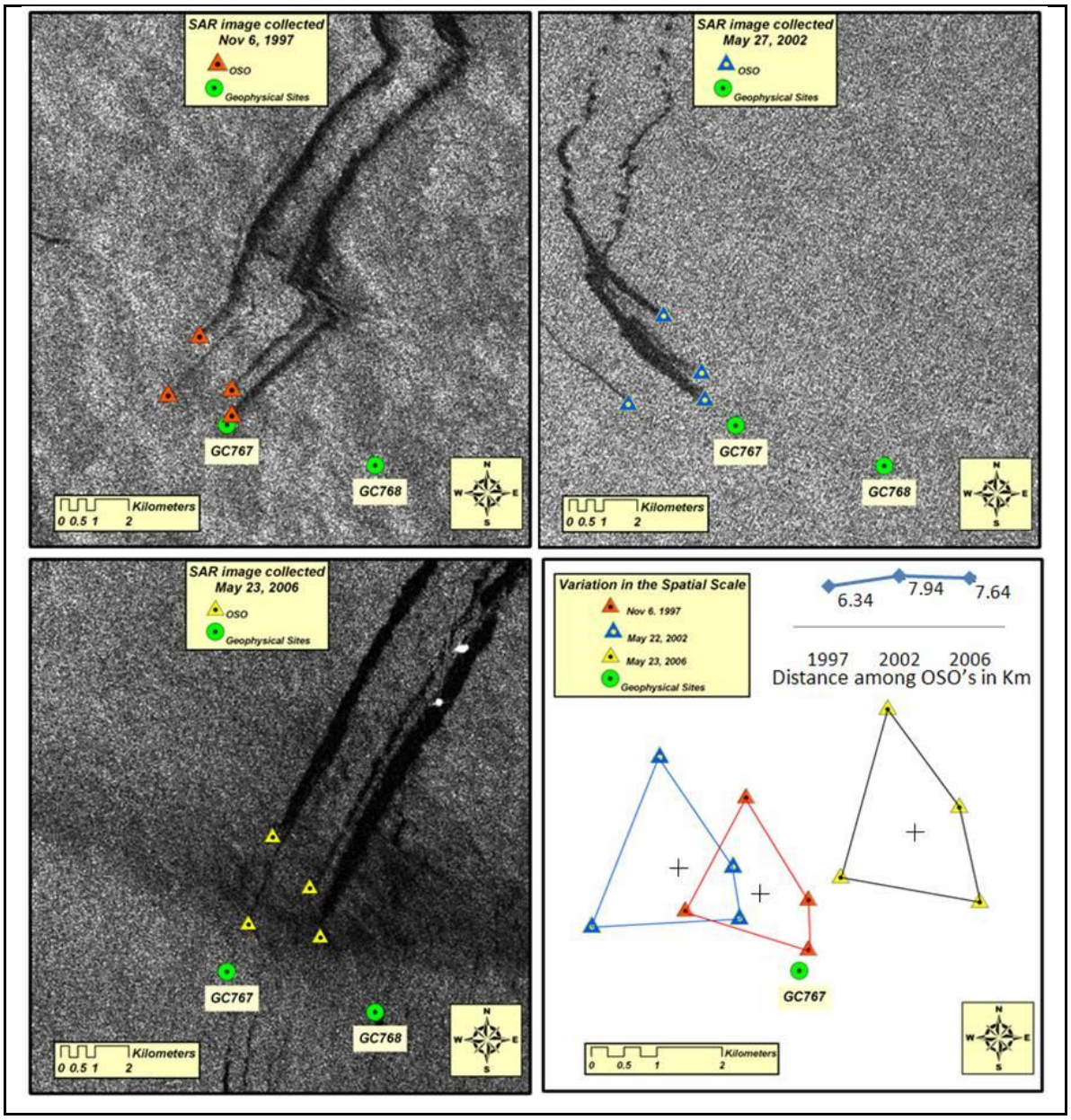

Figure 7-7. Geophysical site GC767, showing a decade of observations of the natural seepage in this area.
Figure 7-8A shows a subset of a SAR image collected in November 6, 1997. At intervals of four and nine years later, the seepage of this formation continues to show similar pattern of the oil slick offset.

The detection of OSO points in SAR images over the study region is consistent with previous work focused at shallower sites on the upper slope (De Beukelaer et al., 2003). The relationship between OSO points, active vents, and geologic formations was also confirmed. From this example, two questions arise: 1) Within a geophysical formation, is there a typical spacing between active vents that can be used to threshold clusters of OSO points? and 2) Is it possible to

characterize the regional offset of oil rising in the water column to identify seafloor seep locations based on their satellite signatures?

A full hierarchical cluster tree links all the OSO points together. Figure 7-8A and 7-8B show the mean and the standard deviation of the distances between those OSO pairs detected in Figure 6A and 6B, respectively. A non-linear increase in pair-wise distances between OSO points were observed in both cases. In the calculation of the IC, the means and standard deviations of the distances between all original points in a new sub-cluster were computed. Since the inconsistency index alone is an insufficient decision criterion from cutoff distances, these means and standard deviations as well as the maximal distances within a cluster were studied. Determination of maximal distance cutoffs for clusters was based on changes in the maximal distance between two OSO points within the same cluster.

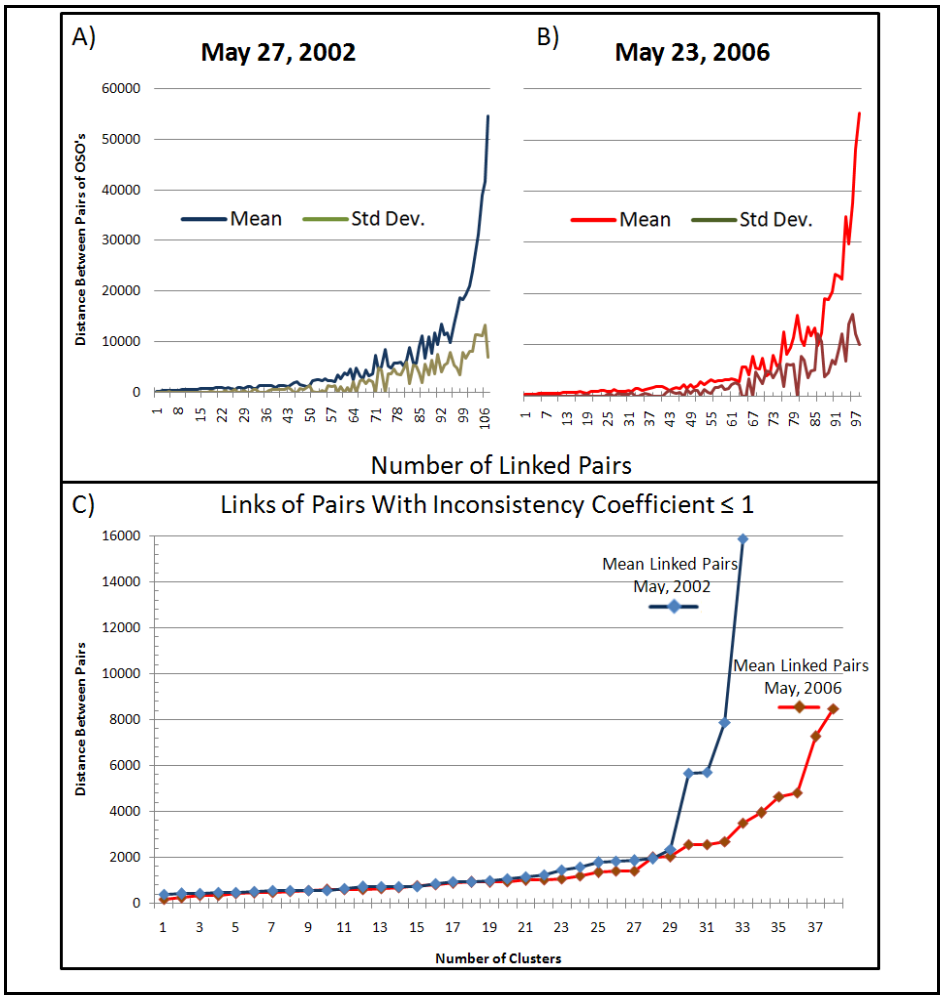

Figure 7-8. Cluster analysis results for OSO points in individual images. (A) Mean and standard deviation of distances between linked OSO points from Figure 3A. (B) Mean and standard deviation of distances between linked OSO points from Figure 3B. (C) Distance between linked OSO points with

inconsistency coefficient less than 1, shows the same linear pattern in those OSO points linked in distances no greater than 2500 m.

The variance of distances between OSO points were explained by the number of linked pairs. As the number of linked pairs increased, the standard deviation also increased, because less similar objects are connected by the links. Based on IC values less than 1, Figure 7-8C showed the distance between a subset of linked pairs in Figure 7-8A and 7-8B, which have similar length on the same level of hierarchy on their cluster tree. In Figure 7-8C, when the maximal distances between any two OSO points in the sub-cluster were greater than 2500 m, the slope of both means increased. This result was consistently noted in virtually all images that were compared. We therefore chose 2500 m as the maximal distance between any two OSO points that can be assigned to the same cluster. This confined clusters of OSO points to be within circles of a radius of 1250 m. With this specific cutoff the OSO points in every individual image were clustered and the clusters were saved in a database.

For each cluster in each of the SAR images, the OSO cluster centroids were computed by averaging the latitude and longitude of all of the OSO points clustered together in an image. An OSO centroid points database were then constructed, containing the maximum and minimum quantity of OSO points detected in each image, and all the environmental variables (sea-surface height and wind conditions) associated with them.

7.3.2. Deflection by Subsurface Currents

The oil drops are deflected in their trajectory form the seafloor vents to the OSO points observed in a given SAR image (MacDonald et al., 2002). The magnitude of deflection is determined by subsurface currents acting over the depth of the water but this offset has not been previously quantified. To estimate deflection by subsurface currents, the OSO centroid point database was used to cluster all OSO centroid points for all time frames in order to find the appropriate cutoffs by different depths, and to examine the offset range for OSO points arising from seep formations at different locations in the GoM. This followed the same procedure explained in the previous section, constructing and computing a hierarchical cluster tree and the IC at some of the most persistent seepage formation sites in the Northern GoM, which were used as a training set and to find patterns of deflection by depth. Computed IC values less than 1 were used to plot the mean distance between pairs of OSO centroids.

As water depth increases, subsurface currents produce an increasing deflection on the rising of oil coated bubbles. Figure 7-9 shows a linear trend pattern in the deflection of the rising coated bubbles influenced by subsurface currents as water depth increases. Therefore, for the observation in the GoM dataset, the radial deflection of streams of oily hydrocarbons as a function of depth is defined as:

$$C = 1.2346z + 796.86$$

Where C is the cutoff for clustering OSO centroid points at a given depth z.

This linear relationship was used to set the cutoffs in each of the sites under investigation described in Table 7-1. The last two columns in Table 7-1 include the maximum observed

deflection distance and the calculated cutoffs per site. For those sites with active seeps, clusters of OSO centroid points were hence contained within circles of radius between 1950 m and 3036 m. These results were validated by comparing the offset of OSO points over sites where submersible operations and geophysical data provided the evidence of the locations of the geophysical formation, thus evidencing patterns due to deflection by subsurface currents.

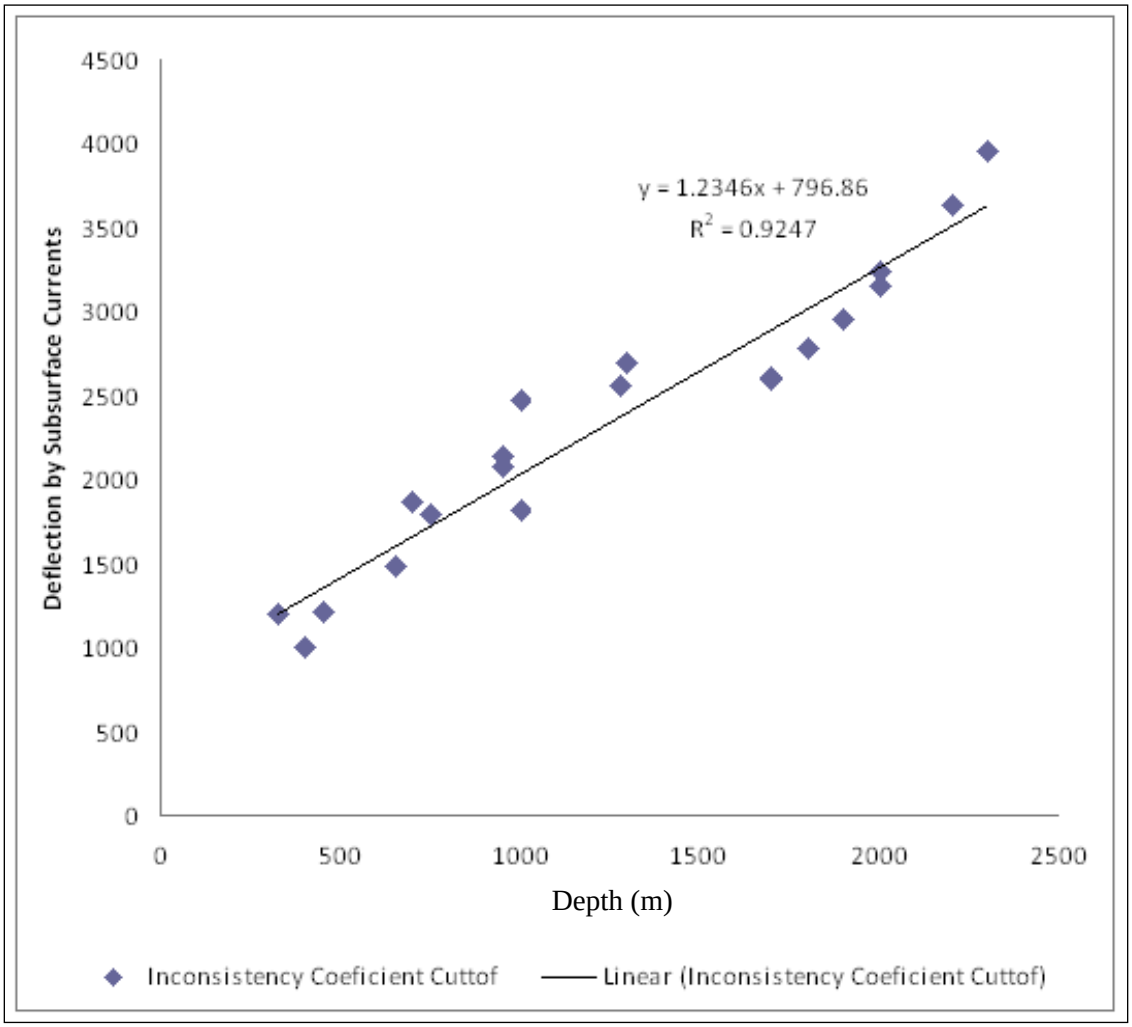

Figure 7-9. Deflection from bottom location by depth with linear fit.
As the water depth increases, subsurface currents produce an increasing deflection on the rising oil. Values were calculated from thresholding cluster analysis.

The clustering scales provide an objective method for generalizing the results from a large number of OSO points observed among multiple images. A case study of one of the study sites illustrates this approach.

7.3.3. Dive Site GC600

This site is situated on a low-relief ridge at a depth of about 1250 m. Direct observational data from submersible operations at this site confirmed the geologic and biologic complexity of the area. In areas of high surface reflectivity mapped from seismic data, massive hydrocarbon seep-related carbonate hardground pavements and isolated blocks were present (TDI-Brooks, 2006). Gas was observed bubbling from cracks in the carbonates during *Alvin* dive in the area, where high seismic amplitude was previously observed from seismic records (Figure 7-10). The location of the dive site was 90º 22' 51"W and 27º 21' 59"N. Oil slicks were also observed from the R/V *Atlantis* during the sampling survey by *Alvin*.

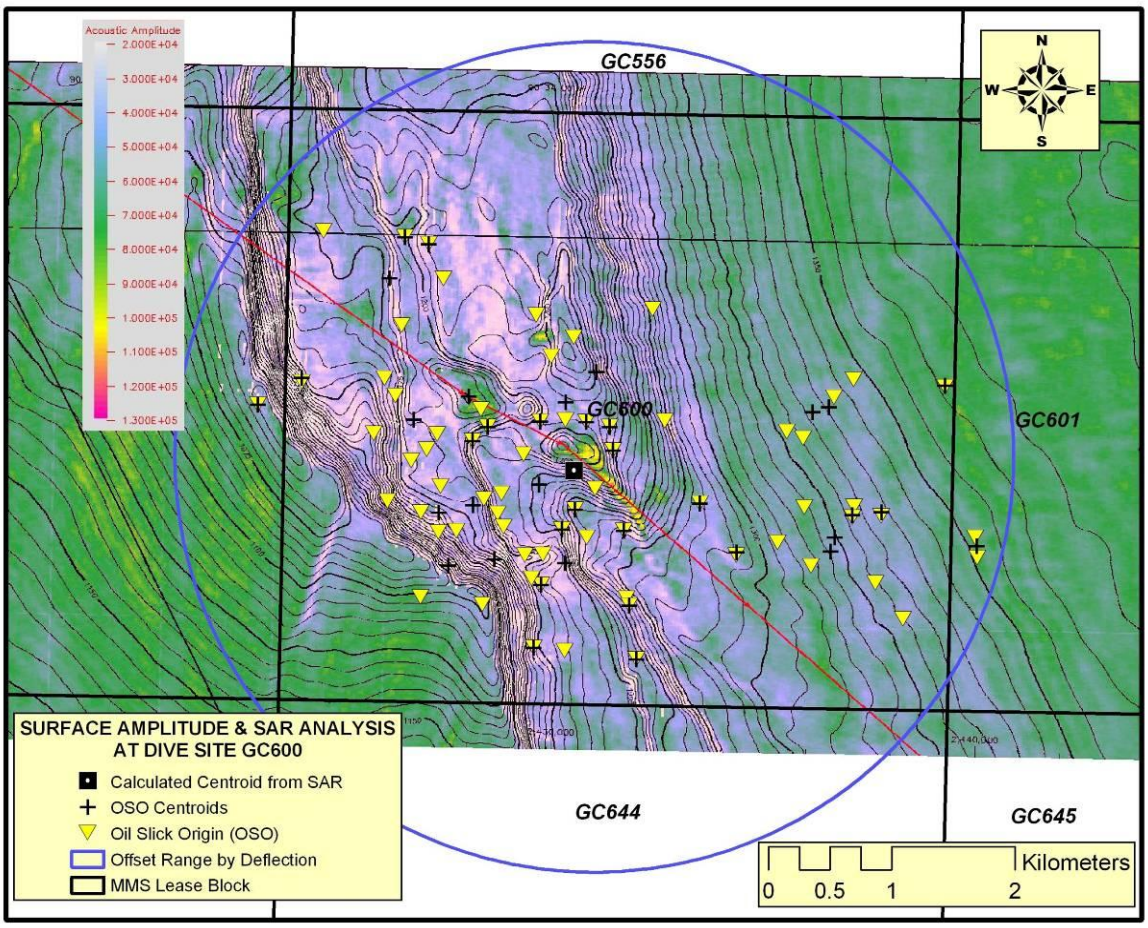

Figure 7-10. Dive Site GC600. Cluster analysis of oil slicks observed in the region plotted over a display of bathymetric contours and surface reflectance amplitude. These geophysical data suggest an anomaly is located on the bathymetric high near the center of the plot. The OSO centroid calculated from SAR data corresponds very closely to this anomaly, which was a persistent source of oil (Table 7-1).

In the study archive of SAR images, the GC600 region was covered 74 different times. In this site with persistent seepage, about 60% of the images did not meet wind and incidence angle conditions to clearly detect the OSO points or in some cases oil slicks were covered only partially by the SAR images, in which case these oil slicks were excluded from the analysis. However, in 31 SAR images of the total of 74, OSO points and oil slicks were clearly detected by RADARSAT (Figure 7-10). The longest slick ever observed in all SAR images occurred at this site, and had a length of 54 km and covered an area of 26 km^2 (Table 7-1).

In total, 65 OSO points associated with GC600 were detected in the 31 images. Figure 7-10 shows the seafloor reflectivity (or surface amplitude) map of the region (Roberts, 2006). This image showed a relatively low reflectivity of the venting center and the "bright" and highly reflective flows extending downslope from the center. The highly reflective flows (SBSs) are often related to authigenic carbonates and bivalve shells. The existence of gas in sediments of the venting sites like GC600, are the reason of their low reflectivity. The greatest distance from an OSO centroid to the selected site was 2742 m.

7.4. Discussion

Remote sensing detection of oil slick signatures at the sea-surface by SAR satellites, combined with TCNNA outputs and cluster routines, has been used to quantify the abundance, distribution and temporal variability of active oil seeps in the northern GoM. This analysis was used to study relationships between oil slicks visible at the sea surface and vent distribution within selected geophysical anomalies. Using the criterion of repeated detection of oil slicks origins within local areas, the results confirmed the relationship between active oil seepage and geophysical anomalies (Fisher et al., 2007; Frye, 2008). Seafloor observations with submersibles, showed that in 100% of the cases, the calculated seep formations matched with anomalies interpreted from surface amplitude maps and migration pathways in the seismic data. The results demonstrate consistent patterns in seep activity and provide a means for correlating occurrence of active oil seeps with geophysical and topographic anomalies and with chemosynthetic communities.

From the 32 sites selected previously for their geophysical characteristics, 16 were confirmed to contain active oil seeps. These results showed that active oil seeps detected by SAR only represented 50% of the geophysical sites selected. When the frequency and consistency of oil slick detection was normalized to the number of SAR scenes analyzed, the results confirmed that active oil seeps detectable by SAR represent a subset of the total geophysical features in the GoM. These findings illustrate the potential utility of satellite detection as well as some limitations for the technique.

Not all the sites with active hydrocarbon seepage showed the same level of oil discharge. Some seep formations showed relatively constant activity. In some cases, the identical vents remained active over a decadal scale (Figure 4). Sites GC600, GC767, GC415, GB647, and MC462 showed the highest frequency of oil slick detection (Figure 8A). The detection of oil at these persistently seeping sites was limited mainly by environmental factors and sensor configurations. Other active seep formations showed inconsistent releases of oil; that is, oil slicks were detected in a fraction of images collected under suitable environmental conditions (i.e., GB829, Keathley

Canyon (KC)243, GC296, GB741, and KC295). This indicates episodic releases of oil or non-continuous upward migration of hydrocarbon fluids from deeper sediments.

An example of episodic release was seen at dive site GC852. This site is located along the southeast margin of a large mini-basin that was formed from recent deepwater sedimentation (Miocene, Pliocene, and Pleistocene) and salt withdrawal (Fisher et al., 2007). This site was selected because of a series of seafloor amplitude anomalies that are aligned along the eastern margin of the basin coincident with locally positive bathymetric features on the seafloor (TDI-Brooks, 2006). These features were interpreted to be high-flux vents capable of extruding sediments and hydrocarbons. In addition, during submersible operations, the presence of hydrocarbon migration was confirmed by massive mussel beds, tube worms and carbonate outcrops. However, in 11 years of SAR records within 73 images, only eight images showed oil slicks which were positively associated with this seep formation (Table 7-1). However, similar chemosynthetic communities were detected at dive sites GB829, GC647, GC415, GB647 and GC600, which are sites with the highest frequency of oil slicks observed. At these sites, a different amount of oily hydrocarbon releases was also observed (i.e. GC767 Figure 7-4). There does not appear to be a direct relationship between seep activity detected in SAR and chemosynthetic communities.

Episodic seepage is apparent in the amount of oil discharged through persistent seep formations as well as in seeps that were intermittent. Under similar meteorological (wind) and detection conditions (wind speed, resolution, and incidence angle) Figure 7-4 showed that the distribution of active seeps did not change over a 9-year time frame, but a relative flux in the amount of oil coming out from this formations was evident by calculating the area covered by the oil slicks. In our SAR archive, the largest amount of oil released from a single seep formation was observed at site GC767. This oil slick (detected in May 2006) covered an area of 34.27 km^2, while the area of the slicks in the remaining 27 SAR images over the site averaged only 9.2km^2. Figure 7-8B shows the areas of the largest oil slicks released per site.

Sites GC767, GC600, GC852, GC415 were the sites with the largest amount of oil released (Figure 7-8B) and with persistent seepage (Figure 7-8A). However, site KC295 was an episodically active site. This site was covered 80 times by SAR images (Table 7-1) and only 4 times were oil slicks positively observed near with this site. The areas of oil slicks at this site ranged from 1.3 to 10.24 km^2 confirming the variation in flux of hydrocarbon migration from deeper sediments to surface sediments.

This variation in the flux could be driven by oily hydrocarbons that are aggregated in subsurface sediments and are suddenly released by break of the equilibrium of the trap that contains them. These events could also be associated with processes affecting the seafloor stability like tectonism or variations in regional temperature and pressure affecting the hydrate stability zone. In addition, warm-core eddies have been detected by satellite altimetry and in most cases coincided with SAR detections of episodic releases. In other investigations, swell, tides, and earthquakes have been also associated as processes playing a role in the amount of oil released from natural seepage in other basins (Del Sontro et al., 2004; Zatyagalova et al., 2007). Future work is required to determine the influence of geophysical, oceanographic, meteorological or astronomical factors that could trigger these events in the GoM.

The cluster analysis indicates that in a typical active seep formation, oil vents would be found within a seep formation of approximately 2.5 km in diameter. This scale may be significant for biological processes such as reproduction and larval settlement at active seeps. The cluster analysis for seep formations reveals processes resulting from water column circulation (deflection is a depth-dependent function), not geological structures.

7.5. Summary

With use of a semi-automated image processing algorithm, it was possible to search for floating oil slicks released from natural seeps by analyzing a large number (579) SAR images from the GoM. Detection of oil in SAR data is sensitive to weather conditions and to sensor configurations. However, the large archive of SAR data provides highly replicated coverage over areas of interest for investigating geology and ecology of natural hydrocarbon seeps. The SAR data allowed us to localize areas where floating oil (slicks) were regularly seen. In many cases these sites could be compared to areas containing geophysical anomalies believed to be caused by seepage, i.e. seep formations. We were also able to complete geostatistical analysis of clusters of oil slicks and OSO to investigate the spatial and temporal variability of oil output from seep formations.

The geostatistical analysis among multiple images detected 6209 OSOs. We believe that clustering in these points caused by two distinct processes, each with characteristic spatial scale. Within seep formations, individual vents (which are these seafloor sources of OSOs) tend to be located nearer to each other than to active vents in different hydrocarbon migration systems. Among the OSOs found an average clustering scale of 2.5 km was determined. This scale is generally consistent with the geophysical data and may be a geological characteristic of GoM hydrocarbon seeps. Comparing the clustering of oil released from unique seep formations (OSO centroids) we found a depth-dependent spatial variation with offsets, for example of 2.0 km at ~1,000 m and 3.0km at 1,820 m depth.

In summary, it was found that many seep formations generate perennial output. Evidence from our 14-year record demonstrated that individual patterns of vents within individual seep formations had consistent output over a decadal time scale (e.g., GC767). Overall, 16 of 32 sites identified in the geophysical data were also evident in the SAR data. However, output from some seeps was more intermittent, when weather and sensor conditions were controlled. These sites would activate episodically followed by periods with no detectable oil output (e.g., GC852) when intermittent sites were activated, the perennial seeps appeared to increase their output and to produce larger slicks than usual.

8. SITES NOT VISITED: RECONNAISSANCE DATA ONLY

The Drift camera Recon Cruise visited 18 sites which had been previously selected from evaluation of core and seismic data for the region. Based on data from that cruise and consideration of project needs such as visiting sites over a large depth range and longitudinal range, six of the sites were chosen for further study using submersible assets. In this section we summarize the data from the Recon Cruise collected on the 12 sites that were not studied further.

8.1. Keathley Canyon 333

This station (KC333) was situated on the crest and eastern flank of a low mound at depths from 1,650 to 1,720 m. The DCS reached bottom at 03:03 hrs on 13 March and collected images with a 120-second repeat rate until 04:33 hrs. A total of 267 images were collected with the bottom in view and acceptable navigation. The site showed some evidence for development of chemosynthetic communities including occasional bacterial mats, scattered dead shells, and a few solitary mussels. Tube worms were observed as solitary individuals in three photographs. Geological indications of seepage included extensive brine-staining and of carbonate boulders. This site was considered as a marginal candidate for additional study (Figures 8-1 and 8-2).

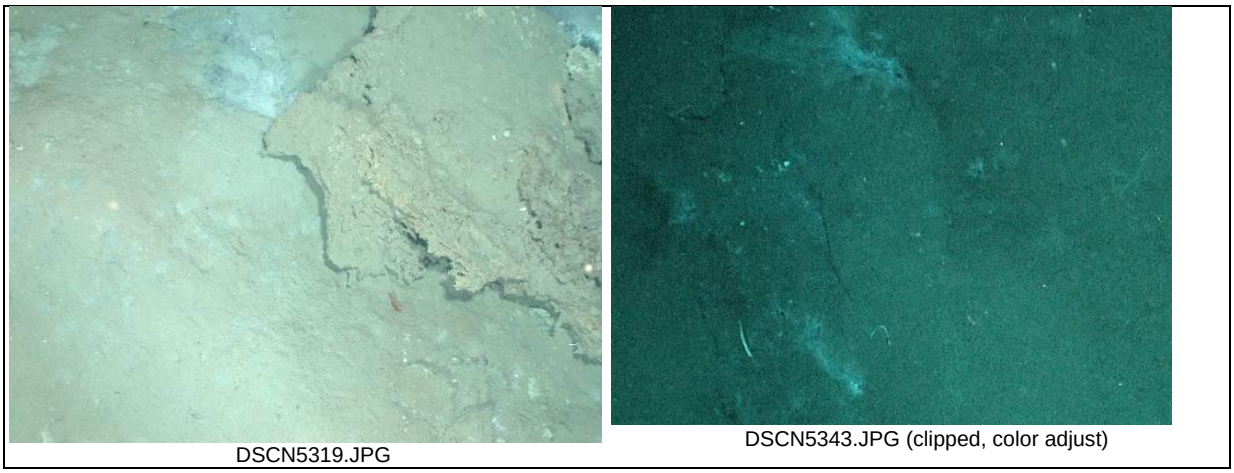
DSCN5319.JPG

DSCN5343.JPG (clipped, color adjust)

Figure 8-1. Representative photography from KC333.

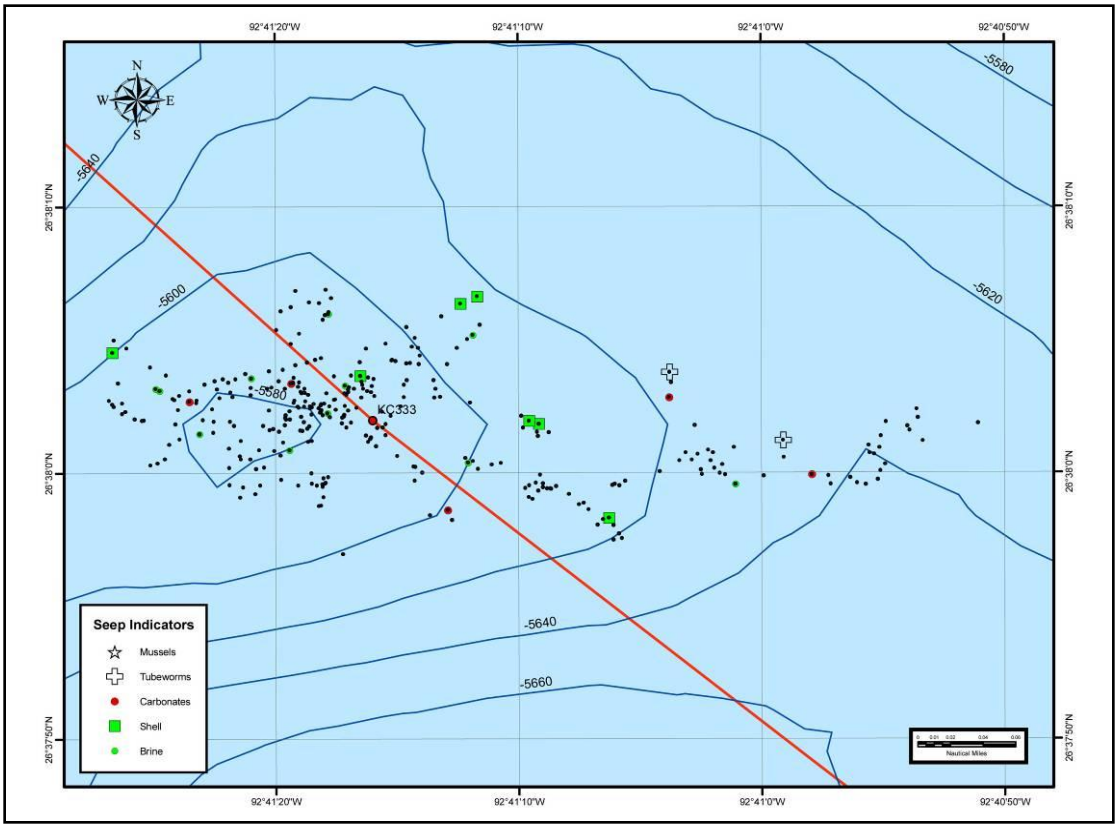

Figure 8-2. Survey results from KC333.

8.2. Keathley Canyon 216

This station (KC216) was situated on the crest and the steeply sloping eastern flank of a mound at 1,750 m. The DCS reached bottom at 00:42 hrs on 14 March and collected images with a 10-second repeat rate until 05:47 hrs. A total of 802 images were collected with the bottom in view and acceptable navigation. The site appeared to be an active mud volcano. It showed some scant evidence for development of chemosynthetic communities, with fauna limited to bacteria, dead shells, and a few solitary mussels. Tube worms were photographed as solitary individuals associated with carbonate outcrops in the eastern portion of the site. Geological indications of active fluid flow included extensive brine-staining, large mud flows, and disturbed sediments. The eastern portion of the site featured more extensive brine and bacteria covered sediments and numerous solitary shells. This site was considered a marginal candidate for additional study (Figures 8-3 and 8-4).

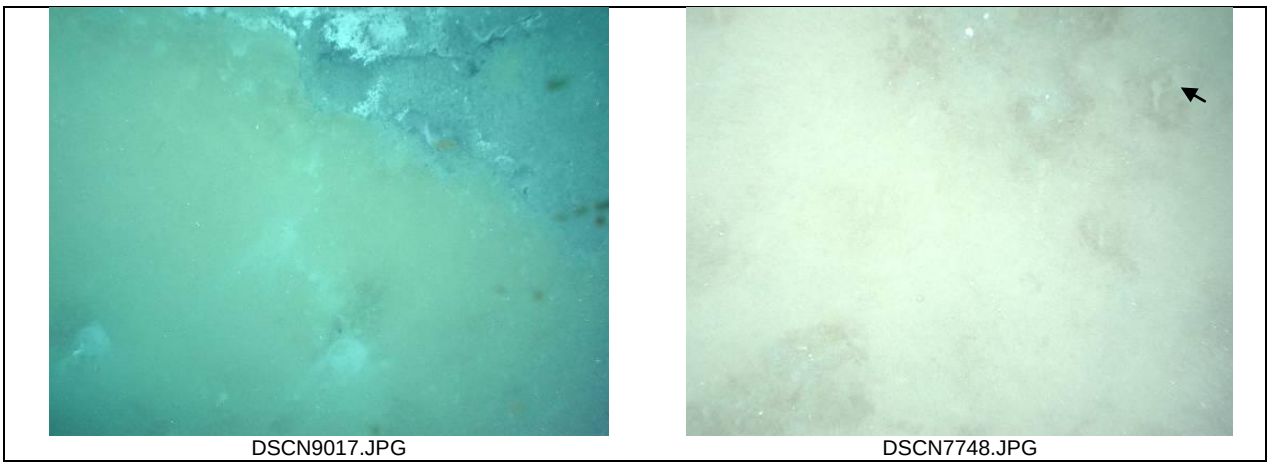

Figure 8-3. Representative photography from KC216.

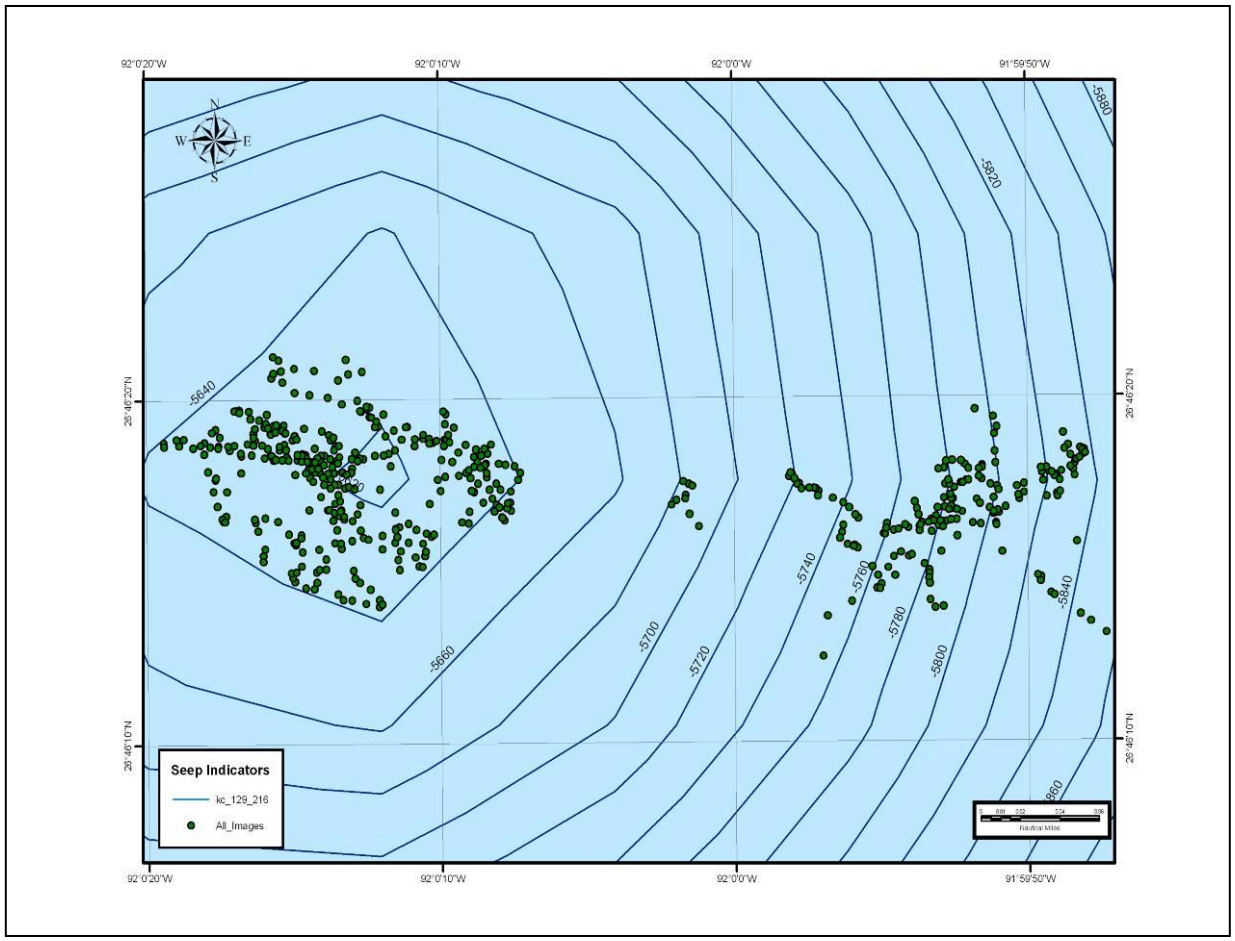

Figure 8-4. Survey results from the KC216 station.

8.3. Keathley Canyon 129

This station (KC129) was situated on the crest and the gradual sloping eastern and southern flanks of a mound at 1,675 m. The DCS reached bottom at 12:39 hrs on 14 March and collected images with a 12-second repeat rate until 03:14 hrs. Survey operations were hampered by heavy seas. A total of 271 images were collected with the bottom in view and acceptable navigation. The site appeared to be an active mud volcano. It showed moderate evidence for development of chemosynthetic communities, with abundant bacteria, dead shells, and a small mussel cluster. A solitary linear object, possibly a tube worm was photographed associated with carbonate outcrops. Geological indications of active fluid flow included extensive brine-staining, large mud flows, and disturbed sediments. Carbonates were developed as large jointed pavements in one area. This site was considered a marginal candidate for additional study (Figures 8-5 and 8-6).

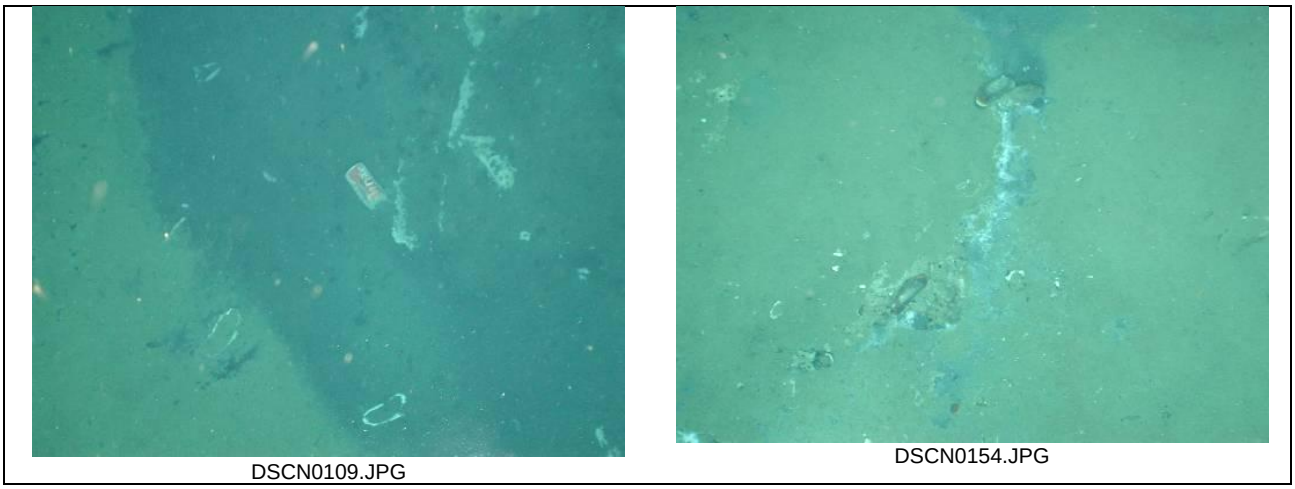

Figure 8-5. Representative photography from KC129.

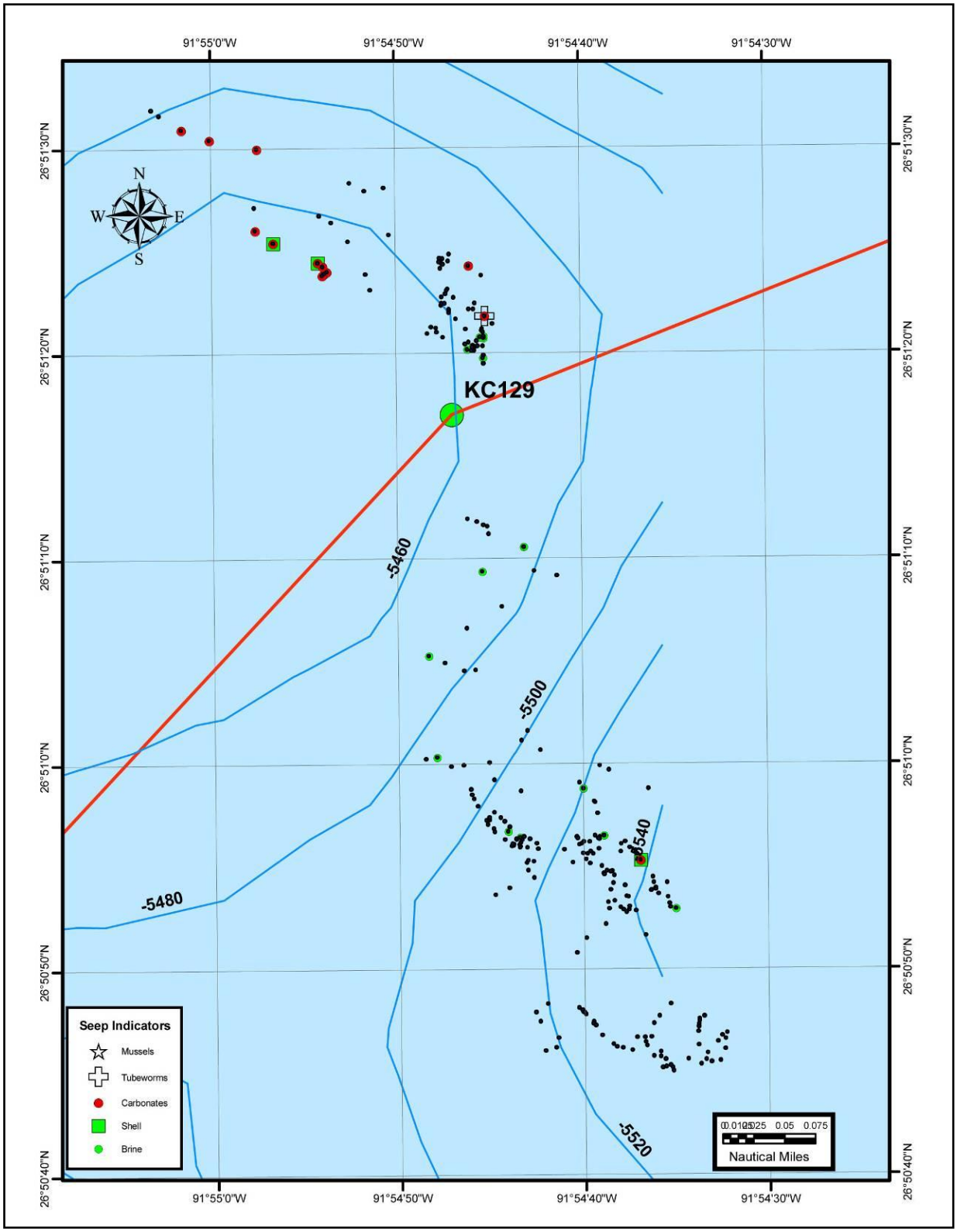

Figure 8-6. Survey results from KC129 station.

8.4. Green Canyon 767

This station (GC767) had a series of seismic anomalies on a steep slope between 1,480 and 1,590 m. The DCS reached bottom at 12:01 hrs on 15 March and collected images with a 10-second repeat rate until 13:58 hrs. A total of 269 images were collected with the bottom in view. The navigation data file for this site was lost and it is not possible to navigate the individual bottom images. The site appeared to be a series of fluid flows on a steep slope. It showed extensive bacterial mats and several brine-channels. This site was considered a poor candidate for additional study (Figures 8-7 and 8-8).

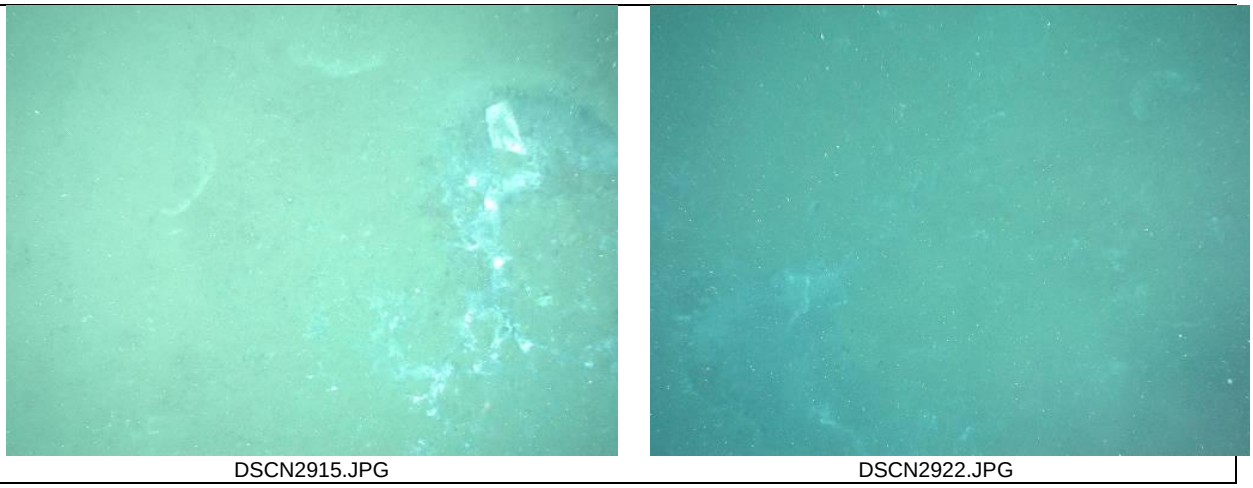

DSCN2915.JPG DSCN2922.JPG

Figure 8-7. Representative photography from GC767.

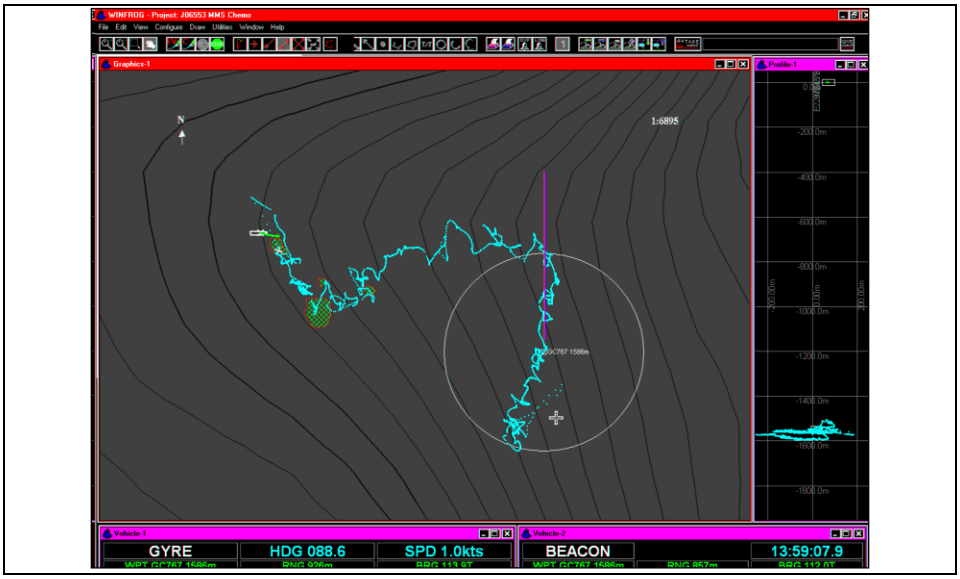

Figure 8-8. Survey results from GC767 station.

8.5. Green Canyon 812

This station (GC812) was situated on a low-relief topographic high at a depth of about 1,800 m. The DCS reached bottom at 18:14 hrs on 15 March and collected images with an 11-second repeat rate until 19:24 hrs. A total of 225 images were collected with the bottom in view and acceptable navigation. The site showed extensive brine flows and frequent bacterial mats. Fresh mud-flows suggest ongoing fluid venting. No chemosynthetic megafauna were seen. This site was considered a poor candidate for additional study (Figures 8-9 and 8-10).

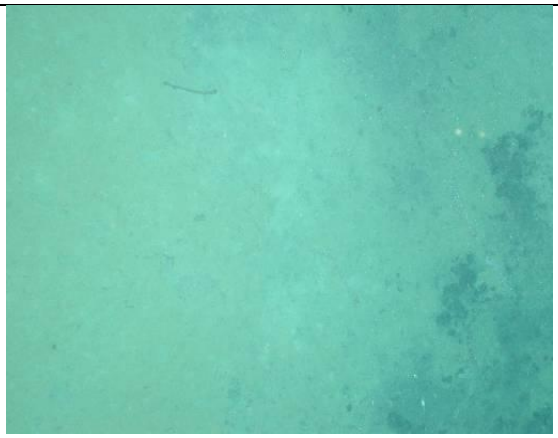

DSCN3725.JPG

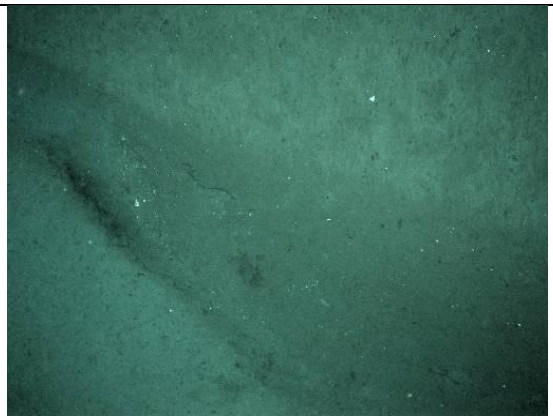

DSCN395.JPG (color adjust)

Figure 8-9. Representative photography from GC812.

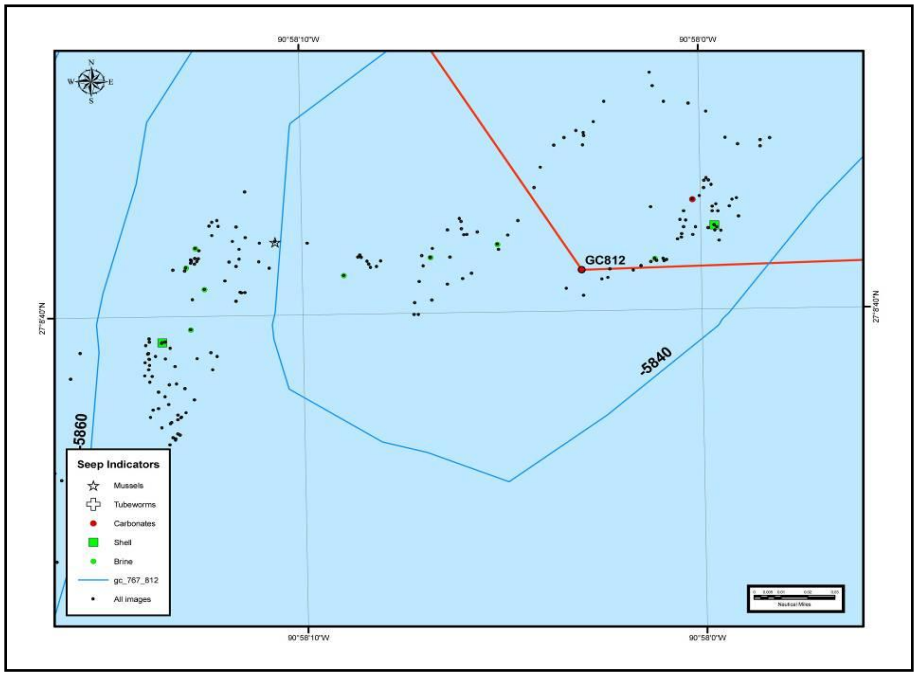

Figure 8-10. Survey results from GC812 station.

8.6. Green Canyon 817

This station (GC817) was situated on a low-relief topographic high at a depth of about 1,800 m. The DCS reached bottom at 02:53 hrs on 16 March and collected images with an 11-second repeat rate until 07:02 hrs. A total of 515 images were collected with the bottom in view and acceptable navigation. Image quality was poor due to aperture setting at *f* 2.5. The site showed occasional bacterial mats. There was a single aggregation of mussels and dead shell with carbonate pavement. This site was considered a marginal candidate for additional study (Figures 8-11 and 8-12).

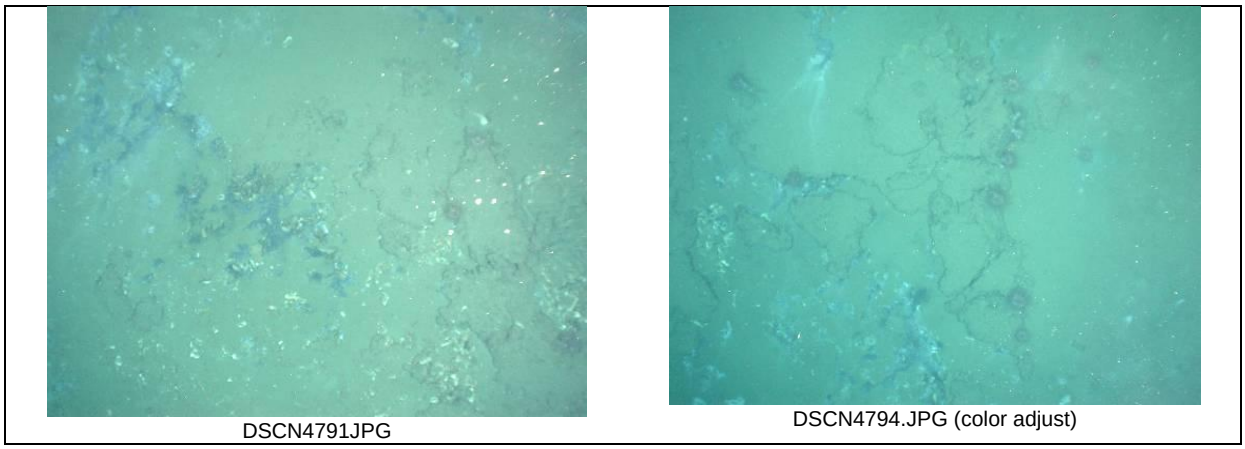

Figure 8-11. Representative photography from GC817.

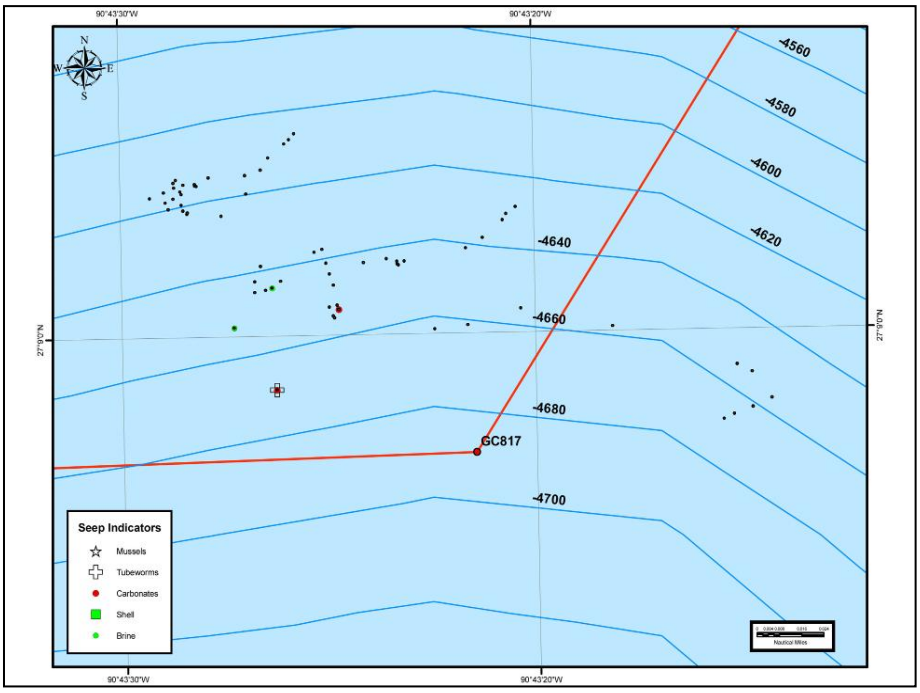

Figure 8-12. Survey results from GC817 station.

8.7. Green Canyon 296

This station (GC296) was previously the site of an exploratory well that was shut in due to fluid flow. The DCS reached bottom at 03:29 hrs on 17 March and collected images with a 12-second repeat rate until 06:30 hrs. A total of 766 images were collected with the bottom in view and acceptable navigation. Calmer seas and level bottom contributed to quality survey collections. The site showed extensive areas of mottled-green depressions suggesting brine-saturated sediments. The well site was characterized by completely featureless bottom, suggesting fluidized mud. Occasional bacteria mats were also seen, as was a solitary mussel shell. Notably there were abundant fish—many more than seen at previous stations—often two or three individuals in a single photograph. This site was considered as a possible candidate for additional biological study to understand what is attracting the fish. However the complete lack of chemosynthetic megafauna argued against submersible dives at this site (Figures 8-13 and 8-14).

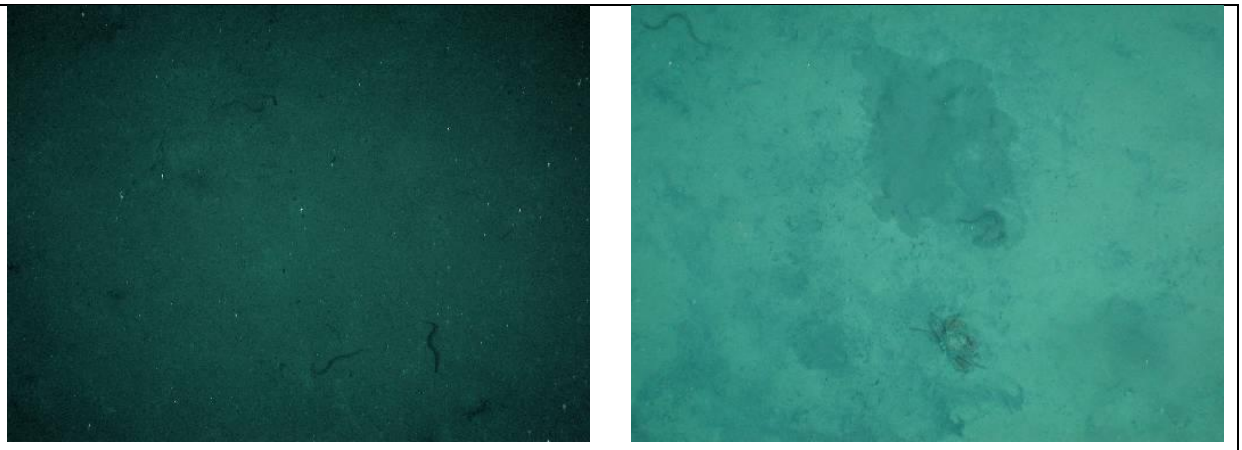

Figure 8-13. Representative photography from GC296.

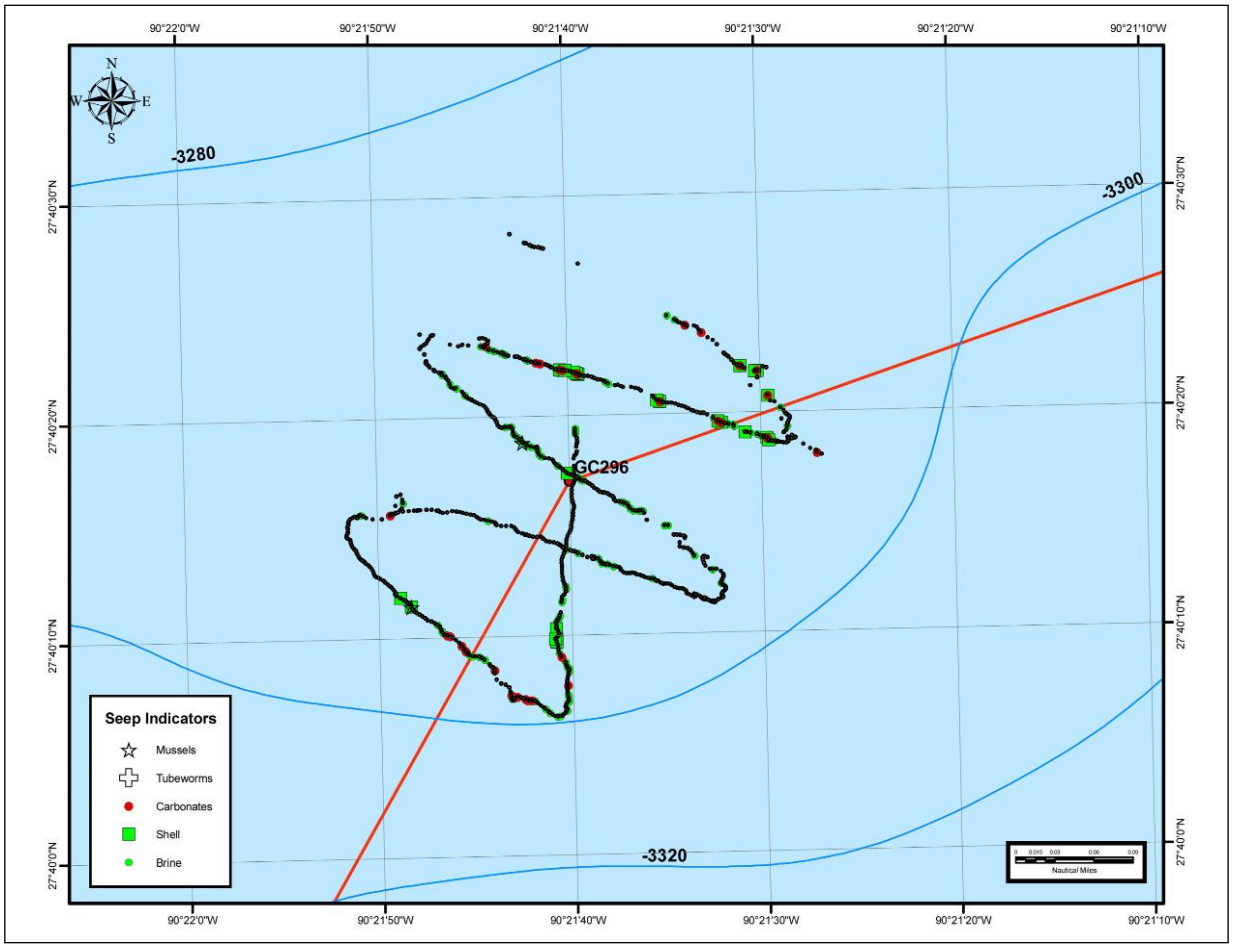

Figure 8-14. Survey results from GC296 station.

8.8. Mississippi Canyon 981

This site (MC981)was a series of anomalies on a west-to-east slope. The DCS reached bottom at 14:47 hrs on 17 March and collected images with a 12-second repeat rate until 17:44 hrs. A total of 825 images were collected with the bottom in view and acceptable navigation. Calmer seas again contributed to quality survey collections. The site featured a large mud-filled pool with extensive mud and brine flows. Development of bacterial mats was quite impressive over much of the site. However, apart from occasional shells and possible solitary tube worms, there was no development of a chemosynthetic community. This site was deemed a poor candidate for further study (Figures 8-15 and 8-16).

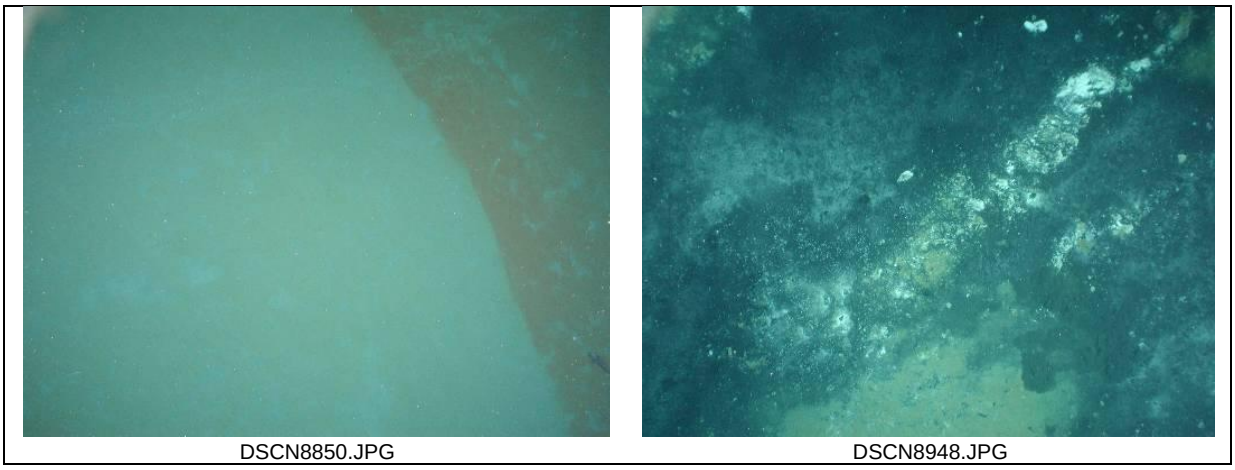

Figure 8-15. Representative photography from MC981.

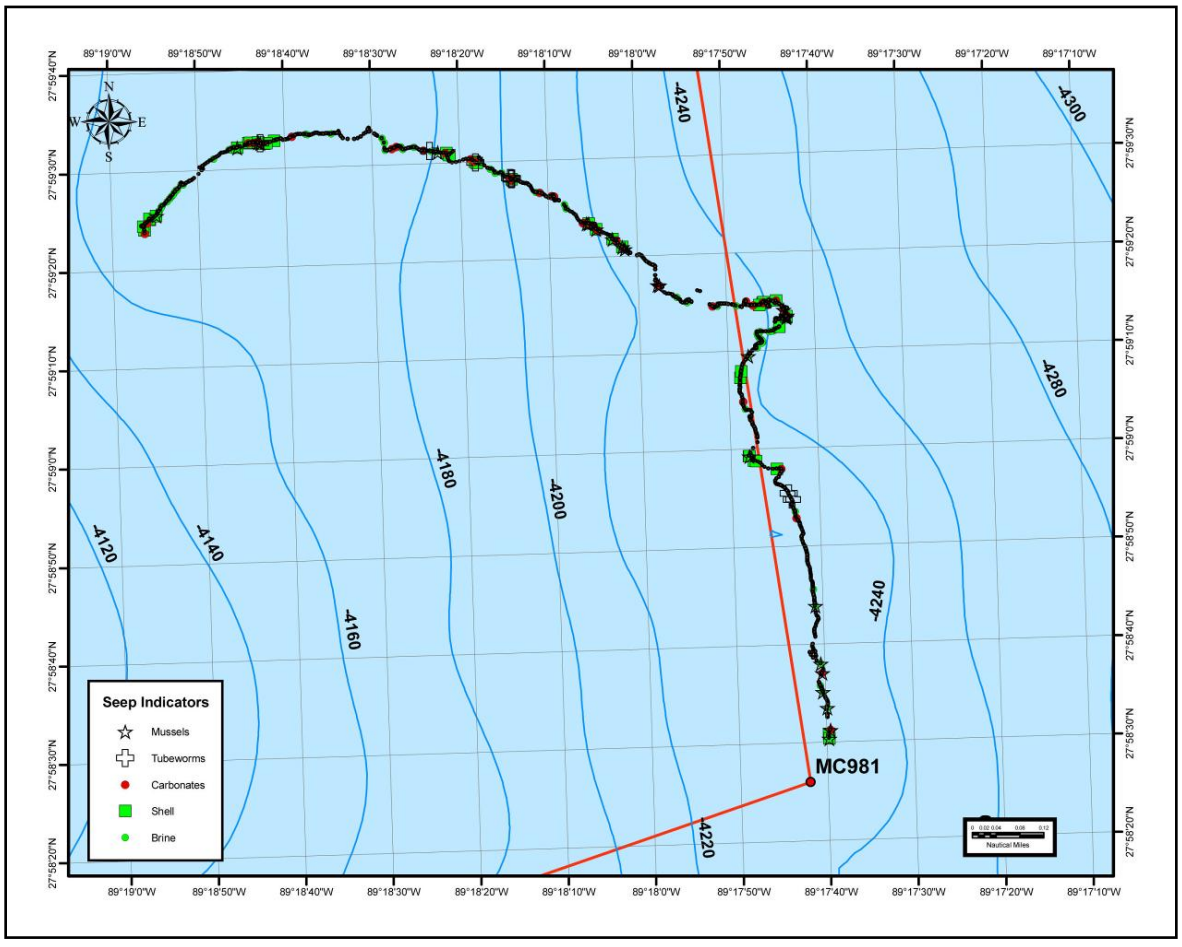

Figure 8-16. Survey results from MC981 station.

8.9. Mississippi Canyon 462

There were two targets at this site (MC462): a low mound and a terrace separated by 1.2 km at a depth of about 985 m. The DCS reached bottom at 02:25 hrs on 19 March and collected images with a 12-second repeat rate until 05:59 hrs. A total of 825 images were collected with the bottom in view and acceptable navigation. This site showed only isolated indications of seepage. Several carbonate outcroppings appeared to have bacteria or precipitate coatings with a few shells. Bacteria were also seen on sediment associated with brine staining. This site was considered a poor candidate for further study; however, a gorgonian colony on a large carbonate boulder was noted (Figures 8-17 and 8-18).

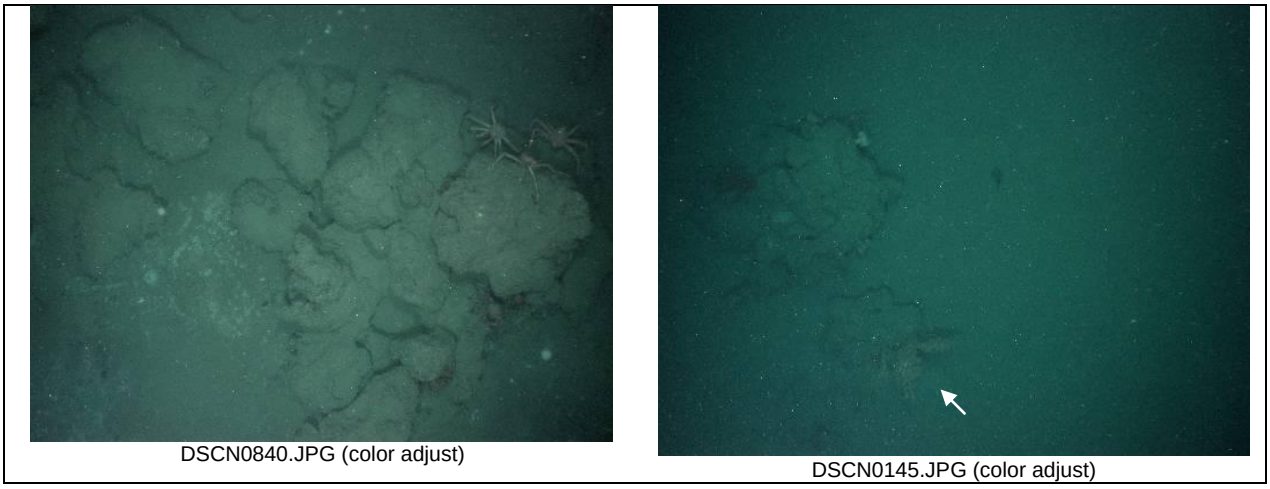

Figure 8-17. Representative photography from MC462.

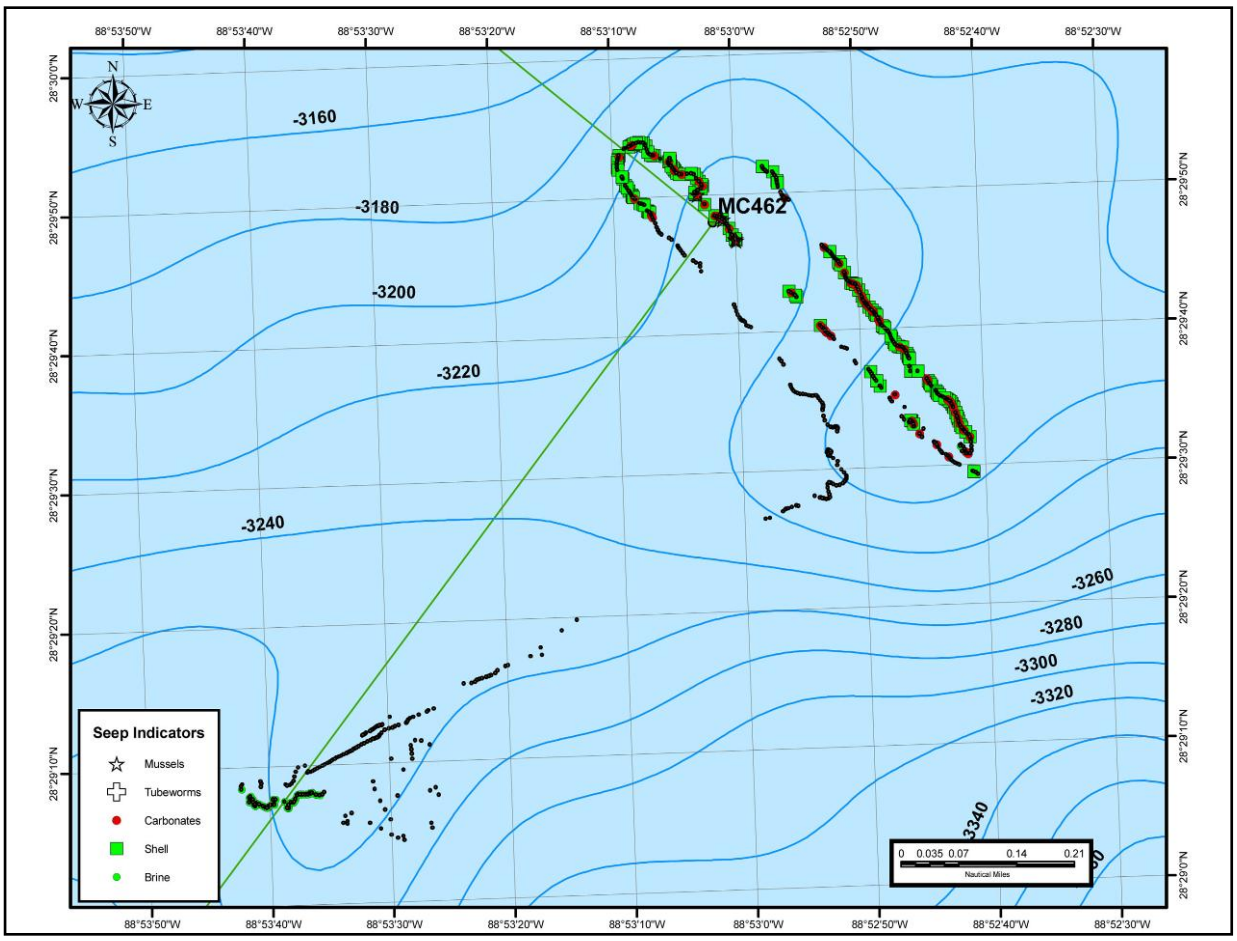

Figure 8-18. Survey results from MC462 station.

8.10. Atwater Valley 342

This site (AT342) was a low-relief mound with numerous geophysical targets distributed to the east and west with a depth of about 2,375 m. This site was the deepest surveyed during the photo Recon Cruise . The DCS reached bottom at 14:20 hrs on 20 March and collected images with a 12-second repeat rate until 16:49 hrs. A total of 516 images were collected with the bottom in view and acceptable navigation. This site included at least two large brine pools with active mud flows and brine channels. Sediment slumping was widespread. Vesicomyid clam shells were widespread, but few living individuals could be identified with certainty. What appeared to be tube worms occurred as individuals. Mussels were common, but not locally dense. This site was considered a good candidate for further study, but not pursued due to the discovery of the nearby extensive community at AT340 (Figures 8-19 and 8-20).

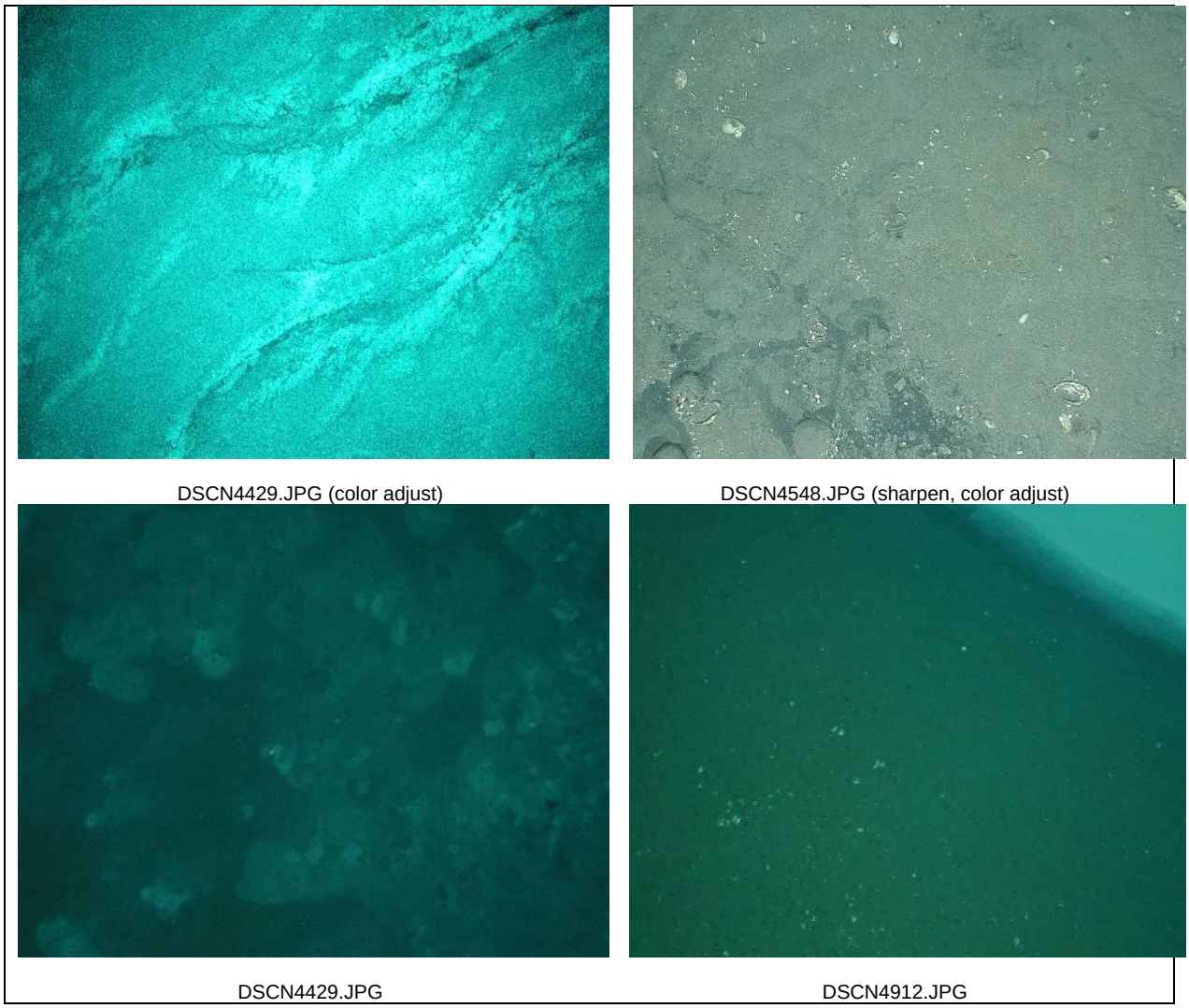

Figure 8-19. Representative photography from AT342.

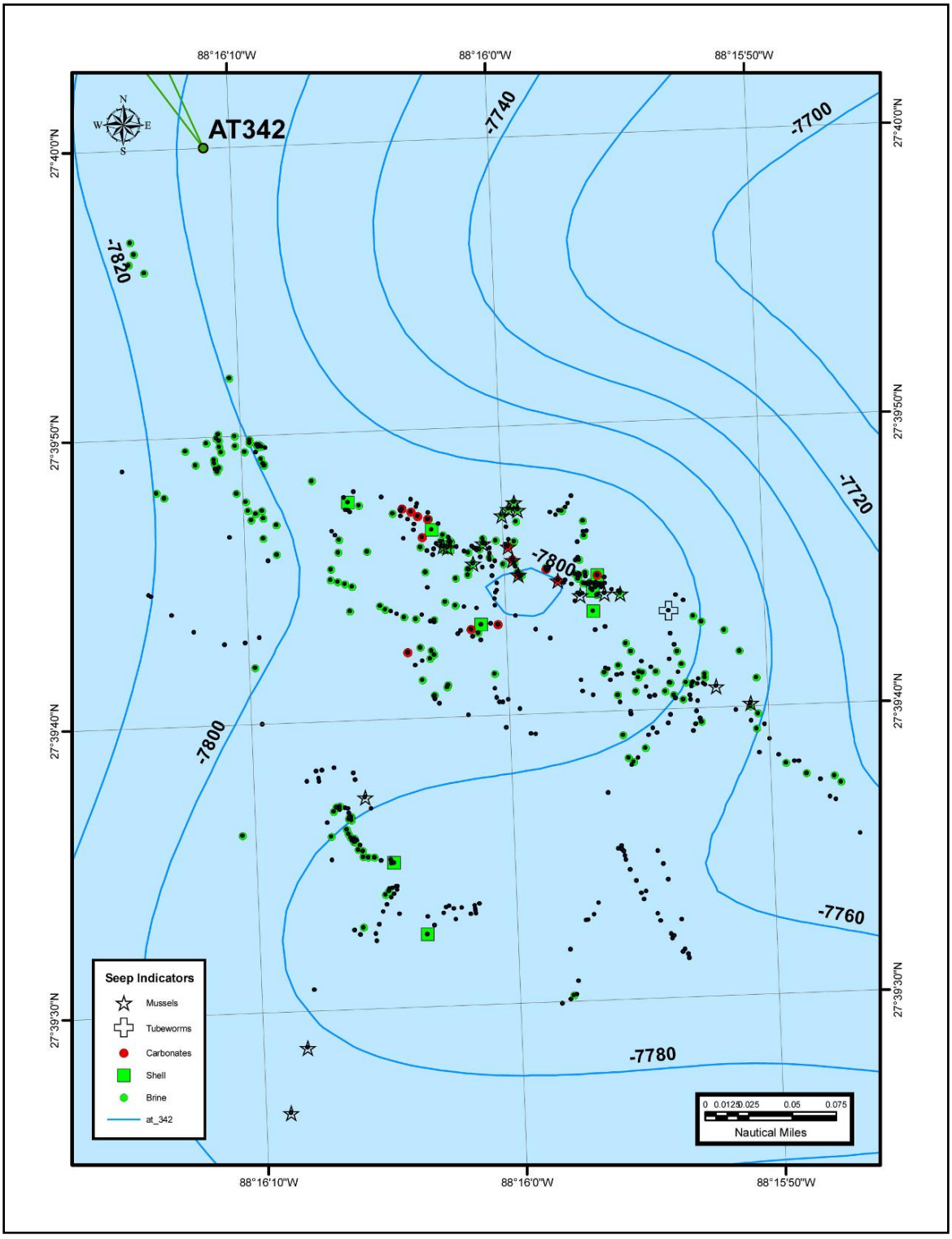

Figure 8-20. Survey results from AT342 station.

8.11. Green Canyon 868

This site (GC868) included a series of geophysical targets distributed over a very steep slope over a depth range of 1,360 to 1,460 m. The steep slope and worsening sea conditions presented particular challenges to effective survey, so the survey track was limited to the upper portion of the escarpment. The DCS reached bottom at 18:16 hrs on 22 March and collected images with a 10-second repeat rate until 19:04 hrs when a minor power malfunction in the DCS prematurely ended the survey sequence. A total of 236 images were collected with the bottom in view and acceptable navigation covering the major part of the targeted area. The sediment here appeared unstable and subject to granular sorting saltation down the visibly steep slope. Apparent small brine flows were seen on upper portion of slope. Fauna included a few fish, an isopod, and several examples of stalked anemones attached to sediment boluses. This site was deemed a poor candidate for further study (Figures 8-21 and 8-22).

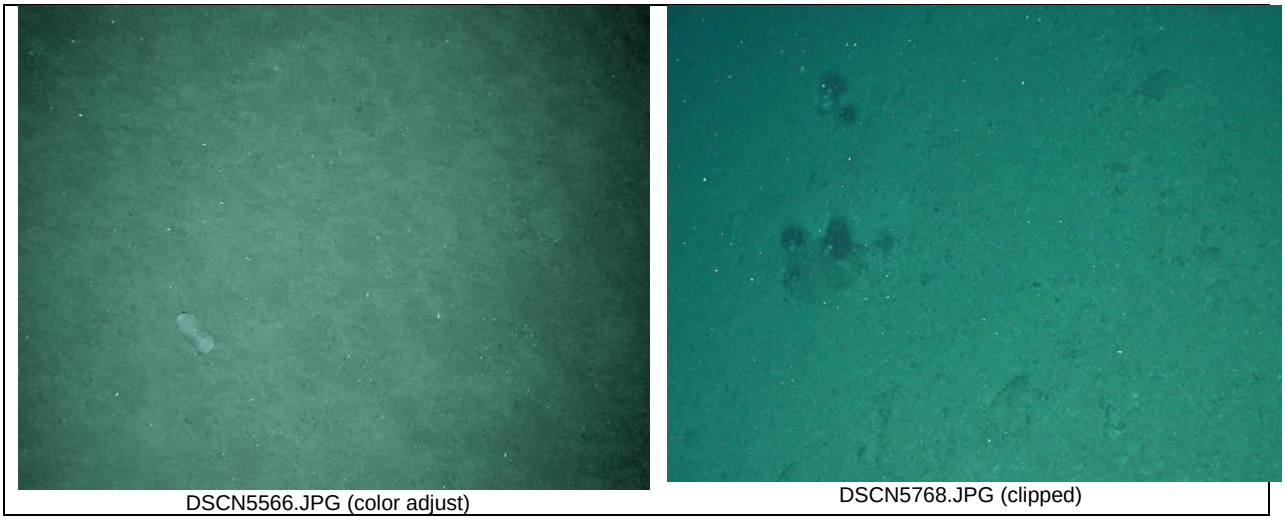

Figure 8-21. Representative photography from GC868.

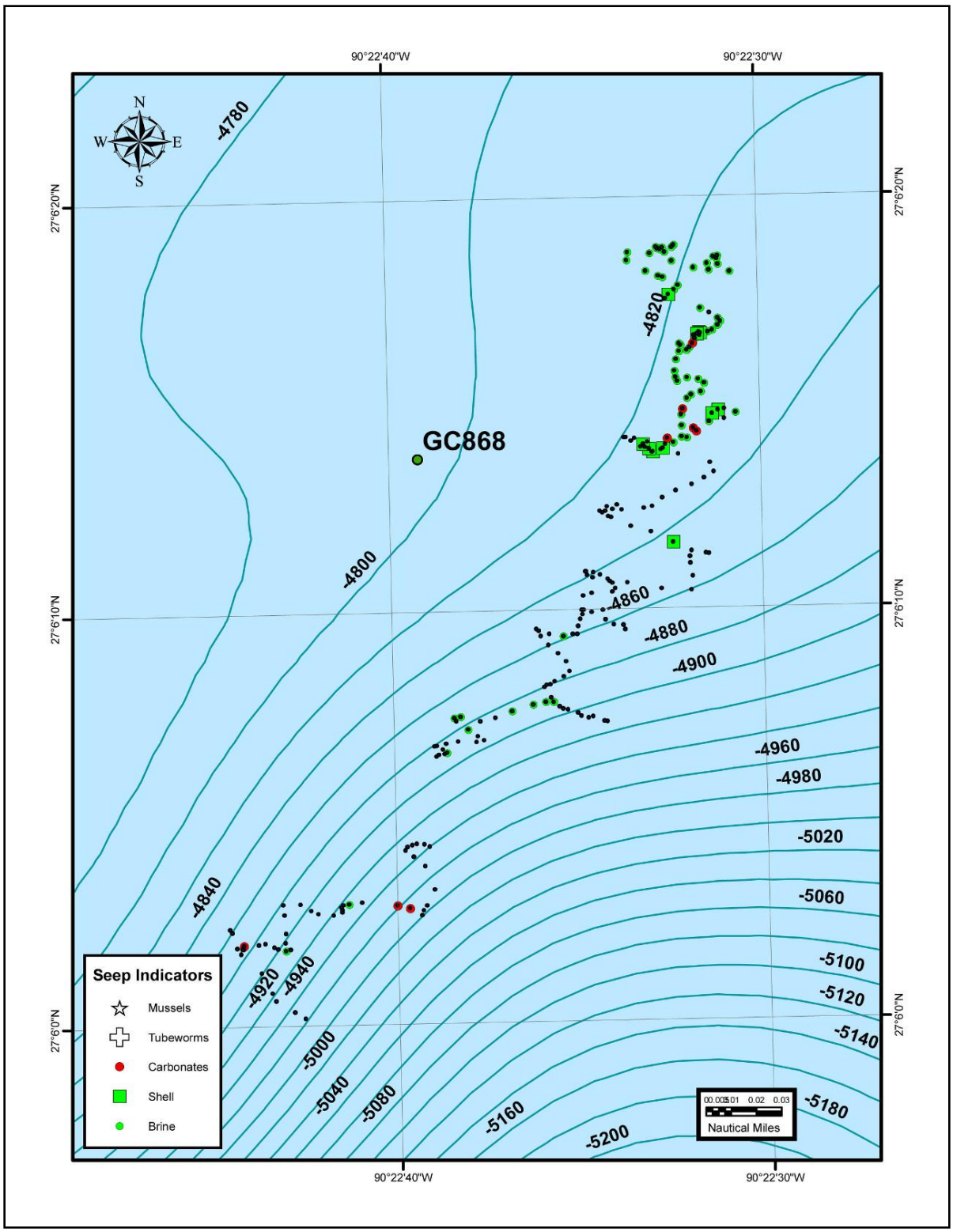

Figure 8-22. Survey results from GC868 station.

8.12. Walker Ridge 268

This site (WR268) was a low mound with a tight focus of geophysical targets at about 1,860 m. Despite continued heavy seas, the survey was completed because the target was concentrated and the ship could hold station in a tight radius while the DCS covered the objectives. The DCS reached bottom at 22:50 hrs on 23 March and collected images with a 10-second repeat rate until 00: 56 hrs on 24 March. A total of 523 images were collected with the bottom in view and acceptable navigation covering the major part of the targeted area. There were widespread indicators of sparse seepage at this site including small bacterial mats, shells, and individual tubes. Some of these "tubes" were probably sea whips misclassified as tube worms, but others appeared to be solitary pogonophorans. This site was considered a very marginal candidate for further study. This was the final station in the photo Recon Cruise (Figures 8-23 and 8-24).

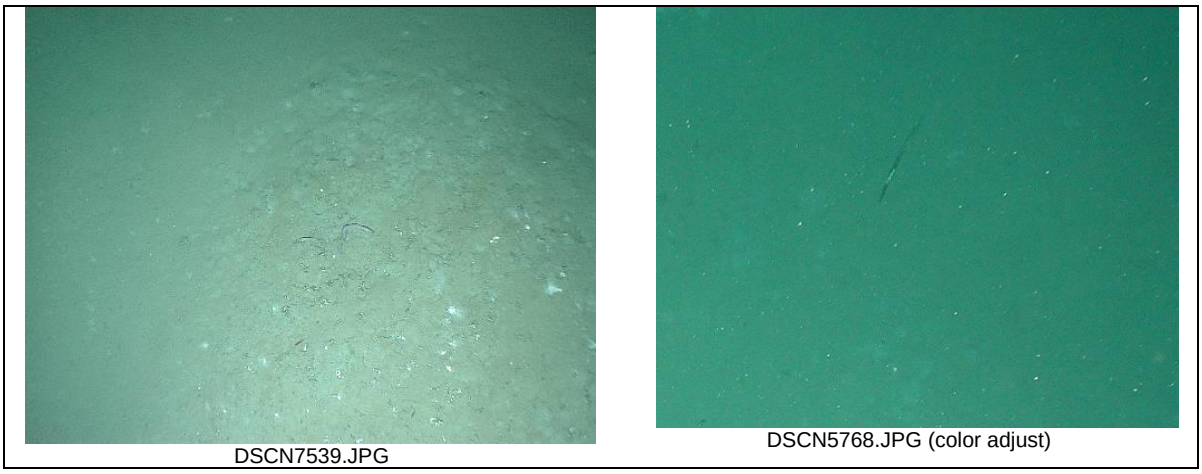

Figure 8-23. Representative photography from WR268.

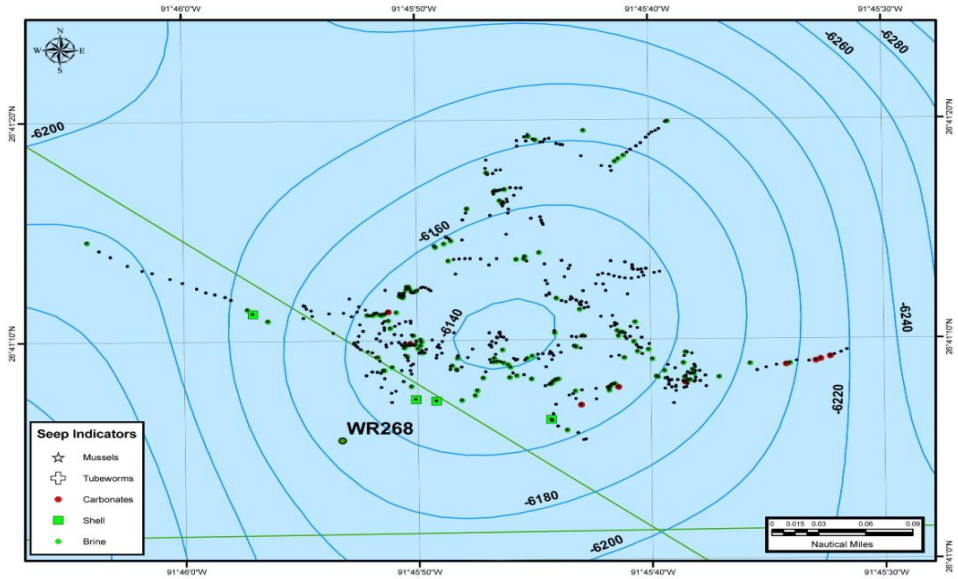

Figure 8-24. Survey results from WR268 station.

9. AUTONOMOUS UNDERWATER VEHICLE (AUV)

The original dive sites for the 2006 *Alvin* cruise were prioritized on the basis of character on 3-D seismic surface reflectivity maps and associated subsurface profiles coupled with bottom photographs acquired on a separate cruise prior to using *Alvin*. Great success was achieved using this pre-dive analysis of existing 3-D seismic data and acquiring bottom photography on transects across critical sites. As a product of these procedures, chemosynthetic communities were found at all 10 of the dive sites visited. These sites ranged from the deep eastern GoM (N 27 38.8': W 88 21.7') to the far western GoM (N 26 11.0'; W 94 37.4').

The major drawbacks of 3-D data, though, are the horizontal and vertical resolution. Most 3-D data have horizontal sample sizes of around 15m by 30m and vertical resolutions of 5–10 m (the contour interval used on the map below is 10m); many of the sub-environments of chemosynthetic communities are smaller than the horizontal sample of 3-D data and bathymetric changes are in the 1–2 m range. To identify these subtle features at the more interesting sites identified after the 2006 *Alvin* dives, and to improve the bathymetry maps to aid in navigation, we obtained high resolution bathymetry surveys over four of our key study sites using the Autonomous Underwater Vehicle (AUV) Hugin.

The AUV was equipped with instrumentation for collecting high-resolution multibeam bathymetry, chirp sonar subbottom profiles, and side-scan sonar swaths. These data are well constrained with excellent navigation and the data sets are acquired as the AUV travels at a constant height, 40 m, above the seabed. The AUV data sets for AT340, GC852, WR269, and AC601 were acquired in February 2007.

Details of the C&C Technologies AUV are given in the AUV Appendices, as are the results of the AUV imaging (Appendix 3).

10. *IN SITU* ACTIVITIES

The following section describes in-situ work for all sites visited by submersible or ROV, organized by site. If the sites were also visited during the Recon Cruise that information is also included for the sites. All dives during the 2006 *Alvin* cruise and the 2007 *Jason II* cruises are summarized. Dive maps showing *Alvin*'s and *Jason* II's track and sampling locations, as well as representative photographs, are presented as individual figures at each site.

Twenty-four dives were completed with *Alvin* at 10 different sites in 2006. Sixteen dives were completed using the ROV *Jason II* at 11 different sites in 2007. At some sites, multiple dives were made while at other sites only a single dive was completed. Table 10-1 and Figure 10-1 summarize the *Alvin* dive activity and Table 10-2 and Table 10-3 summarize the *Jason II* lowerings. Detailed dive information is presented on the pre-dive planning (Appendix 4) samples collected (Appendix 5), and dive activities (Appendix 6).

Table 10-1

Alvin Dive Summary

DIVE_NUM	Site	Depth(m)	Date	Dive Time	Lat Mean	Lon Mean
4173	AT340	2,216	5/9/2006	14:59	27.64532147	-88.36397849
4174	GC600	1,250	5/10/2006	14:04	27.37043846	-90.56947755
4175	WR269	1,950	5/11/2006	16:20	26.68598286	-91.66054682
4176	KC243	1,610	5/12/2006	14:29	26.73075164	-92.83065783
4177	GC852	1,450	5/13/2006	15:27	27.10628141	-91.16609942
4178	MC853	1,070	5/14/2006	14:35	28.12471393	-89.14148176
4179	AT340	2,200	5/15/2006	14:47	27.64507002	-88.36439901
4180	AT340	2,200	5/16/2006	16:45	27.64477891	-88.36475654
4181	AT340	2,200	5/17/2006	16:22	27.64648744	-88.36891570
4182	MC640	1,410	5/18/2006	15:37	28.35677424	-88.79270267
4183	AT340	2,175	5/19/2006	14:58	27.64634439	-88.37037384
4184	GC600	1,250	5/20/2006	14:25	27.36961335	-90.56930234
4185	GC852	1,410	5/21/2006	14:45	27.10911676	-91.16565528
4186	GC852	1,410	5/22/2006	15:56	27.10614074	-91.16601572
4187	GC852	1,410	5/23/2006	14:19	27.11026061	-91.16568461
4189	GC852	1,410	5/24/2006	16:39	27.11002842	-91.16590412
4190	GC852	1,410	5/25/2006	14:33	27.10836764	-91.16621835
4191	WR269	1,950	5/26/2006	15:25	26.68606157	-91.66147458
4192	AC818	2,740	5/27/2006	16:34	26.18030207	-94.62308449
4193	AC601	2,340	5/28/2006	14:27	26.39123684	-94.51446418
4194	AC645	2,240	5/29/2006	14:32	26.35448427	-94.49977357
4195	AC818	2,740	5/30/2006	14:42	26.18026385	-94.62294105
4196	AC601	2,330	5/31/2006	15:11	26.39164934	-94.51394832
4197	AC645	2,200	6/1/2006	14:29	26.35403655	-94.49670376

Site Abbreviations: AC= Alaminos Canyon; AT= Atwater Valley; GB= Garden Banks; GC- Green Canyon; KC= Keathley Canyon; MC= Mississippi Canyon; WR= Walker Ridge

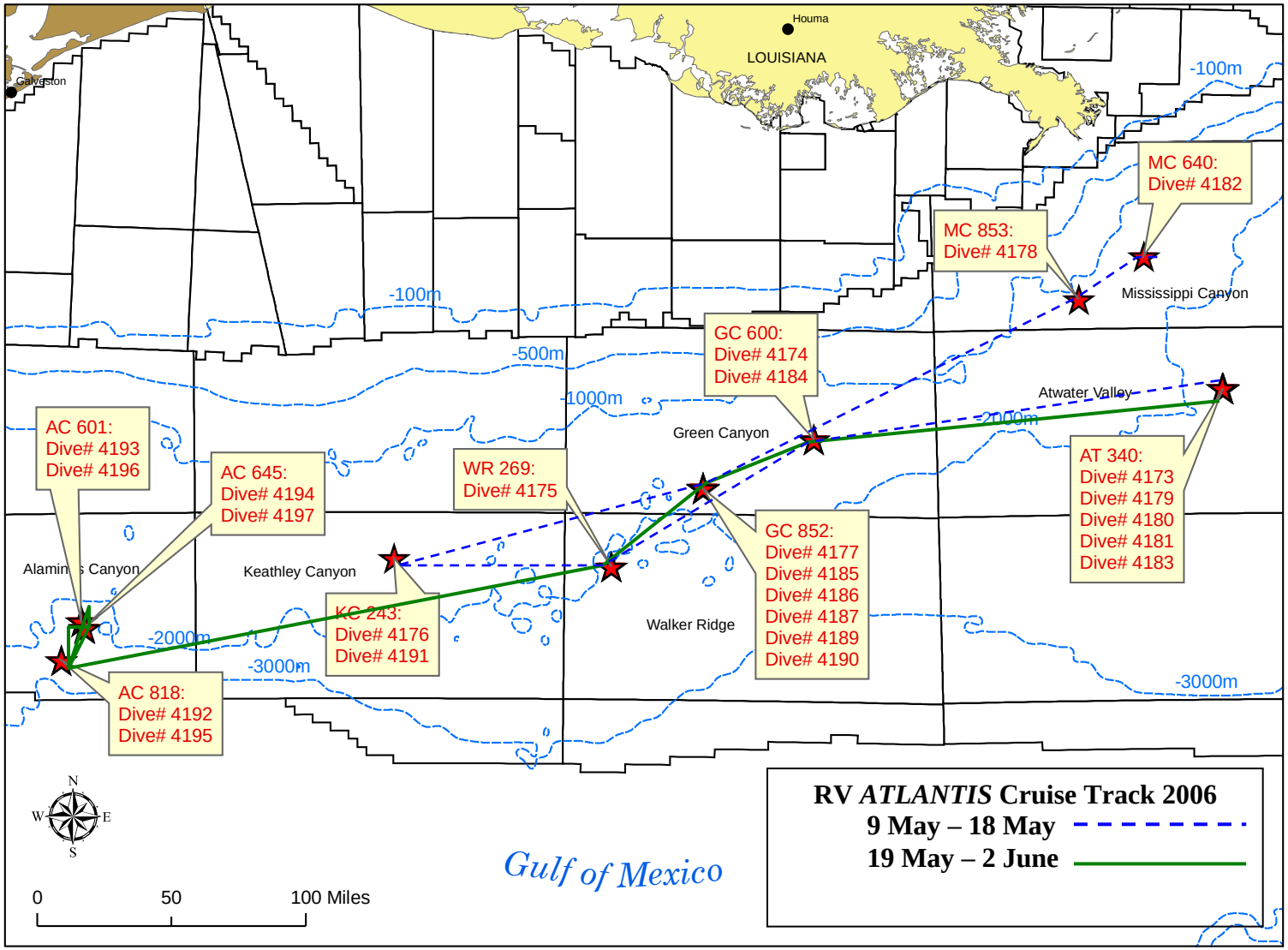

Figure 10-1. Site locations of *Alvin* dives.

Table 10-2

Jason II Dive Data

Site	Lowering ID	Start/Launch	End/ On Deck	Data Time	Lowering Time	Max Depth (m)
AT340	J2-269	2007/06/07 11:58	2007/06/09 06:02	37:58:00	4:06:00	2,212
AT340	J2-270	2007/06/09 16:48	2007/06/11 04:30	32:22:00	3:20:00	2,213
MC462	J2-271	2007/06/11 21:37	2007/06/12 13:16	13:49:00	1:50:00	973
GC415	J2-272	2007/06/13 01:10	2007/06/13 12:11	0:00:00	11:01:00	1,107
GC852	J2-273	2007/06/14 00:00	2007/06/15 19:10	41:09:00	2:01:00	1,633
GB697	J2-274	2007/06/16 05:05	2007/06/17 12:50	29:43:00	2:02:00	1,281
WR269	J2-275	2007/06/18 00:05	2007/06/18 20:06	17:42:00	2:19:00	1,964
AT340	J2-276	2007/06/19 12:36	2007/06/20 17:21	25:31:00	3:14:00	2,213
AT340	J2-277	2007/06/21 04:04	2007/06/22 12:10	29:13:00	2:53:00	2,213
GC852	J2-278	2007/06/23 06:15	2007/06/24 20:09	36:06:00	1:48:00	1,426
GB829	J2-279	2007/06/25 12:09	2007/06/25 22:31	8:18:00	2:04:00	1,303
GB647	J2-280	2007/06/26 09:59	2007/06/27 00:17	12:49:00	1:29:00	1,014
AC645	J2-281	2007/06/28 05:36	2007/06/29 23:02	38:30:00	2:56:00	2,223
AC818	J2-282	2007/06/30 12:31	2007/07/01 19:41	27:51:00	3:19:00	2,750
AC601	J2-283	2007/07/02 11:57	2007/07/04 10:09	42:41:00	3:31:00	2,338
AC818	J2-284	2007/07/04 21:06	2007/07/05 13:26	12:44:00	3:36:00	2,747
16			**Totals:**	**406:26:00**	**51:29:00**	

Table 10-3

Dive Summary

SITE	Dive	LEASE_AREA	SEQ	DEPTH_(M)	LATITUDE	LONGITUDE
Y1	269, 270, 276, 277	AT340	1,7	2,242	27.646389	-88.365833
Y5	273, 278	GC852	4,8	1,448	27.112500	-91.164167
Y6	275	WR269	6	1,862	26.684444	-91.671389
Y8	283	AC601	13	2,366	26.362500	-94.510278
Y9	281	AC645	11	2,226	26.371389	-94.496944
Y10	282, 284	AC 818	12	2,875	26.161389	-94.576667
Y11	280	GB 647	10		27.331389	-92.435000
Y14	271	MC 462	2		28.494444	- 88.881389
Y15	272	GC415	3		27.542222	- 90.990278
Y	279	GB829	9			
Y16	274	GB697	5		27.283611	- 92.112778
2		MC640		1,404	28.355833	-88.793056
3		MC853		1,082	28.123333	-89.139722
4		GC600		1,249	27.366389	-90.564167
7		KC243		1,610	26.750278	-92.829167
12		GB741			27.248611	-92.112778
13		GC559			27.426667	-90.434167

Table 10-4

Dive Activity over the Program

Lease Area	**Dates Sampled**
AC601	June 2006, June 2007
AC645	June 2006
AC818	June 2006, June 2007
AT340	June 2006, June 2007
GB647	June 2007
GB697	June 2007
GB829	June 2007
GC415	June 2007
GC852	June 2006, June 2007
MC462	June 2007
WR269	June 2006, June 2007
GC600	June 2006
MC640	June 2006

10.1. Atwater Valley 340

This site (AT340) was surveyed as part of the 2005 Recon Cruise and mapped by the AUV Hugin. There were five *Alvin* dives and four *Jason II* lowerings at this site. *Alvin* dives included AD4173 on 5/9/2006, AD4179 on 5/15/2006, AD4180 on 5/16/2006, AD4181 on 5/17/2006, and AD4183 on 5/19/2006. *Jason II* dives included J2-269 from 6/7/2007 to 6/9/2007 for a total of 37 hrs and 58 minutes, J2-270 from 6/09/2007 to 6/11/2007 for a total of 32 hrs and 22 minutes, J2-276 from 6/19/2007 to 6/20/2007 for a total of 25 hrs, 31 minutes, and J2-277 from 6/21/2007 to 6/22/2007, for a total of 29 hrs and 13 minutes.

10.1.1. 2005 Reconnaissance Cruise (Recon Cruise)

The portion of this site surveyed in 2005 included two low-relief mounds with numerous geophysical targets distributed down-slope to the east with a depth of about 2,240 m. The DCS reached bottom at 14:20 hrs on 20 March and collected images with a 12-second repeat rate until 16:49 hrs. A total of 502 images were collected with the bottom in view and acceptable navigation. This site showed a high diversity of chemosynthetic fauna and habitat variations. Brine flows and channels were common. Carbonates included large boulders and solitary pieces. Tube worms occurred as individuals or tufts, but also as small bushes in one location. The community appears to be spread over a large area, implying that there may be yet more variability to discover. This site was selected as an excellent candidate for further study (Figures 10-2 and 10-3).

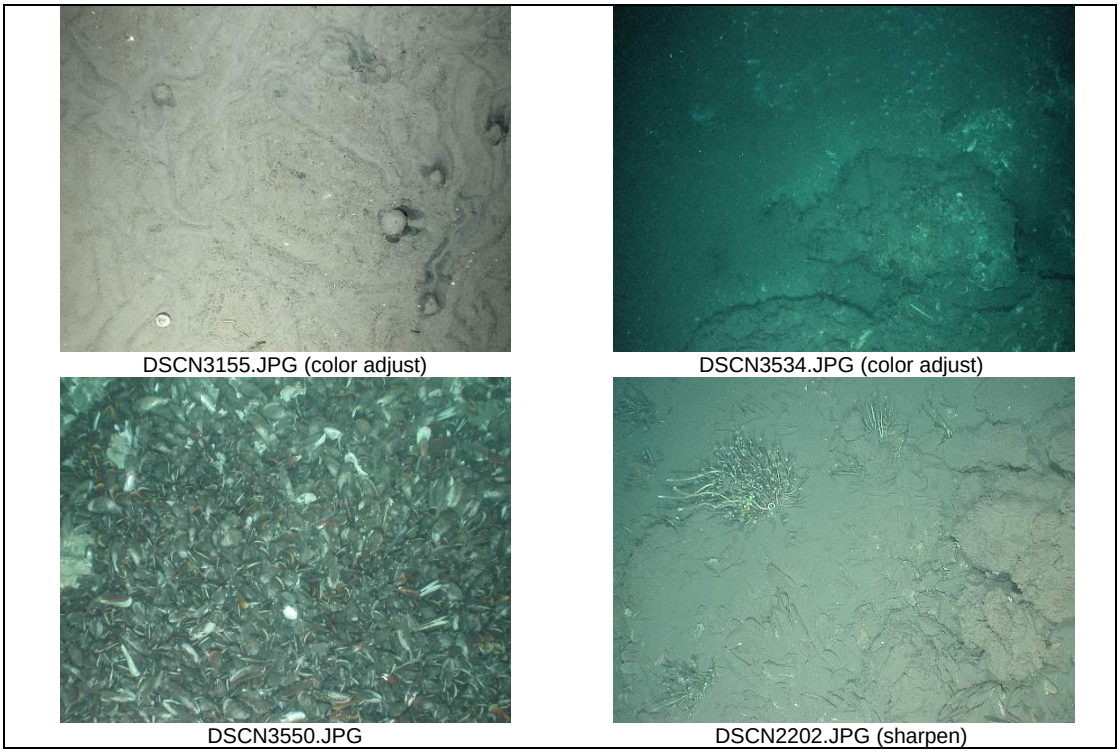

Figure 10-2. Representative photography from AT340.

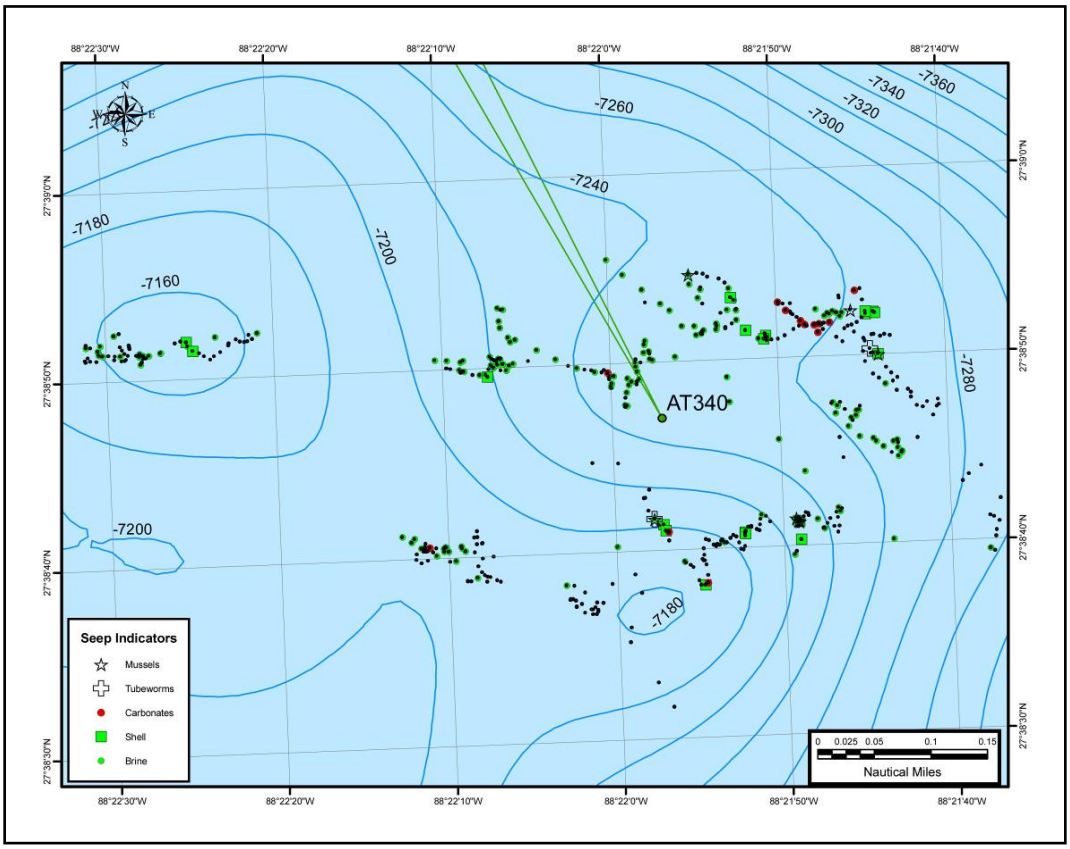

Figure 10-3. Survey results from AT340 station.

10.1.2. Navigation Considerations

From our *Alvin* dives, we had a lingering perception that the positions reported by the navigation system on *Alvin* for this site were offset from their true position by perhaps 25 to 35 m (refer to the Navigation section of this report for a detailed discussion of multi-vessel navigation and geodetics reconciliation issues). Due to the importance of reconciling positions reported by the navigation systems on the four survey vessels involved in this multi-year program, our first *Jason II* dive priority was to perform a detailed survey of a prominent geologic feature revealed by our recent AUV survey. This feature is shown as a crater in Figure 10-4, as derived from the AUV dataset.

The crater is shown as a circular depression of depth 2,200 m in the center of the contour map. The diameter of the crater at the fourth and outer-most concentric 2-m contour line (i.e., up to 2,194 m water depth) is about 67 m. We were confident that we could find the center of this crater using *Jason* II, so we defined the crater center as our Central Reference Point (CRP) for the site work at AT340. We defined the AUV survey positions as the assumed true positions of all features at the site, and then used the AUV survey to measure the position of the center of the crater. The latitude in World Geodetic System 1984 WGS84 for the crater center from the AUV survey was measured as N27 38.67010. The longitude was measured as W088 22.08535. We used this position as the *defined-as-true* position of the site CRP.

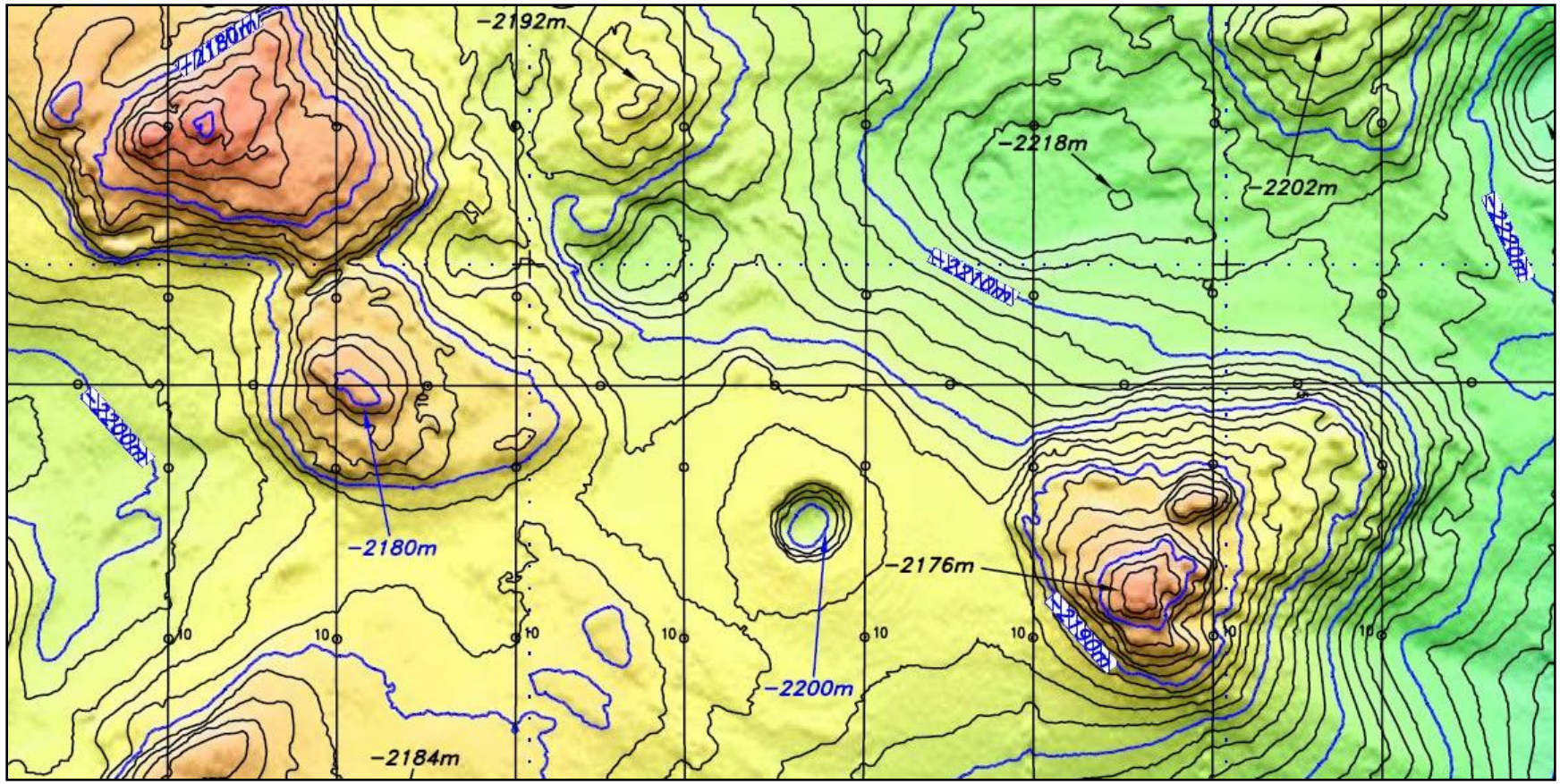

Figure 10-4. The crater used for defining a Central Reference Point at site AT340.

We then determined the Northing (Y) and Easting (X) in m for this CRP for the local coordinate system in which *Jason II* would work. We did this by applying a geodetic False Northing (-3,058,258.71 m) and a False Easting (135,152.2 m) to the standard UTM Zone 16 projection for the WGS84 datum, then calculating the local X and Y from the latitude and longitude of the site CRP as measured from the AUV survey. These are the same Falsings used for the local projection of the dives at this site with *Alvin* last year. These Falsing shifts had been selected for the *Alvin* dives at this site in order to place a "Local Origin" in X,Y space near the targets of interest at the site. The latitude of this Local Origin is N27 38.50000 and the longitude is W088 22.20000. The local coordinates thus calculated and assigned to the site AT340 CRP were X = 192 m and Y = 312 m. We placed this CRP target into *Jason* II's navigation system along with targets of interest positioned by *Alvin* last year and targets positioned by a geologic review of the AUV contour map.

Targets developed for this site are listed in Table 10-5. Targets appended with "*Jason* II" in their name have listed their position fixes logged by *Jason II* after each marker or target was found. Targets appended with "Predicted" have listed the predicted position of the marker, though the marker was not found by *Jason* II. To predict each such marker position, we applied an X and Y shift to the old *Alvin* positions (see note at bottom of table) in order to transform each of them to predicted locations for *Jason II* and the future. The method and justification for deriving this transformation offset is detailed in the following *Dive Summary* for Dive 269.

Table 10-5

Target Locations for Site AT340

Target	Latitude	Longitude	Local X (m)	Local Y (m)	Depth (m)
Local Origin	N27 38.500000	W088 22.200000	0	0	2,194
Cent Ref Point	N27 38.670102	W088 22.085353	192	312	2,201
BenchMarker #1 Jason	N27 38.678012	W088 21.887194	518	323	2,194
BallMarker #2 Jason	N27 38.699431	W088 21.857052	568	362	2,190
Marker #11 Jason	N27 38.690605	W088 21.873362	541	346	2,183
Blue Flight Bag Jason	N27 38.702626	W088 21.862565	559	368	2,190
Urchins #1 Jason	N27 38.702751	W088 21.959871	399	370	2,193
Cores in Urchins Jason	N27 38.701794	W088 21.947088	420	368	2,193
Marker #12 Jason	N27 38.841125	W088 22.425623	-384	621	2,175
Marker #15 Jason	N27 38.697320	W088 21.851550	577	358	2,191
Harry's Rock Jason	N27 38.838844	W088 22.437150	-383	630	2,173
SW Mound	N27 38.623116	W088 22.564597	-597	234	2,184
Marker #3 Predicted	N27 38.697199	W088 21.863714	557	358	2,192
IanMarker #6 Predicted	N27 38.696217	W088 21.853363	574	356	2,190
Marker #8 Predicted	N27 38.839494	W088 22.426211	-385	618	2,175
Urchins #2 Predicted	N27 38.737589	W088 22.216339	-22	439	2,192
Marker #5 Predicted	N27 38.669931	W088 21.772760	706	306	2,206

Alvin to Jason local transform: 24m at 95deg, or add 24m to x and subtract 5 m from y.

10.1.3. *Alvin* Dive 4173

Upon arriving on station at midnight before the dive, Bob Carney ran a trawl about 1 km from the site that recovered a variety of holothurians, shrimp, crabs, and snails. Also recovered were some coal, a small piece of iron or steel, and some wood and perhaps bone. Speculation ran high that we trawled an old shipwreck. This first dive went extremely well. Bernie Bernard and Erik Cordes were in the sub. It was the very first solo dive for their pilot, and both scientists reported that he is very good and that the dive went very well. Launch was right on time at 08:00, and the sub resurfaced about 15 minutes early (16:45 hrs) because the battery ran down. The map that Bernie put together, linking the geophysics data, bathymetry, and targets derived from the photo recon cruise was used to navigate the dive, which seemed to go very efficiently (Figure 10-5). They found the site very shortly after arriving on the bottom and were able to sample both mussel beds and tube worms. They also took two sets of six push cores. One set in a bacterial mat and another near the tube worm collection. Erik reported that there are 3–4 tube worm aggregations suitable for staining and Bushmaster collection, so this is likely to become one of our alpha sites for intensive study. They did not have time to conduct a formal photo survey for the mosaic on this dive, but did test the down looking camera by running it for about two hours of the dive.

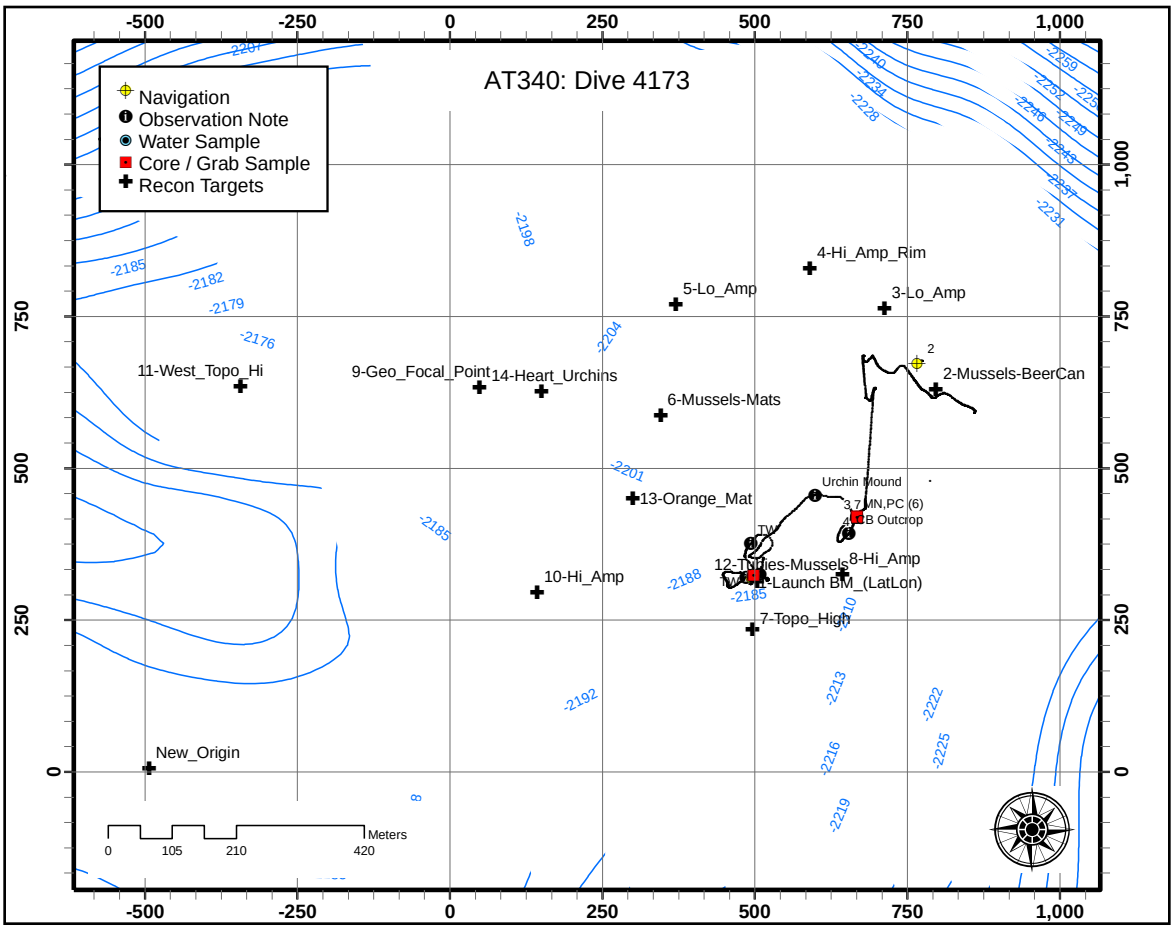

Figure 10-5. Dive 4173 on 5/9/2006 at an average depth of 2,216 m.

10.1.4. *Alvin* Dive 4179

Between dives, Bob Carney conducted a trawl off the AT340 site. He was successful in bringing up numerous holothurians, a fish, and small numbers of other benthic fauna. The *Alvin* dived on schedule with Chuck Fisher and Stephanie Lessard-Pilon. The dive was again focused on AT340 at a general depth of 2242 m. This was a very productive dive.

We have had some issues resolving the location differences between our seismic surface reflectivity-bathymetry maps and the ship's/sub's navigation net. The first task, once the sub hit the bottom, was to go to our benchmark deployed from another dive and get the X-Y position. In addition, a coil of fishing line seen in the March photo survey was found and marked with an X-Y position. Bernie Bernard is using these known points to understand and rectify the offset in our two sets of navigation data. Tasks accomplished during the dive included: 1) staining of four tube worm bushes, 2) acquisition of one Bushmaster sample, 3) collection of mussels by using the scoop, 4) collection of one tiger holothurian, 5) Collection of shrimp and crabs using the slurp gun, 6) collection of water over the seep using a Niskin bottle, 7) shooting of a photo mosaic over the collection sites, and 8) deployment of a baited crab trap for Bob Carney. This was also an extremely productive dive with regard to sampling and staining tube worms for growth rate studies. After the *Alvin* was on deck, Mandy Joye conducted a CTD cast over the site in order to assess methane concentrations in the water column over this productive site (Figure 10-6).

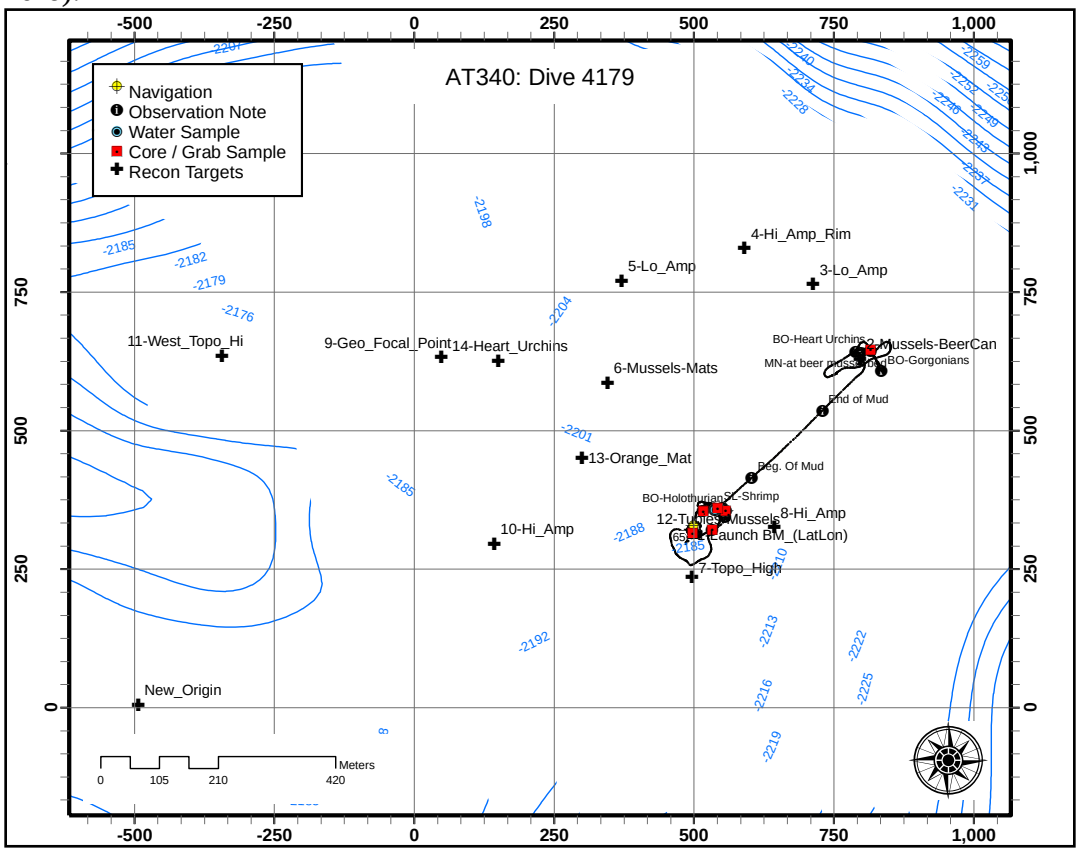

Figure 10-6. Dive 4179 on 5/15/2006 at an average depth of 2,200 m.

10.1.5. *Alvin* Dive 4180

Erik Cordes and Jillian Petersen were the observers. They had a very productive dive that followed the successful sampling protocols from the previous dive. A problem developed when they attempted to stain a tube worm bush for eventual growth rate studies. The stainer pump did not work so no stain could be put into the chamber. The staining task was aborted, and the dive team moved on to other tasks. The following samples were acquired: 1) one Bushmaster sample, 2) one big mussel net scoop, 3) one tube worm grab sample, 4) two authigenic carbonate samples (a large one and a small one), and 5) four Niskin bottle samples.

During the dive a very large and densely populated mussel bed was discovered. Because of its linear shape, the observers name it the "mussel brick road." Following the dive a trawl was conducted adjacent to the site and north-south and east-west multibeam bathymetry swaths were collected over the AT340 site (Figure 10-7).

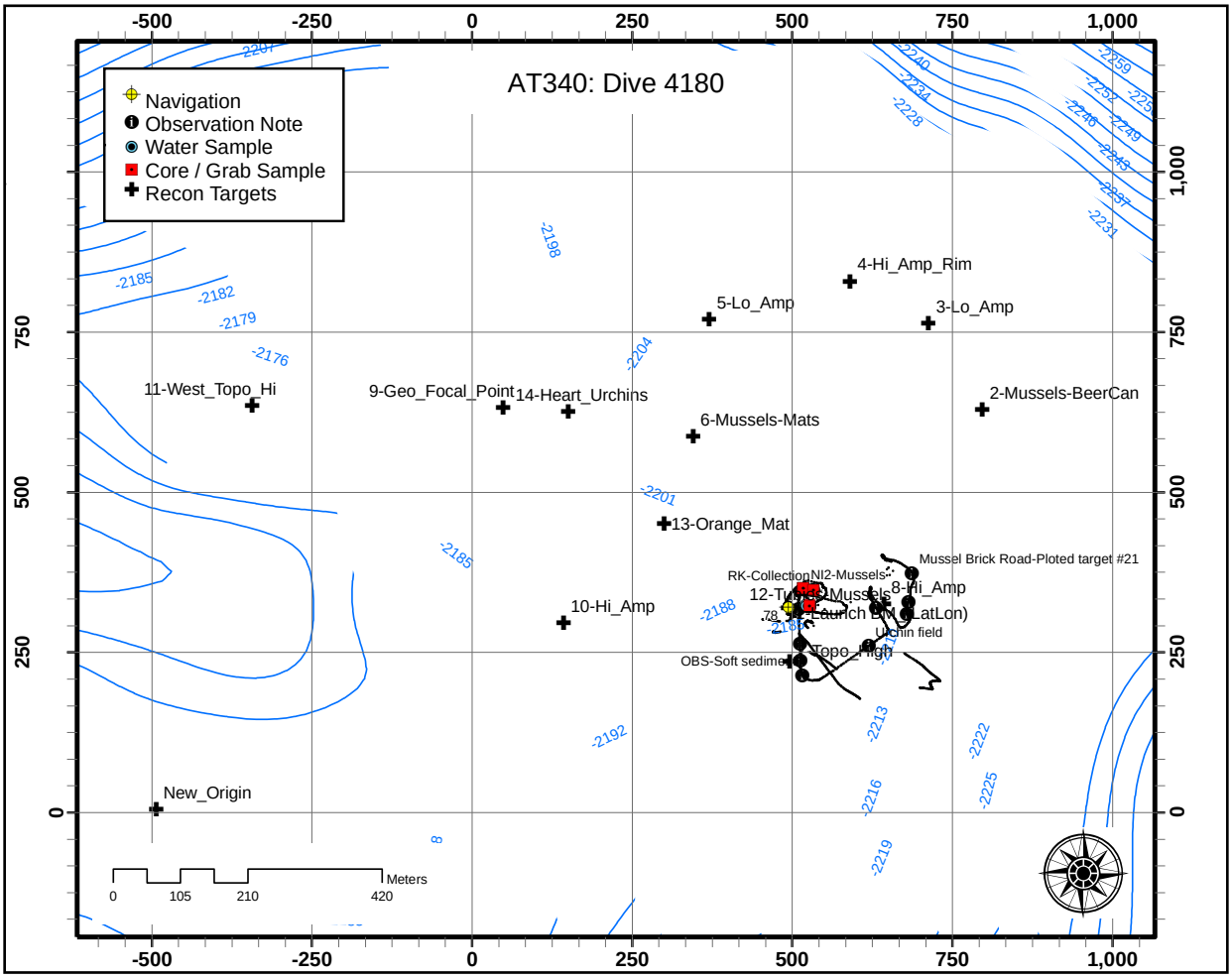

Figure 10-7. Dive 4180 on 5/16/2006 at an average depth of 2,200 m.

10.1.6. *Alvin* Dive 4181

The pilot was Mark Spear, and the two observers were Harry Roberts and Guy Telesnicki. The purpose of this dive was to investigate a rather distinct reflectivity anomaly in the northwest part of the study area. The geophysical data suggested that this site would be a good one, and our interpretations were supported by the results of today's dive. After reaching the bottom, we proceeded to the apex of the northwest mound. Upon approaching the mound, the scattered mussel shells and tube worms suggested that there were interesting things ahead. As we approached the upper part of the mound, it became apparent that the entire mound was composed of one cemented mussel shell horizon after another. The top and upper flanks of the mound were covered with tube worm bushes and both living and dead mussels. Since we had other areas to sample, we left the mound and traveled to the east where we encountered a brine flow and pool and many associated mussel beds. After sampling the mussels, we moved on to the original benchmark to the SE. At this point, we took cores around a tube worm bush and picked up *in situ* experiments as well as a fish trap. It was a very instructive and productive dive.

The following samples were acquired: 1) one mussel pot, 2) two mussel scoops, 3) three push cores, 4) three Niskin bottle samples, and 5) pick-up of fish trap and small *in-situ* experiments. Even though we thought this would be our last dive at AT340, the new site to the northwest was so good that another dive is being planned (Figure 10-8).

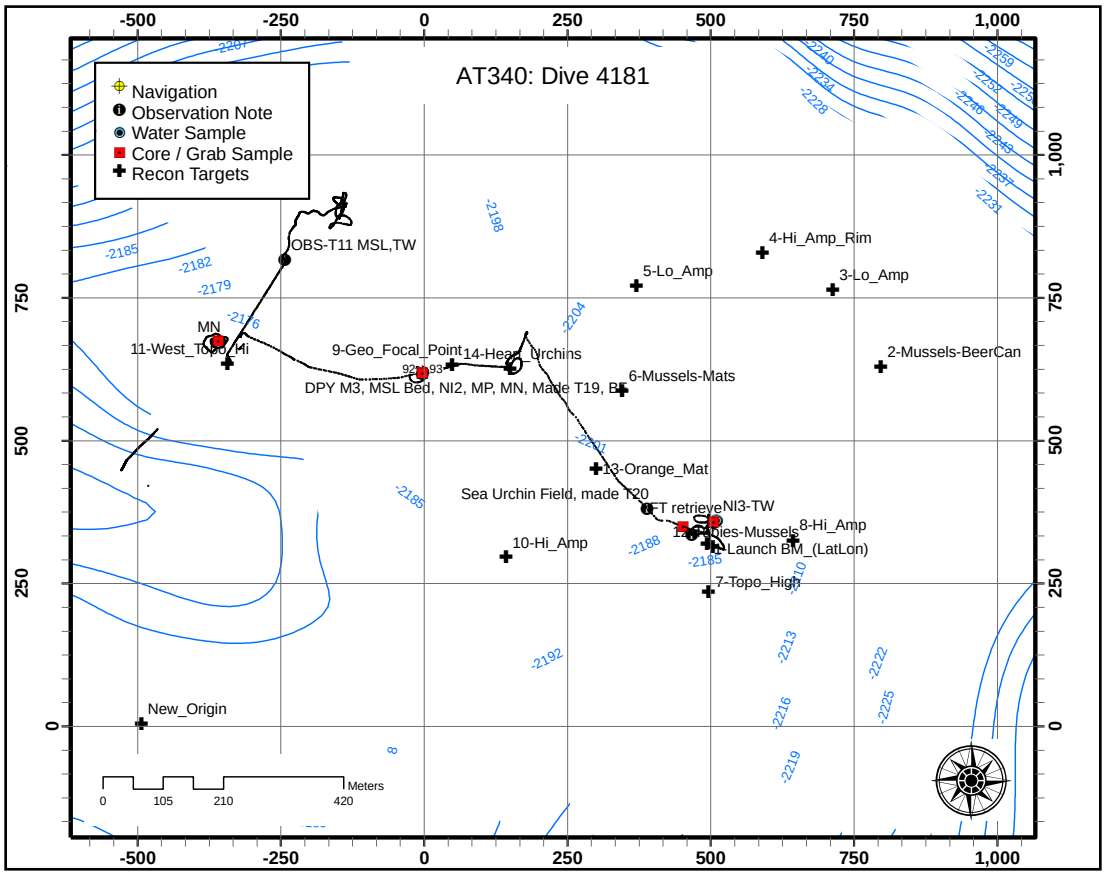

Figure 10-8. Dive 4181 on 5/17/2006 at an average depth of 2,200 m.

10.1.7. *Alvin* Dive 4183

We began this dive at X-389 m, Y-609 m, a nice area with tube worm clumps all around. We sized one tube worm bush up for a Bushmaster collection but decided against it. We two control push cores about 2 m from tube worms. There were some large pockmarks about 2 m in diameter and 1 m deep. We covered the flanks of the mound back and forth and found that at the top it got thick with carbonates and lots of tube worms, but not a very good spot for a Bushmaster collection. At 15:15 hrs, we set up to stain some large (not giant) tube worms and dropped digital target 18. In looking at the tube worms on the video, it seems that *Escarpia* rarely stick out their plume while *Lamellibrachia* has it out often. Physical Marker 12 was deployed here at X-388 m, Y-639 m. We set up again nearby to stain a second clump of tube worms. This clump consisted of small worms with mostly unclonoized anterior ends. Marker 8 was deployed at this clump. We stained a third bush about 0.5 m to the west of Marker 8; no new marker was deployed for this one. We looked around for a clump of tube worms of appropriate Bushmaster size and stopped to grab some baby tube worms on a rock. We returned to the original clump of tube worms from the beginning of the dive and collect a Bushmaster of these. At 17:42 hrs, we headed to "urchin acres" X-375 m, Y-375 m. We passed a carbonate ridge with tube worms on the way. At 18:15 hrs X-46 m, Y-444 m, we took 10 push cores in urchins, collected some urchins, and dropped digital target 19. While coring, we took some good video of hermit crabs. We slurped some shrimp from the basket and two of the hermit crabs and headed to Mussel Brick Road. En route we saw an urchin field and marked it with digital target 20. We also pass some pogonophorans. At 19:16 hrs, we begin to see a lot of tube worms, all up on the ridge. We dropped Marker 5 on the Mussel Brick Road at the southern end X-682 m, Y-311 m. We start the first transect of the photomosaic at altitude 3-4 m at an initial heading of 3º. A couple of ball markers were dropped within the mosaic for scale. We made two more overlapping transects, continued on about 40 m past the end, dropped the weights and headed up (Figure 10-9).

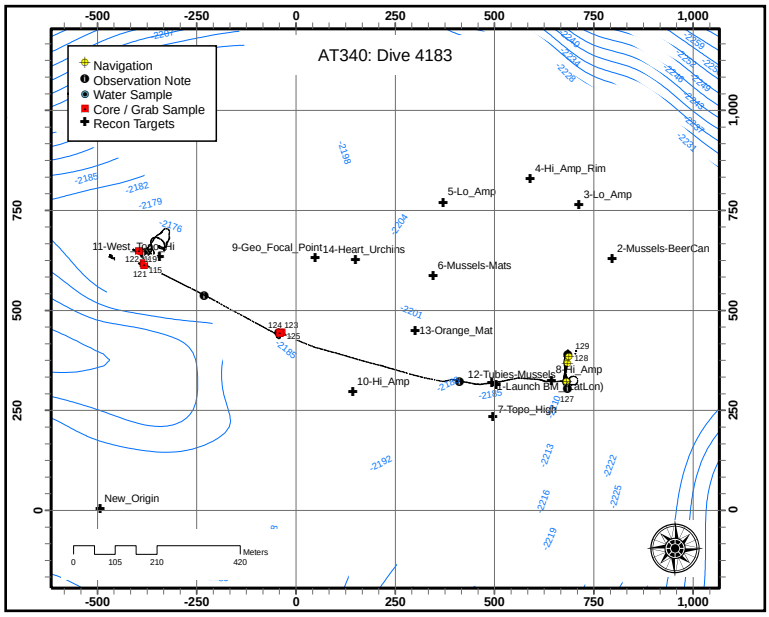

Figure 10-9. Dive 4183 on 5/19/2006 at an average depth of 2,175 m.

10.1.8. *Jason II* Lowering 269

Time in water:	2007/06/07 11:58
Time on bottom:	2007/06/07 14:01
Time off bottom:	2007/06/09 03:59
Time out of water:	2007/06/09 06:02
Water time:	42 hrs 4 minutes
Bottom time:	37 hrs 58 minutes
Minimum working depth:	1,873.96 m
Maximum working depth:	2,212.51 m
Produced	12GB of raw vehicle data

After the long baseline (LBL) navigation net was calibrated at this site, *Jason II* was deployed into the water at 08:04 hrs local on 07 June. All times and dates in this summary are reported in Eastern Daylight Time (EDT), local time. The sea-bed at 2,199 m was reached at 10:07 hrs and event logging was initiated by the watch-stander on duty using *Jason* II's VV event logger system. Refer to *Dive Observations* for this dive in Appendix 7 for a detailed log of the observed events and their times in Greenwich Mean Time (GMT).

Jason II transited to perform a bathymetric survey of the crater that was defined as containing the CRP for this site. Before arriving at the crater, we transited over a very flat seabed surrounding the crater. This crater-flanking environment was characterized by many tracks and trails made primarily by heart urchins. The edge of the crater appeared very abrupt and the break in slope was noted on the ROV log. The bottom of the crater had dark reducing sediments and scattered white bacterial mats. In some areas of the crater floor holothurians and especially heart urchins were in high-density groupings (Figure 10-10) and the crater floor was thoroughly worked by this community.

Figure 10-10. Urchins in bacterial mats.

In the northern part of the crater before reaching the lip, some unusual localized hummocky areas were observed. It is possible that these areas were near-surface expressions of shallow gas hydrate. After we confidently located the center of the crater with visual and depth-sensor reconnaissance, we then began an SM-2000 multibeam survey of the bathymetry of the crater. By later comparing the bathymetry reported by the AUV survey with the bathymetric measurements generated by our crater survey using the LBL navigation in conjunction with *Jason* II's Doppler navigation algorithm, we concluded that there was no significant offset between positions measured by *Jason II* and the AUV-reported positions. It also appeared that the crater was a little elliptical as opposed to the beautifully circular feature that appears on the map of the AUV data. At this point, we concluded that we could rely on the positions reported by the *Jason II* navigation system without needing to apply offset corrections to derive accurate working positions.

However, a comparison of the final processed *Jason II* SM2000 multibeam data and the Hugin AUV data shows an apparent positional offset of approximately 20 m in the X-axis between the two datasets (see Figure 10-11). It is not definitively known whether this apparent offset is an artifact (i.e., possible projection error during plotting in GIS) or if the error is real.

We completed the crater survey at 13:49 hrs, and proceeded to try to find Bench Marker #1 that had been deployed last year on *Alvin* dive 4173. Finding and logging a position fix on this marker would allow us to begin to accumulate a set of comparative position measurements between *Alvin* navigation and *Jason II* navigation. Because we had already concluded that *Jason II* navigation did not deviate from the AUV-reported positions (which we defined to be the true positions for the sake of this project), any significant variance in measured positions of the Bench Marker #1 between *Jason II* and *Alvin* gear would tend to indicate an offset error in *Alvin*'s positioning system.

We transited along the sea-bed toward the presumed (*Alvin*) location of Bench Marker #1 at an altitude of about 2 m, logging information as we proceeded. As we approached the mound in the eastern part of the study area where Bench Marker #1 was deployed last year with *Alvin*, the seafloor characteristics changed dramatically. The transit from the crater to the base of the mound was over rather featureless mud bottom with scattered holothurians and occasional urchin communities. Upon arriving at the mound base, the seafloor changed to one dominated by highly variable topography related to the occurrence of large carbonate pavements and blocks. We arrived in its vicinity of the marker about 14:30 hrs. The area had numerous scattered tube worm colonies (Figure 10-12) and mussel beds. We looked for the marker until about 15:00 hrs. Not finding it, we proceeded to attempt to find one or more of the other markers we had deployed from *Alvin* on this eastern side of the site. We found Marker #11 by accident at 15:20 hrs as we were transiting to the presumed location of a group of other markers we deployed with *Alvin*. We did not immediately have the *Alvin* position of this marker in our dive plan, so we logged a position fix and proceeded on to the area of the other markers while looking for the logged position in our records. When we obtained the *Alvin* position from that cruise report, we saw that the *Jason II* position was to the east of the *Alvin* position about 24 m and to the south of it about 4 m.

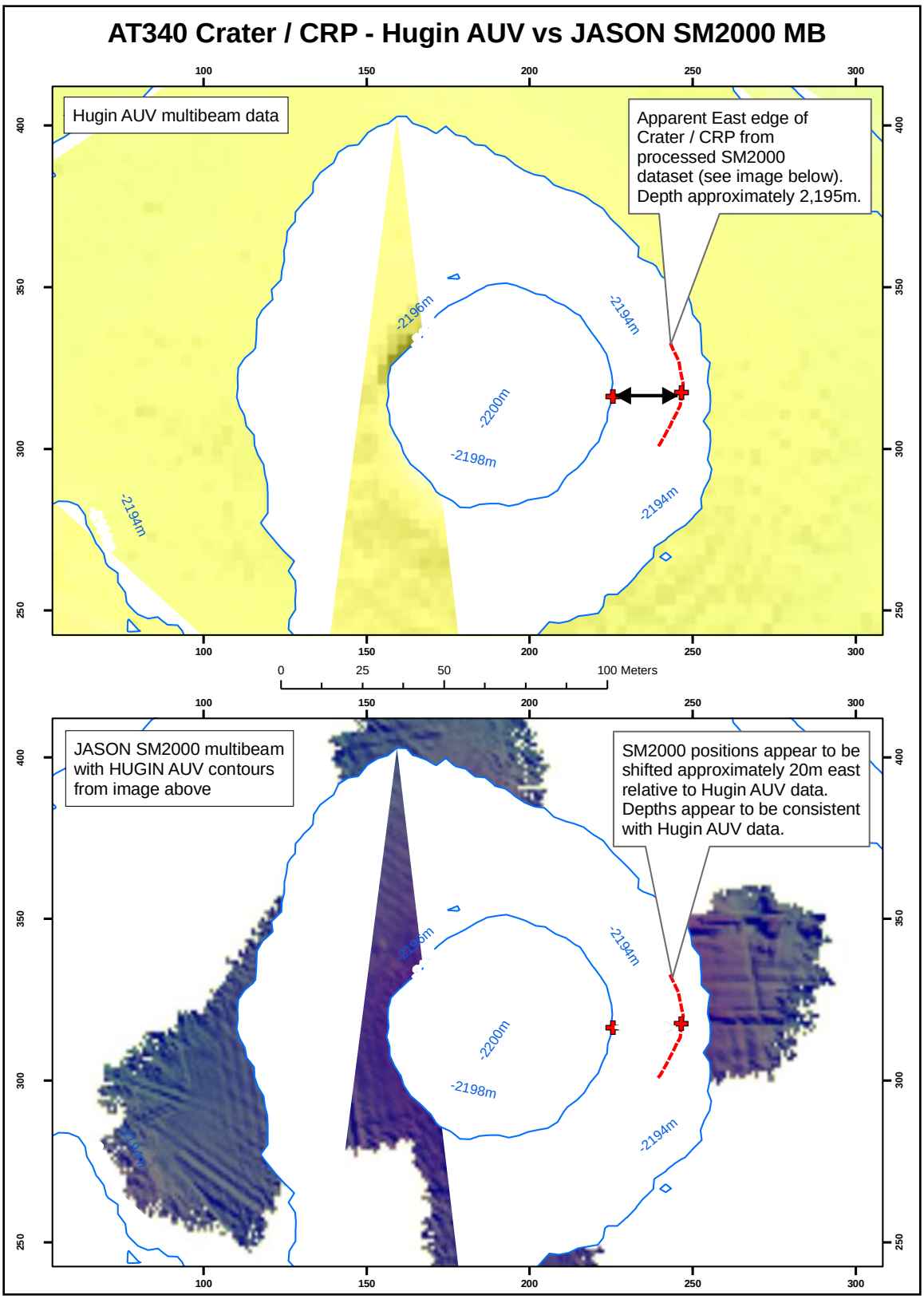

Figure 10-11. Apparent offset between processed SM2000 and Hugin AUV multibeam data.

Figure 10-12. Tube worm colony.

We found BallMarker #2 at 16:01 hrs and logged a position fix. We noted that the *Jason II* position was to the east of the *Alvin* position about 24 m and to the south of it about 8 m. We also noted that the float attached to this marker (intended as an aid in spotting it) was no longer floating, but rather, lying beside the ball-marker. If other such floats were compromised in this way, they would be much harder to find.

With no success finding the other markers in the area, we returned to the vicinity of Bench Marker #1 and looked in the area about 24 m to the east and 5 m to the south of its *Alvin* position. We found the marker with little effort at 17:12 hrs, and logged a position fix. It was positioned by *Jason II* about 26 m to the east and 3 m to the south of its *Alvin* position. Now having three sets of comparative points that indicated a fairly consistent error-offset in *Alvin*'s position fixes, we applied an offset correction to all of the remaining *Alvin* target positions at this site. We added 24 m to their local X value and subtracted 5 m from their local Y value. Presumably, this would help us find the other markers left at this site with *Alvin* last year.

We began a test of the digital camera systems and their lighting at different altitudes at 17:34 hrs and finished at about 18:00 hrs. On the basis of this test we worked out methods to use the DSC in aperture priority mode adjusting f-stop to optimize for different altitudes. We then transited to an urchin field took a set of 16 cores from about 19:00 hrs to 20:48 hrs. This included a set of cores for microbiology and geochemistry (Joye group) and a set for meiofauna and analysis of urchin impact on meiofauna community. We developed a leak in the highly maneuverable Kraft manipulator arm while coring and decided that we should not use it to acquire any more samples.

The remainder of this dive thus involved accumulating information that we could gather with minimal or no collection of physical samples.

We performed an SM-2000 multibeam survey over a 200 x 375 m rectangle in the eastern area of the site from 22:36 hrs until about 07:40 hrs the next day (08 June). The survey grid was set up for east-west lines. During the survey, we developed positioning problems and trouble staying on line. The bridge indicated they were fighting a strong surface current. However, after a software modification we were able to occupy our survey lines. We then transited to the western area of the site to perform a similar 200 x 325 m rectangle survey, and logged visual information while we transited. We began the western SM-2000 survey at 09:20 hrs and completed it at 20:37 hrs, after some problems keeping the mother vessel on track with the survey maneuvering requirements. We had to re-orient the lines to run north-south instead of east-west as an aid to the helmsmen.

We then transited to the vicinity of Marker #12 in the western area to see if we could find it by applying the offset corrections we had derived for the eastern part of the site. The area was characterized by broken carbonate slabs with tube worms occupying most of the cracks. We found the marker at 22:24 hrs and logged a position fix for it. The *Jason II* position was 4 m to the east and 18 m to the south of the original *Alvin* position, so the offset correction matched the range of the offset correction needed, but did not match the bearing of the correction needed for the east side of the site. In the east, the position had to be moved 24 m essentially to the east, and in the west, it had to be moved the same distance essentially to the south. This difference is potentially explained by considering that the *Alvin* survey of the western side of this site (when Marker #12 was deployed) was a separate dive (#4180) from that of the eastern side (#4173). Even though the LBL net had been left down for both dives, there could have developed a change in error-offset between these two dives performed more than a week apart. Based on information we have received subsequent to this dive it is also possible that either a different baseline (between three transponders) was used on these two *Alvin* dives, or that the *Jason II* navigator switched the baseline being used to determine positions on the western and eastern end during this dive. All positions recorded during this dive will be re-navigated to a single baseline for consistency.

Observations of non-seep fauna were made during transits between seep locations. The bottom sediments were very fine and poorly consolidated. Surface color was primarily grey. Bioturbation structures are small except for occasional rings on holes. By far the most common large organisms were holothuroids (*Benthodytes gigantea*, *B. typica*, *B. lingua*, and *Benthothuria sp.*) Shrimp 2–3cm in length were common but often hard to see in the video. Tripod fish were encountered on the mud surface. Other fish seem restricted to rocky areas. Local vagrant fauna at seeps was conspicuously sparse and seemingly limited to very few fish. Large crustaceans were not observed.

We transited to help release the elevator with *Jason* II, and then began ascending at about midnight of 08 June. We left the LBL net in place in anticipation of upcoming dives at this site. Figure 10-13 shows the dive track for dive 269.

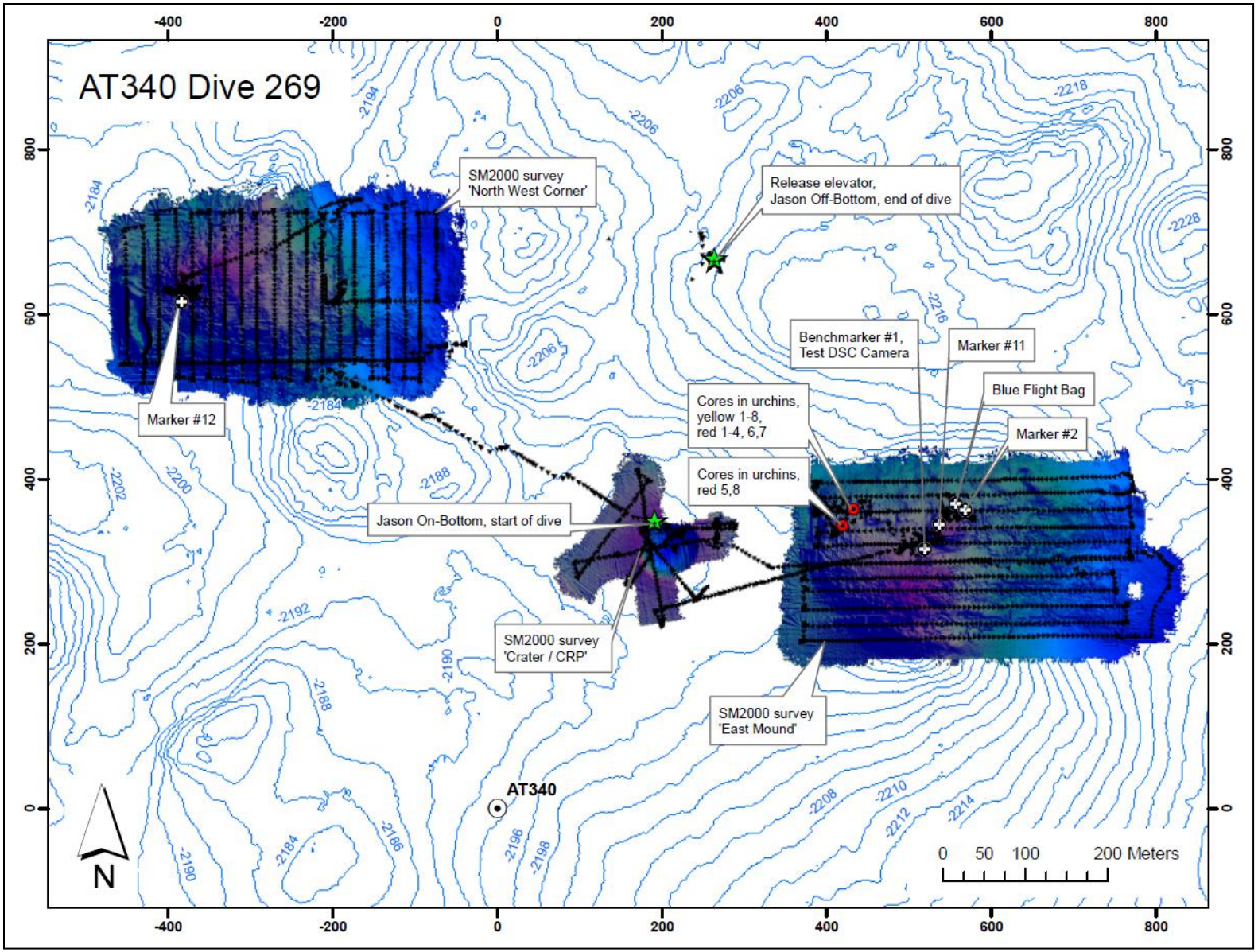

Figure 10-13. Dive 269 dive track.

10.1.9. *Jason II* Lowering 270

Time in water:	2007/06/09 16:48
Time on bottom:	2007/06/09 18:28
Time off bottom:	2007/06/11 02:50
Time out of water:	2007/06/11 04:30
Water Time:	35 hrs 43 minutes
Bottom Time:	32 hrs 23 minutes
Min. working depth:	2094.58 m
Max. working depth:	2213.85 m
Produced	3.7GB of raw vehicle data
Produced	~52 DVDs of Science video
Produced	~52 DVDs of Archive video

The calibrated LBL net had been left in place at this site from Dive 269 (see *LBL Calibration* section for details of the procedure). Target locations had already been developed for this site during Dive 269 (refer to Target Selection, AT340 for background).

Jason II was deployed into the water at 12:48 hrs local on 09 June. All times and dates in this summary are reported in EDT, local time. The sea-bed at 2,207 m was reached at 14:24 hrs and event logging was initiated by the watch-stander on duty using *Jason* II's VV event logger system. Refer to Dive Observations for this dive in the Appendix 7 for a detailed log of the observed events and their times in GMT.

Jason II was launched in the area identified as the most probable location for the missing fish trap. The launch area was a relatively flat stretch of sea floor. Sonar and the Homer beacon receiver were used to search for the fish trap as the *Jason II* made a transit from this area to the location identified for the elevator launch. The elevator was launched at 16:06 hrs and mobile fauna were collected using the suction sampler in this area and during transit to the elevator.

The normal deep-sea fauna in the vicinity of the seeps was dominated by elasipod holothuroids typical of lower slope and abyssal plain environments: *Benthodytes typica*, *Benthodytes lingua*, and a synallactid *Benthothuria sp.* Both *Benthodytes* were collected by slurp sampler for trophic analysis. In addition, three seastars and a hermit crab were collected for the same analysis.

The elevator was moved at 17:42 hrs (X-585 m, Y-341 m) approximately 25 m south-southeast of the big mussel bed and Marker #2. A rotary camera, confirmed to be operating, was removed from the elevator, and deployed in a seep community of tube worms and mussels (Figure 10-14). This camera will remain on the sea floor at X-557 m, Y-354 m for approximately 2 weeks, taking a picture every 5–6 minutes. We then transited to the mussel bed and set up for acquisition of images for a mosaic of this bed, using the "blue flight bag" marker at the north-northwest edge of the mussel bed as a beginning location. The mussel bed occurred in a separation between extensive carbonate pavements, slabs, and boulders.

Rotary time-lapse camera L (Louie) is set to record pictures at 6 min intervals with 36deg rotation between shots. Deployment site includes carbonates, mussels and tube worms within

the probable visible area. This camera will be left in place for approximately 14 days. It will be recovered autonomously by releasing its anchor weight with a burn wire.

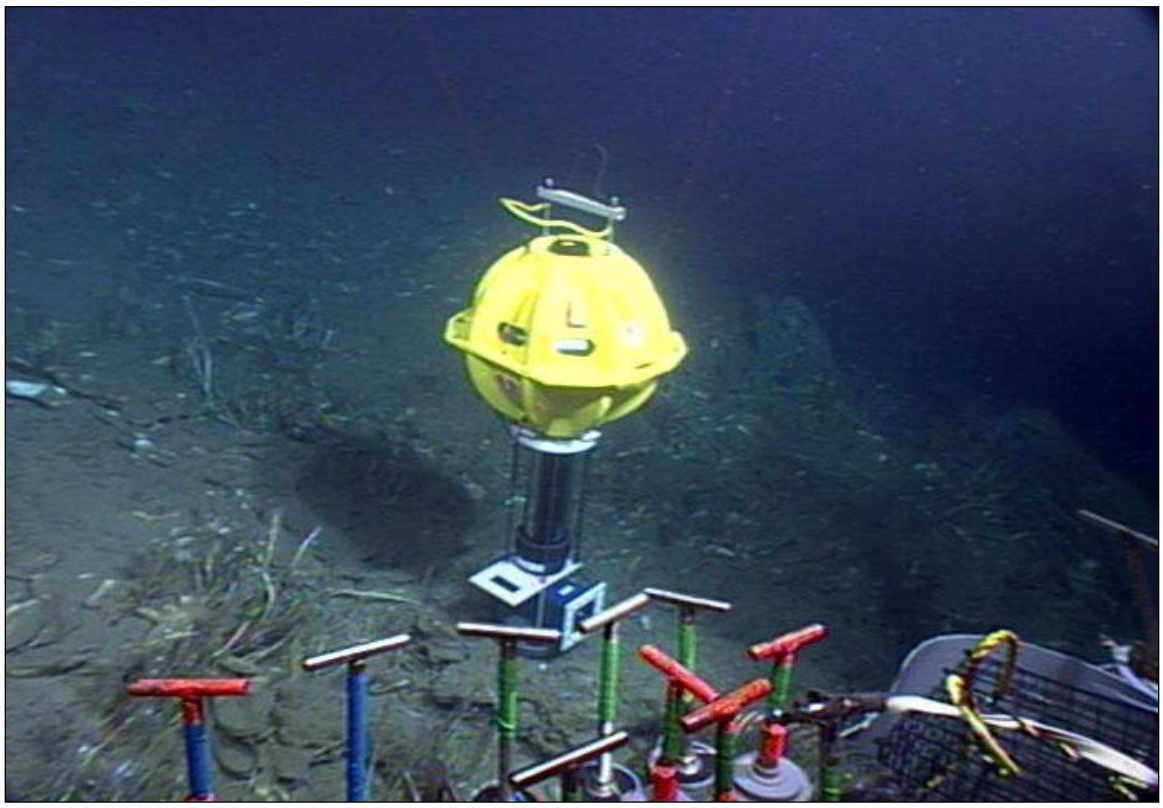

Figure 10-14. Rotary camera "Louie" deployed in seep community of tube worms and mussels.

After completing the mosaic, a transplant experiment was initiated by placing mussels from different parts of this bed in cages and moving them to other parts of the bed. The transplanted mussels will be collected in two weeks and analyzed to determine if the symbiont complement (methanotrophic or chemoautotrophic) changes after movement between different chemical environments. A collection of mussels from each location was also made and loaded onto the elevator. The CONTROS methane sensor was tested in several locations in this mussel bed and was determined to be unresponsive. A Niskin bottle was triggered over this bed (at 23:36 hrs) at X-567 m, Y-362 m and a carbonate collected from beneath the mussels.

The elevator was then moved at 02:24 hrs of 10 June to an area exhibiting a high density of urchins at X-356 m, Y-286 m for deployment of the second rotary camera and coring. The urchin beds were located in calibration crater where the initial navigation calibration at AT340 was done using the AUV multibeam maps compared with *Jason* II's navigation (see Target Selection, AT340). The second rotary camera was no longer functioning and was left on the elevator. Six cores were taken in this urchin area at X—366 m, Y-87 m, followed by 8 control cores taken from nearby sediment with no visual indication of seep impact (X-408 m, Y-355 m). The 16 cores already taken were loaded onto the elevator and exchanged for 16 empty core samplers.

The elevator was released (with mussel collections, cores, and one rotary camera) from the sea floor at 06:10 hrs and the *Jason II* laid back until 07:37 hrs.

At 08:51 hrs a random set of ten, 40 m photo transects, were initiated over the area of the eastern-most SM-2000 area. This operation proved to be very time efficient and was completed at 10:52 hrs. Each transect was 40 m in length. Control of the DSC was manual with images fired every ~10 sec, while avoiding overlapping images when *Jason II* was stationary. Each transect comprised 15–20 images. DSC images were also recorded in the transit between transects. Orientation of transects was approximately northwest to southeast. All transects were parallel. Placement was random within a 360 m east-west and 200 m north-south box at the center of the SM2000 survey area.

Jason II then transited to the crater (CRP) to set up experiments and gather images for a photo mosaic to study urchin feeding and movement. The artificial urchin trails were created using a custom tool and cement filled yellow Whiffle balls deployed to mark the ends of the trails (Figure 10-15).

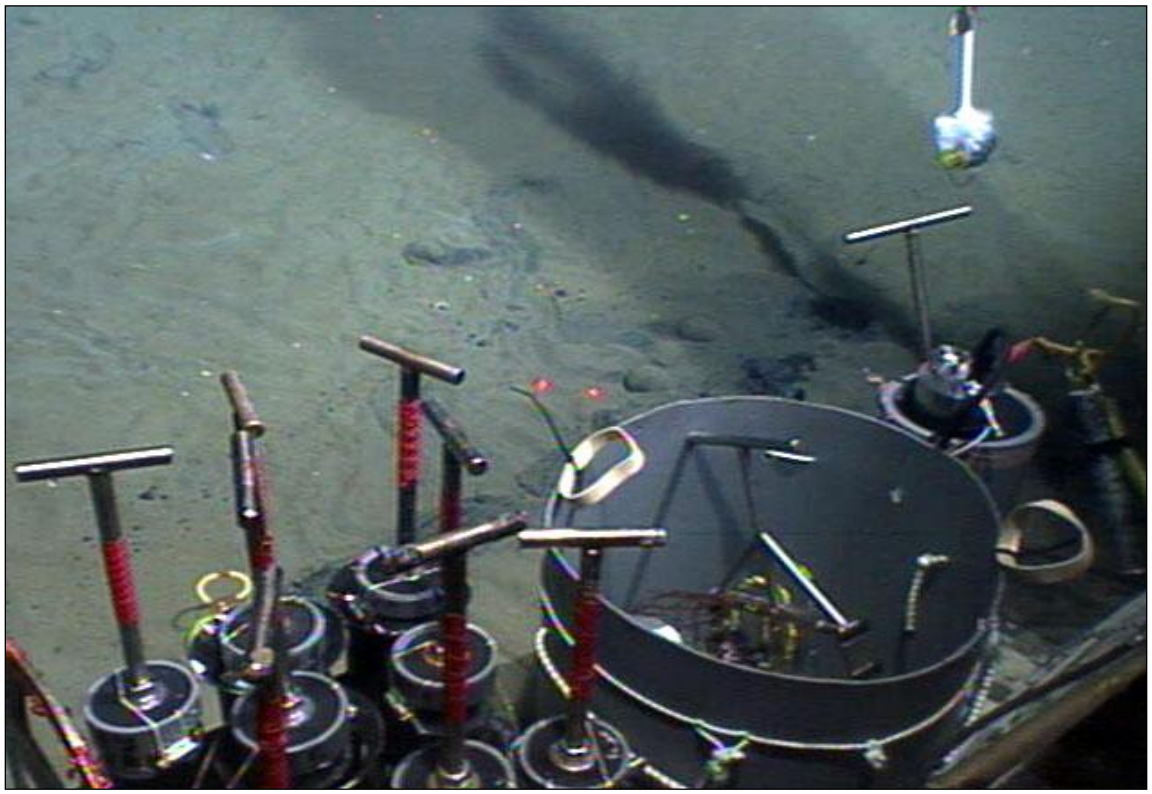

Figure 10-15. Creating artificial urchin trails with "custom tool" (upper right).

An area of approximately 100 m^2 was imaged with a total of seven markers in the images for re-visitation of this photo-mosaic site in two weeks. The second Niskin was triggered here at 15:50 hrs. After completion of the imaging, an additional 1.5 hours were spent taking push cores of isolated bacterial mats and different mud flows in this crater. A total of nine cores was taken in the crater. A lone small carbonate was collected from an urchin area of the crater shortly before leaving the crater for transit back to the eastern work area.

We transited back to the eastern work area and began the search for one of the markers associated with stained tube worms. After careful searching, Marker #15 was found within one m of the location predicted from applying the navigation corrections to the *Alvin* position, but was not floating. This tube worm aggregation was collected with the Bushmaster collection device. Based on review of last year's log and images of the second stained aggregation in this area it was located (even though the marker "Ian 6" was no longer present), and was subsequently collected into the port bio box.

The final task under consideration for this dive was another search for the missing fish trap. Before embarking on this search the sonar was tested using the glass ball associated with the rotary camera approximately 25 m away. This test indicated that a sonar search would not be fruitful as the sonar did not detect the ball unless the vehicle was on the ground and canted down. The *Jason II* dive was terminated at 22:50 when the vehicle lifted off the bottom, initiating its ascent. The dive track for dive 270 is shown in Figure 10-16.

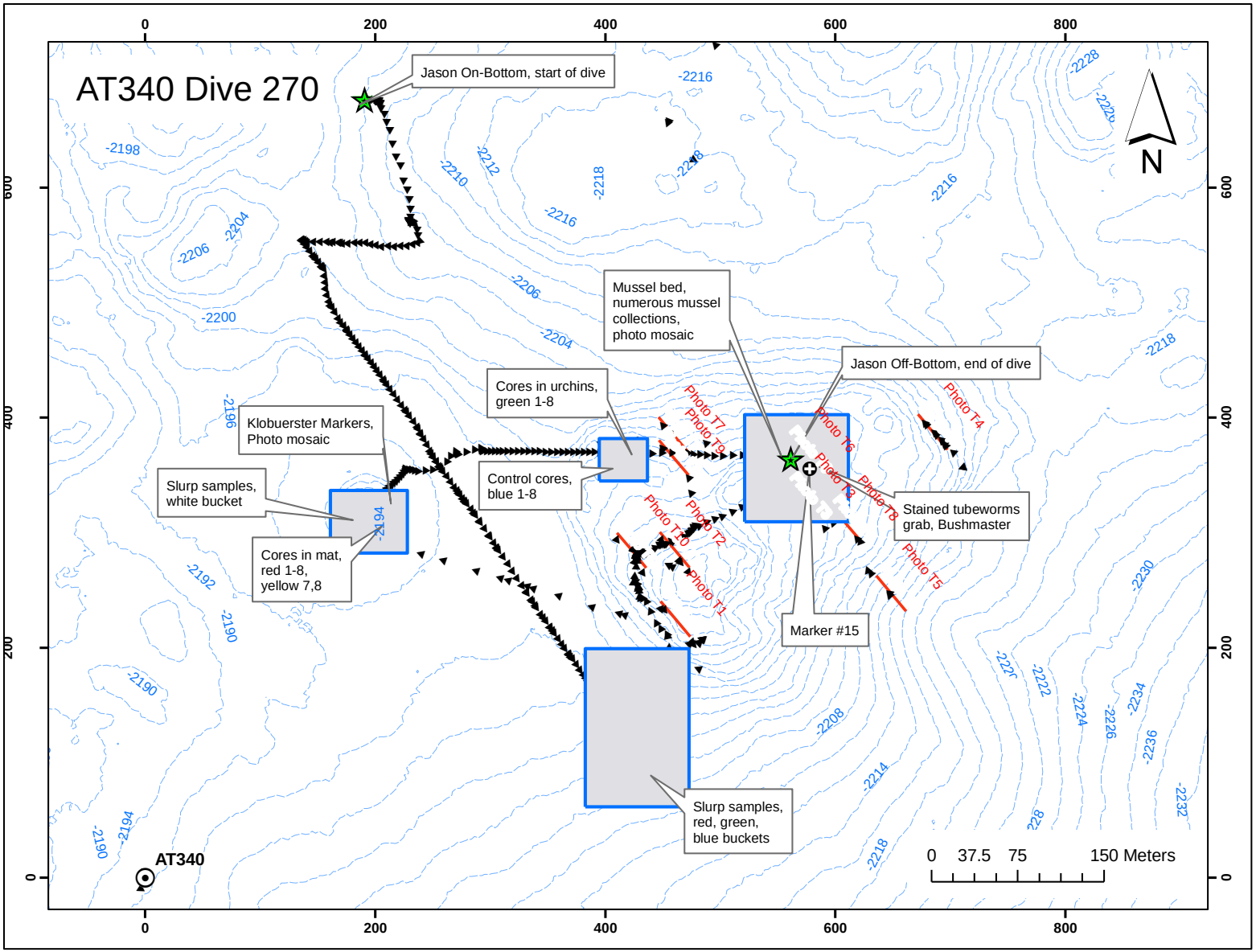

Figure 10-16. Dive 270 dive track.

10.1.10. *Jason II* Lowering 276

Time in water:	2007/06/19 12:36Z
Time on bottom:	2007/06/19 14:14Z
Time off bottom:	2007/06/20 15:45Z
Time out of water:	2007/06/20 17:21Z
Water Time:	28 hours 45 minutes
Bottom Time:	25 hours 31 minutes
Min. working depth:	2033 m
Max. working depth:	2213.97 m
Produced	3.0 GB of raw vehicle data
Produced	~41 DVDs of Science video
Produced	~41 DVDs of Archive video

The calibrated LBL net had been left in place at this site from previous dives. Most target locations had already been developed for this site during Dive 269 (refer to Target Selection, AT340 for background).

All times and dates in this summary are reported in EDT, local time. *Jason II* reached the seafloor at 10:15 local time and event logging was initiated by the watch-stander on duty using *Jason II*'s VV event logger system. Refer to Dive Observations for this dive in the Appendix **7** for a detailed log of the observed events and their times in GMT. We proceeded towards the CRP and the nearby urchin mosaic site. One of the first features noticed on the seafloor was a high-density urchin bed centered at approximately X-193 m, Y-290 m. As this bed was explored more, a number of ball markers were found, indicating that this was the site of the photomosaic taken during J2-270. We then took a second photomosaic of the urchin bed at the same location to track the movement of the urchins over the previous two weeks. It was obvious that the urchins had traveled more than anticipated, as many had crossed the experimental tracks made a number of times. Therefore, a third, short-term mosaic in this location was planned for the next lowering.

Following the completion of the mosaic, a series of push cores were taken within and next to the experimental trails. While taking this series of cores, the core rack fell off of the basket. It was recovered and stowed over the course of 30 minutes, but was unstable and fell off of the basket again. At this time, we noticed that there was a slight hydraulic fluid leak from the Bushmaster. While trying to adjust the position of the slurp hose on the basket, the core rack fell off once again. This time one of the quivers containing an empty push-core fell out of the rack. There were attempts to recover the core, but they were unsuccessful. We relocated the urchin bed and completed the series of cores over the course of the next two hours, assuming that the four cores taken prior to the core rack fumble were unsuitable for detailed analysis. The left manipulator was used to hold the core rack in place the entire time. At 18:34, *Jason II* transited to the elevator and swapped out the core rack. During this process, the second core rack was dropped and then recovered (Figure 10-17). [It was determined that the core-rack fumbles were a result of a combination of overly long bolts securing the core quivers to the rack (and protruding from the bottom), and an insufficient restraining brace in front of the core rack on *Jason II*. Both problems will be addressed before future dives]

Figure 10-17. Core rack dropped.

Once the core rack was in place, *Jason II* picked up the elevator and proceeded to the large mussel bed. We arrived at the mussel bed at 20:50 and found an appropriate place for the elevator. The experimental mussel transplants were located in the mussel bed and a series of down-looking still pictures were taken. The four mussel cages (Figure 10-18) were then recovered from the bed and placed in the elevator. The elevator was released at 22:57. Time on deck was not logged.

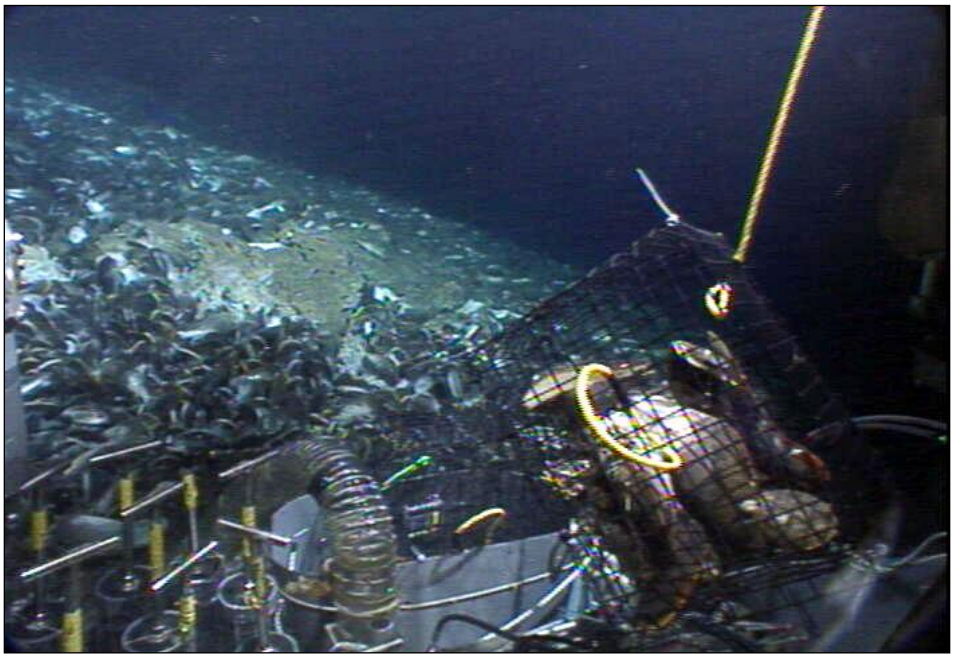

Figure 10-18. Recovering mussel cages.

Jason II began transit towards the northwest area to look for the fish trap using the homer beacon at 00:45 hrs on 20 June in lay-back mode. At about 02:25 hrs observations of the sea floor resumed (X-279 m, Y-696 m) and the search for the fish trap continued. While searching, a number of holothurians, mussel beds, and urchin beds were observed. A possible mud vent was also noted and some down-looking still pictures were taken. At 03:31 hrs the search for the fish trap was terminated (X-336 m, Y-1100 m), and Ian was awakened for the photo survey. At 05:13 hrs, the photo survey began with transect #T9 (X-368 m, Y-752 m). The first five of planned ten transects were complete at 07:28 hrs. At this time, the chief scientist decided to postpone the second half of the survey until a future dive and transit back to the southeast corner of the site began.

Jason II arrived at the blue bag in the large mussel bed (mosaic site) at 08:45 hrs, passing by one of the time-lapse camera deployments on the way (about X-560 m, Y-352 m). A mussel pot sample was attempted, but mussel pot B suffered a mechanical failure and the collected was aborted. *Jason II* was moved to another location within the bed and the other mussel pot (F) was used to make a successful collection (Figure 10-19). Following the collection, the ring that was left behind was inspected and found to contain a number of small tube worms and brittle stars. These were subsequently collected with the slurp gun into the white bucket and the mussel pot ring retrieved. One of the small ball markers was deployed in this location to mark the site of collection. A series of down-looking photographs of the mussel bed were taken at different heights to locate the collection in the mosaic.

Figure 10-19. Mussel pot collection.

At 10:05 hrs we moved to marker 5 at the edge of the mussel bed at X-555 m, Y-364 m to collect stained tube worms with the Bushmaster collection device (Figure 10-20). It was determined that the hydraulic leak was not too severe and this was one of the last tasks on the dive so we proceeded with the Bushmaster collection. The collection was successful and the Bushmaster was stowed at 10:47 hrs and a small ball marker deployed in the collection location. Down looking images were again collected to locate this site on the mosaic. Two carbonate collections were also made in this location.

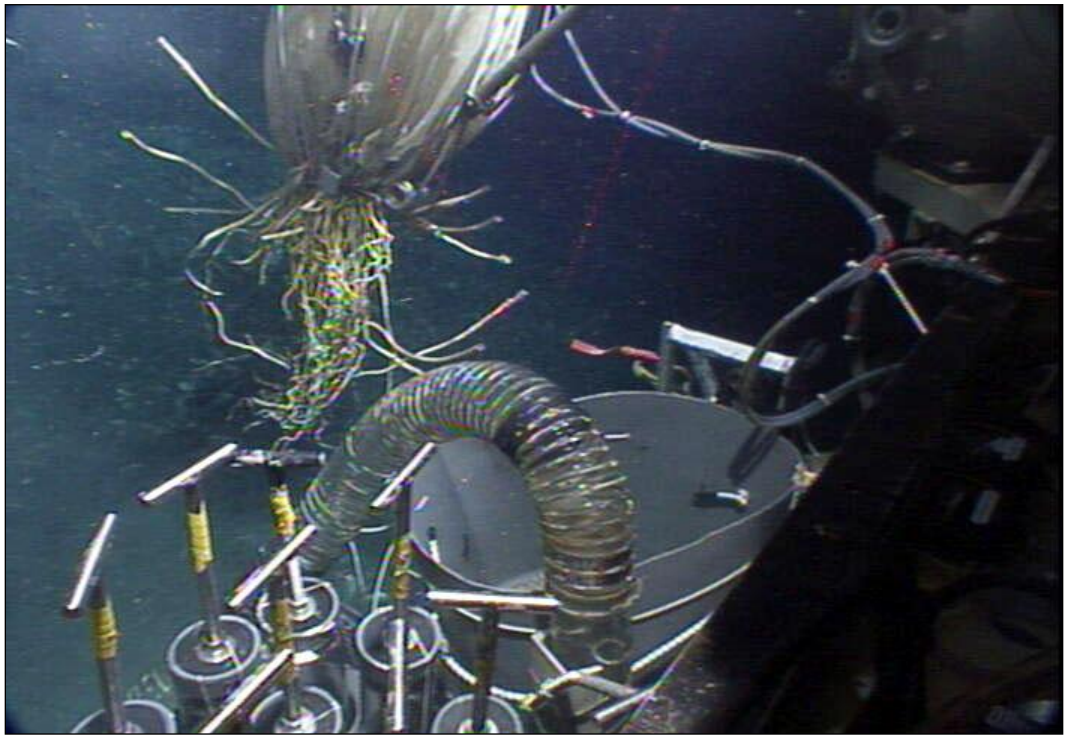

Figure 10-20. Successful tube worm collection with Bushmaster.

Jason II moved a short distance to the location of the time lapse camera (X-563 m, Y-361m) and the camera was released from the seafloor. Once the camera was safely away, *Jason II* left the bottom at 11:45 hrs.

Non-seep mobile fauna was sparse but typical of the depth. This lower slope fauna was dominated by elasipod holothurians. Fish and crabs were also present. The dive track for dive 276 is shown in Figure 10-21.

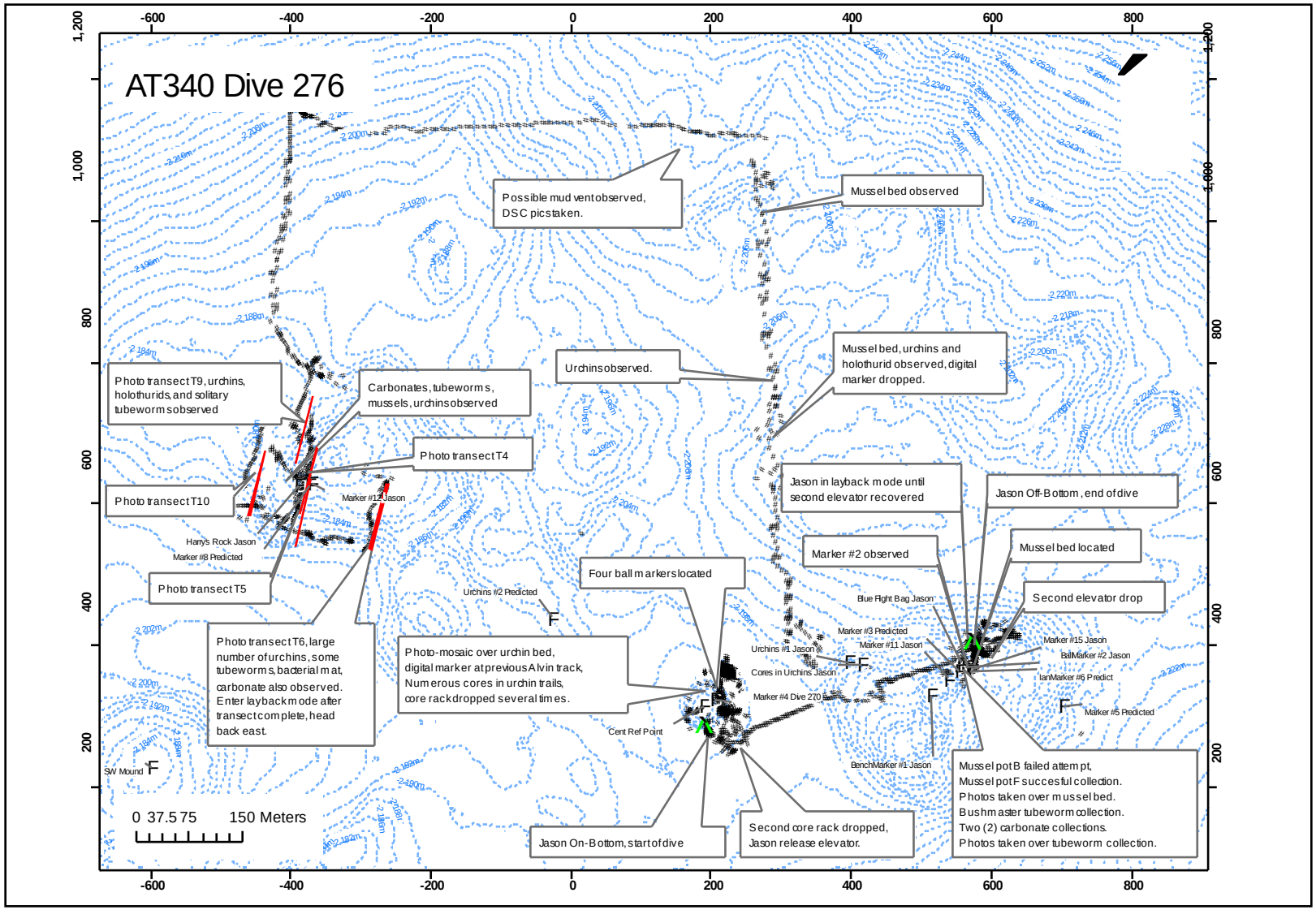

Figure 10-21. Dive 276 dive track.

10.1.11. *Jason II* Lowering 277

Time in water:	2007/06/21 04:04Z
Time on bottom:	2007/06/21 05:24Z
Time off bottom:	2007/06/22 10:37Z
Time out of water:	2007/06/22 12:10Z
Water Time:	32 hrs 7 minutes
Bottom Time:	29 hrs 13 minutes
Min. working depth:	2164.28 m
Max. working depth:	2214.56 m
Produced	3.3GB of raw vehicle data
Produced	~48 DVDs of Science video

All times and dates in this summary are local, i.e., Coordinated Universal Time (UTC) minus 4 hours.

The *Jason II* reached the bottom at 01:24 hrs on June 2 and proceeded to the predicted location of marker #5, which marked the Southern End of the "Mussel Brick Road." Marker 5 was found near its predicted location (X-700 m, Y-290 m). At 01:54 hrs we began the first objective of this dive; to acquire images to mosaic the portions of this mussel-populated brine flow which we first imaged in 2006. After completing this task (at 02:54 hrs) the new CONTROS Methane Sensor was again tested (Figure 10-22). (It had been rebuilt since its first dive (#275 at WR269), because it flooded during that dive.) It appeared to be working and will be used extensively during this dive.

Figure 10-22. Testing CONTROS Methane Sensor near bacterial mat.

After testing the sensor, attempts were made to core in several locations with apparent brine flows near the mussels. The cores would not penetrate sufficiently at the original site. A site with evident bacterial mats was tried and although core penetration was only about 10 cm, Chris Kellogg indicated this was sufficient for analyses of viruses and 2 were taken from this mat location (X-694 m, Y-306 m; 04:27 hrs). We then moved north on the Mussel Brick Road to X-706 m, Y-318 m (05:40 hrs), an area with more extensive brine flow and mats, and what appeared to be a reddish mud flow overlying some of the brine, mats, and mussels. Five cores were taken in blackish sediment (brine) and the last two in the reddish mud flow.

The *Jason II* then moved to the Big Mussel Bed (site of ball marker 2, the "blue flight bag," and the big mussel mosaic). The methane sensor was used in nine locations (starting at X-539 m, Y-376 m at 06:31 hrs) and then two mussel pots were successfully taken. These went very smoothly as a result of slight modification (shortening) of the anti-rotation arms to better interact with the *Jason II* hydraulic ram. The ring of the second pot was left in place to give the water a chance to clear, and the *Jason II* left for scheduled "Engineering dive time" to run tests on the new 56 m tether and various navigation tests at 10:15 hrs. Science operations resumed shortly after noon, with initiation of a series of photo transects over the southeast mounds (and our primary work area). The ten 100 m photo transects were completed at 16:13 hrs and *Jason II* returned to the Big Mussel Bed to resume methane measurements. We set up for the first methane scan at 16:56 hrs.

The methane sensor gave consistent measurements within locations (Figure 10-23), but after extensive testing it was determined that there must be another gas interfering with methane that causes readings to drop significantly in some locations. This will make interpretation of the data either difficult or impossible. The methane sensor was stowed at about 20:15 hrs, the previously deployed ring from the mussel pot was collected, and a ball marker left to mark the spot of this collection. The carbonates identified by Harry Roberts on the Big Mussel Bed Mosaic were targeted for collection. The first carbonate on the list (Harry's #1) was too robust to break despite a concerted effort by the *Jason II* pilots, so it (and considerable dust) was left on the sea floor. Harry's carbonate "#2" (as indicated on the print out of the mussel mosaic) was collected at 20:41hrs into the milk crate. Harry's carbonate "#4" was collected at 20:54 hrs. This collection consisted of three small pieces of carbonate placed on top of the starboard mussel pot (A).

Figure 10-23. Methane Sensor deployed in mussel bed.

The next objective was to collect mobile fauna while in transit to the Urchin Mosaic area near the CRP. Mobile non-seep fauna was collected under the direction of Dr. Carney during this transit. Lower-slope holothuroids predominated (*Benthodytes typica* and *lingula*). Shortly after arrival at the Urchin Mosaic area (at 22:41 hrs) it was noticed that the strobes were not evenly illuminating the sea floor. Subsequent inspection (after recovery of the vehicle) confirmed that they had been displaced during one of the times the *Jason II* sat on the sea floor. To assure complete coverage of the mosaiced area images were obtained with increased overlap, which will allow cropping of the darker area.

After completing this mosaic at 00:23 hrs, the *Jason II* transited to the northwest working area for completion of the last five lines of photo transect imaging under the direction of Ian MacDonald. This effort was completed at 02:30 hrs and the *Jason II* began looking for the stained tube worms at markers 8 and 12. Marker 8 was located at 03:01 hrs (X-379 m, Y-630 m): it was not floating, like many of the other markers at this site), and the two stained tube worm aggregations at this location were collected into the port bio box. Marker 12 was visible (floating) during these collections, and *Jason II* proceeded straight to Marker 12 (X-377 m, Y-630 m) at 03:40 hrs. The stained aggregation at Marker 12 was collected using the Bushmaster collection device (Figure 10-24). This collection proceeded in text-book perfect fashion.

After the full Bushmaster was secured to the vehicle (04:17 hrs), we initiated a transit to explore the mound immediately southeast of the northwest working area. The downlooking scorpio

camera was turned on with a 25-second flash interval. Our target ("morning exploration") was the top of this mound. While in transit an area with numerous small carbonates with small (and young appearing) tube worm aggregations were seen and one was collected along with the carbonate it was attached to at X-248 m, Y-453 m (05:47 hrs). [after recovery the mobile fauna was removed by hand and the entire carbonate and tube worm aggregation pickled].

Figure 10-24. Carbonate-Tube worm collection.

We then proceeded to the top of this mound, where several large carbonates were exposed, but there was only scattered chemosynthetic fauna. The area around the top of the mound was explored (efficiently using the new 56 m tether on the *Jason II*) but only scattered tube worms and chemosynthetic fauna were observed until we proceeded to the Southern flank of this mound. We then discovered an area with lush chemosynthetic communities of both young and old tube worms and mussels (X-216 m, Y-347 m). This area had some of the most healthy looking tube worm aggregations of any area visited at AT340. This area was imaged and some high quality "best of" tube worms and mussel video was obtained during the last 20 minutes of this dive. Noteworthy was the large amount of trash also visible in this otherwise beautiful area: Budweiser can, Fanta can, fishing line, bag. The *Jason II* left the bottom at about 06:30 hrs local time on June 22 for an "on time" 08:00 hrs recovery. After recovery the transponders were recovered and transit to GC852 begun. The dive track for dive 277 is shown in Figure 10-25.

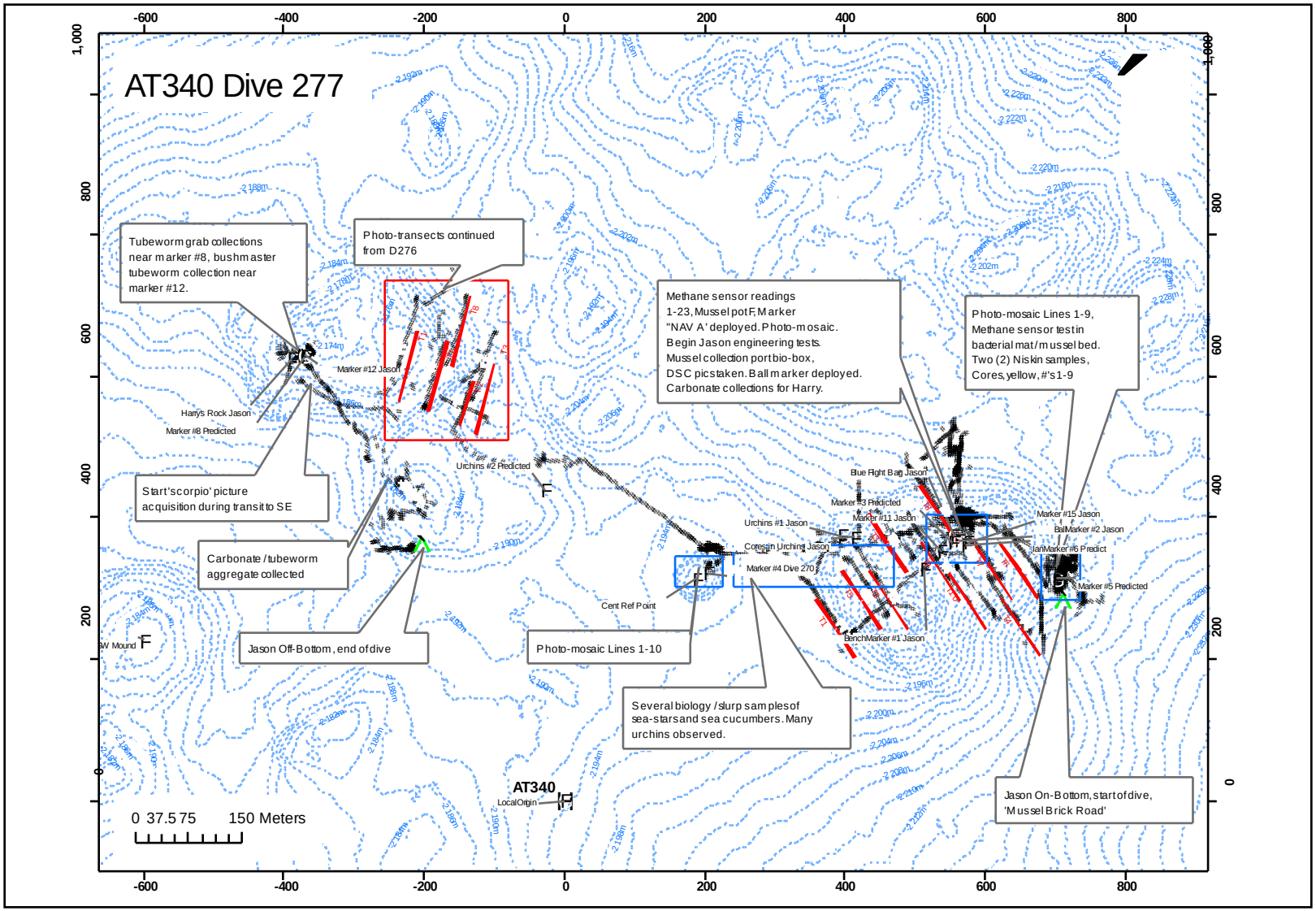

Figure 10-25. Dive 277 dive track.

10.2. Green Canyon 600

This site was surveyed during the Recon Cruise and explored during *Alvin* Dives 4174 on 5/10/06 and 4184 on 5/20/2006. There were no *Jason II* dives at this site.

10.2.1. Reconnaissance Cruise

This station is situated on a low-relief ridge at a depth of about 1,250 m. The DCS reached bottom at 17:40 hrs on 16 March and collected images with an 11 second repeat rate until 20:44 hrs. A total of 694 images were collected with the bottom in view and acceptable navigation. The site showed extensive hard ground and carbonate boulders. There were several sparse aggregations of tube worms growing under the carbonates. Scattered living mussels and extensive dead shells were also seen. Despite the extensive hard ground, no coral colonies were observed. This site should be considered as a possible candidate for additional biological study. The degree of lithification may have geological significance (Figures 10-26 and 10-27).

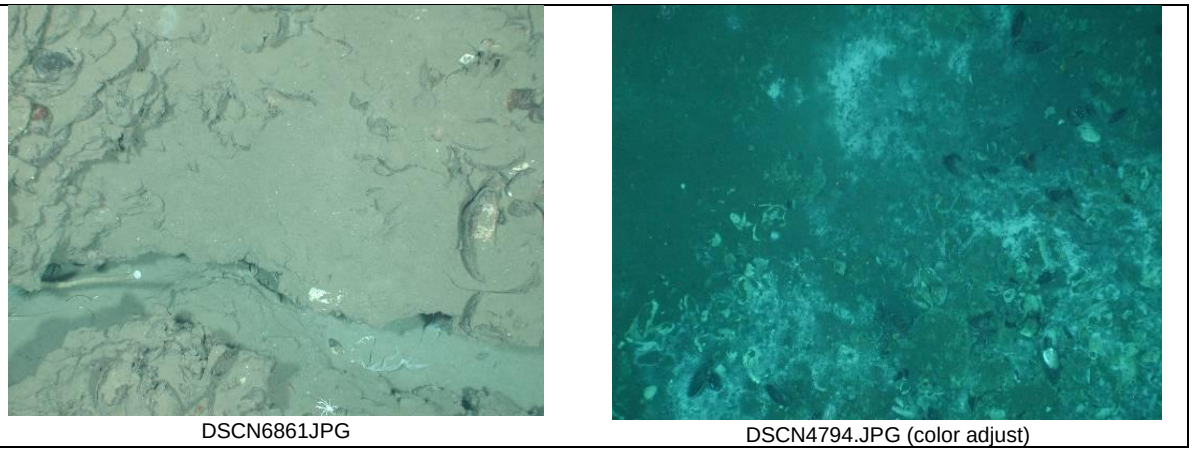

Figure 10-26. Representative photography from GC600.

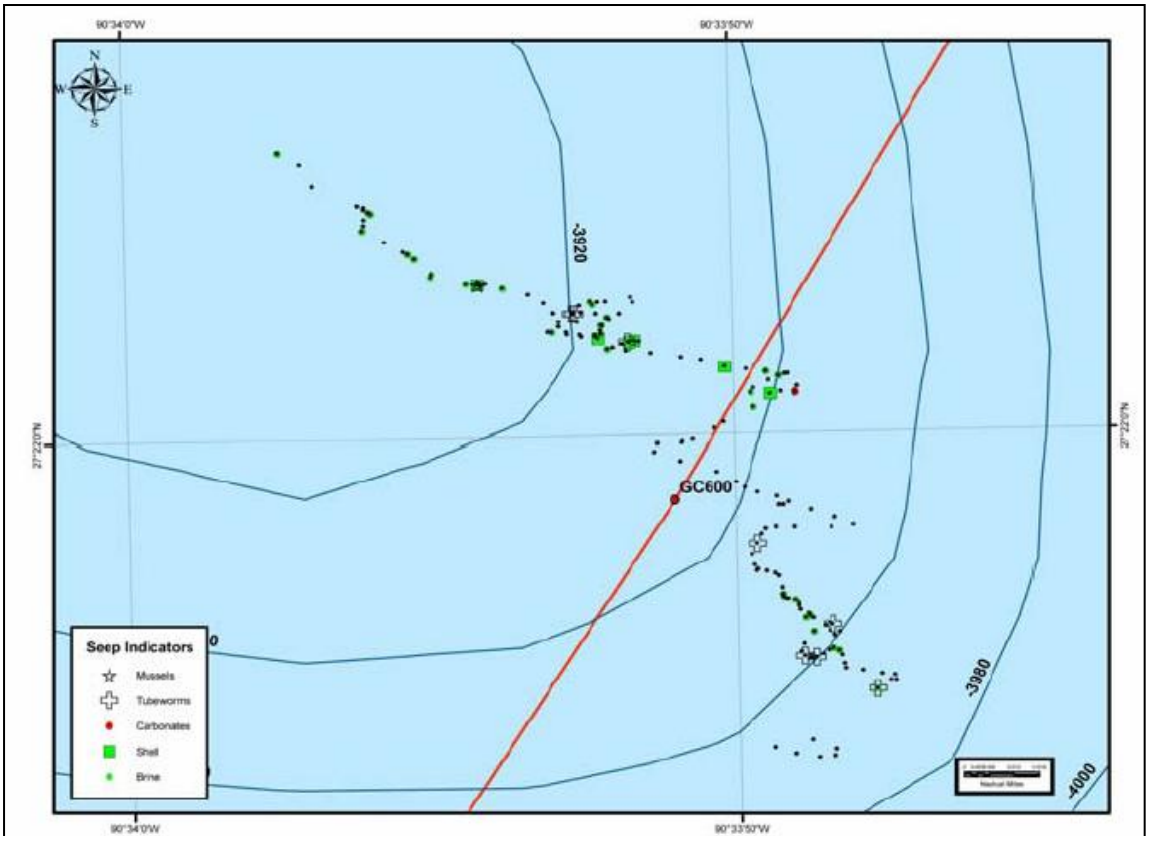

Figure 10-27. Survey results from GC600 station.

10.2.2. *Alvin* Dive 4174

Started dive at 14:04 at X-2667 m, Y-2594 m. There are carbonates, bacterial mat patches, dead clams and mobile fauna (crabs) around. We tried out the chemical sensor over carbonate, but O_2, pH, and H_2S sensor values were far below calibration range and began the transit to Target 1, which is isolated tube worms. At Target 1, there are massive carbonate pavements and some tube worms growing out of fissures and also some mussels in the cracks. We tried the chemical sensor again above the tube worms, but the readings are still below calibration. We moved to a site that looks like a small pockmark crater about 5 m in diameter with white and orange bacterial mats in the crater. We tried to take push cores but the sub does not fit in the crater. We saw oil seeping out after the sub hit the sediment and headed toward Target 8. We collected six push cores in a circular ring of white bacterial mats about 0.5 m across and headed back to Target 1 to collect some mussels, but had some trouble with navigation. After unsuccessfully hunting for Target 1, we headed to the cluster of targets in the south. We collected 6 cores in bacterial mat close to a seepage site (X-333 m, Y-2071 m). When pulling cores out of sediment, huge gas eruptions followed. We did not observe any live mussels during this dive but took a mussel pot in dead shells hoping to retrieve a few live ones (X-3332 m, Y-2071 m). We deployed yellow Marker 5 next to the mussel pot collection site. We slurped some shrimp and galatheids from the carbonate surface close by and pick up a venus fly trap anemone. Left bottom at 18:40 hrs (Figure 10-28).

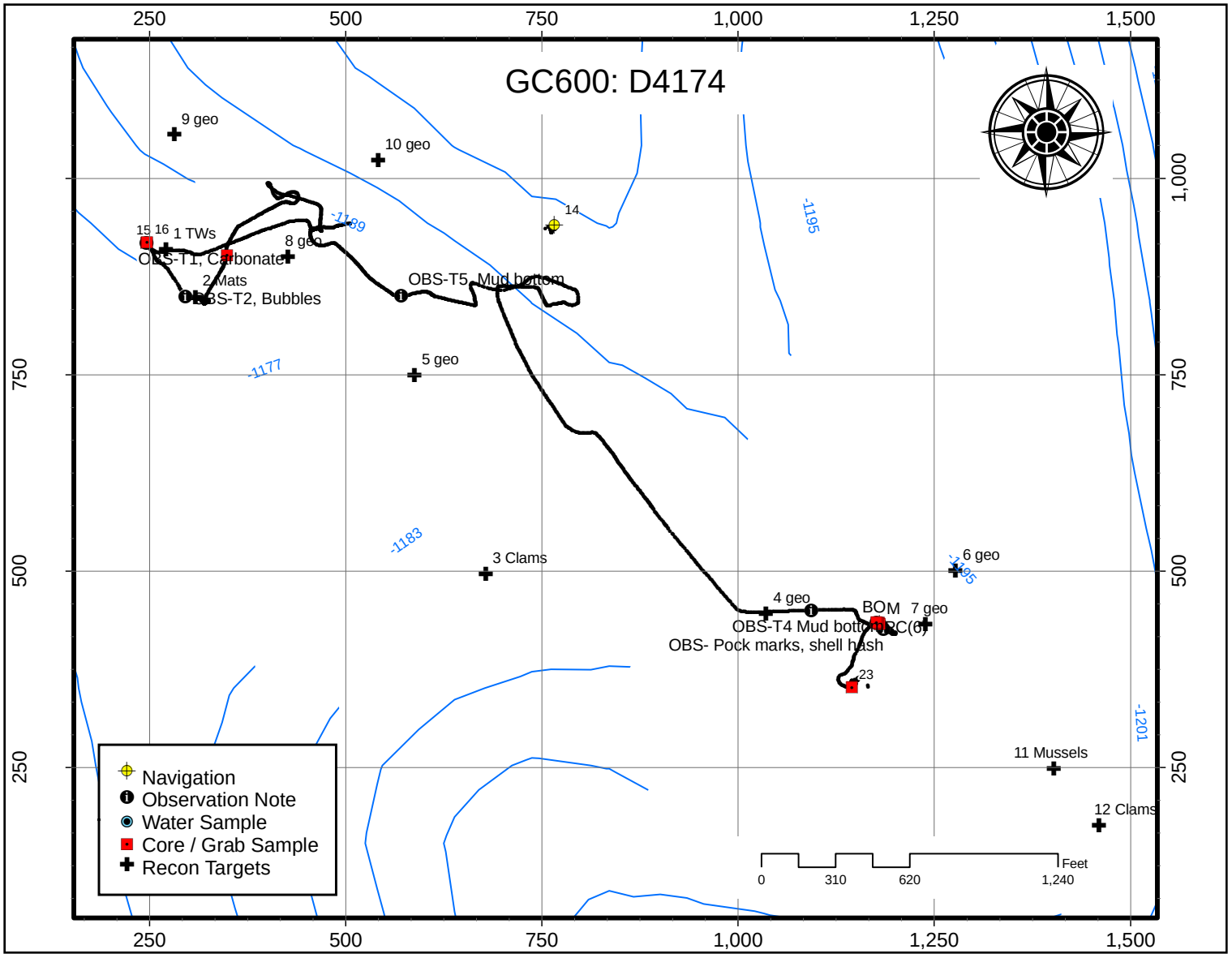

Figure 10-28. Dive 4174 on 5/10/2006 at an average depth of 1,250 m.

10.2.3. *Alvin* Dive 4184

The object of this day's dive was a northwest-southeast trending ridge with a distinct mound at the southeast end, water depth approximately 1250 m. Gavin Eppard was the pilot and Stephane Hourdez and Marshall Bowles were observers. The dive track started at the southeast end of the study area where tube worms had been spotted from a previous dive by Bob Carney. The dive progresses toward the northwest until the sub ran out of power near the extreme northwest end of the designated work site. Pockmarks and craters up to 10 m in diameter and over a meter deep were observed at various places along the sub's track. Living mussels were observed in the bottoms of some craters. Authigenic carbonate ledges, blocks and pavements were observed. Tube worms were frequently spotted growing out of cracks in the carbonates or from the edges of rock exposures. One of the prime tasks of the dive was to use the Bushmaster to collect an entire tube worm colony and all the secondary animals associated with it. This task was not accomplished because a stand-alone bush could not be found. Rock samples from the site contained biodegraded crude oil. This area seems to have a rather persistent slick over the site as monitored with RADARSAT data. There was an oil slick over the site during the dive (Figure 10-29).

The following samples were collected: 1) two samples of the authigenic carbonate, 2) two clams, 3) one scoop of clams, 4) five Niskins, 5) 12 push cores, and 6) one slurp sample of shrimp and crabs. Tonight we are transiting to one of our prime sampling sites, GC852.

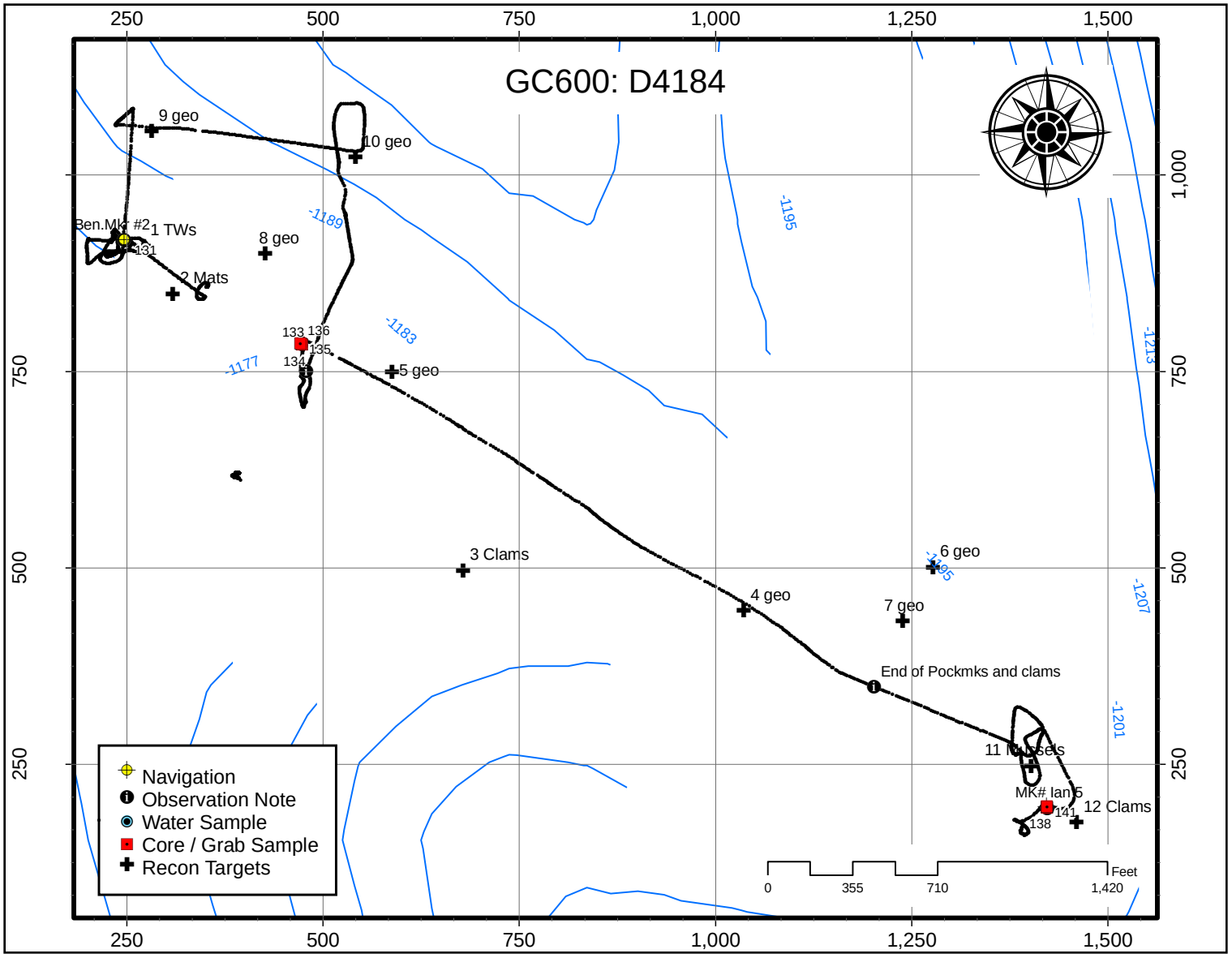

Figure 10-29. Dive 4184 on 5/20/2006 at an average depth of 1,250 m.

10.3. Green Canyon 415

This site was not visited during the Recon Cruise and there was no *Alvin* dive at this site, and only one *Jason II* lowering J2-272, on 6/13/2007 for 11 hours and 57 minutes.

10.3.1. Navigation Considerations

There are two separate areas with distinct geophysical characteristics at the GC415 dive site (Figure 10-30). The southern area is a large mound with moderately high positive amplitude response on top of a northeast-southwest trending bathymetric ridge supported by diapiric salt. Sediment flows extend down-slope for over 3 km and pond in the adjacent intersalt basin. The amplitude response is quite consistent across the mound. The northern area is broken up into smaller, discrete highs and lows with highly variable amplitude response. The small highs have the strong positive amplitude response of low- to moderate-flux seep sites and the intervening lows have the low positive background response of typical, non-seep hemipelagic mud. No flows are associated with the northern amplitude anomalies.

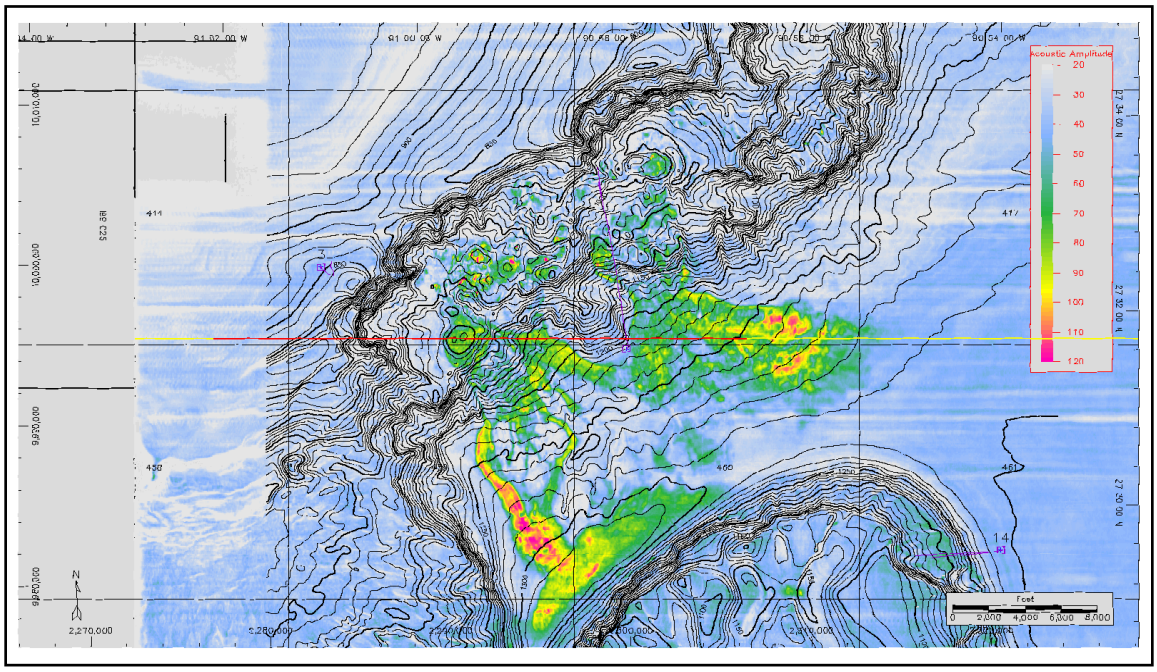

Figure 10-30. 3-D seismically derived bathymetric map with amplitude overlay (C.I.=10m) used for selecting targets at site GC415. Used by permission, Veritas.

We did not visit this site last year with *Alvin*, so we had not developed a list of targets or a point of local origin. We also did not have bathymetry at this site from the AUV-multibeam bathymetric survey dataset developed for this project. We did, however, have access to the BOEM bathymetric and surface anomalies maps, so we used these geo-referenced graphics (Figure 10-30) to establish a local origin, to define a site CRP, and to select targets for the site.

We defined the following for this site in WGS84 datum:

Geodetics False Northing: -3,046,554.27 m
Geodetics False Easting: -197,847.03 m
Local Origin Northing: 3,046,554.27 m
Local Origin Easting: 697,847.03 m.

These Falsing shifts were selected at this site in order to place a Local Origin in X,Y space near the targets of interest at the site. The latitude of this Local Origin is N27 31,70000 and the longitude is W090 59.80000. We then defined an X,Y in the resulting local coordinate system in m for a southern CRP and a northern CRP. We did this by applying the geodetic False Northing and False Easting defined above to the standard UTM projection for the WGS84 datum, then calculating the local X and Y from the latitude and longitude of each site CRP as measured using the BOEM map represented by Figure 10-30. A requirement of such a defined site is the ability to locate it by visual means with *Jason II*. We identified such a topographic high in the north and in the south part of the site on the map and chose a location on top of each.

The local coordinates thus calculated and assigned to the south CRP were X = 345 m and Y = 250 m. The local coordinates thus calculated and assigned to the north CRP were X = 590 m and Y = 1,721 m. We placed these two CRP targets into *Jason* II's navigation system along with targets of interest positioned by a geologic review of the BOEM bathymetric/anomaly map. Targets developed for this site are listed in Table 10-6.

Table 10-6

Target Locations for GC415

Target	Latitude	Longitude	Local X (m)	Local Y (m)	Depth (m)
LocalOrigin	N27 31.700000	W090 59.800000	0	0	1,060
CRP South	N27 31.832310	W090 59.588040	345	250	1,038
geo 1	N27 31.907301	W090 59.419034	621	393	1,055
geo 2	N27 31.730427	W090 59.619657	296	61	1,045
geo 3	N27 31.807676	W090 59.682032	191	202	1,038
geo 4	N27 31.985094	W090 59.631432	269	531	1,055
CRP North	N27 32.626472	W090 59.424777	590	1,721	1,040
geo 5	N27 32.607828	W090 59.146891	1,048	1,694	1,025
geo 6	N27 32.601367	W090 59.074719	1,167	1,684	1,025
geo 7	N27 32.543572	W090 59.121942	1,091	1,576	1,035
geo 8	N27 32.420132	W090 59.310078	785	1,343	1,030
geo 9	N27 32.432605	W090 59.461109	536	1,362	1,045
geo 10	N27 32.434194	W090 59.571031	355	1,362	1,050
geo 11	N27 32.367335	W090 59.853499	-108	1,231	1,045

We did not deploy the LBL net at this site because it was relatively shallow and we felt that we could establish *Jason II*'s position on the CRP without the net. This technique had worked at the previous site MC462. The time saved by not deploying and calibrating an LBL net could be better used in the survey of this site.

Our plan for calibrating *Jason II*'s navigation system was to position the vessel's stern A-frame sheave directly over the CRP ($1{,}000^{+}$ m above it) and allow *Medea* to settle into a position directly under its sheave, suspended by its main cable. We would then position *Jason II* directly under *Medea* while within sight of the seabed. We would monitor *Jason II*'s stability of position by watching the seabed and by using its seabed-position-hold navigation feature. We would then monitor the lateral movement of *Medea* using its downward-looking camera aimed at *Jason II*, to confirm that *Medea* had settled into a stable, equilibrium position with respect to the vessel's stern A-frame sheave.

When we were satisfied that all three vehicles (vessel sheave, *Medea*, and *Jason II*) were vertically aligned to within one meter, and all directly over the defined CRP position, we would reset *Jason II*'s navigation system to re-define its location as the X,Y of the CRP. Then we would drop a marker on that location in order to physically set a benchmark at this site. At this site there would be two such markers, one in the south and one in the north.

The timing of implementation of this plan is outlined below

10.3.2. *Jason II* Lowering 272

Time in water:	2007/06/13 00:14
Time on bottom:	2007/06/13 00:10
Time off bottom:	2007/06/13 11:26
Time out of water:	2007/06/13 12:11
Water Time:	11 hrs 57 minutes
Bottom Time:	10 hrs 15 minutes
Min. working depth:	786.92 m
Max. working depth:	1107.06 m
Produced	1.2G of raw vehicle data
Produced	~16 DVDs of Science video
Produced	~16 DVDs of Archive video

Jason II was deployed into the water at about 20:40 hrs local on 12 June. All times and dates in this summary are reported in EDT, local time. The seabed at 1,076 m was reached at 21:10 hrs and event logging was initiated by the watch-stander on duty using *Jason II*'s VV event logger system. Refer to Dive Observations for this dive in the Appendix 7 for a detailed log of the observed events and their times in GMT.

We first determined the top of the topographic high designated as containing the location of our CRP South by maneuvering a few m in each direction and monitoring water depth. We deployed Marker #2 at a top-of-the-mound location suitable for a CRP at 21:33 hrs. We then reset *Jason II*'s navigation system at X-345 m, Y-250 m using the method described in Target Selection, GC415. Before the dive the observation of oil on the water was made. Several members of the

scientific party confirmed an oil slick over the dive site. This observation was considered a good indication that we would find chemosynthetic communities at the surface reflectivity targets established by analyzing 3-D seismic data from the area.

After looking around the mound where the CRP was established it became apparent that the seafloor was rather featureless and no indicators of seepage were observed. *Jason II* then headed to target Geo 1 at 21:35 hrs. The transit to Geo 1 was uneventful in terms of seepage indicators. After logging biological observations and arriving in the vicinity of Geo 1 at 22:02 hrs, we headed for target Geo 2 at 22:09 hrs. Pockmarks were encountered and clearly displayed on the forward-looking sonar between the CRP site and Geo 1. We explored and logged observations of fish, shrimp, and eels in this region and arrived at Geo 2 at 22:33 hrs. No significant geologic features were observed on the transit. We then headed to target Geo 3 at 22:34 hrs. On the way, we observed and logged more fish before arriving at Geo 3 at 22:48 hrs. We then went back to the CRP to check the performance of our Doppler navigation, and found the offset to be about 1 meter. This was excellent. We picked up the ball marker because the south area was not worth a permanent marker, and then headed for target Geo 4 at 23:10 hrs while logging observations of fish and bacterial mats. These bacterial mats were the only notable seepage indicators encountered on the transit. We arrived at Geo 4 at 23:32 hrs, and then called the completion of this survey of the south area of the site. The mound we had just observed in reconnaissance mode was not a highly reflective target on the 3-D seismic data. Observations from *Jason II* confirmed that hydrocarbon and brine seepage associated with the feature was minimal and certainly not sufficient to support abundant and diverse chemosynthetic communities. Occasional small bacterial mats were the only indicators that we were in a hydrocarbon seep setting. We put *Jason II* in tow-mode, and headed north for 1.2 km.

After arriving in the vicinity of CRP North, we first determined the top of the topographic high designated as containing the location of our CRP North by maneuvering a few m in each direction and monitoring water depth. We re-deployed Marker #2 at a top-of-the-mound location suitable for a CRP at 00:44 hrs on 13 June. We then reset *Jason II*'s navigation system at X-590 m, Y-1,721 m using the method described in Target Selection, GD415. This area north of the initial dive site had many highly reflective, but small targets as determined from the 3-D seismic data. We expected these areas and its features to be much more productive in terms of hydrocarbon seep features and associated chemosynthetic fauna.

The CRP target area was a low relief mound approximately 300 m diameter that displayed a very bright reflectivity zone on the southern flank. After arriving at the mound and looking around , *Jason II* headed to target Geo 5 at 00:46 hrs. During the transit we logged biological observations of fish, bacterial mat, crabs, clams, and holothurians. We arrived in the vicinity of Geo 5 about 01:07 hrs. While approaching this target, a field of numerous pockmarks was encountered. They were impressively displayed on the forward-looking sonar. We proceeded to core (X-777 m, Y-1,071 m) at 01:20 hrs in a large bacterial mat (Figure 10-31). We eventually obtained 3 cores at this site. Coring was completed at 01:29 hrs. We then went on to the east observing some biology, including holothurians, fish, bacterial mats crab, clams, shrimp, and a shark. We then acquired three more cores at X-1026m, Y-1695 m, in another bacterial mat.

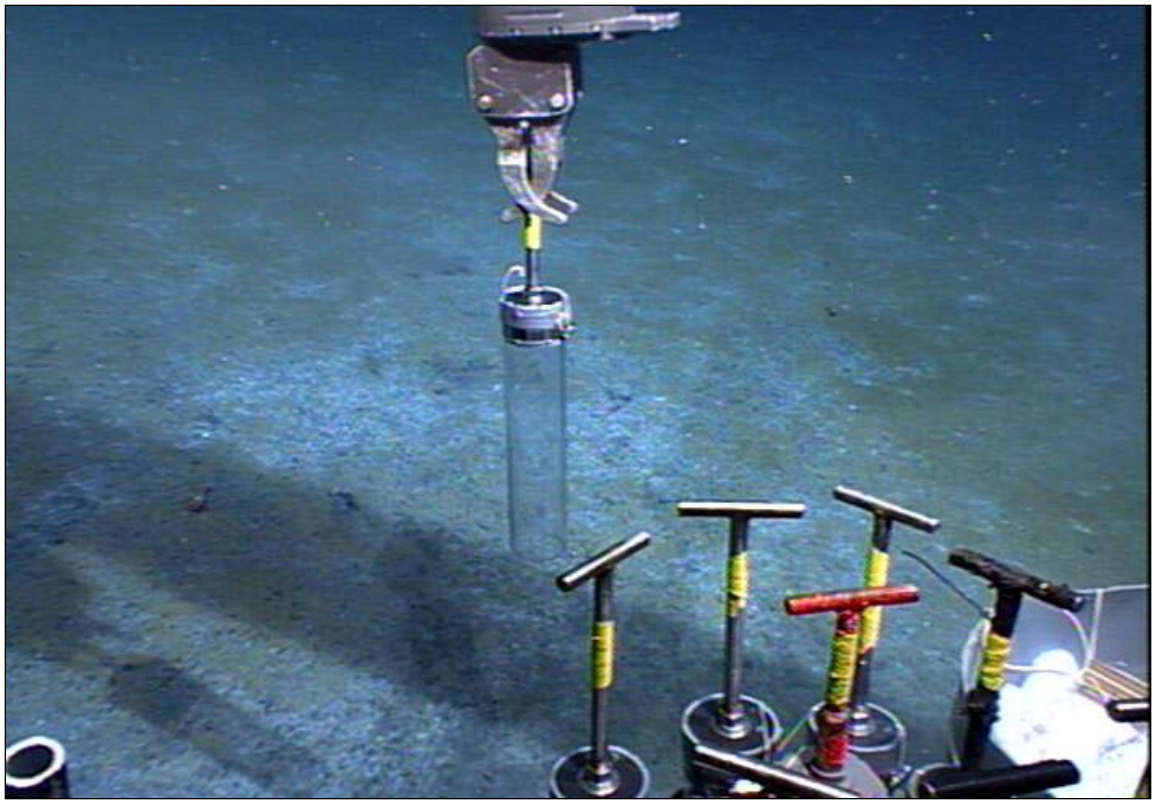

Figure 10-31. Push-cores taken in bacterial mat.

We continued on to target Geo 6 at 02:22 hrs, then on to target Geo 7 at 02:32 hrs, and on to target Geo 8 at 02:44 hrs, observing fish and other fauna along the way. We headed to target Geo 9 at 03:31 hrs making more such observations, stopping to take 3 more cores in a mat at X-516-m, Y-1,349-m. We also started sampling with the mass spectrometer in this mat.

At approximately 04:00 hrs we arrived at target Geo 9 and a large "bacterial mat" was identified for the last three push cores. When the first core was taken, it only penetrated about 4 inches and gas bubbles were released from the sea floor. Underlying hydrate was suspected. A second core in this central area also stopped hard at 4 inches and released gas. A third core off to what appeared to be near the edge of this mound also hit hydrate and released gas. During the coring operations a small area of about 50 cm^2 of brown fine grain "sediment" with "blue fuzz" around its perimeter was seen in the video. These resembled, and were later confirmed to be, a colonial ciliate in the family Folliculinidae, that is thought to have chemoautotrophic symbionts. The hand held cool pix camera was used to take about 80 close up images of these colonies, bacterial mat, and the push core holes. It became apparent that this area was actually a thin carbonate crust, over 4 inches of sediment, overlying a buried hydrate.

When imaging was complete several unsuccessful attempts were made to core the ciliates. (Although we did not recover these impressive and visible colonies, isolated (tiny) groups were later confirmed in some of the other mat push cores). We then used a push core to break up an area of the crust and scoop mud, followed by scooping with a net lined with linen to collect

several liters of the mud (for bulk analyses by the Joye group) and pieces of the carbonate crust. During this operation bubbles were released almost constantly and numerous pieces of white hydrate floated up and past the three cameras (this is most apparent in the down looking "Brow cam"). The net full of mud and carbonate was stored in the port bio box and the sub proceeded to Geo 10 before ending the dive. We deployed Marker #5 here (X-505 m, -1378 m), then transited to target Geo 10 while logging biological and geological observations. *Jason II* lifted off of the bottom at 07:26 hrs to begin its ascent.

Logged soft-bottom fauna were typical for this depth in the northern GoM. Rattails and eels were common but not notably abundant. Holothurians were dominated by the large white *Mesothuria lactea* although the purple *Paelopatides* was also present. Crabs were dominated by Geryonids.

NOTE: During post-cruise dive track chart creation it was noticed that the latitude and longitude values in the *Jason II* VV table appear to be shifted over 300 m to the east (Figure 10-32). The local XY's appear to be correct relative to the target locations visited during this dive.

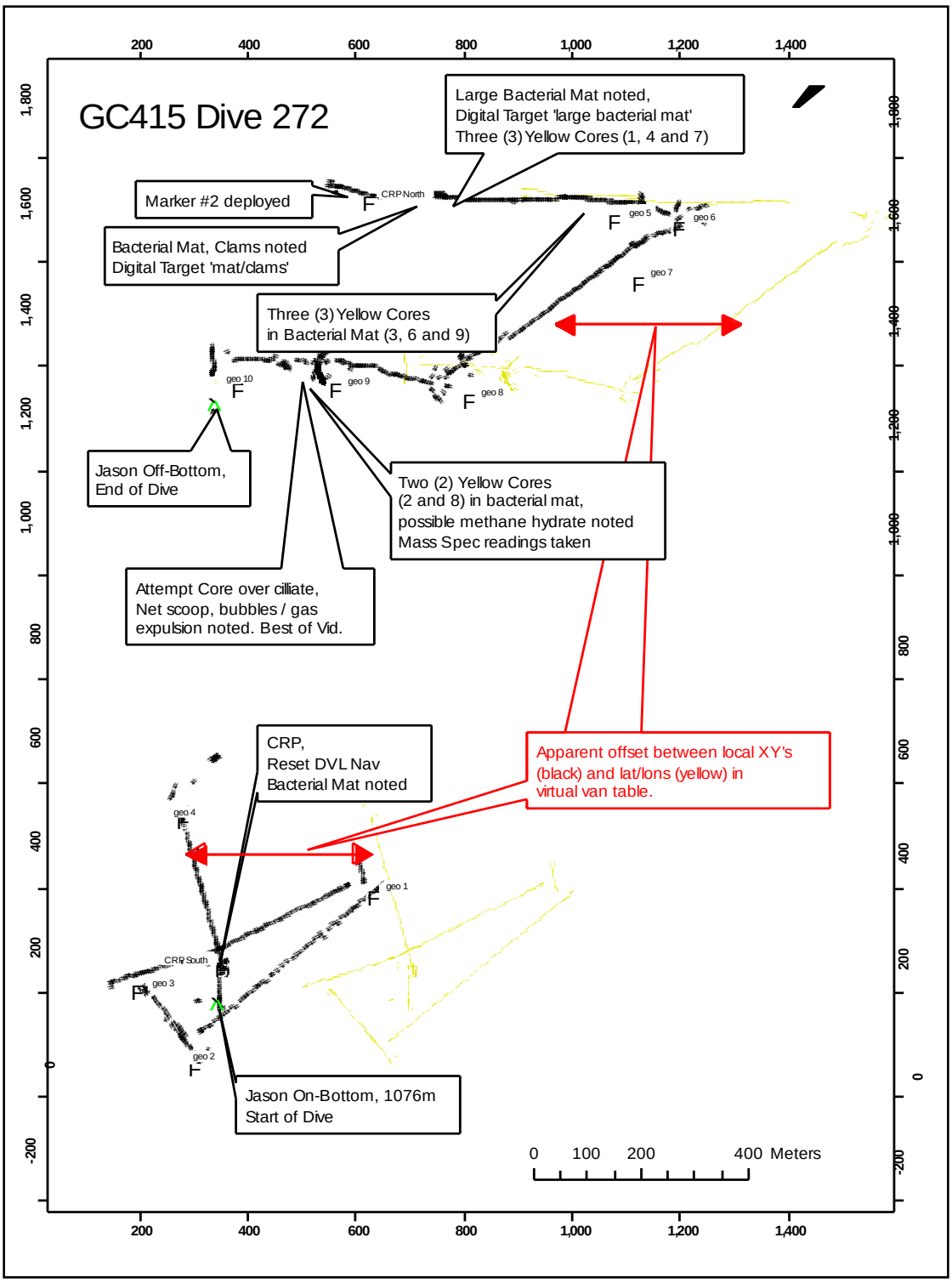

Figure 10-32. Dive track for D272.

10.4. Mississippi Canyon 462

This site (MC462) was not visited during the Recon Cruise and there were no *Alvin* dives at MC462. There was one *Jason II* lowering from 6/11/2007 to 6/12/2007 for a duration of 15 hours and 39 minutes.

10.4.1. Navigational Considerations

We did not visit this site last year with *Alvin*, so we had not developed a list of targets or a point of local origin. Because we didn't visit this site and designate it as one of our primary sampling sites during the *Alvin* cruise, we did not have bathymetry at this site from the AUV-multibeam bathymetric survey dataset acquired for this project in March 2007. We did, however, have access to the BOEM bathymetric and surface anomalies maps, so we used these geo-referenced graphics (Figure 10-33) to establish a local origin, to define a site CRP, and to select targets for the site. Prior to this year's cruise, the site was selected from review of the BOEM 3-D seismic database to meet the needs of the biologists who needed a chemosynthetic community site in the 1,000 m depth range to firmly establish depth-distributions of key species.

We defined the following for this site in WGS84 datum:

Geodetics False Northing: -3,153,114.37 m
Geodetics False Easting: 184,345.02 m
Local Origin Northing: 3,153,114.37 m
Local Origin Easting: 315,654.98 m.

These Falsing shifts were selected at this site in order to place a Local Origin in X,Y space near the targets of interest at the site. The latitude of this Local Origin is N28 29.50000 and the longitude is W088 53.00000. We then defined an X,Y in the resulting local coordinate system in m for the CRP. We did this by applying the geodetic False Northing and False Easting defined above to the standard UTM projection for the WGS84 datum, then calculating the local X and Y from the latitude and longitude of the site CRP as measured using the BOEM map represented by Figure 10-33. A requirement of such a defined site is the ability to locate it by visual means with *Jason II*. We identified such a topographic high on the map and chose a location on top of it.

The local coordinates thus calculated and assigned to the site CRP were X = 391 m and Y = 66 m. We placed this CRP target into *Jason* II's navigation system along with targets of interest positioned by a geologic review of the BOEM bathymetric/anomaly map. Targets developed for this site are listed in Table 10-7.

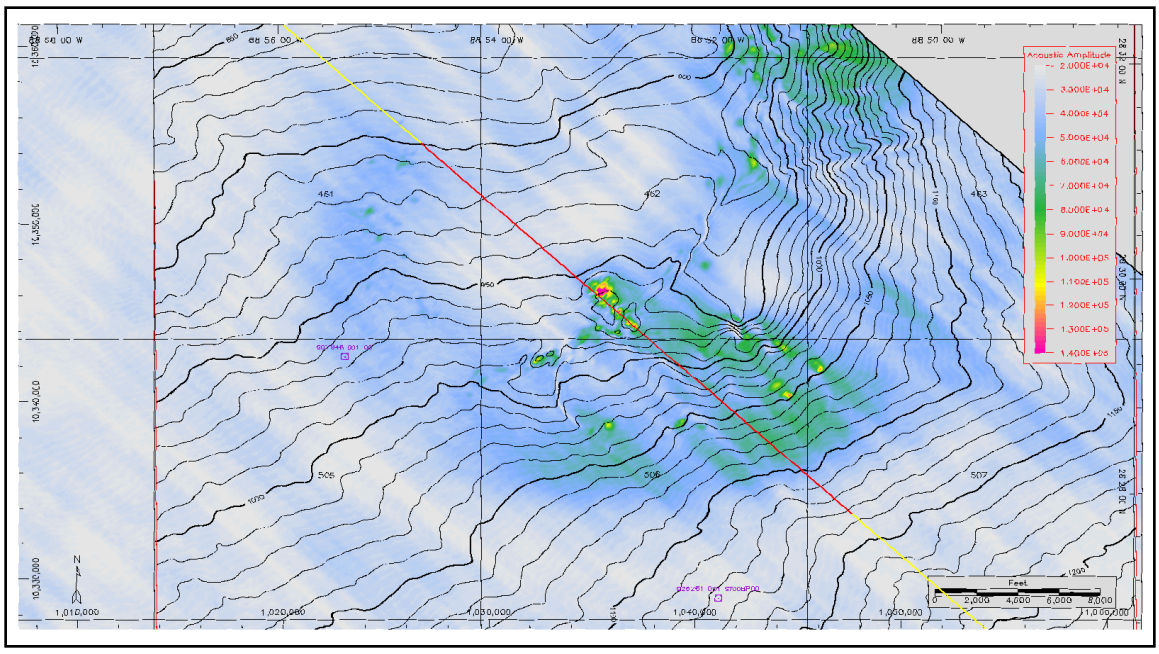

Figure 10-33. 3-D seismically derived bathymetric map (C.I.=10 m) with amplitude overlay used for target selection at site MC462. Used by permission, TGS.

Table 10-7

Target Locations for Site MC462

Target	Latitude	Longitude	Local X (m)	Local Y (m)	Depth (m)
Local Origin	N28 29.500000	W088 53.000000	0	0	965
CRP	N28 29.544530	W088 52.755640	400	76	960
geo 1	N28 29.651806	W088 52.867860	220	277	965
geo 2	N28 29.661142	W088 52.897444	172	295	960
geo 3	N28 29.715721	W088 52.905154	161	396	960
geo 4	N28 29.726042	W088 53.019946	-26	418	955
geo 5	N28 29.754366	W088 53.046803	-69	471	960
geo 6	N28 29.828180	W088 53.034020	-46	607	960
geo 7	N28 29.452258	W088 52.889449	179	-91	965

We did not deploy the LBL net at this site because it was a reconnaissance dive and relatively shallow. We felt that we could establish *Jason II*'s position on the CRP without the net. The time saved by not deploying and calibrating an LBL net could be better used in the survey of this site.

Our plan for calibrating *Jason II*'s navigation system was to position the vessel's stern A-frame sheave directly over the CRP (960^{+} m above it) and allow *Medea* to settle into a position directly under its sheave, suspended by its main cable. We would then position *Jason II* directly under

Medea while within sight of the seabed. We would monitor *Jason II*'s stability of position by watching the seabed and by using its seabed-position-hold navigation feature. We would then monitor the lateral movement of *Medea* using its downward-looking camera aimed at *Jason II*, to confirm that *Medea* had settled into a stable, equilibrium position with respect to the vessel's stern A-frame sheave.

When we were satisfied that all three vehicles (vessel sheave, *Medea*, and *Jason II*) were vertically aligned to within one meter, and all directly over the defined CRP position, we would reset *Jason II*'s navigation system to re-define its location as the X,Y of the CRP. Then we would drop a marker on that location in order to physically set a benchmark at this site. The timing of implementation of this plan is outlined in the beginning of the Dive 271 Summary.

The 3-D seismic surface amplitude map of the MC462 site, prepared before the cruise at the New Orleans, LA BOEM office, indicates a line of bright anomalies arranged roughly in a line oriented in a northwest-southeast direction. In plan view, the area is a low-relief mound to the southeast and a broad shallow depression to the northwest. The mound rises to a water depth of about 955 m, as determined from seismic data, and the depression reaches a depth of about 965 m. In profile view, the subsurface directly beneath the depression is acoustically opaque and appears a "gas chimney" that extends far into the sedimentary section. Prominent subsurface reflection horizons disappear in the chimney-like zone. The surface reflector is a strong positive and broken into highly reflective segments and there is some suggestion of a small phase reversal. There is a suggestion of a bottom simulating reflector , but this observation is certainly not conclusive.

10.4.2. *Jason II* Lowering 271

Time in water:	2007/06/11 21:37
Time on bottom:	2007/06/11 22:38
Time off bottom:	2007/06/12 12:27
Time out of water:	2007/06/12 13:16
Water Time:	15 hrs 39 minutes
Bottom Time:	13 hrs 49 minutes
Min. working depth:	921.95 m
Max. working depth:	973.96 m
Produced	1.6 GB of raw vehicle data
Produced	~21 DVDs of Science video
Produced	~21 DVDs of Archive video

Jason II was deployed into the water at 17:37 hrs local on 11 June. All times and dates in this summary are reported in EDT, local time. The seabed at 953 m was reached at 18:38 hrs and event logging was initiated by the watch-stander on duty using *Jason II*'s VV event logger system. Refer to Dive Observations for this dive in the Appendix 7 for a detailed log of the observed events and their times in GMT.

We first determined the top of the topographic high designated as containing the location of our CRP by maneuvering in each direction and monitoring water depth. This area was found to be

very flat as suggested by the seismic profile. We deployed Marker U at a top-of-the-mound location suitable for a CRP at 19:33 hrs (Figure 10-34). We then reset *Jason II*'s navigation system at X-400 m, Y-76 m using the method described in Target Selection, MC462.

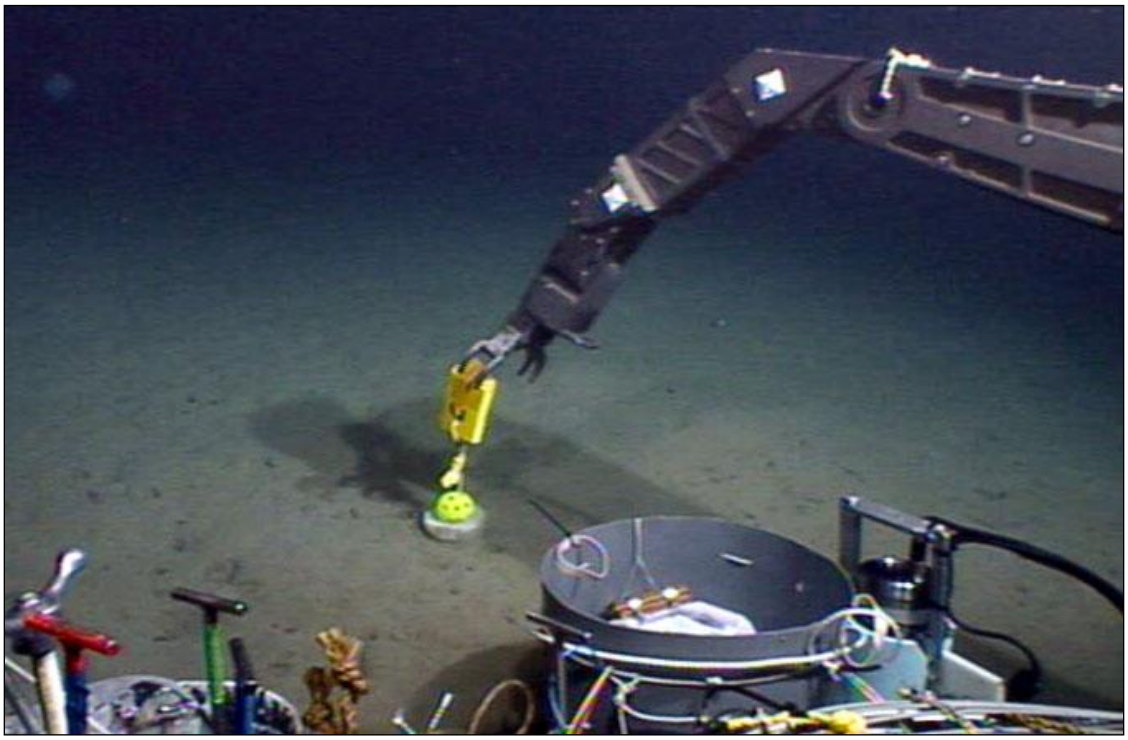

Figure 10-34. Marker "U" deployed at CRP.

After looking around the mound and logging biological observations, *Jason II* headed to target Geo 1 at 21:37 hrs. The surface character of the mound top and flanks appeared to be primarily burrowed hemipelagic mud. After arriving in the vicinity of Geo 1 at 21:55 hrs, we headed for target Geo 2 at 22:03 hrs. We explored and logged observations in this region and then headed to target Geo 3 at 22:14 hrs. We observed and logged a brine seep with a bacterial mat (X-168 m, Y-334 m) at 22:19 hrs, before arriving at Geo 3 at 22:26 hrs. We then headed for target Geo 4 while logging observations of rat-tail and other fish, star fish, eels, and holothurians. We then headed for target Geo 5 at 22:41 hrs, logging more fish and eels. At 22:47 hrs we headed for target Geo 6, noticing a few outcropping carbonates with gorgonians on them, and arriving at 22:56 hrs. After logging more fish, we headed south at 23:30 hrs, and stopped at what we were calling the brine seep to take some cores. The bacterial mats (Figure 10-35) occurred at the base of a low-relief mound. The mound had a smooth surface with thin bacterial mats and evidence of small slope failures derived by fluid expulsion. We proceeded to core (X-172 m, Y-337 m) at 23:55 hrs in the bacterial mat, and disturbed the sediment enough that hundreds of gas bubbles, hydrate fragments, and oil droplets floated up into the water. Some of the oil droplets stuck on the camera lenses. We also saw yellow hydrate floating out of the disturbed coring area and layered gas hydrate in the areas we had cored. We eventually obtained 5 cores out of 8 tried, as we broke 3 of the core rigs with the manipulating arm. We completed the coring at 01:01 hrs of 12 June, and went on to collect some biological samples. During coring, we noticed a few shells on the periphery of the bacterial mat. These were collected and turned out to be *Calyptogena*

ponderosa, the same species of chemosynthetic clam that is on the upper slope. We also were sampling with the mass spectrometer and the methane sensor in this area. The high amplitude observed for this area did not result in finding carbonates, mussel beds, or colonies of tube worms in the area. After coring of the bacterial mats and finding abundant gas hydrate, it is likely that the high reflectivity is from shallow gas hydrate under the sizeable areas of high surface amplitude.

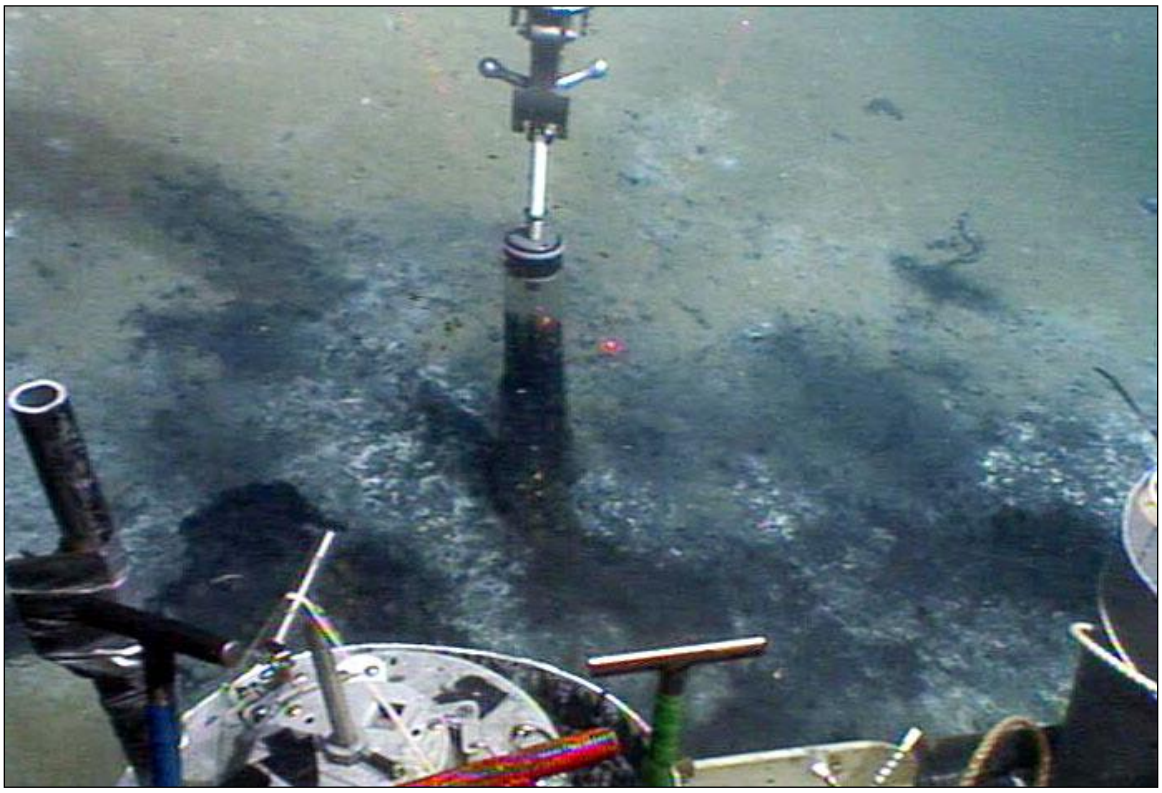

Figure 10-35. Collecting push-core samples in bacterial mat.

After physical sampling, we began a photo acquisition at 04:03 hrs, in order to test some of the settings on the down-looking Scorpio camera. We made a series of coral collections in this area including the colonial hard coral *Madrepora oculata*, a purple gorgonian, and a yellow octocoral. We also collected a piece of carbonate that contained two *Caryophila* sp. individuals, a solitary hard coral. We then completed a set of 10 random photo transects distributed in a 200 x 200 area from 05:53 hrs to 08:04 hrs. We then navigated back to the CRP to check the navigation stability of the Doppler navigation over this entire time period, and found that we were within 4 m (X-401 m, Y-72 m) of the original position of this dive. We considered this to be excellent control over our navigated fixes. *Jason II* lifted off of the bottom at 08:21 hrs to begin its ascent. Figure 10-36 shows the dive track for dive 271.

Logged soft-sediment megafaunal can be considered typical for this depth in the northern GoM. Rattails and eels were quite common followed by the large white holothurian *Mesothuria lactea* . Less common were Geryoind crabs (red or golden crabs) and Lithodid crabs (cf. *Paralomis*).

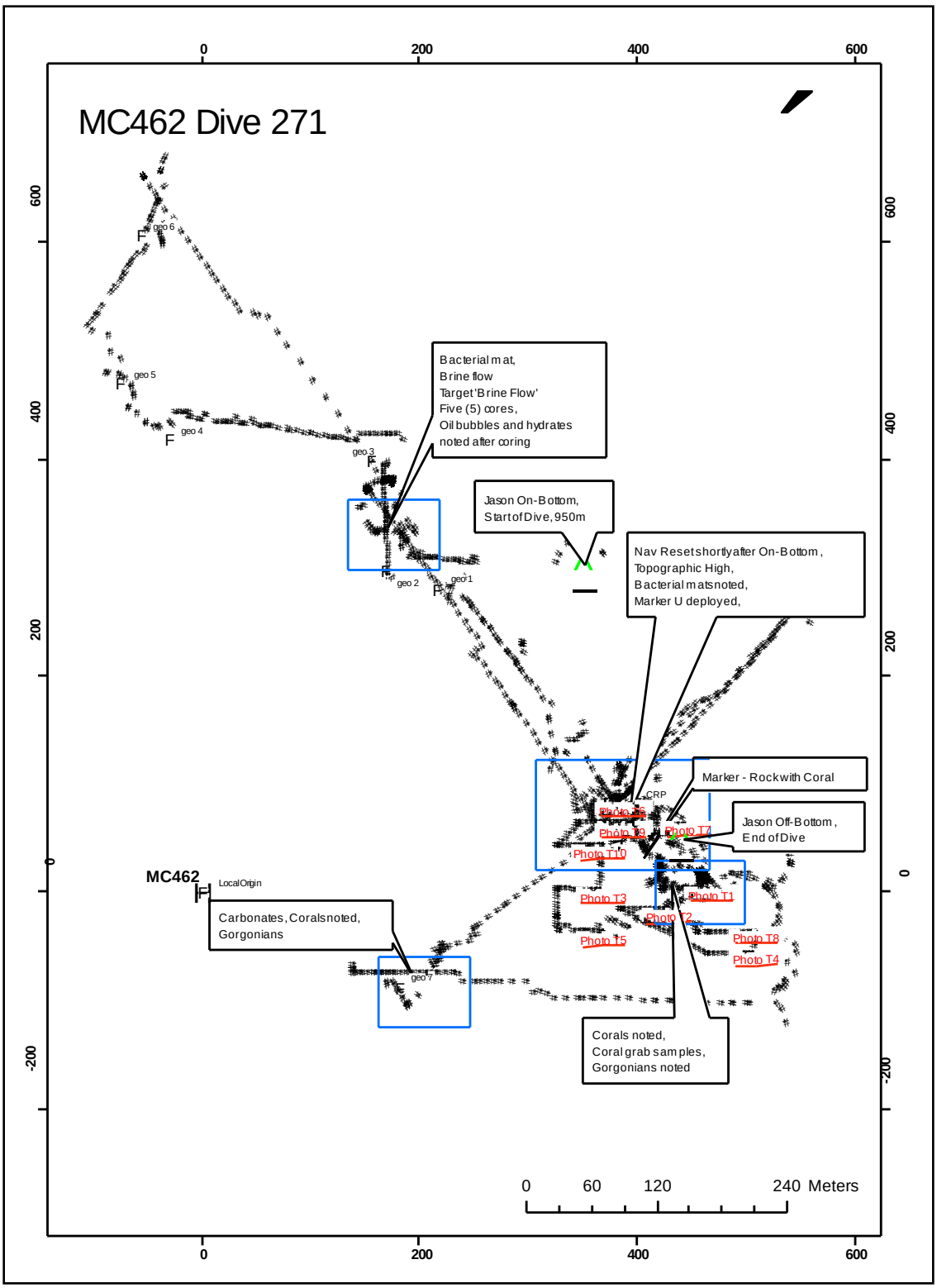

Figure 10-36. Dive track for D271.

10.5. Walker Ridge 269

This site (WC269) was surveyed during the Recon Cruise , and there were two *Alvin* dives at Walker Ridge 269, including AD4175 on 5/11/06 and AD4191 on 5/26/06 as well as one *Jason II* dive on 6/18/07 that lasted for 17 hours and 42 minutes.

10.5.1. Reconnaissance Cruise

This site was a series of geophysical targets distributed over sloping terrain at a depth of about 1,950 m. The sea conditions were at the limit of what could be tolerated as can be seen from the very numerous bottom strikes where several images in a row would be obscured by sediments. The DCS reached bottom at 10:48 hrs on 23 March and collected images with a 10 second repeat rate until 13:11 hrs when a minor power malfunction in the DCS prematurely ended the survey sequence. A total of 467 images were collected with the bottom in view and acceptable navigation covering the major part of the targeted area. There were definitive indicators of seepage at this site including small, but widespread bacterial mats, shells, and several individual mussels. This site is a very marginal candidate for further study (Figures 10-37 and 10-38). However, after review of the camera tract from the survey cruise and H. Roberts and W. Shedd concluded that some features of interest were not covered well and that this site deserved a closer look even though there was no direct evidence of chemo communities evidenced in the survey cruise photos.

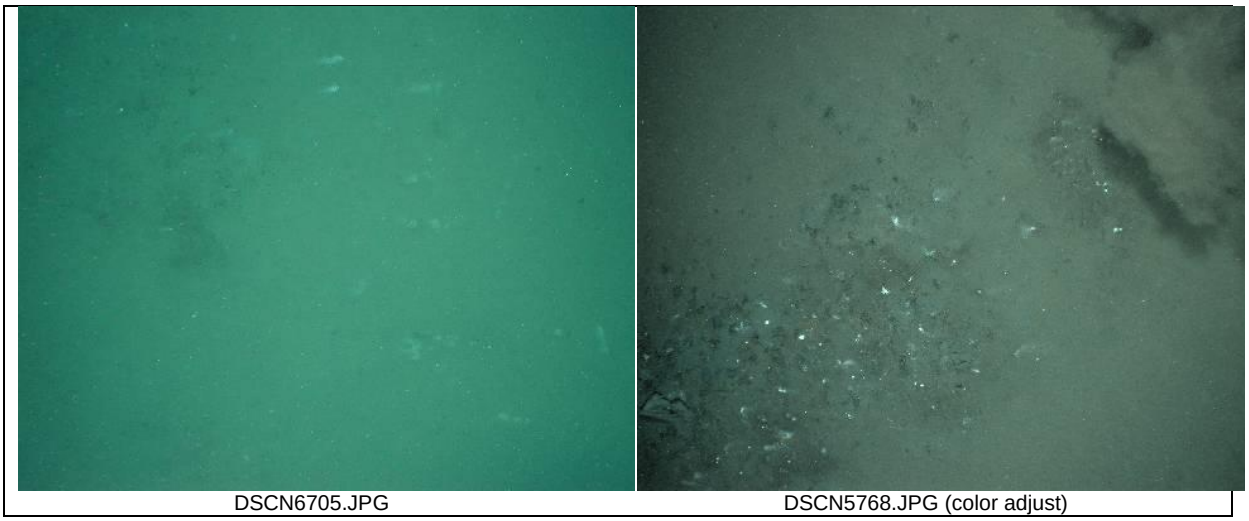

Figure 10-37. Representative photography from WR269/270.

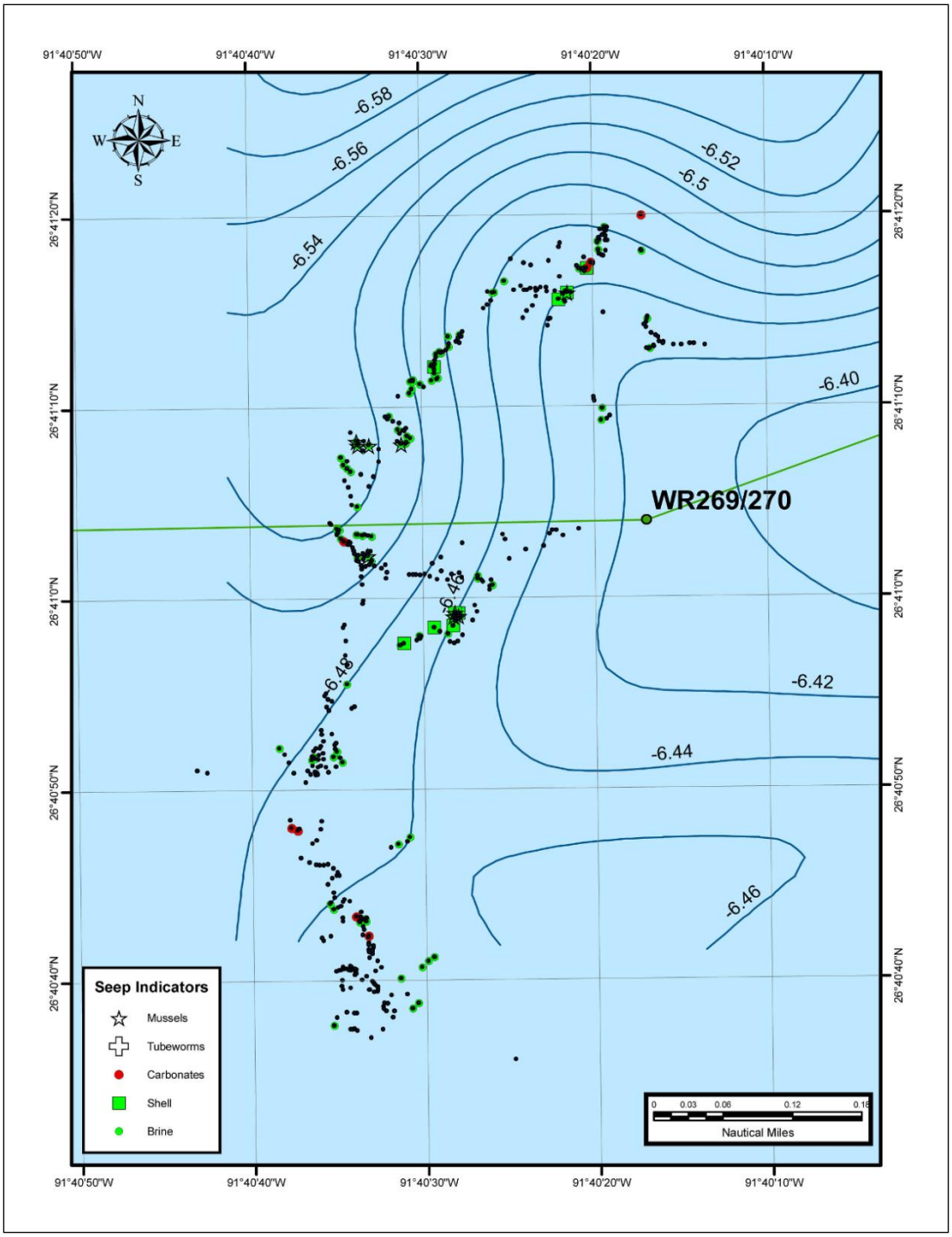

Figure 10-38. Survey results from WR269/270 station.

10.5.2. Navigational Considerations

This site is 1,910–2,000 m of water and is approximately 3,000 m long by 1,000 m wide (Figure 10-39). Moderate-to-high positive amplitude covers the entire feature except at a discrete, circular high that appears to be a mud volcano with distinctly lower positive amplitude (either due to steeper slopes and attenuated return signal or less lithification). Subsurface active gas migration is clear from the blanking of sedimentary bedding below the entire feature.

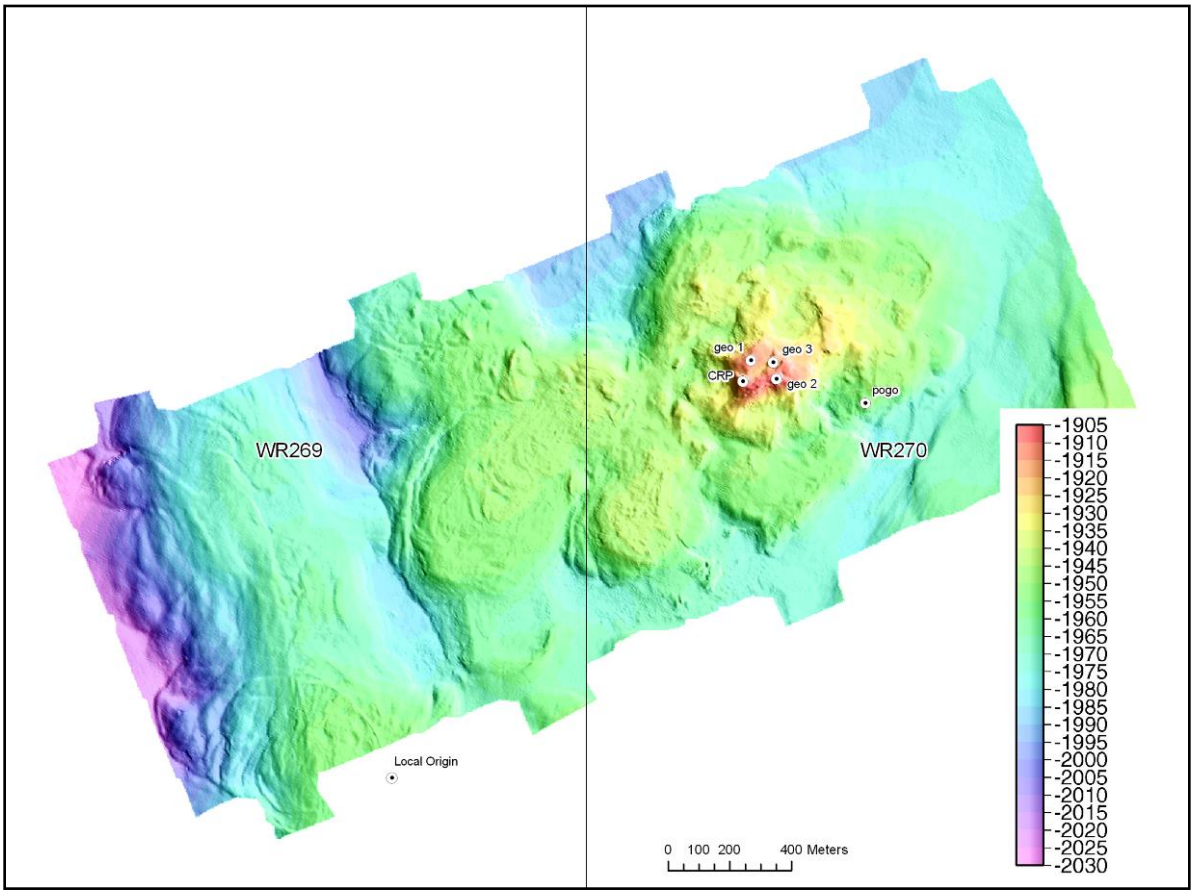

Figure 10-39. AUV derived map of bathymetry at site WR269/270.

The Recon Cruise in March 2006 and the *Alvin* dives in May 2006 confirmed that the locations chosen from the 3-D seismic maps were active seeps that contained variable population sizes and diversity of chemosynthetic organisms. The major drawbacks of 3-D data, though, are the horizontal and vertical resolution. Most 3-D data have horizontal sample sizes of around 15 m by 30 m and vertical resolutions of 5–0 m; many of the sub-environments of chemosynthetic communities are smaller than the horizontal sample of 3-D data and bathymetric changes are in the 1–2 m range. To identify these subtle features at the more interesting sites from last year's *Alvin* dives with improved bathymetry maps to aid in navigation, we obtained high resolution bathymetry surveys over WR269/270 and three other sites using the AUV Hugin.

Before our first *Jason II* dive at this site we located a prominent geologic feature revealed by our recent AUV survey. This feature is shown as a topographic high labeled as -1,920 m in Figure

10-40 below, as mapped from the AUV dataset. We were confident that we could find the center of this topographic high using *Jason II*, so we defined its center as our CRP for the site work.

We determined the Northing (Y) and Easting (X) in m for this selected CRP in the local coordinate system in which *Jason II* would work. We did this by applying a geodetic False Northing and Easting to the standard UTM Zone 15 projection for the WGS84 datum, then calculating the local X and Y from the latitude and longitude of the site CRP as measured from the AUV survey. These are the same Falsings used for the local projection of the dives at this site with *Alvin* last year. The local coordinates thus calculated and assigned to the site CRP were X = 424 m and Y = 2,190 m. We placed this CRP target into *Jason II*'s navigation system along with targets of interest positioned by *Alvin* last year and targets positioned by a geologic review of the AUV contour map.

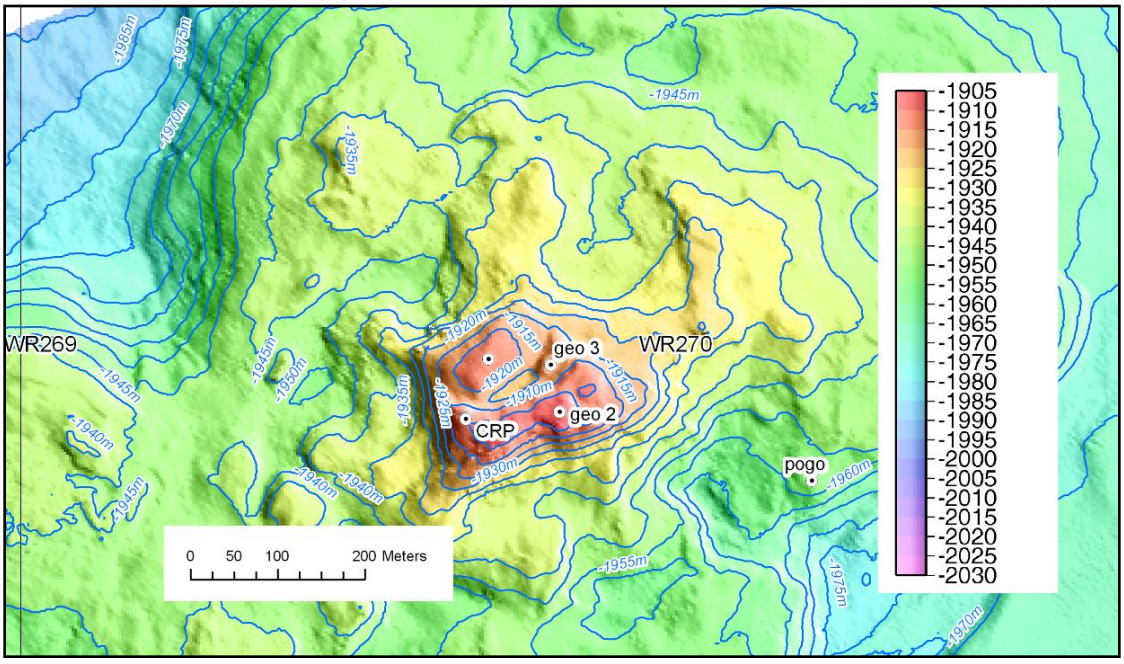

Figure 10-40. The Central Reference Point at site WR269/270.

We defined the following for this site in WGS84 datum:

Geodetics False Northing: -2,951,123.79 m
Geodetics False Easting: -131,843 m
Local Origin Northing: 2,951,123.79 m
Local Origin Easting: 631,843 m

Targets developed for this site are listed in Table 10-8. Targets listed prior to the CRP are targets from the *Alvin* cruise last year. Their position fixes are those logged by *Jason II* after each marker or target was found. Targets listed after the CRP (the "geo" targets) are ones selected on this cruise by a review of the geophysical information available to us on the cruise.

Table 10-8

Target Locations for Site WR269/270

Target	Latitude	Longitude	X (m)	Y (m)	Depth (m)
Local Origin	N26 40.50000	W091 40.50000	0	0	
CRP	N26 41.191685	W091 39.805804	1,138	1,289	1,905
geo 1	N26 41.228907	W091 39.789692	1,164	1,358	1,910
geo 2	N26 41.195399	W091 39.740035	1,247	1,297	1,905
geo 3	N26 41.224710	W091 39.746930	1,235	1,351	1,912
pogo	N26 41.150970	W091 39.566293	1,536	1,218	1,954

10.5.3. *Alvin* Dive 4175

The evening before the dive Bob Carney conducted a trawl about two miles away from the site with a nice recovery of benthic animals. This dive was heavily impacted by weather. The site was Walker Ridge 269 and the divers were Harry Roberts and Vladimir Samarkin. The launch was delayed until 0900 because of high winds. The dive was called up early for the same reason and was on deck at 1400. At the first target they saw very little, but did collect what looked like "white fuzz" that turned out to be very thin pogonophorans with an associated community of very small snails and mussels. They moved to the second target on their dive plan, inside the crater, and found a lush community of tube worms and mussels. Unfortunately, at that point, they were called off the bottom and no physical collections were made at this location. Navigation was excellent and they deployed a benchmark marker. We planned to revisit this site later in this cruise (Figure 10-41).

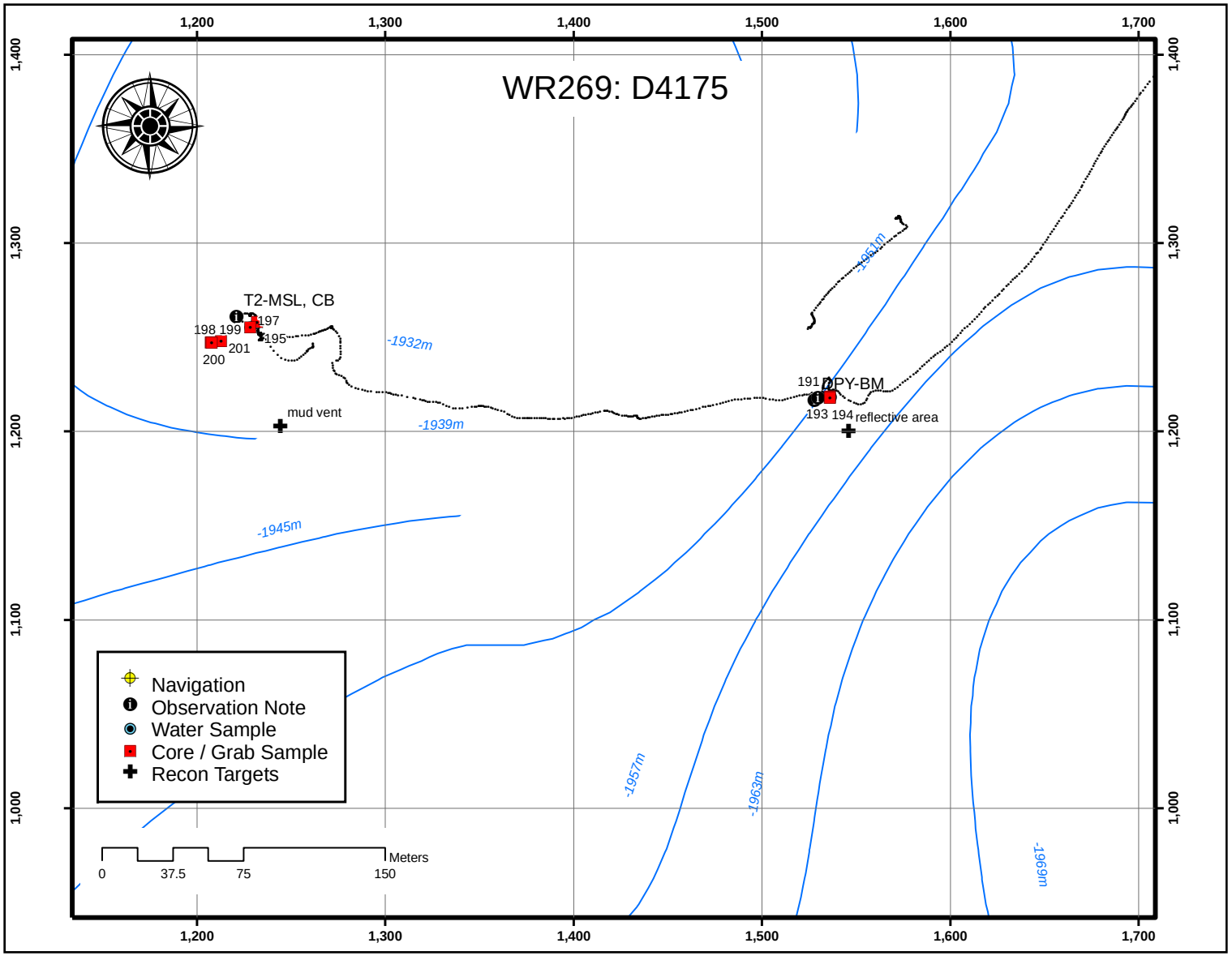

Figure 10-41. Dive 4175 on 5/11/2006 at an average depth of 1,950 m.

10.5.4. *Alvin* Dive 4191

The pilot was Patrick Hickey, and the observers were Harry Roberts and Matt Kupchik. The dive started on time at 0800 and arrived at the seafloor near our first target which was a field of small pogonophorans on the flank of the eastern mounded area. We set out a benchmark float there the first dive. Even though our navigation seems to have improved, we had a difficult time finding the pogonophoran site. It took the better part of an hour before we found our benchmark. The first thing accomplished was a mosaic of the area. We took close-up pictures of the pogonophorans and holothurians eating them. Water samples and push cores were also taken. We wanted to "slurp" sample the pogonophorans, but the slurp gun malfunctioned. After finishing at this area, we moved to the central crater area where we sampled tube worms, mussels, and carbonates. This was a productive dive and we determined that this site deserved more intensive study on a later cruise (Figure 10-42).

The following samples were collected at this site: 1) photos for a photomosaic, 2) close-up pictures of the pogonophorans, 3) five Niskin bottle samples, 4) 12 push cores, 5) tube worms, 6) one mussel pot, 7) one scoop of mussels, and 8) one carbonate rock sample.

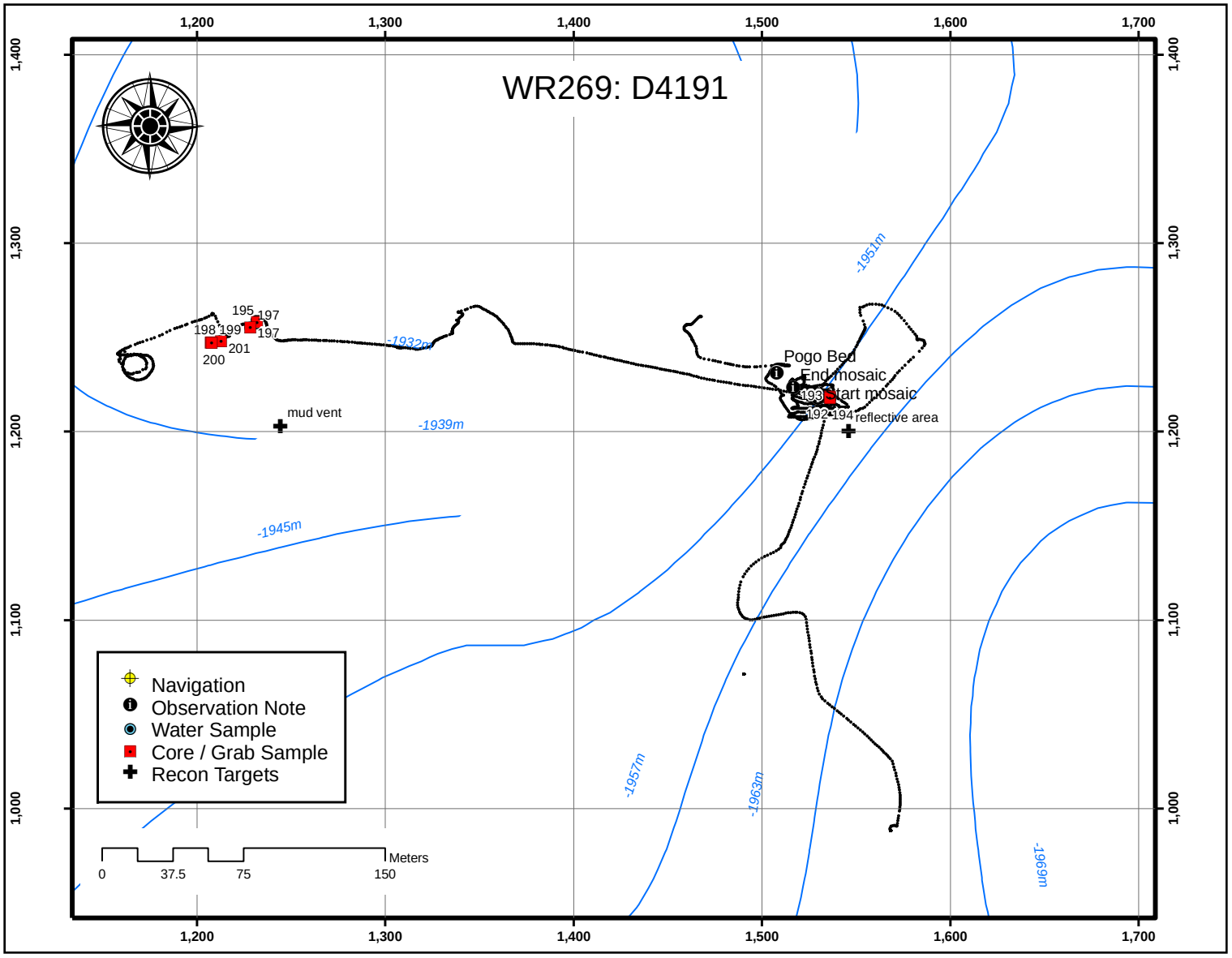

Figure 10-42. Dive 4191 on 5/26/2006 at an average depth of 1,950 m.

10.5.5. *Jason II* Lowering 275

Time in water:	2007/06/18 00:05
Time on bottom:	2007/06/18 00:12
Time off bottom:	2007/06/18 18:54
Time out of water:	2007/06/18 20:06
Water Time:	20 hrs 2 minutes
Bottom Time:	17 hrs 41 minutes
Min. working depth:	1883.04 m
Max. working depth:	1964.25 m
Produced	2.1 GB of raw vehicle data
Produced	~28 DVDs of Science video
Produced	~28 DVDs of Archive video

Jason II was deployed into the water at about 20:00 hrs local on 17 June. All times and dates in this summary are reported in EDT, local time. The sea-bed at 1,965 m was reached at 21:13 hrs and event logging was initiated by the watch-stander on duty using *Jason* II's VV event logger system. Refer to Dive Observations for this dive in the Appendix 7 for a detailed log of the observed events and their times in GMT.

The core rack was top heavy with two long cores and fell off the basket upon (a slightly rough) arrival on the bottom (Figure 10-43). It was fully recovered and at 22:00 hrs we began the transit to the pogonophoran field that should be near the Marker 1. The CONTROS hydroC Methane sampler was turned on at 22:17 and gave a spike as it should, but it developed a ground fault and was giving very high readings at 23:00 hrs. The power was cycled but the ground fault got worse and the sensor was turned off at 23:15. Meanwhile, Marker 1 was found at 23:09 hrs (X-1483 m, Y- 1222 m). It was no longer floating. [Note that the Doppler navigation is moving quite a lot since event 19736, although the ROV is stationary during these coring operations]. The large pogonophoran patch extends to the northwest and a little to the northeast of Marker 1. We planned to mosaic the area around Marker 1, so we moved north to do the sampling. We found a patch of pogonophorans that appeared to have white tubes on the camera, which we later found out to be the tubes of another polycheate, possibly a sabellid, whose white tubes were attached to the tops of the pogonophoran tubes. The purple sea cucumber *Chirodota heheva* was fairly abundant in this patch. We took one long core here at 23:29 hrs (logged in the VV under "carbonate collection"; X-1528 m, Y-1234 m). The rubber band was holding the valve open at the top of the core, so it was only half full. We took two wide cores in this same location at 23:34 and 23:37 hrs. The rubber bands were broken off of these first, so the cores were filled completely. We used the suction sampler to collect associated fauna into the blue container (started at 23:53). We collected two sea cucumbers, a *Munidopsis*, amphipods and tiny white snails. After slurping for some time, we could see a brittle star near the base of the pogonophorans near the sediment. Attempts to slurp this failed because the fine mesh on the slurp was clogged and the suction was weak. We also failed to collect any anemones with the slurp sampler.

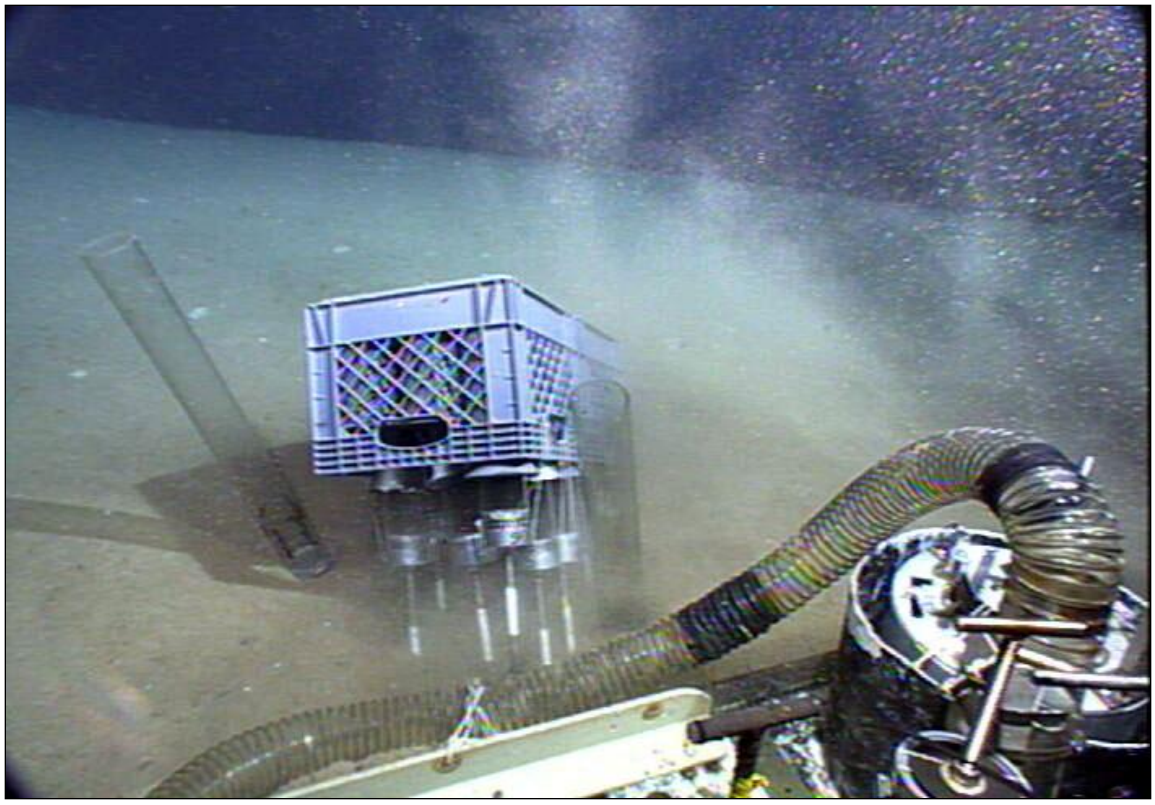

Figure 10-43. The core rack falls off *Jason II*.

We then moved to the northwest in search of a non-white-looking patch of pogonophorans. We found a non-white patch at 00:12 hrs (X-1502 m, Y-1239 m; this time is an ASNAP in the VV). This patch lacked the white-tube polychaetes as well as the purple sea cucumber. The small white snails were more visible on these pogonophorans. We took the other long core, two fat cores, and two short cores here. The second short core contained the rarer straight species of pogonophoran. [Unfortunately, all four fat cores were empty upon recovery; they apparently emptied during recovery of *Jason II* on the surface]. There was no large associated fauna, so we generally slurped around the patch to catch the tiny amphipods that were swimming around the pogonophorans (00:55 to 01:20 hrs). At 01:27 hrs, we fired the red Niskin while still sitting down at this location.

We moved back to Marker 1 and fired the green Niskin over the pogonophorans at 0.7 m altitude (01:40 hrs; X-1493 m, Y-1231 m). This patch was similar to the patch where the first cores were taken, with white tubes and Chirodota. We did an approximately 2.5 x 2.5-meter Scorpio mosaic of this area (01:52 to 03:02 hrs). At 3:11 moved a few m away from the pogonophoran bed and collected 7 control cores (X-1486 m, Y-1228 m). We returned to the pogonophoran bed around Marker 1 to collect the remaining cores. The vehicle had accumulated a lot of mud during the control coring and a cloud of suspended mud obstructed vision every time the vehicle or manipulator arm moved. The pilot moved *Jason II* up 7 m and spun it in circles for a few minutes to remove mud. At 04:33 we sat back down and collected 2 pogonophoran cores that were chosen to contain the rare straight-tubed species. We left this area to go back to the second coring location (non-white tubes) and take another mosaic. The VV gave an X,Y that was far to

the southeast (used the red Niskin event: 19997), so this objective was aborted at 05:28 hrs to head for the CRP and slurp mobile fauna along the way under the direction of Dr. Carney.

After collection of mobile fauna and upon arrival in the vicinity of the CRP at 08:15 hrs, extensive chemo communities, including dense aggregations of tube worms and apparently thriving mussel communities were seen on the flanks of the central crater. Mussel Pot F (Figure 10-44) was attempted but failed due to clockwise rotation past the anti-rotation post (the handle just spun after this) [to fix this for future dives the antirotation posts were shortened by 1 inch after recovery]. A mussel collection was taken into the Blue net and placed into the starboard bio box. Marker 7 was deployed as a CRP in this mussel bed (X-1155 m, Y-1248 m). At 09:38 hrs a mussel pot collection (MP A) was taken in a different mussel bed (X-1194 m, Y-1269 m). At 10:36 hrs (X-1189 m, Y-1266 m) a tube worm collection was made into the white net and placed in the port bio box (Figure 10-45).

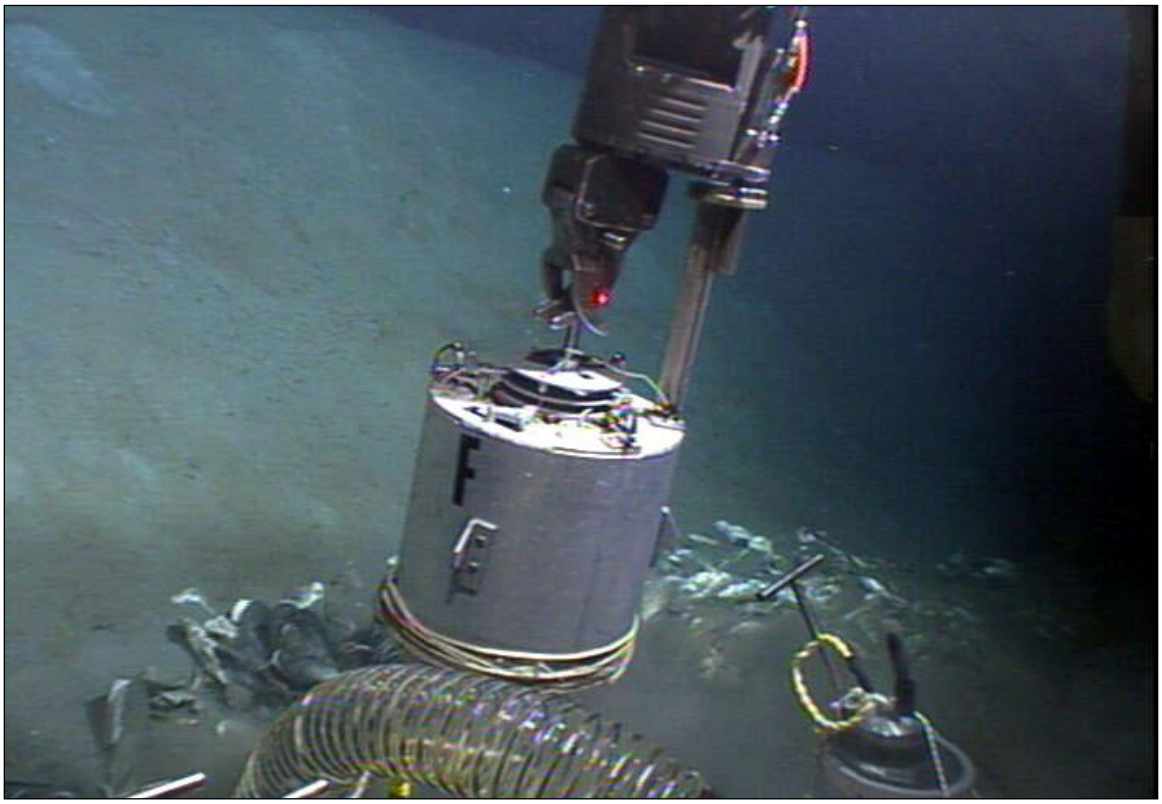

Figure 10-44. Mussel Pot F attempted collection.

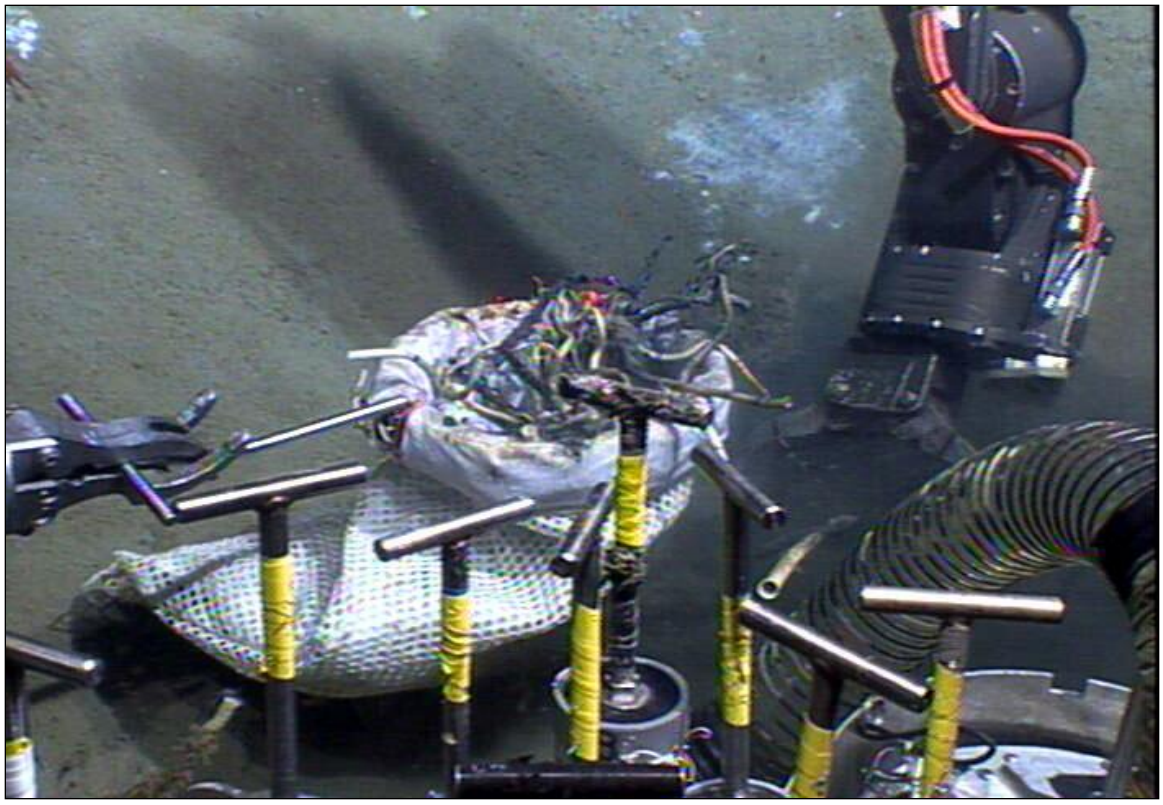

Figure 10-45. Tube worm collection with net.

At this point, transits between geo targets were initiated and Ian was contacted for initiation of Photo transects. The first photo transect started at 12:22 hrs. As is normal for the photosuvey, there were ten transects. Each transect was 50 m long at this site. The last photo transect ended at 14:49 and the *Jason II* left the bottom at 14:54 hrs. The dive track for dive 275 is shown in Figure 10-46.

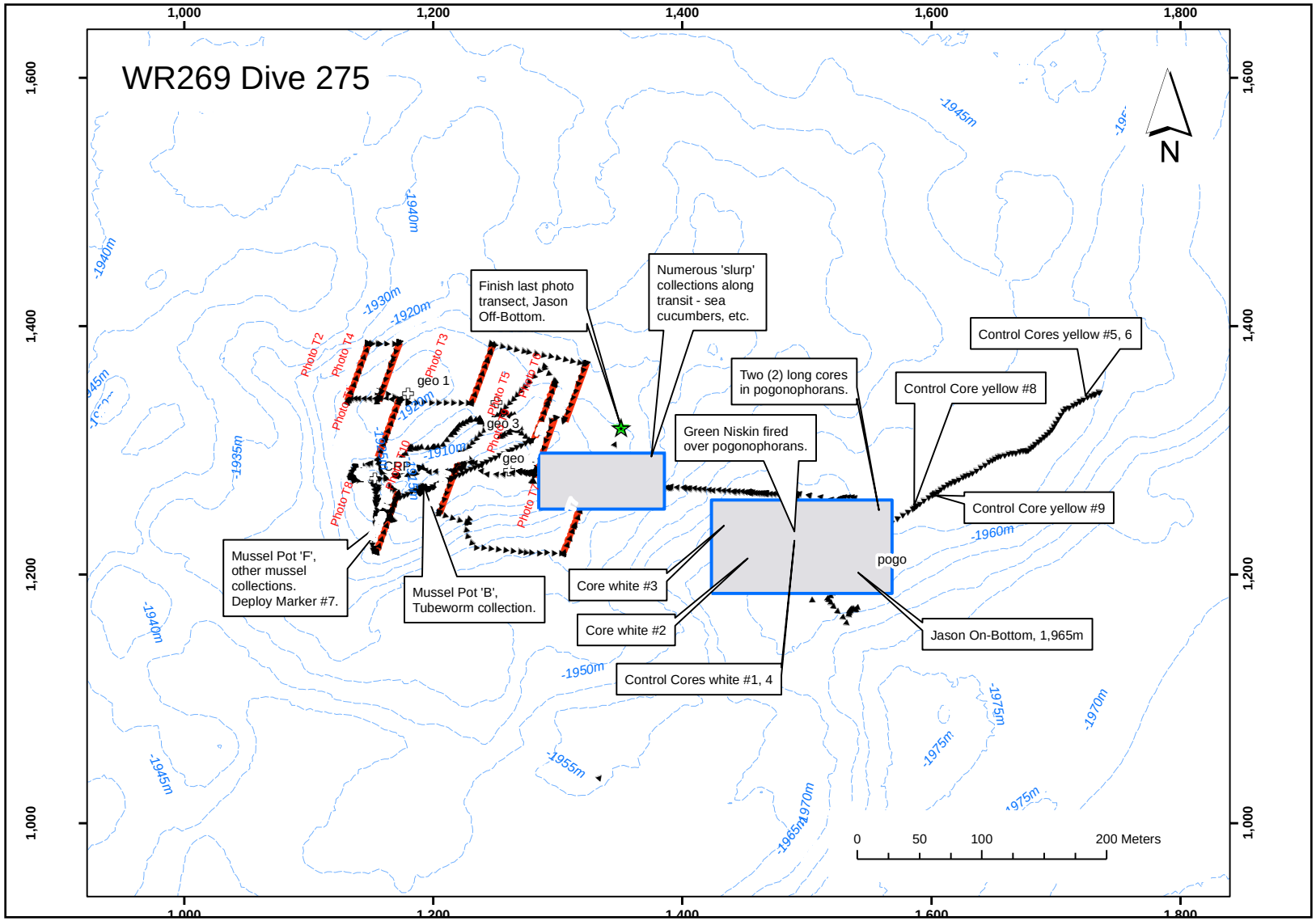

Figure 10-46. Dive 275 dive track.

10.6. Keathley Canyon 243

This site (KC243) was surveyed during the Recon Cruise and one *Alvin* dive took place at this site (AD4176) on 5/12/06. There were no *Jason II* dives at this site.

10.6.1. Site/Target Selection

This station is situated on a level area on a southwest oriented slope at approximately 1,610 m depths. The DSC reached the bottom and at 16:10 hrs on 12 March and collected images with a 12 second repeat rate until 19:13 hrs. A total of 747 images were collected with the bottom in view and acceptable navigation. The site showed good evidence for development of chemosynthetic communities including extensive bacteria mats, scattered and concentrated dead shells, and small patches of living mussels. Tube worms were observed as solitary individuals or small clusters in six photographs. Geological indications of seepage included extensive brine-staining and patches of carbonate. This site was considered as a good candidate for additional study (Figures 10-47 and 10-48).

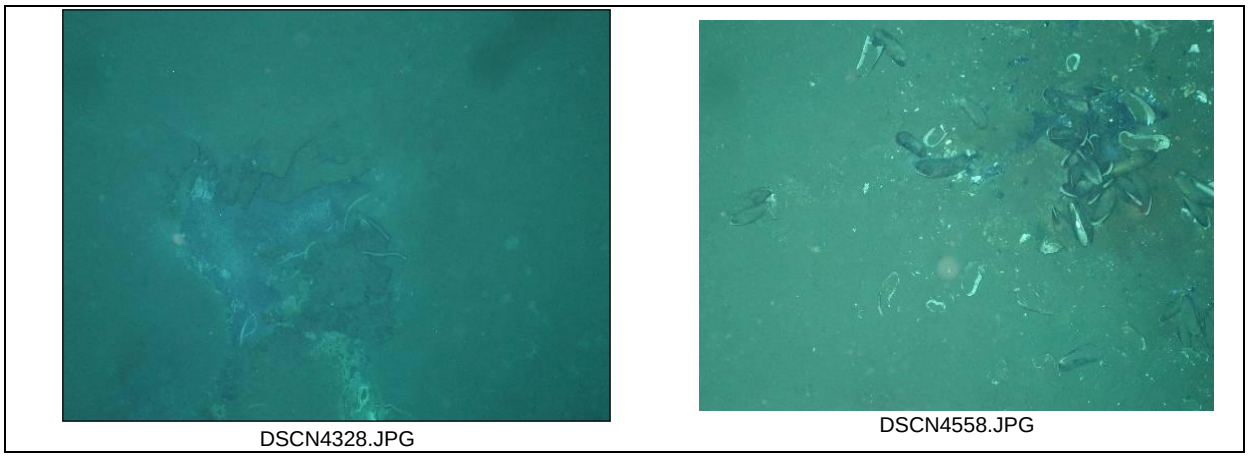

Figure 10-47. Representative photography from KC243.

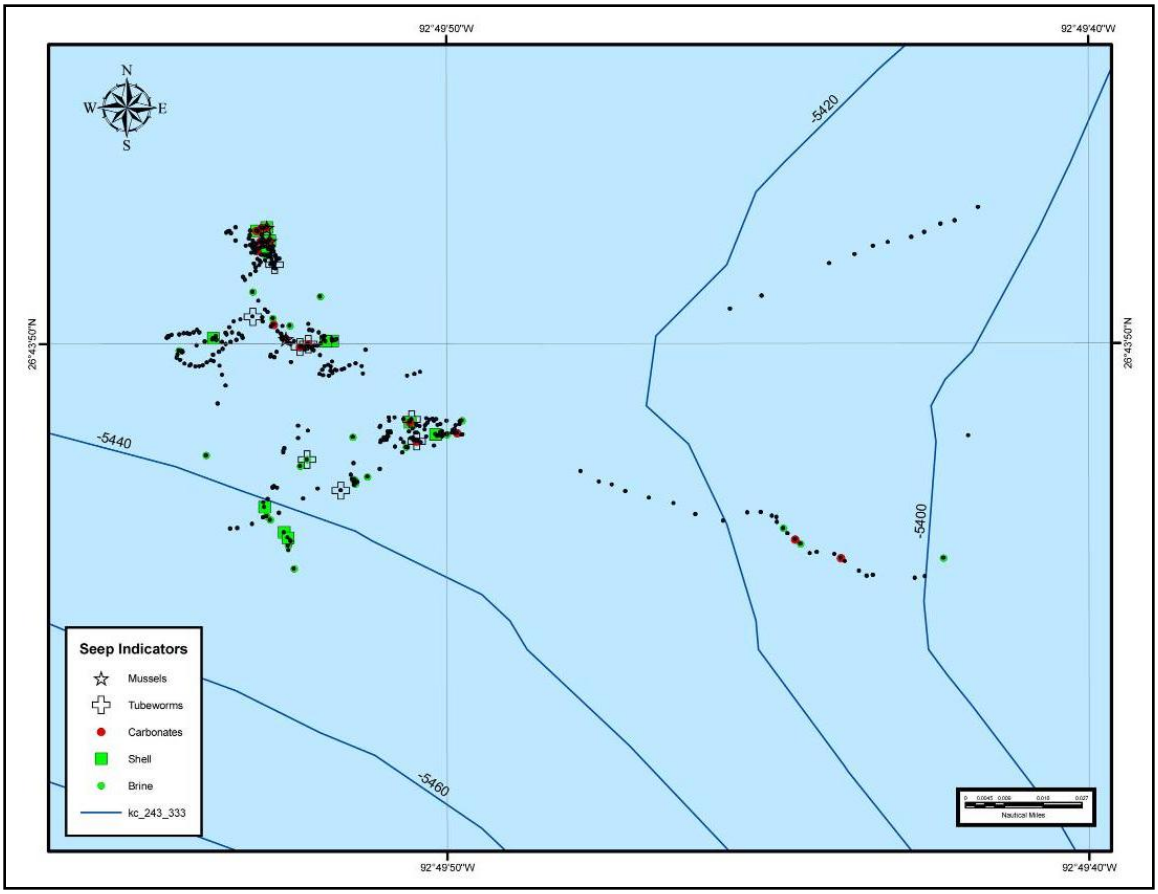

Figure 10-48. Survey results from KC243 station.

10.6.2. *Alvin* Dive 4176

Some dive navigation issues plagued the dive, but it was nonetheless quite successful. Dive 4176 was to the Keithley Canyon 243 site in 1,610 m water depth. This was a pilot-in-training dive, with only a single scientist on board. The scientist was Stephane Hourdez, who has extensive *Alvin* experience as well as GoM seep experience. Early in the dive the pilot was reaching for a site marker in the basket and hooked an oil compensation hose for the port manipulator. As a result this manipulator was compromised and could not be used at all during the dive and the oil leakage mandated a much-shortened dive. Several additional problems arose because the port manipulator is the primary manipulator for push coring and delicate tasks. The seep was located, tube worms (*Lamellibrachia sp nov*) and mussels (*B. brooksi*) were imaged. A bench marker was deployed. One mussel pot collection was made, additional mussels were collected using a net, and a single push core was taken, and two carbonates were collected. The down-looking digital camera was used to collect two lines of images for mosaicking, but time limitations prevented further work. The sub was called up early because of the hydraulic leak and surfaced at 14:30 hrs. Seawater incursion into the oil compensation system was slight and the sub was ready to dive on schedule on 13 May. This site is relatively small. We explored only part of it, due to a torn boot at the beginning of the dive and some issues with navigation and target positions. Most of the exploration was centered on markers 1 and 2. *Alvin* was called to the surface just after reaching Target 3 and little of that area was explored. Bench Marker 1 (X-162 m, Y-293 m) was

dropped at the beginning of the dive, about 160 m west of the mussel beds. A ball marker was dropped on the mussel bed as a reference for a mosaic. The biological findings were initially tantalizing. Some of the fauna are the same as we find at shallower sites and some are the same as the deeper sites The disappointment for the dive was the fact that the Chemical profiler from our German colleagues failed at depth. However, no damage was done, and we will be trying it again on the next dive. At the time, we planned to dive at this site one more time, in connection with one of our remaining transits to or from Mississippi Canyon. However, other discoveries and considerations made this our only visit to KC243. Figure 10-49 shows the dive track of *Alvin* and activities performed during the dive.

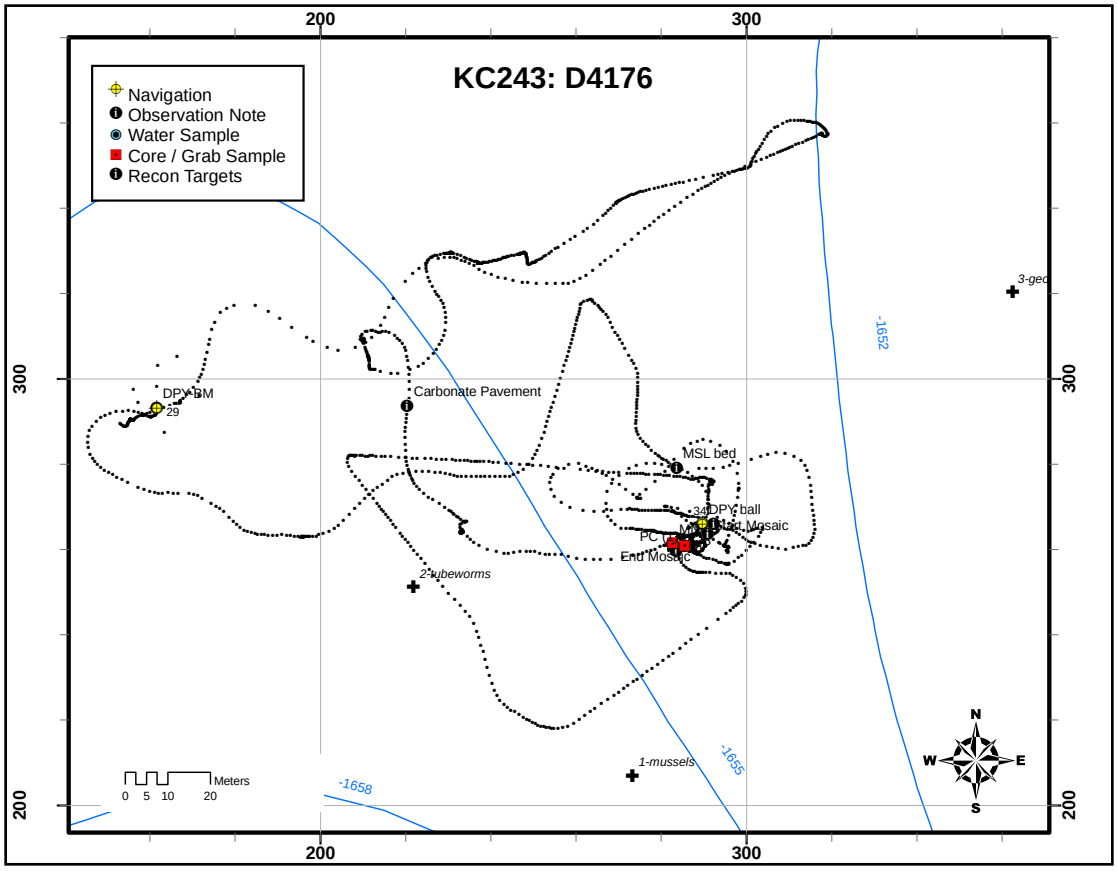

Figure 10-49. Dive 4176 on 5/12/2006 at an average depth of 1,610 m.

10.7. Green Canyon 852

This site (GC852) was surveyed during the Recon Cruise and was mapped by the Hugin AUV. There were 6 *Alvin* dives at GC852, including AD4177 on 5/13/06, AD4185 on 5/21/06, AD4186 on 5/22/06, AD4187 on 5/23/06, AD4189 on 5/24/06, and AD4190 on 5/25/06. There were also two *Jason II* dives, including J2-273 from 6/14/07 to 6/15/07 (41 hours, 9 minutes) and J2-278 (6/23-24/09, 36 hours and 6 minutes).

10.7.1. Reconnaissance Cruise

This station is arrayed along a steep-sided, north-south oriented ridge at 1,450 m. The DCS reached bottom at 04:04 hrs on 15 March and collected images with a 12-second repeat rate until 07:58 hrs. Survey coverage was focused along ridge-crest with relatively favorable sea conditions. A total of 1,054 images were collected with the bottom in view and acceptable navigation. The site contained probably the most prolific chemosynthetic community seen during the cruise and included a comparatively diverse array of chemosynthetic and heterotrophic fauna. Tube worms were widespread, mostly associated with large carbonates. Mussels were locally dense at several points. Development of carbonates was impressive and clearly indicates prolonged seepage at this site. The combination of hard substrata and topographic relief favored the colonies of deepwater coral. Gorgonians of several species were widespread. Live bamboo coral was seen at several points and pieces of another species of branching coral could be seen on the bottom around the boulders. This site was considered to be a high-priority candidate for additional study (Figures 10-50 and 10-51).

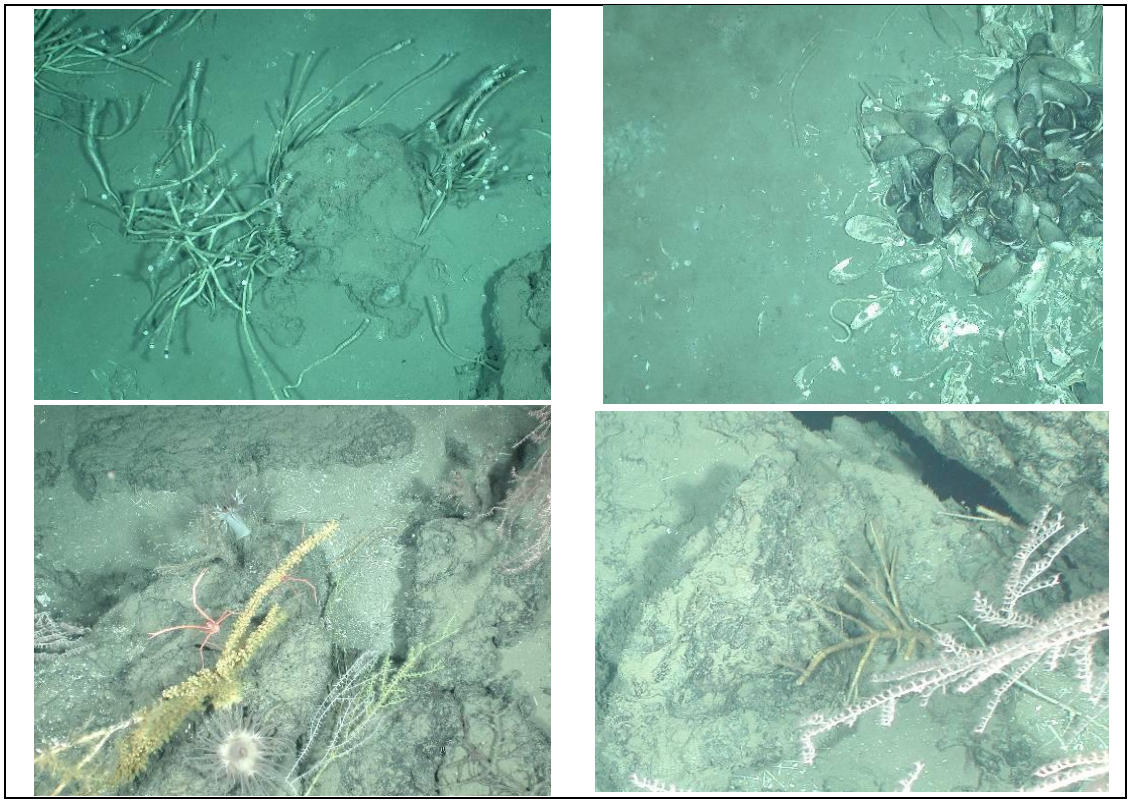

Figure 10-50. Representative photography from GC852.

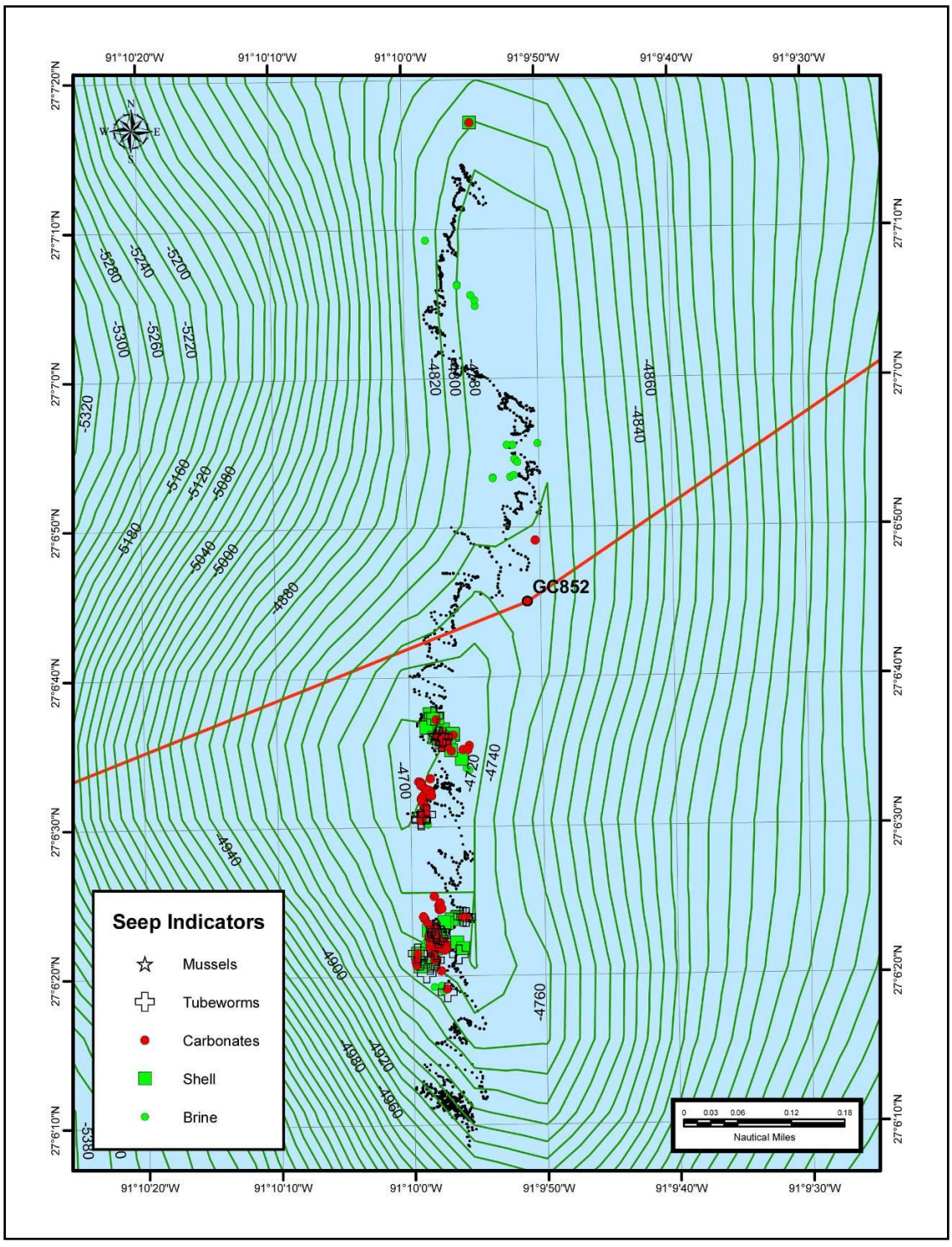

Figure 10-51. Survey results from GC852 station.

10.7.2. Navigation Considerations

We determined the Northing (Y) and Easting (X) in m for this selected CRP in the local coordinate system in which *Jason II* would work. We did this by applying a geodetic False Northing and Easting to the standard UTM Zone 15 projection for the WGS84 datum, then calculating the local X and Y from the latitude and longitude of the site CRP as measured from the AUV survey. These are the same Falsings used for the local projection of the dives at this site with *Alvin* in the previous year. The local coordinates thus calculated and assigned to the site CRP were X = 424 m and Y = 2,190 m. We placed this CRP target into *Jason II*'s navigation system along with targets of interest positioned by *Alvin* last year and targets positioned by a geologic review of the AUV contour map (Figure 10-52).

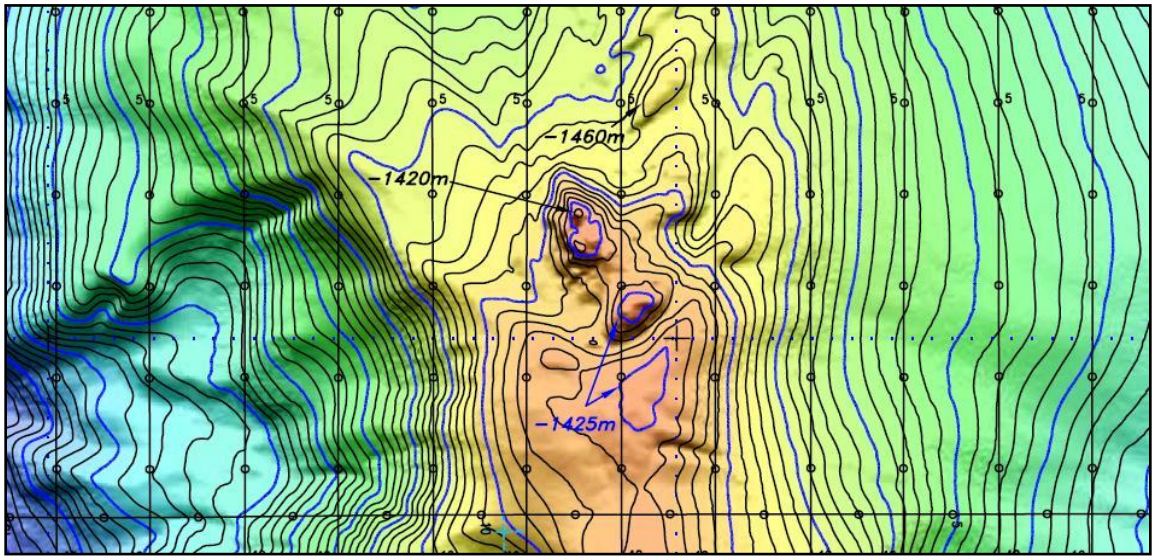

Figure 10-52. The topographic-high used for defining a Central Reference Point at site GC852.

We defined the following for this site in WGS84 datum:

Geodetics False Northing: -2,999,016.02 m
Geodetics False Easting: -181,418.40 m
Local Origin Northing: 2,999,016.02 m
Local Origin Easting: 681,418.40 m.

Targets developed for this site are listed in Table 10-9.

Table 10-9

Target Locations for Site GC852

Target	Latitude	Longitude	Local X (m)	Local Y (m)	Depth (m)
Local Origin	N27 06.100000	W091 10.200000	0	0	
1-tubes_mussels	N27 06.320018	W091 09.962236	387	412	1400
Marker #1	N27 06.378595	W091 09.969147	374	520	1407
Marker #2	N27 06.639749	W091 09.937658	419	1,003	1405
Marker #5	N27 06.662141	W091 09.910665	463	1,045	1409
Marker #6	N27 06.370928	W091 09.962616	385	506	1407
Marker #8	N27 06.649550	W091 09.941734	412	1,021	1405
Coral Site	N27 06.600533	W091 09.961898	380	930	1398
CRP	N27 07.282385	W091 09.924148	424	2,190	1420
geo 1	N27 07.223863	W091 09.921471	430	2,082	1440
geo 2	N27 07.198850	W091 09.872252	512	2,037	1423
geo 3	N27 07.121873	W091 09.866247	524	1,895	1428
geo 4	N27 07.152695	W091 09.945630	392	1,950	1422
geo 5	N27 07.049405	W091 09.915240	445	1,760	1433

Targets listed prior to the CRP are targets from the *Alvin* cruise last year. Targets listed after the CRP (the "geo" targets) are ones selected on this cruise by a review of the geophysical information available to us on the cruise.

10.7.3. *Alvin* Dive 4177

Ian MacDonald was the port observer and Monika Bright the starboard observer. This site has both chemo communities and coral communities. The primary objectives of this dive centered on imaging. MacDonald's rotary time-lapse camera was deployed in an active seep area with both mussels and tube worms in the field of view. A baited trap was also deployed in the field of view of the camera. The camera deployment was documented with the down looking digital still camera. A bench marker was deployed. This was also the first dive with a functioning hand held Cool Pix macro camera. Thirty-six macro photos of tube worms and mussels were taken, and the new lighting system produced very nice pictures. A mussel pot was attempted, but the giant size of the mussels at the site made this difficult and operator error resulted in a partially closed pot. A net of mussels and associated fauna was collected as a backup, and six push cores were taken in this area. A small tube worm collection was also made. Navigation was excellent throughout the dive. Bernie Bernard's ongoing efforts to merge navigation files and improve compatibility between *Alvin* and other navigation systems have paid off. The dive ended early because the batteries were depleted. The sub surfaced at 14:20 hrs. The short dive was in part a result of the fact that the dive was to a relatively shallow site (with resultant longer working bottom time) and in part due to the relative inexperience of the new pilot and a heavy hand on the stick. We will revisit this site with 3–4 additional dives (Figure 10-53).

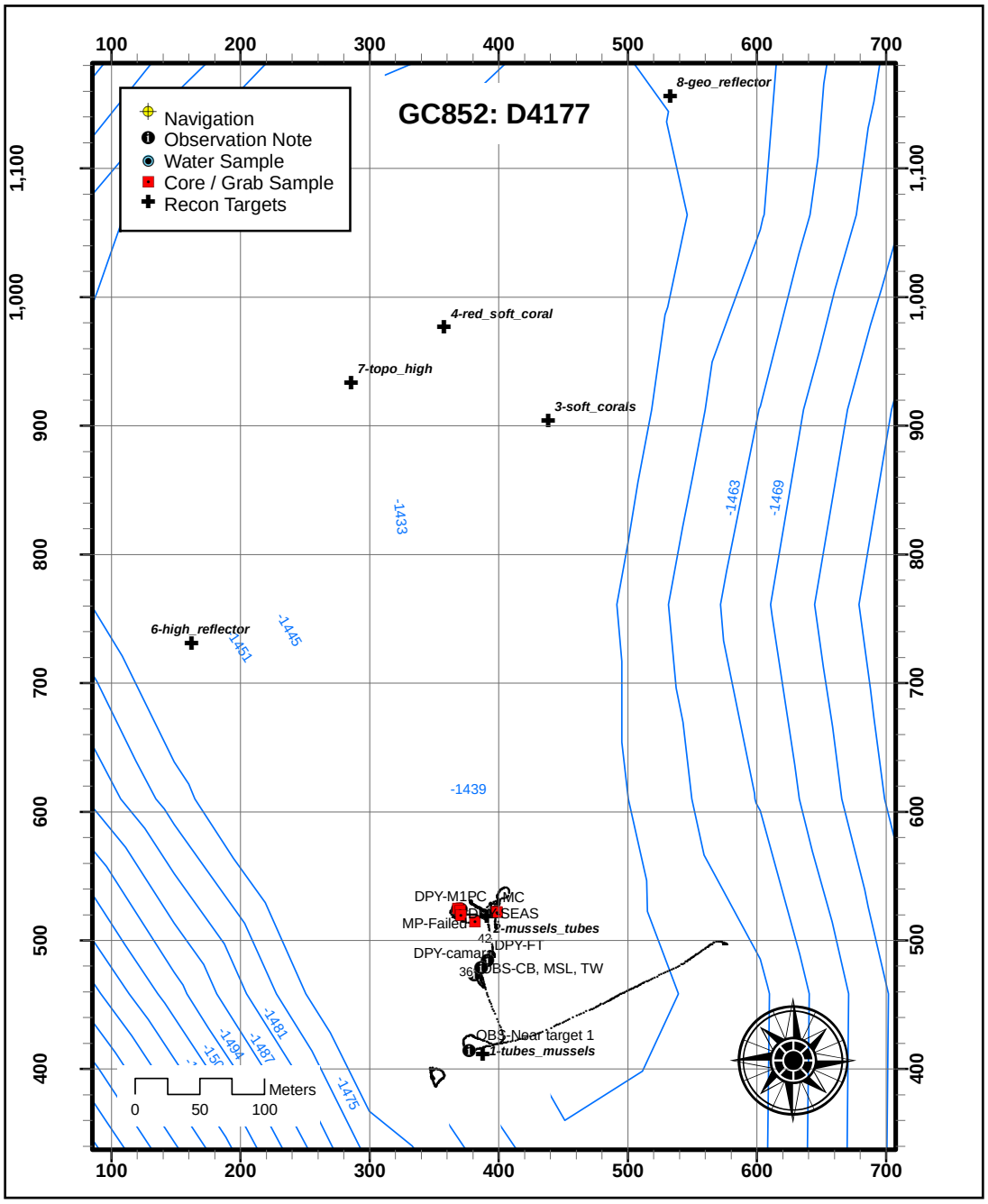

Figure 10-53. Dive 4177 on 5/13/2006 at an average depth of 1,450 m.

10.7.4. *Alvin* Dive 4185

The pilot for this dive was Mark Spear. Observers were Monika Bright and Cheryl Morrison. This was not a very productive dive, as a lot of time was spent in transit. The first activity was to attach floats to Ian MacDonald's camera that had been deployed on an earlier dive. The camera floated to the surface, was retrieved without problems, and the pictures were downloaded once on deck. A lot of time was spent in reconnaissance of the area looking for coral communities. The following samples were acquired during the dive: 1) one crab trap that was in front of the camera, 2) two rocks with attached anemones, 3) one rock with attached sponge, 4) one large crab, and 5) one large soft coral colony. The coral colony was not spotted until the end of the dive. Therefore, only one colony was sampled. An additional dive was planned for the following day (Figure 10-54).

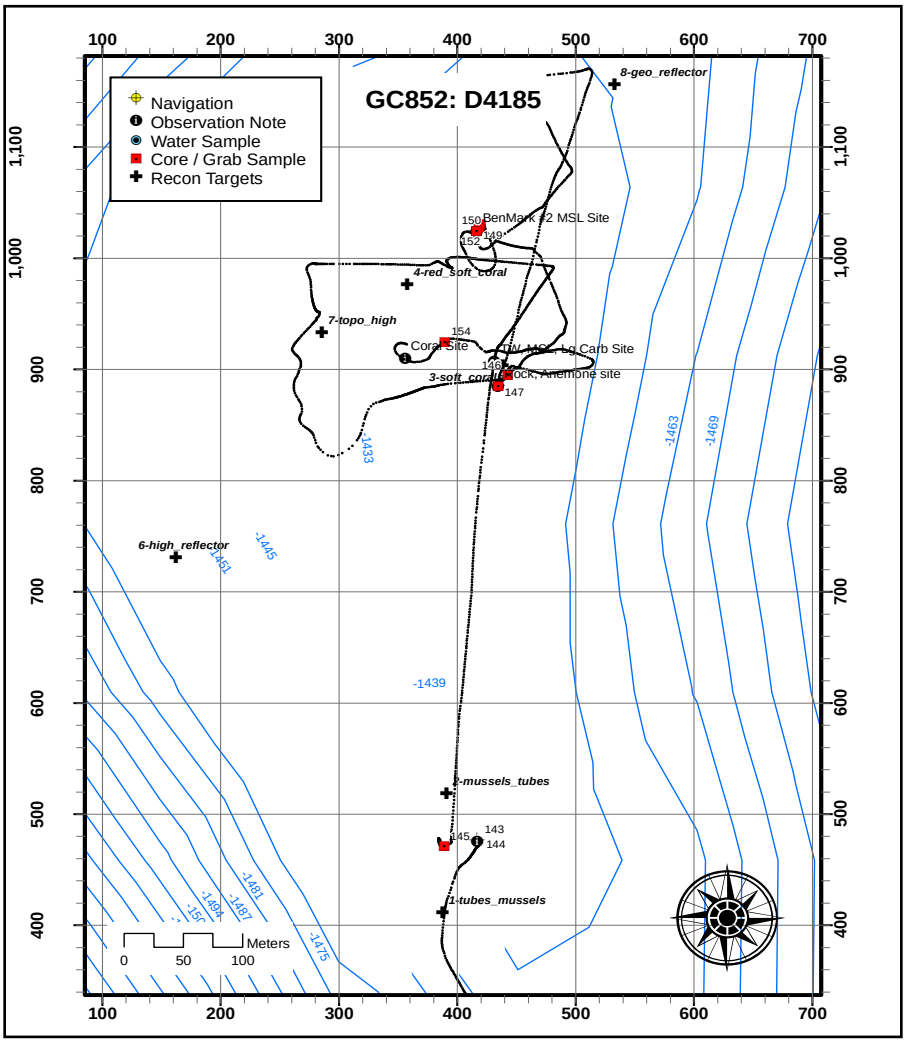

Figure 10-54. Dive 4185 on 5/21/2006 at an average depth of 1,410 m.

10.7.5. *Alvin* Dive 4186

The pilot was Pat Hickey. The observers were Chuck Fisher and Erin Becker. The focus area of the dive was the mounded area at the south end of the overall anomaly. This is the area where most of the collections have been made so far. This is also the area where the initial benchmark and Ian's camera were deployed. Somewhere in this region is an active oil seep. Prior to the dive this morning, we watched oil droplets rise to the sea surface spread into elongate shapes as they were acted on by the wind and local surface currents. We have observed oil on the surface all day.

Today the dive objectives centered on staining tube worms and collecting a whole tube worm bush with the Bushmaster sampler. The following samples were collected: 1) one Bushmaster sample, 2) one mussel pot sample, 3) one slurp sample containing scale worms and a shrimp, 4) one authigenic carbonate sample. We also deployed the fish trap and stained two tube worm bushes. At the end of the dive, the *Alvin* transited to near the crest of the southern mound. A soft coral was collected on a rocky surface, but the dive did not reach the top of the mound where the oil seep may be occurring. We planned to dive at this very productive site again the following day (Figure 10-55).

10.7.6. *Alvin* Dive 4187

The pilot was Bruce Strickrott and the observer was Stephane Hourdez. Only one observer was on this dive because it was a pilot-training dive . The pilot-in-training was Sean Kelley. The objectives of the dive were to collect tube worms, stain tube worm bushes, take digital pictures with the Cool Pix camera, and explore the areas where soft corals were spotted and sampled on yesterday's dive. Sampling activities centered around the mound-like topographic feature at the southern end of the overall area for surface anomalies identified on the 3-D seismic reflectivity maps. Most of the sampling took place close to the benchmark site that was occupied at the beginning of the dive for navigation purposes. Some pilot-training dives are not very productive because time is spent training the new pilot and sampling may not be as efficient as it could be with an experienced pilot. Today was a notable exception. Many samples were collected and the overall dive turned out to be highly productive. The following samples were collected during Dive 4187: 1) one Bushmaster sample of a tube worm colony, 2) one mussel pot, 3) one scoop of mussels, 4) one authigenic carbonate sample. Two tube worm aggregations were stained and a variety of digital and high-resolution photos taken. At the end of the dive, a mosaic was shot of the hard-bottom area at the top of the mound where soft corals were observed and sampled (Figure 10-56).

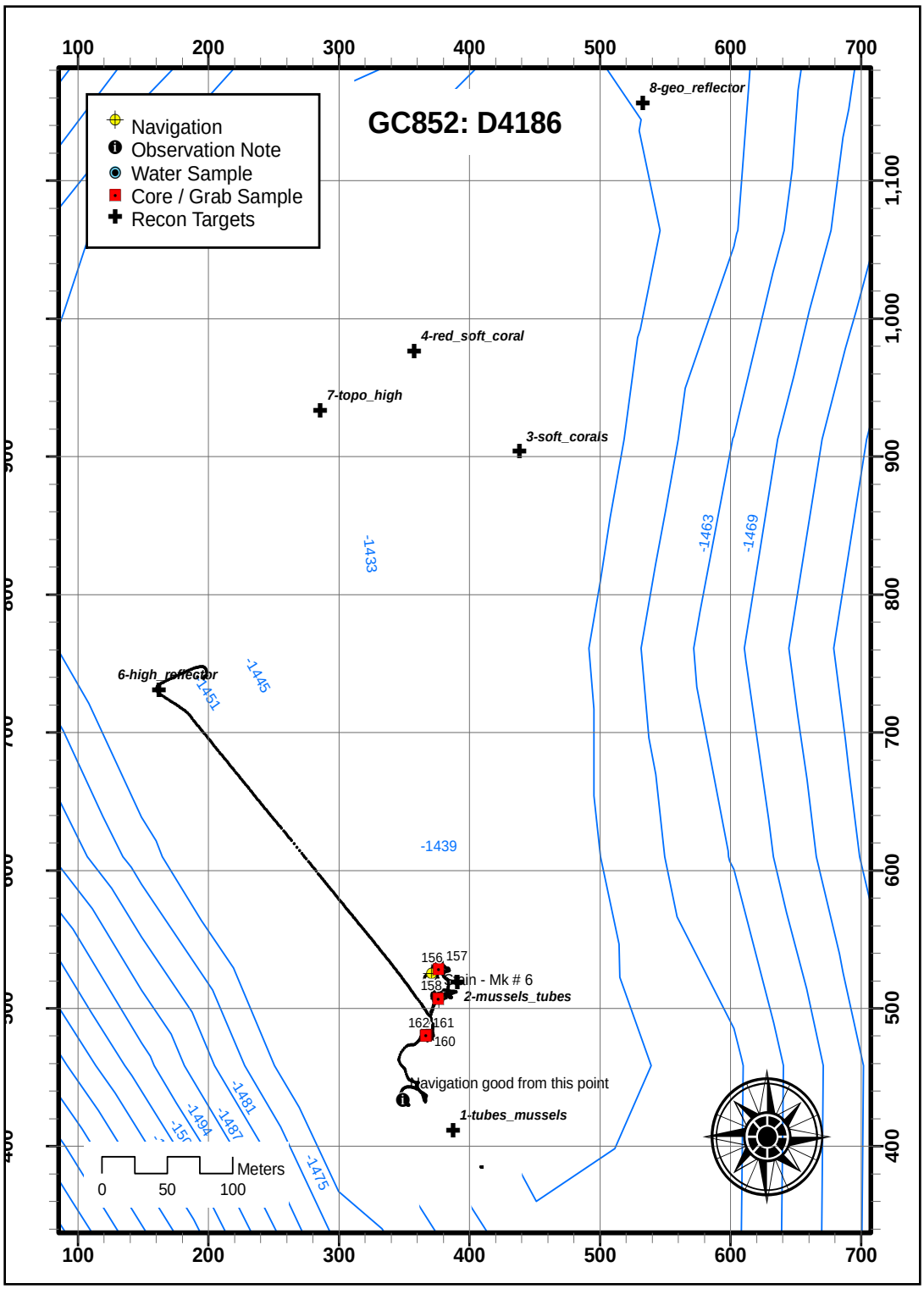

Figure 10-55. Dive 4186 on 5/22/2006 at an average depth of 1,410 m.

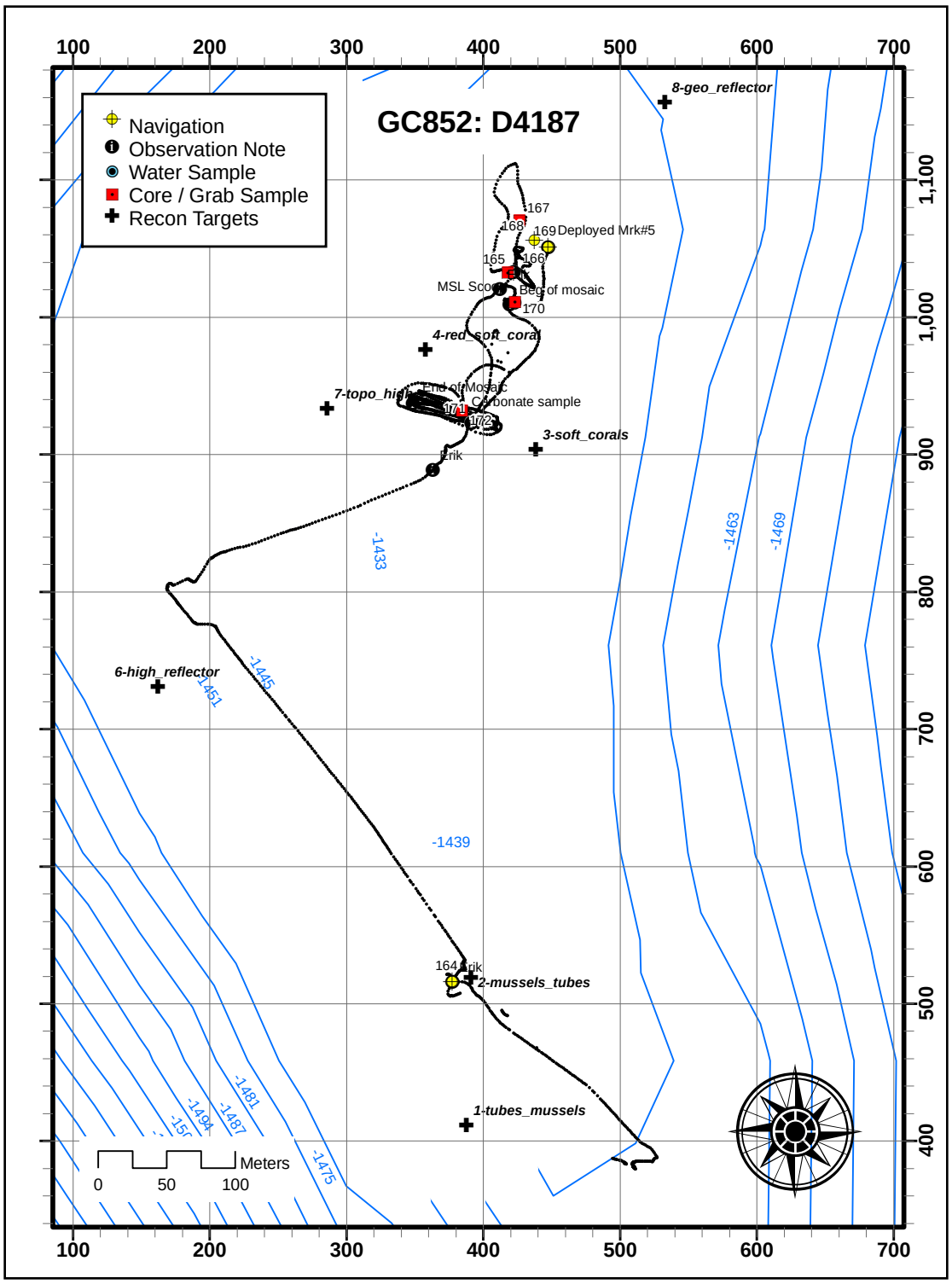

Figure 10-56. Dive 4187 on 5/23/2006 at an average depth of 1,410 m.

10.7.7. *Alvin* Dive 4188/89

The pilot was Gavin Eppard and the observers were Cheryl Morrison and Ian MacDonald. A short on *Alvin* battery A necessitated aborting the first dive at 500 m depth and recovering the *Alvin*. It was relaunched about 1.5 hours later. The objectives for the dive were to recover a time-lapse camera, image, collect corals and carbonates, and take pushcores with an associated Niskin water sample. Most objectives were accomplished despite the shortened dive. The following samples were collected during Dive 4189: 1) 10 pushcores in bacterial mats, 2) 2 Niskins, 3) assorted corals and carbonates, and 4) a variety of digital and high-resolution photos (Figure 10-57).

10.7.8. *Alvin* Dive 4190

The pilot was Mark Spear and the observers were Bob Carney and Meaghan Bernier. This has been such a productive site that it is hard to leave. By the end of the last dive the hard coral site had not been found, even though we had a position from Dive 4187. So, today one of the objectives was to find the hard coral site and photograph, as well as sample them. It was thought from previous dives that two species were observed. In addition, during this dive, Ian's camera was to be deployed and the Seas experiment and the fish trap were to be picked up. Push cores were also to be taken. Unfortunately, because of navigation problems, some of the dive time was spent trying to rectify the sub's navigation net. The strong current we encountered on previous dives was also a factor. It made positioning the sub for sampling a difficult task. Regardless they were able to sample the soft and hard corals. The hard coral was an unknown species to those onboard (Figure 10-58).

The following tasks performed: 1) collected two soft corals and one hard coral, 2) picked up the Seas experiments, 3) deployed Ian's camera (will pick up next year), 4) collected five Niskin bottle samples, 5) took Cool Pix pictures, and 6) picked up fish trap (contained one crab and one isopod). A final trawl sample will be taken over GC852 before making the 4-hour transit to the Walker Ridge site.

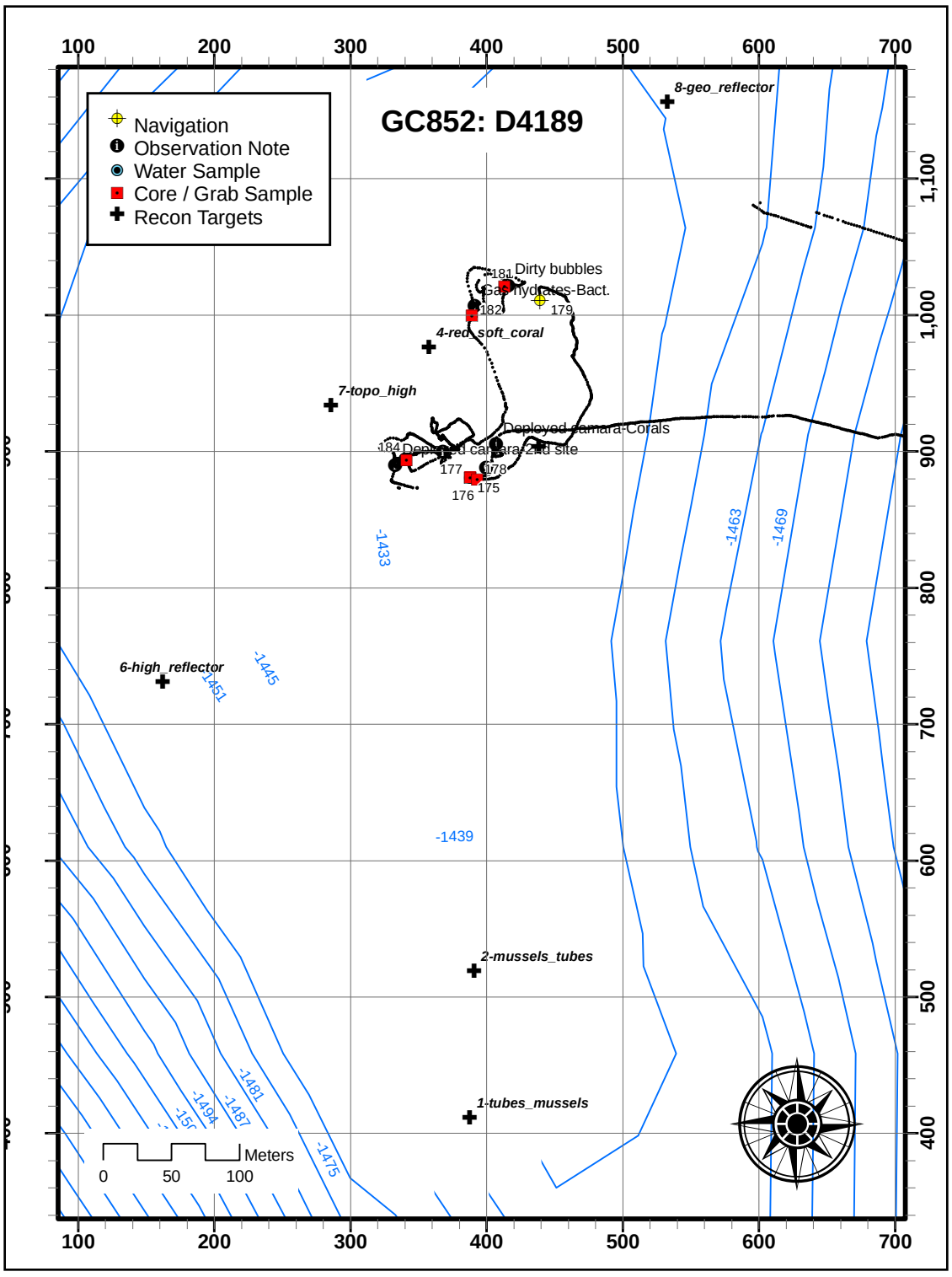

Figure 10-57. Dive 4189 on 5/24/2006 at an average depth of 1,410 m.

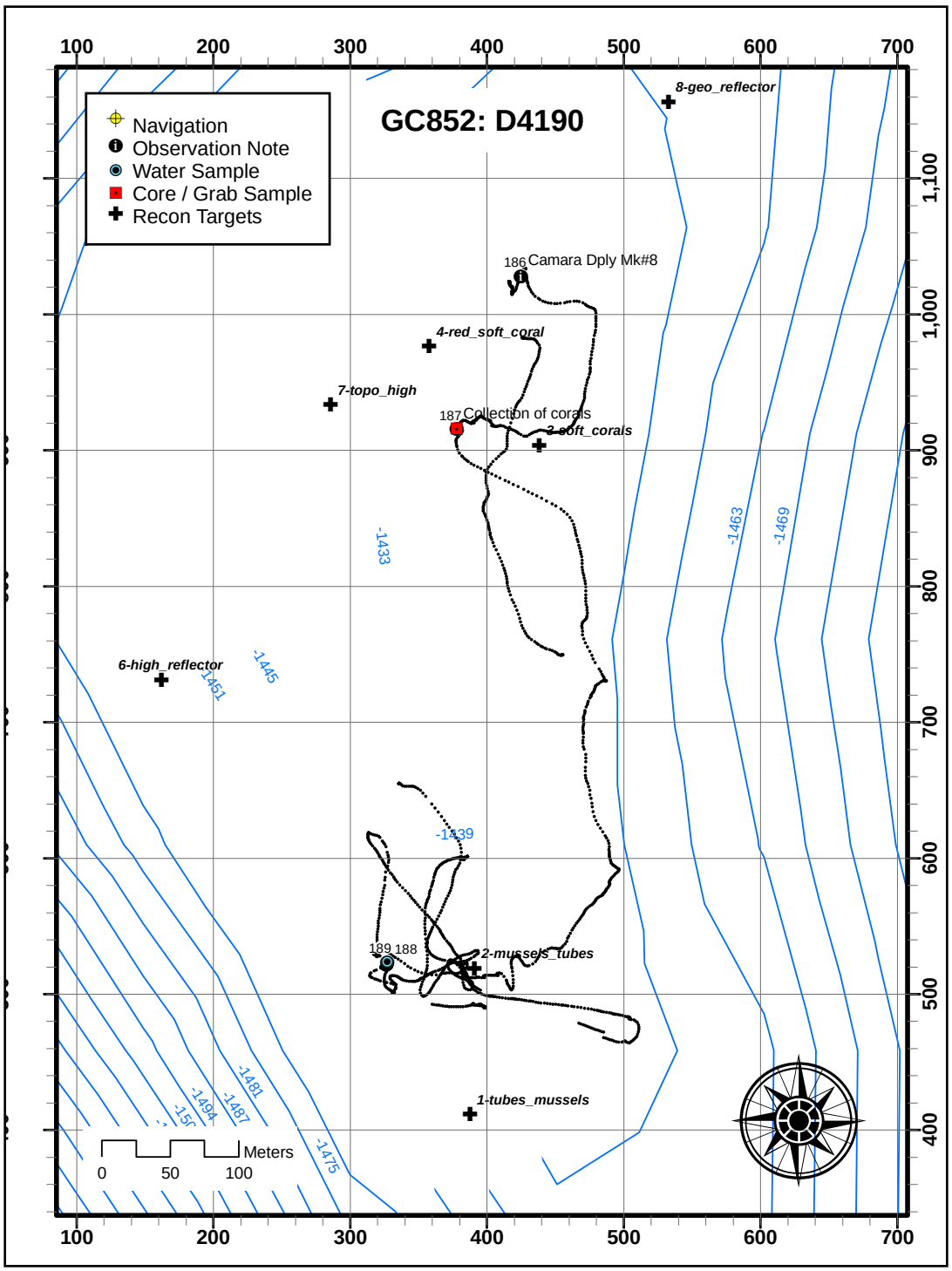

Figure 10-58. Dive 4190 on 5/25/2006 at an average depth of 1,410 m.

10.7.9. *Jason II* Lowering 273

After the LBL net was calibrated at this site (see the *LBL Calibration* section for details of the procedure), *Jason II* was deployed into the water at 20:44 hrs EDT (local time) on 13 June. All times and dates in this summary are reported in EDT. The sea-bed at 1,457 m was reached at 20:55 hrs and event logging was initiated by the watch-stander on duty using *Jason II*'s VV event logger system. Refer to Dive Observations for this dive in the Appendix 7 for a detailed log of the observed events and their times in GMT.

We occupied the location of the tentative CRP at 21:01 hrs and reset the Doppler navigation to this point. We then verified that we were on the top of the topographic dome and deployed Marker #3 at this revised CRP point (X-470 m, Y-2,183 m) at 21:31 hrs. We then headed for target Geo 1 at 21:34 hrs while logging observations of fish, gorgonians, anemones, and shrimp. We occupied Geo 1 at 21:53 hrs, and then headed to target Geo 2. We arrived in the vicinity of Geo 2 at 22:24 hrs, continued to explore, and stopped to collect a Munidopsis with the suction sampler at X-538 m, Y-2,034 m. We also grab-sampled an anemone, a crab, and a small branch of bamboo coral (Figure 10-59). We logged a "best-of" marker for the video footage we gathered in this process. We headed toward target Geo 4 at 23:35 hrs. We started moving to target Geo 3 at 00:00 hr of 14 June, while logging observations of skate, bacterial mats, ctenophores, shrimp and black coral. We collected a carbonate collection with apparently attached tube worms (X-188 m, Y-1795 m) at 01:48 hrs. We made collections of various benthic fauna by suction sampler from 03:18 (X-389 m, Y-968 m) until about 04:20 hrs.

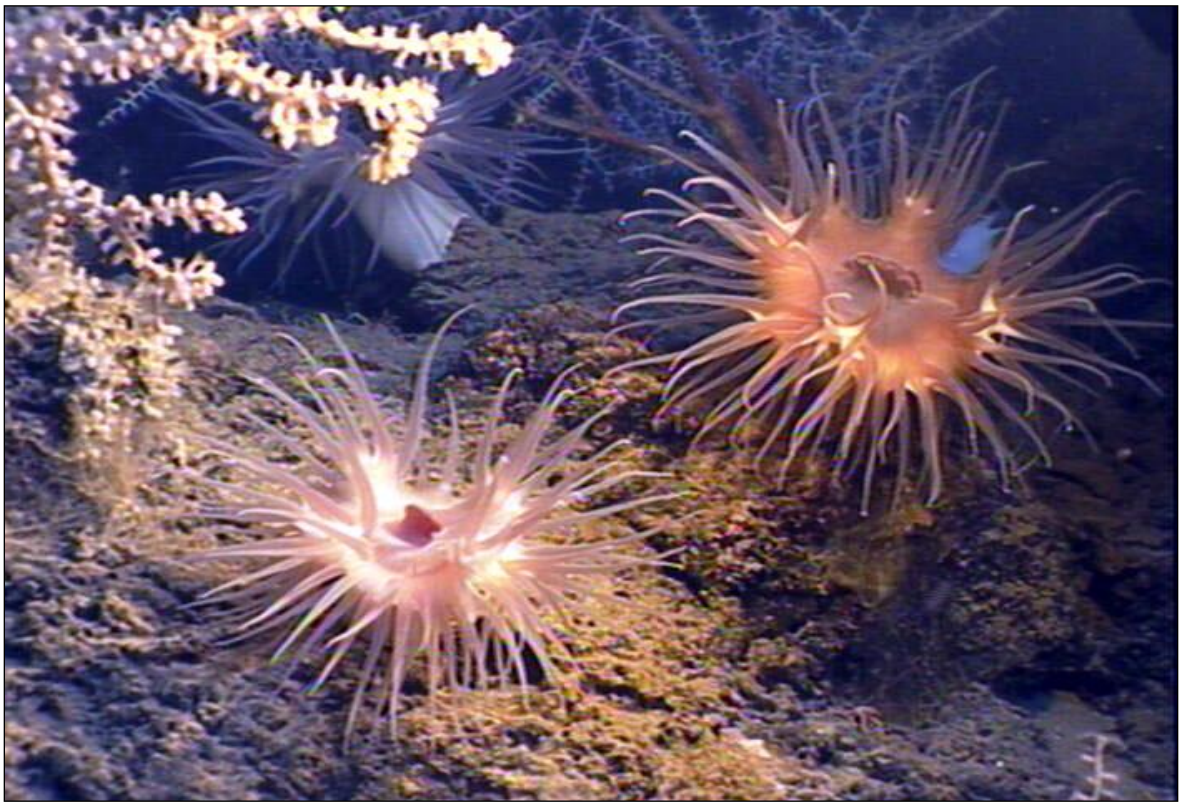

Figure 10-59. Anemones and coral.

Shortly after this, we arrived at the central coral site and then took a navigation fix on some golden coral (X-361 m, Y-918 m) at 04:53 hrs. We began to head for the elevator at 05:18 hrs. The elevator was located at 06:10. The camera on the elevator is not functioning and will not be deployed. We helped the elevator come free of the sea-bed at 06:36 hrs and moved it to the vicinity of Ian's camera, where it was set on the bottom at 07:18 (X-387 m, Y-1029 m). We then looked for Ian's camera which had been previously deployed at Marker #8, and came across Marker #2 at 08:12 hrs (X-425 m, Y-1026 m). We spotted Marker # 8 and occupied it (X-454 m, Y-1038 m) at 08:16 hrs. Mussels were collected into the white net from the bed within 2 m of Marker #8 and a Ball Marker with blue tape on the polypro line was deployed at this site, X-451 m, Y-1031 m, into the spot of our mussel collection. [Note that the navigation fixes were off by about 1 km from this point during the dive until after return to the sea floor following the elevator recovery. These were fixed during a second post-dive renavigation of the data] The stained tube worms associated with marker 8 were then collected (X-454 m, Y-1032 m) at 09:36 hrs (Figure 10-60). We fixed a new position for Marker #8 at X-454 m, Y-1029 m, then occupied Marker #5 (X-462 m, Y-1054 m) at 09:58 hrs. (After renav, this position is about 20 m different from the fix taken on D278).

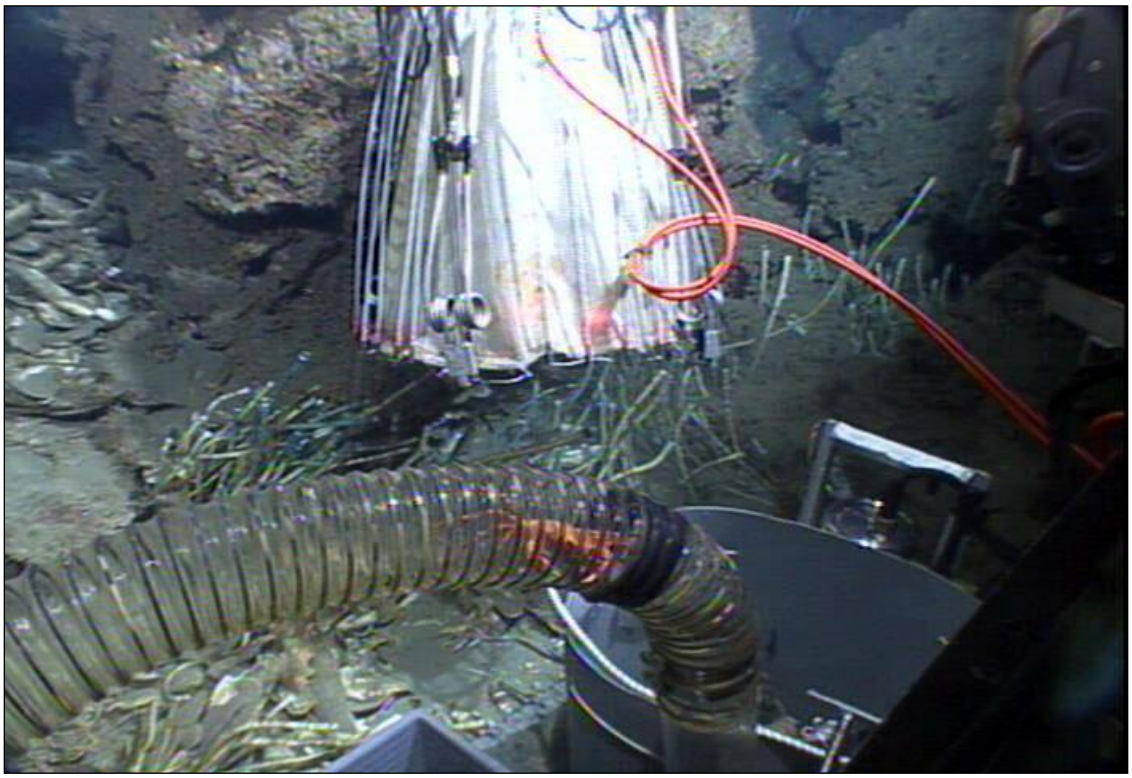

Figure 10-60. Bushmaster collection at stained tube worm site.

We collected a "red" core set at X-463 m, Y-1051 m in a bacterial mat, from 10:14 to 10:51 hrs, then acquired video and still pictures of mussels. Mussels were collected into the blue/black net and a Ball Marker deployed here for future chemistry (X-466 m, Y-1052 m) at 11:46 hrs. We moved to Ian's camera deployed in 2006 and confirmed it was flooded. The homer probe was operational. We retrieved Ian's camera from X-442 m, Y-1,020 m at 12:11 hrs, and placed it on the elevator. We confirmed that Ian's new camera was not flashing and needs to be sent back to

the surface. We swapped core racks at the elevator so we could take another set of cores at this site. The mussel collections and some of the coral collections were loaded on the elevator into its bioboxes. The elevator was released at 13:58 hrs and *Jason II* went into lay-back mode, waiting for recovery of the elevator. The elevator was secured on the deck of the ship at 15:15 hrs and *Jason II* began transit to the coral site.

We arrived near the northern edge of the main coral site at 15:37 hrs and decided to take a series of fixes to delineate the perimeter of the coral area. For this operation the *Jason II* heading is always in towards the center of the coral site and we crabbed around its entire perimeter, using the sonar to watch locations of carbonates and the drop-off in elevation, while keeping all significant coral colonies in front of *Jason II*. A total of 12 coral fixes ("coral 1" to "coral 12") were taken between 15:37 and 16:40 hrs. Number 12 was adjacent coral 1 (imaging the same carbonate and corals). The corals are abundant and dense on the north, west and southwest edges of this patch. The bathymetry drops off immediately on the west edge (the corals are thick right up to the drop-off). On the southwest corner of the patch the corals extend off the top of the hill and down off the edge for about 15 m. On the east edge, the corals do not extend to the edge of the topographic high, and the density of the corals is generally lower. All of this was well documented on video during this survey. After finishing the perimeter run, we obtained images for a photo-mosaic in the central area of the coral community beginning at 17:17 hrs. *Jason II* was tugged off-site by the ship at 20:43 hrs and resumed the mosaic at 21:53 hrs. The mosaic was completed at 22:22 hrs. We began acquiring macro-camera photographs of corals at 22:24 and used this camera until it was stowed at 00:48 hrs. A series of photo transects that centered on the coral area began at 01:18 hrs of 15 June and was completed at 03:54 hrs. We identified a site suitable for coring of briney sediments at 04:50 hrs, took a few DSC images and then triggered the Niskin bottles 1.3 m off the sea floor at 05:07 hrs, (X-449 m, Y-912 m).We then collected 8 cores in this area. We saw gas bubbles emanating from the sediment due to our coring activities. This coring effort was completed at 05:51 hrs and we initiated transit to Marker 5 for a stained tube worm collection.

The stained tube worms at Marker 5 were located at 06:15 and macro images were acquired of the stained worms until 06:31 hrs. The previously stained tube worms (from Marker 5, at X-448 m, Y-1066 m), were then collected in several grabs and stowed in the starboard biobox, ending at 06:54 hrs. We then transited south towards Marker #1 for other planned collections. We occupied Marker #1 at 08:11 hrs, fixing its position at X-378 m, Y-518 m. We then located a site for a mussel-pot collection, but had inadvertently pinned the mussel pot with one of *Jason II*'s front-spikes, and ended up shearing the set-screw that engages the T-handle with the sprocket of the mussel pot. This meant that we could not effectively close the pot after insertion, so we abandoned this effort at 08:58 hrs. We then found Marker #6 (stained worms) at 09:11 hrs (and identified its location as X-380 m, Y-498 m). We used the suction sampler to collect shrimp for hemolymph analyses and also began the collection of a red crab at 09:32 hrs. The red crab fought the sampler and remained in the hose for hours, occasionally getting our attention and the attention of the pilot. Although the pilot was unable to force the crab into the chamber of the sampler during the dive, it was recovered in the sampler on the surface. At 09:40 hrs we set up to Bushmaster a stained tube worm collection. The Bushmaster collection was completed at 10:13 (X-384 m, Y-499 m). One additional stained aggregation remains at this location, about 2 m away from Marker #6. We began our transit to the dead (ops) transponder at 10:26 hrs, and the

competition between the *Jason II* pilot and the crab captured our attention for over an hour as we continued to work, with the crab (Figure 10-61) finally outlasting the pilot (still in the house at this time), as the pilot ended his shift at 11:45 hrs. This saga is documented in the Observations log of this dive.

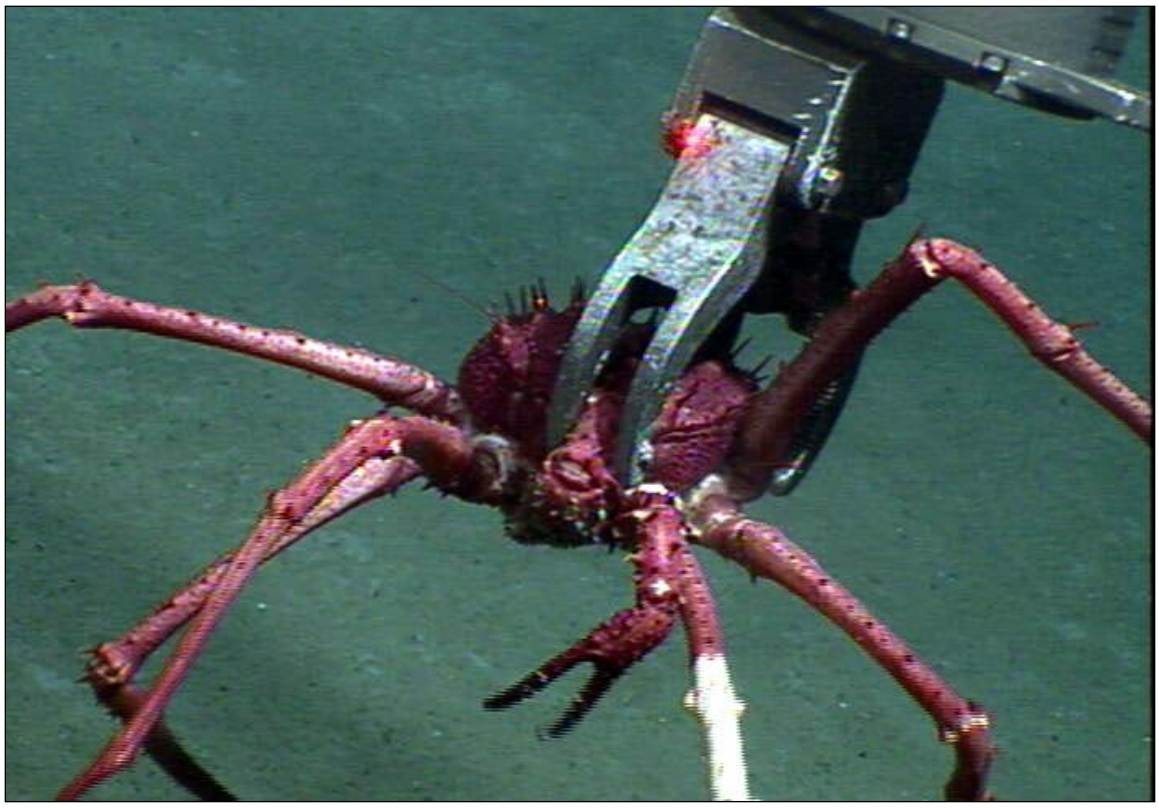

Figure 10-61. The one that got away.

The non-responsive LBL transponder was located at 13:17, and *Jason II* headed to the surface at 13:57 hrs. on 15 June.

The background fauna at GC852 was found to be extremely sparse on mud bottom. On a transect from the southern to northern end, only 3 possible holothuroids were observed. Mobile animals were largely restricted to rocky areas. Legs from a large Paralomis-type crab were sampled in a rocky area at the southern end of the transect. At the northern end where corals and chemosynthetic organisms were found, rattails and Geryonid crabs were observed. One crab was sampled along with several galatheids off the rock surfaces. The dive track for dive 273 is shown in Figure 10-62.

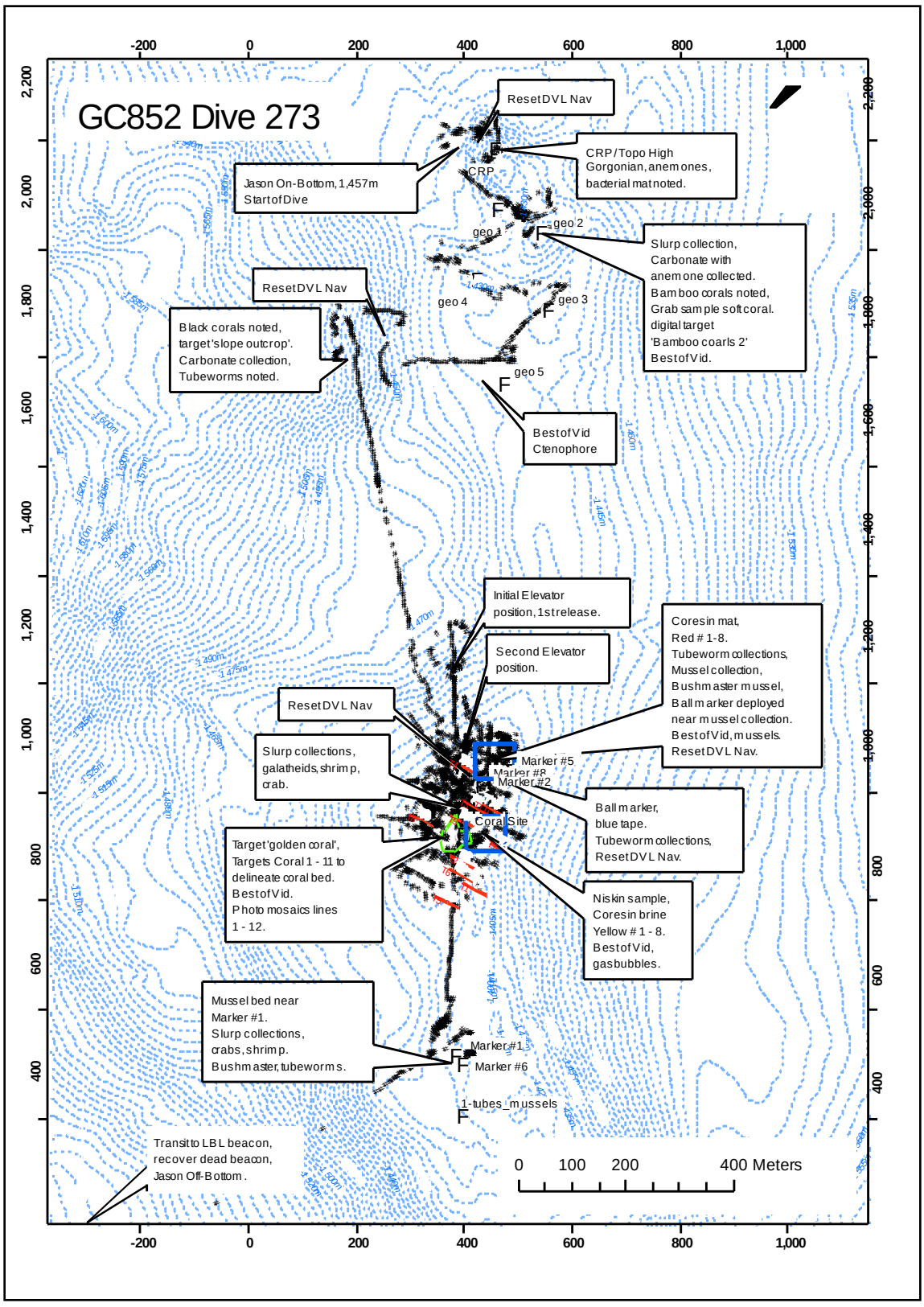

Figure 10-62. Dive track for D273.

10.7.10. *Jason II* Lowering 278

Time in water:	2007/06/23 06:15Z
Time on bottom:	2007/06/23 07:05Z
Time off bottom:	2007/06/24 19:11Z
Time out of water:	2007/06/24 20:09Z
Water Time:	37 hrs 55 minutes
Bottom Time:	36 hrs 6 minutes
Min. working depth:	1336.89 m
Max. working depth:	1426.02 m
Produced:	3.8 GB of raw vehicle data
Produced:	~59 DVDs of Science video
Produced:	~59 DVDs of Archive video

We arrived on station for our final planned dive at GC852 at 0100 local time on 6/23. An elevator was planned to deploy two rotary cameras and recover push cores and a set of hard corals early in the dive. Due to a last-minute failure of a connector on one of the cameras, the elevator was deployed with only a single camera (Figure 10-63) at 0130 hrs local time. *Jason II* was launched shortly afterward and arrived at the sea floor at about 0300. During descent, the mass spectrometer was initiated and determined to be functioning.

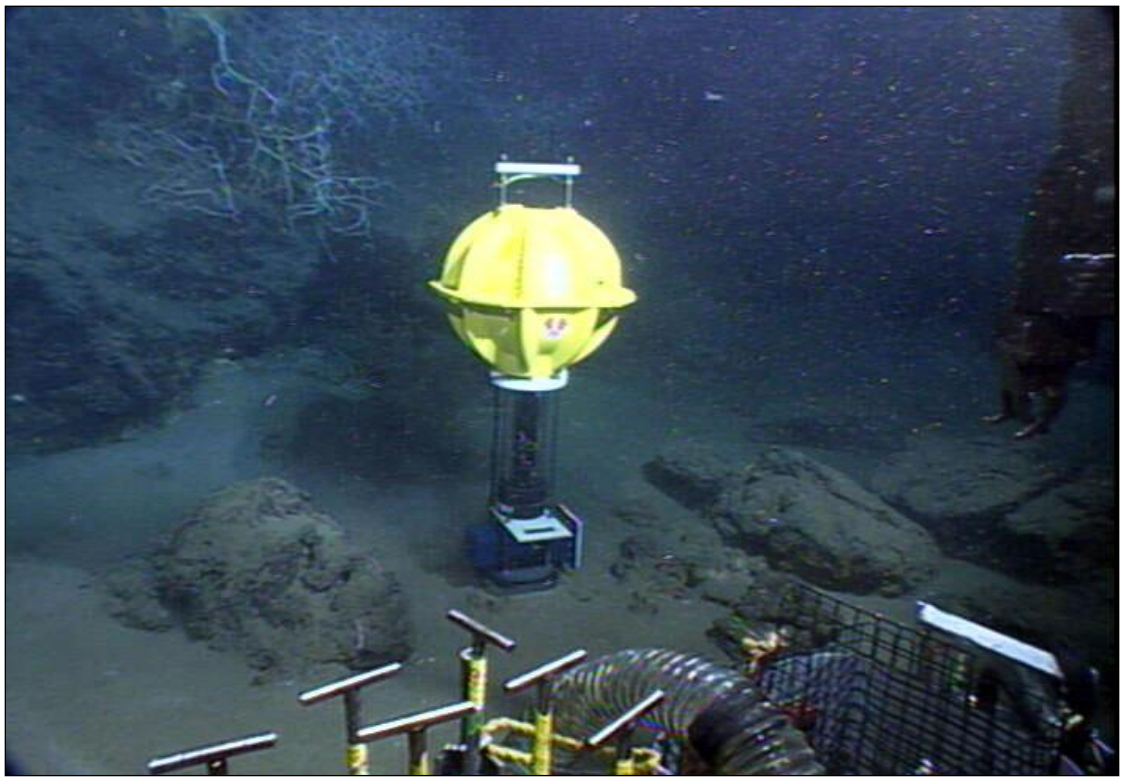

Figure 10-63. Rotary camera deployed for 2 months at coral bed.

The rotary camera was offloaded and deployed for a two-month deployment among corals at 04:49 hrs (X-373 m, Y-923 m.). The decision was made by Ian and Chris in the van to make the coral collections without waking Chuck or Erik because Chris was aware of Cheryl Morrison's

project requirements. Attempts were made to collect pieces of different colonies of *Madrepora* and *Lophelia* into separate compartments of the transfer basket, as well as what appeared to be another hard coral (Figure 10-64). This did not go smoothly and was rather destructive to the corals due to their extreme fragility. Upon recovery, there was one small piece each of living *Madrepora* and *Lophelia* in one compartment of the basket, and a specimen of a calcareous gorgonian in the other side. Coral collections were completed at 06:30. *Jason II* returned to the vicinity of the elevator and the control pushcores for this site were taken under the direction of Marshal between 06:41 and 06:51 hrs. The coral basket was loaded into one of the bioboxes on the elevator, and the pushcores into the wooden box and the elevator released for ascent to the surface at 07:36. While waiting for the elevator, a spider crab was collected into the port biobox for Dr. Carney. The elevator was recovered onto *Ronald Brown* and *Jason II* got underway back towards the general area of marker numbers 8, 5, and 2.

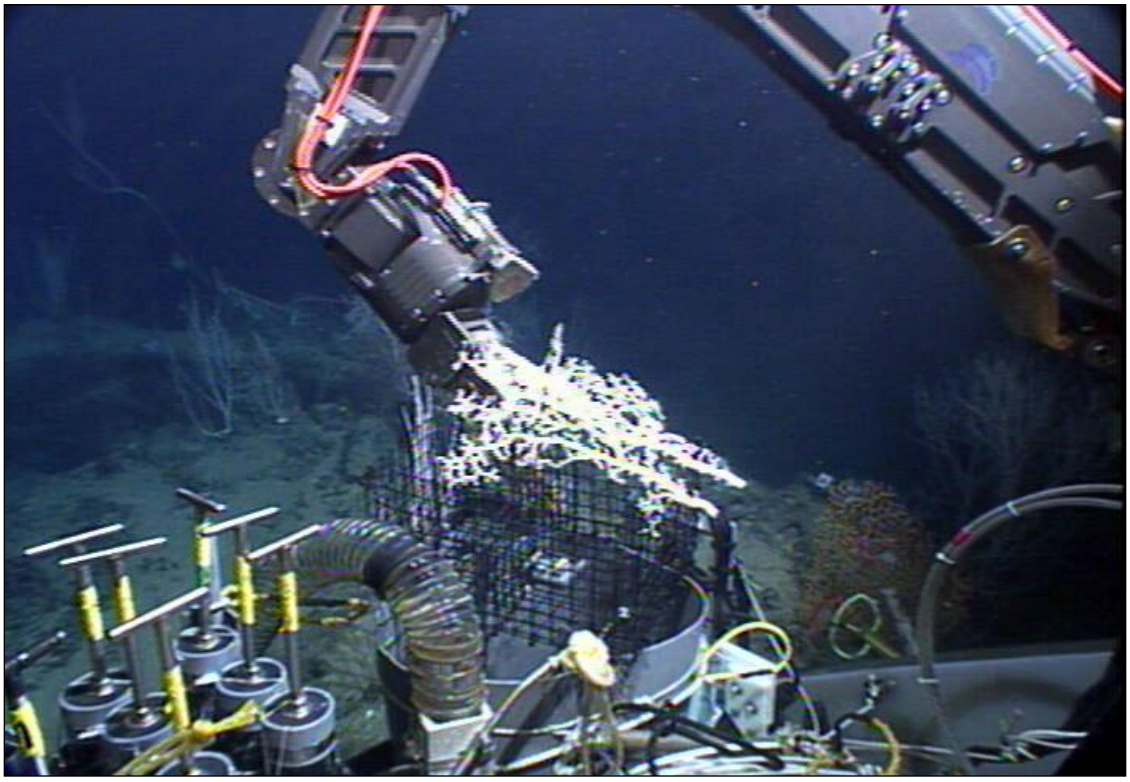

Figure 10-64. Coral collections.

We took three mass spectrometer scans in a small mussel near Marker 5 beginning at 09:40. This fix is approximately 24 m to the east of where it was expected, so we began to look for Marker 8 with this offset. Marker 8 was located with about a 17 m offset to the east, along with the ball marker indicating the mussel bed sampled on *Jason II* dive 273. This mussel bed was scanned with the mass spectrometer four times from 10:10 to 10:53 hrs. We then moved to X-466 m, Y-1034 m and began to survey another group of mussels whose shells showed obvious white staining. These were surveyed with the mass spectrometer (Figure 10-65) from 11:00 until 11:57 hrs. It was not possible to achieve a secure set-up with *Jason II* to make a mussel pot collection here, although it was attempted for about 10 minutes.

Figure 10-65. Mass spectrometer readings over mussel bed.

After firing both of the Niskin bottles in this location, we began the search for another group of mussels with obvious white staining. Most of the mussel aggregations in this area are found among the carbonates and difficult to reach. A likely group was located at X-459 m, Y-1051 m and the group was surveyed with the mass spectrometer from 13:11 until 14:34 hrs. After completing the chemical characterization of this group, a mussel pot collection was made and then the port biobox opened for collection of a few additional mussels under conditions of temperature insulation (for symbiont ribonucleic acid (RNA) analyses). Upon opening the box, this watch was surprised to find it occupied by the large spider crab. In order to make room for the mussels, a leg was removed from the crab (for stable isotope analyses) and it was set free. The additional mussels from this white patch were collected into the small white net and stored in the port bio box. Two additional mass spectrometer scans were completed beneath the mussel collection to determine if the chemistry at the sediment surface beneath the mussels was different from that analyzed previously. *Jason II* then proceeded to another patch of mussels (X-457 m, Y-1015 m) and the group was chemically surveyed from 17:07 until 18:09 hrs. After surveying this group, 6–8 of them were collected into the port biobox (on top of the net). During this collection, some very young mussels were spotted among the carbonates about 10 m away. After the collection. the *Jason II* proceeded towards these and found they were in the middle of a very large (approx 8 x 20 m) and thriving patch of mussels on the underside of a small carbonate ledge.

Very distinctive in this area were large patches of small mussels apparently partially encased in carbonates and covered with a white fluffy material that appeared to be a sponge. A carbonate ledge covered with small mussels and this "fluff," with good access for the submersible was located (X-464 m, Y-1014 m) and identified for chemical scanning (from 18:44 to 20:01 hrs, macro camera photography, and sampling (of carbonates and mussels). We then searched for another group of mussels to chemically survey, passing by Marker #2 again en route. During the transit, background readings were recorded with the mass spectrometer wand in the water column. Another small, dark patch of mussels was located at X-458 m, Y-1015 m and chemically profiled from 21:32 to 22:35 hrs.

Following the chemical sampling, *Jason II* transited to the coral site to image and sample another patch of hard corals. We traveled at a heading of approximately 225 degrees in the direction of the western edge of the photomosaic where we had previously observed a large colony of *Madrepora* that had not been previously sampled. In transit, we passed over another carbonate outcrop containing bamboo corals and other gorgonians at X-439 m, Y-1008 m. We reached the coral site at 22:59 hrs. We began imaging the corals with the macro camera at X-362 m, Y-916 m. We noticed the area where *Enallopsammia rostrata* had been collected with *Alvin* the previous year only a few m away. After taking images, a small piece of *Madrepora* was collected into the starboard biobox at 23:33 hrs. *Jason II* lifted off the bottom and a careful survey of the area was conducted to ensure that it was all part of one Madrepora colony, and did not consist of separate settlement events. After we were satisfied with this conclusion (indicating that it was unnecessary to continue physical sampling of the same coral colony), we proceeded to the central point for the SM2000 survey.

Calibration of the SM2000 began at 00:01 hrs, and the survey began at 00:27 at X-279 m,Y-816 m at a heading of 0° and 5 m altitude. After 12 lines, with the odd-numbered lines heading north and the even-numbered lines heading south, the survey was completed at 05:10 and a tie line was run parallel to the rest at a heading of 270°.

After comparing the processed SM2000 and Hugin AUV multibeam data, it appears that a positional offset similar to that observed in AT340 (see Figure 3, D269 AT340) exists between the two surfaces (see Figure 10-66).

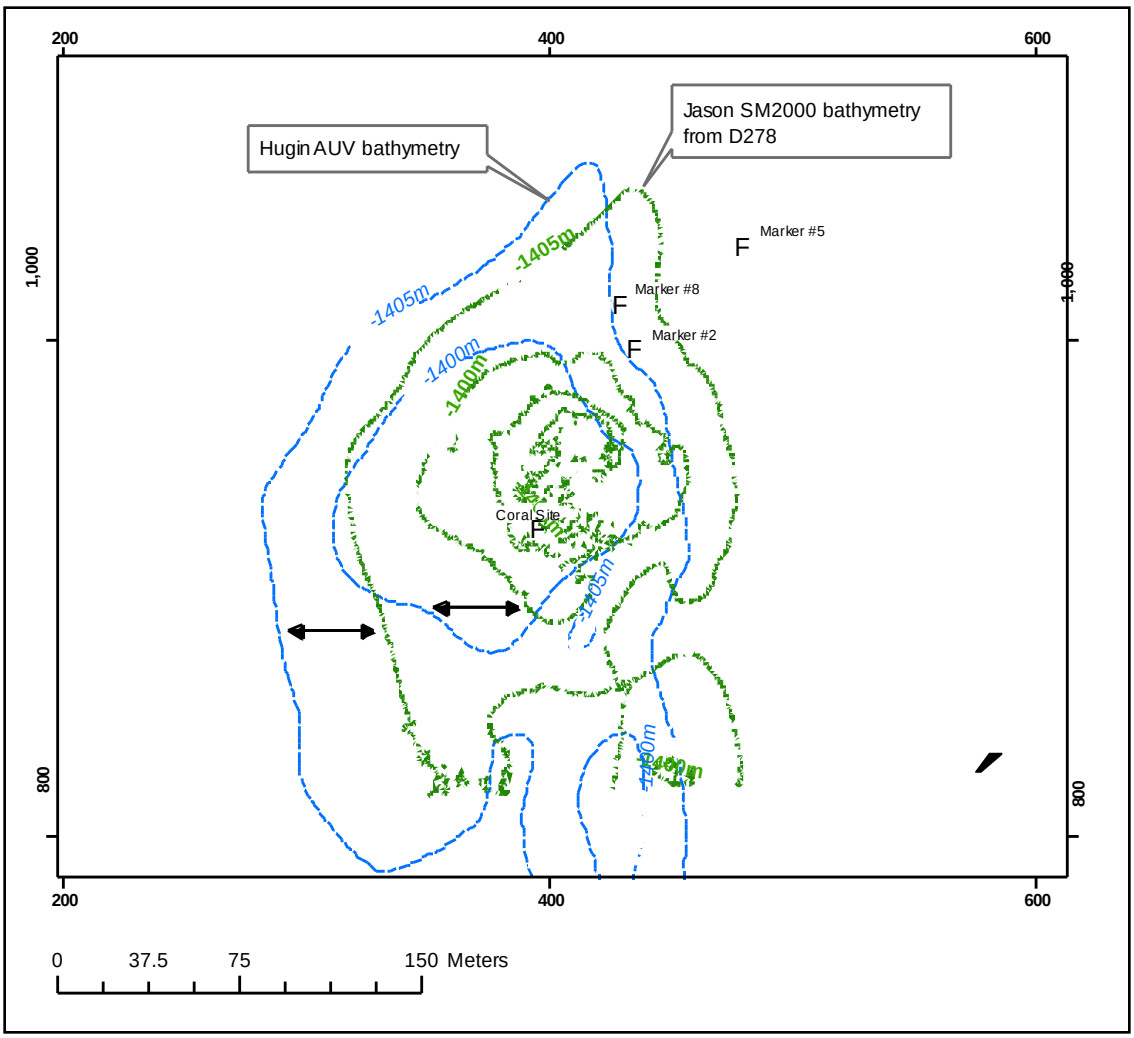

Figure 10-66. Apparent offset between processed SM2000 and Hugin AUV multibeam data.

At 6:08 hrs, *Jason II* began transit to Marker 1, searching for mobile fauna to slurp on the way under the direction of Dr. Carney. We arrived at Marker 1 at 07:42 hrs (X-392 m, Y-495 m), then proceeded to Marker 6 and the stained tube worms. Mass spectrometer sampling of stained tube worms began at 08:28 hrs (X-410 m, Y-492 m) and finished at 09:13 hrs. The stained tube worms were collected into the starboard bio box at 09:31 and we then slurped shrimp for about 15 minutes. We moved to mussel bed at Marker 1 (previously scooped), for another mass spectrometer followed by collections. The first mass spectrometer scan started at 10:11 hrs (position 38) and was done with "position 41" at 10:58. Mussel pot F taken smoothly and done by 11:10 hrs. We then moved towards the southwest and collected a few vesicomyid clams into the bio box (X-373 m, Y-422 m at 11:54 hrs). At 12:44 a Bushmaster collection of a tube worm aggregation was completed (X-381 m, Y-470 m) and we began transit to the first of 10 photo-transects (labeled photo-mosaics in the log). These began at 13:07 hrs (X-385 m, Y-469 m). These were completed at 15:00 hrs and we left the bottom at 15:12 hrs. The dive track for dive 278 is shown in Figure 10-67.

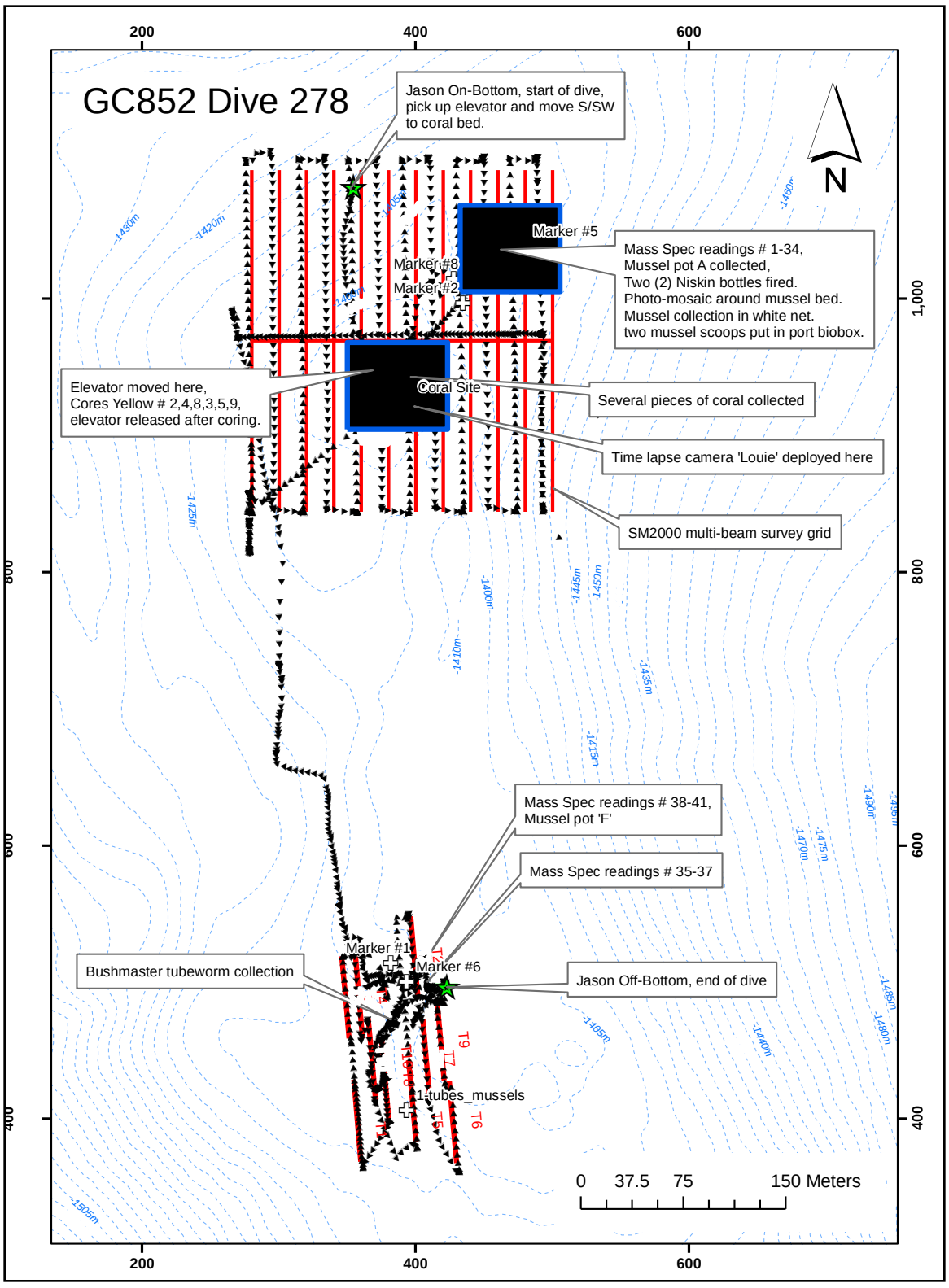

Figure 10-67. Dive track for Dive 278.

10.8. Garden Banks 697

This site (GC697) was not visited during the Recon Cruise and there were no *Alvin* lowerings at this site, but there was one *Jason II* lowering, from 6/16/07 to 6/17/07 for a duration of 31 hours and 45 minutes. It was chosen for visitation during the *Jason II* cruise because of its geographic location and depth for the community analyses.

10.8.1. Navigational Considerations

We did not visit this site last year with *Alvin*, so we had not developed a list of targets or a point of local origin. We also did not have bathymetry at this site from the AUV-multibeam bathymetric survey dataset developed for this project. We did, however, have access to the BOEM bathymetric and surface anomalies maps, so we used these geo-referenced graphics (Figure 10-68) to establish a local origin, to define a site CRP, and to select targets for the site.

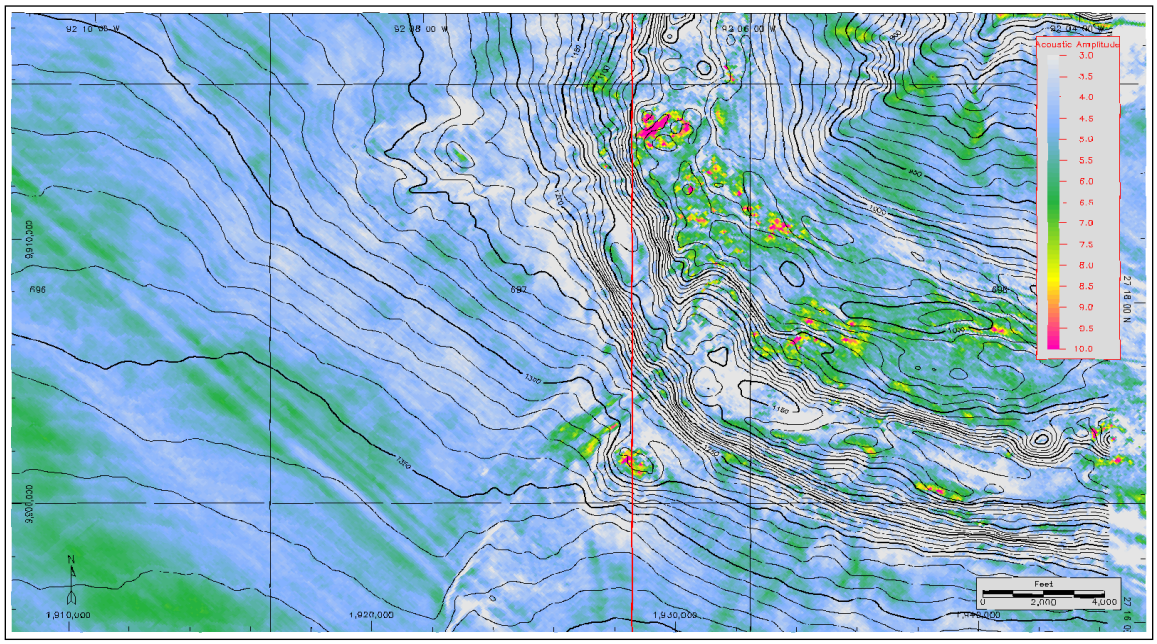

Figure 10-68. 3-D seismically derived bathymetric map with amplitude overlay (C.I.=10m) used for selecting targets at site GB697; used by permission.

We defined the following for this site in WGS84 datum:

Geodetics False Northing: -3,017,944.28 m
Geodetics False Easting: -87,752.61 m
Local Origin Northing: 3,017,944.28 m
Local Origin Easting: 587,752.61 m

These Falsing shifts were selected at this site in order to place a Local Origin in X,Y space near the targets of interest at the site. The latitude of this Local Origin is N27 16.90000 and the longitude is W092 06.80000. We then defined an X,Y in the resulting local coordinate system in m for a northern and a southern CRP. We did this by applying the geodetic False Northing and False Easting defined above to the standard UTM Zone 15 projection for the WGS84 datum,

then calculating the local X and Y from the latitude and longitude of each site CRP as measured using the BOEM map represented by Figure 10-68. A requirement of such a defined site is the ability to locate it by visual means with *Jason II*. We identified two such topographic highs on the map, one in the north and one in the south, and chose location on top of each.

The local coordinates thus calculated and assigned to the south CRP were X = 153 m and Y = 224 m. The local coordinates thus calculated and assigned to the north CRP were X = 398 m and Y = 3,385 m. We placed these two CRP targets into *Jason II*'s navigation system, along with targets of interest positioned by a geologic review of the BOEM bathymetric-anomaly map. Targets developed for this site are listed in Table 10-10.

Table 10-10

Target Locations for Site GB697

Target	Latitude	Longitude	Local X (m)	Local Y (m)	Depth (m)
Local Origin	N27 16.90000	W092 06.80000	0	0	
CRP South	N27 17.020734	W092 06.706285	153	224	1,278
geo 1	N27 16.959546	W092 06.709196	149	111	1,280
geo 2	N27 17.039112	W092 06.785555	22	257	1,280
geo 3	N27 17.083506	W092 06.782171	27	339	1,280
geo 4	N27 17.084697	W092 06.713657	140	342	1,280
geo 5	N27 17.009848	W092 06.697884	167	204	1,278
CRP North	N27 18.731873	W092 06.544099	398	3,385	1,015
geo 6	N27 18.993458	W092 06.623875	263	3,867	1,025
geo 7	N27 19.179328	W092 06.636946	239	4,210	1,015
geo 8	N27 19.119317	W092 06.399707	631	4,102	1,025
geo 9	N27 19.186951	W092 06.473149	509	4,226	1,025

We did not deploy the LBL net at this site because it was relatively shallow and we felt that we could establish *Jason II*'s position on the CRP without the net. This technique had worked at the previous sites that had no LBL positioning. The time saved by not deploying and calibrating an LBL net could be better used in the survey of this site.

Our plan for calibrating *Jason II*'s navigation system was to position the vessel's stern A-frame sheave directly over the CRP ($1{,}000^{+}$ m above it) and allow *Medea* to settle into a position directly under its sheave, suspended by its main cable. We would then position *Jason II* directly under *Medea* while within sight of the seabed. We would monitor *Jason II*'s stability of position by watching the seabed and by using its seabed-position-hold navigation feature. We would then monitor the lateral movement of *Medea* using its downward-looking camera aimed at *Jason II*, to confirm that *Medea* had settled into a stable, equilibrium position with respect to the vessel's stern A-frame sheave.

When we were satisfied that all three vehicles (vessel sheave, *Medea*, and *Jason II*) were vertically aligned to within one m, and all directly over the defined CRP position, we would reset

Jason II's navigation system to re-define its location as the X,Y of the CRP. Then we would drop a marker on that location in order to physically set a benchmark at this site. At this site there would be two such markers, one in the south and one in the north.

The timing of implementation of this plan is outlined in the beginning of the Dive 274 Summary section.

10.8.2. *Jason II* Lowering 274

Time in water:	2007/06/16 05:05
Time on bottom:	2007/06/16 06:08
Time off bottom:	2007/06/17 11:51
Time out of water:	2007/06/17 12:50
Water Time:	31 hrs 45 minutes
Bottom Time:	29 hrs 43 minutes
Min. working depth:	674.36 m
Max. working depth:	1281.50 m
Produced:	3.2 GB of raw vehicle data
Produced	~48 DVDs of Science video
Produced	~48 DVDs of Archive video

Jason II reached the seafloor at 02:08 EDT and event logging was initiated by the watch-stander on duty using *Jason II*'s VV event logger system. All times and dates in this summary are reported in EDT, local time. Refer to Dive Observations for this dive in the Appendix 7 for a detailed log of the observed events and their times in GMT. Upon arrival at the sea floor, we started transiting to the southern CRP. Numerous signs of seepage such as mats, carbonates and even tube worms were seen shortly after arrival on the sea floor (Figure 10-69).

Figure 10-69. Bacterial mat-chimney.

Marker 2 was deployed at 02:36 hrs for our southern CRP and was adjusted slightly (final logged position X-155 m, Y-222 m). We then began transit to Geo 2 target. Biological and geological indications of seepage were also logged while in transit to Geo 2. We then transited to Geo targets 3 and 4 and continued to see mats and assorted signs of chemosynthetic communities.

The first push core of four to be taken at this location was taken at 03:54 hrs at X-72 m, Y-341 m. The fourth core of this set was completed at 04:08 and one "non-carbonate" rock was collected into the empty milk crate. At 04:16 hrs, a brine flow (Figure 10-70) was found (the digital target "Brine River" was entered at 04:48 X-143 m, Y-339 m). Four additional push cores were taken at this location.

Figure 10-70. "Brine River."

On the way to Geo 4, we encountered fairly lush communities of tube worms. Numerous macro camera photographs were taken and several grabs were made from an aggregation (X-141 m,Y-323 m) into the starboard bio box at 06:00 hrs. We then proceeded towards Geo 5 and the CRP. We reoccupied the Marker 2 at 06:23 X-170 m, Y-235 m. This is approximately 20 m offset after 4 hours of work without a navigation net, which is not bad. We continued the transit to Geo 5 and arrived there at 06:38 hrs.

We then went into lay-back mode for the tow to the northern site 3 km away. We arrived on bottom in the northern area and reset our Doppler navigation at about 0900 hrs to X-427 m, Y-3382 m (by assuming *Medea* is under the ship). We decided to head to the topographic high

about 300 m east to define our CRP. Marker #3 was deployed at 09:36 hrs at X-713 m, Y-3347 m at CRP North. We explored this topographic high and found a large community of live mussels, a single tube worm, and a big ugly fish. We investigated the fish and spent 20 minutes, starting at 10:19, taking macro photos of this sculpin (X-680 m, Y-3420 m). We then headed to the single tube worm and shot macro camera shots of this Escarpid (X-679 m, Y-3420 m). [Note that these last two locations are about 10–15 m apart, with the fish to the north, although this is not seen in the nav log.] The tube worm was collected into the port bio box (Figure 10-71) and a soft coral of a species that had not been collected before was collected into the starboard bio box. The crater seen in the sonar was investigated and found to harbor shell hash and perhaps a few living vesicomyids. We began preparation for a series of photo transects over this chemo area at 12:26 hrs and started the first transect at 12:53 hrs. The last transect was completed at 14:23 hrs and a final line was run towards the mussel bed (which did not appear in the random transect lines) and finished photo surveying at 14:47 hrs (X-666 m, Y-3430 m). We began transit to Geo 5 at 14:48 hrs on a heading of 310°.

Figure 10-71. Tube worm collection placed in bio box.

After arriving at geotarget 6 at about 15:40 hrs, we continued past the target to run over an area of high reflectivity. We began transit to Geo 9 on a heading of 55° along the path of high reflectivity. We stopped at what appeared to be a small outcropping gas hydrate. When *Jason II* came to a halt over the feature, we encountered bad visibility. We waited over that position for 15 minutes for the visibility to improve, but it did not. We continued to Geo 9, approximately 150 m at a heading of 55°. The visibility was still bad at Geo 9 and we changed heading to 250°

towards Geo 7. We stayed in bad visibility for about another 200 m and a mud volcano is hypothesized somewhere between Geo 6 and 9.

Carbonates and scattered seep fauna were observed as we neared Geo 7 and we began to chase sonar targets and found lush seep communities. A digital target "tube worm carbonates" entered at 18:12 hrs marked this area (X-259 m, Y-4230m) and we stopped to collect tube worms and a carbonate at this site. In the vicinity of Geo 7, we observed bacterial mats, clam shell hash, and live vesicomyid clams. We arrived at Geo 7 and chased sonar targets to the north. We observed recent mud flows and small mounds (but not the large mud volcano we will discover later). A site with live clams was found at X-283 m Y-4309 m and we set down to collect a few clams and 3 push cores in the vicinity of the clams. Continuing to chase sonar targets south of Geo 7, a mussel bed was found. The mussel bed consists mainly of *B. childressi*. The upper slope species of *Munidopsis* was also noted, but was not collected. A mussel pot sample was attempted, but was unsuccessful and the scoop was used instead to collect this community. We explored the area more, observing a number of small pockmarks with shell hash and bacterial mats.

We completed a photosurvey of the central portion of the site. Start time for survey was 16:53Z; end time was 18:30 hrs. The random survey lines were 40 m in length. They largely overlooked the large mussel bed.

We returned to Geo 7 and continued on across our previous track towards Geo 8 at a heading of approximately 100° to look for the mud volcano. We ran into cloudy waters again at X-450 m, Y-4115 m in the same area as the previous transit across this area. We then began the search for the source of the mud plume. After running through the plume for a while, *Jason II* began to ascend, trying to get out of the cloud. We progressed in the direction that we believed was the source, looking for a plume of rising bubbles. We found the top of the volcano, having risen about 30 m from the surrounding bottom. At the summit, there were active mud flows, billowing fluidized mud coming out of the crater at the top, and a large column of rising methane bubbles (09:17 hrs, X-543 m, Y-4133 m). A number of still photographs of the summit were taken and one push core of the mud adjacent to the flowing channel was obtained. The Niskin bottles were also fired right above the plume coming out of the volcano. We spent about an hour there and then began to transit towards Geo 8 at 00:15 hrs.

After arriving at Geo 8 (00:15 hrs, X-662 m, Y-4098 m) we decided to investigate additional geo targets (areas of high reflectivity) to the south-southeast before returning to our final CRP and the mussel bed. We transited at 150° down to X-932 m, Y-3650 m (at 01:20 hrs) and the only indication of seepage were occasional bacterial mats and carbonates. We chased sonar targets in this area (and encountered scattered tube worms, mats and carbonates. Plumes of mud were encountered during this exercise and speculation of another mud volcano ensued. No evidence of such was encountered and review of dive tracks (Fisher) suggests the possibility of encountering *Jason II* silt. We continued in a generally southeastern direction and continued to encounter scattered and sparse indications of chemosynthetic communities down to about X-1350 m, -3000 m (at 05:20 hrs). We then turned west towards a geo target immediately south of our northern CRP, about 600 m away. No significant chemosynthetic communities were encountered during this transet west to about X-700 m, Y-3050 m, nor during the north 300 m leg back to the CRP. We reoccupied the north CRP marker at 07:03 hrs (X-716 m, Y-3356 m). This is less than a 15 m offset from the original logged deployment location 22 hours earlier (X-713 m, Y-3347 m), again, excellent navigation without a transponder net. A mussel pot collection was made at 07:35 hrs in the mussel bed located here 22 hours ago (current X-685 m,

Y-3424 m), the big ugly fish (sculpin, Figure 10-72) had only moved about a m and was revisited, and *Jason II* left the bottom at 07:52 hrs.

Non-seep mobile fauna was typical for the depth. Holothuroids were dominated by the white *Mesothuria lactea*. Fish were common and diverse. Crabs included both Geryonids and lithodids.

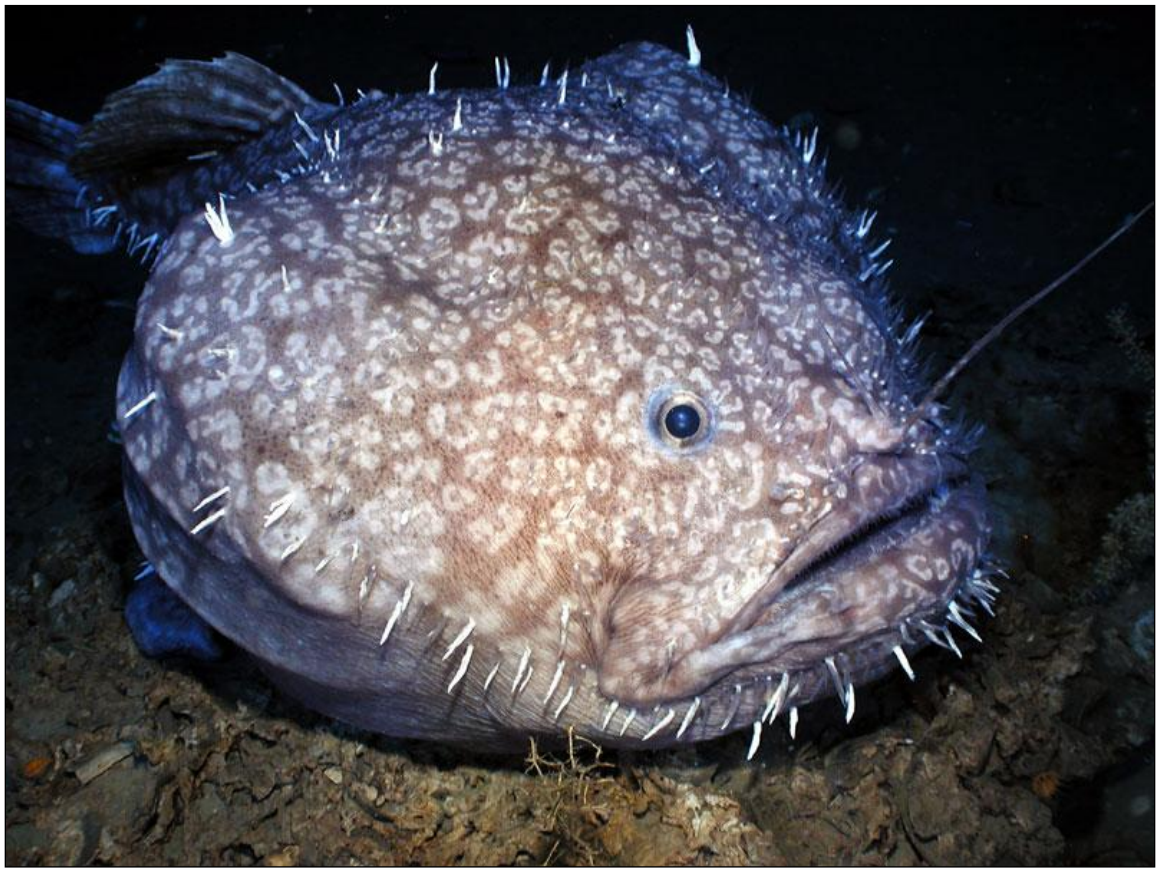

Figure 10-72. "Big ugly fish" (sculpin).

The dive track for dive 274 is shown in Figure 10-73.

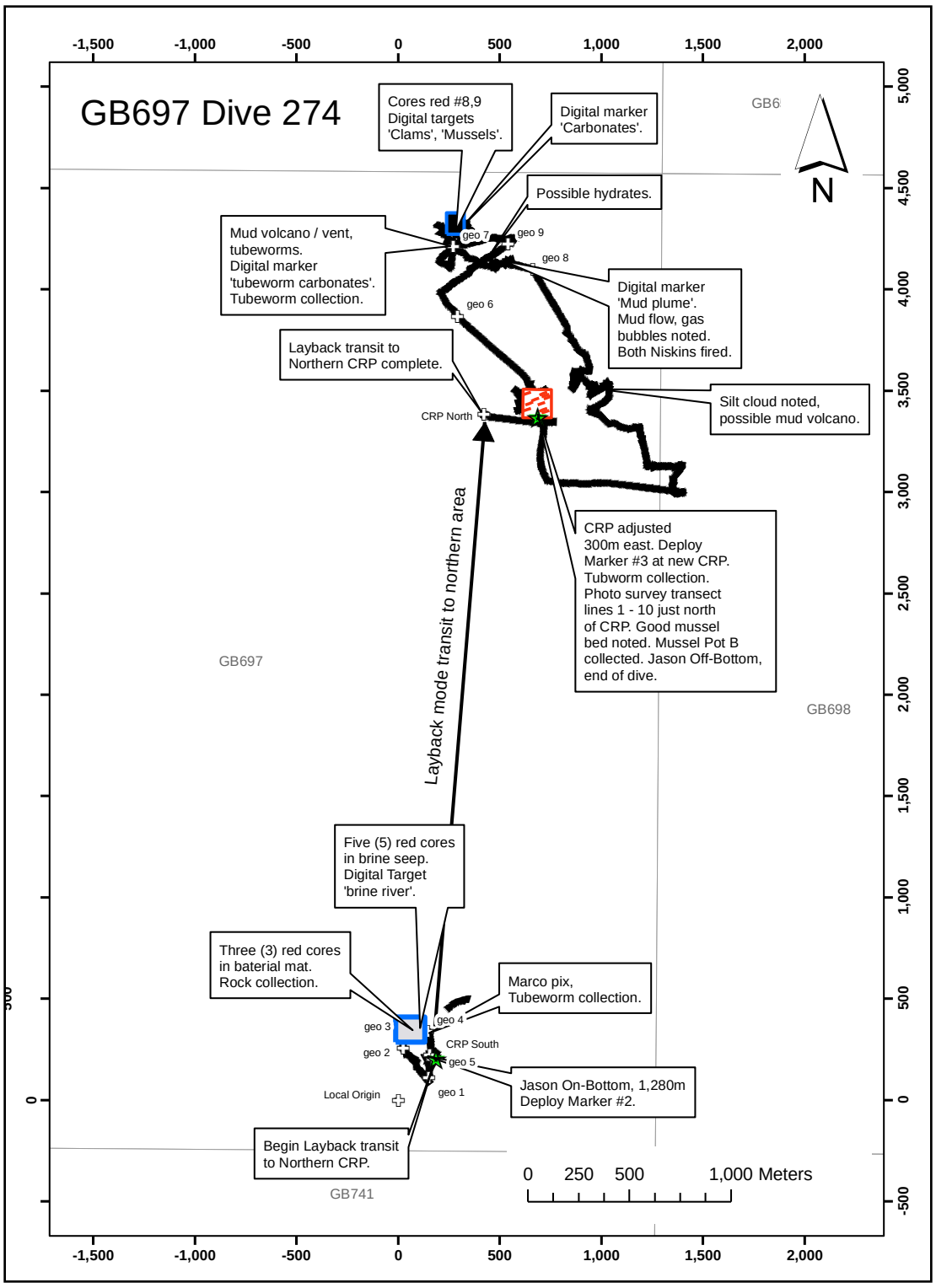

Figure 10-73. Dive track for D274.

10.9. Garden Banks 829

This site (GB829) was not visited during the Recon Cruise and there were no *Alvin* dives at this site. There was one *Jason II* lowering on 6/25/2007 for a duration of 10 hours and 22 minutes.

10.9.1. Navigation Considerations

An approximate target location for the high-relief mound was selected from a paper BOEM chart (no digital BOEM chart was available prior to the dive) and digital bathymetry data from the NOAA National Geophysical Data Center database. Prior to ROV deployment, a single pass over this approximate dive site was made using the SeaBeam multi-beam system on *Ronald Brown* starting at 05:30 EDT. Based on the multibeam data, a slightly revised dive target location was selected. A local origin was selected just to the southwest of the CRP (see Table 10-11 and Figure 10-74).

Table 10-11

Target Locations for Site GB829

Target	Lat	Lon	Depth m	LatDD	LonDD
Local Origin	27 10.650 N	92 7.820 W		27.177500	-92.130333
Peak - CRP	27 11.0844 N	92 7.4302 W	1,291	27.184740	-92.123837
East Mnd	27 10.8689 N	92 6.9784 W	1,326	27.181148	-92.116307

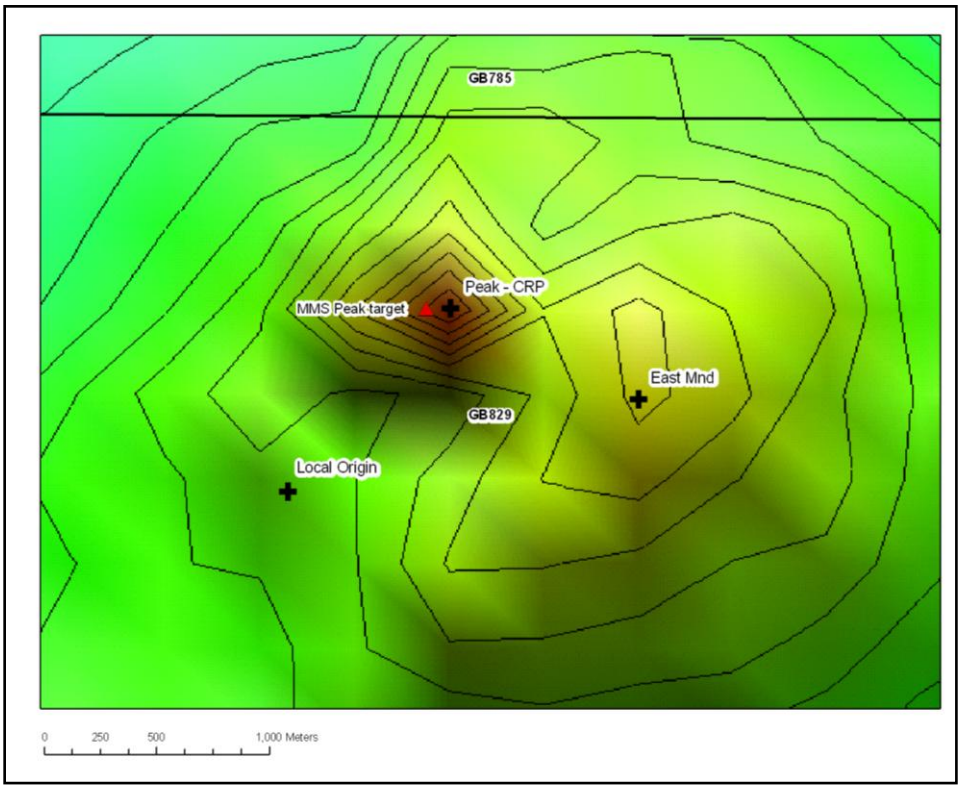

Figure 10-74. SeaBeam multi-beam data used to confirm dive target.

10.9.2. *Jason II* Lowering 279

Time in water:	2007/06/25 12:09Z
Time on bottom:	2007/06/25 13:14Z
Time off bottom:	2007/06/25 21:32Z
Time out of water:	2007/06/25 22:31Z
Water Time:	10 hrs 22 minutes
Bottom Time:	8 hrs 18 minutes
Min. working depth:	1216.46 m
Max. working depth:	1303.88 m
Produced:	1.1 GB of raw vehicle data
Produced	~13 DVDs of Science video
Produced	~13 DVDs of Archive video

At 9:06 EDT hrs *Jason II* reached the seafloor at the CRP. Depth was approximately 1,255 m. *Jason II* then began a transit to the west-north-west up a steep slope (approximately 30 degrees) and reached a local high of approximately 1,222 m which was believed to be the top of the "Christmas Tree" high-relief mound. The site marker was placed here, near the summit of the mound. *Jason II* then transited approximately 200 m to the north and then descended to find the sea floor (this avoided dragging the tail of the ROV down the mound and creating mud clouds). *Jason II* turned 180° and proceeded approximately 100 m back up the slope to the south in search of the source of a high reflector indicated on the BOEM charts.

A dense mussel bed extending over approximately 3.5 m east to west and 2 m north to south was located on a slope near the expected location of the high reflector at a depth of approximately 1,260 m. The mass spectrometer unit was deployed to take readings in five locations (#42–46) in the mussel bed from 11:00 to 12:40 hrs (Figure 10-75). At 12:45 hrs mussel pot A was collected for analysis of the community composition and samples were also collected with a net into the temperature-insulated bio box for genetic analyses. The bed and surrounding briney sediments were imaged via a photo mosaic from 01:11 to 01:51 hrs to allow future measurement of the bed dimensions.

Figure 10-75. Mass spectrometer readings taken over dense mussel bed.

At 01:52 hrs, *Jason II* began to move west-southwest towards the next suspected high reflector noted on the BOEM amplitude anomaly map. After approximately 140 m, an area of carbonate outcrops, mussels, and tube worms was found. From 02:26 to 02:43 hrs, a series of macro camera photos was taken (tube worms and mussels). Between 02:47 to 02:54 hrs, a carbonate sample with a sponge attached, a tube worm grab sample, and another carbonate sample (associated with the tube worms) were collected. Scientists in the *Jason II* Van speculated that the sponges covering the carbonates might facilitate carbonate deposition above the sediment surface here as was also speculated in the community of young mussels at AT340.

At 03:05 hrs the *Jason II* returned east to the large mussel bed and at 03:31 hrs mussel pot F was collected in the same mussel bed visited 4 hours earlier (Figure 10-76).

At 03:51 *Jason II* proceeded east on a heading of approximately 90 degrees to find the third high-amplitude anomaly. After approximately 140 m, *Jason II* turned to a heading of 145 degrees following a sonar target. Several large carbonate outcrops were noted. Tube worms and mussels were also noted in these areas. *Jason II* then headed northwest upslope towards the topographic high. A carbonate sample was collected near the summit and at 05:32 hrs *Jason II* began its ascent to the surface.

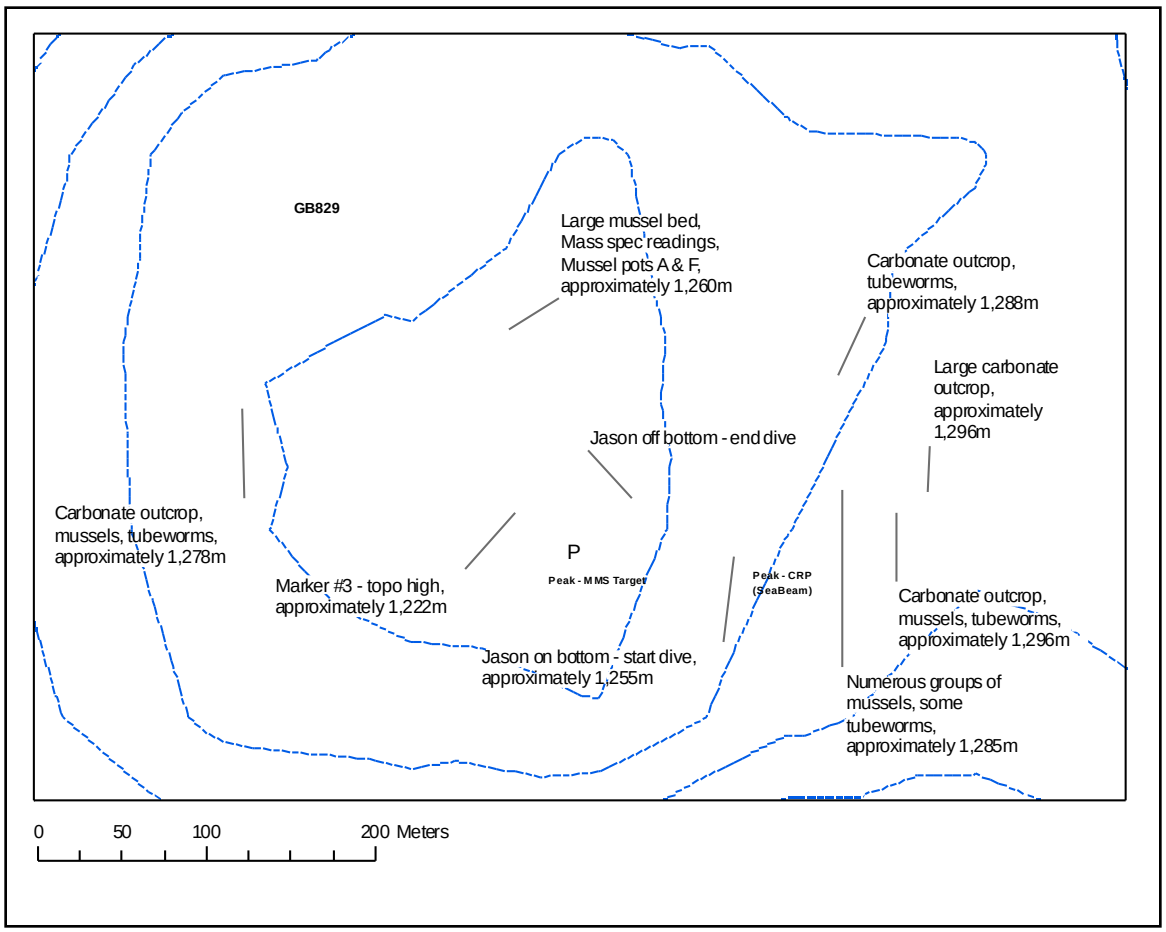

Figure 10-76. Dive track for Dive 279.

10.10. Garden Banks 647

This site (GB647) was not visited during the Recon Cruise and there were no *Alvin* dives at this site. There was one *Jason II* lowering (J2-280) on 6/26/07 for a duration of 14 hours and 18 minutes.

10.10.1. Navigational Considerations

As with several of our previous relatively shallow sites in Garden Banks, we did not visit this site last year with *Alvin*, so we had not developed a list of targets or a point of local origin. We did, however, have access to the BOEM bathymetric and surface anomalies maps, so we used these geo-referenced graphics (Figure 10-77) to establish a local origin, and to select targets for the site (Table 10-12).

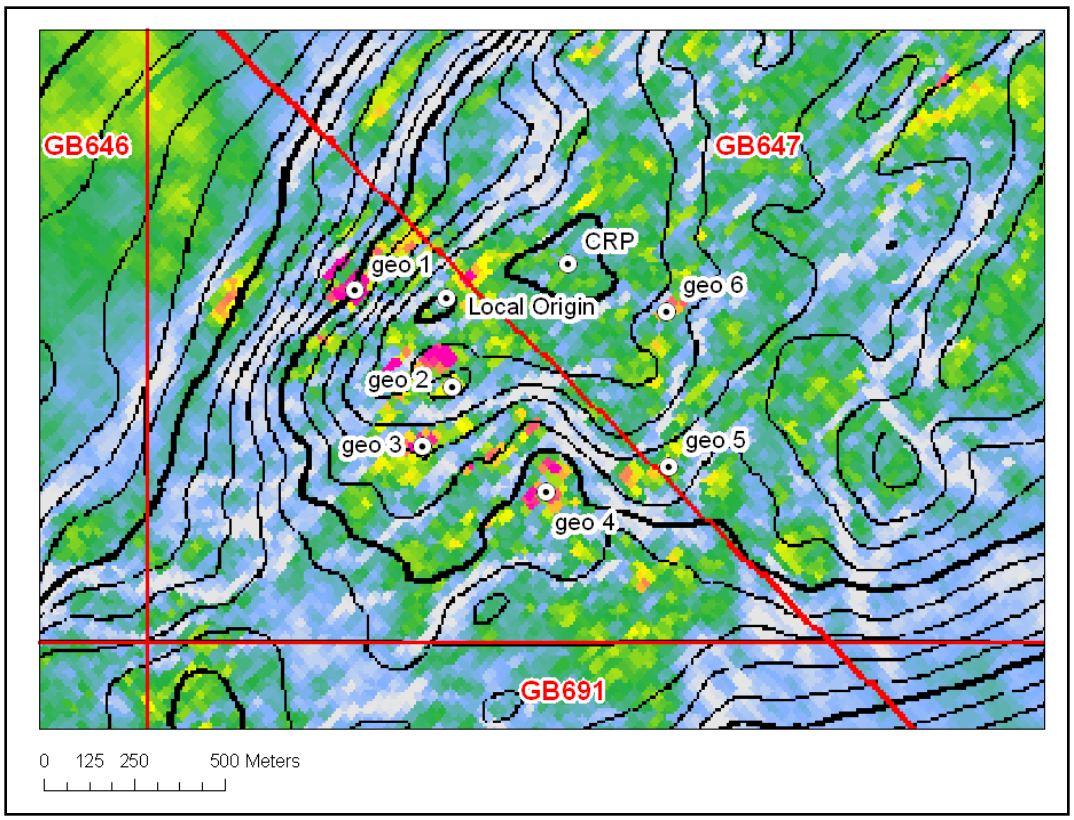

Figure 10-77. Target locations for site GB647 on 3-D seismically derived bathymetric map with amplitude overlay (C.I.=10m). Used by permission.

Table 10-12

Target Locations for Site GB647

Target	Latitude	Longitude	Local X (m)	Local Y (m)	Depth (m)
Local Origin	N27 20.00000	W092 26.00000	0	0	
CRP	N27 20.051172	W092 25.796552	335	96	945
geo 1	N27 20.012004	W092 26.155817	-257	21	1,000
geo 2	N27 19.866171	W092 25.991583	15	-247	965
geo 3	N27 19.777003	W092 26.042983	-69	-412	980
geo 4	N27 19.706283	W092 25.835312	274	-541	1,003
geo 5	N27 19.743898	W092 25.628909	614	-470	985
geo 6	N27 19.977914	W092 25.631952	607	-38	965

10.10.2. *Jason II* Lowering 280

Time in water:	2007/06/26 09:59Z
Time on bottom:	2007/06/26 10:44Z
Time off bottom:	2007/06/26 23:33Z
Time out of water:	2007/06/27 00:17Z
Water Time:	14 hrs 18 minutes
Bottom Time:	12 hrs 49 minutes
Min. working depth:	932.09 m
Max. working depth:	1004.95 m
Produced:	1.5 GB of raw vehicle data
Produced	~20 DVDs of Science video
Produced	~20 DVDs of Archive video

This is the shallowest of the study sites. During the dive, we transited from the north end to the south end, across a topographic high (a carbonate mound). Abundant microbial mats, live clams and giant mussels were observed consistently along the dive path. Numerous pockmarks and carbonate pavements were evident. Exposed gas hydrate was observed in the crater where clams were collected towards the end of the dive (southern end of the site).

- Bench Marker (X-367 m, Y-1167 m) near target #1.
- Marker #2 (X-342 m, Y-1171 m) in epic mat area.
- Marker #3 (X-548 m, Y-706 m) near mussel collection area

Jason II reached the bottom at 10:44 GMT at a subsea depth of 945 m, on top of the local topographic high. Immediately next to the landing site was an asphaltic rock with several gorgonian corals growing on it (Figure 10-78). The rock was sampled and one coral was taken. Marker #2 was deployed at this site and identified as new CRP.

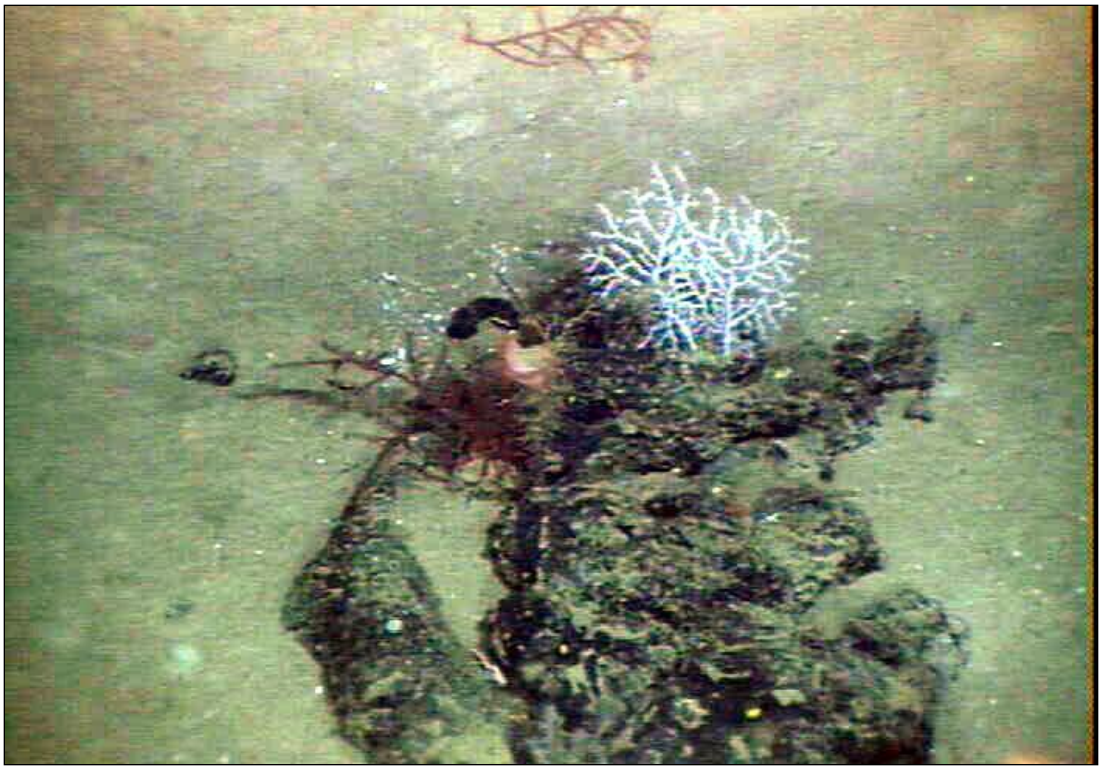

Figure 10-78. Asphalt with coral collected.

The *Jason II* transited west to geo-marker #1. At 12:17 hrs, a gorgonian was observed prior to Geo 1, and a marker was deployed. When we arrived at Geo1, a vast outcrop of both carbonate rocks and asphalt was observed. Samples of asphalt and carbonate rocks were taken. The rocks had the appearance of laterally elongate burrows (Figure 10-79). Several white-stained soft-bottom patches were observed and cores were taken. Possible brine flows and bacterial mats were observed. Regular urchins, gorgonians, and sponges were observed on the outcrops. SM 2000 sonar in side-scanning mode was useful in locating targets. We traversed to the western (downdip) margin of the outcrops, then turned back to the east and headed 159 to geo-marker #2.

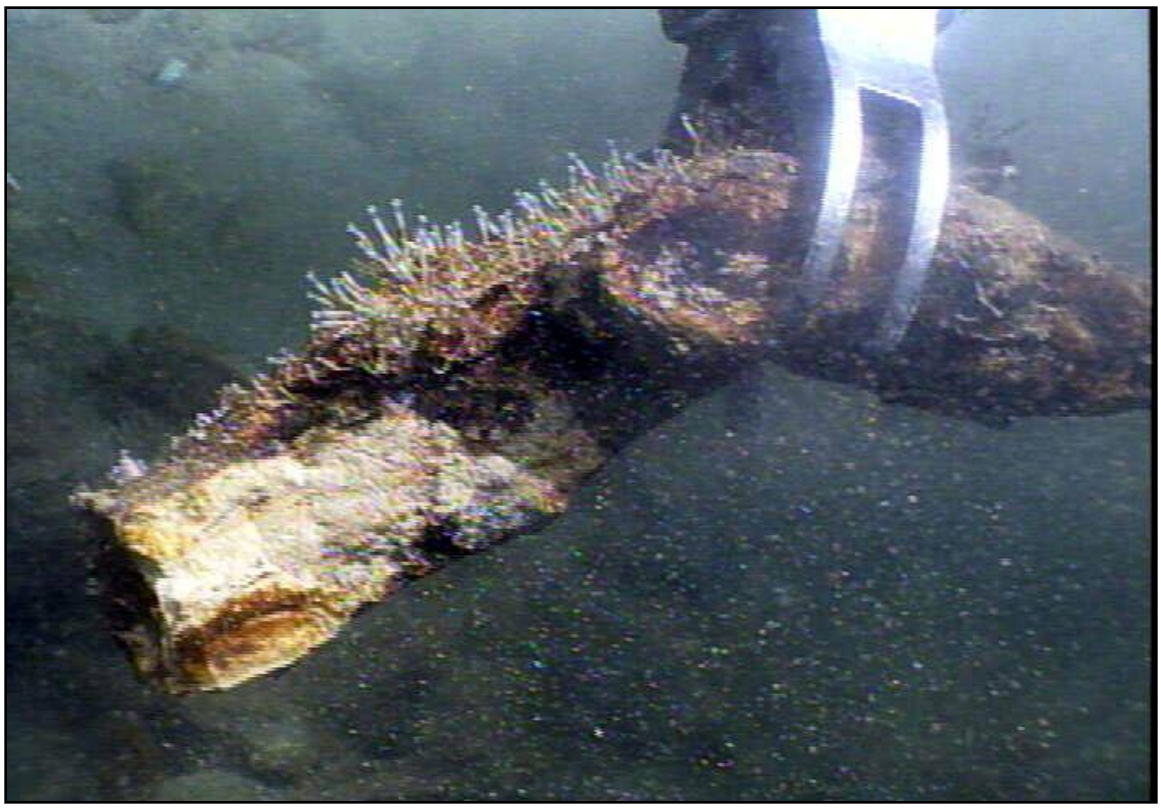

Figure 10-79 Carbonate collection.

Geo-marker #2 and #3 yielded very little. Associated sponges and isolated tube worms were noted in very limited quantities, as well as carbonate rocks and bacterial mats.

In transit to Geo 4, small clusters of 3–5 tube worms were encountered at 16:17 hrs and were sampled. When one of the tube worms was pulled, asphalt, tar, or an oily substance was dripping from the base of the tube worm. Also, the same black substance was floating up from the disturbed sandy bottom (Figure 10-80). Also, some tar or oil landed on the science cam, partially blocking vision. This location corresponded nicely with geophysical amplitude anomalies that had not been pre-selected as a geo-target. Also at the pre-Geo 4 location, cores were taken in a bacterial mat; these yielded a very oily substance.

Figure 10-80. Tar-like substance oozing from site of tube worm collection.

Geo-target #4 had very expansive carbonate outcrops and possible asphalt. Topographically, the outcrops were located in a valley that trends roughly north-south. The exposures were along strike, dipping slightly off the mound. Incisions were noted in the valley, indicating flow. Briney flows (bright white) were flowing downhill along the bedding planes. Several cores were recovered from the white bottom. The only live mussel community of the dive was observed living at the base of one of the flows. This small mussel aggregation was mostly buried in the sediment. Samples were taken using the *Jason II* claw into starboard biobox at 18:05 hrs. A traverse was made back to the west and muddy bottom was found. Re-calibration of the Doppler navigation indicates that the large carbonate outcrops in the valley corresponded to the high-amplitude response on the seafloor geophysical map.

We traversed east to geo-marker #5. This area had mostly muddy sediment, with an occasional bacterial mat and sponge, and an occasional carbonate outcrop. We turned nearly due north for geo-marker #6 at 21:09 hrs. We then traversed for nearly 400 m to north, encountering very sparse carbonate outcrops, bacterial mats, and sponges. We arrived at Geo 6 at approximately 22:00 hrs. Again, very few organisms or outcrops were observed. Two samples of lone tube worms were collected to the west of Geo 6 at 22:17 and 22:26 hrs. We traversed to the west and encountered the CRP at 22:48 hrs.

The decision was made to traverse west back to geo-marker #1 to attempt to collect Niskin data. As this was the end of the dive, we transited as quickly as possible to the previous asphalt site. When cobbles of carbonates and asphalt were encountered, both Niskins were fired at 23:23 hrs.

Once *Medea* settled out (because of the rapid transit to this location), eight hand-held macro camera images were acquired of the asphalt cobbles. *Jason II* was off of bottom at 23:33 hrs.

Asphalt samples collected during dive included soft, malleable material. The dive track for dive 280 is shown in Figure 10-81.

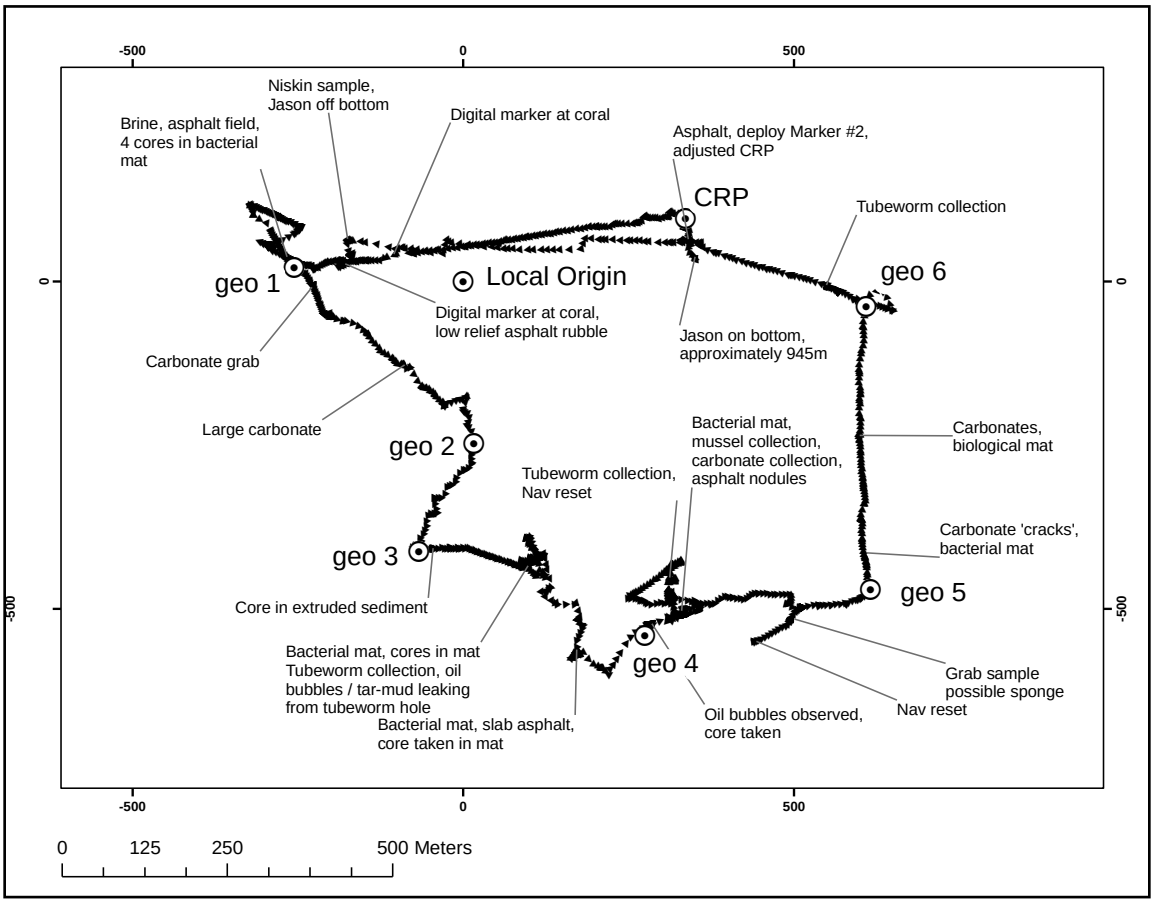

Figure 10-81. Dive track for dive 280.

10.11. Mississippi Canyon 853

This site (MC853) was not visited during the Recon Cruise but had been visited in 2000 with *Alvin*. One *Alvin* dive, AD4178 on 5/14/06 took place at this site. There were no *Jason II* dives at this site.

10.11.1. *Alvin* Dive 4178

This site was the shallowest site visited by *Alvin*, with water depths as shallow as 1,050 m. Mandy Joye and Bill Shedd were the divers. Brine was abundant on the top where numerous small mussel patches were found. Both mussels and clams were very abundant at this site and present along most of the dive track. Also extremely abundant during the dive were bacterial mats. We worked from the northern edge of the top of the mound, across the mound, down the

western edge and across to the southern edge. The *in-situ* chemical profiler was successfully used.

Twelve push cores were taken, six from each of two locations. Four water samples were taken with a Niskin array mounted on the sub. Two mussel pot samples were attempted, and one was fully successful; the other caught a seep fish. In addition, the pilot made several collections with a net and vesicomyid clams were collected (*Calyptogena ponderosa*). A community of giant *Bathymodiolus brooksi* was also sampled. Neither of these had been sampled by the previous 2000 *Alvin* cruise. Some *B. brooksi* were so large that they could not be collected with either the mussel pots or the collection nets, and the pilot picked up several with the manipulator. These are the largest mussels sampled to date in the GoM (over 25 cm in length and about 2 lbs in weight) and the known depth range of this species is now the largest of any endemic GoM seep species (from 1,050 to 3,200 m). One of the most interesting creatures observed during the dive was a large, colorful siphonophore (1525 in dive log), which was slurped up by Pat. During the dive, black streams of liquid emanating from topographic highs were assumed to be brine flows, but geochemical examination of sediment cores back in the lab showed no evidence of brine (the pore water salinity at all sites was ~35).

This was a very successful dive that will provide important data on depth distributions of numerous species and highlighted the importance of additional dives to this depth in the future (Figure 10-82).

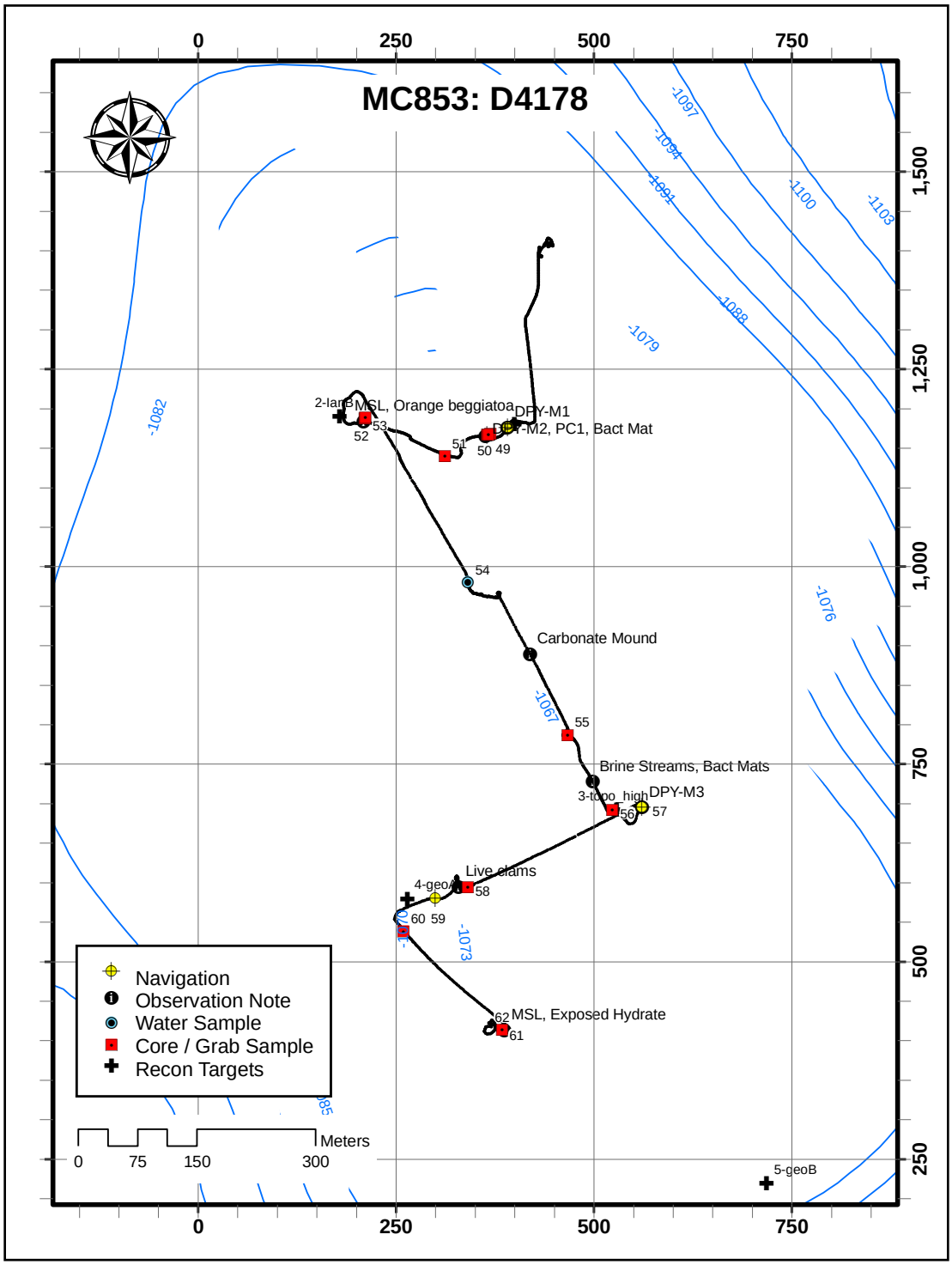

Figure 10-82. Dive 4178 on 5/14/2006 at an average depth of 1,070 m.

10.12. Mississippi Canyon 640

This site (MC640) was surveyed on the Recon Cruise and there was one *Alvin* dive, AD4182, on 5/18/06. There were no *Jason II* dives at this site.

10.12.1. Reconnaissance Cruise

This site was a large, low-relief mound with numerous geophysical targets distributed across its crest. The DCS reached bottom at 00:50 hrs on 20 March and collected images with a 12-second repeat rate until 04:11 hrs. Calmer seas and favorable winds provided good survey conditions. A total of 976 images were collected with the bottom in view and acceptable navigation. Many of these images occur in sequences that can be mosaicked to cover larger areas. This site showed only abundant chemosynthetic fauna—predominantly mussels. Carbonates were low, jointed pavements or solitary pieces. Bacteria were also seen associated with brine channels and near what appeared to be brine pools. Only one solitary cluster of tube worms was observed and this specimen was of an unusual growth form. Large areas of the bottom were covered with very numerous, small tubes on open sediment. This site is a good candidate for further study (Figures 10-83 and 10-84).

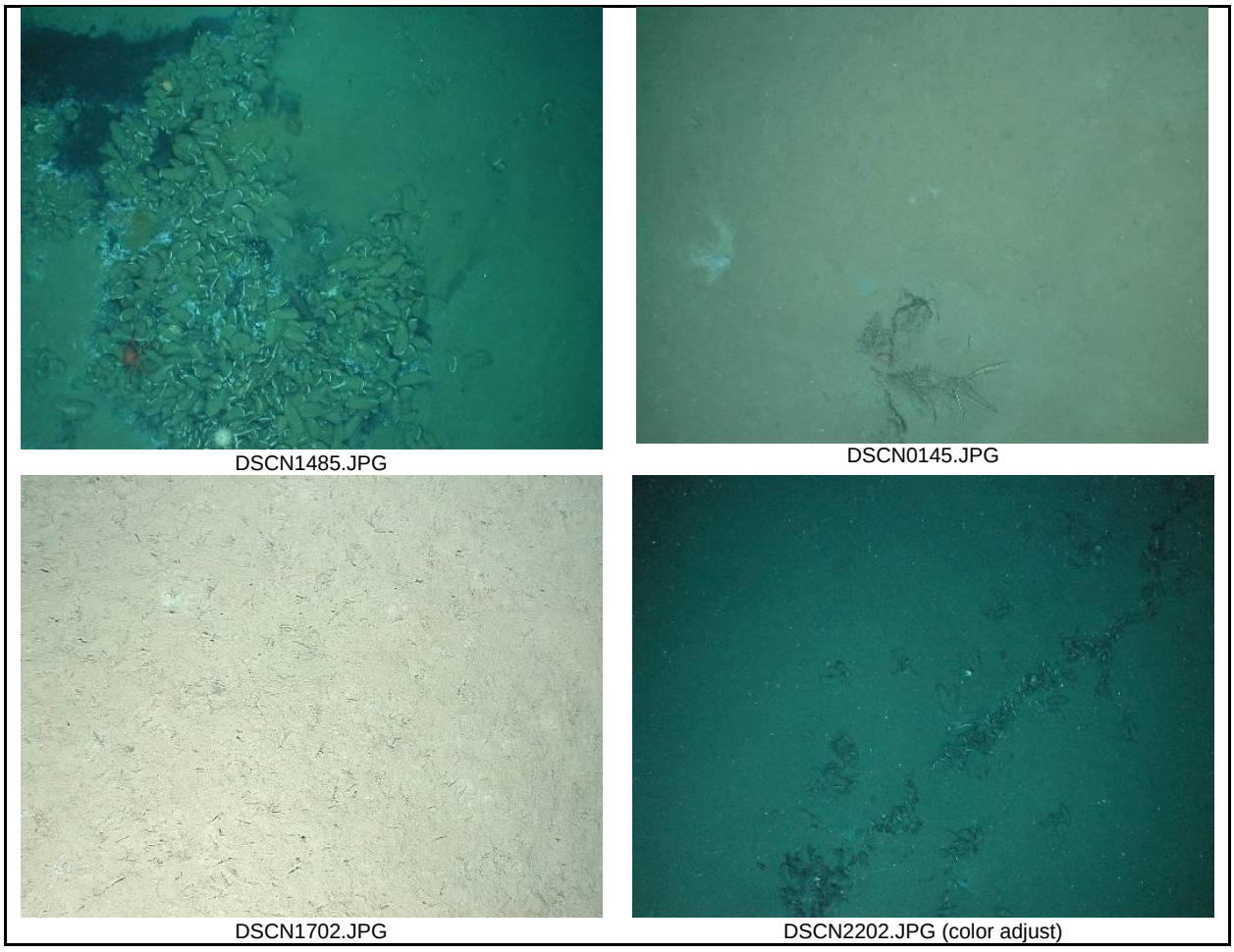

Figure 10-83. Representative photography from MC640.

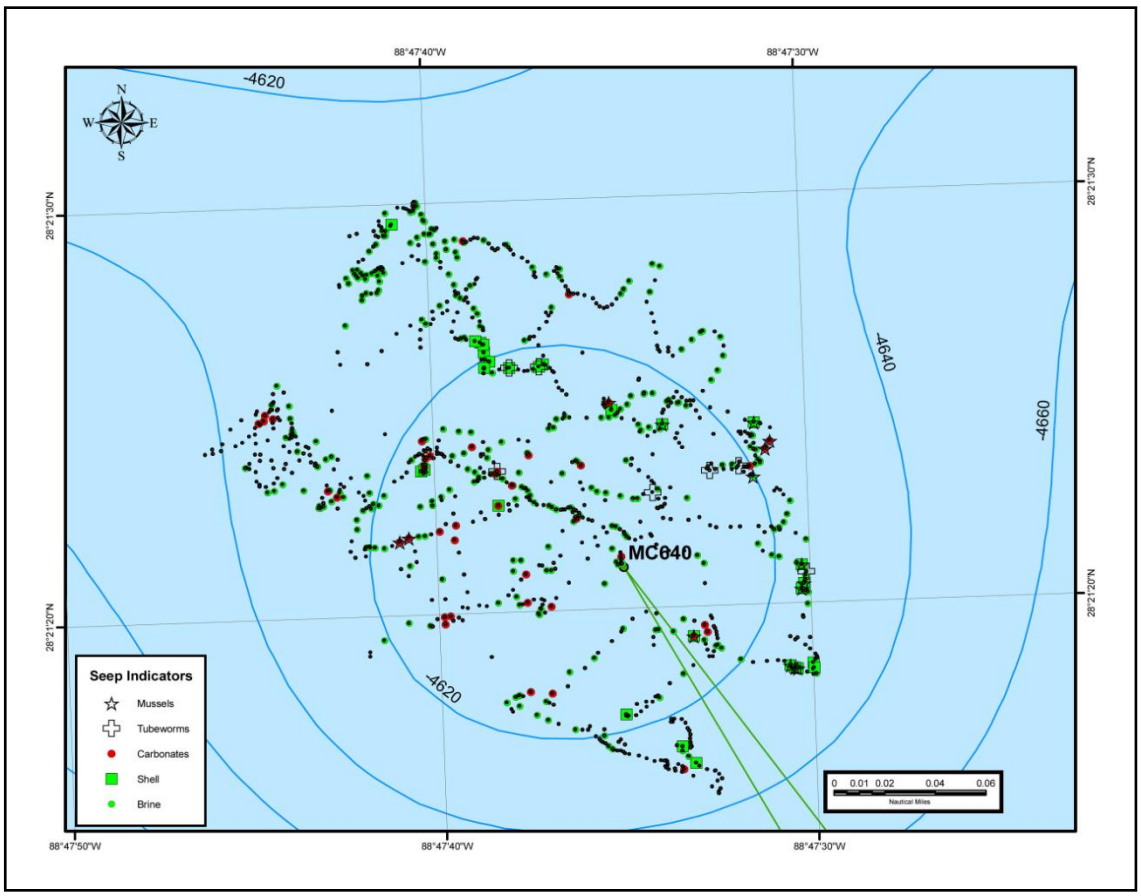

Figure 10-84. Survey results from MC640 station.

10.12.2. *Alvin* Dive 4182

The pilot was Patrick Hickey, Anton Zafereo was the pilot-in-training, and Bob Carney was the lone observer. The data from the March camera cruise suggested that this target area was characterized primarily by brine flows. The *Alvin* observations substantiated this interpretation of the area and added the details of venting craters and many pockmarks. Within the craters were mussel communities but no tube worms. Large depressions had sharp edges and were at least 10 m across (exact size hard to determine) and greater than2 m deep. *Alvin* could fit within these and still have limited room to maneuver. In addition, there was very little evidence of seafloor lithification. However, one sizeable rock was collected. The dive often had visibility problems because the bottom was very easily disturbed. Even though there was a current, it took a while for the area to clear, once the bottom was encountered. It was also noted that a "haze" hung over the craters, perhaps a chemical precipitate. The following samples were collected: 1) one mussel pot, 2) two mussel scoops, 3) one slurp sample, 4) 12 push cores, 5) five Niskin bottle samples, and 6) one large rock. Upon returning to the surface, a CTD cast was taken at the MC640 site (Figure 10-85).

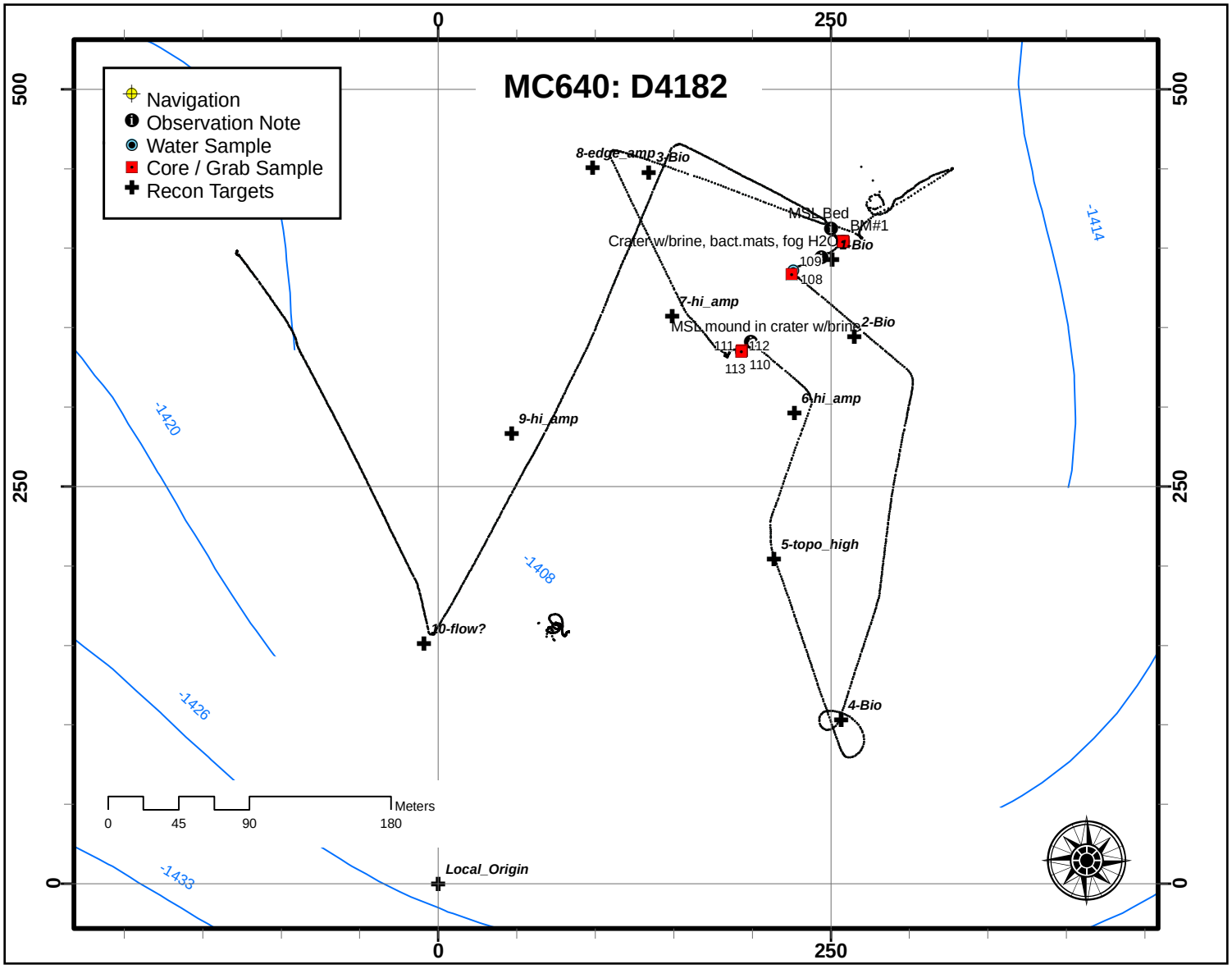

Figure 10-85. Dive 4182 on 5/18/2006 at an average depth of 1,410 m.

10.13. Alaminos Canyon 818

This site (AC818) was not visited during the Recon Cruise, but was chosen because an industry survey around a well-head had encountered tube worms and associated seep fauna. There were two *Alvin* dives at AC818, including AD4192 on 5/27/06 and AD4195 on 5/30/06 and two *Jason II* lowerings, including J2-282 from 6/30/07 to 7/1/07 for a duration of 27 hours and 51 minutes, and J2-284, from 7/4/07 to 7/5/07 for a duration of 12 hours and 44 minutes.

10.13.1. Navigational Considerations

The principal targets for *Jason II* dive 281 at AC818 were the well head and bench markers deployed during the previous *Alvin* dives (numbers 1, 3, and 4) located north of the well head. Other targets included the elevator drop site and *Jason II* launch site. An array of six survey lines for an SM2000 bathymetric survey was established over the site. Targets information is detailed in Table 10-13 and illustrated in Figure 10-86.

Table 10-13

Targets for Dive 281 at AC818, WGS84 Except for Wellhead.

Target	Latitude	Longitude	Depth (m)	Note
Local Origin	N26° 10.3	W094° 37.7		From 2006 *Alvin* cruise
Wellhead-Chevron	*26° 10' 47.398" N (NAD27)*	*94° 37' 22.414" W (NAD27)*		Chevron proprietary location given in NAD27, target converted to WGS84
3-geo	N26° 10.87071'	W094° 37.35272'		2006 *Alvin* cruise target
7-geo	N26° 10.39953'	W094° 37.61391'		2006 *Alvin* cruise target
2-geo	N26° 10.99434'	W094° 37.36435'		2006 *Alvin* cruise target
1-geo	N26° 11.10067'	W094° 37.32450'		2006 *Alvin* cruise target
5-geo	N26° 10.73630'	W094° 37.37069'		2006 *Alvin* cruise target
WELLHEAD	N26° 10.78663'	W094° 37.37362'		2006 *Alvin* cruise target
6-geo	N26° 10.60057'	W094° 37.50598'		2006 *Alvin* cruise target
ROV chemo	N26° 10.80933'	W094° 37.38367'		2006 *Alvin* cruise target
BenchMkr #1				2006 *Alvin* Dive Logs
BenchMkr #3			2,744	2006 *Alvin* Dive Logs
BenchMkr #4			2,745	2006 *Alvin* Dive Logs
Drop Elevator Here				
Launch Site				

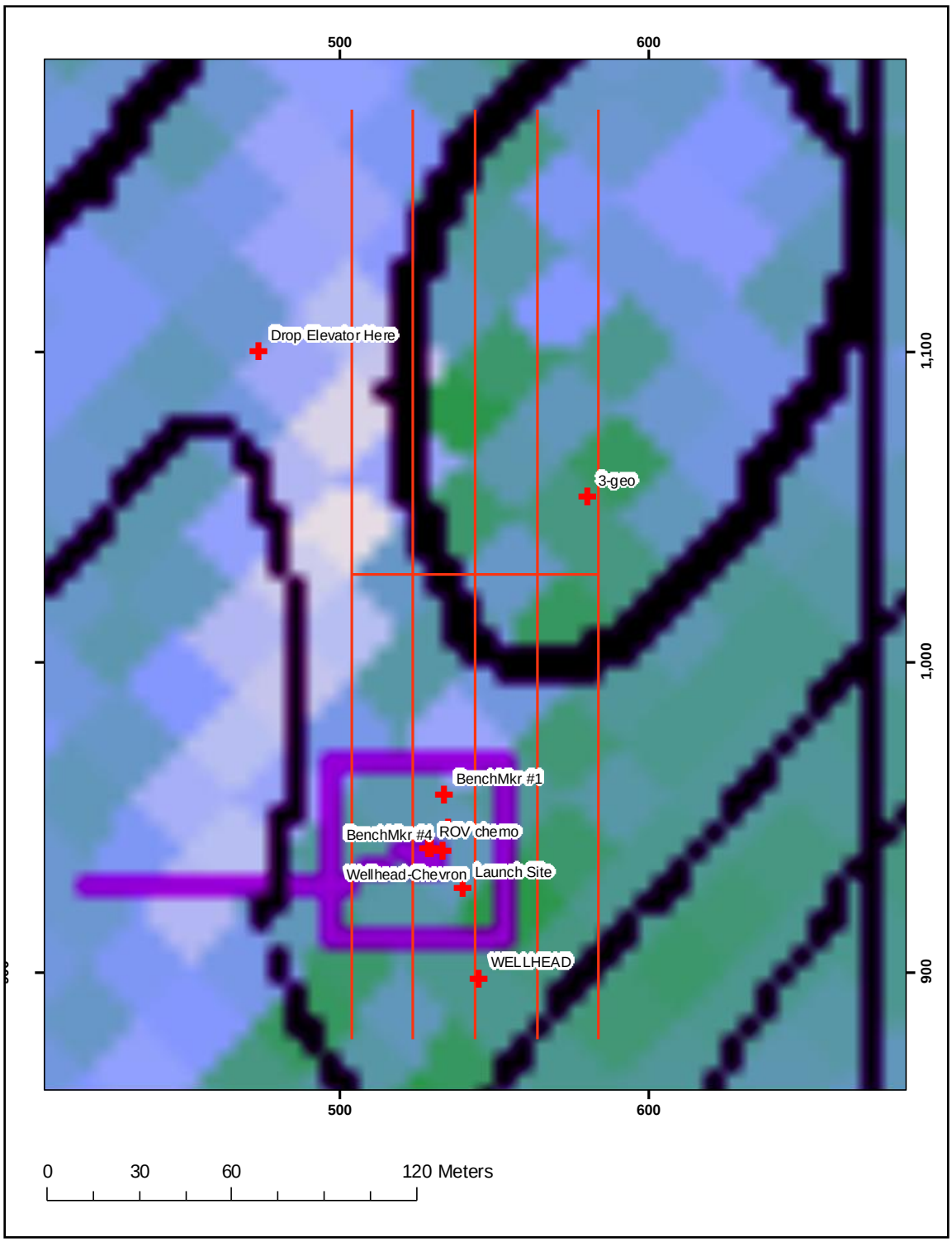

Figure 10-86. Targets for dive 282 at AC818 on 3-D seismically derived bathymetric map with amplitude overlay (C.I.=10 m). Used by permission, Veritas. Lines are target tracks for SM2000 bathymetric survey. Coordinates are *Jason II* local XY m.

10.13.2. *Alvin* Dive 4192

This was the deepest dive made during the *Alvin* cruise at 2,805 m. The pilot for this dive was Bruce Strickrott and the observer was Stephane Hourdez. It was a pilot-training dive and Mike McCarthy was the pilot-in-training. The *Alvin* landed on the seafloor near the wellhead, got navigational information, and then proceeded toward the wellhead, which is a known point to which the sub's navigation can be calibrated. On the way to the wellhead, they encountered a clam bed, but all the clams appeared to be dead. After they arrived at the wellhead, it was a short time before they found the chemosynthetic community that had been documented by the ROV. From our coordinates of the site, the community is only about 40 m from the wellhead. The rest of the dive was spent sampling this relatively small area of chemosynthetic communities. The size of this community is the reason that it does not appear as a distinct anomaly on the 3-D seismic reflectivity data. There are probably several of these small communities along the fault. At this one productive community site, the following samples were collected: 1) 12 push cores (six in mussel/ tube worm areas and six in an urchin area), 2) one mussel pot sample, 3) one scoop sample of mussels, 4) one grab sample of small tube worms, and 5) one carbonate rock sample. After the dive, a trawl sample was taken over this site (Figure 10-87).

10.13.3. *Alvin* Dive 4195

The pilot was Pat Hickey and the observers were Erik Cordes and Liz Goehring. The objective of the dive was to head to the wellhead area, acquire navigational information, and then travel north to the northernmost reflectivity anomaly along the regional fault along which the hydrocarbon seepage is occurring. This transit was made without finding densely populated chemosynthetic communities. The sub returned to the known site near the wellhead and started a rather intensive sampling program. The objective was to collect tube worms and mussels as well as stain tube worm bushes for growth studies.

The following samples were collected: 1) one Bushmaster collection, 2) one scoop sample of mussels, 3) one large rock sample, 4) one and a half push cores, and 5) slurp samples including a sea cucumber, sea star, squid, crab, and pogonophoran. Four tube worm bushes were stained and assorted Cool Pix macro pictures acquired. Although we had planned another dive at this site, it was decided that no more meaningful collections could be made at this site so we left for additional dives in the Alaminos Canyon area (Figure 10-88).

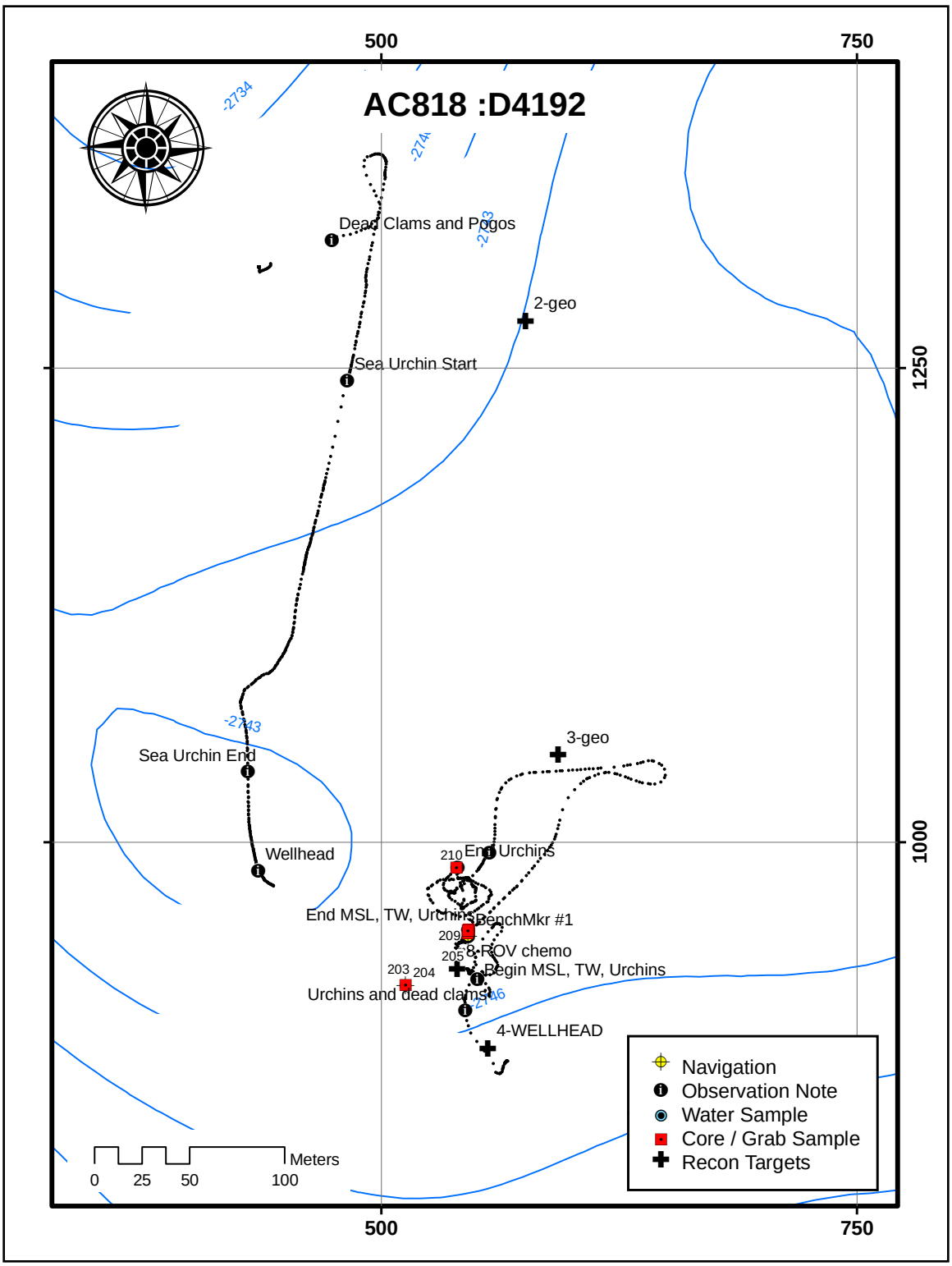

Figure 10-87. Dive 4192 on 5/27/2006 at an average depth of 2,740 m.

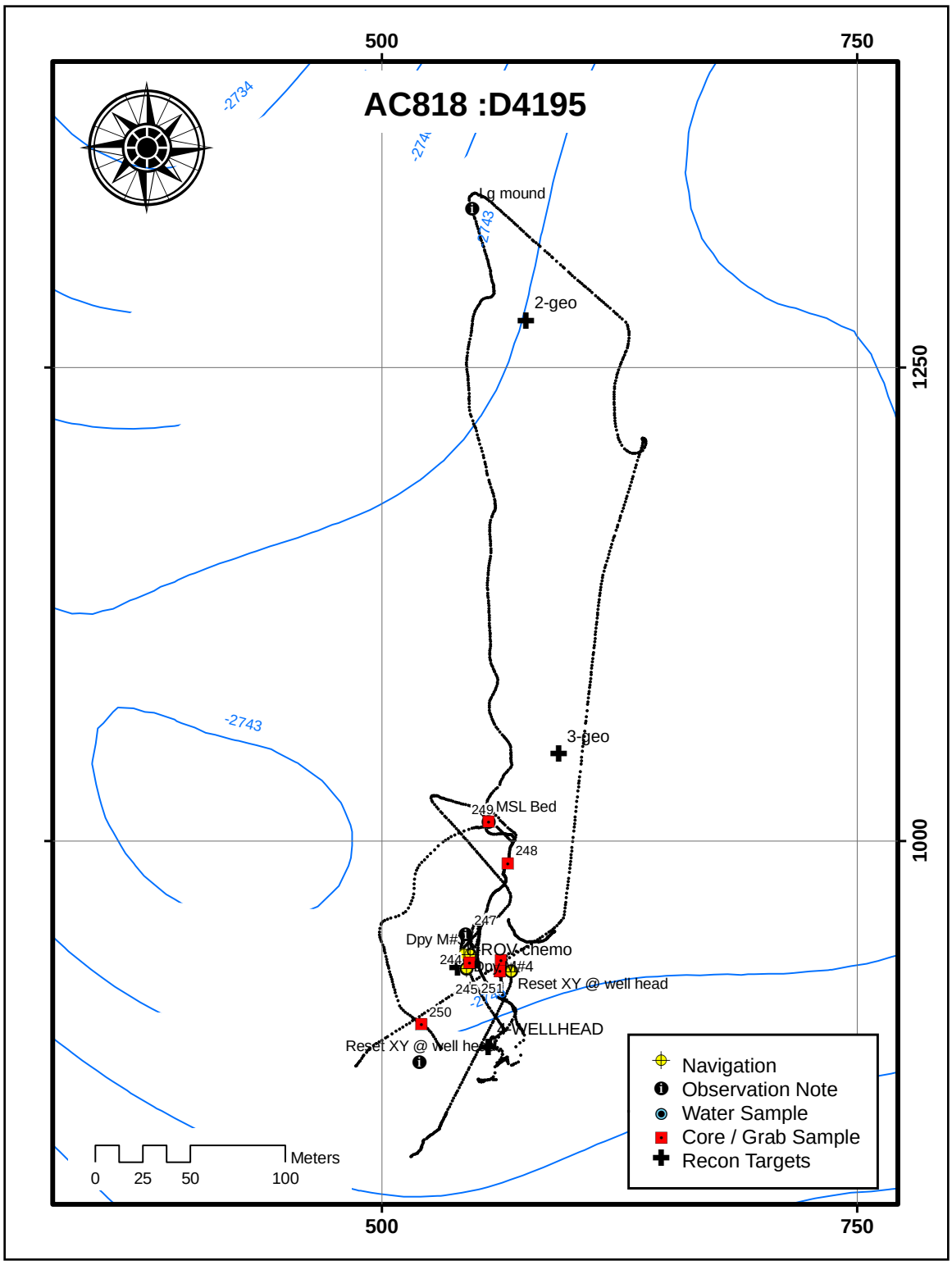

Figure 10-88. Dive 4195 on 5/30/2006 at an average depth of 2,740 m.

10.13.4. *Jason II* Lowering 282

Time in water: 2		007/06/30 12:31
Time on bottom:		2007/06/30 14:10
Time off bottom:		2007/07/01 18:01
Time out of water:		2007/07/01 19:41
Water Time:		31 hrs 9 minutes
Bottom Time:		27 hrs 52 minutes
Min. working depth:		2688.41 m
Max. working depth:		2750.31 m
Produced	:	2.9 GB of raw vehicle data
Produced:		~44 DVDs of Science video
Produced:		~44 DVDs of Archive video

The elevator was launched at about 06:00 hrs with rotary time-lapse camera Huey and a rack of replacement push cores. *Jason II* was launched at 07:30 hrs. All times in this summary narrative are Central Daylight Savings Time , which is UTC minus 5 hours.

The mass spectrometer was tested on the way down and seemed to be operable. *Jason II* reached bottom at 11:10 hrs and began a search for a coring station to collect pogonophorans and associated sediment. The wellhead was occupied at 09:36 hrs (Figure 10-89). Comparing the observed *Jason II* position to the Chevron wellhead location provided by BOEM (26 10 47.398 N, 94 37 22.414 W NAD27) yielded a difference of approximately 24 m to the east-northeast (Figure 10-90).

Figure 10-89. Chevron wellhead observed during JII-282, at AC818.

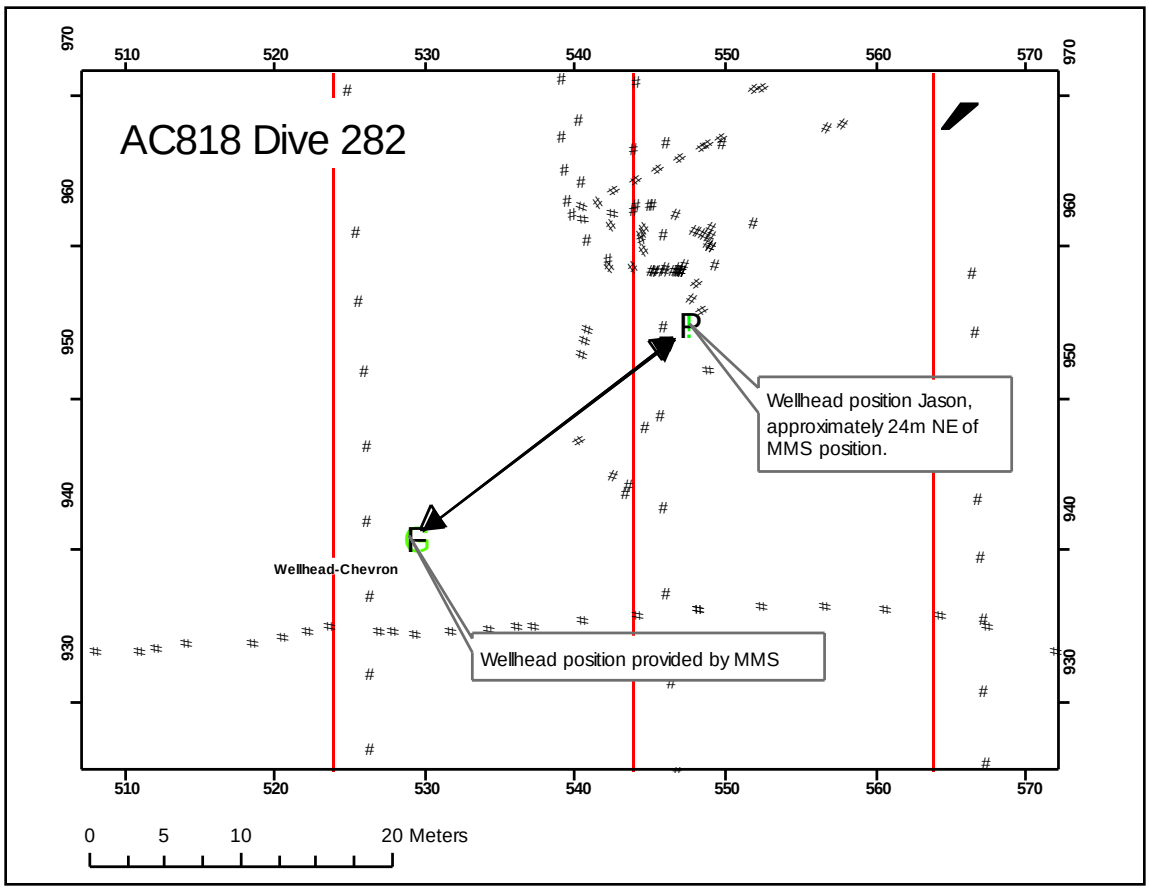

Figure 10-90. Observed *Jason II* position to the Chevron wellhead location.

Marker #4 was found at 09:43 hrs. *Jason II* continued north and reached marker #1 at 09:52.

A suitable pogonophoran field was found at 10:40 hrs at position X-563 m, Y-1198 m. Between 10:40 and 11:20 hrs, (VV events 40744-40917) collection of 11 pogonophoran cores was logged.

Jason II then moved to an area of sea urchins and commenced collection of sediment cores in the sea urchin field until 12:07 hrs (VV event 40893-40917). At this time *Jason II* moved to the elevator site to send push cores up to surface (Figure 10-91) and to remove elevator. *Jason II* arrived at elevator at 12:29 hrs. After the cores were loaded and the rotary time-lapse camera was removed, the anchor was released to send the elevator to the surface. Because the elevator legs were buried in mud, the pilot had to grasp the elevator with the Schilling arm to free it from the bottom. When it lifted off, the jaws of the arm were snagged. Freeing the Schilling arm was a 20-minute operation that entailed having to drop the rotary time-lapse camera from an altitude of about 3 m. The arm was freed without being damaged and the camera remained functional.

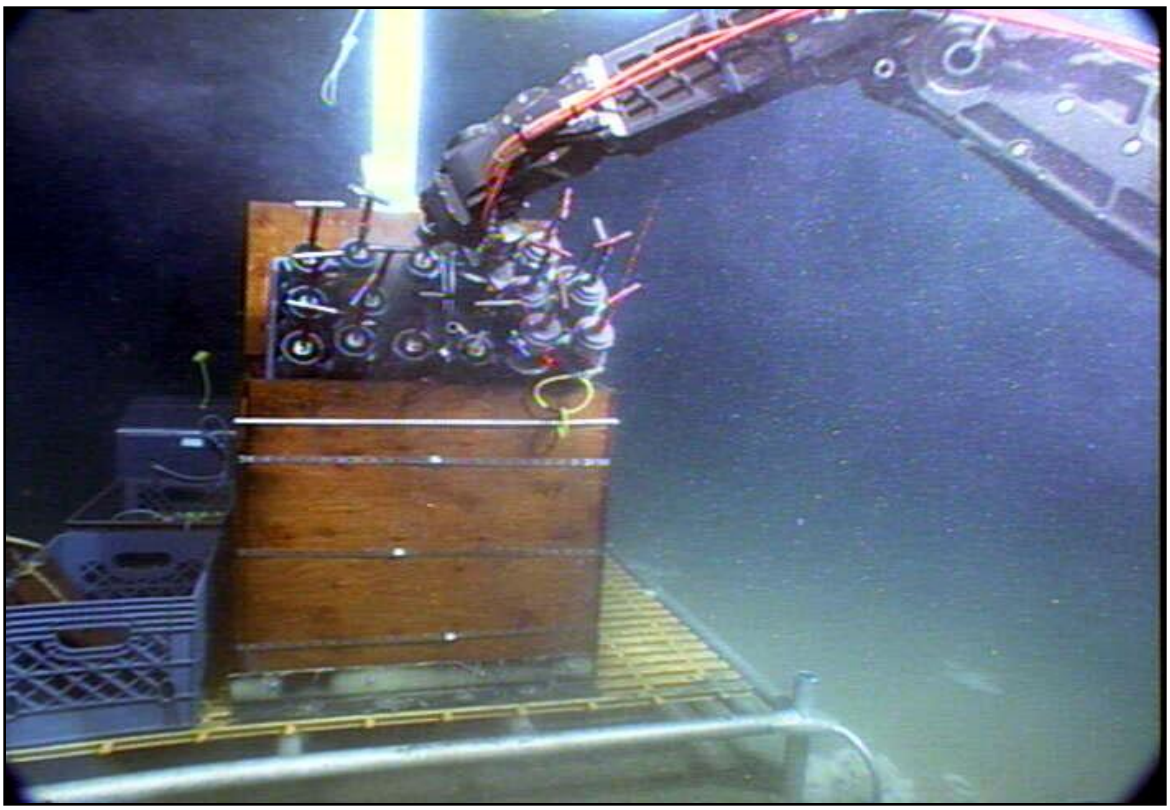

Figure 10-91. Loading core racks onto elevator.

Rotary time-lapse camera Huey was deployed next to Marker #1 at 13:34 hrs (VV event 41100). Its strobe was observed to flash after deployment.

Jason II then went into lay-back mode for elevator recovery. The elevator was taken on deck at 15:04 hrs. *Jason II* then positioned to begin SM2000 bathymetric survey. The SM2000 survey was conducted between about 16:32 and 20:02 hrs (VV event 41241-41673).

At the conclusion of the SM2000 survey, the rotary time-lapse camera was moved from Marker #1 to a position just north of the well head approximately 4 m from the main structure. The camera was deployed at 20:30 hrs (VV event 41709). The flash was observed to fire.

Jason II moved north and prepared a photo-mosaic of the tube worm, mussel and urchin communities situated from south of Marker 4 to north of Marker 1. This mosaic will comprise five, long, north-south lines passing through the main axis of the communities. Actual mosaicking began at 20:58 and continued through 21:44 hrs (VV event 41802-41901).

At the conclusion of the photo-mosaic, *Jason II* moved closer to the mussel beds to carry out measurements with the mass spectrometer. The position is X-536 m, Y-1017 m; depth is 2,744 m. Observations with the mass spectrometer commenced at 22:00 and continued through 22:44 hrs (VV event 41933-41951). Readings were logged as position 68 through position 70. At 23:03 hrs, mussel pot D was successfully used to collect the mussel community at the position of the chemical measurements. A scoop of mussels was also collected and stowed in the port

(insulated) biobox in the vicinity of mass spectrometer readings 72–74. During measurement 72, the probe was accidentally inserted into the sediment, so the valve on the basket was turned and the lines leading to the inlet of the mass spectrometer switched.

Jason II continued operations with collection of mussel pot using pot B, commencing 00:50 hrs (VV event 42014-42036). Difficulties were encountered with use of this device due to the ram not extending to the stop on the mussel pot. It was stowed at 01:04 hrs and collections of mussels were made with jaws of manipulator, continuing until 01:20 hrs. The mass spectrometer wand was then deployed to measure dissolved gases in the sediment scars created by the mussel collection activities. Mass spectrometer readings were collected as positions 74 and 75.

Jason II was repositioned slightly to collect stained tube worms near Marker #3. The marked tube worms were collected by the manipulator arm and stowed in the biobox. Collection was completed at 02:28 hrs.

Jason II was then repositioned to a bacterial mat located near position X-542 m, Y-1003 m, depth 2743m. Mass spectrometer readings were collected into positions 76-79. Five bacterial mat cores were collections were logged, followed by three control cores. Coring concluded at 03:58 hrs (VV event 42286-42409).

Jason II moved about 20 m east while making biological observations of mobile fauna—eventually locating an area occupied by sea urchins—brine-stained sediments were visible in the vicinity. At 05:01 hrs we commenced coring operations collect sediment from urchins. Coring concluded at 05:17 hrs, with 3 core collections logged.

Suction and grab collection of mobile fauna and video observations were carried out until 08:17 hrs. At this time, *Jason II* moved back to the elevator which had been relaunched. All cores and mussel pots B and D were stowed on elevator. Elevator was released at 09:09 hrs (VV event 43043). *Jason II* then made biological observations and grab samples until 10:31 hrs but was in lay-back mode for elevator recovery. *Jason II* moved to well head at 11:18 hrs. At the well head, the rotary camera was picked up and moved to a position north of marker #3 (VV event 43353).

Jason II then moved to near Marker #4 to collect stained tube worms with Bushmaster. Collection was complicated because there was a tangle of monofilament fishing net partly entangled in the cluster of stained tube worms and in base of Marker #4. After consultation with the *Jason II* pilots, an attempt was made to use Marker 4 to clear the net and allow collection. The marker was dragged through the net and the net was moved approximately 5 m to the west. Mass spectrometer readings started at 11:59 hrs at position 80. Collection with Bushmaster proceeded smoothly from 12:20 to 12:30 hrs. [This tube worm aggregation contained over 100 young, stained tube worms, most of which exhibited significant growth.]

Jason II then moved north toward Geo targets 1 and 4. At 12:59 a field of pogonophorans was noted. There were also many clam shells at this site—most appeared to be dead. The position is X-567 m, Y-1232 m, depth is 2738 m. *Jason II* left bottom at 13:01 hrs on 2007-07-03.

Non-seep fauna was typical for the lower slope and was dominated by elasipod holothuroids. Crabs were not observed and fishes limited to a few rattails. Eleven holothuroids and asteroids were collected. The dive track for dive 282 is shown in Figure 10-92.

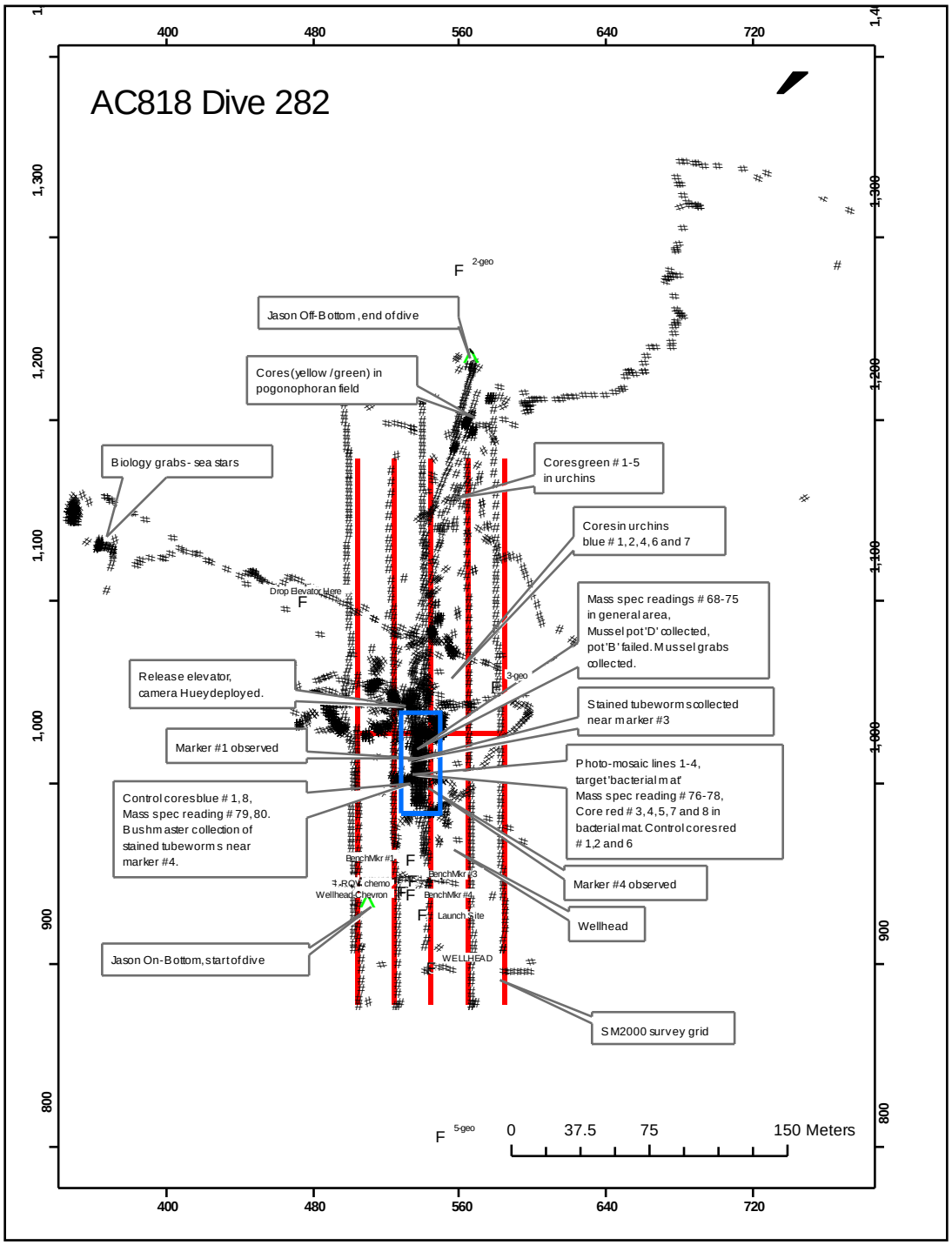

Figure 10-92. Dive track for D282.

10.13.5. *Jason II* Lowering 284

Jason II was launched at 16:07 and reached the bottom at 17:45 hrs on July 4. All times in this summary narrative are Central Daylight Savings Time , which is UTC minus 5 hours. *Jason II* then began to search for camera Huey, which was located at 18:10 and released to the surface at 18:19 hrs. There was some difficulty in releasing Huey during this time.

Five sea stars were grabbed between 18:28 and 18:51 hrs (one of the five eventually escaped from the bio-box). A "Best of" video of a pelagic sea cucumber feeding on the bottom was taken at 19:12 hrs. Doppler navigation was reset at 20:04 hrs. A sea cucumber was collected at 20:12 hrs. Pogonophorans and clams were noted at 20:17 hrs, and a digital marker fix was taken on this site at 20:18 hrs. The presence of pogonophorans was noted along *Jason* II's path until 20:41 hrs.

At 20:44 hrs *Jason II* was in site of Marker #4 and began to run photo-mosaic lines in the area. Four photo-mosaic lines were run from 21:11 to 22:03 hrs. *Jason II* then moved to Marker #1, arriving at 22:05 hrs. A grab of stained tube worms was made at 22:09 hrs (a "Best of" video of these tube worms was also taken at 22:11 hrs).

Camera Huey was scheduled for a long-term deployment after recovery, but problems with the camera's strobe (possibly caused during the attempts to release Huey at the beginning of the dive) forced this plan to be abandoned and a planned elevator launch was aborted.

At 23:10 hrs *Jason II* arrived at the northern urchin site (EVT49555, X-539 m, Y-1,048 m) and took eight (8) push cores (yellow) as well as collecting 4 individual urchins from 23:13 to 00:12 hrs on July 5th. *Jason II* then moved a short distance to Marker #1 (X-541 m, Y-1018 m).

Mass spectrometer readings 96–101 were taken within the vicinity of Marker #1 from 00:25 to 02:06 hrs. Readings 97 and 98 were taken in an area with brown mussels, reading 99 in an area of white stained mussels. Readings 100 and 101 were taken near a large tube worm bush. Doppler navigation was reset during reading 101 at 02:05 hrs.

After completing the mass spectrometer readings, *Jason II* moved to Marker #4 (X-533 m Y-1,006 m). Two Niskin samples were taken over a mussel bed near marker #4 at 02:19 hrs. Mass spectrometer reading 102 was taken from 02:29 to 02:44 hrs. Mussel pot D and B were collected in the same location (area of white mussels) at 02:55 and 03:20 hrs respectively.

At 03:48 hrs *Jason II* began to head north looking for clams to sample. Numerous biological observations were made from 03:56. Two net scoops of mussels were taken at 04:34 and 04:37 hrs near X-551 m, Y-1,078 m.

Jason II then began to move south again, making numerous biological observations and taking macro camera pictures from 04:56 to 05:28 hrs. From 05:30 to 06:26 hrs *Jason II* moved around a small area making biological observations and taking seventeen slurp samples of tube worms, sea stars, and sea cucumbers (Figure 10-93). At 06:26 hrs the mass spectrometer was turned on to take readings during the ascent to the surface, and at 06:27 hrs *Jason II* left the bottom to begin its return to the surface.

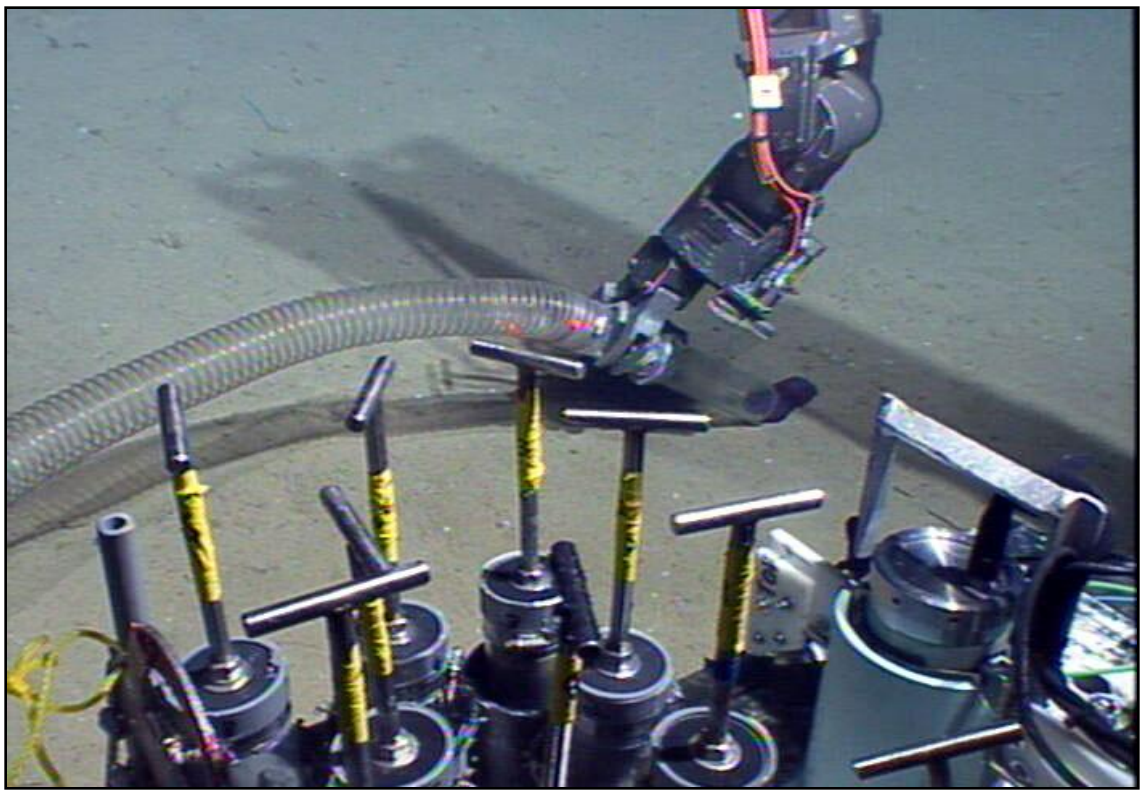

Figure 10-93. Slurp collection of sea cucumber.

Non-seep fauna has been previously described. Eighteen samples were taken for background analysis consisting of elasipod holothuroids, and asteroids. The dive track for dive 284 is shown in Figure 10-94.

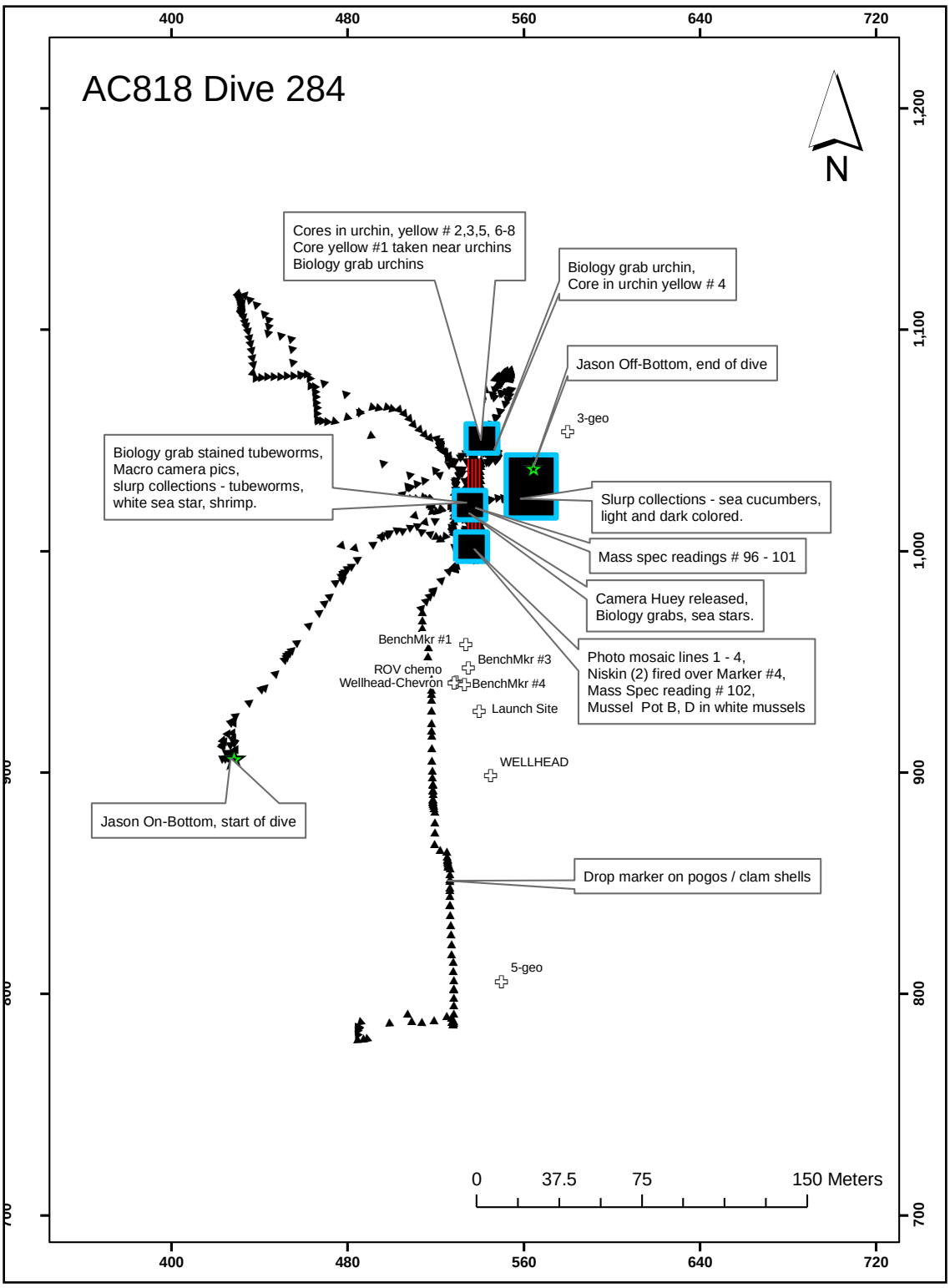

Figure 10-94. Dive track for D284.

10.14. Alaminos Canyon 601

This site (AC601) was not visited during the Recon Cruise, but was visited during ROV reconnaissance of the area previously by Harry Roberts. There were two *Alvin* dives at AC601, including AD4193 on 5/28/06 and AD4196 on 5/31/06. There was also one *Jason II* lowering at this site from 7/02/07 to 7/04/07 for 42 hours and 41 minutes.

10.14.1. *Alvin* Dive 4193

The pilot for this day's dive was Gavin Eppard. The observers were Harry Roberts and Mandy Joye. The objective was a large mound-like feature in the northwest part of AC601. Previous side-scan data indicated that the mound had flow deposits radiating from the mound top. However, the expulsion center does not seem to be active now or in the recent past. A depression on the northern side of the mound was found to be a brine lake by the 2005 ROV survey. The *Alvin* dive proved that this site is much more productive regarding chemosynthetic communities than the ROV survey data revealed. We found abundant tube worm colonies around the mound rim, but no mussels. Carbonates, tube worm colonies, localized bacterial mats, and pogonophoran colonies characterized the mound top. We did not explore the whole top, so there may be more than reported here. Off the mound to the north we found the brine lake. It was an amazing feature with what we think is elemental sulfur floating at the interface and at the "shoreline." We mapped the perimeter of the lake with the sub. It was about 150 m in diameter and roughly circular in plan-view. An urchin field paralleled the shoreline of the lake and was about 5–10 m wide. Numerous urchins inhabited this zone along with some small clumps of mussels. Broad areas of pogonophorans were also observed along the western shoreline of the lake. This was a very interesting dive, and there were many areas that we did not get a chance to observe. We finished the dive thinking the area is potentially more productive than we have thus far shown (Figure 10-95).

The following samples were collected and activities conducted: 1) 12 push cores, 2) one tube worm bush, 3) five Niskin bottle samples (in the brine lake), 4) two carbonate rock samples, 5) one scoop mussels and urchins, 6) Cool Pix pictures of tube worm associated fauna, and 7) video of the brine lake and its rafts of crystalline material (maybe elemental sulfur).

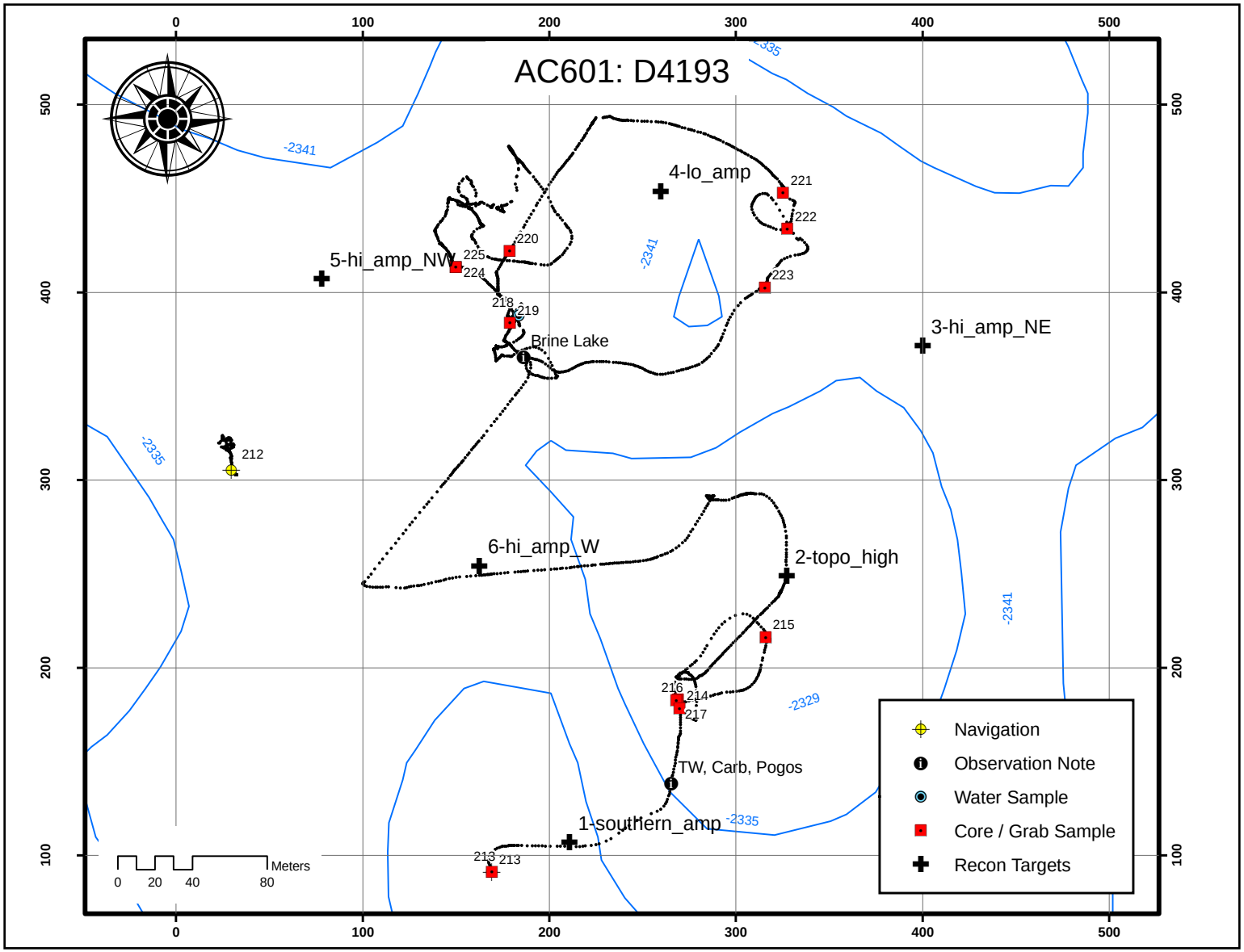

Figure 10-95. Dive 4193 on 5/28/2006 at an average depth of 2,330 m.

10.14.2. *Alvin* Dive 4196

The pilot for this dive was Bruce Strickrott and the observers were Chuck Fisher and Jeremy Potter. The main objectives for the dive were to map the perimeter of the lake a second time (some navigation problems had obscured the results of the first mapping effort), to take uncontaminated samples of the brine, and to complete faunal sampling including a Bushmaster sample. These objectives were met and it was found that the lake was about 160 m in diameter and that the brine salinity was about 90 practical salinity units. Samples were also taken during this dive to determine the origin of the white clots that are floating in the brine and that accumulated at the lake shoreline. Both suction pump sampling and coring addressed this issue.

The following samples were collected: 1) one Bushmaster sample, 2) two suction pump samples of brine, 3) one slurp sample, 4) 12 push cores, 5) one scoop of mussels, 6) two rocks, and 7) one octopus. This very interesting dive collected some critical data to help understand the characteristics of the brine lake and surrounding area. The last dive of the cruise will go back to AC645 for final collections (Figure 10-96).

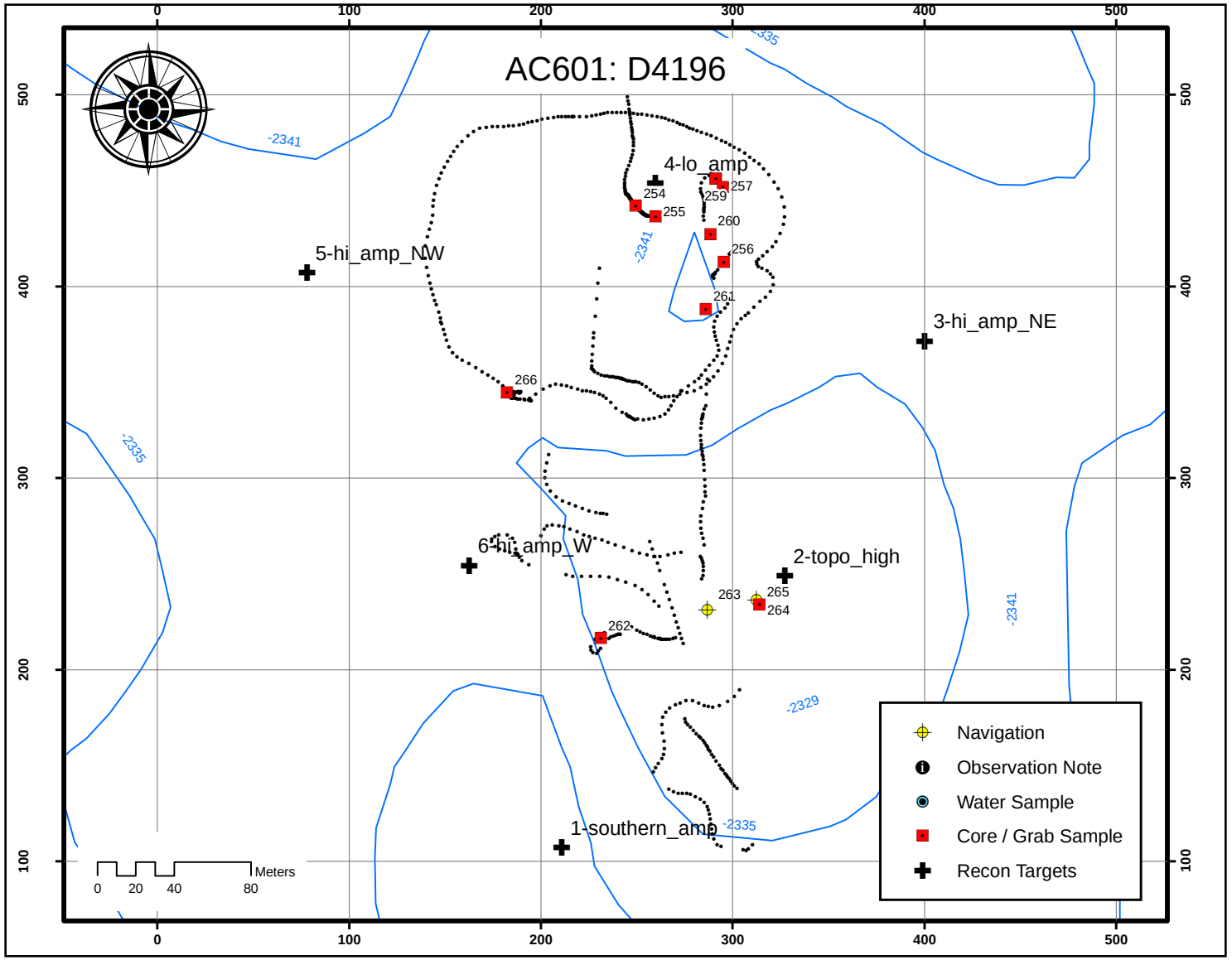

Figure 10-96. Dive 4196 on 5/31/2006 at an average depth of 2,330 m.

10.14.3. *Jason II* Lowering 283

Jason II launched at 07:00 hrs on a dive target selected to be the northern edge of the brine pool at (XY). The bottom was in sight at 08:27 hrs and *Jason II* was in the middle of the brine pool. *Jason II* headed due north to the edge of the pool and conducted survey around the perimeter with the DSC on 15-second intervals. This survey followed the contour of the AUV survey very closely. The survey was completed at 09:55 hrs and core sampling commenced. The first set of cores was taken 5 m from the barite shore-line from 1011 to 1019 (EVT43746). The second set of cores was taken within the barite zone from 1050 to 1105 (EVT43812). The third set of cores was taken in knee deep brine (Figure 10-97) on the edge of the pool from 11:45 to 11:58 hrs (EVT43938). Both Niskin bottle samples were taken in this area by using a t-handle to dip the bottles into the brine from 12:12 to 12:28 hrs (EVT44000).

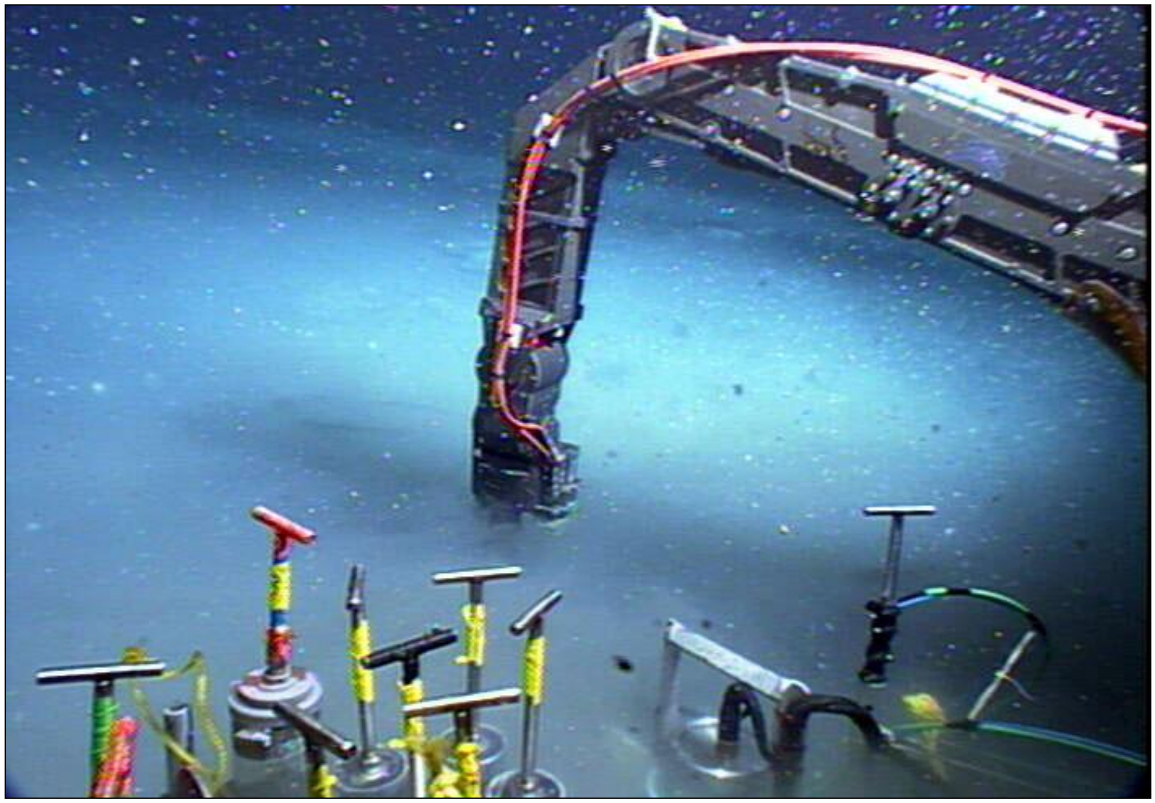

Figure 10-97. Taking cores "knee deep" in brine pool.

Jason II transited to the elevator, arriving at 12:56 (EVT44097). The core racks were swapped and Niskin bottles were deposited on the elevator and the elevator released at 13:15. While in lay-back mode, 3 sea cucumbers and a sponge were slurped from 13:15 to 14:51 hrs. When the elevator was on deck at 14:51, *Jason II* transited to the start of the photo transect survey. This survey was a set of lines centered around the middle of the brine pool and extending from the shore line out. The survey lasted from 15:09 to 18:30. During the survey, 2 background scans were conducted with the mass spectrometer. At the end of the survey, the macro camera was used in down-looking mode to retrace transect line #9 from the center of the pool to the end of

the line. This was begun at 18:46 (EVT44723), continued at 19:27 with a number of images of the shore-line.
Slurping and grabbing (in starboard biobox) of mobile fauna proceeded from 20:14 to 21:40 at which point *Jason II* approached the shoreline of the pool once again. Two push cores were taken in the barite zone for Harry Roberts from 21:42 to 21:49 (EVT45115). The mass spectrometer was then used to take samples above the barite shore line from 21:49 to 22:46, taking readings in positions 83–85 (EVT45119). *Jason II* then headed towards the interior of the pool and took scans 86–89 within the brine from 22:53 hrs on July 02 to 00:16 hrs on July 03 (EVT45259). During this time, there were a number of significant hits of methane and sulfide detected within the brine. The mass spectrometer appeared to be working very well.

Jason II then transited back to the shoreline to continue following the path of photo transect #9 with the macro camera. A series of macro pictures were taken from 00:36 until 01:31. A slurp collection of mussels on barite was made at 01:36 (EVT45620) [although upon recovery these mussels were not present in the slurp container], and a grab of an urchin was made at 01:50 (EVT45660). The macro photo-transect was continued from 01:52 to 02:23 hrs.

Jason II then returned to the shore line to core urchins. A series of cores were taken in and out of urchin trails from 02:41 to 03:36 hrs (EVT45763). A mass spectrometer reading (#90) was taken inside the core hole from the first core at 03:09 (EVT45817). A search for pogonophorans began at 03:36 hrs passing over the northern, western, and southern edges of the pool and continuing to the south. Three cores were taken in a small patch of pogos at 06:35 hrs (EVT46363). Finally, a large, dense bed was found at 07:08 (EVT46446) and 3 cores and the 2 fat cores were taken in this location, concluding at 07:23. Another patch was found and the remaining 2 fat cores and 2 more pogo cores taken at 07:45 (EVT46527). This was followed by macro pictures until 08:23 hrs.

Jason II transited back to the pool and took one urchin core for Harry Roberts at 08:44 (EVT46640), a series of pictures were taken of *Jason II* and the brine pool, then *Jason II* transited to the elevator. Five control cores were taken next to the elevator (EVT46763) from 09:34 to 09:40. The cores were placed on the elevator and the good mussel net removed from one of the wooden boxes. The elevator was released at 10:03 at which time the feed from *Medea* was recorded to get some good video of *Jason II* and the brine pool. The elevator was recovered at 11:55 and *Jason II* went back to a position where strange-looking mussels were noted to collect a scoop. The mussel scoops were taken at 12:24 hrs in a mussel bed on top of a large barite formation (EVT47121) [Upon recovery, this was found to be slightly radioactive, so the mussels were removed from the barite and the minerals jettisoned overboard. The mussels appear to be the same species that was sequenced last year and found to not belong to the genus *Bathymodiolus*.]

At 0551, *Jason II* came up to 150 m off the bottom and went into tow mode, transiting approximately 1.5 km to the south to a large mound feature in the AUV survey corresponding to a circle of high reflectivity bounding a low reflectivity center. The bottom was back in sight at 14:23 (EVT47166) and *Jason II* approached the feature from the north transiting up the side of the mound. At 14:40 (EVT47202), *Jason II* crossed over the lip of the crater on the top of the mound and found the border of what appeared to be a large brine lake. This was subsequently

named Lake Eerie (Figure 10-98) by the *Jason II* pilots due to the very odd appearance of the white "sand dunes" on the edge of the lake.

Figure 10-98. The northern edge of "Lake Eerie."

Jason II traced the outer edge of the lake with the DSC firing on a 20-sec interval. The perimeter corresponded very well to the bathymetry in the AUV survey. At 14:47, a few isolated mussel beds and interspersed urchin trails were noted, and these continued until a very large mussel bed was noticed at 14:57 (Figure 10-99). The mussel bed extended from (EVT47245) to (EVT47253).

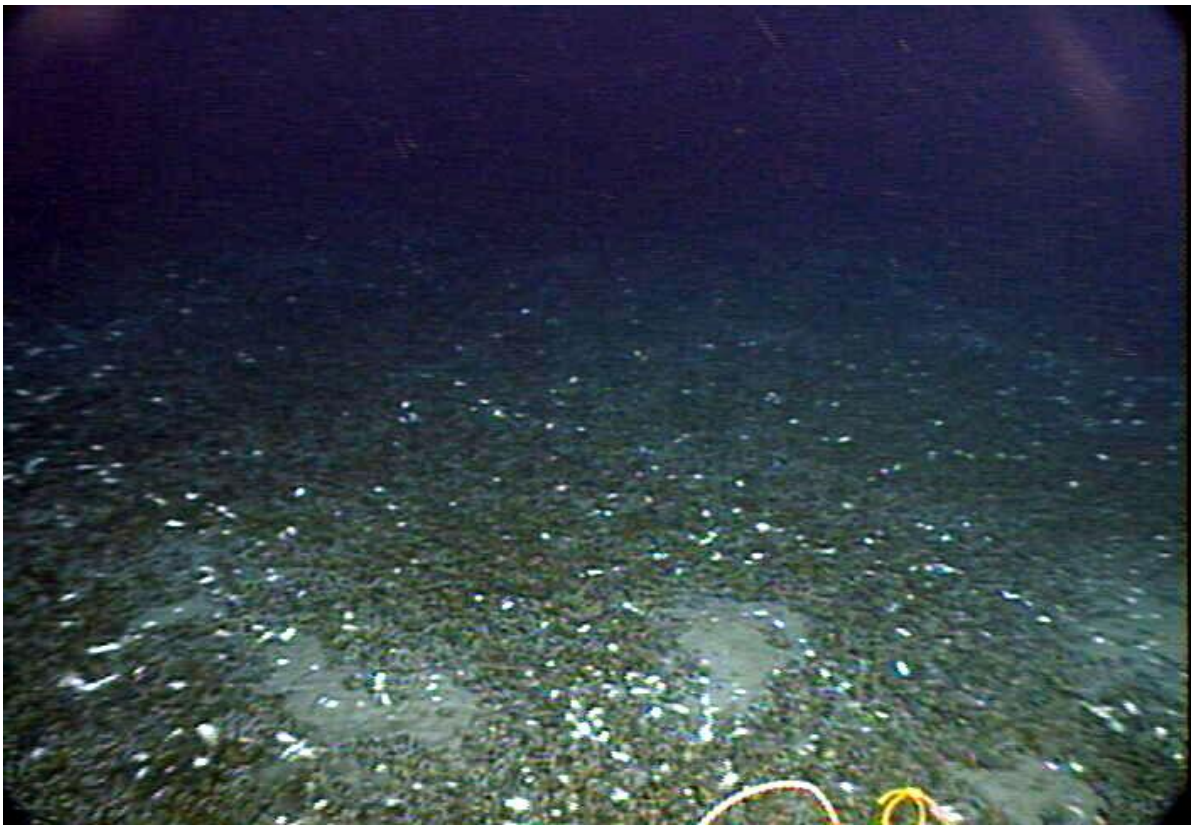

Figure 10-99. After closer review of the AUV data, scientists spotted another geological target of potential interest. They discovered what is probably one of the largest-known mussel beds in the deep GoM; a small portion of the bed is shown in this image.

At this point, it was decided to launch an elevator at this target. The elevator was equipped with two mussel pots, nine cores, a mussel scoop, and two hand-held Niskin bottles. The survey around the perimeter continued while the elevator was prepped and launched. Patchy mussel beds continued around the western edge of the feature, and became less dense on the southern rim (EVT47343) where large mud flows were noted at a depth of 2,283 m. Stained sediments and strange bed formations continued around the southern and eastern edges of the lake. A series of macro pictures were taken of the shoreline beginning at 1649 (EVT47492) and continuing as *Jason II* traced the shoreline.

Once the perimeter trace was completed (17:12 hrs, EVT47533), *Jason II* headed to the elevator launch site. The elevator was launched at 17:39, and was in site at 18:40 (EVT47718). The elevator was picked up at 18:50 and moved to the large mussel bed (Mussel Manhattan), arriving at 19:29. The mussel pots were retrieved at 19:56 (EVT47873). The first (mussel pot D) was taken right next to the elevator in Mussel Manhattan at 20:05 (EVT47894), and placed back in its holster on the elevator at 20:17, and Marker 1 deployed in its location. The second (mussel pot B) was taken at an isolated patch of mussels just to the east near the shoreline at 20:37 (EVT47960), Marker 2 deployed, and the mussel pot returned to the elevator at 20:52. The push

core rack and the Niskin bottles were then removed from the elevator and placed on the basket at 21:22 hrs.

Jason II then started to look for brine to take pushcores and sample some brine in Niskins. On the way south from the elevator, *Jason II* ran over strange formations with "dunes" of mud and dark channels that looked like they contained brine (EVT48106). From the shore, *Jason II* headed towards the center of the crater in search for brine deep enough for cores and Niskin bottles. At 22:00 hrs, *Jason II* was moving over extensive red stains (EVT48133) with some signs of downhill flows (22:03, EVT 48141). At 22:10 hrs, a set of cores was taken in the area. The mud is very fluid and some cores came out of the cores before they were in the holsters. The long slim Niskin was used upright in the fluid mud to get a sample (22:36, EVT 48217). The lower end of the Niskin touched a harder layer underneath while 10 cm were still out of the mud (Figure 10-100).

Figure 10-100. Using Niskin to take core sample in soft red-stained sediment.

Jason II then headed south to follow the flow of brine and find deep brine areas (Figure 10-101). At 22:53, *Jason II* is back in areas with mud dunes and dark channels between them (EVT48255). A set of four cores was then collected in this area in the brine channel (EVT48266-48276). AT 23:03, *Jason II* started heading back to the mussel bed. Numerous white shells were observed, many snails and clams, some of these latter alive (EVT48297). A close-by channel is overlaid with a mist (EVT 48315) in which the large Niskin was fired, but no obvious interface between the two fluids was observed (23:24, EVT48334). Another set of cores was then taken,

moving every time to avoid contamination of the overlying water of the cores by the resuspended mud (EVT48381). Some clams and white snails were then scooped at 00:02 (EVT48417). At 00:40, *Jason II* was back at the large mussel bed (EVT48497), and some snails were collected in the white net at 00:45 (EVT48511). AT 00:53, *Jason II* is at the elevator (EVT48530) and the core rack was transferred to the elevator, along with the white net in the core rack.

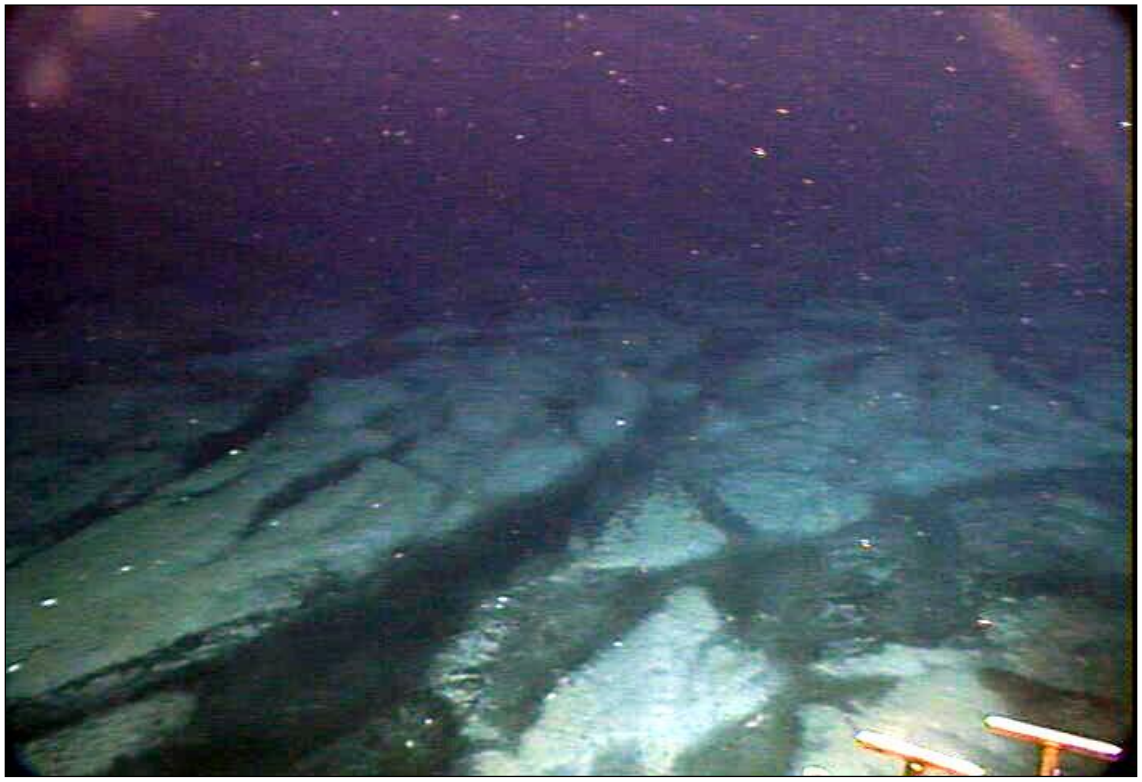

Figure 10-101. Area of apparent brine flows.

At 0102 (EVT48552), a mass spectrometry background scan (#91) was started in the water about 1.5 m above the bottom near marker 1 right next to the elevator. At 01:20, the mass spectrometer wand was placed in the mussel pot D sampling scar to scan (#92) (EVT48590). The wand was then placed among mussels (scan #93) at 01:37 (EVT48623). The mussels had their siphons very extended (EVT48625). Mussels from location of mass spectrometer scan #93 were then collected for genetics studies (01:55, EVT48662) and placed into the port biobox. At 02:00, *Jason II* then headed to the brine shore area to do some mass spectrometry measurements. At 02:28, mass spectrometer scans began at positions #94 and 95 near some tube polychaetes [likely to be Onuphids] in a transition zone (EVT48728) that may have been a gradual brine interface [both methane and sulfide were present in relatively high quantities here.] At 02:48, *Jason II* headed to the elevator to release it and come to the surface. At 02:54, *Jason II* was at the elevator (EVT48790), the Niskin bottles were transferred, and the elevator released at 03:05. *Jason II* left bottom at 03:08. During ascent, the mass spectrometer recorded a depth transect of scans for calibration.

Non-seep fauna at the dive site was typical for the depth and dominated by elasipod holothurians. Ten specimens were collected. Fish were limited in numbers and crabs not observed. The fauna

near the crater was not well surveyed, but seemed to be similar to the dive site and dominated by elasipod holothuroids. The dive track for dive 283 is shown in Figure 10-102.

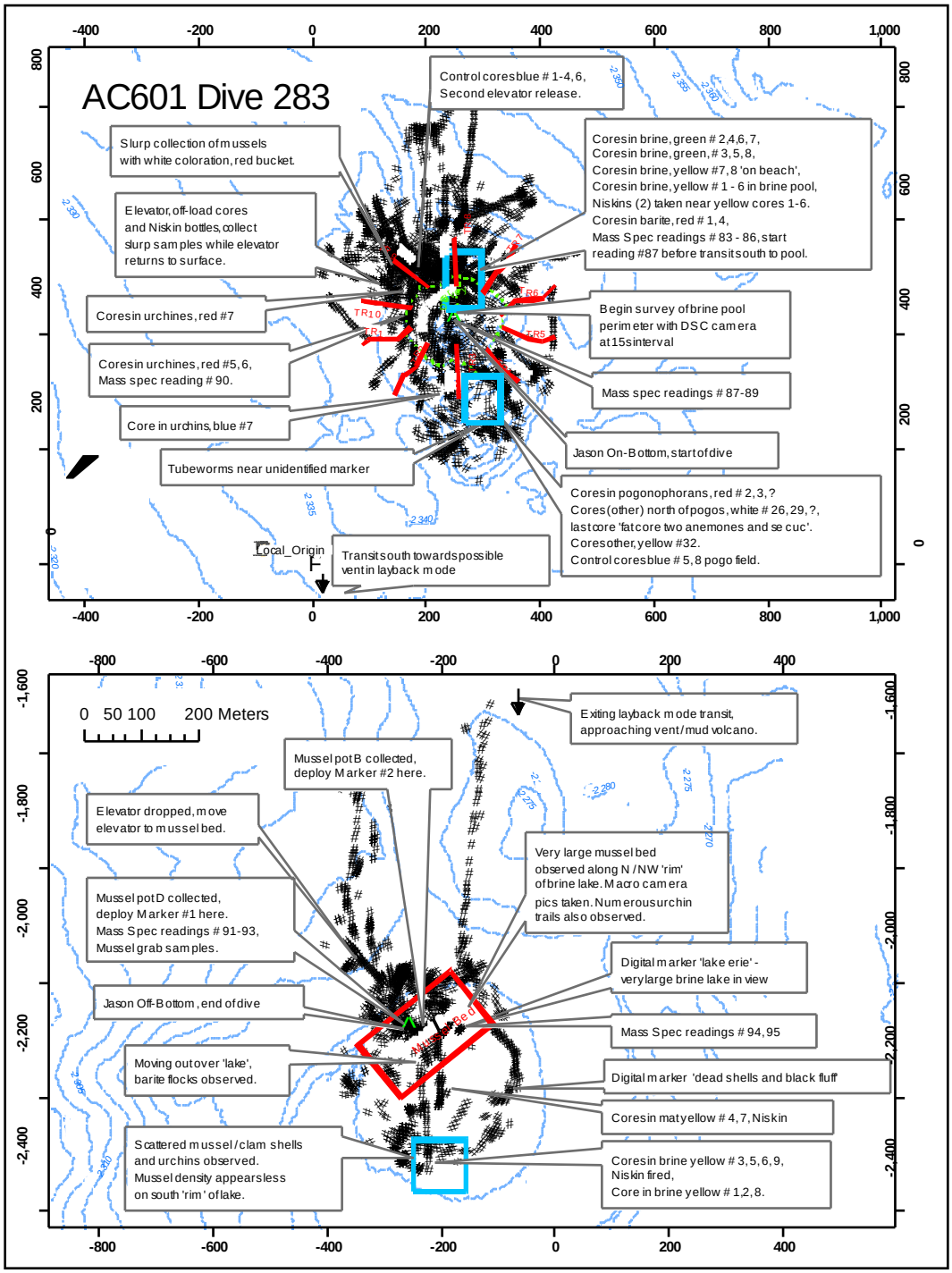

Figure 10-102. Dive track for J2-283.

10.15. Alaminos Canyon 645

This site (AC645) was discovered in 1990 during an *Alvin* dive series led by James Brooks. It was again visited in 1992 during an expedition led by Ian MacDonald. Additional dives at this site were made here in 2003 during an expedition led by Robert Carney. In 2006, we made two *Alvin* dives at AC645, including AD4194 on 5/29/06 and AD4197 on 6/1/06. There was also one *Jason II* lowering at this site. J2-281 took place from 6/28/07 to 6/29/07 for 38 hours and 30 minutes.

10.15.1. Site/Target Selection

Targets for the *Jason II* dive were selected from the 2006 *Alvin* dive logs, and the local origin defined for the 2006 *Alvin* dive was also used (see Table 10-14). This area has been extensively explored and mapped since the early 1990's and the current targets were selected to revisit previous sampling areas. An SM2000 multi-beam survey grid was also laid out to cover the target area of interest (see Figure 10-102). Prior to 2006, the site had last been visited with *Alvin* in 1992. At that time a number of floating markers were deployed. The most abundant markers are rectangular sheets of white, buoyant plastic measuring 15 cm wide and 30 cm high. They have numbers cut into their sides and tops. Hereafter they are referred to as *Alvin*-92 markers. A few additional syntactic foam markers with letters were left in 1992 to precisely identify the location of tube worms banded for growth studies at that time (Figure 10-103).

Table 10-14

Target Locations for Site AC645

Target	Depth	Lat	Lon	Note
Local Origin		26.351667	-94.501667	From 2006 Alvin cruise
Marker #1	2,208	26.354448	-94.498345	2006 Alvin Dive Logs
Marker # 42 - 46	2,202	26.354088	-94.497959	2006 Alvin Dive Logs
TW and MSL	2,221	26.355165	-94.498652	2006 Alvin Dive Logs
Banded Tubeworms	2,195	26.354396	-94.497264	2006 Alvin Dive Logs

10.15.2. *Alvin* Dive 4194

This dive targeted an area of AC645 where previous *Alvin* dives have been made. The site is an east-west trending area with a low relief mound on the western end and a higher and more distinct mound on the eastern end. The eastern mound is the one that has been the subject of previous dives. The two mounds are about 1 km apart and in slightly over 2,200 m water depth. The pilot for today's dive was Mark Spear and the observers were Bob Carney and Cynthia Petersen. The dive plan called for the dive to start on the unknown western mound and, if good sites could not be found in this location, to transit to the eastern mound for collections. On 3-D seismic surface reflectivity maps, the eastern mound was a "bright star" while the western mound had only a moderate level of reflectivity. Both sites show good migration pathways in the subsurface leading to the seafloor. At the start of the dive, *Alvin* and its observers did not encounter much regarding chemosynthetic communities. After looking around the top of the western mound and dive targets 3 and 4, they started the long transit to the eastern mound. While

transiting to target 5, a western-facing slope was encountered with fractured carbonate pavement. Tube worms were abundant either as clusters among boulders or as a large field. Mussel beds were also present among and adjacent to the carbonates (Figure 10-104).

Sediments were chemically stained. Although west and south of target 5 coordinates, this area of lush growth may represent that location from previous dives (Figure 10-105). Progressing up slope to northeast additional carbonate fields and seep fauna were encountered. Markers left in 1992 were encountered. Soft corals were scattered along the carbonates (Figure 10-106). Progressing northwest and downslope towards target 2, seep fauna and carbonates became less common and large expanses of bottom were again dominated by holothuroid and whip seapen. In the vicinity of target two, an area of carbonate, tube worms, dead clams, and mixed live/dead mussels was encountered. Following seep fauna sampling, we explored westward, southward, eastward, and northward to determine extent of seep area. No new seeps were encountered. Only typical non-seep habitat exists surrounding the previously found communities (Figure 10-107).

The following samples were collected: 1) 12 push cores, 2) one tube worm clump, 3) five Niskin bottle samples, 4) two rocks, 5) two mussel pots, 6) three soft corals, and 7) one scoop holothurians.

Figure 10-103. Study site with marked tube worms from 1992 was re-sampled during the final *Alvin* dive (4197).

Figure 10-104. Mussels at AC645 were often coated with a white precipitate not seen at other sites.

Figure 10-105. Community at AC645 was sampled by *Alvin* divers in 1993.

Figure 10-106. Soft coral colonies were observed on the rocky slope to the north of the main sampling station and marker field at AC64.

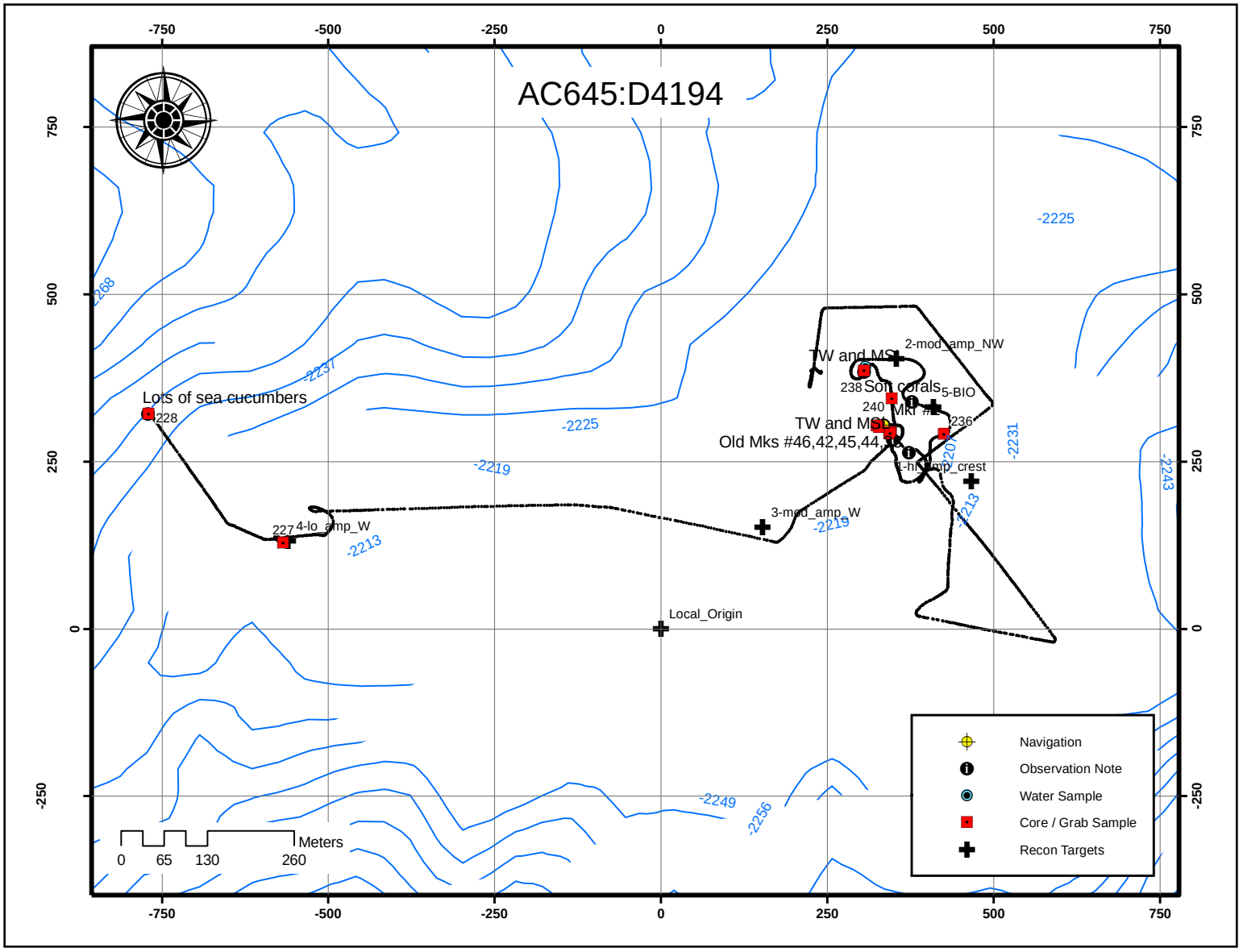

Figure 10-107. Dive 4194 on 5/29/2006 at an average depth of 2,240 m.

10.15.3. *Alvin* Dive 4197

The scientist was Ian McDonald with observer Kazumi and Gavin as pilot. This was a very short last dive before transiting back to land, with a total bottom time of 1.5 hrs (Figure 10-108). The area where markers from 1992 were discovered was the object of the dive. We collected rocks for Harry Roberts and took two mussel pots at markers 4 and 5 at the site where we made mosaics in 1992. There were markers everywhere from this previous cruise. We took some Cool Pix photos of mussels, tube worms and associated mobile fauna. We found Marker E and photographed two banded tube worms. At least one was alive. We left for the surface after 1 1/2 hrs on bottom.

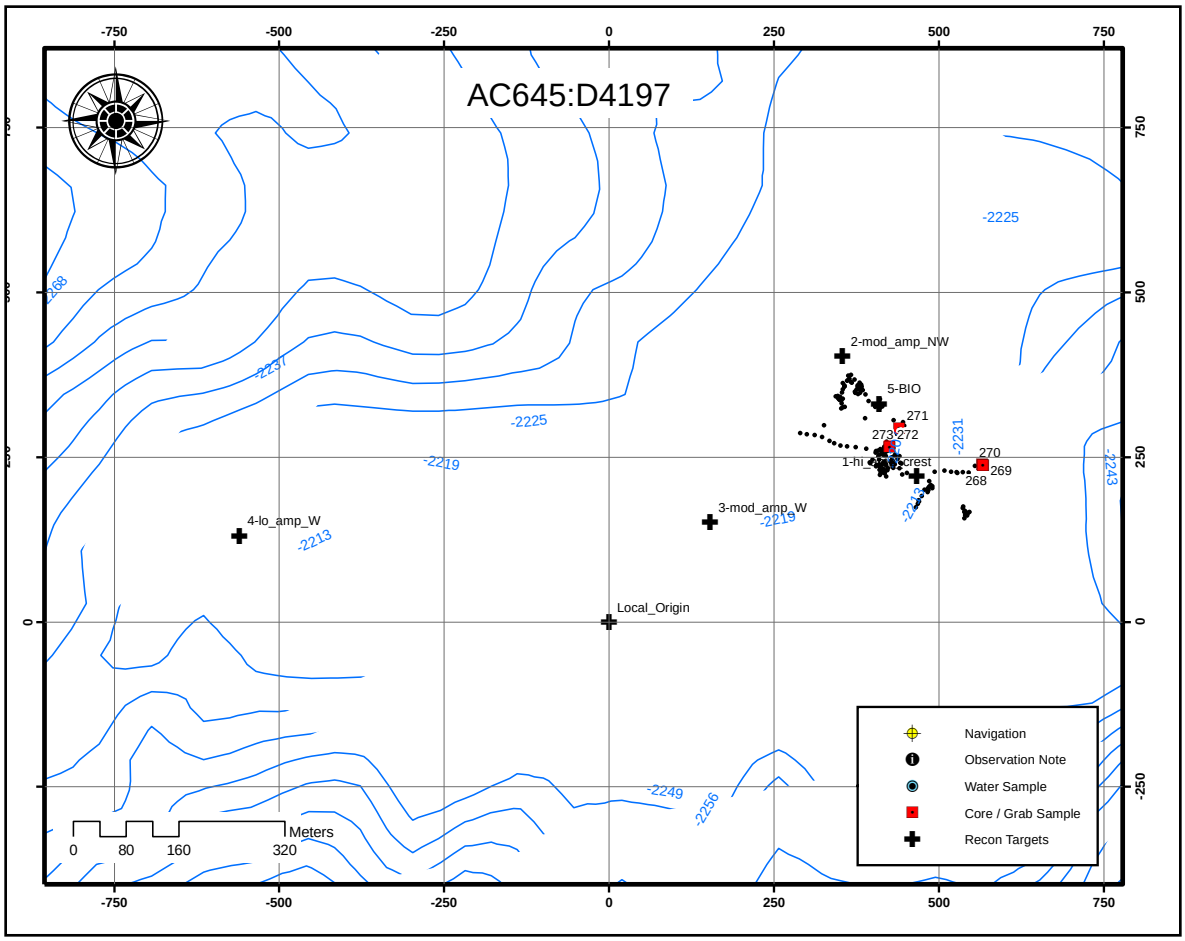

Figure 10-108. Dive 4197 on 6/01/2006 at an average depth of 2,200 m.

10.15.4. *Jason II* Lowering 281

Time in water:	2007/06/28 05:36Z
Time on bottom:	2007/06/28 06:47Z
Time off bottom:	2007/06/29 21:17Z
Time out of water:	2007/06/29 23:02Z

Water Time:	41 hours 27 minutes
Bottom Time:	38 hours 30 minutes
Min. working depth:	2176.38 m
Max. working depth:	2223.54 m
Produced:	4.2GB of raw vehicle data
Produced:	~62 DVDs of Science video
Produced:	~62 DVDs of Archive video

After the LBL net was calibrated at this site (see *LBL Calibration* section for details of the procedure), *Jason II* was deployed into the water at 00:39 hrs on June 28, 2007. All times and dates in this summary are reported in CDT, local time. The sea-bed at 2,225 m was reached at 01:49 hrs, at which point *Jason II* began moving towards the SM2000 multi-beam survey area. Refer to Dive Observations for this dive in the Appendix 7 for a detailed log of the observed events and their times in GMT.

After reaching the SM2000 survey area the Doppler navigation was reset, then a series of multi-beam calibration lines were run at 20, 15, 10, and 5 m altitudes from 01:57 to 02:13 hrs. The Doppler navigation system was then reset again, and multi-beam survey operations began. A total of 17 survey lines (see Figure 10-111) were run from 02:24 to 11:21 hrs. Doppler navigation was then reset again at 11:28 hrs and *Jason II* descended towards the seafloor to begin observation and sample collection.

Jason II began to transit towards the approximate elevator location 200 m south of *Alvin*-92 markers 42–46. A number of sea pen, sea whip and holothuroid observations were made. Doppler navigation was reset again at 11:44 hrs. At 11:48 hrs, a small area of pogonophorans was observed, and at 01:51 this area was fixed with a digital marker in Doppler velocity log navigation. Eight red push cores were taken at this site from 12:08 to 12:22 at a depth of approximately 2,215m. Two of the eight cores were "control" cores taken just outside of the pogonophoran field. Doppler navigation was then reset at 02:26 and *Jason II* continued its transit to the elevator. *Jason II* arrived at the elevator at 12:49 and began to offload core samples. The elevator was released at 13:27. The elevator was recovered on the surface at 14:49 hrs.

Doppler navigation was again reset at 14:56 hrs and *Jason II* began to try to find *Alvin*-92 Markers 42-46 for camera deployment. A large area of carbonates and tube worms was observed and the presence of markers deployed during a 1992 dive was noted. These markers were surveyed and at 15:47 hrs a digital marker fix was taken near *Alvin*-92 Markers 12 and 13 (Figure 10-109). Rotary time-lapse camera Huey was deployed at 16:05 hrs in a mussel bed within sight of *Alvin*-92 markers 4 and 5 at a depth of approximately 2,197m.

From 16:43 to 19:18 hrs, *Jason II* searched the local area for tube worms that were banded in 1992 as part of a growth study (Figure 10-110). During this time, background readings were acquired for the mass spectrometer. Tube worms B23WS, G57WT, and W3 were found at 16:43 hrs in the vicinity of Marker E at XY and were imaged with the macro camera to determine their growth over the last 16 years.

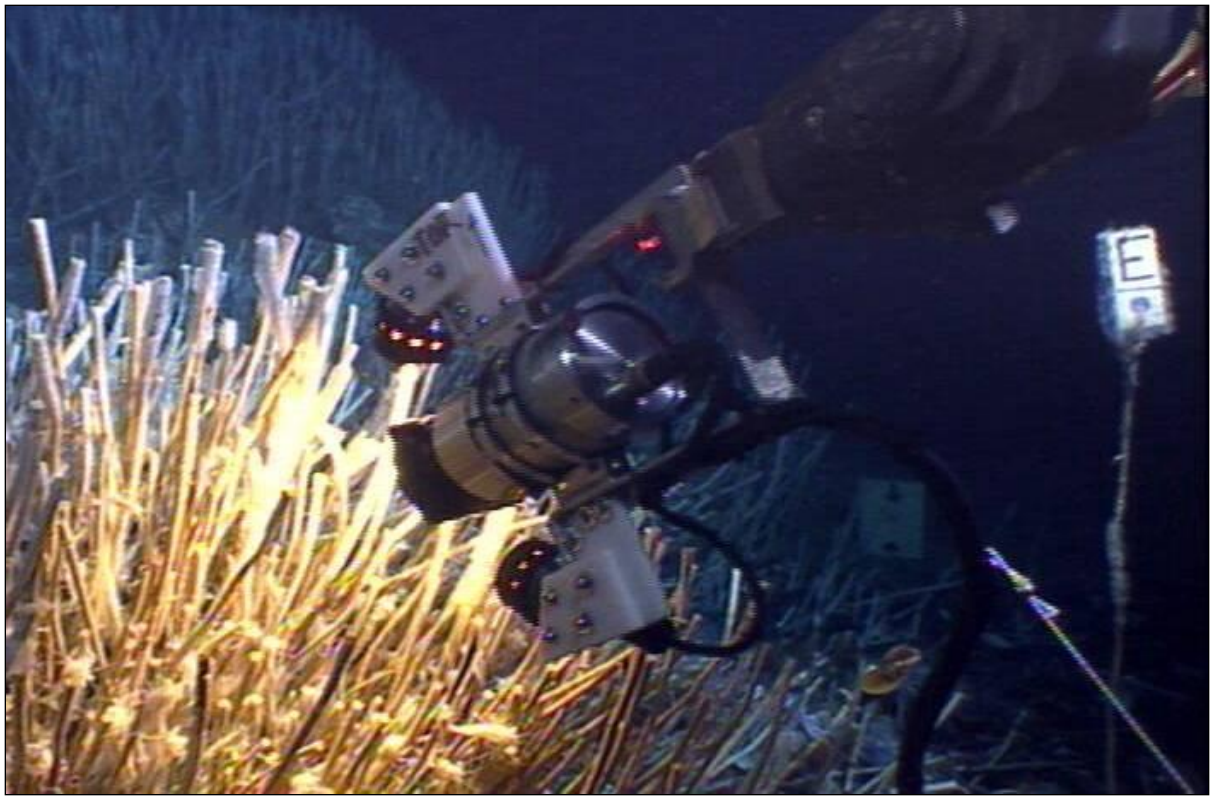

Figure 10-109. Imaging banded tube worms near Marker E with macro camera.

While it was being used, the ground in the macro camera began to worsen until, during the second set of pictures of G57WT, the ground in the camera went to 1.0, indicating that it was a complete ground fault. After consultation with the pilots, we were allowed to continue using the camera for this objective despite the hard ground in the camera. The decision was made to complete all of the imaging of the tube worms as quickly as possible, shutting down the camera during transits, then isolate the camera once finished and proceed with the chemistry measurements over the same sites. After the third tube worm near marker, we shut down the camera and proceeded to marker F at XY at 17:12 and located one tube worm (R47TS). We proceeded to *Alvin*-92 marker 10 at 17:36 hrs (37359) where tube worms W2WP and B20WG were imaged from 17:39 to 17:57 hrs. Two other banded tube worms near this marker could not be located. Marker A (XY EVT37458) was reached at 18:25 and 2 more banded tube worms (W4 and R8) were located and imaged. An effort was made to locate tube worm #28 at (EVT37555), but it was not found.

Mass spectrometer readings 48–57 were then taken in the same tube worm aggregations where growth of the banded tube worms was photographically sampled from 20:04 June 28 to 01:52 on June 29. There was a persistent peak on the mass spectrum in the vicinity of higher hydrocarbons (oil).

Upon recovery, this was discovered to be a spot of some kind of oil on the membrane inlet of the instrument. The membrane and the entire sampling line were replaced and the instrument redeployed. The hydrocarbon peak was still present following this work, but is not likely to

interfere with methane or sulfide readings, so it was decided to continue use of the mass spectrometer.]

Figure 10-110. Old marker # 29 in tube worm bed.

Once the chemistry measurements were complete, *Jason II* searched for the markers contained in the video mosaic obtained in 1992 from 01:56 to 02:31 when *Alvin*-92 marker 41 was observed approximately 20 m to the north of the area containing the banded tube worms. At this time, *Jason II* transited back to the location of the time lapse camera deployment, collected the camera from this position (XY EVT38518) at 02:40 hrs and deployed it in the area to be re-mosaicked at 02:46 (XY EVT38534). The perimeter was surveyed, and the entire area mosaicked at 4 m from 03:07 to 03:33 hrs.

A series of 10 photo transects were then run from 03:54 to 07:11 hrs. The transect lines were 100 m in length, oriented 345°–165°, and contained within a 150x150.m perimeter centered at 26° 21’ 6.0” 94° 30’ 6.0”

We found a suitable mussel bed for mussel pot sampling (XY EVT39324) near the banded tube worms, within the mosaic to be taken later in the dive. Chemical sampling of the mussel bed proceeded from 08:09 to 09:29 hrs, taking samples 62 to 65. During this time, “Best of” tube worm and mussel video was obtained. Following the chemical sampling, Mussel Pot B was used (very successfully) to sample this patch of mussels at 09:34 hrs. The remaining mussel pot ring was imaged and nothing was seen to have been left behind (the two mussel shells inside were

knocked in by the sub). At 10:10 and XY (EVT39591), carbonates associated with tube worms at the top of the mound were sampled into the starboard biobox.

Jason II collected mobile fauna: and 5 sea cucumbers, a sea star, a sponge, and a sea whip were collected between 10:20 and 11:40 hrs. We attempted to find the Marker 1 site to continue sampling, but after searching from 11:35 to 12:15, we returned to the main site where we had been working.

Another mussel bed was found and was chemically sampled from 12:45 until 12:51 hrs, but due to the high readings for hydrocarbons the decision was made to end the scans early. Two Niskin bottles were fired in this location (XY EVT39952). An attempt was made to sample the mussel bed, but the handle of mussel pot F spun freely and the mussel pot sample was aborted. Another photomosaic was then initiated over the area containing all of the banded tube worms and previous chemical measurements. The mosaic contained 9 lines over the northeast corner of the banded tube worm site and lasted from 13:12 until 14:02 hrs. Two different Bushmaster samples were attempted, one within the banded tube worm mosaic and one within the replicate of the 1992 mosaic. However, the support rods connected to the springs on one of the hydraulic cylinders came free, and a portion of the net was not completely connected to the steel drawstring around the bottom of the Bushmaster device. This made collection very difficult, and in the end, impossible. [After the dive, it was discovered that one of the brackets connecting the rod to the spring was corroded through. This was replaced and the net was reattached.] The second attempt was near the time lapse camera deployment (XY EVT40277), so *Jason II* moved a few m, released the camera, and it was followed most of the way to the surface. *Jason II* left the bottom at 16:17 hrs.

Non-seep fauna was consistent with the depth and was dominated by elasipod holothuroids. Specimens of *Benthodytes typica*, the seastar *Hymenaster*, an anemone, and a soft coral were collected for background fauna analysis (Figure 10-111).

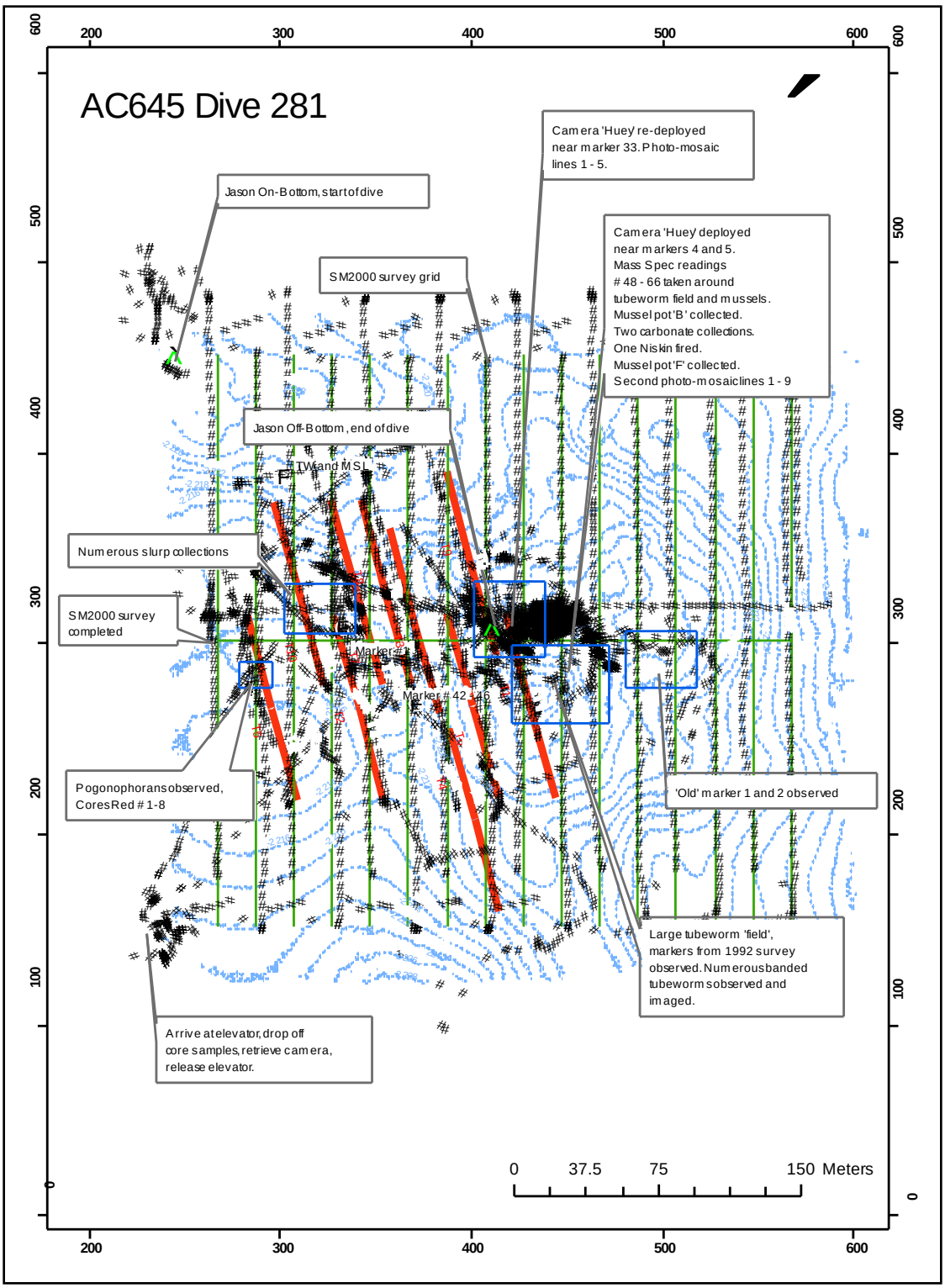

Figure 10-111. Dive track for J2-281, with photo transect lines shown in red.

.

11. MICROBIOLOGY/BIOGEOCHEMISTRY

11.1. Water Column Biogeochemistry

11.1.1. Results and Discussion

Oxygen and methane concentrations were quantified on board ship. Nutrient concentrations were determined within 10 days of returning from the cruise. All sites were characterized by a pronounced oxygen minimum (concentrations <4 mg L^{-1} O_2) in the midwater, between about 500 and 1,400 m water depth. This oxygen minimum did not appear to correspond to temperature or salinity anomalies, suggesting it resulted from elevated rates of biological respiration. Within the oxygen minimum zone, nitrate concentrations peaked, suggesting active nitrification in this depth interval. Water column methane concentrations were elevated significantly (between 10 nanomolar (nM) and 100 nM) compared to the concentration expected from equilibrium with atmospheric methane (~ 2 nM). Highest methane concentrations were always observed in the deepest samples and the concentrations at depth at AC601 exceeded those at GC852 and AT340 by an order of magnitude. At the AC601 site, methane was supersaturated throughout the 2,300 m water column, even at the surface, suggesting that this site is a source of methane to the atmosphere.

The water column at all sites examined was thermally stratified and a pronounced oxygen minimum zone was observed. At GC852, the oxygen minimum zone was present between about 300 and 800 m (Figure 11-1). In this same zone, nitrate concentrations increased, suggesting active water column nitrification (middle panel). Methane concentrations were slightly above 100 nM near the bottom, similar to concentrations observed at other sites in the GoM, and methane oxidation rates accounted for a turnover of up to 1% of the methane pool per day, which is quite high for the oceanic water column (right panel). However, this minimal amount of methane consumption means that the water column likely serves as a substantial source of methane to the atmosphere.

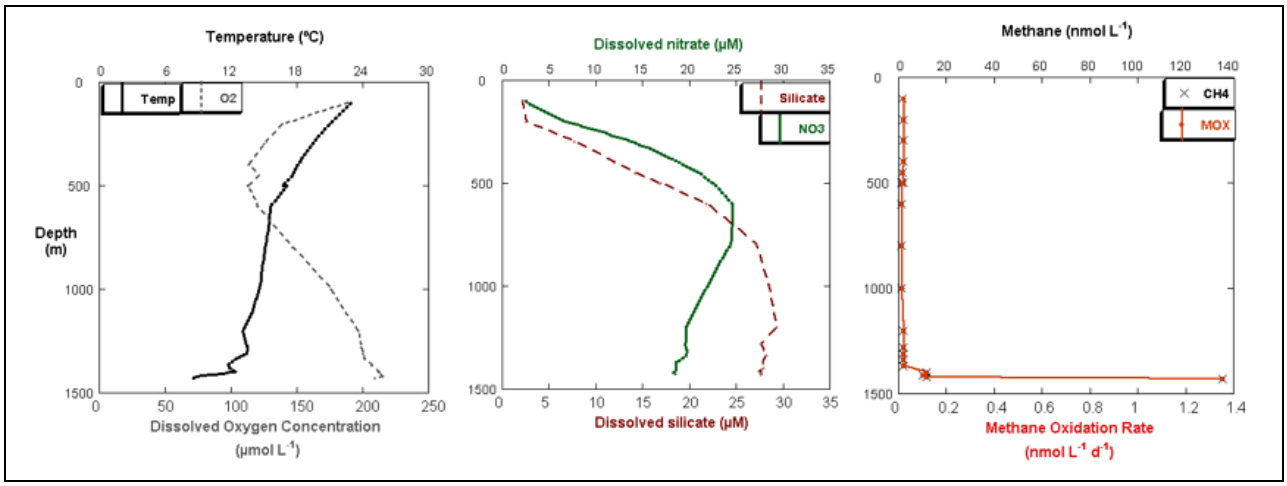

Figure 11-1. Water column temperature and O_2 (left), nitrate and silicate (middle), and dissolved methane and methane oxidation rate at GC852.

Similar profiles of oxygen, nitrate, and methane were found at the other sites sampled (AT340, AC601). Methane concentration and oxidation rates were highest at AC601. There, bottom water methane concentrations were about 35 micromolar (µM) (as opposed to nM at other sites) and methane concentrations were extremely supersaturated throughout the water column (Wankel et al., 2010). The profile shown for AC601 in Figure 11-2 shows results from a CTD cast where bottles were tripped several m above the bottom. Methane concentrations attenuate rapidly in the water column, likely more so by lateral advection than via microbial consumption, given the low oxidation rates measured.

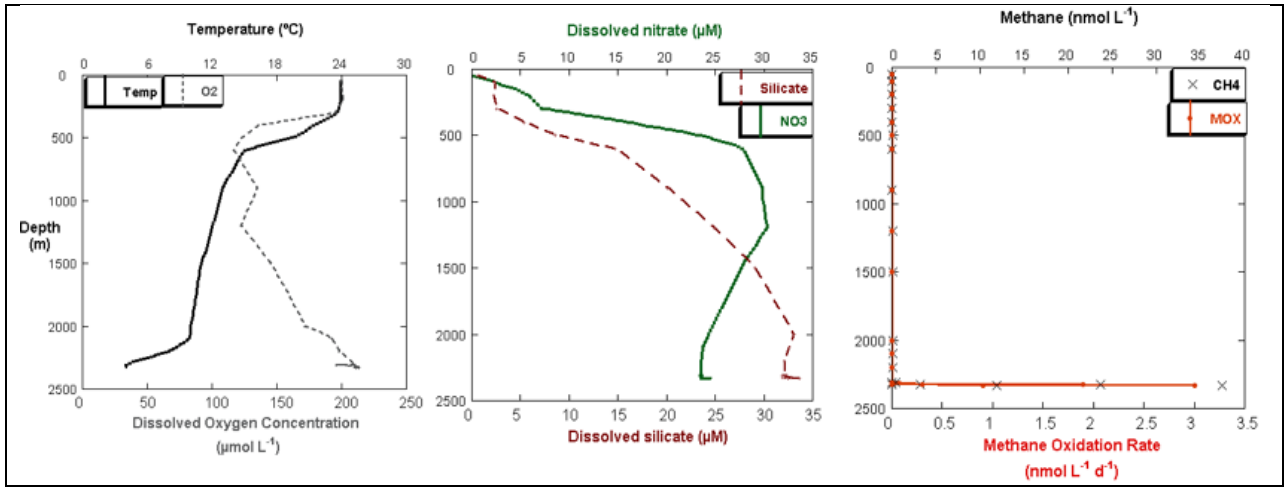

Figure 11-2. Water column temperature and O_2 (left), nitrate and silicate (middle), and dissolved methane and methane oxidation rate at AC601.

11.2. Sediment Biogeochemistry

11.2.1. Results and Discussion

11.2.1.1. Salinity and pH

Cores were categorized as normal to low salinity (35–40‰), intermediate salinity (40–75‰) and high salinity (>75‰). Most of the cores collected fell into the normal to low salinity range. Three cores (4178-R4 [75‰, MC853], 4182-R2 [75‰, MC640] and 4193-R2 [62‰, AC601]) were categorized as intermediate salinity and six cores were categorized high salinity (4173-Y1 [122‰, AT340], 4178-Y2 [115‰, MC853], 4182-Y4 [88‰, MC640], 4193-Y1 [90‰, AC601], 4196-Y5 [90‰, AC601], and 4196-R5 [76‰, AC601].

Most of these sediments were extremely sulfidic and exhibited peculiar pH profiles. Core-to-core variability in pH distribution was significant but generally speaking, three types of profiles were noted. The lowest pH values (down to 6.5) were observed in the high salinity sediments from AC601. In intermediate salinity sediments, pH tended to increase with depth below the top of the core, possibly because of increased sulfide concentration at depth. In low salinity sediments, a pH maximum was observed in the upper 2–4 cm and the pH decreased below that depth.

11.2.1.2. Methane Concentrations

On dive 4173 to AT340, cores were collected near tube worm bushes and from near a mussel bed. Methane concentrations in the pore water near the tube worm bush were low (< 20 µM), while concentrations near the mussel bed were extremely high, up to 3 mM. Most of the cores from dive 4174 to GC600 were oil stained. Both sets of cores were collected from white bacterial mats but the red set was taken near mussel beds and the yellow set was taken near tube worms. Methane–as well as concentrations of higher alkanes up to C_5–was extremely high (up to 7 mmol CH_4) in the yellow cores; concentrations in the red cores were over an order of magnitude lower (max ~300 µM). Concentrations of methane in the sediment core collected from mussel beds at GC852 (dive 4177) were extremely low (< 20 µM).

Methane concentrations in the cores from MC853 (dive 4178) were extremely elevated (up to 7.5 mM). Ethane (but no alkanes $>C_3$) was also detected in these cores. These cores were collected from areas of dense white bacterial mats. The first set of cores retrieved from AT340 (dive 4181) were from alongside a tube worm and methane concentrations ranged from 50µM to 1.2 mM. Dive 4182 to site MC640 retrieved two sets of cores from bacterial mats alongside brine flows. Concentrations of methane in these cores were quite high (up to 6 mM). On dive 4183 to AT340, control cores were collected from areas having no oil staining or chemo fauna. The methane concentration in these cores was < 8 µM. Another set of cores was collected from an urchin field. Methane concentrations here were also low (12 to 40 µM). On dive 4184 to GC600, two sets of cores were collected, one from a dead clam bed and one from an area of live clams. Neither set of cores had elevated methane concentrations. In fact, in the upper ~10 cm, methane was below detection and below 10 cm , concentrations reached only 10 µM.

Site GC852 was home to deepwater corals. Two sets of cores were collected here on dive 4189, red cores over "gray" mats with mussel shell debris in area and yellow cores from an area of patchy white mat. Methane concentrations in both sets of cores were > 1 mmol over the entire depth of the core. Dive 4191 was to WR269/270 and cores were retrieved from a pogonophoran field. Methane concentrations increased over depth below the top of the core, reaching 1.5 mmol at 6 cm and having a maximum concentration of 2.6 mmol at 12 cm. Dive 4192 at AC818 retrieved a set of cores from an urchin field and a set of cores from a mussel bed. Methane concentrations were low (<50 µM) in the upper 10 to 14 cm but reached concentrations of 1.3 to 1.7 mmol at depths >18 cm. On dive 4193 to AC601, three sets of cores were taken. Four control cores were taken at the edge of the site. Methane concentration in the control cores was < 5 µM. Cores collected from the bottom and edge of the brine lake were extremely supersaturated with methane (concentrations > 1.5 mM) even though continual degassing was observed during return of the submersible to the surface. Methane concentrations in the brine (determined in sub-samples obtained using small Niskin bottles) were >1.5 mM.

Dive 4194 retrieved one set of cores from AC645. Methane concentrations were < 30 µM at all depths in this core. Dive 4196 returned to AC601. One set of cores was collected from the "floc" zone at the edge of the brine lake. Methane concentration in these cores was high, but did not exceed 1 mM. The other set of cores was collected from beneath the brine, about 2 m out into the lake. These cores had much higher methane concentrations (up to 3 mM). All cores degassed significantly during ascent to the surface.

In the following section, core profiles and microbial activity are discussed by habitat type. During the 2006 cruise, only 1 core per habitat per site was analyzed, while 2–3 cores were analyzed for rates.

To evaluate the impact of habitat and gas, oil, and brine seepage on microbial activity and biogeochemistry, we compared active seep sites with control sites where the sediments lacked any visible evidence of current or recent seepage, e.g., oil stained sediments, black reducing sediments, microbial mats, authigenic carbonates, chemosynthetic animals (bivalves or tube worms).

11.2.1.3. Control Sediments

In control sediments, porewater methane and DIC concentrations were lower (<50 μM and <6 mM, respectively) than the values typically observed at seep sites and the average pH was around 8.2 (Figure 11-3, Table 11-1). The isotopic composition of CH_4 at the GC852 control site was -56.6 (Table 11-1). At control sites, no Cl^- gradient was apparent but SO_4^{2-} concentrations decreased steadily with depth below the top of the core and H_2S concentrations increased with depth (Figure 11-3) (Joye et al., 2010).

The percent organic matter in control sediments (between 6 and 7%) was similar to that observed in some active sediments (Table 11-2), and it is likely that oxidation of this particulate organic matter and/or DOC(Figure 11-3, Table 11-1) fueled SO_4^{2-} depletion, and the ensuing H_2S accumulation with depth, in these sediments. However, SR rates in off-seep or "inactive" control sediments were generally lower (by a factor of 10 to 100; Figure 11-3) than rates observed at active seep sites (Table 11-1). It is noteworthy however, that some sites (e.g., urchin meadows) with signs of active seepage exhibited SR rates which were in the same range as the control sites (Table 11-1). Rates of AMO were below detection at all control sites.

At control sites on the upper slope, rates of both SR and AMO were substantially lower at control sites than at actively seeping sites and biogeochemical signatures indicated reductant-limited sediments (Arvidson et al., 2004; Joye et al., 2004). The control sites we sampled on the lower slope were "on-site" controls, that is, they were not located significant (>0.5 km) distances from actively seeping sites. In contrast, the upper slope control sites sampled by Joye et al. (2004) were located from >0.5 to 1 km from known active seeps and this might explain why rates of SR were so much lower in those control samples (Joye et al., 2010).

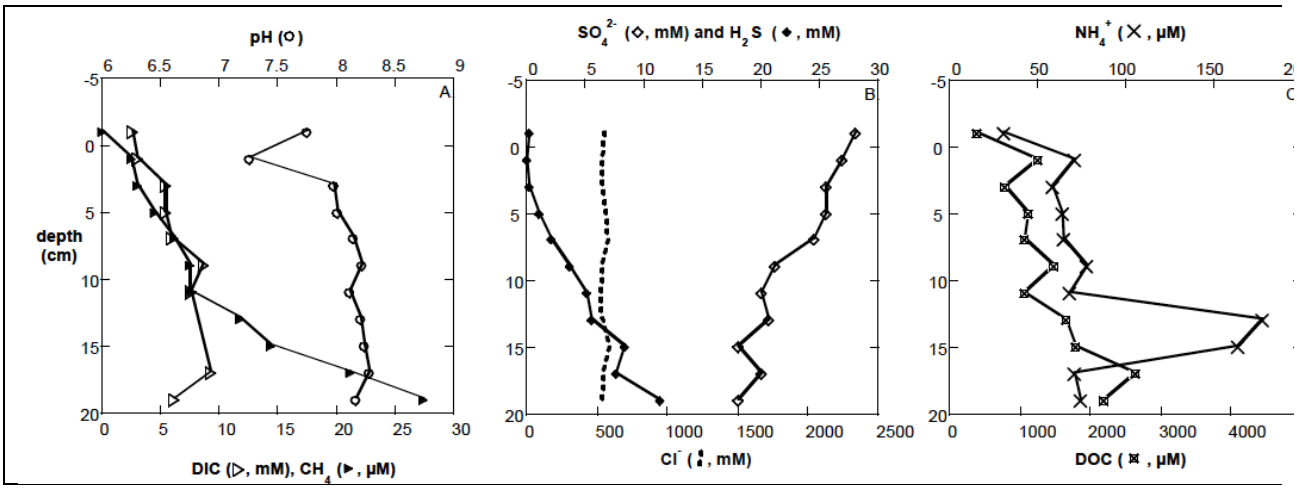

Figure 11-3. Depth profiles of (A) pH (upper axis) and methane and dissolved inorganic carbon (lower axis) concentration; (B) sulfate and sulfide (upper axis) and chloride (lower axis) concentration; (C) ammonium (upper axis) and DOC (lower axis) concentration; and (D) sulfate reduction rate (upper axis) in the GC852 control core. Data from the 2006 *Alvin* cruise

.

Table 11-1

Summary of Average Geochemistry (µM for methane, ammonium, and dissolved organic carbon; mmol for dissolved inorganic carbon, hydrogen sulfide, sulfate and chloride) and Integrated Rates of Sulfate Reduction and Anaerobic Methane Oxidation (mmol m^{-2} d^{-1})

SITE	CORE	TYPE	CH_4	max CH_4	$\delta^{13}C$-CH_4	DIC	H_2S	SO_4^{2-}	min SO_4^{2-}	Cl	NH_4^+	DOC	‡ SRR	‡ AOM	AOM/SR
AT340	4183-R2	control	4.0	7.3	n.d.	4.70	0.40	26.80	23.10	621.3	192.4	1149.5	n.d.	n.d.	n.d.
GC852	4177-R1	control	5.2	7.5	-56.6	6.00	2.00	27.30	23.60	586.7	67.3	1123.9	0.32	0.00	0.00
AT340	4173-Y1	brine	1340.4	1881.7	-75.6	5.10	7.78	7.53	1.57	1557.5	1173.6	3207.7	3.26	1.49	0.46
MC640	4182-R2	brine	353.4	621.5	-72.6	6.60	3.40	16.20	0.30	861.1	1080.8	1800.7	1.15	0.32	0.28
MC853	4178-Y2	oily	964.2	1417.3	-68.4	6.00	4.80	5.30	0.30	1299.5	4334.9	3069.0	5.26	0.93	0.18
GC600	4174 Y2	oily	3174.2	7177.0	-46.9	22.11	18.74	2.45	0.66	623.6	140.7	2512.6	0.48	1.19	2.50
GC600	4184-R	clam	1.7	6.0	-62.9	5.90	2.10	24.80	17.60	570.2	181.3	1707.3	0.56	0.00	0.00
GC600	4184-Y	clam	1.5	5.3	-54.8	5.10	3.10	25.40	19.50	579.6	118.8	1468.8	0.44	0.01	0.01
AT340	4173-R1	white mat	8.5	21.7	n.d.	3.57	0.00	28.50	25.63	585.5	62.9	1341.8	10.57	0.01	0.00
GC852	4189-R	white mat	1932.0	2509.0	-75.3	13.20	20.70	11.30	6.40	565.2	99.8	3404.2	0.25	0.32	1.28
MC853	4178-R4	white mat	280.6	1229.3	-52.2	7.90	6.30	14.10	5.10	778.3	1804.6	2188.0	8.74	0.05	0.01
GC852	4189-Y	orange mat	1773.4	3080.6	-75.0	10.50	14.30	14.60	5.80	569.4	63.7	1994.5	3.88	0.35	0.09
WR 269/270	4191-Y5	pogonophoran	1309.2	2646.0	-88.8	9.20	8.60	12.90	2.20	559.2	53.7	2858.6	9.85	2.68	0.27
AC645	4194-Y6	pogonophoran	19.4	26.2	-56.5	3.80	0.40	22.40	21.60	548.5	56.8	1196.6	0.29	0.06	0.21
AC818	4192-R5	Lamellibranchia	9.2	20.5	-70.3	7.50	3.30	23.00	18.30	553.1	91.0	3744.2	2.44	0.01	0.00
AT340	4183-R2	urchin	25.4	39.8	-74.2	4.80	4.90	25.60	19.70	610.8	62.7	1235.5	0.24	0.01	0.04
AC818	4192-Y5	urchin	48.8	130.5	n.d.	9.10	11.20	16.00	6.50	579.3	86.5	1716.8	0.40	2.00	5.00

Table 11-2

Summary of Solid Phase Geochemistry Percent Organic Carbon (%C), Percent Organic Nitrogen (%N), Organic Carbon-Nitrogen Ratio (C:N) and Percent Organic Matter (%OM)

Data from 2006 Cruise

SITE	CORE	TYPE	%C	%N	C:N	%OM
AT340	4183-R2	control	0.82	0.23	17.96	7.1
GC852	4177-R1	control	1.27	0.14	9.11	6.1
AT340	4173-Y1	brine	1.68	0.20	8.50	6.7
MC640	4182-R2	brine	1.82	0.23	7.84	5.2
GC600	4184-R	clam	4.84	0.17	29.15	10.1
GC600	4184-Y	clam	6.13	0.35	17.61	12.6
AT340	4173-R1	white mat	1.99	0.20	10.16	6.0
GC852	4189-R	white mat	1.96	0.25	7.86	7.4
MC853	4178-R4	white mat	1.35	0.15	8.72	4.2
GC852	4189-Y	orange mat	2.54	0.26	9.92	6.2
MC853	4178-Y2	oily	1.84	0.23	7.94	6.1
GC600	4174 Y2	oily	7.89	0.40	19.97	9.7
WR 269/270	4191-Y5	pogonophoran	1.82	0.23	7.84	5.1
AC645	4194-Y6	pogonophoran	1.42	0.19	7.51	2.1
AC818	4192-R5	Lamellibranchia	2.56	0.35	7.37	5.4
AT340	4183-R2	urchin	1.47	0.13	10.94	5.5
AC818	4192-Y5	urchin	1.89	0.26	7.26	3.9

11.2.1.4. Sediments Influenced by Brine Seepage or Brine and Oil Seepage

A common feature of cold seeps on the upper and lower slope is brine seepage. We sampled four sites along the lower slope where brine was present at depth (AT340, MC640, MC853 and Alaminos Canyon lease Block 601, AC601); three of those sites are discussed in this section (AT340, MC640, MC853) and the remaining site (AC601) is discussed in the 2007 cruise section. At AT340, gas-laden brine flows were common and at MC640 and MC853, gas-laden brine co-migrated with oil. The AT340 brine-influenced sediments were noted by black coloration, reflecting reducing conditions, abundant microbial mats and, often, dense communities of methanotrophic mussels (Fisher et al. 2007). Generally, brine-influenced sediments were characterized by high CH_4 concentrations (>500 µM), rapid SO_4^{2-} depletion, intermediate H_2S concentrations (usually < 8 mM), lower DIC concentrations (<8 mM), steep Cl^- gradients, and significant increases in both DOC and NH_4^+ concentration with depth (Table 11-1, Figure 11-4, Figure 11-5). The $d^{13}C$-CH_4 at brine sites was highly depleted (-72 to -75 ‰ PDB (Pee Dee Belemnite); Table 11-1), illustrating a strong contribution of biogenic methane. Sediments from brine sites contained about 1.7% organic carbon, 0.2% organic nitrogen and between 5 and 7% organic matter (Table 11-1) (Joye et al. 2010).

Brine sediments from AT340 had a lower pH than control sediments (~7.5) and DIC concentrations were fairly uniform with depth (Figure 11-4A). The deepest sediment contained higher CH_4 concentrations (Figure 11-4A), while AMO was only detected in the upper 5 cm. Thus the low CH_4 concentrations in the upper 15 cm cannot be explained by AMO and are likely result of degassing during core recovery. As Cl^- concentrations increased, SO_4^{2-} concentrations rapidly decreased (Figure 11-4B). Unlike SO_4^{2-}, concentrations of NH_4^+ and DOC increased with depth and were positively correlated to Cl^- concentration (Figure 11-4C). Ammonium concentrations reached >2000 µM and DOC concentrations were >3500 µM (Joye et al., 2010).

Sulfate depletion in brine-influenced sediments results from a combination of microbial consumption of SO_4^{2-} via SR and upward advection of SO_4^{2-}-free fluids (Joye et al. 2009; Orcutt et al. 2005). GoM brines are most commonly derived from halite dissolution so the endmember brine contains no SO_4^{2-} (Joye et al. 2005). This feature was also observed at the Håkon Mosby mud volcano where rapid upward advection of SO_4^{2-}-free fluids also limited SR in some parts of the system (De Beer et al. 2006; Niemann et al. 2006a). More rapid rates of upward advection generate sharp gradients in SO_4^{2-} and Cl^- concentration and may restrict rates of microbial activity, particularly SR (Joye et al. 2009). Evidence for limited SR is apparent in the H_2S concentrations that increased to a maximum slightly below the sediment surface, but then decreased (Figure 11-4B, Figure 11-5B). The H_2S concentration profile can be explained by high SR rates in the upper 5 cm of the sediment, and, below this depth, SR rates are low and likely are limited by SO_4^{2-} availability since concentrations of DOC are comparably high (Figure 11-4C, 2D) (Joye et al., 2010).

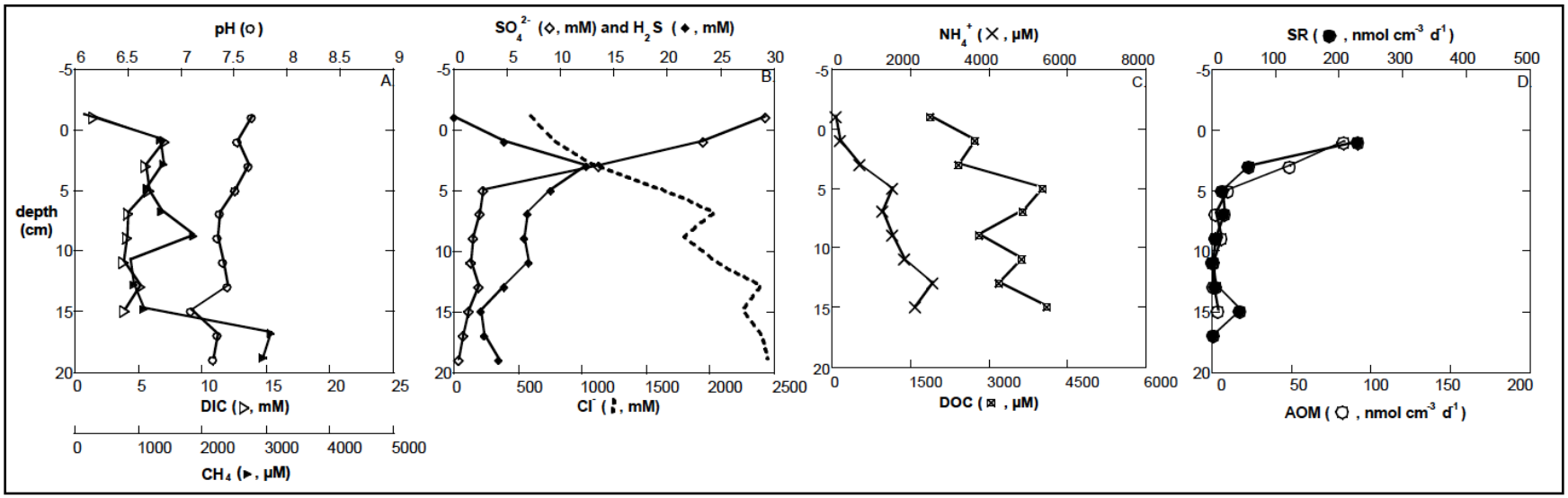

Figure 11-4. Depth profiles of (A) pH (upper axis) and methane and dissolved inorganic carbon (lower axis) concentration; (B) sulfate and sulfide (upper axis) and chloride (lower axis) concentration (note different scale for CH4 compared to figure 3); (C) ammonium (upper axis) and dissolved organic carbon (lower axis) concentration (note different upper and lower axis scales compared to figure 1); and (D) sulfate reduction rate (upper axis) and anaerobic oxidation of methane AOM, also known as AMO (lower axis) in the AT340 brine flow core. Data from the 2006 *Alvin* cruise.

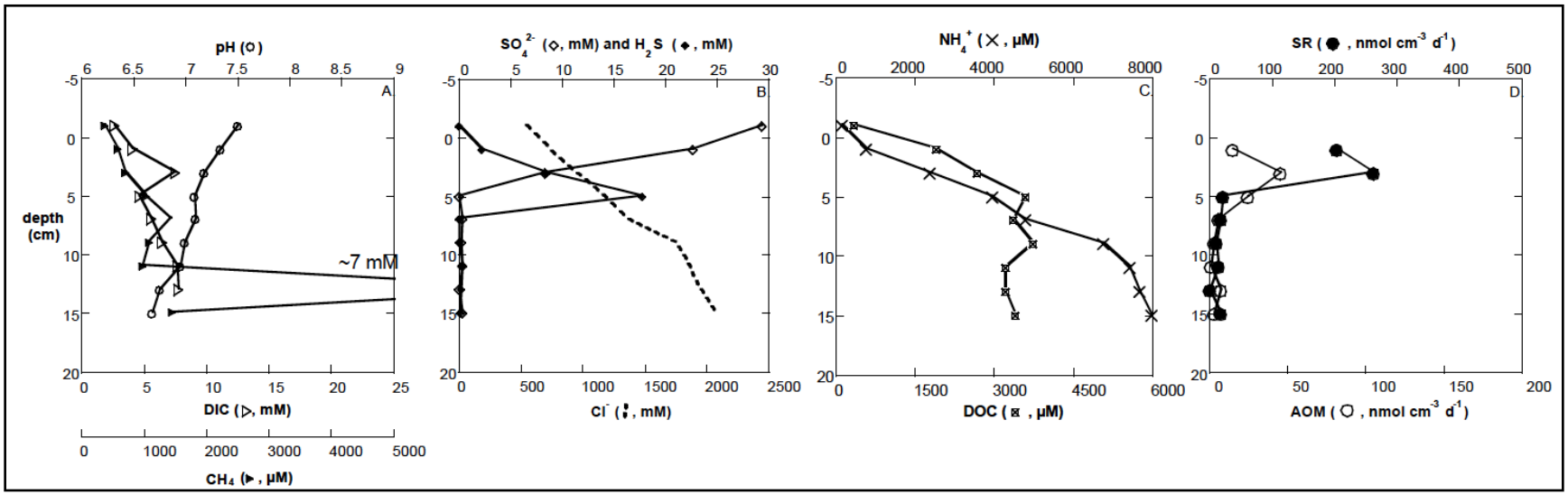

Figure 11-5. Depth profiles of (A) pH (upper axis) and methane and dissolved inorganic carbon (lower axis) concentration; (B) sulfate and sulfide (upper axis) and chloride (lower axis) concentration (same axis scales as figure 4); (C) ammonium (upper axis) and dissolved organic carbon (lower axis) concentration (same axis scales as figure 2); and (D) sulfate reduction rate (upper axis) and anaerobic oxidation of methane AOM, also known as AMO (lower axis) in the MC853 oily brine flow core. Data from the 2006 *Alvin* cruise.

The integrated SR rate in the AT340 brine was 3.3 mmol m^{-2} d^{-1} and the integrated AMO rates was 1.5 mmol m^{-2} d^{-1}, amounting to just under 50% of SR rates. The depth profile of AMO and SR mirrored one another, suggesting that the two processes are possibly coupled, to some extent. In brine-influenced sediments on the upper slope, Orcutt et al. (2005) found much higher SR rates (154 mmol m^{-2} d^{-1}) that exceeded AMO rates (0.1 mmol m^{-2} d^{-1}) by several orders of magnitude, suggesting that the processes were not coupled. In contrast to the lower slope brine habitats presented in this study (Figures 11-4 and 11-5; Table 11-1), Joye et al. (2009) found that AMO was absent in upper slope brine fluids that supported large SR rates. A possible explanation for this difference is that different methanotrophic communities populate the upper and lower brine habitats or that other factors favor AMO in the deeper habitats (see below).

The oily brine sediment collected from MC853 was distinct from the AT340 brine sediment discussed above. The MC853 sediment had a lower pH (around 7) and much higher CH_4 concentration at the bottom of the core (Figure 11-5). The steep nature of the Cl^- gradient suggests rapid upward brine advection at this site, as also noted at AT340. Sulfate was rapidly depleted by 5 cm and H_2S was absent below that depth. Concentrations of DOC and NH_4^+ were significantly higher in the MC853 brine compared to the AT340 brine (Figure 11-5; discussed further below). SR rates were measurable only in the upper 5 cm where SO_4^{2-} was available. AMO rates (0.9 mmol m^{-2} d^{-1}) accounted for about 18% of SR (5.3 mmol m^{-2} d^{-1}) (Figure 11-5, 3-D). Unlike AT340, AMO and SR are very loosely coupled at this site. The oil at this site may have fueled more SR and resulted in decoupling of AMO and SR as observed on the upper slope (Joye et al. 2004; Orcutt et al. 2005) as well as at other cold seeps (Niemann et al. 2006b). Previous documentation of anaerobic hydrocarbon oxidation by SRB in enrichment cultures from the GoM (Kniemeyer et al. 2007) shows that SRB are capable of oxidizing a variety of substrates in these settings.

The three brine sites shared some similarities but there were also some notable differences (Table 11-1). Brine advection rates were apparently faster at MC853 and AT340 compared to MC640, based on the shape of the Cl^- profile (profile not shown for MC640). At MC853, SO_4^{2-} was completely consumed by 5 cm but SO_4^{2-} penetrated to 12 cm (or deeper) at both AT340 and MC640. This suggests that mechanism of anaerobic H_2S oxidation replenishes SO_4^{2-} at depth at the latter two sites. Joye et al. (2005, 2009) proposed that deep SO_4^{2-}penetration into brine fluids resulted from efficient oxidation of H_2S at depth. They originally proposed an abiotic mechanism, i.e., H_2S oxidation coupled to Fe-mineral reduction (Joye et al. 2005), but later documented a population of sulfide oxidizing bacteria in the Green Canyon 233 brine (Joye et al. 2009), suggesting that microbial processes also play a role in SO_4^{2-} recycling. Whether abiotic or biotic processes mediate H_2S recycling at these lower slope brine sites remains unknown (Joye et al., 2010).

Rates of SR and AMO in brine sediments were significantly higher than rates in control sediments (Table 11-1). Generally speaking, SR in brines is limited by the SO_4^{2-} depth penetration (Arvidson et al. 2004; Joye et al. 2009), which is controlled by the upward flux of SO_4^{2-}-free brine. The rates of SR at lower slope brine seeps (range: 0.5 to 5 mmol m^{-2} d^{-1}, average = 3.8 ± 3.3 mmol m^{-2} d^{-1}) were much lower than SR rates documented at upper slope brine seeps (57 to 250 mmol m^{-2} d^{-1}, Arvidson et al. 2004; 154 mmol m^{-2} d^{-1}, Orcutt et al. 2005). In contrast, rates of AMO in the lower slope (0.05 to 1.5, average: 0.8 ± 0.6 mmol m^{-2} d^{-1}) were

substantially higher than rates documented in brines on the upper slope (0.1 mmol m^{-2} d^{-1}, Orcutt et al. 2005). While AMO and SR were effectively uncoupled at upper slope brine sites (Orcutt et al. 2005; Joye et al. 2009), AMO and SR were coupled about 70% of the time at lower slope sites (Table 11-1).

The reasons for the observed difference in SR and AMO rates and coupling between the processes between upper and lower slope brine sites are unclear. Possible driving factors include microbial abundance, microbial community composition, depth (pressure), brine advection rate, presence/absence of oil, DOC concentration, and CH_4 concentration. Microbial abundance in sediments from lower slope sites is similar to that observed at upper slope sites (Joye, unpublished data) so this is unlikely the driving factor. Studies are currently underway to evaluate the potential role of differences in microbial community composition and that possibility cannot be ruled out at present. Reduced rates of SR at lower slope sites are in contrast to the higher observed rates of AMO, so pressure related-impacts on microbial activity probably are not an issue. While we cannot constrain brine advection rates at these sites, it is likely that advection limits SO_4^{2-} penetration and may thereby regulate both SR and AMO rates. The lowest SR rates were observed in the core with the shallowest depth to brine and thus the shallowest SO_4^{2-} penetration depth (Table 11-1) (Joye et al., 2010).

The amount and type of reductant–CH_4 versus oil versus labile DOC–is likely to be important. At the lower slope sites, the average, but not the maximum, CH_4 concentration was positively correlated with AMO rates (but not SR rates). DOC concentration was not correlated with SR or AMO rates, supporting the above hypothesis that the DOC pool is refractory in these anoxic sediments. Oily samples had somewhat lower AMO rates but often exhibited the highest SR rates (Table 11-1). Of the oily sites discussed here (GC600 and MC853), oil co-migrated with brine, so is not possible to isolate the impact of oil seepage on microbial activity. However, since oil plays a key role in regulating microbial activity at upper slope sites (Joye et al. 2004), it is likely to play a similar role at lower slope sites.

All brines had elevated concentrations of NH_4^+ and DOC (Table 11-1) but the relationship between NH_4^+ and Cl^- concentration varied substantially between sites (Figure 11-6). The highest NH_4^+ concentration was observed in brines from Mississippi Canyon. The MC640 and MC853 brines exhibited a similar relationship between NH_4^+ and Cl^- concentration [$NH_4^+ = 5.43(Cl^-) - 2874$; $R^2 = 0.94$, $p < 0.0001$], with the highest NH_4^+ concentrations (~8,000 µM) observed in the oily brine core from MC853. The brine sample from Atwater Valley 340 (AT340) had lower NH_4^+ concentrations in general and a significantly different relationship between NH_4^+ and Cl^- concentration [$NH_4^+ = 1.23(Cl^-) - 688$; $R^2 = 0.92$, $p < 0.0001$]. Also shown on Fig. 4 are NH_4^+-Cl^- concentration relationships for the Alaminos Canyon 601 (AC601) [$NH_4^+ = 6.11(Cl^-) - 7323$; $R^2 = 0.63$, $p < 0.01$] brine and an upper slope brine, Garden Bank 425 (GB425) [$NH_4^+ = 2.65(Cl^-) - 1079$; $R^2 = 0.979$, $p < 0.001$]. The GB425 brine NH_4^+-Cl^- concentration relationship lies in between that observed for the MC and AT brines. The AC601 sample differs from the other sites in that the core sample was collected from the bottom of a brine lake (Roberts et al. 2007). While the Cl^- concentration range in this core was quite narrow compared to that observed in other cores, for a given Cl^- concentration, the NH_4^+ concentration was similar to that observed at AT340.

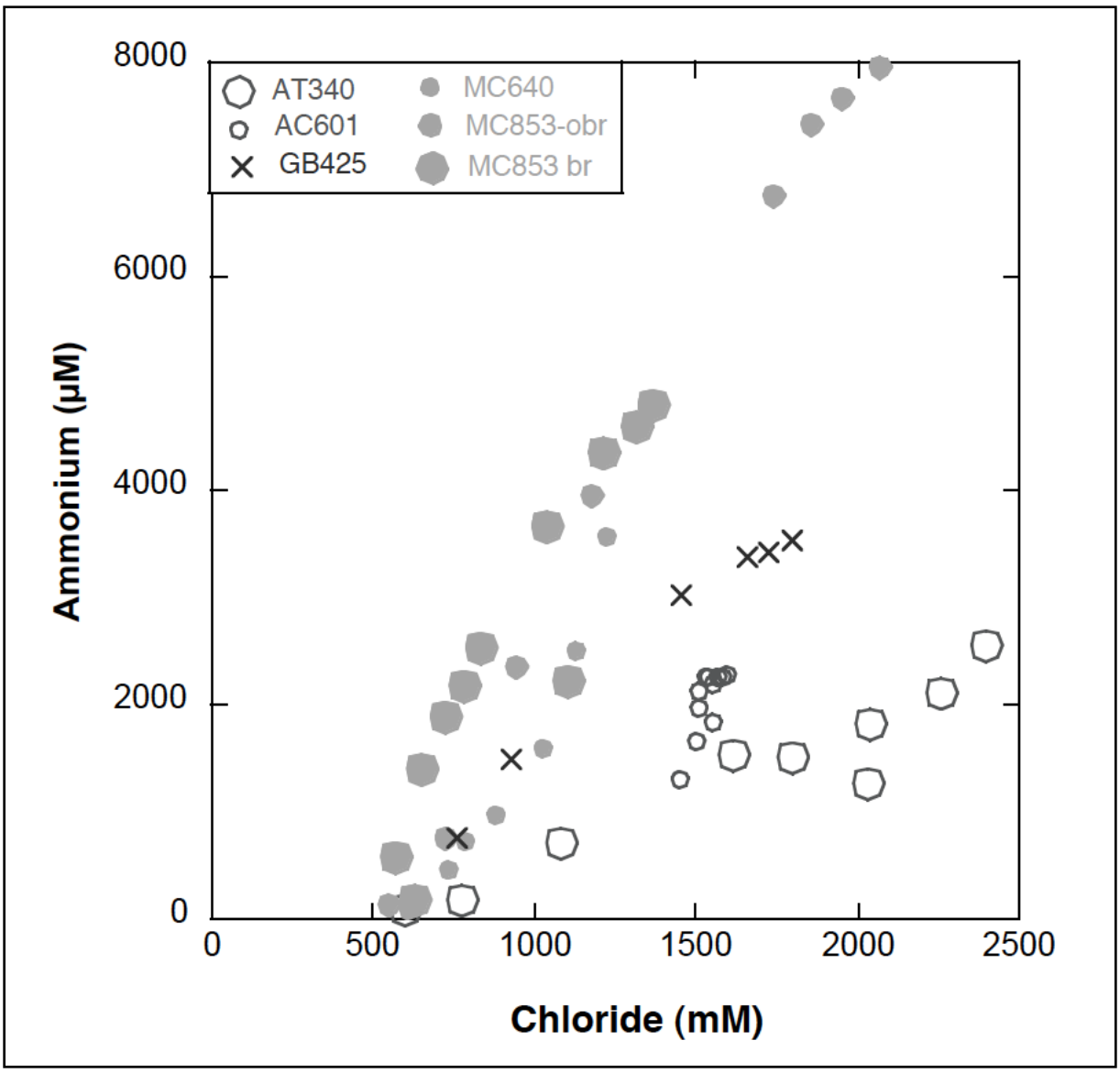

Figure 11-6. Scatter plot of ammonium concentration versus chloride concentration for the AT340, AC601, GB425, MC640, and MC853 brines. Data from the 2006 *Alvin* cruise.

Joye et al. (2005) were the first to document elevated NH_4^+ concentrations of in GoM brine fluids. Brines from other locations (e.g., the Mediterranean) also exhibit elevated concentrations of NH_4^+ (Joye et al. 2005 and references therein). Joye et al. proposed that the high ionic strength of brines leaches NH_4^+ from the sediments as the brines migrate up from deep reservoirs to the sediment-water interface. If this is correct, then the depth of the salt diapirs beneath the different sites could influence the observed patterns. The depth to salt at the MC sites (MC640: 760m, MC853: 1067 m) exceeded that of GB425 (667 m), which exceeded that of AT340 (233 m) (H. H. Roberts, personal communication). Ammonium concentrations were highest at MC sites, followed by GB425 and AT340, suggesting that perhaps depth-to-salt does play a role in governing NH_4^+ load of the brine. However, the deepest salt was at AC601 (3000 m) and

AC601 exhibited the lowest NH_4^+ concentrations of all the brines sampled. A combination of depth-to-salt, diapir geometry and surface area, and the overlying sediment composition, through which the brine migrates and which serves as the source for the NH_4^+, likely interact to generate a unique NH_4^+ signature for each province (Joye et al., 2010).

A similar salt-induced desorption mechanism for DOC removal from sediment was proposed by Joye et al. (2005) but DOC dynamics are further complicated by inputs from animals in near-surface habitats (Joye et al. 2009). Surprisingly, the MC and AT brines had similar DOC concentrations (Figure 11-4, 3) and showed a surprising similarity in the relationship of DOC concentration versus Cl^- concentration (Figure 11-7). Regression analysis of DOC concentration versus Cl^- concentration were highly significant for each site (MC: $DOC=2.65*Cl^- + 507$; $R^2=0.58$, $p<0.00001$ and AT: $DOC=0.88*Cl^- + 1732$; $R^2=0.57$, $p<0.017$) but regressing the pooled DOC data for MC and AT sites yielded a more significant regression (AC+MC: $DOC=1.39*Cl^- + 808$; $R^2=0.6$, $p<0.0000001$). This is somewhat surprising, since the brines are derived from different depths and may reflect the fact that the measured DOC reflects refractory DOM that is not metabolized during transit. Thus, the measured DOC is that which was not microbially utilized; this fraction may be somewhat independent of site. At oily sites, a large part of the oil is removed during pore water extraction and more is removed by filtration (oil sticks to membrane filters) so oil, per se, is not quantified in any of our various analyses. Though the measured DOC is not labile under the anoxic conditions present in the sediments, it may be metabolized upon reaching the oxic water column (Joyet et al., 2010). This possibility deserves further study.

11.2.1.5. Sediments Inhabited by Microbial Mats

Some sediments at AT340, MC853 and GC852 were overlain by thin (0.5 cm thick) patches (often <1 m^2 in diameter) of microbial mats of white or orange *Beggiatoa*. Microbial mat-influenced sediments were characterized by a distinct pH minimum of ~6.6 at approximately 3 cm (Figure 11-8). DIC concentrations were elevated (up to 5 mM) relative to the overlying water (2 mM) but were low compared to typical concentrations observed in upper slope microbial mat-influenced sediment (>10 mM; Joye et al. 2004; Orcutt et al. 2005; Joye et al. in review). Methane concentrations in microbial mat cores ranged from extremely low (< 10 µM) to extremely high (> 1 mM) (Table 11-2; Figure 11-6) and likewise the $d^{13}C\text{-}CH_4$ ranged from -52 to -75 ‰ PDB. Methane from GC852 was predominantly biogenic (lighter than -70‰) while that from MC853, which was not strongly brine influenced, was heavier (-52.2‰). AMO rates did not correlate with the $d^{13}C\text{-}CH_4$ suggesting that different sources of CH_4 (e.g. acetoclastic vs. hydrogenotrophic methanogenesis) were a more important factor.

Sulfate concentrations in microbial mat-influenced sediments were never fully depleted in the upper 12 cm, most likely due to the efficient reoxidation of H_2S to SO_4^{2-} by the *Beggiatoa* (Figure 11-8). Compared to brine-habitats, NH_4^+ concentrations were much lower in microbial mat-influenced sediments (usually < 100 µM except for the elevated concentrations in 4178-R4, which was also brine-influenced) (Figure 11-8). DOC concentrations were variable and did not appear related to the presence of microbial mats (Figure 11-8) because the highest concentrations were found in deeper sediments. Microbial mat sediments contained about 1.96% organic carbon and 0.22% organic nitrogen and the organic matter content was about 6% (Table 11-2).

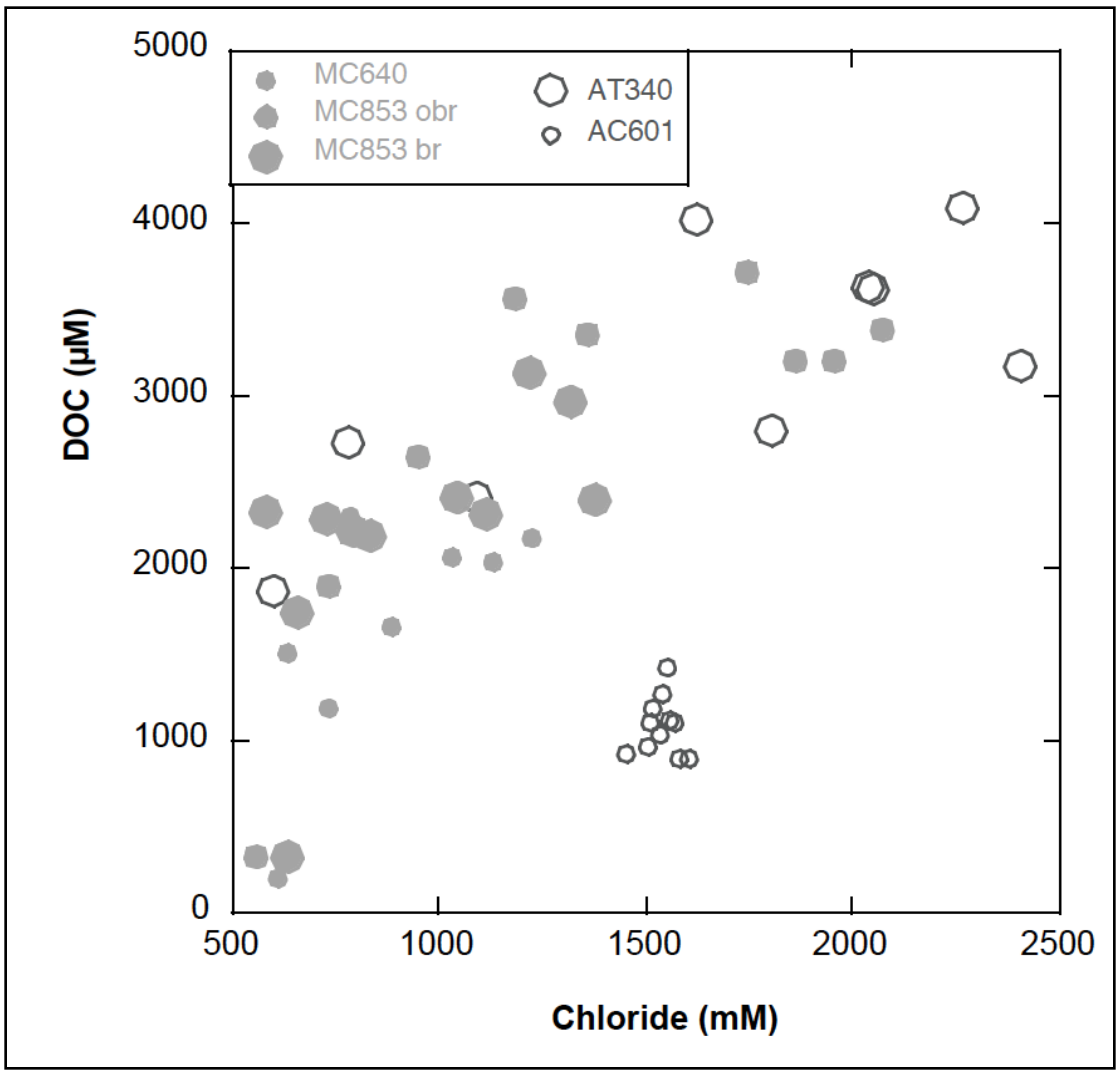

Figure 11-7. Scatter plot of dissolved organic carbon concentration compared with chloride concentration for the AT340, AC601, GB425, MC640 and MC853 brines. Data from the 2006 *Alvin* cruise.

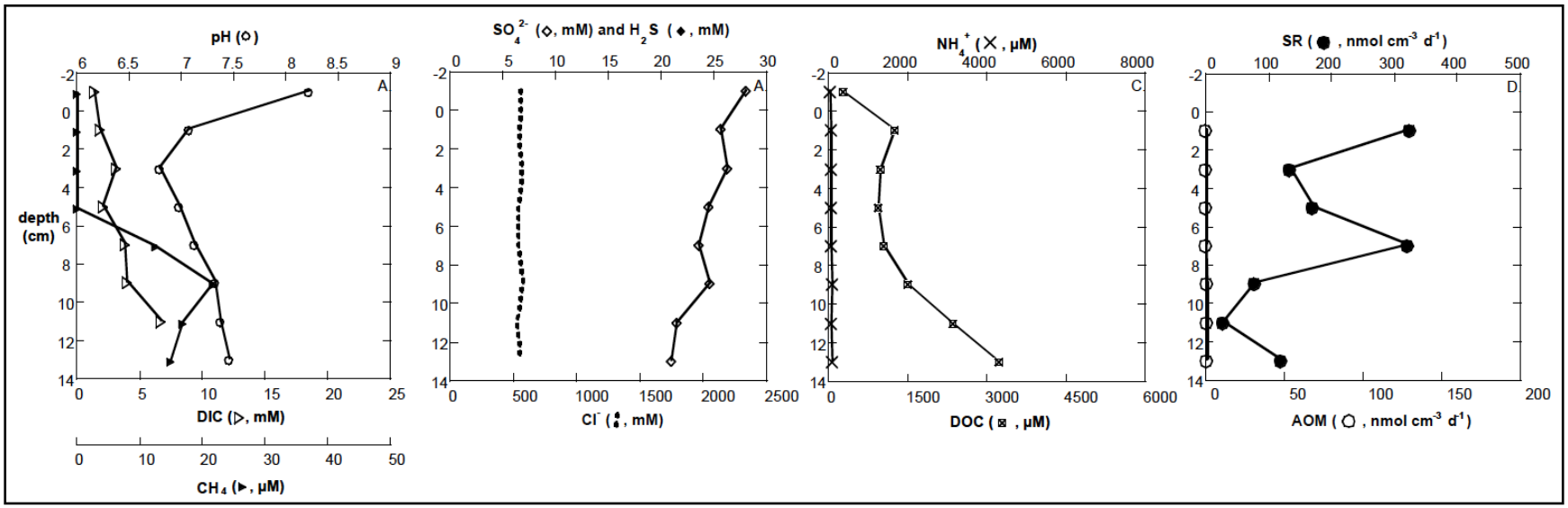

Figure 11-8. Depth profiles of (A) pH (upper axis) and methane and dissolved inorganic carbon (lower axis) concentration; (B) sulfate (upper axis) and chloride (lower axis) concentration (no hydrogen sulfide data is available for this core); (C) ammonium (upper axis) and dissolved organic carbon (lower axis) concentration; and (D) sulfate reduction rate (upper axis) and anaerobic oxidation of methane (AOM; also termed AMO) (lower axis) in the AT340 microbial mat core. Data from the 2006 *Alvin* cruise.

Rates of SR in microbial mat-influenced sediments were among the highest measured of the explored habitats on the lower slope (Figure 11-8; Table 11-1). However, similar to the brine cores discussed above, SR rates in lower slope microbial mat-influenced sediments (5.86 ± 4.68 mmol m^{-2} d^{-1}) were substantially less than those observed in upper slope microbial mat-influenced sediments [321.6 ± 315 mmol m^{-2} d^{-1} (Arvidson et al. 2004) or 54 ± 94 mmol m^{-2} d^{-1} (Joye et al. 2004)]. Likewise, AMO rates in lower slope microbial mat-influenced sediments (0.18 ± 0.17 mmol m^{-2} d^{-1}) were substantially less than those observed in upper slope microbial mat-influenced sediments [2.8 ± 4.6 mmol m^{-2} d^{-1} (Joye et al. 2004)]. Similar to the upper slope microbial mat-influenced sediments, however, AMO was very loosely coupled to SR, possibly because sulfate reducing bacteria were involved in the oxidation of non-methane hydrocarbons. It is also possible that SRB were consuming the particulate or dissolved organic carbon present in these sediments (Joye et al., 2010).

Despite abundant and dense chemosymbiotic and free-living animal communities documented at lower slope sites (Fisher et al. 2007), the lush, abundant microbial mats typically observed on the upper slope were a rarity on the lower slope (Joye, personal observation). Mats were most commonly observed at the more shallow sites (MC853, GC600 and GC852) but even at these sites, mats were limited in distribution (patches of 1 to 2 m^2 were common but larger patches were not observed; larger patches covering 10s of m^2 are common on the upper slope; Joye, personal observation; Joye et al., 2010). The paucity of mats is most possibly due to limited reductant supply at lower slope site, as H_2S concentrations were substantially reduced at lower slope sites compared to upper slope sites (Table 11-2; Arvidson et al. 2004; Joye et al. 2004; Orcutt at al. 2005). Since H_2S is produced by microbial SR in these sediments, this infers that lower slope sediments are generally less active than those on the upper slope, which is what we observed in the measured SR rates. The specific reason(s) for this decrease in microbial activity remains elusive, since reductant (oil and CH_4) and oxidant (SO_4^{2-}) are abundant. One possibility is that the flux of oil and/or gas is reduced at the deeper sites, which would lead to lower SR rates, but that remains to be quantified in an absolute sense.

11.2.1.6. Sediments Inhabited by Animals

Tube worms. One of the most common features of gas and oil seeps on the upper and lower slope is the presence of lush fields of chemosymbiotic tube worms. On the lower slope, several types of tube worms are common: the Vestimentiferans, including *Lamellibranchia* and *Escarpia*, pogonophorans and Monoliferans. We obtained sediment core samples from a *Lamellibranchia* habitat and habitats characterized by a mixture of pogonophorans (*Oligobrachia* sp.) and monoliferans (*Sclerolinum* sp.) on this cruise. *Sclerolinum* was usually dominant in these mixed assemblages so we refer to these habitats as *Sclerolinum* hereafter (E. Becker and C. Fisher, Pers. Comm.). All of these tube worms have sulfide-oxidizing symbiotic bacteria in their respective trophosomes and have long vertical "roots" that penetrate deep into the sediment, mining H_2S to nourish their symbionts (Fisher et al. 2007).

The biogeochemistry and microbial activity patterns in sediments from *Lamellibranchia* versus *Sclerolinum* habitats were distinct (Joye et al., 2010). However, we note that while different *Sclerolinum* habitats were sampled, only one *Lamellibranchia* habitat was sampled. Concentrations of DIC were significantly elevated above seawater values (10 to 15 mmol versus

2 mmol in seawater) in sediments inhabited by both *Sclerolinum* and *Lamellibranchia* and pH increased similarly with depth (Figures 11-7 and 11-8). Methane concentrations were substantially higher at shallower depths in sediments inhabited by *Sclerolinum* than in *Lamellibranchia* (Figures 11-7 and 11-8) and the $d^{13}C\text{-}CH_4$ of methane was about -70‰, on average, in both habitats, showing a strong input of biogenic CH_4. However, a large range of $d^{13}C\text{-}CH_4$ was noted at *Sclerolinum* sites; this is probably related to CH_4 source differences between sites (AC645 is more strongly influenced by thermogenic CH_4 than is WR269/270) (Joye et al., 2010).

Sediments inhabited by *Sclerolinum* showed more rapid SO_4^{2-} depletion and H_2S accumulation (Figure 11-9) than sediments inhabited by *Lamellibranchia* (Fig. 8B); H_2S concentrations were highest in sediments inhabited by *Lamellibranchia*. Solid phase organic carbon content was higher in sediments inhabited by *Lamellibranchia* (2.56% for *Lamellibranchia* vs. 1.6% for *Sclerolinum*; Table 11-2). Concentrations of DOC were elevated in both *Sclerolinum* and *Lamellibranchia* cores (Figures 11-7 and 11-8) but the *Lamellibranchia* cores had the highest DOC concentrations measured at any site/habitat (~7 mM). Concentrations of NH_4^+ were low in sediments inhabited by both *Sclerolinum* and *Lamellibranchia* with *Sclerolinum*-inhabited sediments having the higher absolute concentrations (Figures 11-7 and 11-8). Rates of SR were about four times higher in the *Sclerolinum*-inhabited sediments than in the *Lamellibranchia*-inhabited sediments (Figures 11-9 and 11-10; Table 11-1). Rates of AMO were highest in one of the *Sclerolinum* cores (Figure 11-9) and were extremely low in the *Lamellibranchia* core and the other *Sclerolinum* core (Table 11-1) (Joye et al., 2010).

Urchins and Clams. Dense populations of urchins (*Sarsiaster griegii*, up to 20 individuals per m^2; S. Lessard-Pilon, Personal Communication; Roberts et al. 2007) were found at some active seep sites (AT340, AC818, AC601). So far, relation between the sediment biogeochemistry and the urchins is unknown. However, the urchins may be attracted by sedimentary microbial biomass, which they could utilize as a nutrition source. Sediments inhabited by urchins exhibited unique patterns of biogeochemistry and microbial activity (Figure 11-11). These sediments were characterized by extremely high concentrations of DIC (up to 20 mM) and CH_4 concentrations were as high as 1 mM, though concentrations were lower on average in the upper 12 cm (Figure 11-11, Table 11-1). Methane carbon isotope data is only available for one urchin site (AT340) and there the $d^{13}C\text{-}CH_4$ was -72.4‰, again showing the importance of biogenic CH_4 (Table 11-1) (Joye et al., 2010).

Pore water SO_4^{2-} was rapidly depleted, H_2S accumulated to high concentrations (up to 25 mmol at 15 cm), and there was no change in Cl^- concentration over depth (Figure 11-11). The rapid accumulation of H_2S shows that the sediments were anoxic despite obvious urchin bioirrigation activities (urchin motion was visible as obvious dark lines marking their movement) (Figure 11-11). Concentrations of NH_4^+ were low and DOC concentrations increased slightly with depth; DOC concentrations in particular were much lower than observed at other habitats (Figure 11-11). *Sarsiaster*-inhabited sediments contained a similar amount of organic carbon (~1.6%) and organic nitrogen (~0.2 %) as tube worm inhabited sediments (Table 11-2) (Joye et al., 2010).

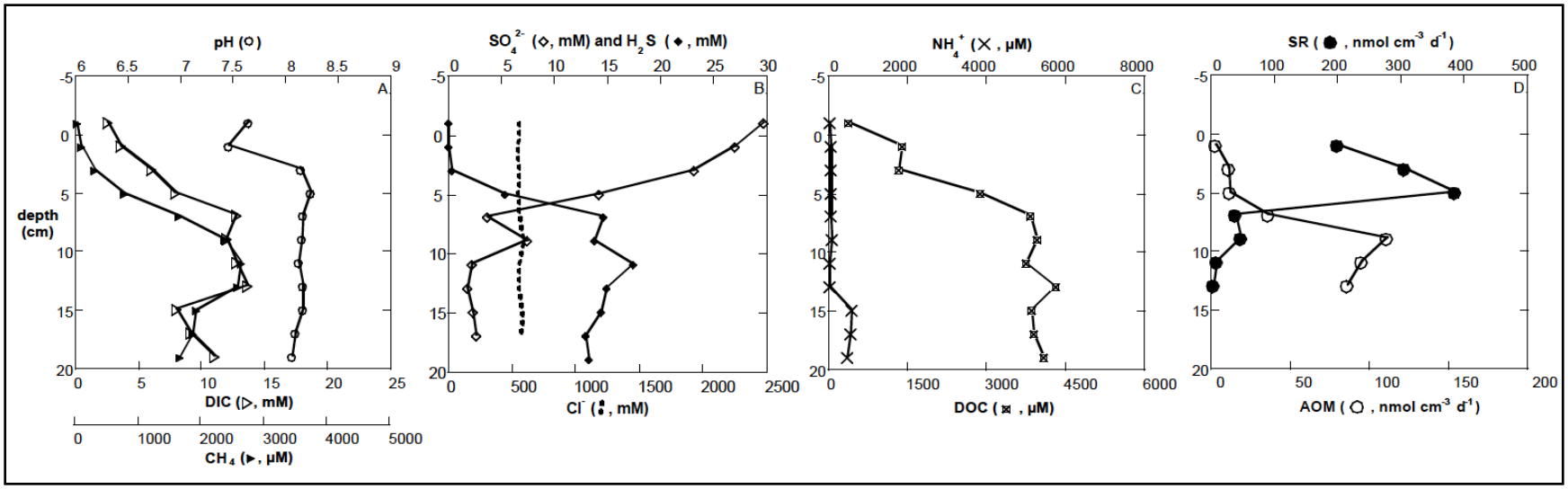

Figure 11-9. Depth profiles of (A) pH (upper axis) and methane and dissolved inorganic carbon (lower axis) concentration; (B) sulfate and hydrogen sulfide (upper axis) and chloride (lower axis) concentration; (C) ammonium (upper axis) and dissolved organic carbon (lower axis) concentration; and (D) sulfate reduction rate (upper axis) and anaerobic oxidation of methane (AOM, also called AMO) (lower axis) in the WR269/270 *Sclerolinum* core. Data from the 2006 *Alvin* cruise.

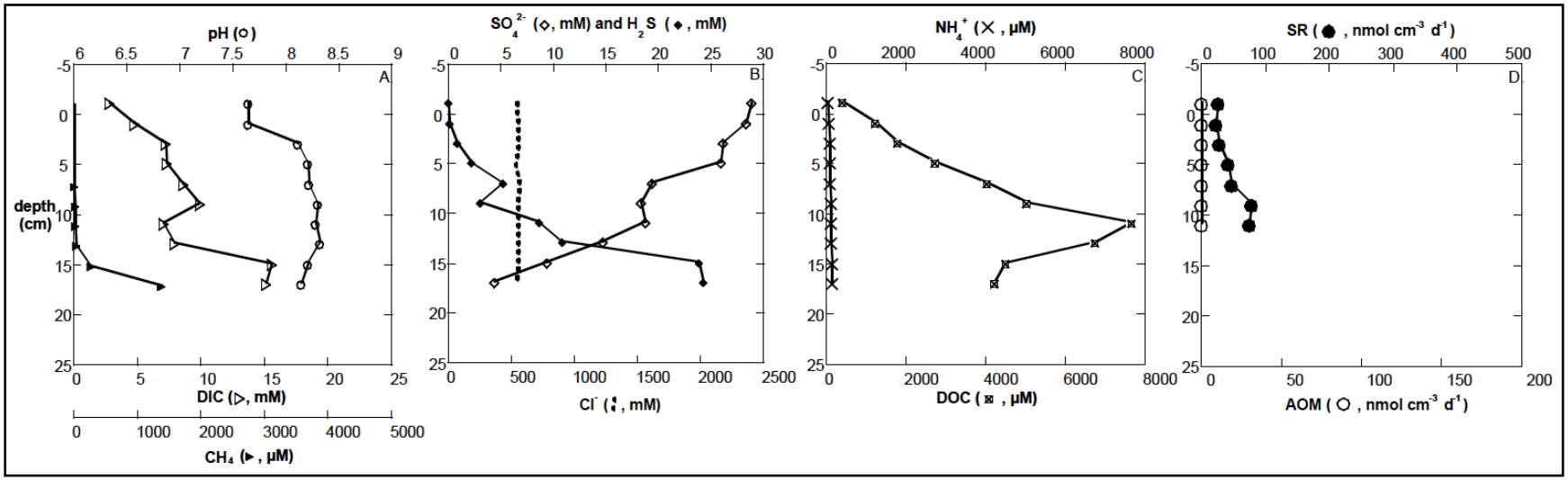

Figure 11-10. Depth profiles of (A) pH (upper axis) and methane and dissolved inorganic carbon (lower axis) concentration; (B) sulfate and hydrogen sulfide (upper axis) and chloride (lower axis) concentration; (C) ammonium (upper axis) and dissolved organic carbon (lower axis) concentration; and (D) sulfate reduction rate (upper axis) and anaerobic oxidation of methane (AOM, also called AMO) (lower axis) in the AC818 *Lamellibranchia* core. Data from the 2006 *Alvin* cruise.

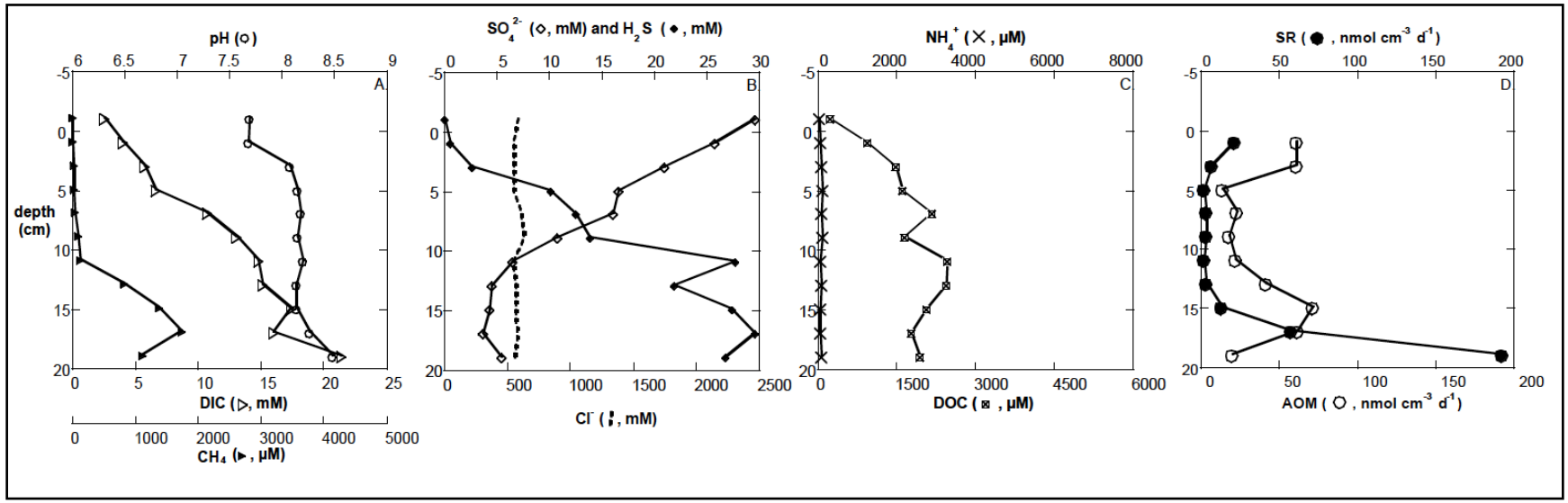

Figure 11-11. Depth profiles of (A) pH (upper axis) and methane and dissolved inorganic carbon (lower axis) concentration; (B) sulfate and hydrogen sulfide (upper axis) and chloride (lower axis) concentration; (C) ammonium (upper axis) and dissolved organic carbon (lower axis) concentration; and (D) sulfate reduction rate (upper axis) and anaerobic oxidation of methane (AOM, also called AMO) (lower axis; note that upper and lower axes have the same scale on this figure) in the AC818 Urchin core. Data from the 2006 *Alvin* cruise.

Sarsiaster-inhabited sediments exhibited a unique pattern of SR and AMO rates. AMO rates significantly exceeded SR rates throughout much of the core until at the bottom of the core (17 and 20 cm depths), where SR rates increased substantially (Figure 11-11). When integrated over the top 12 cm of the core, SR rates were substantially lower (by 5 times) the AMO rates (Table 11-2). Possibly, CH_4 consumption in uppermost sediments was mediated by aerobic methanotrophs. However, a rapid increase of H_2S with depth and the fact that O_2 and H_2S are not mutually stable means that another electron acceptor for AMO is required (elaborated on by Joye et al., 2010).

Sediments inhabited by clams (*Calyptogena ponderosa*) contained the lowest concentrations of CH_4 measured (Table 11-1) and the methane was of mixed thermogenic-biogenic origin (-54 to -62‰). Concentrations of DIC and H_2S were also low and SO_4^{2-} was only moderately depleted (Table 11-1). Concentrations of NH_4^+ were higher in *Calyptogena*-inhabited sediments than any other animal habitat (Table 11-1). Rates of SR were low and rates of AMO were near detection limits. Surprisingly, the percent organic carbon (%OC) noted at clam-inhabited sediments (4–6%) was the highest measured at any site (Table 11-1). *Calyptogena*-inhabited sediments also exhibited the highest carbon-nitrogen (C:N) ratios. The high organic content (10–12 % organic matter) of the sediments could result from release of organic matter by the clams; it is unclear why the high %OC and organic matter do not translate into high rates of microbial activity. Overall, the data show that clam-inhabited sediments are characterized by moderate rates of microbial activity and efficient re-cycling of H_2S produced via SR (Joye et al., 2010), as noted by Treude et al. (2003).

11.2.1.7. Summary for 2006 Biogeochemistry Results

At sites on the lower slope of the GoM, sediment biogeochemical signatures were unique and rates of microbial metabolism were substantially less than previously noted at upper slope sites. Rates of SR and AMO reported here were 1 to 3 orders of magnitude lower than those reported for upper slope sites. Brine-seepage was associated with substantial release of NH_4^+ and DOC to associated habitats, potentially impacting a suite of geobiological processes. Animal habitats were distinct from each other and from other habitats and suggested unique interactions between animals and sediment microorganisms. Biogenic methane was abundant at lower slope sites, suggesting a previously unrecognized role for microbial methanogenesis in these habitats.

11.2.1.8. 2007 Cruise

The main biogeochemistry-microbiology goal for the 2007 cruise was to evaluate within and between habitat variability at key sites. We determined that significant differences were present between habitats within a given site and to some extent at similar habitats between sites. Generally speaking, this means that specific habitats have specific features–across sites–and that some sites have features that imprint across habitats.

11.2.1.9. AT340: Cross Habitat

At AT340, four habitats were examined: control, urchin, microbial mat and brine. The pH of sediment pore water was, on average, 1.5 units higher at urchin and mat sites relative to the control. This increase in pH is largely due to elevated concenrations of hydrogen sulfide and poly sulfide in the porewater at urchin and mat sites compared to control sites (data not shown) (Table 11-3). The pore water salinity was significantly higher at mat (82 ‰) and brine (>100 ‰)

sites compared to urchin and control sites. The percent combustible organic matter (COM) was similar across sites (5–6%; Table 11-3). Particulate organic carbon content was high and variable (~1.5%) and was significantly lower at microbial mat sites (Table 11-3). Particulate nitrogen content was significantly higher (by 2X) in brine sediments relative to control, mat or urchin sediments. This could be the result of elevated concentrations of DIN in brine fluids (see above). This DIN is subsequently incorporated into particulate organic matter by microbial activity. The C:N ratio of the sediment was lowest at brine sites (8.3) and both brine and mat sites had lower C:N ratios than control sediments (Table 11-3).

Pore water profiles further illustrated significant differences between habitats (Figure 11-12). Sodium concentrations in brine and mat pore water were significantly higher than those from control and urchin cores at depth. Sulfate concentrations and the profile over depth were unique at brine sites, illustrating the rapid upward advection of sulfate-free fluids. Sulfate draw down by microbial activity was surprisingly similar in urchin and microbial mat habitats (Figure 11-12). Methane concentrations were highest in brine followed by mat habitats. Concentrations in urchin and control pore waters were low (Figure 11-12). Concentrations of DIC, a metabolic by product that indicates relative rates of microbially-mediated organic matter oxidation, were significantly higher in urchin, mat and brine cores relative to control cores. There were no significant differences observed in DIC concentration between these three habitats (Figure 11-12). SR rates were significantly higher in brine sediments while rates in both mat and urchin habitats were similar and higher than those in the control sediments (Figure 11-12, Table 11-4).

These data clearly show distinct habitat-specific biogeochemical signatures. Brine sediments supported the highest rates of microbial SR, despite rapid drawdown of sulfate due to the combination of microbial activity and upward advection of sulfate-free brine fluids. Brines also exhibited the highest concentrations of methane and DIC. Rates of anaerobic oxidation of methane were extremely low and were comparable across habitats (though significantly lower in microbial mats).

11.2.1.10. GC852: Cross Habitat

At GC852, three habitats were examined: control, gassy microbial mat and brine. Unfortunately, the cores collected from a supposed brine flow were too short (~14 cm) to actually penetrate into the elevated salinity sediments. Still, both microbial mat and brine sediments had elevated pH (8.2) compared to control (6.8) sediments. The COM was somewhat higher than that observed at AT340 (8 compared to 5) as was the POC (20 compared to 12; Table 11-3). In contrast to the brine at AT340, the mat and brine sediments from GC852 contained lower particulate organic nitrogen (PON) than control sediments (Table 11-3). The C:N ratio of sediments was between 8 and 9 and not significantly different between sites.

No difference in chloride concentrations was noted between the three sites but rapid and significant drawdown of pore water sulfate was noted at mat and brine sites relative to the control (Figure 11-13). Methane and DIC concentrations were similar in brine and mat sediments and were significantly higher than those in control sediments (Figure 11-13). SR rates were also comparable in mat and brine sediments and were significantly higher than those observed in control sediments (Figure 11-13; Table 11-4).

Table 11-3

Pore Water pH and Salinity and Combustible Organic Matter (COM), Particulate Organic Carbon (PC), Particulate Organic Nitrogen (PN) and the Particulate C:N Ratio (C:N)

Averages and standard deviations (in parenthesis) over depth for each site are shown (n=number of cores or depths (total data points) averaged to generate the values shown).

Site	**Habitat**	***n* cores**	***n* depths**	**pH**	**Salinity *(‰)***	**COM *(weight %)***	**PC *mg/ g dry sed***	**PN *mg/ g dry sed***	**C:N *g:g***
AT340	Control	4	20	6 (±0.1)	36.2 (±0.9)	5.3 (±0.7)	12.4 (±1.3)	0.8 (±0.1)	16.1 (±1.5)
AT340	Urchin	4	20	**7.7 (± 0.2)**	35.1 (±0.9)	6.2 (±0.8)	13.5 (±1.9)	1 (±0.2)	13.4 (±1.6)
AT340	Mat	4	20	**7.8 (±0.2)**	**82.3 (±13.7)**	5.3 (±0.3)	**7.8 (±1.5)**	0.8 (±0.1)	**10.4 (±1.9)**
AT340	Brine	4	20	7.2 (±0.5)	**103.8 (±24)**	5.2 (±0.9)	14.9 (±2.6)	**1.9 (±0.4)**	**8.3 (±0.7)**
GC852	Control	2	10	6.8 (±0.1)	36.4 (±0.5)	7.9 (±0.3)	19.6 (±0.7)	2.3 (± 0.01)	8.4 (±0.3)
GC852	Mat, gassy	4	20	**8.2 (±0.3)**	34.9 (±0.6)	7.1 (±0.8)	**12.2 (±2.3)**	**1.5 (±0.4)**	8.6 (±1.3)
GC852	Brine	4	20	**8.3 (±0.1)**	35.3 (±0.3)	**3 (±0.6)**	**12 (±1.9)**	**1.4 (±0.6)**	9.5 (±1.1)
GB697	Brine	2	8	7.4 (±0.1)	48 (±0.7)	4.1 (±0.6)	18.8 (±1.4)	2.4 (±0.2)	7.9 (±0.2)
WR269	Control	3	20	7.1 (±0.2)	35.6 (±0.2)	2.8 (±1.3)	9.4 (±0.4)	1.1 (0.1)	8.9 (±0.2)
WR269	Pogo	3	20	6.9 (±0.4)	35.2 (±0.8)	3.3 (±0.7)	11.1 (±2.7)	1.3 (±0.4)	8.6 (±0.6)
GB647	Oily	2	10	6.8 (±1)	123.5 (±100)	15.4 (±8)	70 (±88)	1.8 (±1.6)	29.2 (±25)
AC645	Pogo	4	20	7.2 (±0.3)	36 (±0.4)	5.9 (±1.4)	8.9 (±0.5)	1.1 (±0.1)	8.5 (±0.2)
AC818	Control	4	20	7.2 (±0.2)	35.3 (±0.3)	6.2 (±0.6)	13.6 (±0.4)	1.6 (±0.01)	8.7 (±0.1)
AC818	Urchin	4	20	**8 (±0.1)**	35.7 (±0.4)	7.1 (±0.7)	19.3 (±1.2)	2.4 (±0.2)	8.2 (±0.2)
AC818	Pogo	4	20	7.9 (±0.5)	35.9 (±0.4)	6.4 (±0.5)	19.5 (±0.5)	2.4 (±0.2)	8.3 (±0.6)
AC601	Control	4	20	7.5 (±0.2)	37.6 (±0.9)	9.6 (±0.5)	11 (±0.3)	1.3 (±0.05)	8.5 (±0.1)
AC601	Lake Interior	3	15	**6.8 (±0.05)**	**86.1 (±4.7)**	**7.2 (±0.8)**	**21.6 (±0.7)**	**2.6 (±0.1)**	8.3 (±0.2)
AC601	Lake Edge	3	15	7.5 (±0.1)	**52.4 (±6.2)**	**6.4 (±0.5)**	**20.3 (±0.7)**	**2.4 (±0.1)**	8.6 (±0.1)
AC601	Urchin	3	15	7.3 (±0.2)	39.1 (±3.1)	7.8 (±1.7)	16 (±4.2)	1.8 (±0.5)	8.7 (±0.1)
Red Crater	Pogo	2	10	7.9 (±0.05)	39.8 (±0.05)	9 (±0.3)	12 (±0.1)	0.8 (±0.05)	16 (± 0.7)
Red Crater	Old MV	2	10	7.3 (±0.05)	41.4 (±1.6)	8.7 (±0.3)	11.9 (±0.3)	0.7 (±0.1)	16.7 (±1)

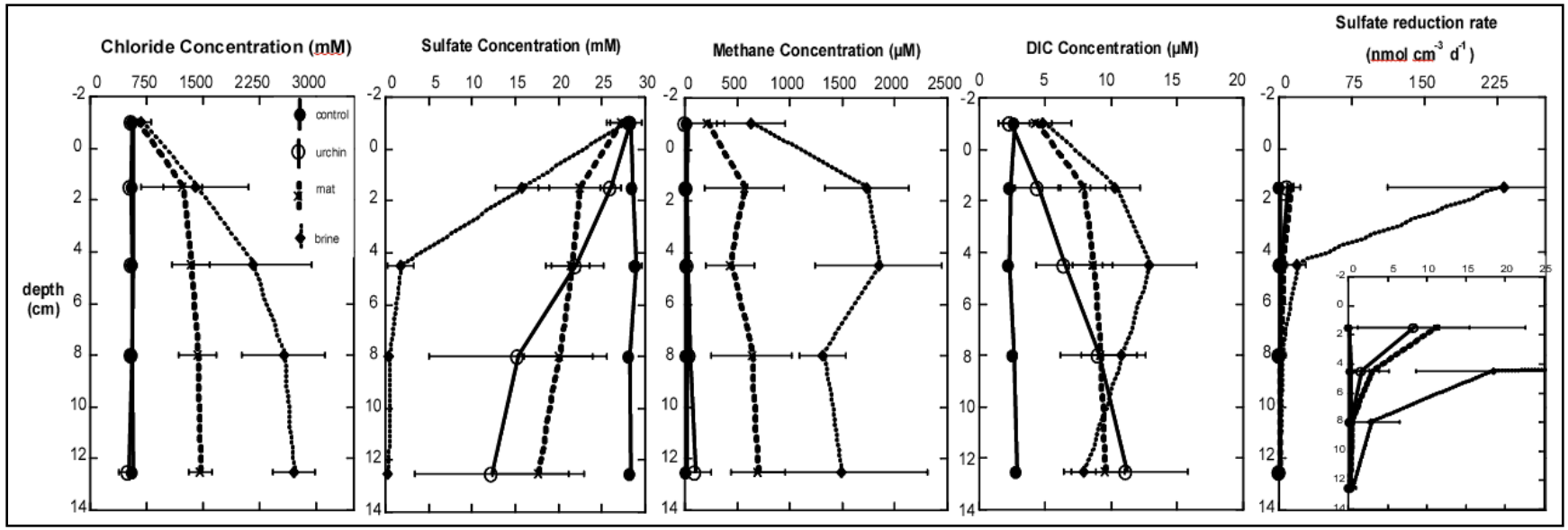

Figure 11-12. Comparative geochemical profiles and sulfate reduction rates of habitats (control, urchin, mat, brine) from AT340. Data are from 2007 *Jason II* cruise. Symbols denote average and error bars denote standard deviation of the mean.

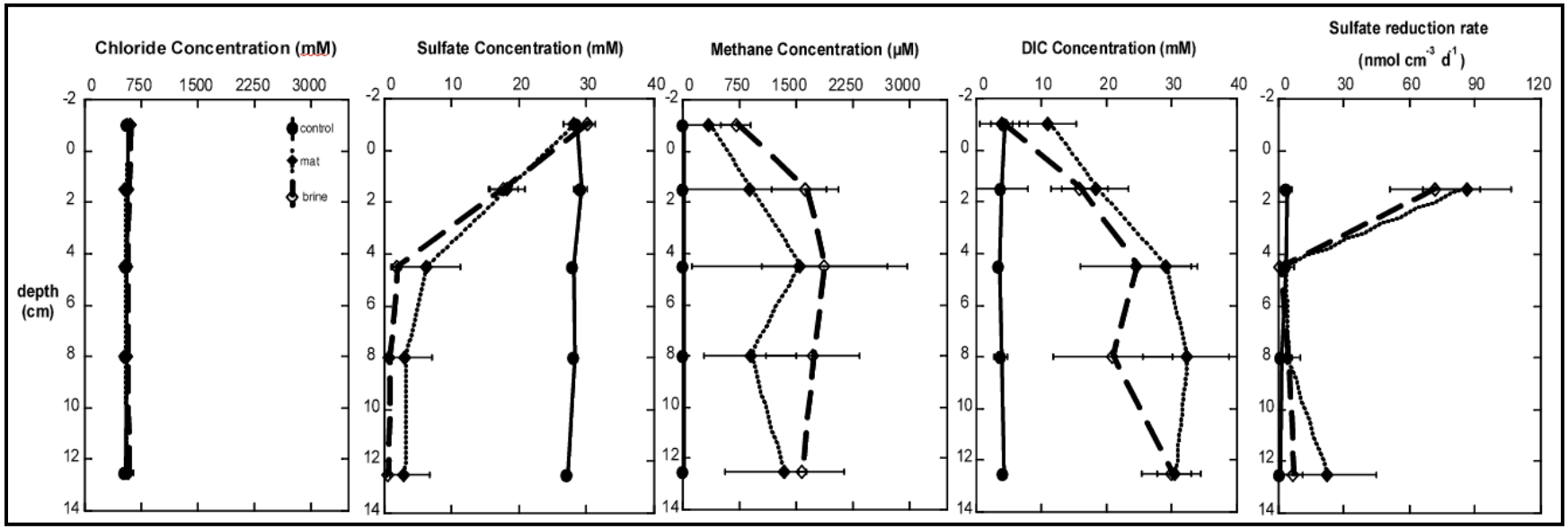

Figure 11-13. Comparative geochemical profiles and sulfate reduction rates of habitats (control, mat, brine) from GC852. Data are from 2007 *Jason II* cruise.
Symbols denote average and error bars denote standard deviation of the mean. Note that while the brine cores were collected from an apparent brine seep, the cores were not deep enough (14 cm) to penetrate into the higher salinity sediments.

SR rates in the GC852 brine cores were comparable to those observed in the AT340 brine cores (Table 11-4). In contrast, SR rates in GC852 mat cores were significantly higher than those in AT340 mat cores (Table 11-4). Rates of AMO were highest in GC852 gassy mat sediments (but not significantly different from rates in brines) and were much higher than those observed in brine or mat sites at AT340. The ratio of SR:AMO was lower at GC852 than AT340 (Table 11-4).

11.2.1.11. WR269: Cross Habitat

At WR269, two habitats were examined: control and *Sclerolinum*. These cores were slightly deeper (17 cm) that the cores collected from other habitats because results from the 2006 cruise revealed that *Sclerolinum* impacted biogeochemical signatures to substantial depth (>20 cm; Joye et al., 2010). In terms of solid phase characteristics, the control and *Sclerolinum* were similar (Table 11-3). Similarly, depth profiles of biogeochemical constituents (chloride, sulfate, methane, and DIC) were comparable (Figure 11-14). Rates of SR were significantly higher in the *Sclerolinum* core relative to the control but AMO rates in *Sclerolinum* and control cores were not significantly different (Figure 11-14; Table 11-4). If deeper cores had been examined, more differences between control and *Sclerolinum* cores would likely have been observed (Joye et al., 2010).

11.2.1.12. AC818: Cross Habitat

At AC818, three habitats were examined: control, urchin, and *Sclerolinum*. Solid phase particulate organic carbon (POC) and PON were higher in urchin and *Sclerolinum* compared to control cores (Table 11-3). Chloride concentration profiles were comparable at all habitats (Figure 11-15). Sulfate was depleted in similarly urchin and *Sclerolinum* cores relative to control cores (Figure 11-15). Methane exhibited a subsurface peak in *Sclerolinum* cores, while concentrations in urchin cores increased gradually with depth (Figure 11-15). Methane and DIC concentrations in control cores were significantly lower than those from animal habitats. As noted at other sites, SR rates were higher in animal habitats than in control habitats (Table 11-4).

11.2.1.13. AC601: Cross Habitat

At the AC601 brine lake, four habitats were examined: control, inside the lake, the barite precipitation zone at the lake edge, and urchins. The pH was comparable at all habitats, except the lake interior, where it was significantly lower (Table 11-3). Salinity was highest in the lake interior and both the lake interior and lake edge pore waters had higher salinity than control or urchin sites. The lake interior and lake edge also had lower contents of combustible organic matter than the control site, suggesting elevated rates of microbial activity at these sites relative to the control. The POC and PON content of the lake interior and lake edge habitats were significantly higher than those of control or urchin habitats (Table 11-3).

Table 11-4

Integrated Rates of Sulfate Reduction (SR), Anaerobic Oxidation of Methane (AMO) and the Rates Over Depth For Each Habitat/Site

(n=number of cores or depths (total data points) averaged to generate values shown)

Site	**Habitat**	***n* cores**	***n* depths**	**SR** *mmol m^{-2} d^{-1}*	**AMO** *mmol m^{-2} d^{-1}*	**SR:AMO**
AT340	Control	4	16	0.016 (±0.008)	0.021 (±0.002)	0.8 (±0.4)
AT340	Urchin	4	16	**0.190 (±0.174)**	0.021 (±0.002)	**8.6 (±7)**
AT340	Mat	4	16	**0.279 (±0.005)**	**0.005 (±0.005)**	**69 (±23)**
AT340	Brine	4	16	**4.212 (±1.953)**	0.019 (±0.013)	**553 (±70)**
GC852	Control	2	8	0.193 (±0.03)	0.026 (±0.003)	7.7 (±2.2)
GC852	Mat, gassy	4	16	**2.062 (±1.144)**	0.077 (±0.043)	**38 (±36)**
GC852	Brine	4	16	**1.399 (±1.434)**	0.047 (±0.020)	**26 (±14)**
GB697	Brine	2	8	2.579 (±2.306)	0.008 (±0.003)	429 (±50)
WR269	Control	3	16	0.073 (±0.001)	0.045 (±0.017)	1.8 (±0.7)
WR269	Pogo	3	16	**1.587 (±0.921)**	0.067 (±0.029)	**22 (±4.6)**
GB647	Oily	2	8	14.6 (±20.3)	0.016 (±0.021)	563 (±50)
AC645	Pogo	4	16	0.239 (±0.108)	0.010 (±0.0.004)	27.4 (±19)
AC818	Control	4	16	0.289 (±0.039)	0.030 (±0.001)	9.7 (±1.3)
AC818	Urchin	4	16	1.78 (±2.30)	0.031 (±0.035)	108 (±11)
AC818	Pogo	4	16	0.825 (±0.393)	0.015 (±0.007)	69 (±54)
AC601	Control	4	16	0.080 (±0.010)	0.028 (±0.027)	5.2 (±3.7)
AC601	Lake Interior	3	12	0.692 (±0.69)	0.005 (±0.001)	127 (±100)
AC601	Lake Edge	3	12	2.804 (±0.773)	0.067 (±0.04)	52 (±33)
AC601	Urchin	3	12	4.418 (±1.373)	0.078 (±0.015)	16.4 (±14)
Red Crater	Pogo	2	8	4.517 (±1.635)	0.082 (±0.023)	54.7 (±4.3)
Red Crater	Old MV	2	8	2.766 (±0.867)	0.015 (±0.011)	290 (±200)

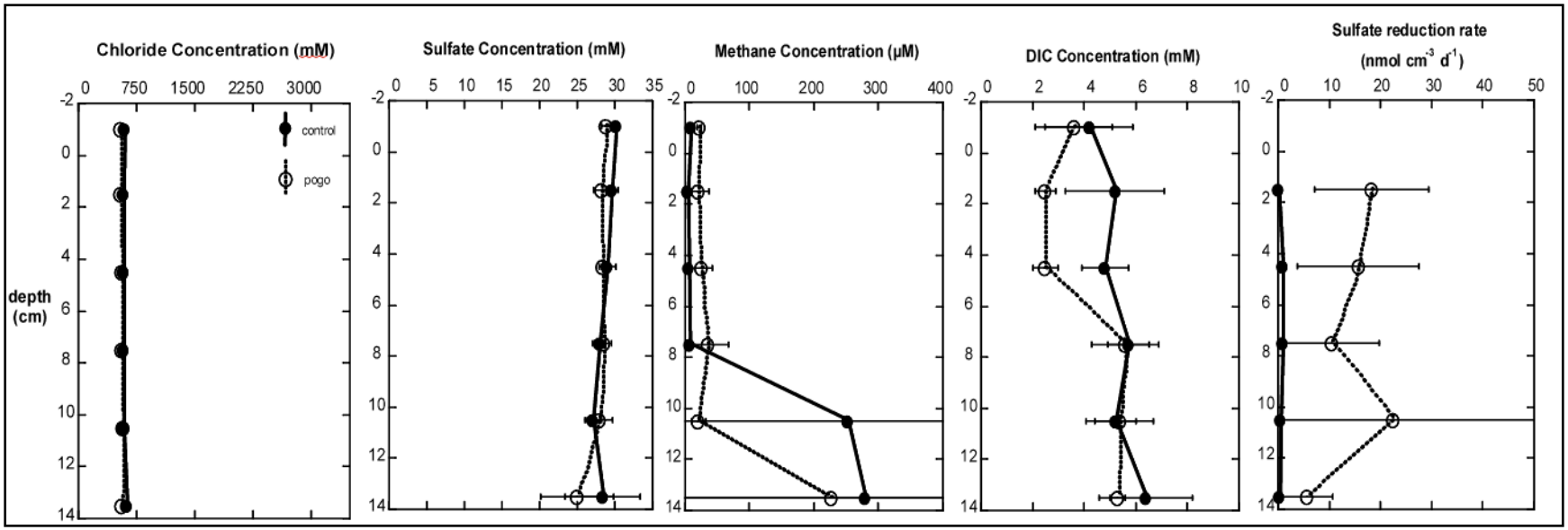

Figure 11-14. Comparative geochemical profiles and sulfate reduction rates of habitats (control, pogonophoran) from WR269. Data are from 2007 *Jason* II cruise. Symbols denote average and error bars denote standard deviation of the mean.

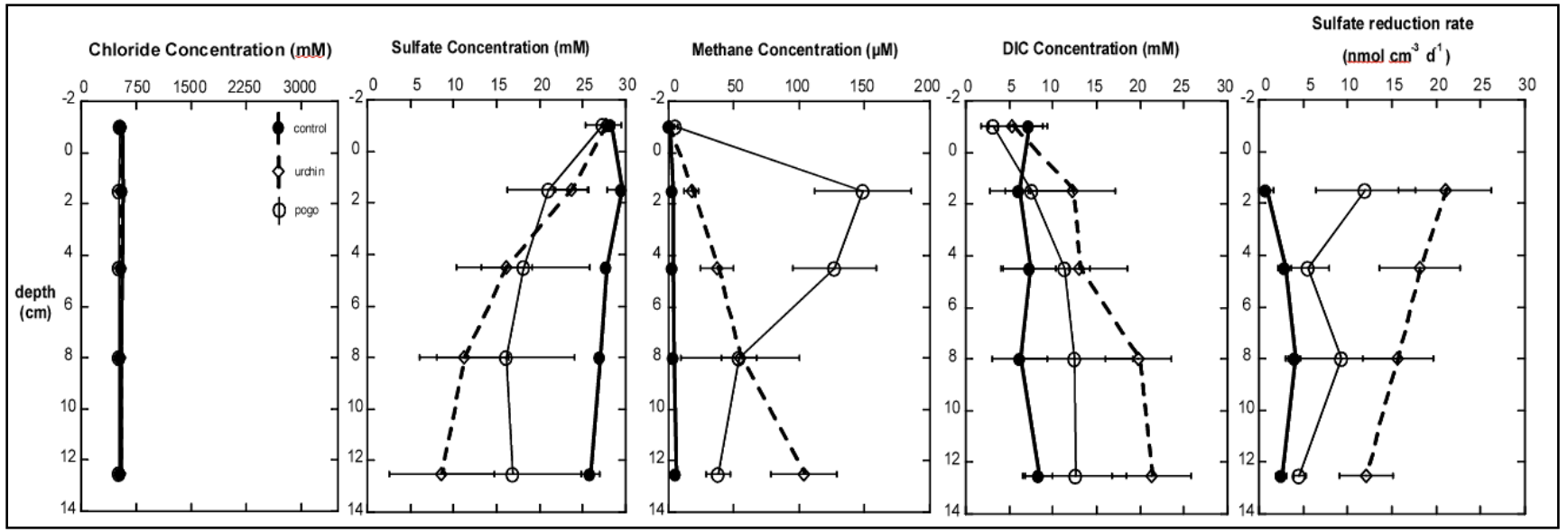

Figure 11-15. Comparative geochemical profiles and sulfate reduction rates of habitats (control, urchin, pogo) from AC818. Data are from 2007 *Jason II* cruise. Symbols denote average and error bars denote standard deviation of the mean.

Pore water biogeochemical signatures clearly showed differences between sites. Pore water chloride content was highest in cores from the lake interior, followed by the lake edge, urchins and finally control sites (Figure 11-16). Sulfate concentrations in the overlying water of the brine lake were about 10 mM, comparable to concentrations observed in 2006 (15 mmol albeit at a different part of the lake) and were significantly lower than concentrations at other sites. Sulfate consumption was rapid at both lake interior and lake edge sites; sulfate was near zero by 8 cm (Figure 11-16). Sulfate depletion in urchin sediments exceeded that in control cores, as well. Methane concentrations were highest in lake interior sediments followed by lake edge sediments and then urchin sediments. Methane concentrations in control sediments were much lower (single digit µM; Figure 11-16). Similarly, DIC concentrations were highest and comparable in lake edge and lake interior pore waters. Pore waters from urchin habitats contained significantly more DIC than did pore waters from control habitats. Rates of SR were highest in lake edge sediments, followed by urchin sediments and then finally lake interior sediments (Figure 11-16).

Rates of SR in control sediments were significantly lower than observed in the other sites (Table 11-4). Highest rates of SR were observed in the urchin and lake edge habitats. Rates in lake interior sediments were limited by sulfate. Rates of AMO were higher in lake edge and urchin sites than in lake interior or control sediments (Table 11-4).

11.2.1.14. Control Habitats: Across Site

Control habitats were examined at four sites: AT340, GC852, AC818, and AC601. We also obtained control cores from WR269 but different depths were samples so are not discussed here. Overall, control cores were similar (Table 11-5). The most pronounced site-specific difference in control cores was the higher COM, particulate carbon, and particulate nitrogen content observed at GC852 (Table 11-5). The C:N ratio was twice as high at AT340 (16) compared to the other sites.

Chloride concentrations were not significantly different among control habitats (Figure 11-17). Sulfate depletion and DIC concentration were highest at AC818, though not nearly as substantial as that noted in other habitats. Methane concentrations were highest at AC601 and AT340 and lowest at GC852 and AC818. SR rates over depth were highest at AC818 and GC852. Though integrated SR rates at control habitats were much lower than at other habitats, some variability was observed between sites. SR rates at GC852 and AC818 were significantly higher than rates at AT340 and AC601 (Table 11-6). AMO rates were comparable at all the control sites.

11.2.1.15. Urchin Habitats: Across Site

Urchin habitats were examined at three sites: AT340, AC818, and AC601. The solid phase characteristics of urchin habitats were similar across sites (Table 11-5). A notable exception was the POC and PON content of AC818 urchin meadows: these sediments contained significantly more POC and PON than AT340 (but POC at AC818 and AC601 was similar). The C:N ratio was significantly higher (13.4) at AT340 compared to AC818 or AC601 (Table 11-5).

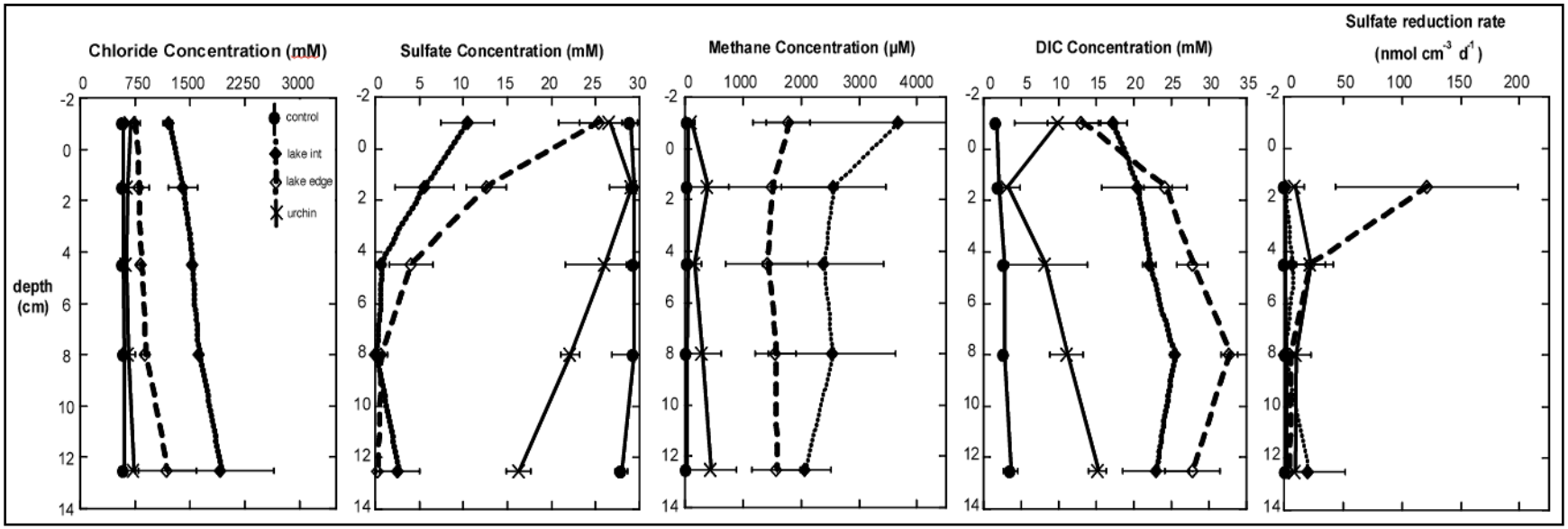

Figure 11-16. Comparative geochemical profiles and sulfate reduction rates of habitats (control, lake interior (lake int), lake edge, urchin) from the AC601 Brine Lake. Data are from 2007 *Jason II* cruise. Symbols denote average and error bars denote standard deviation of the mean.

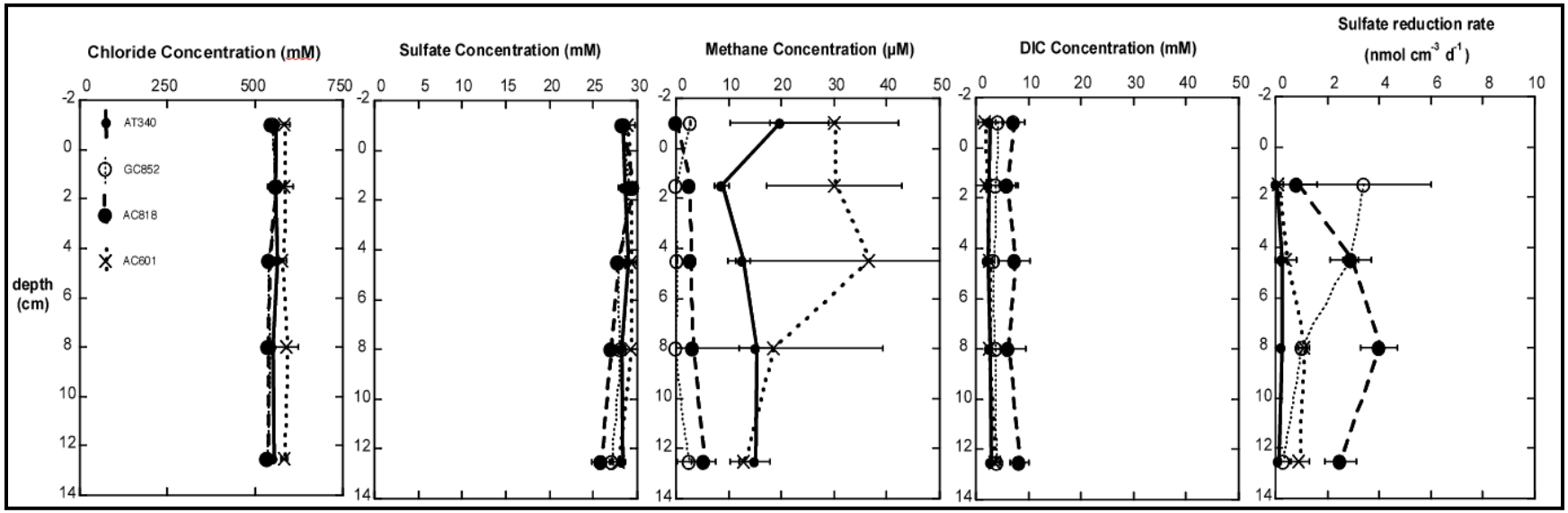

Figure 11-17. Comparative geochemical profiles and sulfate reduction rates in control cores collected at different sites (AT340, GC852, AC818, AC601). Data are from 2007 *Jason II* cruise. Symbols denote average and error bars denote standard deviation of the mean.

Table 11-5

Pore Water pH and Salinity and Combustible Organic Matter (COM), Particulate Organic Carbon (PC), Particulate Organic Nitrogen (PN) and the Particulate C:N Ratio (C:N)

Averages and standard deviations (in parenthesis) over depth for each habitat are shown (n=number of cores or depths (total data points) averaged to generate the values shown).

Habitat	**Site**	***n* cores**	***n* depths**	**pH**	**Salinity** *(‰)*	**COM** *(weight %)*	**PC** *mg/ g dry sed*	**PN** *mg/ g dry sed*	**C:N** *g:g*
Control	AT340	4	20	6 (±0.1)	36.2 (±0.9)	5.3 (±0.7)	12.4 (±1.3)	0.8 (±0.1)	**16.1 (±1.5)**
Control	GC852	2	10	**6.8 (±0.1)**	36.4 (±0.5)	**7.9 (±0.3)**	**19.6 (±0.7)**	**2.3 (± 0.01)**	8.4 (±0.3)
Control	AC818	4	20	**7.2 (±0.2)**	35.3 (±0.3)	6.2 (±0.6)	13.6 (±0.4)	1.6 (±0.01)	8.7 (±0.1)
Control	AC601	4	20	**7.5 (±0.2)**	37.6 (±0.9)	**9.6 (±0.5)**	11 (±0.3)	1.3 (±0.05)	8.5 (±0.1)
Urchin	AT340	4	20	7.7 (± 0.2)	35.1 (±0.9)	6.2 (±0.8)	13.5 (±1.9)	1 (±0.2)	**13.4 (±1.6)**
Urchin	AC818	4	20	8 (±0.1)	35.7 (±0.4)	7.1 (±0.7)	**19.3 (±1.2)**	**2.4 (±0.2)**	8.2 (±0.2)
Urchin	AC601	3	15	7.3 (±0.2)	39.1 (±3.1)	7.8 (±1.7)	16 (±4.2)	1.8 (±0.5)	8.7 (±0.1)
Pogos	WR269	3	20	6.9 (±0.4)	35.2 (±0.8)	**3.3 (±0.7)**	11.1 (±2.7)	1.3 (±0.4)	8.6 (±0.6)
Pogos	AC645	4	20	7.2 (±0.3)	36 (±0.4)	5.9 (±1.4)	*8.9 (±0.5)*	1.1 (±0.1)	8.5 (±0.2)
Pogos	AC818	4	20	7.9 (±0.5)	35.9 (±0.4)	6.4 (±0.5)	**19.5 (±0.5)**	**2.4 (±0.2)**	8.3 (±0.6)
Brine	AT340	4	20	7.2 (±0.5)	**103.8 (±24)**	5.2 (±0.9)	14.9 (±2.6)	1.9 (±0.4)	8.3 (±0.7)
Brine	GC852	4	20	**8.3 (±0.1)**	35.3 (±0.3)	*3 (±0.6)*	12 (±1.9)	**1.4 (±0.6)**	9.5 (±1.1)
Brine	GB697	2	10	7.4 (±0.1)	48 (±0.7)	4.1 (±0.6)	**18.8 (±1.4)**	2.4 (±0.2)	7.9 (±0.2)
Brine	GB647	2	10	6.8 (±1)	**123.5 (±100)**	**15.4 (±8)**	**70 (±88)**	1.8 (±1.6)	**29.2 (±25)**
Brine	AC601	3	15	*6.8 (±0.05)*	**86.1 (±4.7)**	**7.2 (±0.8)**	**21.6 (±0.1)**	2.6 (±0.1)	8.3 (±0.2)

Table 11-6

Integrated Rates of Sulfate Reduction (SR), Anaerobic Oxidation of Methane (AMO) and the Ratio of SR to AMO (SR:AMO)

Averages and standard deviations (in parentheses) of rates over depth are shown for each habitat. (n=number of cores or depths (total data points) averaged to generate values shown).

Site	**Habitat**	***n* cores**	***n* depths**	**SR** *mmol m^{-2} d^{-1}*	**AMO** *mmol m^{-2} d^{-1}*	**SR:AMO**
AT340	Control	4	16	0.016 (±0.008)	0.021 (±0.002)	0.8 (±0.4)
GC852	Control	2	8	**0.193 (±0.03)**	0.026 (±0.003)	7.7 (±2.2)
AC818	Control	4	16	**0.289 (±0.039)**	0.030 (±0.001)	9.7 (±1.3)
AC601	Control	4	16	0.080 (±0.010)	0.028 (±0.027)	5.2 (±3.7)
AT340	Urchin	4	16	*0.190 (±0.174)*	0.021 (±0.002)	**8.6 (±7)**
AC818	Urchin	4	16	1.78 (±2.30)	0.031 (±0.035)	108 (±11)
AC601	Urchin	3	12	**4.418 (±1.373)**	**0.078 (±0.015)**	16.4 (±14)
WR269	Pogo	3	16	1.587 (±0.921)	**0.067 (±0.029)**	22 (±4.6)
AC645	Pogo	4	16	0.239 (±0.108)	0.010 (±0.0.004)	27.4 (±19)
AC818	Pogo	4	16	0.825 (±0.393)	0.015 (±0.007)	69 (±54)
AT340	Brine	4	16	4.212 (±1.953)	0.019 (±0.013)	553 (±70)
GC852	Brine	4	16	1.399 (±1.434)	**0.047 (±0.020)**	**26 (±14)**
GB697	Brine	2	8	2.579 (±2.306)	0.008 (±0.003)	429 (±50)
GB647	Oily Brine	2	8	**14.6 (±20.3)**	0.016 (±0.021)	563 (±50)
AC601	Brine	3	12	0.692 (±0.69)	0.005 (±0.001)	127 (±100)

Chloride concentrations were similar in urchin habitats at all sites (Figure 11-18). Sulfate depletion was most rapid at AC818 and was comparable at AT340 and AC601 (Figure 11-18). Methane concentrations were highest at AC601 while DIC concentrations were highest at AC818. Volumetric SR rates were comparable at AC601 and AC818 (Figure 11-18). Integrated SR and AMO rates were significantly higher in urchin sediments from AC601. Rates of SR in AT340 urchin sediments were the lowest measured (Table 11-6).

11.2.1.16. Sclerolinum Habitats: Across Site

Sclerolinum habitats were examined at three sites, WR269, AC645 and AC818. The pH and pore water salinity was comparable at all sites (Table 11-5). As noted for urchin cores, the POC and PON content at AC818 *Sclerolinum* sites was higher than those noted at other sites (Table 11-5). Pore fluid salinities were comparable at all *Sclerolinum* sites (Figure 11-19). Sulfate depletion and methane and DIC concentrations were highest at AC818. Integrated rates of SR were lowest at AC645 and rates were comparable at WR269 and AC818 (Table 11-6). Integrated rates of AMO were highest at WR269, as was observed in the 2006 core collections as well.

11.2.1.17. Brine Habitats: Across Site

Brine habitats were examined at five sites, AT340, GC852, GB697, GB647, and AC601. A surprising amount of variability was noted in brine habitats between sites. The porewater pH was lowest at GB647 and AC601 and highest at GC852 (Table 11-5). Pore water salinity was highest at GB647; this site was both oily and brine-charged. The combustible organic matter (COM) content was highest in the oily sediments of GB647 (15 weight percent) and these sediments also contained the highest amount of POC (70 mg/g dry sediment). Because of the high POC content of these sediments, the C:N ratio in them was almost 30, the highest value noted in any of the cores (Table 11-5).

Pore water biogeochemistry differed between brine sites, largely as a function of fluid advection rate (Figure 11-20). Highest pore water salinities and steepest chloride profiles were observed at AT340. The AC601 brine showed only slight chloride gradients with depth, suggesting negligible rates of fluid advection at this site. Sulfate was rapidly depleted in the sediments of AT340, GC852 and AC601. Sulfate depletion was much less substantial at GB697 than at the other brine sites (Figure 11-20). Methane concentrations, though variable, were highest in AC601 brines. Concentrations of methane in AT340 and GC852 brine sediments were comparable. DIC concentrations were highest in AC601 brines but high variability obscured differences between sites (except that GB697 brines had the lowest DIC) (Figure 11-20). SR rates were highest in AT340 sediments and lowest in AC601 sediments (Figure 11-20); volumetric rates in GB647 sediments were even higher (data not shown).

Integrated rates of SR were significantly higher in the oily, briney sediments of GB647 (Table 11-6). These rates were about 4 times higher than those measured at other sites (Tables BGC8 &10). Rates of SR in brine habitats generally were among the highest measured during the project (the highest SR rates in both 2006 and 2007 were observed in oily sediments). Integrated rates of AMO were highest at GC852; AMO rates were generally low in brines being comparable to rates in control sediments.

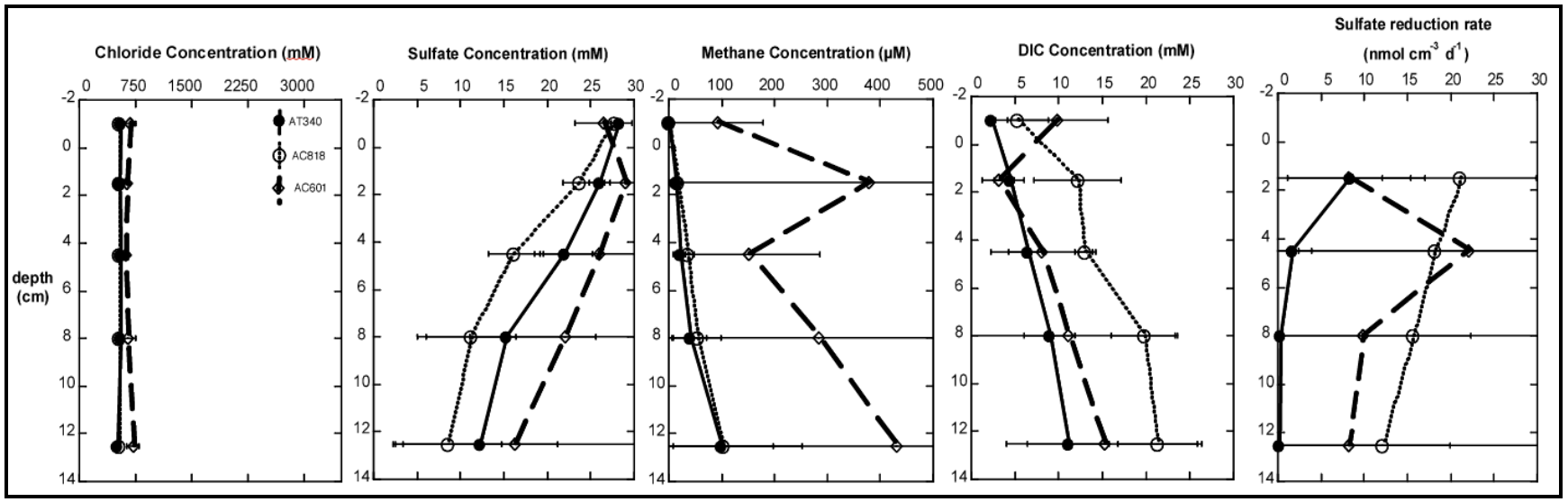

Figure 11-18. Comparative geochemical profiles and sulfate reduction rates in urchin cores collected at different sites (AT340, AC818, AC601). Data are from 2007 *Jason II* cruise. Symbols denote average and error bars denote standard deviation of the mean.

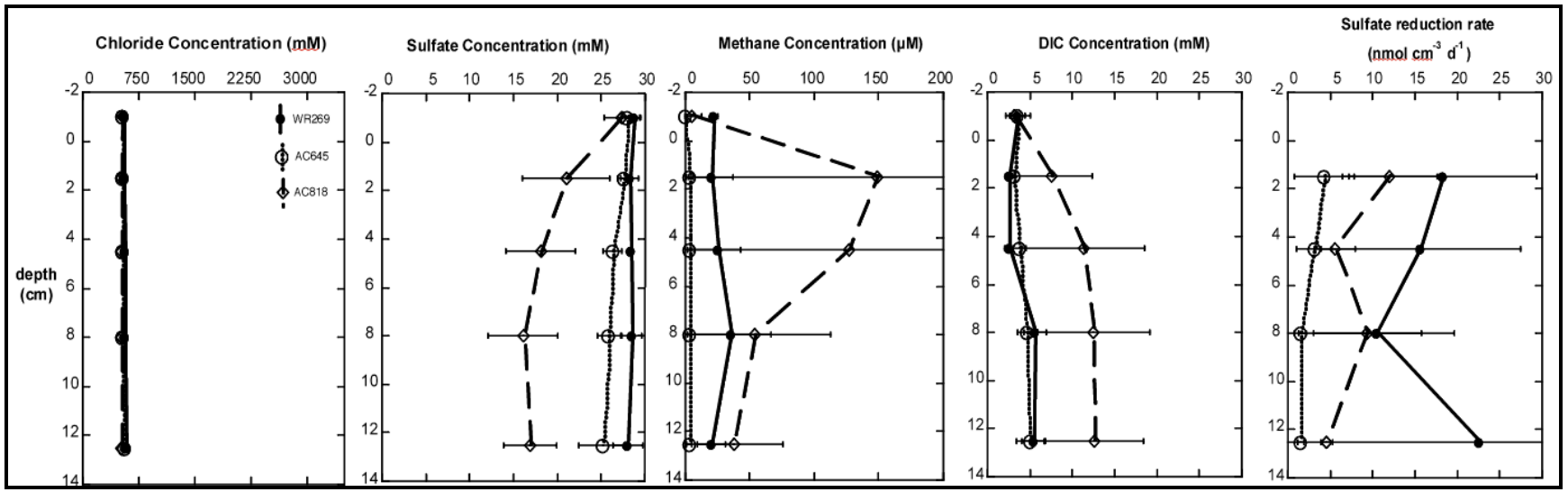

Figure 11-19. Comparative geochemical profiles and sulfate reduction rates in Sclerolinum cores collected at different sites (WR269, AC645, AC818). Data are from 2007 *Jason II* cruise. Symbols denote average and error bars denote standard deviation of the mean.

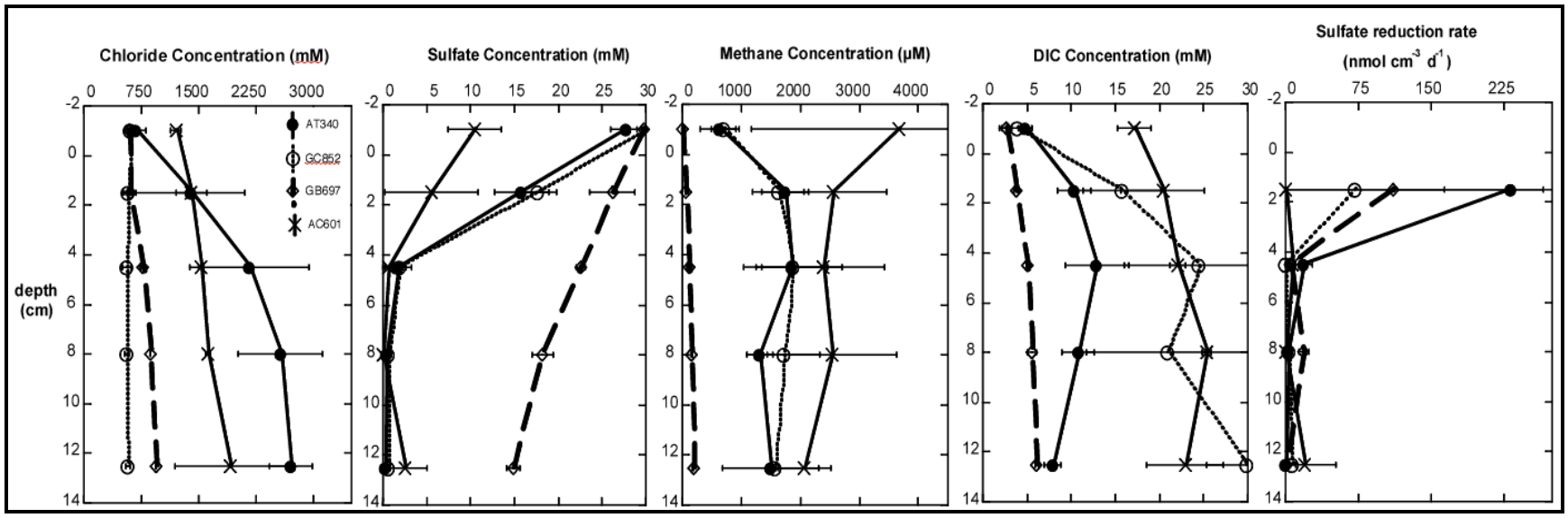

Figure 11-20. Comparative geochemical profiles and sulfate reduction rates in brine cores collected at different sites (AT340, GC852, GB697, AC601). Data are from 2007 *Jason II* cruise. Symbols denote average and error bars denote standard deviation of the mean.

High rates of microbial activity in brine sediments was fueled partially by the high concentrations of DOC present in brine fluids (Joye et al. 2009, Joye et al., 2010). Low rates of AMO in brines are possibly due to high concentrations of dissolved hydrogen, which makes AMO thermodynamically unfavorable (Joye et al. 2009). Brines are very inefficient filters for methane, thus this methane can support chemosynthetic macrofauna (mussels) in brine habitats. Similarly, the high SR rates supported brines generates hydrogen sulfide that can be used as an energy source by chemosynthetic clams and tube worms.

11.2.1.18. Bacterial Diversity around the AC601 Brine Lake

Due to the distinct habitats around the AC601 brine lake, we evaluated bacterial diversity in lake bottom sediments, inner edge sediments, outer edge sediments and in urchin inhabited sediments (Figures 11-21 and 11-22). Distinct differences in microbial community composition were noted among these habitats. Lake bottom sediments were highly diverse but the community was dominated by Gammaproterobacteria and Deltaproterobacteria. Deltaproteobacteria are often involved in SR while Gammaproterobacteria are involved in the oxidation of reduced sulfur species. Roles for the other bacterial species observed are unclear. In inner lake edge sediments, Deltaproteobacteria decreased in relative abundance while Epsilonproteobacteria, Planctomycetes, and Chloroflexi increased in relative abundance. The largest increase in abundance was of the Epsilonproteobacteria; the ecological role of these organisms is unclear but they may be involved in organic matter fermentation. In outer edge (barite zone) sediments, Deltaproteobacteria increased in abundance, which is not surprising since these organisms are involved in SR. Gammaproteobacteria, who are involved in sulfide oxidation, also increased in abundance in this zone. Surprisingly, Chloroflexi increased substantially within this zone. These organisms may also be involved in sulfur cycling. In the urchin sediments, Deltaproteobacteria, gammaprotobacteria, and episonproteobacteria were abundant (gammaprotobacteria more so than others). Interestingly, planctomycete and symbiont sequences were also abundant. These data are being combined with biogeochemical and microbial activity data.

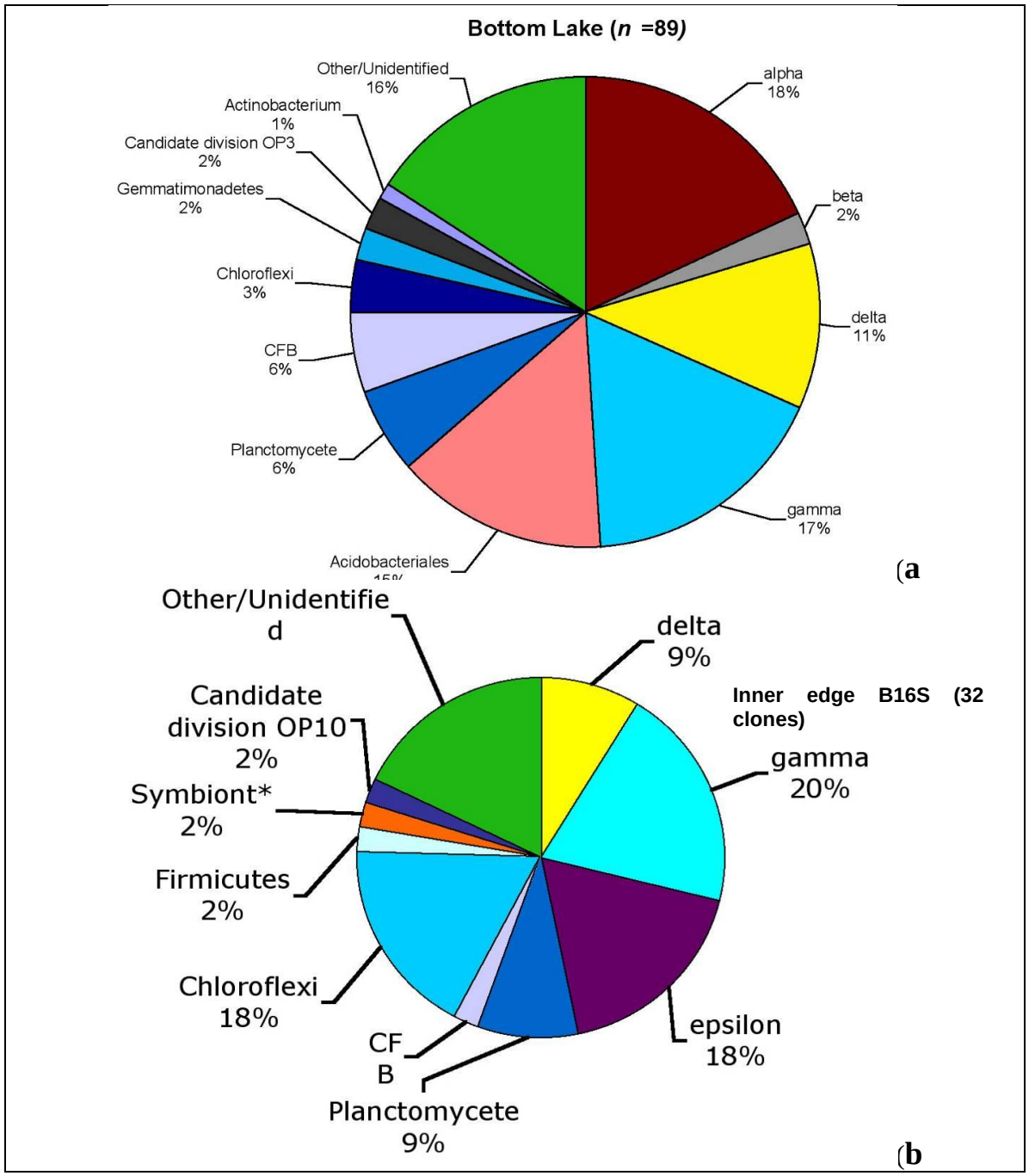

Figure 11-21. Diversity of eubacteria in sediments collected from the (a) bottom, (b) inner edge, at AC601 Brine Lake.

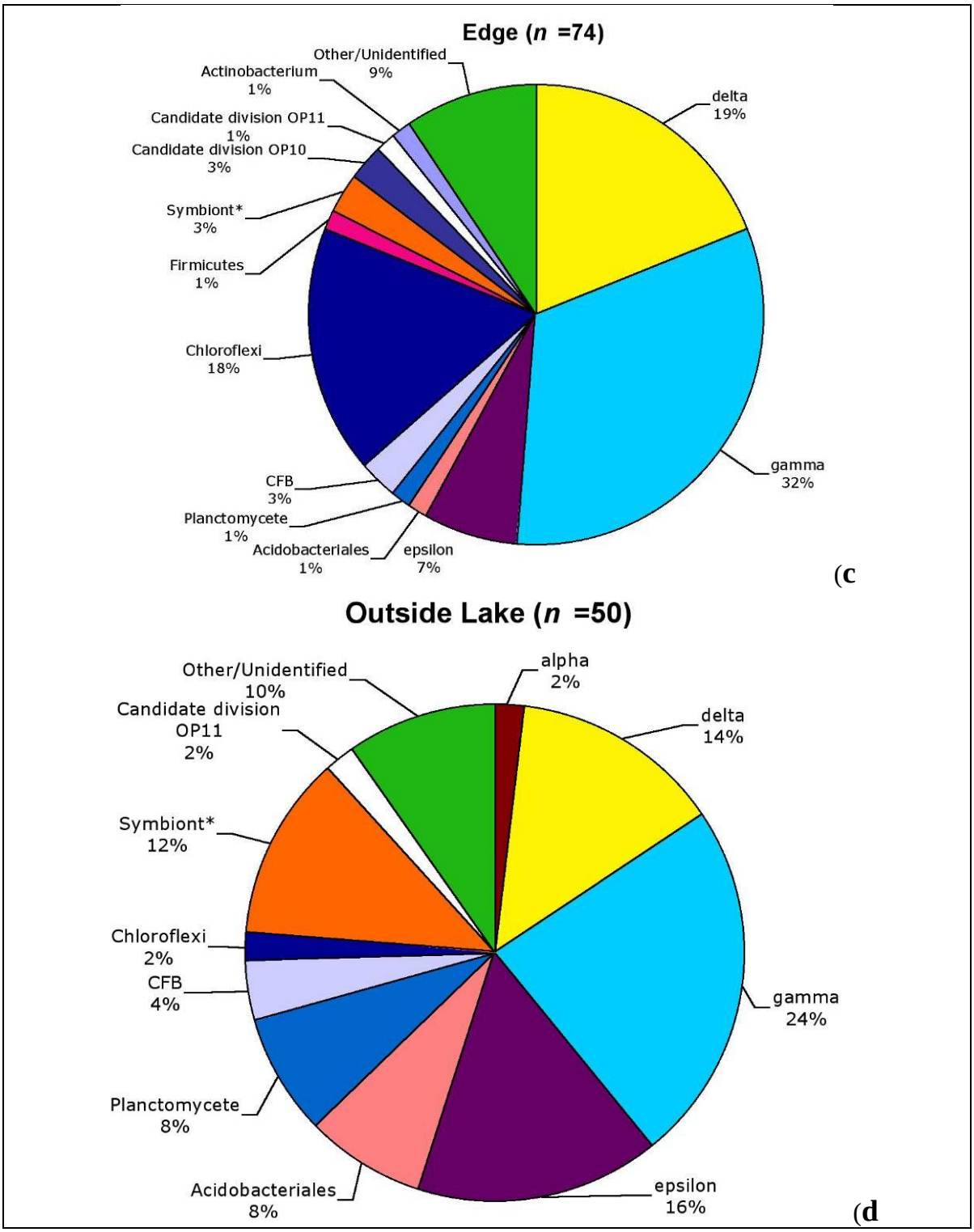

Figure 11-22. Diversity of eubacteria in sediments collected from the (c) outer edge and (d) off site control (d) at AC601 Brine Lake.

12. IDENTIFICATION AND DISTRIBUTION OF VESTIMENTIFERAN TUBE WORMS

12.1. Introduction

During our dives on the lower slope, we encountered three morphospecies of vestimentiferan tube worms, two of which appeared to be undescribed. As a result, six morphospecies of vestimentiferan tube worms have been reported for the GoM (Fisher et al., 2007; Roberts et al., 2007; Cordes et al., 2009). Two of described species, *Lamellibrachia luymesi* (Vander Land and Narrevang, 1975) and *Seepiophila jonesi* (Gardiner et al., 2001), are relatively well studied, and their ecology and physiology are well understood (Bergquist et al., 2002; Cordes et al., 2007a; Cordes et al., 2007b). These species occur on the upper Louisiana slope between about 500 and 950 m and occasionally co-occur with a rare undescribed species, escarpiid sp. nov.. One species from the lower slope, *Escarpia laminata*, has been described, while the other two morphospecies of *Lamellibrachia* spp. appeared undescribed. Surprisingly, one of the *Lamellibrachia* sp (Sp 1) cannot be distinguished from *Lamellibrachia luymesi* by conventional genetic markers.

As a result, we are working on constructing a multigene phylogeny based on the large ribosomal subunit rDNA gene (16S), mitochondrial Cytochrome Oxidase 1 (COI) mitochondrial Cytochrome B (CytB), and nuclear protein genes Elongation Factor 1 alpha and Globin A1 Intron 1 from the six morphospecies that occur in the GoM. This work tests whether any of these genes can be used as "barcodes" that are able to identify these species based on a unique genetic signature. In this report, phylogenetic trees based on 16S and COI genes are used to examine the distribution of vestimentiferans in the GoM and their relations to other vestimentiferans from around the world. We also compare between and within species 16S and COI genetic distances and suggest that these two mitochondrial genes have little utility as "barcoding molecules" for seep vestimentiferans in general.

12.2. Material and Methods

12.2.1. Collection of Material

Vestimentiferans were collected in the deep GoM from 12 sites, during two cruises in 2006 and 2007, using the DSV *Alvin* and R/V *Atlantis* in 2006 and the ROV *Jason II* and the NOAA R/V *Ronald Brown* in 2007 (Figure 12-1). Vestimentiferans were collected either using the Bushmaster Jr. collection device (for samples destined also for community ecology analyses, see Cordes et al., this volume), or using the submersible manipulators and placed directly into a collection box. Aboard the ship, all vestimentiferans were identified using morphological criteria and subsamples of vestimentum tissue were frozen for subsequent analyses at The Pennsylvania State University. Additional frozen vestimentiferan tissue samples collected previously from shallower sites on the upper Louisiana slope using the DSV *Johnson Sea Link* were also analyzed for this study (See Table 12-1 for a complete list of specimens).

12.2.2. DNA Sequencing

DNA was extracted by either boiling a small amount of frozen tissue in 600 µL of 10% Chelex solution (Bio-Rad) or using a CTAB+PVP method modified from (Doyle and Doyle, 1987) followed by a standard ethanol precipitation.

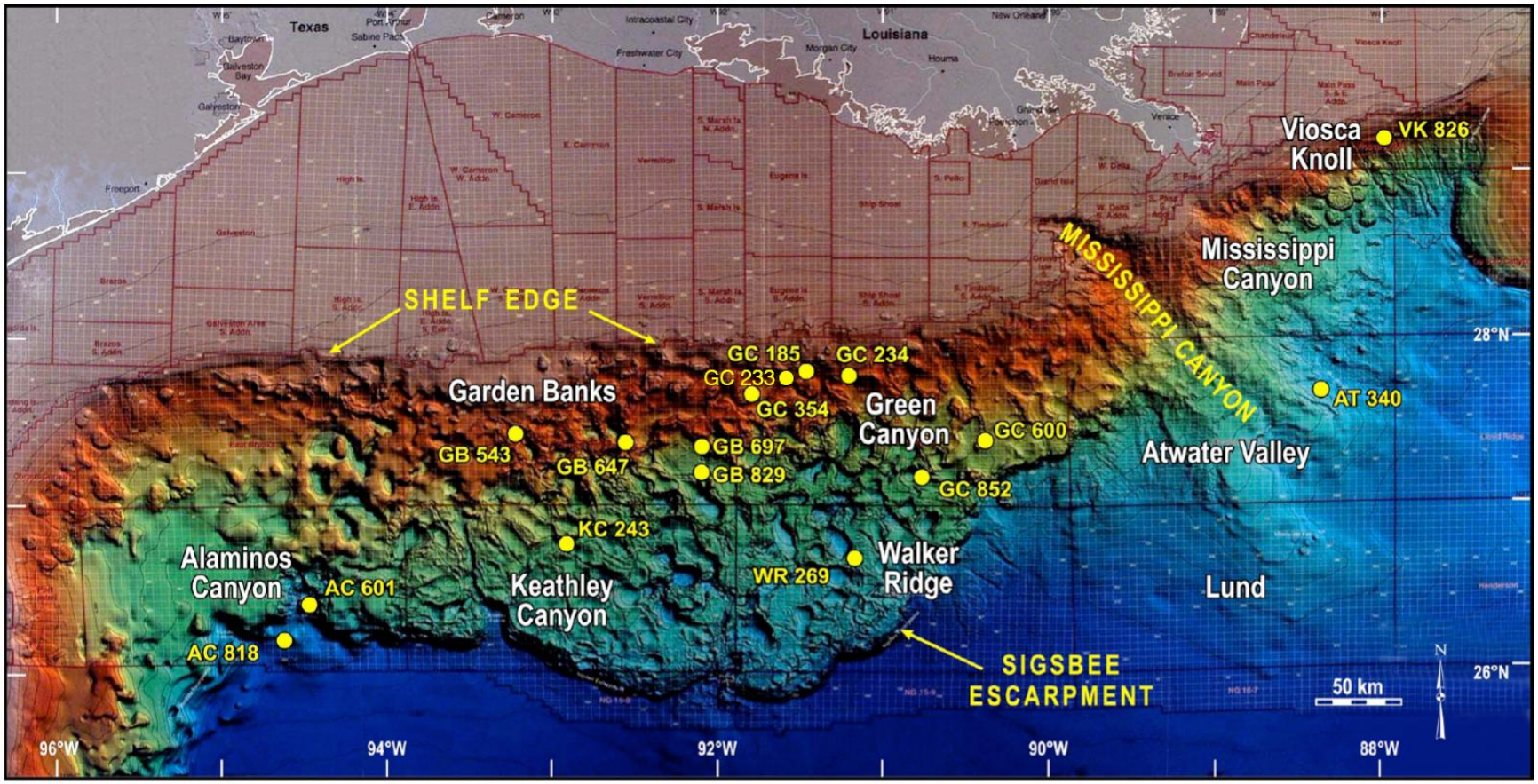

Figure 12-1. Map of new deepwater collection sites in the GoM.

A 524 base pair (bp) fragment of the mitochondrial 16S gene was amplified using primers 16Sar and 16Sbr (Kojima et al., 1995). A 689 bp fragment of the mitochondrial gene COI was amplified using the primers HCO and LCO (Folmer et al., 1994). Amplification was performed under the following polymerase chain reaction (PCR) conditions: 94ºC (1 min); 50ºC (2 min); 72ºC (2.5 min) for 30 cycles. All PCR reactions were performed using 0.5 µl of each primer, 2.5 µl of 10XBuffer, 2.0 µl of 10µM dNTPs, 2µl of taq, 16.5 µl of water and 3 µl of template. The PCR product was first purified with the ExoSap-it protocol (USB, Affimetrix) and then run on a 2% agarose gel stained with ethidium bromide to check the quantity and quality of the product. The purified PCR product was used as a template for double stranded sequencing that was carried out at The Pennsylvania State University Sequencing Core Facility, University Park, Pennsylvania.

The fragment of the mitochondrial gene CytB gene has been successfully amplified using published primers (Bleidorn et al., 2006) and similar PCR conditions as with the 16S and COI genes. Direct sequencing is performed from ExoSap-it purified PCR products.

The Globin AI Intron 1 (800pb) is being amplified using primers LamA1I1R and LamA1I1F newly designed by S. Hourdez. These primers are specific for species of the genus *Lamellibrachia* only. PCR conditions were: 94ºC (1 min); 51ºC (2 min); 72ºC (2.0 min) for 30 cycles. Due to the presence of accessory bands, the PCR product is cloned in a pGEM-T vector by using the pGEM-T cloning kit. Ten clones per individual are amplified using the same specific primers. PCR product is then selected depending on length, purified with the ExoSap Protocol and used for double stranded sequencing at The Pennsylvania State University Sequencing Core Facility.

Elongation Factor 1 alpha is amplified using universal primers (Roderick and Palumbi, in Palumbi 1992). The Globin A1 Intron 1 gene requires that the PCR product be cloned in a pGEM-T vector because of the presence of several accessory bands. At least ten clones per individual are amplified with the same specific primers. PCR products are then selected depending on length, purified with the ExoSap Protocol and used for double stranded sequencing at the at The Pennsylvania State University Sequencing Core Facility.

12.2.3. Phylogenetic Analyses

For each gene, sequences were first assembled and edited using Geneious Pro 4.0.4 (Biomatters Ltd.), and then aligned using ClustalX (Thompson et al., 2002). All alignments were confirmed and edited by eye in MacClade 4.06 OS X (Maddison and Maddison, 2000) to insure that indel variation was aligned consistently among all sequenced genes.

Phylogenetic analyses of the aligned sequences were conducted using the Maximum Parsimony (MP) optimality criterion and Neighbour Joining (NJ) (Saitou and Nei, 1987) (NJ) in PAUP* version 4.0b10 for Macintosh (Wilgenbusch and Swofford, 2003), and the Maximum Likelihood (ML) optimality criterion in GARLI v0.951.OsX-GUI (Zwickl, 2006) and PhylML (Guindon and Gascuel, 2003). The best-fit model used in PhyML and PAUP* was assessed using the Akaike Information Criterion as implemented in Modeltest (Posada, 2003; Posada and Crandall, 1998). The best-fit model was (HKY+I+G) for the COI dataset and (GTR+G) for the 16S dataset. Clade

stability was assessed by ML bootstrap analysis (Felsenstein, 1985) in GARLI (100 bootstrap replicates) and NJ (1000 replicates) in PAUP*. The ML analyses in GARLI were performed using random starting trees and default termination conditions. Within and between species distances were estimated in MEGA 4 (Tamura et al., 2007).

12.3. Results and Discussion

12.3.1. Phylogenetic Trees and Morphospecies

The complete COI dataset includes 146 sequences (Table 12-1) of the six GoM cold seep morphospecies, the available GenBank sequences of *E. southwardae, E. spicata,* and *Lamellibrachia* species collected from around the world. Sequences from the hydrothermal-vent dwelling genera, *Riftia*, *Oasisia*, *Tevnia*, and *Arcovestia* were used as outgroups. The complete and aligned COI dataset included 690 bp, 460 of which were invariant sites, 207 were phylogenetically-informative sites, and 23 sites had unique variants to a particular vestimentiferan lineage (autapomorphies). The complete 16S dataset consisted of 133 sequences (see Table 12-1 for the complete list of samples), 127 of which from the GoM. Sequences from the vent dwelling genera, *Tevnia* and *Ridgeia*, were used as outgroups. The aligned 16S ribosomal ribonucleic acid dataset consisted of 524 bp, of which 433 were invariant sites, 72 were phylogenetically-informative, and 19 were autapomorphies. We restricted our analyses to the species' boundaries for *Lamellibrachia*, *Escarpia* and *Seephiophila* and do not infer higher level phylogenetic relationships among genera because neither the 16S or COI genes offer sufficient resolution at deeper nodes.

The Globin Gene dataset consists of 40 sequences from all of the GoM *Lamellibrachia* species. The CytB data set include 30 sequences of GoM *Lamellibrachia* and *Escarpia*. The phylogenetic analysis of these two datasets should be considered preliminary because data collection is still underway.

MP, ML, and NJ analyses produced congruent trees and the GARLI ML 16S and COI phylogenyes are presented in Figures 12-2 A-B and Figures 12-4A-B. Maximum Parsimony phylogeny based on the Globin A1 Intron 1 sequences is presented in Figure 12-3 and the Cytochrome B neighbor-Joining tree is shown in Figure 12-5.

Both 16S and COI phylogenies identify five distinct monophyletic clades of vestimentiferans in the GoM. Four of the clades represent single morphospecies, *Seepiophila jonesi*, *Escarpia laminata*, *Lamellibrachia* sp. 2, and escarpiid sp. nov. from the upper slope. However, the fifth clade includes both *Lamellibrachia* sp.1 from the collections in the deeper GoM and *L. luymesi* from the upper Louisiana slope sites. They were, therefore, considered a single species when within- and between- species distances for the 16S and COI datasets were estimated. Additionally, COI sequences of *Escarpia laminata* did not differ from those of *E. spicata* and *E. southwardae* from the East Atlantic and East Pacific, respectively. We were unable to obtain 16S sequences for *E. spicata* or *E. southwardae*.

Table 12-1

Genbank Accension Numbers and Genes Analyzed

Sample*	Clade	Location**	GenBank Accession #	Genes
1.AC818	*Escarpia laminata*	GoM AC818	16S: GU068165COI: GU059163	16S/COI
2.AC818	*Escarpia laminata*	GoM AC818	COI: GU059196	COI
3.AC818	*Escarpia laminata*	GoM AC818	16S: GU068166COI: GU059205	16S/COI
4.AC818	*Escarpia laminata*	GoM AC818	16S: GU068167COI: GU059214	16S/COI
5.AC818	*Escarpia laminata*	GoM AC818	16S: GU068168COI: GU059222	16S/COI
6.AC818	*Escarpia laminata*	GoM AC818	16S: GU068169COI: GU059228	16S/COI
7.AC818	*Escarpia laminata*	GoM AC818	16S: GU068170COI: GU059234	16S/COI
8.AC818	*Lamellibrachia luymesi*/sp. 1	GoM AC818	16S: GU068171	16S
10.GB697	*Escarpia laminata*	GoM GB697	16S: GU068172COI: GU059164	16S/COI
11.GB829	*Escarpia laminata*	GoM GB829	16S: GU068173COI: GU059170	16S/COI
12.GB829	*Escarpia laminata*	GoM GB829	16S: GU068174COI: GU059174	16S/COI
13.GC600	*Escarpia laminata*	GoM GC600	16S: GU068175	16S
14.GC852	*Escarpia laminata*	GoM GC852	16S: GU068176COI: GU059185	16S/COI
17.GC852	*Escarpia laminata*	GoM GC852	16S: GU068177COI: GU059192	16S/COI
18.GC852	*Escarpia laminata*	GoM GC852	COI: GU059193	COI
19.GC852	*Escarpia laminata*	GoM GC852	16S: GU068178COI: GU059194	16S/COI
19B.AC818	*Escarpia laminata*	GoM AC 818	COI: GU059195	COI
20.WR269	*Escarpia laminata*	GoM WR269	16S: GU068179COI: GU059197	16S/COI
21.WR269	*Escarpia laminata*	GoM WR269	16S: GU068180COI: GU059198	16S/COI
22.WR269	*Escarpia laminata*	GoM WR269	16S: GU068181COI: GU059199	16S/COI
23.WR269	*Escarpia laminata*	GoM WR269	COI: GU059200	COI
24.WR269	*Escarpia laminata*	GoM WR269	COI: GU059201	COI
26.AT340	*Escarpia laminata*	GoM AT340	16S: GU068182	16S
27.AT340	*Escarpia laminata*	GoM AT340	16S: GU068183COI: GU059202	16S/COI
28.AT340	*Escarpia laminata*	GoM AT340	16S: GU068184COI: GU059203	16S/COI
29.AT340	*Escarpia laminata*	GoM AT340	16S: GU068185COI: GU059204	16S/COI
30.AT340	*Escarpia laminata*	GoM AT340	16S: GU068186COI: GU059206	16S/COI
31.AT340	*Escarpia laminata*	GoM AT340	16S: GU068187 COI: GU059207	16S/COI

Table 12-1. Genbank Accension Numbers and Genes Analyzed (continued)

32.AT340	*Escarpia laminata*	GoM AT340	16S: GU068188COI: GU059208	16S/COI
33.AT340	*Escarpia laminata*	GoM AT340	16S: GU068189COI: GU059209	16S/COI
34.WR264	*Escarpia laminata*	GoM WR269	16S: GU068190	16S
35.WR269	*Escarpia laminata*	GoM WR269	16S: GU068191COI: GU059210	16S/COI
37.AC601	*Escarpia laminata*	GoM AC601	16S: GU068192COI: GU059211	16S/COI
38.AC601	*Escarpia laminata*	GoM AC601	16S: GU068193COI: GU059212	16S/COI
39.AC601	*Escarpia laminata*	GoM AC601	16S: GU068194COI: GU059213	16S/COI
40.AC601	*Escarpia laminata*	GoM AC601	16S: GU068195COI: GU059215	16S/COI
41.AC601	*Escarpia laminata*	GoM AC601	16S: GU068196	16S
42.AC601	*Escarpia laminata*	GoM AC602	16S: GU068197COI: GU059216	16S/COI
43.AC601	*Escarpia laminata*	GoM AC601	16S: GU068198COI: GU059217	16S/COI
44.AC601	*Escarpia laminata*	GoM AC602	16S: GU068199COI: GU059218	16S/COI
45.AC601	*Escarpia laminata*	GoM AC601	16S: GU068200COI: GU059219	16S/COI
46.AT340	*Escarpia laminata*	GoM AT340	16S: GU068201	16S
47.AC601	*Escarpia laminata*	GoM AC601	16S: GU068202COI: GU059220	16S/COI
48.AC601	*Escarpia laminata*	GoM AC601	16S: GU068203	16S
49.AC601	*Escarpia laminata*	GoM AC601	16S: GU068204COI: GU059221	16S/COI
50.AC601	*Escarpia laminata*	GoM AC601	16S: GU068205COI: GU059223	16S/COI
51.AT340	*Escarpia laminata*	GoM AT340	16S: GU068206	16S
52.AT340	*Escarpia laminata*	GoM AT340	16S: GU068207	16S
54.AC601	*Escarpia laminata*	GoM AC601	16S: GU068208COI: GU059224	16S/COI
55.L. luymesi BH	*Lamellibrachia luymesi*/sp. 1	GoM GC185	16S: GU068209COI: GU059225	16S/COI
56.L. sp.1 GB697	*Lamellibrachia luymesi*/sp. 1	GoM GB697	16S: GU068210	16S
57.L. luymesi GC234	*Lamellibrachia luymesi*/sp. 1	GoM GC234	16S: GU068211COI: GU059226	16S/COI
58.L. sp.1 GC852	*Lamellibrachia luymesi*/sp. 1	GoM GC852	16S: GU068212COI: GU059227	16S/COI
59.L. sp.1 AC601	*Lamellibrachia luymesi*/sp. 1	GoM AC601	16S: GU068213	16S
60.L. luymesi BH	*Lamellibrachia luymesi*/sp. 1	GoM GC185	16S: GU068214	16S
61.L. luymesi BH	*Lamellibrachia luymesi*/sp. 1	GoM GC185	16S: GU068215	16S
62.L. luymesi BH	*Lamellibrachia luymesi*/sp. 1	GoM GC185	16S: GU068216COI: GU059229	16S/COI

Table 12-1. Genbank Accension Numbers and Genes Analyzed (continued)

63.L. luymesi BH	*Lamellibrachia luymesi*/sp. 1	GoM GC185	16S: GU068217	16S
64.L. luymesi BH	*Lamellibrachia luymesi*/sp. 1	GoM GC185	16S: GU068218COI: GU059230	16S/COI
65.L. luymesi BH	*Lamellibrachia luymesi*/sp. 1	GoM GC185	16S: GU068219	16S
66.L. luymesi BH	*Lamellibrachia luymesi*/sp. 1	GoM GC185	16S: GU068220COI: GU059231	16S/COI
67.L. luymesi BH	*Lamellibrachia luymesi*/sp. 1	GoM GC185	16S: GU068221	16S
68.L. luymesi BH	*Lamellibrachia luymesi*/sp. 1	GoM GC185	16S: GU068222COI: GU059232	16S/COI
69.L. luymesi BH	*Lamellibrachia luymesi*/sp. 1	GoM GC185	16S: GU068223COI: GU059233	16S/COI
70.L. luymesi BH	*Lamellibrachia luymesi*/sp. 1	GoM GC185	16S: GU068224COI: GU059235	16S/COI
71.L. luymesi BH	*Lamellibrachia luymesi*/sp. 1	GoM GC185	16S: GU068225	16S
72.L. luymesi BP	*Lamellibrachia luymesi*/sp. 1	GoM GC233	16S: GU068226COI: GU059236	16S/COI
73.L. sp.1 GB697	*Lamellibrachia luymesi*/sp. 1	GoM GB697	16S: GU068227COI: GU059237	16S/COI
74.L. sp.1 GB697	*Lamellibrachia luymesi*/sp. 1	GoM GB697	16S: GU068228	16S
75.L. sp.1 GB697	*Lamellibrachia luymesi*/sp. 1	GoM GB697	16S: GU068229	16S
76.L. sp.1 GB829	*Lamellibrachia luymesi*/sp. 1	GoM GB829	16S: GU068230COI: GU059238	16S/COI
77.L. sp.1 GB829	*Lamellibrachia luymesi*/sp. 1	GoM GB829	16S: GU068231	16S
78.L. sp.1 GB829	*Lamellibrachia luymesi*/sp. 1	GoM GB829	16S: GU068232COI: GU059239	16S
79.L. sp.1 GB829	*Lamellibrachia luymesi*/sp. 1	GoM GB829	16S: GU068233	16S
80.L. sp.1 GB829	*Lamellibrachia luymesi*/sp. 1	GoM GB829	16S: GU068234	16S
81.L. luymesi GC234	*Lamellibrachia luymesi*/sp. 1	GoM GC234	16S: GU068235	16S
83.L. luymesi GC234	*Lamellibrachia luymesi*/sp. 1	GoM GC234	16S: GU068236COI: GU059240	16S/COI
84.L. luymesi GC234	*Lamellibrachia luymesi*/sp. 1	GoM GC234	16S: GU068237	16S
85.L. luymesi GC234	*Lamellibrachia luymesi*/sp. 1	GoM GC234	16S: GU068238	16S
86.L. luymesi GC234	*Lamellibrachia luymesi*/sp. 1	GoM GC234	16S: GU068239COI: GU059241	16S/COI
88.L. sp.1 GC600	*Lamellibrachia luymesi*/sp. 1	GoM GC600	16S: GU068240COI: GU059242	16S/COI
89.L. sp.1 GC600	*Lamellibrachia luymesi*/sp. 1	GoM GC600	16S: GU068241COI: GU059243	16S/COI

Table 12-1. Genbank Accension Numbers and Genes Analyzed (continued)

90.L. sp.1 GC852	*Lamellibrachia luymesi*/sp. 1	GoM GC852	16S: GU068242COI: GU059244	16S/COI
91.L. sp.1 GC852	*Lamellibrachia luymesi*/sp. 1	GoM GC852	16S: GU068243	16S
92.L. sp.1 GC852	*Lamellibrachia luymesi*/sp. 1	GoM GC852	16S: GU068244COI: GU059245	16S
93.L. luymesi BH	*Lamellibrachia luymesi*/sp. 1	GoM GC185	16S: GU068245COI: GU059246	16S/COI
94.L. luymesi BH	*Lamellibrachia luymesi*/sp. 1	GoM GC185	16S: GU068246	16S
95.L. luymesi BH	*Lamellibrachia luymesi*/sp. 1	GoM GC185	16S: GU068247	16S
96.L. luymesi BH	*Lamellibrachia luymesi*/sp. 1	GoM GC185	16S: GU068248	16S
97.L. luymesi GC234	*Lamellibrachia luymesi*/sp. 1	GoM GC234	16S: GU068249	16S
98.L. luymesi GC234	*Lamellibrachia luymesi*/sp. 1	GoM GC234	16S: GU068250	16S
99.L. luymesi GC234	*Lamellibrachia luymesi*/sp. 1	GoM GC234	16S: GU068251COI: GU059247	16S/COI
100.L.sp.1. WR269	*Lamellibrachia luymesi*/sp. 1	GoM WR269	16S: GU068252	16S
102.L.sp. 1 WR269	*Lamellibrachia luymesi*/sp. 1	GoM WR269	16S: GU068253COI: GU059165	16S/COI
103.L. sp.1 AT340	*Lamellibrachia luymesi*/sp. 1	GoM AT340	16S: GU068254COI: GU059166	16S/COI
104.L. sp.1 WR269	*Lamellibrachia luymesi*/sp. 1	GoM WR269	16S: GU068255COI: GU059167	16S/COI
105.L. sp.1 WR269	*Lamellibrachia luymesi*/sp. 1	GoM WR269	16S: GU068256COI: GU059168	16S/COI
107.L. sp.1 AC601	*Lamellibrachia luymesi*/sp. 1	GoM AC601	16S: GU068257COI: GU059169	16S/COI
110.L. sp.1 AC601	*Lamellibrachia luymesi*/sp. 1	GoM AC601	16S: GU068258COI: GU059171	16S/COI
112.GB697	*Lamellibrachia* sp. 2	GoM GB697	16S: GU068259	16S
113.GB697	*Lamellibrachia* sp. 2	GoM GB697	16S: GU068260COI: GU059172	16S/COI
114.GB697	*Lamellibrachia* sp. 2	GoM GB297	16S: GU068261	16S
115.GB697	*Lamellibrachia* sp. 2	GoM GB297	16S: GU068262	16S
116.GB829	*Lamellibrachia* sp. 2	GoM GB829	16S: GU068263	16S
117.GC600	*Lamellibrachia* sp. 2	GoM GC600	16S: GU068264	16S
118.GC852	*Lamellibrachia* sp. 2	GoM GC852	16S: GU068265COI: GU059173	16S/COI
119.GC852	*Lamellibrachia* sp. 2	GoM GC852	16S: GU068266	16S
120.GC852	*Lamellibrachia* sp. 2	GoM GC852	16S: GU068267	16S
121.WR269	*Lamellibrachia* sp. 2	GoM WR269	16S: GU068268	16S
122.AT340	*Lamellibrachia* sp. 2	GoM AT340	16S: GU068269COI: GU059175	16S/COI
123.WR2695	*Lamellibrachia* sp. 2	GoM WR269	16S: GU068270COI: GU059176	16S/COI
124.AC601	*Lamellibrachia* sp. 2	GoM AC601	COI: GU059177	COI

Table 12-1. Genbank Accension Numbers and Genes Analyzed (continued)

126.AC601	*Lamellibrachia* sp. 2	GoM AC601	COI: GU059178	COI
128.L. sp.1 AT340	*Lamellibrachia luymesi*/sp. 1	GoM AT340	16S: GU068271COI: GU059179	16S/COI
130.GB697	*Seepiophila jonesi*	GoM GB697	16S: GU068272COI: GU059180	16S/COI
131.GB647	*Seepiophila jonesi*	GoM GB647	16S: GU068273COI: GU05981	16S/COI
132.GC234	*Seepiophila jonesi*	GoM GC234	16S: GU068274COI: GU059182	16S/COI
133.GC234	*Seepiophila jonesi*	GoM GC234	16S: GU068275	16S
134.GC234	*Seepiophila jonesi*	GoM GC234	16S: GU068276COI: GU059183	16S/COI
134b.GC234	*Seepiophila jonesi*	GoM GC234	16S: GU068277COI: GU059184	16S/COI
135.GC234	*Seepiophila jonesi*	GoM GC234	16S: GU068278	16S
136.GC234	*Seepiophila jonesi*	GoM GC234	16S: GU068279	16S
137.BH	*Seepiophila jonesi*	GoM GC185	16S: GU068280	16S
138.BH	*Seepiophila jonesi*	GoM GC185	16S: GU068281	16S
139.GC234	*Seepiophila jonesi*	GoM GC234	16S: GU068282	16S
140. GC234	*Seepiophila jonesi*	GoM GC234	16S: GU068283	16S
141.GB647	*Seepiophila jonesi*	GoM GB647	16S: GU068284COI: GU059186	16S/COI
142.GB647	*Seepiophila jonesi*	GoM GB647	16S: GU068285	16S
143.GB647	*Seepiophila jonesi*	GoM GB647	16S: GU068286COI: GU059187	16S/COI
144.GB647	*Seepiophila jonesi*	GoM GB647	16S: GU068287COI: GU059188	16S/COI
145.AC818	*Escarpia laminata*	GoM AC818	16S: GU068288COI: GU059189	16S/COI
146.BH	*Seepiophila jonesi*	GoM GC185	16S: GU068289	16S
147.GB647	*Seepiophila jonesi*	GoM GB647	COI: GU059190	COI
148.GB647	*Seepiophila jonesi*	GoM GB647	COI: GU059191	COI
149.AC601	*Escarpia laminata*	GoM AC601	COI: GU059248	COI
151.GB697	*Lamellibrachia luymesi*	GoM GB697	COI: GU059250	COI
152.GC234	*Lamellibrachia luymesi*/sp.1	GoM GC234	COI: GU059253	COI
153.GC600	*Lamellibrachia luymesi*/sp.1	GoM GC600	COI: GU059254	COI
154.NewEscarpidGB485	Escarpiid sp. nov.	GoM GB425	16S: GU068290COI: GU059255	16S/COI
155.NewEscarpidGC234	Escarpiid sp. nov.	GoM GC234	16S: GU068291COI: GU059256	16S/COI
157.L. sp.1 GB697	*Lamellibrachia luymesi*/sp.1	GoM GB697	COI: GU059229	COI
159.GB697	*Seepiophila jonesi*	GoM GB697	COI: GU059251	COI
160.GB697	*Seepiophila jonesi*	GoM GB697	COI: GU059252	COI
161.GC234	*Lamellibrachia luymesi*/sp. 1	GoM GC234		COI
162.GC600	*Lamellibrachia luymesi*/sp. 1	GoM GC600		COI
165.GC852	*Lamellibrachia* sp. 2	GoM GC852		COI
166.L.sp1 AT340	*Lamellibrachia luymesi*/sp. 1	GoM AT340		COI
S.jonesiBH	*Seepiophila jonesi*	GoM GC185	AF317287	COI

Table 12-1. Genbank accension numbers and genes analyzed (continued)

S.jonesiGB425	*Seepiophila jonesi*	GoM GB425	AF317288	COI
LamluymesiGC234	*Lamellibrachia luymesi*	GoM GC234	AY129136	COI
Basibranchia Mariana 1	*Basibranchia mariana*	West Pacific	U74078	COI
Arcovestia	*Arcovestia ivanovi*	West Pacific	AB073491	COI
E.laminata	*Escarpia laminata*	West Atlantic	U74063	COI
E.southwardae1	*Escarpia southwardae*	West Africa	AY326304	COI
E.southwardae2	*Escarpia southwardae*	West Africa	AY326303	COI
E.spicata	*Escarpia spicata*	East Pacific	U84262	COI
L. sp1_b	*Lamellibrachia luymesi*/sp. 1	GoM AT340	U74061	COI
OasisiaHaploA	*Oasisia Alvinae*	East Pacific	AY646001	COI
OasisiaHaploP	*Oasisia Alvinae*	East Pacific	AY646016	COI
Lam2000Nanaki	*Lamellibrachia* sp.	West Pacific	D50592	COI
Lam300Sagami	*Lamellibrachia* sp.	West Pacific	AB088674	COI
Lam300Sagami 1	*Lamellibrachia* sp.	West Pacific	D38029	COI
Lambarhami10b	*Lamellibrachia barhami*	East Pacific	AY129137	COI
Lambarhami11b	*Lamellibrachia barhami*	East Pacific	AY129138	COI
Lambarhami4b	*Lamellibrachia barhami*	East Pacific	AY129147	COI
Lambarhami7	*Lamellibrachia barhami*	East Pacific	AY129146	COI
Lambarhami8b	*Lamellibrachia barhami*	East Pacific	AY129145	COI
Lambarhami9	*Lamellibrachia barhami*	East Pacific	AY129141	COI
Lambarhamib L. barhami2 L. barhami3	*Lamellibrachia barhami* *Lamellibrachia barhami* *Lamellibrachia barhami*	East Pacific East Pacific East Pacific	U74054AF315045AF315045	COI16S16S
Lamcolumna	*Lamellibrachia columna*	West Pacific	U74061	COI
Lamcolumna 1	*Lamellibrachia columna*	West Pacific	AB055210	COI
Lamjuni	*Lamellibrachia juni*	West Pacific	AB242858	COI
LamjuniHaplo1	*Lamellibrachia juni*	West Pacific	AB264601	COI
LamjuniHaplo2	*Lamellibrachia juni*	West Pacific	AB264602	COI
LamjuniHaplo3	*Lamellibrachia juni*	West Pacific	AB264603	COI
LamjuniHaplo4	*Lamellibrachia juni*	West Pacific	AB264604	COI
LamjuniHaplo5	*Lamellibrachia juni*	West Pacific	AB264605	COI
LamL4	*Lamellibrachia* sp.	West Pacific	AB055209	COI

Table 12-1. Genbank Accension Numbers and Genes Analyzed (continued)

LamL5	*Lamellibrachia* sp.	West Pacific	AB055210	COI
LamL6	*Lamellibrachia* sp.	West Pacific	AB088674	COI
LamL7	*Lamellibrachia* sp.	West Pacific	AB088675	COI
LamluymesiBH 2	*Lamellibrachia luymesi*	GoM GC185	AY129133	COI
LamluymesiBHb	*Lamellibrachia luymesi*	GoM GC185	AY129132	COI
LamluymesiBP	*Lamellibrachia luymesi*	GoM GC233	AY129139	COI
LamluymesiGB4252	*Lamellibrachia luymesi*	GoM GB425	AY129135	COI
LamluymesiGC354	*Lamellibrachia luymesi*	GoM GC354	AY129126	COI
LamluymesiVK	*Lamellibrachia luymesi*	GoM VK826	AY129124	COI
LamMed	*Lamellibrachia* sp. from Med.	Mediterranean	EU046616	COI
Lamsatsumab	*Lamellibrachia satsuma*	West Pacific	AF342671	COI
NewEscarpiidGB425	Escarpiid sp. nov.	GoM GB425	AY129134	COI
Oaisisiafujikurai	*Oasisia fujikurai*	South/West Pacific	AB242857	COI
Paraescarpia	*Paraescarpia* cf. *echinospica*	West Pacific	D50594	COI
Ridgeia Ridgei Ridgeia2 Ridgeia3	*Ridgeia piscesae* *Ridgeia piscesae* *Ridgeia piscesae* *Ridgeia piscesae*	Juan de Fuca Ridge Juan de Fuca Ridge Juan de Fuca Ridge Juan de Fuca Ridge	AF022233AF31505 4AF315051AF3150 54	COI16S16S16S
Riftia	*Riftia pachyptila*	East Pacific	AY645989	COI
Tevnia jerichonana	*Tevnia jerichonana*	East Pacific	16S: AF315042COI: AY645995	16S/COI
S.jonesiBH	*Seepiophila jonesi*	GoM GC185	AF317287	COI
S.jonesiGB425	*Seepiophila jonesi*	GoM GB425	AF317288	COI

*Samples analyzed for this study are numbered and labeled as for Figures 12-2 and 12-3. Sequences from Genbank are listed by names assigned in Genbank

**Samples from the GoM are indicated by GoM followed by the abbreviation of their collection sites. VK826, GC185, GC233, GB425, GC234 and GC354 are all on the upper Louisiana Slope at depths <800 m. The other GoM sites are at depths >900 m and are indicated on Figure 12-1.

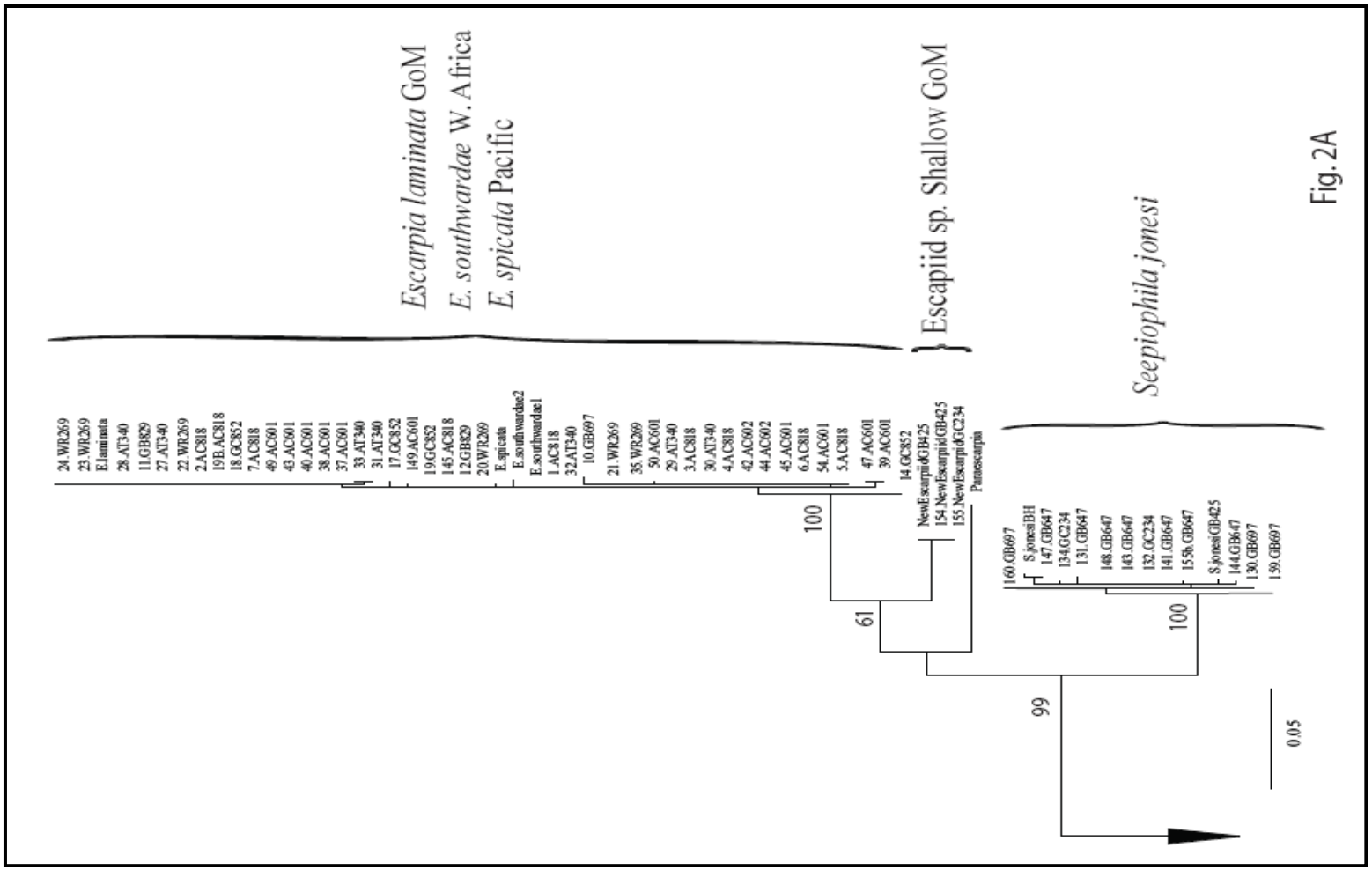

Figure 12-2A. COI Maximum Likelihood (ML) tree. Outgroups are shown in italics and bootstrap support above 50% (NJ 1000 replicates) is indicated below each node. All new sequences are preceeded by a number followed by the abbreviation for the seep site or lease block they were collected from. VK=Viosca Knoll, BH=Bush Hill, BP=Brine Pool. Those sites, together with GB425, GC234 and GC354 are from the Upper Louisiana slope of the GoM (<800 m depth). All other lease blocks are on the lower slope and their locations are indicated in Figure 12-1.

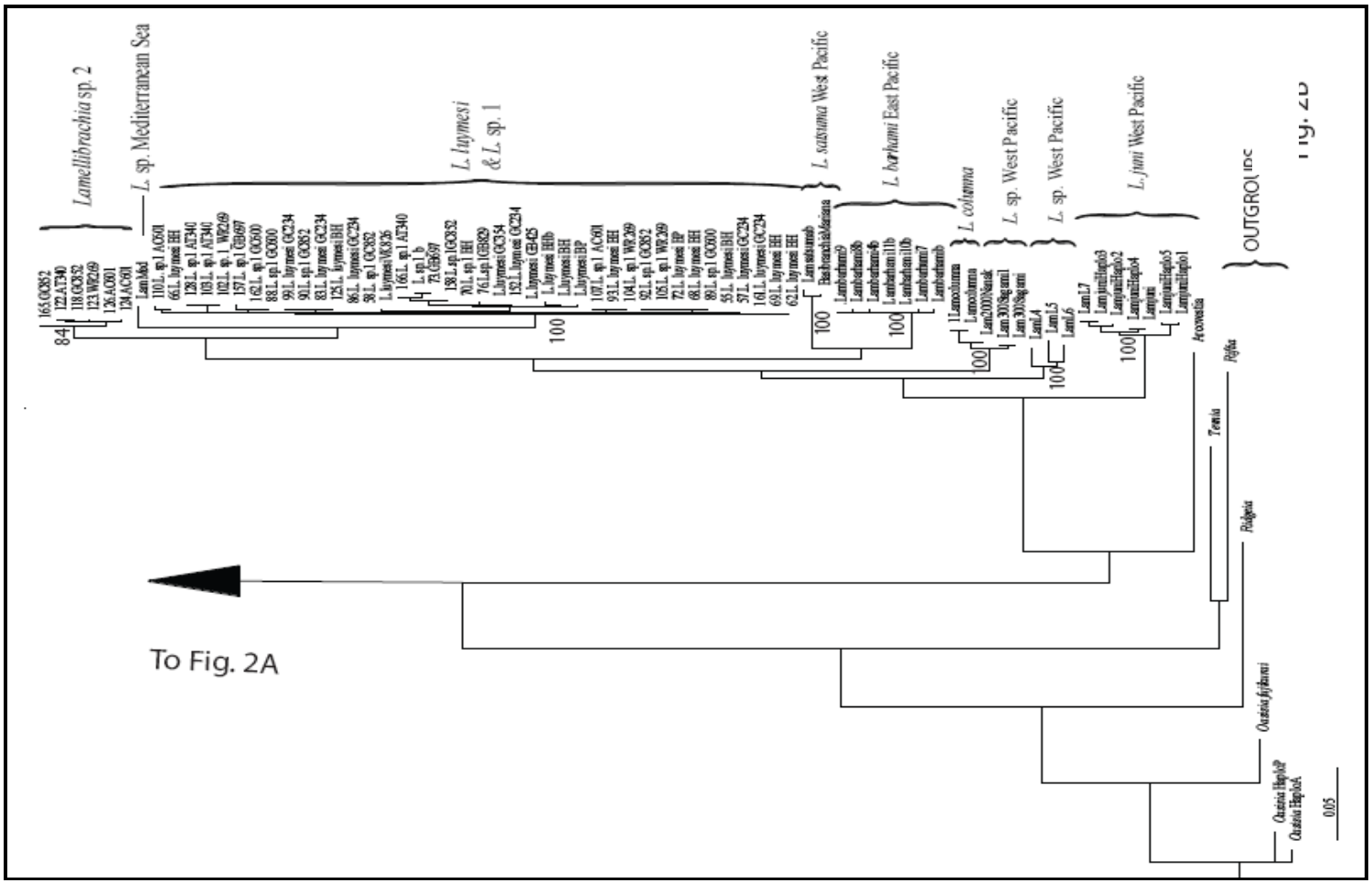

Figure 12-2B. COI Maximum Likelihood (ML) tree. Outgroups are shown in italics and bootstrap support above 50% (NJ 1000 replicates) is indicated below each node. All new sequences are preceeded by a number followed by the abbreviation for the seep site or lease block they were collected from. VK=Viosca Knoll, BH=Bush Hill, BP=Brine Pool. Those sites, together with GB425, GC234 and GC354 are from the Upper Louisiana slope of the GoM (<800 m depth). All other lease blocks are on the lower slope and their locations are indicated in Figure 12-1.

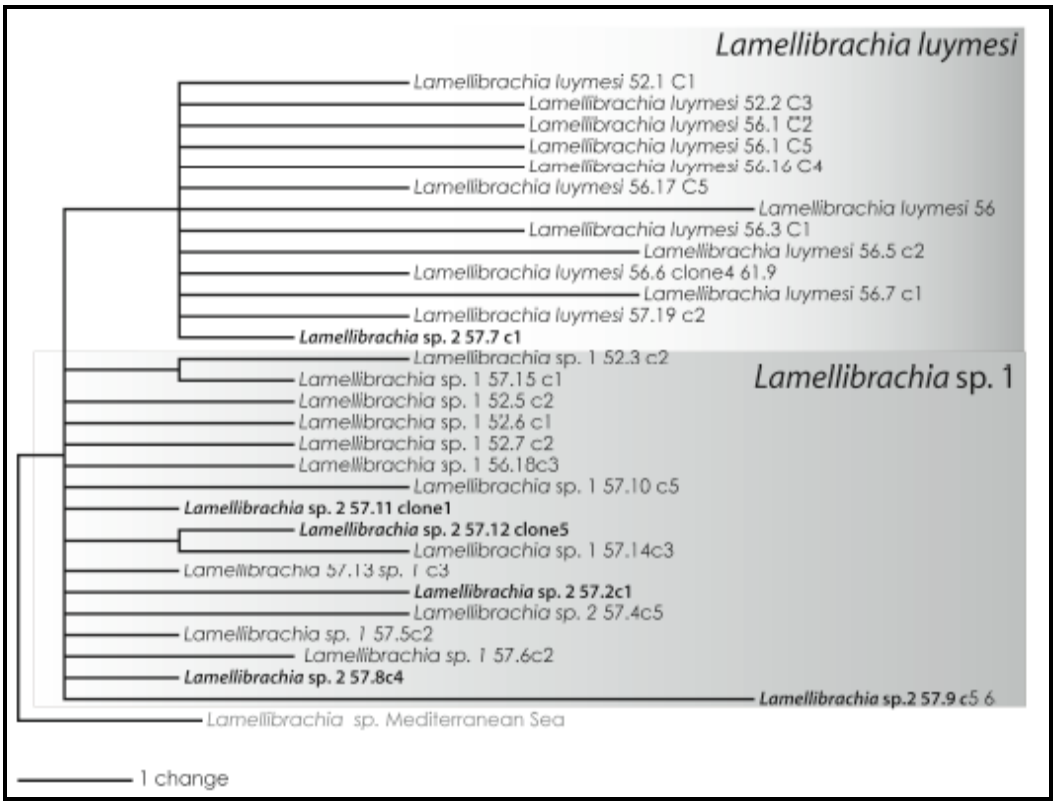

Figure 12-3. Globin 1 Intron 1 Maximim Parsimony (MP) tree.

Estimates of within and between species diversity (*p*) for both genes are shown in Tables 12-2 and 12-3. Within a species, *p* distances range from 0 to 0.1% for 16S, and 0 to 0.9% for the more variable COI. The very low values for the undescribed escarpiid may reflect the small number of individuals of this species analyzed (n=3 for COI and n=2 for 16S).

The 27 clean sequences from Globin A1 Intron 1 we have assembled to date were used to build a phylogenetic tree including individuals of all species of *Lamellibrachia* from the GoM *(L. luymesi, L.* sp.1 and *L.* sp. 2) and one sequence from an undescribed *Lamellibrachia* from the Mediterranean Sea. Figure 12-3 shows the Maximum parsimony phylogenetic tree for this data set. Although this gene seems to distinguish between *Lamellibrachia luymesi* and *L.* sp. 1, albeit by only one variable nucleotide site, sequences identified as *L.* sp. 2 fall within both clades. We are in the process of obtaining sequences from more individuals of each species to produce a more complete dataset and perform a complete set of phylogenetic analyses (MP, ML, and bootstrap analyses).

We also produced 50 CytB sequences from individuals identified as *Escarpia* and *Lamellibrachia* species in the GoM. The CytB fragment is about 310 bp long, and 27 sequences were used to build a phylogenetic tree. This tree includes individuals of all species of *Lamellibrachia* from the GoM *(L. luymesi, L.* sp.1 *and L.* sp2), as well as *Escarpia laminata* and *Seepiophila jonesi*. While we are still in the process of analyzing this dataset, these preliminary results suggest that CytB is unable to distinguish between *L. luymesi, L.* sp. 1, and *L.* sp. 2.

12.4. Distribution of Vestimentiferan Species in the Gulf of Mexico and Relation to Other Seep Species

The vent and seep species of vestimentiferans fall into two distinct clades. However, it should be noted that seep species are sometimes found in sedimented hydrothermal-vent areas with low levels of diffuse flow, and that cold-seep fluids may have temperatures elevated over background (Black et al., 1998; Kojima et al., 1997; MacDonald et al., 2000; Joye et al., 2005) so this separation may reflect more about habitat than about temperature differences, and may not necessarily indicate selection driven by underlying geology. Vestimentiferans found at cold seeps world-wide can be further divided into two clades. One clade includes at least five named and three unnamed species in the genus *Lamellibrachia*. The other clade includes three named species in the genus *Escarpia*, *Seepiophila jonesi*, *Paraescarpia echinospica*, and a rarely collected species (escarpiid sp. nov.) from the shallow GoM. Although *Arcovestia* seems basal to the *Lamellibrachia* clade (Figure 12-2B), this position is not well supported.

Table 12-2

16S Between and Within (in bold) Species p Distances for the 16S Gene of the GoM Species

	[1]	[2]	[3]	[4]	[5]
[1] *E. laminata*	**0.10%**				
[2] *L. luymesi*/ sp. 1	9.60%	**0.00%**			
[3] *L.* sp. 2	9.00%	2.20%	**0.10%**		
[4] *S. jonesi*	2.00%	8.40%	8.10%	**0.00%**	
[5] Escarpid sp. new	3.50%	8.30%	8.90%	3.70%	**0.00%**

Table 12-3

Between and Within (in bold) Species *p* Distances for the COI Gene

	[1]	[2]	[3]	[4]	[5]
[1] *E. laminata/soutwardae/spicata*	**0.9%**				
[2] *L. luymesi*/ sp. 1	13.7%	**0.4%**			
[3] *L.* sp. 2	13.8%	2.8%	**0.3%**		
[4] *S. jonesi*	9.7%	14.2%	14.4%	**0.3%**	
[5] Escarpid sp. new	7.1%	14.8%	14.6%	7.1%	**0.0%**

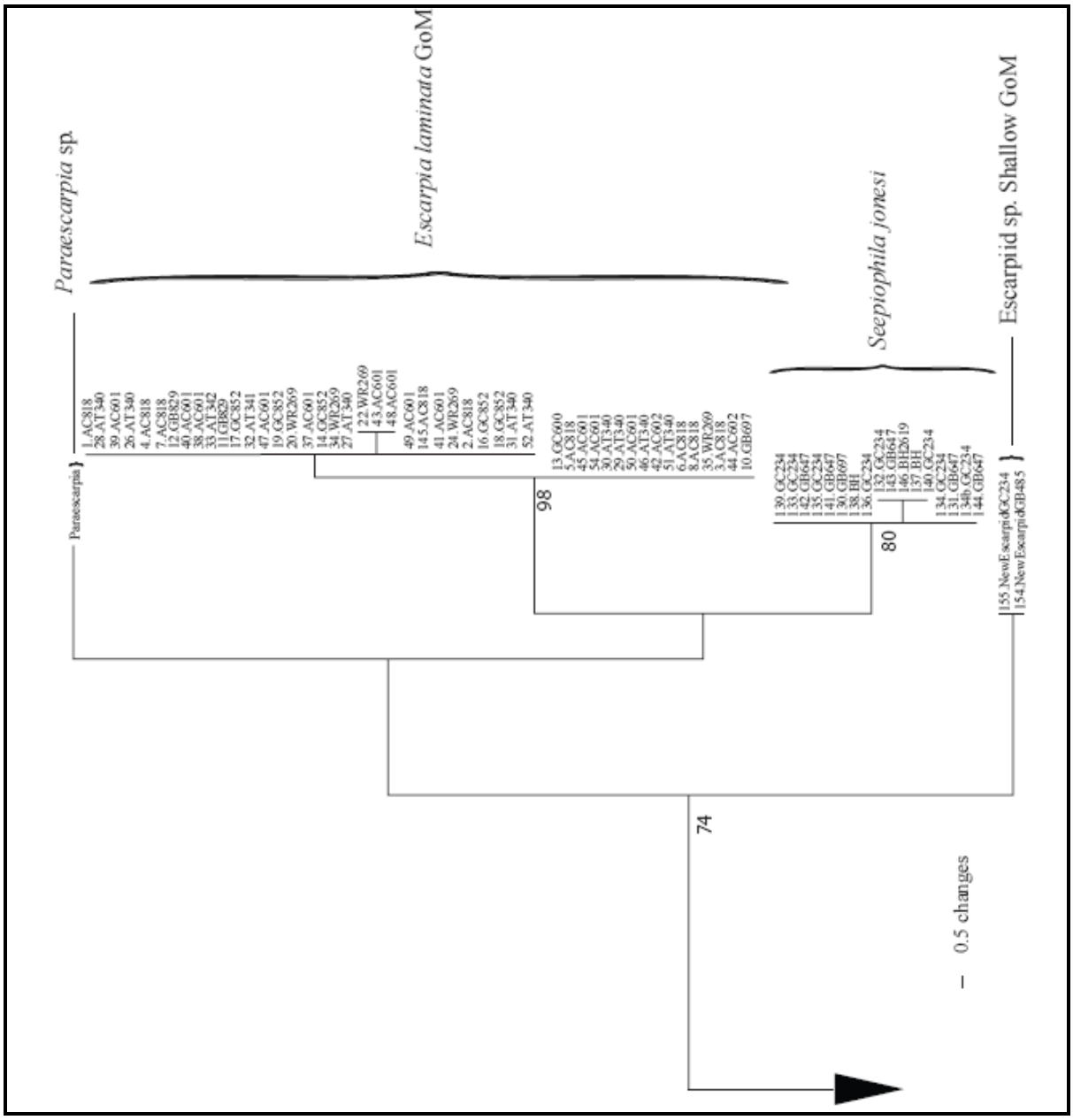

Figure 12-4A. 16S Maximum Likelihood (ML) tree. Outgroups are shown in italics and bootstrap support above 50% (NJ 1000 replicates) is indicated below each node. Sample identifications and abbreviations is as in Figure. 2.

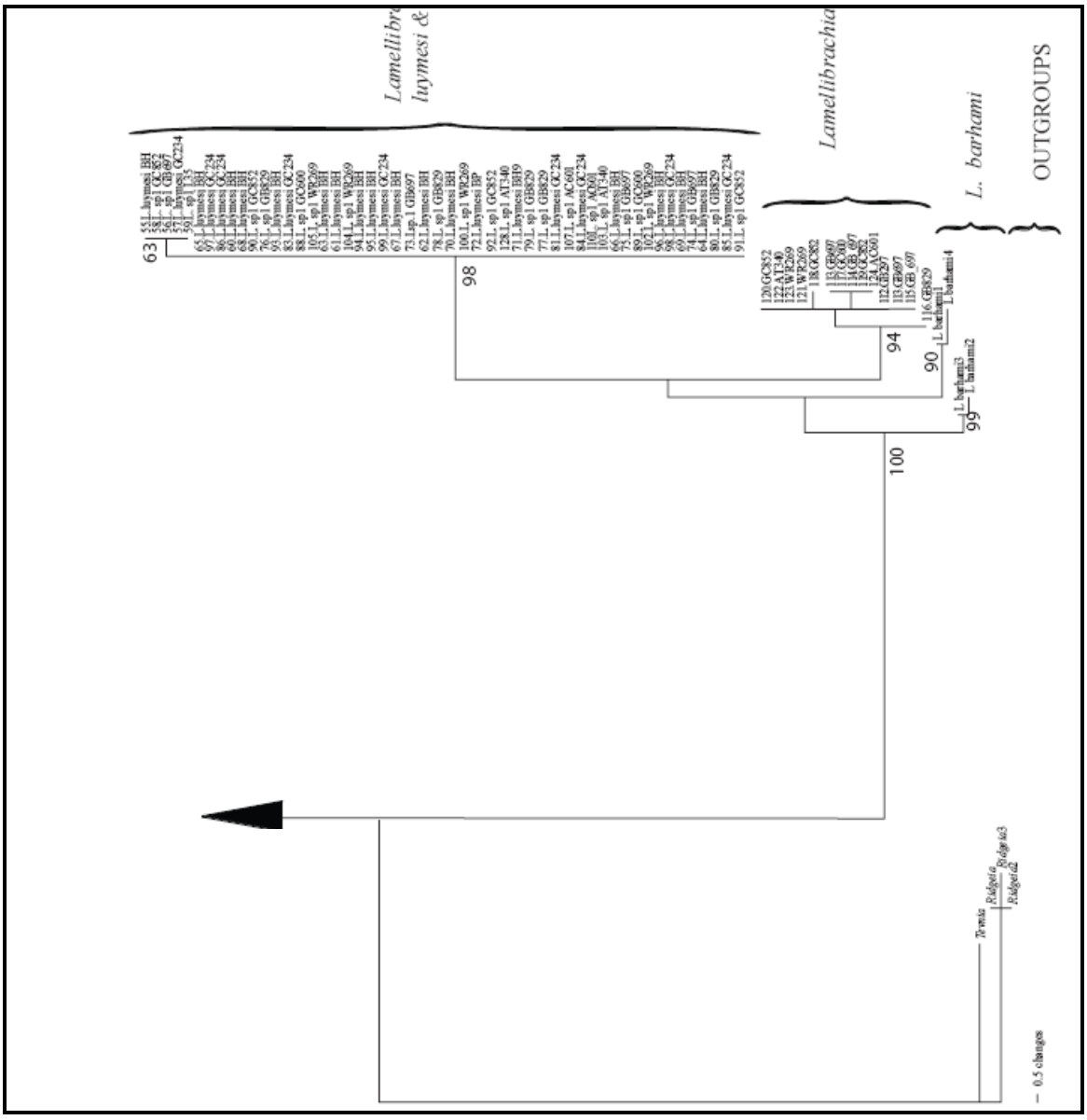

Figure 12-4B. 16S Maximum Likelihood (ML) tree. Outgroups are shown in italics and bootstrap support above 50% (NJ 1000 replicates) is indicated below each node. Sample identifications and abbreviations is as in Figure. 2.

Three species in the escarpiid clade of seep vestimentiferans are found in the GoM: *Seepiophila jonesi* has been collected from numerous sites ranging in depth from 500 to 950 m, escarpiid sp. nov. from two sites ranging in depth from 600 to 640 m where it co-occurs with *Seepiophila jonesi*, and *Escarpia laminata* from 950 to 3,200 m depth. *Seepiophila jonesi* and *Escarpia laminata* co-occurred at only one site, GB647 at a depth of 950 m. The undescribed escarpiid differs morphologically from *Seepiophila jonesi* because it lacks the curl of the ventral vestimental fold, which is a defining character of the genus *Seepiophila* (Gardiner et al., 2001*)*. Additionally, the obturacular process of the undescribed escarpiid forms a spike, but is flat in *S. jonesi* and barely protrudes from the top of the obturaculum.

Both the COI and 16S phylogenetic trees distinguish these three species and place them within the escarpiid clade of seep vestimentiferans (Figures 12-2 and 12-3). Both the 16S tree and the 16S *p* distance matrix suggest *E. laminata* is more closely related to *Seepiophila jonesi* (between-species uncorrected *p*=2%) than to the undescribed escarpiid (between-species uncorrected *p*=3.50%). However, the COI tree groups the undescribed escarpiid with the described *Escarpia* spp. This clade is not well-supported in the COI trees based on a bootstrap value of 61% while in the 16S tree, the bootstrap value is below 50%. Neither tree allows us to clearly state whether this new escapiid is more closely related to *Escarpia*, *Paraescarpia*, or *Seepiophila*.

As previously noted by other authors, COI does not separate *E. southwardae* found in cold seeps on the west coast of Africa in the eastern Atlantic, *Escarpia spicata* from Guymas basin or the coast of California, and *E. laminata* from the GoM (Black et al., 1998) , and there is very little to no intra-clade diversity within this group (Table 12-3). This result may indicate that those three nominal species represent a single biological species with a surprisingly wide geographic distribution and variable morphology. However, this would require a high level of gene flow between quite distant localities, especially since the closing of the Isthmus of Panama 3.5 million years ago followed the closing of the deep sea exchange 10 million years ago (Burton et al., 1997). This level of genetic exchange over these distances seems quite unlikely considering what is known about larval development times for vestimentiferans (Marsh et al. 2001, Young et al., 1996). Although the life span of *Escarpia* larvae has not been determined, the larval life span of the vent species *Riftia pachyptila* is estimated at about three weeks (Marsh et al., 2001) and the larval life span of the seep vestimentiferan *Lamellibrachia luymesi* is estimated to be about one month (Young et al., 1996). Tyler and Young (1999) estimate that the maximal dispersal distances for these species are on the order of 60 km per generation, which is unlikely to support the level of genetic mixing necessary to maintain genetic homogeneity among the three described species of *Escarpia* from such widely separated geographic locations.

The lack of fixed COI differences within *Escarpia spicata*, *E. laminata*, and *E. southwardae* could alternatively be due to different rates of evolution of the COI gene in different taxa. COI has been used for higher level phylogenetic reconstructions in other groups of annelids (Halanych and Janosik, 2006) and has been adopted as an appropriate gene for the "barcode of life" initiative (BOLI). However, the fact that COI fails to identify morphologically distinct populations of *Escarpia* from such widely separated areas implies that, in this clade, the mutation rate may be considerably slower than in other lineages. Slower rates of evolution in the mitochondrial DNA have been recognized in some other groups such as the Cnidarian class Anthozoa where this has been linked to an especially efficient repair system of their mitochondrial DNA (France and Hoover, 2002; Pont-Kingdon et al., 1998); however, no evidence of a similar system has yet to be found for the replication of Vestimentiferan mitochondria. Seep vestimentiferans can also be extremely long-lived (Bergquist et al., 2000; Cordes et al., 2007a), which may contribute to a slower rate of change of mitochondrial DNA (see for example Nabholz et al. (2008) for a consideration of longevity effects on mitochondrial rates of evolution in vertebrates).

In the COI dataset, the *Lamellibrachia* clade is divided into eight distinct groups that represent presumptive species, including five basal species (*L. juni*, *L. barhami*, *L. satsuma*, *L*. sp. Japan, and *L*. sp. West Pacific), all of which are from the Pacific Ocean and four of which are from the western Pacific. This is consistent with the hypothesis that the genus *Lamellibrachia* originated in the Pacific, likely the western Pacific, and subsequently radiated to the eastern Pacific, the Atlantic, and the GoM.

Three morphological species of *Lamellibrachia* were identified in collections from the GoM: *Lamellibrachia luymesi* from the upper slope between about 400 m and 800 m, *L.* sp. 1 from 950 to 2320 m, and *L.* sp. 2 from 1175 to 2320 m. *L. luymesi* and *L.* sp. 1 have a similar number of sheath lamellae but the deep-water *L.* sp. 1 generally has more gill lamellae, ranging between 21 and 27 in the 28 individuals examined, whereas the shallow-water *L. luymesi* has between 15 and 22 gill lamellae in the 20 individuals examined for the species description. The morphological character that allowed rapid identification of animals on board ship was the relatively short and fat vestimentum of *L.* sp. 1. The ratio of the length to the width of the vestimentum of *L*. sp. 1 ranges from 2.4 to 4.7 and from 6.2 to 16.4 in *Lamellibrachia luymesi*. *Lamellibrachia* sp. 2 has a similar number of sheath and gill lamellae as *L.* sp 1, and the vestimentum length to width ratio tends to be shorter (1.9 to 3). The most distinct field character for *L.* sp. 2 is the lack of a ventral vestimental fold, which is present on *L.* sp. 1.

Despite morphological characters that distinguish the three GoM *Lamellibrachia* presumptive species, only two of them were resolved by either the COI or the 16S phylogenetic trees. Specifically, both genes failed to separate *L. luymesi* from the shallow GoM and *L.* sp.1 from the deeper GoM sites. This lack of genetic differences between individuals that span such a wide depth range is unusual (Chase et al., 1998; Zardus et al., 2006) and surprising given the morphological differences. Both 16S and COI genes consistently identify *Lamellibrachia* sp. 2 as a separate clade, sister to the *L. luymesi*/*L.* sp.1 clade.

Our preliminary results from the Globin A1 Intron 1 suggest that this gene can differentiate between L. sp 1 and *L. luymesi*, although only by a single base pair (Figure 12-3). Interestingly, the phylogeny generated with this gene places *L.* sp 2 individuals in both groups, this gene does not distinguish this species, even though both CO1 and 16S genes do so.

There were no apparent geographic distributional patterns that were independent of depth for the seep vestimentiferans in the GoM. The common species present on the upper Louisiana slope (*Lamellibrachia luymesi* and *Seepiophila jonesi*) have been found at both the eastern-most and western-most sites where we have collected vestimentiferans. *Escarpia laminata* from the lower slope ranges from the Alaminos Canyon sites, our most westerly collection sites for this study, to the Florida Escapement in the eastern GoM (Cordes et al., 2009). Both of the *Lamellibrachia* spp. found at the deeper sites occurred over the entire east-west range of sites within their depth range (from the Alaminos Canyon sites in the west to AT340 in the east).

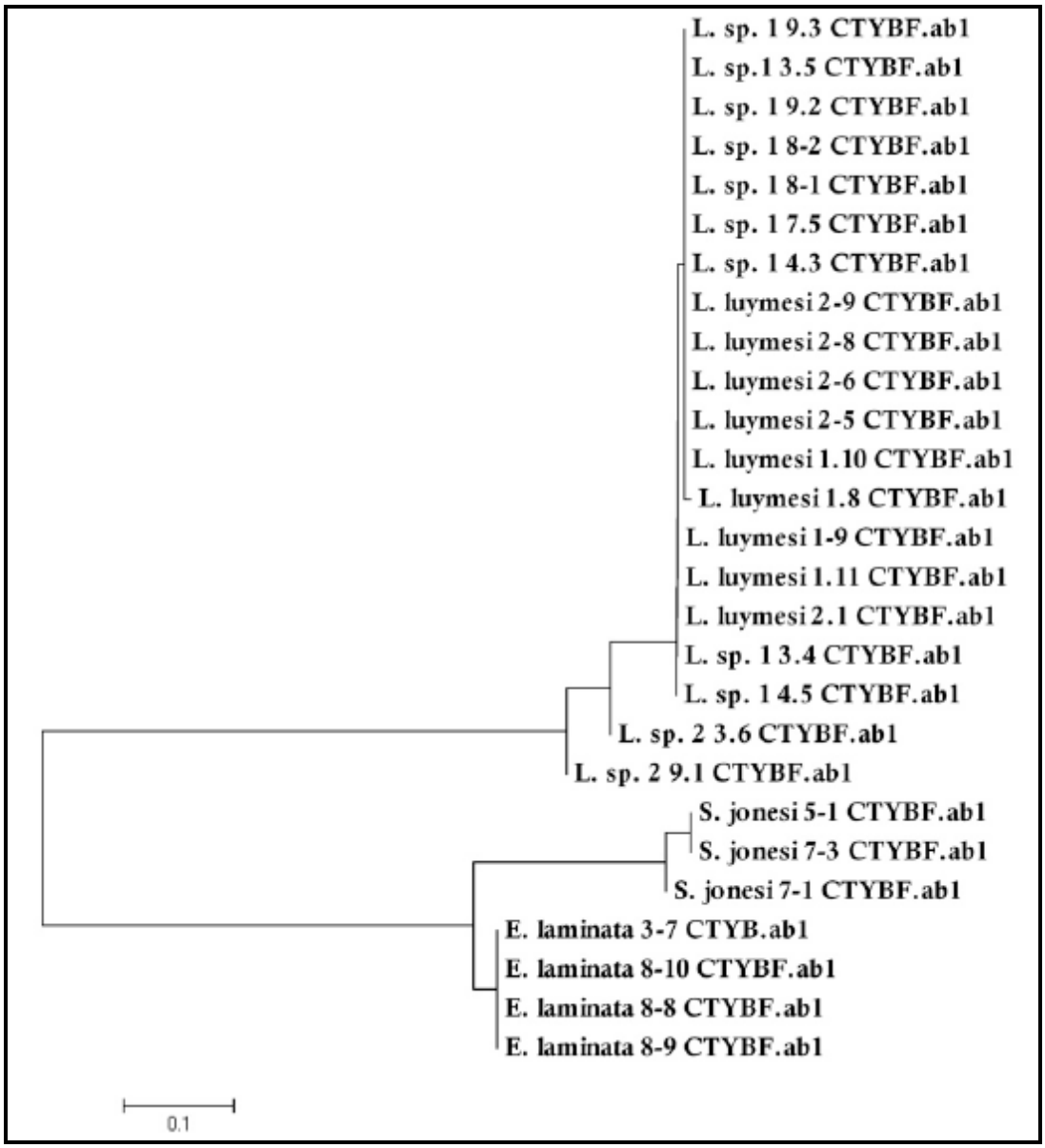

Figure 12-5. Cytochrome B Neighbor-Joining (NJ) tree.

12.4.1. Within Species Diversity of 16S and CO1 Genes

Tables 12-2 and 12-3 report within and between species *p* distance calculated for the GoM genetic species. Within species diversity for both 16S and in the COI genes is strikingly low, which is in contrast to previous studies on deep sea mollusks and echinoderms, where large amounts of genetic variation were observed over small distances (Chase et al., 1998; Howell et al., 2004; Quattro et al., 2001). However, large-scale studies indicate that low within species genetic variation may be typical of deep sea organisms (Bisol et al., 1984) and even suggest that it may decrease with increasing depth (France and Kocher, 1996). Genetic variation has been

suggested to be an important feature of the genome of an organism that allows it to adapt to a changing environment (Powers et al., 1991). Organisms that live in the deep sea may experience a long term stable environment that may result in low levels of within species genetic diversity. Alternatively, low within species genetic diversity may be the result of fewer replication errors, more efficient repair in the germ line, or of repeated population bottlenecks.

The *Escarpia laminata, E. spicata*, and *E. southwardae clade*, and *Lamellibrachia luymesi*/sp.1, and *L.* sp. 2 have a moderate degree of intraclade diversity (Figures 12-2 and 12-3). However, as with all of the GoM vestimentiferans analyzed, none of the within species clades grouped by specific geographic locations or depth. In contrast, genetic breaks and barriers that restrict gene flow were identified in both hydrothermal vent vestimentiferans and mussels along the East Pacific Rise (EPR). Specifically, Won et al. (2003) used COI sequences to identify two highly divergent clades on the EPR on the two sides of the Easter Island Microplate. Similarly, Hurtado et al. (2004) used COI sequences to identify several geographic breaks and barriers that restrict gene flow in three genera of annelids along the EPR, including two species of vestimentiferan (*Riftia pachypitla* and *Tevnia jerichonana*).

12.5. Summary

In this study, our primary goals were to identify and characterize the distributions of vestimentiferans at seep sites covering a wide geographic and depth range in the GoM and to investigate their relation to other seep vestimentiferan species, using phylogenetic analysis of mitochondrial gene sequences. Based on data from other groups, we expected that the widely accepted "barcoding gene" CO1, along with the widely used mitochondrial 16S gene would allow us to accomplish this primary task. Although the genetic analyses confirmed most of the morphological species identified during collections, we also identified an unexpected discrepancy between the morphospecies identified during the collections and genealogical species identified using the mitochondrial genes COI and 16S. Using morphological characters, we identified two new species of *Lamellibrachia* (sp. 1 and 2). However, neither COI nor 16S distinguished the deeper occurring morphospecies *L.* sp. 1 from *L. luymesi*, the common *Lamellibrachia* species on the upper Louisiana slope. Our molecular genetic analyses confirm the presence of three vestimentiferan species within the escarpiid clade in the GoM. However, since COI also does not differentiate between *Escarpia laminata* found in the GoM and the other described *Escarpia* species found off the coast of Africa or in the eastern Pacific Ocean we suggest that COI or 16S genes may not be suitable to reliably distinguish closely-related species of long-lived seep vestimentiferans. We are currently developing a number of additional mitochondrial and nuclear markers and are evaluating their usefulness to clarify the relationships among the named species of *Escarpia* and among the *Lamellibrachia* species in the GoM. These markers are likely to prove quite useful for seep vestimentiferans in general, as this group may include a number of cryptic species not yet detected with more conventional markers.

13. IDENTIFICATION AND DISTRIBUTION OF BATHYMODIOLIN MUSSELS

13.1. Introduction

There are three described species of *Bathymodiolus* mussels in the GoM (*B. heckerae, B. brooksi,* and *B. childressi*) (Gustafson et al. 1998). Based primarily on morphology, we previously indicated that *B. childressi* are found from 400 m to 2200 m depth, *B. brooksi* from approximately 1080 m to 3300 m, and *B. heckerae* from 2200 m to 3300 m (Cordes et al. 2009). Previous phylogenetic analysis of bathymodiolin mussels worldwide revealed that *B. brooksi* and *B. heckerae* are closely-related species and belong in the same clade, whereas *B. childressi* is in another more divergent clade (Iwasaki et al. 2006).

B. childressi are found in a variety of physico-chemical environments on the upper Louisiana slope, including brine-dominated and petroleum-dominated seep sites, exposed to a range of concentrations of methane, oil, and hydrogen sulfide (Bergquist et al. 2004). They are also found on the lower slope and, despite these well differentiated habitats and the large range of depth, there is no previous evidence of significant *B. childressi* population subdivision in the GoM (Carney et al. 2006).

In this section, we use mitochondrial markers to identify and characterize our collections of mussels from a large depth range (530 m to 3288 m) and from various types of habitats. Our results generally validate the previous morphologically based distribution of each of the three species of *Bathymodiolus*, although we found that approximately 10% of the morphologically based identifications were incorrect and some significant differences in sites of occurrence are noted. These data allowed us to confirm that sympatry within a single patch of mussels is common, and allowed discovery a new species of bathymodiolin mussel, *Bathymodiolus* sp. nov. Our more in depth and ongoing analyses suggest that there is detectable genetic structure within individual species of the Bathymodiolinae on the lower Louisiana slope of the GoM.

13.2. Methods

13.2.1. Sample Collection

We extracted DNA and analyzed mussels from 15 discrete sites, ranging from 527 to 3,288 m and from 84°55’ W to 94°34’ W across the GoM (Table 13-1). A total of 231 mussels, collected during 20 dives between October 2002 and August 2009 in the GoM, were included in the analyses. Mussels were collected using either the mussel pot collection device or nets, as described above. Upon recovery of the ROV or submersible, the mussels were transferred to chilled sea water, preliminarily identified using morphological criteria, and dissected on board ship. Pieces of tissue (mantle and gills) were frozen (-80°c) or kept in 70% ethanol until nucleic acid extraction using the CTAB+PVP method (Doyle and Doyle 1987) at The Pennsylvania State University.

Table 13-1

Sampling Information Sorted by Depth

	Site	Latitude	Longitude	Depth (m)	Dive#	Date of collection	B. childressi		B. brooksi		B. heckerae		B. new sp	
							Morpho ID	Genetic ID	Morpho ID	Genetic ID	Morpho ID	Genetic ID	Morpho ID	Genetic ID
Upper Slope	GC 234	27°44.1'N	91°13.5'W	527	JSL 4717	17 July 04	10	10	-	-	-	-	-	-
	MC 929	28°01.1'N	89°43.1'W	636	JSL 3340	08 October 02	15	15	-	-	-	-	-	-
	GC 233	27°43.4'N	91°16.8'W	651	JSL 4711	09 July 04	10	10	-	-	-	-	-	-
	GC 204	27°46.0'N	90°32.7'W	870	JSL 3354	17 October 02	15	15	-	-	-	-	-	-
	GB 647	27°19.8'N	92°25.8'W	1007	J2-280	26 June 07	6	6	-	-	-	-	-	-
	GB697	27°19.2'N	92°06.7'W	1015	J2-274	17 June 07	4	4	-	-	-	-	-	-
	MC853	28°07.6'N	89°08.5'W	1075	AD 4178	14 May 06	3	8	9	4	-	-	-	-
Deeper slope	MC640	28°21.4'N	88°47.7'W	1414	AD 4182	18 May 06	-	3	4	1	-	-	-	-
	AT 425	27°34.16	88°29.6'W	1869	AD 3918	14 October 03	-	-	-	3	3	0	-	-
	AC645	26°21.3'N	94°30.1'W	2195	AD 4197	01 June 06	-	-	-	3	3	0	-	-
				2197	J2-281	29 June 07	-	-	-	3	3	0	-	-
				2200	AD 3923	18 October 03	-	-	-	8	8	0	-	-
				2222	AD 3924	19 October 03	27	25	15	17	-	-	-	-
	AT340	27°38.7'N	88°21.9'W	2190	J2-270	10 June 07	-	-	4	4	-	-	-	-
				2216	AD 4180	16 May 06	-	-	-	1	20	19	-	-
	AC601	26°23.6'N	94°30.9'W	2335	J2-283	07 July 07	3	3	-	-	-	-	-	-
	DC 583	28°23.1'N	87°23.3'W	2445	J2-454	22 August 09	-	-	19	0	13	0	0	32
	AC818	26°11.1'N	94°34.4'W	2744	J2-282	01 July 07	-	-	-	4	4	0	-	-
				2785	AD 4192	27 May 06	-	-	16	16	2	2	-	-
	Flo. Esc.	26°01.8'N	84°55.1'W	3288	AD 3915	11 October 03	-	-	-	1	15	14	-	-
						total:	93	99	67	65	71	35	0	32

13.2.2. PCR Amplification and Sequencing

DNA sequences were obtained for two mitochondrial genes: the CO1 and nicotinamide adenine dinucleotide plus hydrogen (NADH) dehydrogenase subunit 4 (ND4). Fragments of the mitochondrial gene CO1 were amplified using the primers CO1 Bathymodiolus sense/antisense (Olu-Le Roy et al. 2007), and HCO/LCO (Folmer et al. 1994) with the amplification conditions described in Faure et al. (2007). The ND4 segments were amplified with the primers sense ND46S or ArgBL with the anti-sense primer NAP2H and the conditions described in Iwasaki et al. (2006). The primers used in this study are shown in Table 13-2.

Table 13-2

Primers Used to Amplify the CO1 and ND4 Mitochondrial Markers

locus	5'-[size of the tag] primer -3'	References
Sense BathCO1	TGT GGT CTG GAA TAA TTG GAA	Olu et al 2007
Antisense BathCO1	ATA AAA AGA TGT ATT RAA RTG ACG	Olu et al 2007
Sense LCO 1490	GGT CAA CAA ATC ATA AAG ATA TTG G	Folmer 1994
Antisense HCO 2198	TAA ACT TCA GGG TGA CCA AAA AAT CA	Folmer 1994
Sense ArgBL	CAA GAC CCT TGA TTT CGG CTC A	Bielawski and Gold 1996
Sense ND46	GCT CAT GCC CCG AAT ATG TCT	Iwasaki 2006
Antisense NAP2H	TGG AGC TTC TAC GTG RGC TTT	Arevalo et al 1994

The PCR products were run on a 1% agarose gel stained with ethidium bromide to check the quantity and the quality of the products and then purified with the ExoSap-It protocol (USB, Affimetrix). Both strands of the purified PCR products for the two mitochondrial genes CO1 and ND4 were directly sequenced.

13.2.3. Data Analyses

The conflicts from the sequence reads from the two DNA strands were resolved with the Chromas 2.22 computer program (Technelysium Pty. Ltd., Helensvale, Australia). Sequences were aligned with Clustal W (Thompson et al. 1994) in BioEdit program (Hall 1999), with manual adjustments to assure that indels were scored consistently in the alignment. Neighbour-joining trees were constructed using MEGA v4.0 (Kumar et al. 2004) with the Tamura-Nei method (Tamura and Nei 1993) to construct gene genealogies, and the significance of observed clades were examined with 1,000 bootstrap replicates (Felsenstein 1985). For both mitochondrial loci, we included the National Center for Biotechnology Information (NCBI) sequence for *B. thermophilus* (CO1: FJ766893, ND4: AY649808), *B. azoricus* (CO1: FJ766849, ND4: AF128534), and *B. puteoserpentis* (CO1: FJ766949, ND4: AF128533) in the phylogenetic trees. These three species are the most closely related to *B. heckerae and B. brooksi* and were used to allow comparison of our new and the previously published phylogenies (Iwasaki et al. 2006, Jones et al. 2006, Lorion et al. 2009). Additional sequences were included from NCBI in the

general Bathymodiolus phylogeny based on the CO1 marker. Accession numbers of these sequences are indicated in the tree.
The number of haplotypes and nucleotidic diversity (average number of nucleotides differences per site between two sequences (Nei 1987) were estimated using the DnaSP version 4.20.2 software package (Rozas et al. 2003). Pairwise distances between individuals were used to determine genetic differences among populations based on mtDNA sequences (Φst statistic) with Arlequin (Excoffier et al. 2005) and 1,000 permutations of the data were used to evaluate the statistical significance of the differentiation values.

13.3. Results and Discussion

13.3.1. Morphological and Genetic Identification

The rapid identification of closely related mussels at sea is not straightforward, especially for small and broken individuals. As a result, the initial morphological identifications were considered preliminary until later molecular confirmation. We used the widely accepted mitochondrial markers CO1 and ND4 to confirm the species identification of a representative subset of all collections made during this project. The number of mussels analyzed per sampling site varied from 3 to 27 depending on the number of individuals of each species found in the collections. These markers provide a robust separation of the three GoM *Bathymodiolus* spp., *B. childressi*, *B. brooksi*, and *B. heckerae*, as well as numerous other closely related bathymodiolins (Iwasaki et al. 2006) and the results were 100% consistent between the two markers when both were successfully amplified (we were unable to amplify the ND4 loci for 24 of the 231 individuals, but there was no correlation between species or site and failure to amplify). These results and comparison between the morphological and genetic identifications are presented in Table 13-1 and the phylogenetic trees are shown in Figure 13-1.

Table 13-3 summarizes the relation between the shipboard morphological identification and the later molecular based identifications for each species. The molecular analyses confirmed that *B. childressi* identification on board ship was correct 98% of the time, although 12% of the mussels originally identified as *B. brooksi* were later genetically identified as *B. childressi*. Overall the shipboard identifications of *B. brooksi* were confirmed by molecular tests 60% of the time, although if the one collection where the new (and completely unexpected) species was discovered is not considered in this analysis the rate of correct shipboard identification is much higher, at 83%. *B. heckerae* was misidentified 50% of the time at sea. Subsequent molecular analyses identified 31% of these as *B. brooksi*, and another 18% as the new species, *Bathymodiolus* sp nov. Although the misidentifications among species is significant overall, when those associated with *Bathymodiolus* sp nov are excluded, about 90% of those remaining were either noted as troublesome in notebooks at sea or were associated with small individuals or broken shells.

Table 13-3

Assignment of the Species after Genetic Identification (%)

Same estimations without the new species (site DC583) are shown in parentheses

Morphological ID	*B. childressi*	*B. brooksi*	*B. heckerae*	B. new species GoM
From *Bathymodiolus childressi* to…	97.8 (97.8)	2.2 (2.2)	0	0
From *B. brooksi* to...	11.9 (16.7)	59.7 (83.3)	0	28.4
From *B. heckerae* to…	1.4 (1.7)	31.0 (37.9)	49.3 (60.3)	18.3

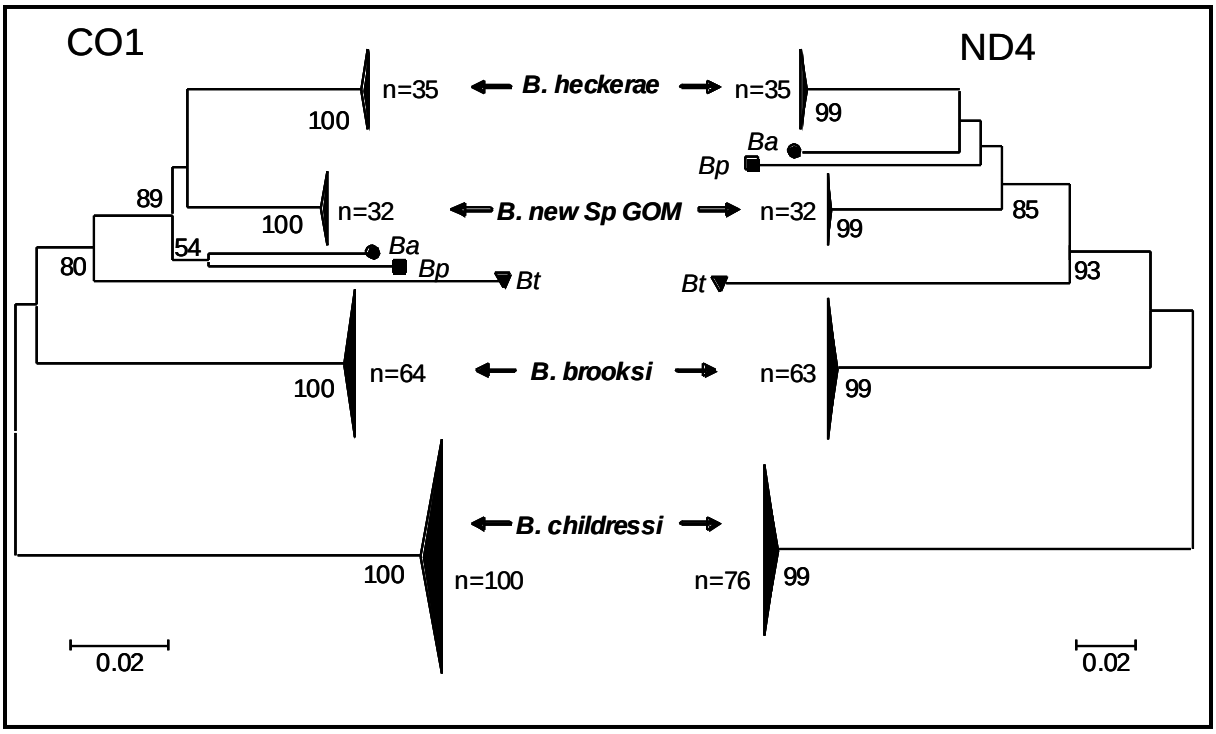

Figure 13-1. Neighbour-Joining trees for the mitochondrial loci (CO1 and ND4) using the Tamura-Nei method (Tamura and Nei 1993). Bootstrap supports above 50% are shown next to the branches (1000 replicates). CO1, n= 231 individuals from the GoM + *Bathymodiolus azoricus* (Ba): FJ766849, *B. puteoserpentis* (Bp): FJ766949, and *B. thermophilus* (Bt): FJ766893; ND4 n= 206 individuals from the GoM, + *Bathymodiolus azoricus* (Ba): AF128534, *B. puteoserpentis* (Bp): AF128533, *B. thermophilus* (Bt): AY649808.

Although the molecular reanalysis of the species identifications changed details with respect to the confirmed sites and relative abundance for the three described species of *Bathymodiolus*, these re-identifications did not result in any significant range extensions for any species from that published in Cordes et al. (2009). However, the molecular analyses only confirmed *B. heckerae* in three of the original nine collections where the preliminary morphology-based identification indicated they occurred. Our molecular identifications are consistent with previous reports of *B. brooksi* and *B. childressi*, but not *B. heckerae* at the relatively well know Alaminos Canyon 645 site (Brooks et al., 1990, Fisher et al. 1993, Craddock et al. 1995, Gustafson et al. 1998). Despite the confirmation of earlier reports of no *B. heckerae* at AC645, the presence of *B. heckerae* at

AC 818 maintains the wide geographic range of this species from east to west across the northern GoM. Our analyses also confirm the wide spread occurrence and large depth and geographic range of *B. brooksi* which we confirmed at 7 of our study sites from 1075 to 3288 m, and from Alaminos Canyon to the Florida Escarpment. Our analyses also slightly extend the already large depth range of the dominant upper slope mussel *B. childressi* from a maximum depth of 2220 m in AC645 (Craddock et al. 1995) to 2335 m in AC601.

A new and exciting result of our molecular analyses of the *Bathymodiolus* spp. collections was the discovery of a chemosynthetic community in DC 583 hosting a new species of *Bathymodiolus* (n=32). This discovery was actually made during the 2009 *Jason II* dives as part of the Lophelia *II* project, but because of the relevance to this study our early results are included here. Theses mussels are clearly divergent from the three other species of *Bathymodiolus* in the GoM, as well as all other *Bathymodiolus* spp. with published CO1 or ND4 sequences, including those on the Blake Ridge, the Mid-Atlantic Ridge, and from west African seeps (Won et al. 2002, Olu-Le Roy et al. 2007, Won et al. 2008, Genio et al. 2008) (Figures 13-1 and 13-2, Table 13-4a). Two other symbiont-containing species of Bathymodiolinae have been described in the GoM: *Idas macdonaldi*, and *Tamu fisheri* (Gustafson et al. 1998). The new species is clearly distinct from these mussels, as well, and phylogenetic analyses including these mussels confirm the new species belongs in the genus *Bathymodiolus*. Discovery of this new species of *Bathymodiolus* at 2,445 m is quite surprising, as this is within the range of depth of all three other species of GoM *Bathymodiolus* (*B. childressi*: 527 to 2335 m, *B. brooksi*: 1075 to 3288 m, and *B. heckerae*: 2216 to 3288 m depth). The DC583 site is one of the eastern-most of our sampling sites but is still within the documented geographic range of *B. brooksi* and *B. heckerae* as both are present further to the southeast on the Florida Escarpment. The limited distribution of this new species within an area with three other widespread species of *Bathymodiolus* strongly suggests that this site or area is in some way oceanographically isolated from the other sites we have visited. *Bathymodiolus* spp. have a planktonic larvae and a long larval life period that allows them to disperse over long distances (Arellano and Young 2009). Such wide dispersal potential is evidenced in the lack of significant population structure of previously detected in *B. childressi* throughout of the GoM (Carney et al. 2006) and the amphi-atlantic distribution of closely related congeners (Olu-Le Roy et al. 2007). It is possible that the sampled population represents a unique recruitment event, however the large size range in our collection (96 to 151 cm in shell length), and presence of very small mussels in the video record of the site suggests this is not the case. It is also possible that this species is capable of using a food or energy source unique to this site that other Bathymodiolids cannot use, but we consider this very unlikely considering the diversity of symbiont physiological types present in *B. brooksi* and *B. heckerae* (Duperron et al. 2007, Duperron et al. 2009). Clearly additional oceanographic, ecological, and physiological studies are needed to understand the distribution of this new species of *Bathymodiolus*.

13.3.2. Genetic Structure within Species

Since (as expected) no genetic differentiation was detected between the different sampling dates within a site (at AC645, AT340 and AC818), we have combined all samples from a site for this analysis. The power to detect differences in these types of analyses is strongly correlated with

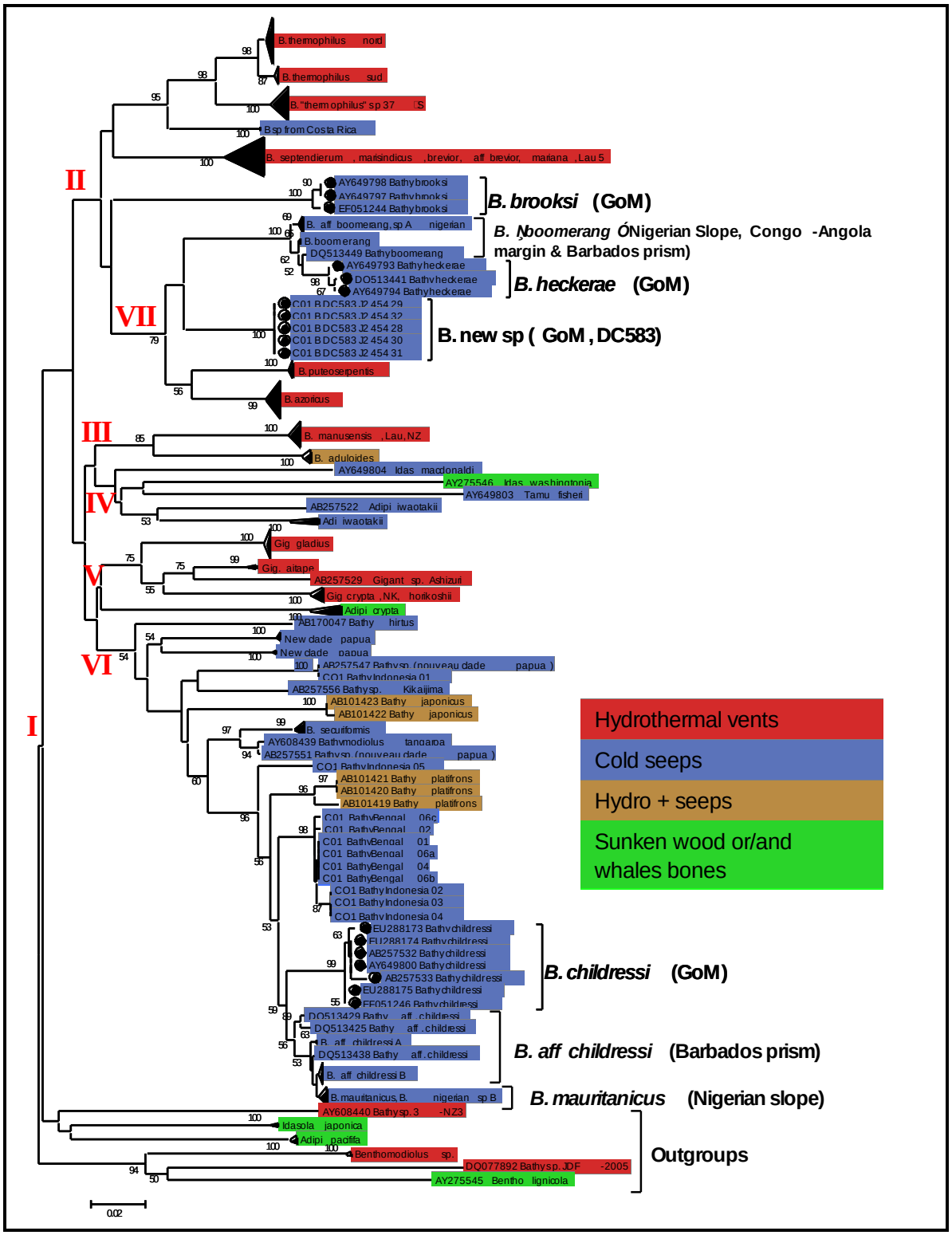

Figure 13-2. Neighbor-Joining tree based CO1 sequences representing 249 sequences from 42 species. Bootstrap values (< 50%) are shown next to the branches.

Table 13-4

Fst Population Differentiation, Tested by 1023 Permutations with the Arlequin Software

(*: p<0.05; **: p<0.01; ***: p<0.001)

A: All species

		CO1			
		B. brooksi (n=64)	*B. childressi* (n=100)	*B. heckerae* (n=35)	B. newSpGoM (n=32)
ND4	*B. brooksi* (n=63)		0.97***	0.98***	0.98***
	B. childressi (n=76)	0.98***		0.97***	0.97***
	B. heckerae (n=36)	0.99***	0.98***		0.99***
	B. newSpGoM (n=32)	0.99***	0.98***	0.99***	

B: *B. childressi*

		CO1									
		Bc_GC234 (n=10)	Bc_MC929 (n=15)	Bc_GC233 (n=10)	Bc_GC204 (n=15)	Bc_GB647 (n=6)	Bc_GB697 (n=4)	Bc_MC853 (n=8)	Bc_MC640 (n=3)	Bc_AC645 (n=25)	Bc_AC601 (n=3)	Bc_AC818 (n=1)
ND4	Bc_GC234 (n=10)		**0.1***	0.15	0.02	-0.01	0.01	-0.01	-0.04	0.05	0.07	0.41
	Bc_MC929 (n=15)	0.06		-0.04	-0.01	0.01	-0.08	**0.11***	-0.07	-0.02	0.01	0.19
	Bc_GC233 (n=10)	0.02	-0.01		-0.02	0.07	-0.11	0.14	-0.01	-0.04	0.06	0.33
	Bc_GC204 (n=9)	-0.01	-0.04	-0.03		-0.01	-0.12	0.01	-0.11	-0.02	-0.03	0.03
	Bc_GB647 (n=0)	-	-	-	-		-0.02	0.02	-0.13	-0.01	-0.03	0.46
	Bc_GB697 (n=4)	0.08	-0.04	-0.07	-0.03	-		0.01	-0.12	-0.12	-0.07	0
	Bc_MC853 (n=7)	0.02	**0.12***	0.07	0.05	-	0.10		0.01	0.05	0.09	0.50
	Bc_MC640 (n=2)	-0.05	-0.16	-0.11	-0.19	-	-0.10	-0.08		-0.08	-0.12	0.50
	Bc_AC645 (n=17)	0.03	-0.01	-0.01	-0.04	-	-0.01	**0.09***	-0.09		-0.01	0.13
	Bc_AC601 (n=2)	0.05	-0.03	-0.04	-0.07	-	0	-0.02	-0.50	-0.01		0.20
	Bc_AC818 (n=0)	-	-	-	-	-	-	-	-	-	-	

Table 13-4. Fst Population Differentiation, Tested by 1023 Permutations with the Arlequin Software (continued)

(*: p<0.05; **: p<0.01; ***: p<0.001)

C: *B. brooksi*

		CO1						
		Bb_MC853 (n=4)	Bb_MC640 (n=1)	Bb_AT425 (n=3)	Bb_AC645 (n=31)	Bb_AT340 (n=5)	Bb_AC818 (n=19)	Bb_FloEsc (n=1)
ND4	Bb_MC853 (n=4)		0.60	**0.23***	-0.01	0.05	-0.01	0.78
	Bb_MC640 (n=1)	-1		-1	-0.26	-0.50	0.01	1
	Bb_AT425 (n=3)	0.07	-1		0.13	0.01	0.22	0.17
	Bb_AC645 (n=30)	-0.06	-0.99			-0.08	-0.02	0.43
	Bb_AT340 (n=5)	-0.03	-1	0.02	0.03		-0.07	0.31
	Bb_AC818 (n=19)	-0.04	-0.95	0.14	-0.01	0.04		0.5
	Bb_FloEsc (n=1)	0.60	1	0	0.34	0.11	0.37	

D: *B. heckerae*

		CO1		
		Bh_AT340 (n=19)	Bh_AC818 (n=2)	Bh_FloEsc (n=14)
ND4	Bh_AT340 (n=19)		-0.33	**0.04****
	Bh_AC818 (n=2)	0.12		-0.3
	Bh_FloEsc (n=14)	-0.01	-0.08	

sample sizes, so our most robust conclusions are necessarily limited to a subset of the sites visited during this and previous projects.

We calculated population differentiation (Fst) for the CO1 and ND4 genes for *B. childressi* (Table 13-4b), *B. brooksi* (Table 13-4c) and *B. heckerae* (Table 13-4d). In these tables the results of pairwise differences for ND4 are presented below the diagonal and the results for CO1 are above it. Despite the relatively small sample sizes for many sites, numerous significant differences were detected. Analysis of CO1 gene in *B. childressi* detected differentiation between MC929 and both GC234 and MC853. The genetic differentiation between MC929 and MC853 was confirmed with ND4, and an additional difference detected between MC853 and AC645. Only a single significant difference was detected among the *B. brooksi* populations; analysis of CO1 indicates differences in the populations from MC853 and AT 425. Despite the small sample sizes, 3 separate analyses suggest that the MC853 mussel population is divergent from at least some others in the GoM, and one of these even detects differences between the population at this site and that at another in the same lease area.

B. heckerae was confirmed in only three of our study sites (AT340, AC818 and Florida Escarpment) and sufficient individuals were collected only at AT340 and from the Florida Escarpment for robust population-level analyses. Using the CO1 gene, we detected a strong genetic differentiation between AT340 and the Florida Escarpment ($p<0.01$). A closer look at this data including consideration of the number of mutations and haplotypes allows a preliminary analysis of the diversity within the populations (Table 13-5). For both loci, the highest diversity is found for the Florida Escarpment population. Although higher than found in the other GoM populations, this diversity is very low compared to that of other species of *Bathymodiolus* (Atlantic: Faure et al. (2009), Pacific: Plouviez et al. (2009)). Mussels from AT340 are almost genetically monomorphic for the CO1 locus (only one mutation and two haplotypes for 19 individuals, $\pi=0.0002$). This diversity is eight times smaller than the diversity detected in the Florida Escarpment population. The ND4 locus shows more diversity than CO1 but like CO1 exhibits lower diversity in the AT340 population than that of the Florida Escarpment.

Table 13-5

B. heckerae Genetic Diversity

Species	Locus	Location	*N*	*Nb haplo*	*S*	*N mut*	π
B. heckerae	CO1 (515bp)	FloEsc	14	6	5	5	0.0016
		AT340	19	2	1	1	0.0002
		AC818	2	1	0	0	0
	ND4 (508bp)	FloEsc	14	5	7	7	0.0020
		AT340	19	5	6	6	0.0012
		AC818	2	2	1	1	0.0020

N : number of individuals
Nb haplo : number of haplotypes
S: number of segregating site
N mut: number of mutations
Π : Average number of nucleotide differences par site between two sequences (Nei 1987)

Although quite preliminary, our results suggest a testable hypothesis we will pursue with additional analyses: a sequential colonization of the GoM by bathymodiolins from East to West with incremental loss of the genetic diversity. This scenario is in agreement with the hypothesis of Won et al. (2002), who suggested a colonisation of the seeps (Florida Escarpment and Blake Ridge) from Mid-Atlantic Ridge vent species. We further suggest colonization the Atlantic seeps were a stepping stone for colonization of the GoM and propagation of the communities within the GoM from east to west.

Although we didn't detect any significant relationship between the genetic structure of populations and depth or geographic distance within any species, taken as a whole our results indicate that mussel populations in the GoM, especially those on the lower slope are not panmictic with unlimited gene flow between populations. Our preliminary analyses indicate there is easily detectable population differentiation among the GoM mussel populations. Additional sampling and analyses are necessary to better understand the patterns and underlying oceanographic causes for these patterns, and these analyses are underway. In particular, the area around DC 583 needs to be more fully explored and sampled as this site in the BOEM planning area may be quite isolated from other seep sites in the GoM.

13.3.3. Phylogenetic Relationship and Ecological Considerations

The last part of our study aimed to understand the evolution of the four *Bathymodiolus* spp. from the GoM using a phylogenetic approach. From previously published phylogenies (Craddock et al. 1995, Iwasaki et al. 2006, Jones et al. 2006, Olu-Le Roy et al. 2007, Won et al. 2008), we know that *B. brooksi* and *B. heckerae* belong in the "thermophilus" group and *B. childressi* belongs in the more divergent "childressi" group. The new species we discovered from the GoM also belongs in the "thermophilus" group (Figures 13-1 and 13-2).

The phylogeny presented in Figure 13-2 is based on the "barcoding" CO1 mitochondrial locus that has been sequenced for most *Bathymodiolus* spp. We used a balanced selection of our own sequences and many others which were directly available from NCBI, including sequences from seven genera of deep-sea Mytilidae. The majority of the species in the phylogeny are *Bathymodiolus* spp., but species from the genera *Gigantidas*, *Benthomodiolus*, *Idas*, *Idasola*, *Adipicola* and *Tamu* are also included. A total of 42 genetically distinct species are included in this analysis, including species from inland seas and the diverse areas of the Atlantic, Indian, and Pacific oceans. Species from three types of reducing environments, hydrothermal vents, cold seeps and biological organic substrates (whale bones and woods) are included.

Despite the use of only one gene locus in this phylogeny (and low bootstrap values for the deepest nodes), our results are consistent with the phylogeny published by (Won et al. 2008) who used three markers in a strong combined analysis.

To clarify our discussion, we will refer to the different clades of the phylogeny using the roman numerals indicated in Figure 13-2. The "thermophilus" and "childressi" groups described in previous publications correspond to our clades II and VI, respectively. We detect 15 species of *Bathymodiolus* in the childressi group and 10 in the thermophilus group. A significant ecological difference between these groups is the habitat occupied by the species in the groups. All the *Bathymodiolus* spp from clade VI (childressi group) are from cold seeps, although two of these

species *B. japonicus* and *B. platifrons* are also described from hydrothermal vents (Iwasaki et al. 2006). In the clade II, five species inhabit seeps and the five others are strictly hydrothermal.

Other species belonging in the less well supported clades (III, IV, V) inhabit a variety of habitats, including hydrothermal vents, seeps, sunken woods or whales' bones and include representatives from additional genera.

Jones et al. (2006) hypothesised an evolutionary colonization of different habitats that included a reversion in the habitats used by Bathymodiolinae. According to these authors, the original habitat of the *Bathymodiolus* spp. was the shallower cold seeps, followed by a subsequent colonisation of the deepest and hydrothermal environments. Reversion of habitat within clade II was suggested for *B. heckerae* which was the only cold seep species strongly supported in the hydrothermal "thermophilus group" at that time. Recent publications (Olu-Le Roy et al. 2007) and (Won et al. 2008) and our discovery of the new GoM species significantly increases the number of seep species confirmed in the "thermophilus" groups and suggests this hypothesis may not reflect the most parsimonious of possibilities.

13.3.4. Large Geographic Distribution and Amphi-Atlantic "Species"

Both the thermophilus and childressi groups are geographically diverse assemblage of deep sea mussels and are a good illustration of the paradox between geographic distance and genetic differentiation. On one hand, we found species showing a clear genetic divergence despite geographically proximity (*B. azoricus* and *B. puteoserpentis*, from the Mid-Atlantic Ridge belonging in the "thermophilus group" as do *B. heckerae* and *B. brooksi* from the GoM). On the other hand, some of the *Bathymodiolus* spp present very little or no genetic differentiation over large geographic distance. Species from around the Atlantic Ocean are excellent examples of this lack of differentiation over large distances and include members in both thermophilus and childressi groups. In the "thermophilus group," (clade II), *B. boomerang* from the Barbados prism and *B. aff boomerang* from the Nigerian slope are very similar genetically and are also closely related to *B. heckerae* in the GoM. Moreover, *B. heckerae* is more closely related to species from the Nigerian slope than to the geographically close *Bathymodiolus* nov. sp. from DC583 or *B. brooksi*. Similarly, *B. aff. childressi* from the Barbados prism is genetically very closely related to *"Bathymodiolus" mauritanicus*. Moreover the "*Bathymodiolus" mauritanicus* species name contains conspecific mussels from geographically distant areas (Nigerian Slope, Gabon margin, from the Gulf of Cadiz) (Genio et al. 2008).

13.3.5. Phylogenetic Position of the Species from the GoM in the Thermophilus Group

B. brooksi, *B. heckerae*, and *B.* nov. sp. from DC583 are in the clade II "thermophilus" but are not sister species. Our phylogeny, like others recently published (Jones et al. 2006, Won et al. 2008), places *B. brooksi* in an independent clade while *B. heckerae* and *B.* nov. sp. are grouped in the strongly supported clade VII with *B. boomerang*, *B. azoricus*, and *B. puteoserpentis* (Figure 13-2). The phylogenetic relationship between the two hydrothermal sister species (*B. azoricus* and *B. puteoserpentis)* is poorly supported in our study (bootstrap value= 56) but is strongly supported in the multigene analyses of Won et al. (2008).

The position of the new GoM species within clade VII is also interesting. This new species does not group cleanly with either the hydrothermal species nor with the seeps species in this clade. Its exact phylogenetic position is uncertain within this clade based on CO1 alone; however, we can confirm that this species is more closely related to the *B. boomerang* (Barbados prism) and *B.* aff. *boomerang* (Nigerian slope) than to *B. heckerae* from the GoM.

The four species previously known in the clade VII harbor a dual symbiosis with sulphur and methane-oxidizing symbionts (Duperron et al. 2009). Won et al. (2008) published a phylogeny of the thiotrophic endosymbionts of the mussels from the clade VII, revealing a well resolved clade for these symbionts. Similar analyses using the GoM symbiont(s) phylogeny will be quite helpful to understand the history and the evolution of the Bathymodiolids.

14. MUSSEL AND TUBE WORM COMMUNITY COMPOSITION AND STRUCTURE

14.1. Introduction

In this chapter, we present data from forty-seven community samples taken during the study to provide a more complete understanding of the biodiversity and biogeography of the seeps of the deep GoM. Previous studies of the GoM seep fauna below 1,800 m suggested that there were very few species in common between the seeps of the upper and lower slope (Carney 1994, Cordes et al. 2007b). A zone of transition between 1,300 and 1,700 m was suggested in the seep fauna based on comparisons to the Barbados Accretionary Prism seep sites (Cordes et al. 2007a), but limited sampling in between 700 and 1,800 m depth in the GoM prevented a more precise determination of the bathymetric zonation or biodiversity patterns in these communities.

Here we examine patterns in biodiversity with respect to depth and the different foundation species of structure-forming fauna. Community composition is also compared among samples and sites to assess the relative importance of the type of foundation species, site of collection, and depth. These data are used to test a series of previous hypotheses based on the more well-known upper-slope (< 1,000 m) seep communities: The high-biomass communities associated with mussel beds are fairly similar to one another and primarily consist of endemic species utilizing the localized seep-related productivity (Bergquist et al. 2005). Communities associated with tube worm-generated habitat structure are initially dominated by endemic species, but these communities proceed through a series of successional stages where overall biomass declines and the proportion of non-endemic species in upper trophic levels increases as epibenthic sulfide concentrations decline (Bergquist et al. 2003a, Cordes et al. 2005).

14.2. Methods

The collection methods are detailed above under Sampling Methodology and Procedures.

Diversity of each sample was estimated using a combination of diversity indices including Shannon-Weiner diversity (natural log), Pielou's index of evenness, and estimated number of species per 50 individuals (rarefaction) calculated using PRIMER v6.0 (Clarke and Warwick 2001). Analyses of diversity at the site-to-site level and within all mussel and tube worm collections were carried out by rarefaction using EcoSim700 (Gotelli and Entsminger 2004). Similarity among communities was assessed by Bray-Curtis similarity index following a fourth-root transformation of species densities in PRIMER 6 (see Cordes et al. 2005 for complete description). This was represented as an ordination plot using non-metric multidimensional scaling (nMDS and significance to the groupings attributed using group-average clustering based on Bray-Curtis similarity, and ANOSIM in PRIMER 6. The species that accounted for the highest proportions of the difference among collections was assessed using the similarity percentage (SIMPER) routine in PRIMER 6 with site and depth interval used as factors in the analysis.

14.3. Results & Discussion

14.3.1. Diversity of the Seep-Associated Fauna

There were 47 community samples taken at 11 sites ranging from 1,005 to 2,746 m depth (Table 14-1). A total of 66 taxa were sampled directly with tube worms or mussels (Table 14-2). Of these taxa, the majority represented morphologically distinct species. However, the taxonomy of the actinarians, nematodes, and amphipods are largely unresolved and are grouped and treated as single taxa. There were up to six species of galatheoids in the collections, which were treated as three taxa on our analyses. We were able to unambiguously distinguish two undescribed species, *Munidopsis* sp. 1 that has been collected frequently on the upper slope (Cordes et al. 2006) and *Munidopsis* sp. nov which was collected for the first time at these deep sites. There are also up to four different species in the *Munidopsis* spp. category whose taxonomy is still under investigation by United States Geologic Survey collaborators (Morrison and Nizinski, pers. comm.). These species include three different species from AC818 that group with the eastern Pacific galatheoids (including *M. bracetosa* and *M. cascadia*) and another species collected at AT340 and GC852 that is aligned with *M. similis*.

Of the 66 taxa collected, 43 (65%) appear to be restricted to water depths over 1,000 m (not collected in previous studies of the shallower seeps), and 39 (59%) of the taxa have not been previously reported from the GoM. Four of the 23 species that have distributions that overlap 1,000 m were collected only at the shallowest sites in this study (Garden Banks 697, 1,010 m; Mississippi Canyon 853, 1,076 m), and two others were collected only at the 1,400 m sites (Green Canyon 852, MC640). Many of these taxa are likely to represent new species, in some cases more than one (e.g., *Munidopsis* spp.) although exact determination of species identity awaits further taxonomic work. Regardless, the high number of species collected here for the first time suggests that these communities represent a pool of biodiversity that may be restricted to the chemosynthetic communities on the lower slope of the GoM.

There were 58 species found in the 35 mussel community collections. The majority of the mussel beds were composed primarily of *B. brooksi* which has been collected between 1,080 and 3,290 m (Cavanaugh et al. 1987, Gustafson et al. 1998, this study). Mussel beds also consisted of *B. heckerae* (depth range 2,180 to 3,290 m) and *B. childressi* (depth range 525 to 2,220 m) either in combination with *B. brooksi* or as monospecific beds (Brooks et al. 1990, Fisher 1993 et al., Gustafson et al. 1998). *Bathymodiolus childressi* and *B. heckerae* were never collected together. The diversity in the mussel community collections was fairly low (H' = 0.206 to 1.924; J = 0.171 to 0.883; Es(50) = 2.0 to 10.9, Table 14-1) with the majority of the collections dominated by the ophiuroid *Ophioctenella acies* followed in order of relative abundance by the common shrimp *Alvinocaris muricola*. Occasionally, a mussel community collection would also contain elevated abundances of another species, for example the fireworm *Eurythoe* sp. (242 individuals) in one Atwater Valley 340 collection and a small epizoic anemone (240 individuals) in another Atwater Valley 340 collection. At the shallowest site sampled in this study (Garden Banks 697, ~1,000 m), two species of upper-slope seep-endemic species, the polychaete *Methanoaricia dendrobranchiata* (139 individuals) and the gastropod *Provanna sculpta* (192 individuals) dominated the collections.

There were 34 species of megafauna and macrofauna collected with the 12 tube worm aggregations. The most common tube worm species were *Escarpia laminata* and *Lamellibrachia spp*. The diversity within individual tube worm aggregations appeared to be slightly higher than

in the mussel community collections (H' = 0.837 to 3.152; J = 0.308 to 0.841; Es(50) = 3.5 to 11.3, Table 14-1). As in the mussel collections, tube worm aggregations were primarily dominated by a limited number of species. The most common species in tube worm aggregations were the two symbiotic (potentially parasitic) polychaetes *Heteromastus* sp. and *Protomystides* sp. followed by the shrimp *A. muricola*.

At the site scale, mussel beds appear to contain greater species richness than tube worm aggregations (Figure 14-1). When all of the communities are pooled within foundation species type (mussel vs. tube worm) from the most completely sampled site Atwater Valley 340 (AT340, 2,200 m, six tube worm aggregations, seven mussel samples), the sampled mussel beds accumulate species at a faster rate than tube worm aggregations. When 1,000 individuals have been sampled, mussel beds contained an average of 23.4 species while tube worm aggregations contained an average of 17.8 species.

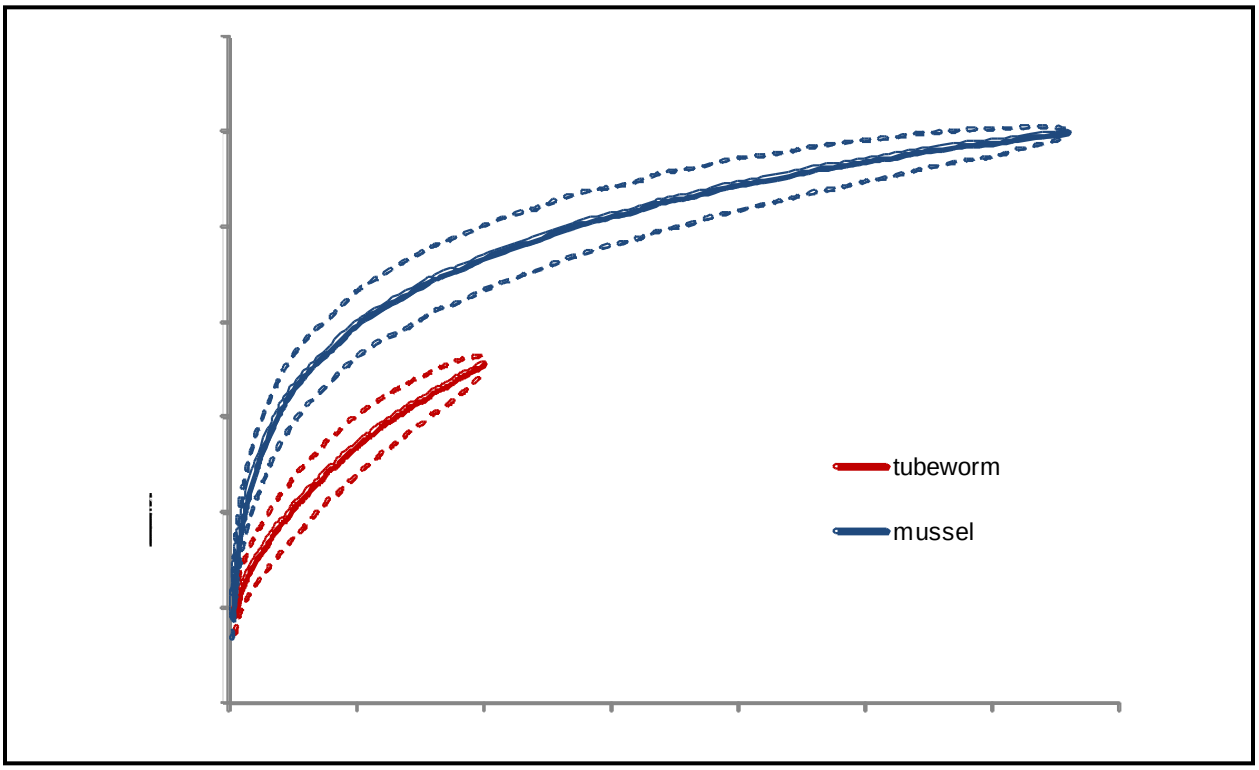

Figure 14-1. Species accumulation curves for tube worm and mussel associated fauna. Average and standard deviation of 1000 replicate curves are shown for all samples included in this study. Mussel bed samples contained more species per number of individuals sampled than tube worm aggregations, and the accumulation curve begins to reach an asymptote.

When species accumulation curves within pooled mussel and tube worm collections are compared among the three most well sampled sites, Green Canyon 852 (GC852, 1410 m, three tube worm aggregations, six mussel collections), AT340, and Alaminos Canyon 818 (AC818, 2,750 m, two tube worm aggregations, five mussel collections), the highest diversity appears to

be at the shallowest site sampled, which corresponds to mid-slope depths (Figure 14-2). The expected number of species for 400 individuals (the extent of sampling at GC852) are 29.6 (GC852), 22.4 (AC818), and 21.3 (AT340). This general trend is also evident when mussel beds are investigated alone among the different sites with multiple samples (Figure 14-3). Higher levels of diversity, measured as Es (100), were found in the samples from GC852 (1,410 m, 15.9 sp) and Walker Ridge 269 (1,910 m, 16.1 sp). Lower diversity was found at the two Alaminos Canyon sites: AC645 (2,210 m, 10.2 sp) and AC818 (2,740 m, 9.8 sp).

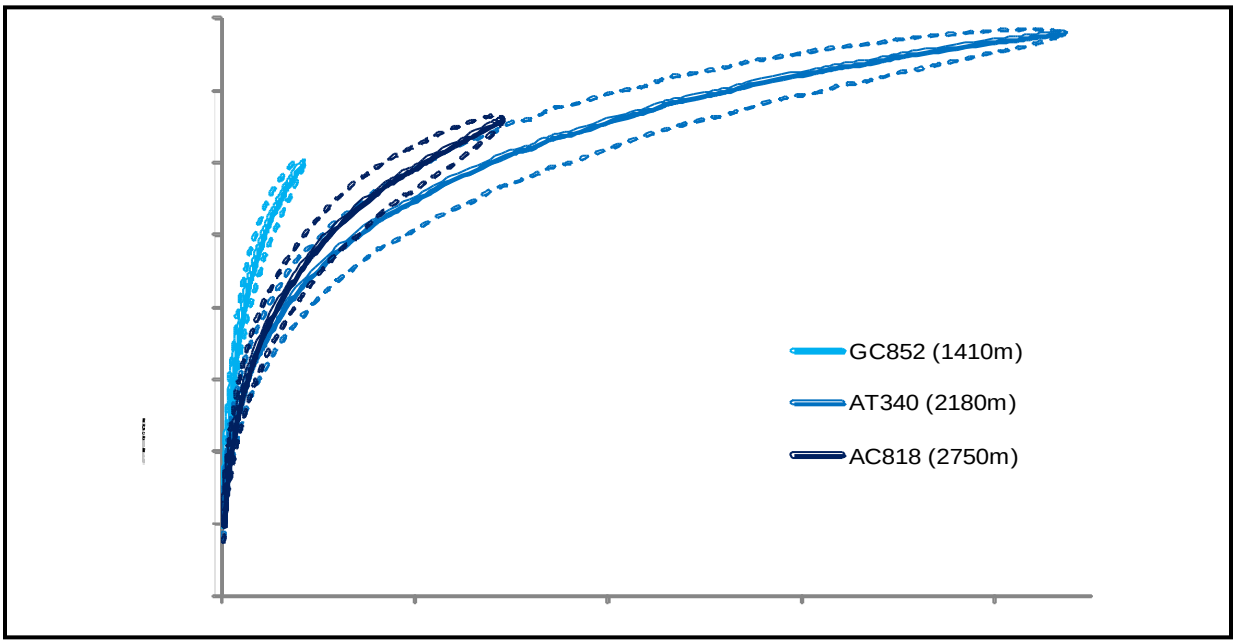

Figure 14-2. Species accumulation curves for tube worm and mussel associated fauna combined within the three sites with the highest sampling effort. Highest diversity was found at the shallowest of the three sites (GC852, 1410 m) followed by the deepest site in the study (AC818, 2750 m) and the intermediate and most comprehensively sampled site (AT340, 2200 m).

Although the most abundant species in a sample were usually the same (*A. muricola* or *O. acies*), the species in the next rank abundance were often different among samples (i.e., anemones, gastropods, different species of polychaetes). This led to greater expected numbers of species in samples pooled within a site and higher beta diversity. This pattern of species accumulation appears similar to that of mussel beds from the Florida Escarpment site at 3,290 m in the GoM with 30–35 species present in a sample of 2,000 individuals (Turnipseed et al. 2004). This level of diversity is greater than that found in mussel beds at hydrothermal vents using similar sampling equipment (Turnipseed et al. 2004). Although collected with different methodology, the diversity of upper slope mussel beds appears to be lower than that found here, with 10–15 species expected in a sample of 2000 individuals pooled among five sites (Bergquist et al. 2005). Diversity within single sites on the upper slope was 6–8 species per 500 individuals (Bergquist et al. 2005), whereas it was at least 18 species per 500 individuals in this study (Figure 14-3).

Despite the extensive sampling effort in this study, there will likely be many more species discovered in the deep-water seeps of the GoM. Only at the site where the most intensive sampling occurred (AT340) did the rarefaction curves begin to level off. At the less comprehensively sampled sites and in tube worm aggregations taken as a whole, the rarefaction curves were quite linear, preventing an accurate estimate of the asymptotic number of species in these habitats. In addition, the very low initial slope of the curve for mussel bed samples at the deepest site (AC818) suggests that there is a high number of rare species in this habitat, as has been shown for numerous other deep-sea systems (for example Hessler and Sanders 1967). The high number of putative new species, the remaining undocumented biodiversity at the sites sampled, and the number of likely additional seep sites that have never been visited, indicate that there is still a wealth of information to be gained from further investigations of the seeps of the lower slope.

14.3.2. Patterns in Community Similarity

The different foundation species harbor distinct communities (Figure 14-4a). In the multidimensional scaling plot, tube worm-hosted communities exhibit a high level of similarity, clustering together in one corner of the ordination. The mussel-hosted communities are far more spread apart and form different clusters in the ordination due to higher rates of species turnover among these samples. This is evidence for higher beta diversity in mussel communities since they occupy a larger area of chemosynthetic community space in the ordination.

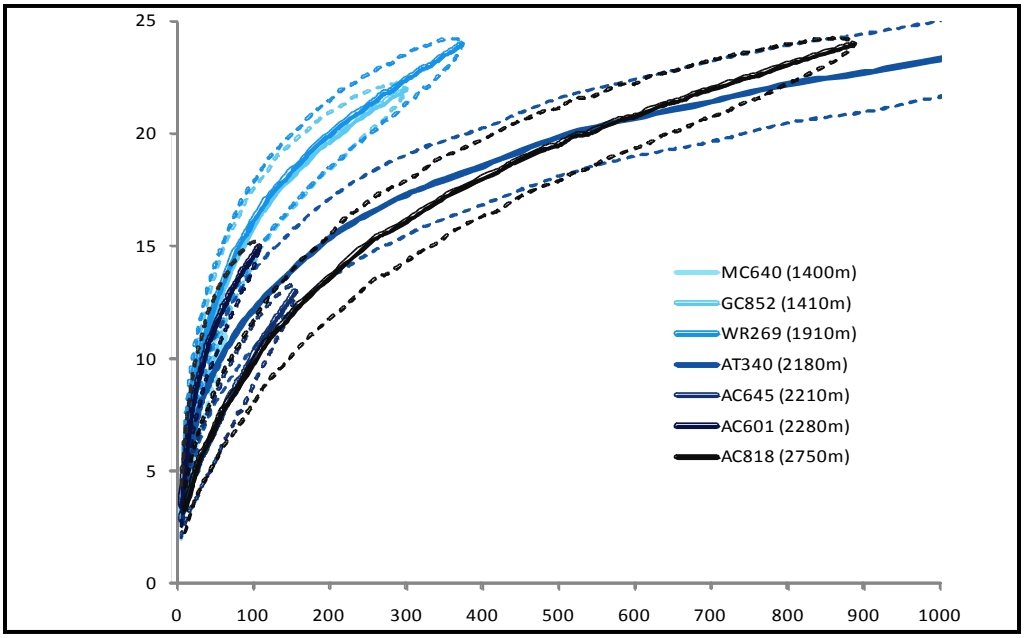

Figure 14-3. Species accumulation curves for mussel beds sampled at seven sites. Highest diversity was present at two of the mid-slope sites, GC852 (1410 m) and WR269 (1910 m). Only a portion of the curve for AT340 is shown, with the curve steadily climbing at approximately the same slope to a total of 30 species found in the complete sample of 3,332 individuals.

To further examine the differences between tube worm and mussel communities, the ordination was repeated after omitting the abundant symbiotic (likely parasitic) polychaetes on the tube worms (*Heteromastus* sp. and *Protomystides* sp.) and the mussel symbiotic polychaete (also a potential parasite, Britayev et al. 2007) *Branchipolynoe seepensis* (Figure 14-4b). The polychaetes on the tube worm tubes are either feeding off of the tube worm blood (*Protomystides* sp.) or infesting senescent tube worms or empty tubes (*Protomystides* sp. and *Heteromastus* sp.).

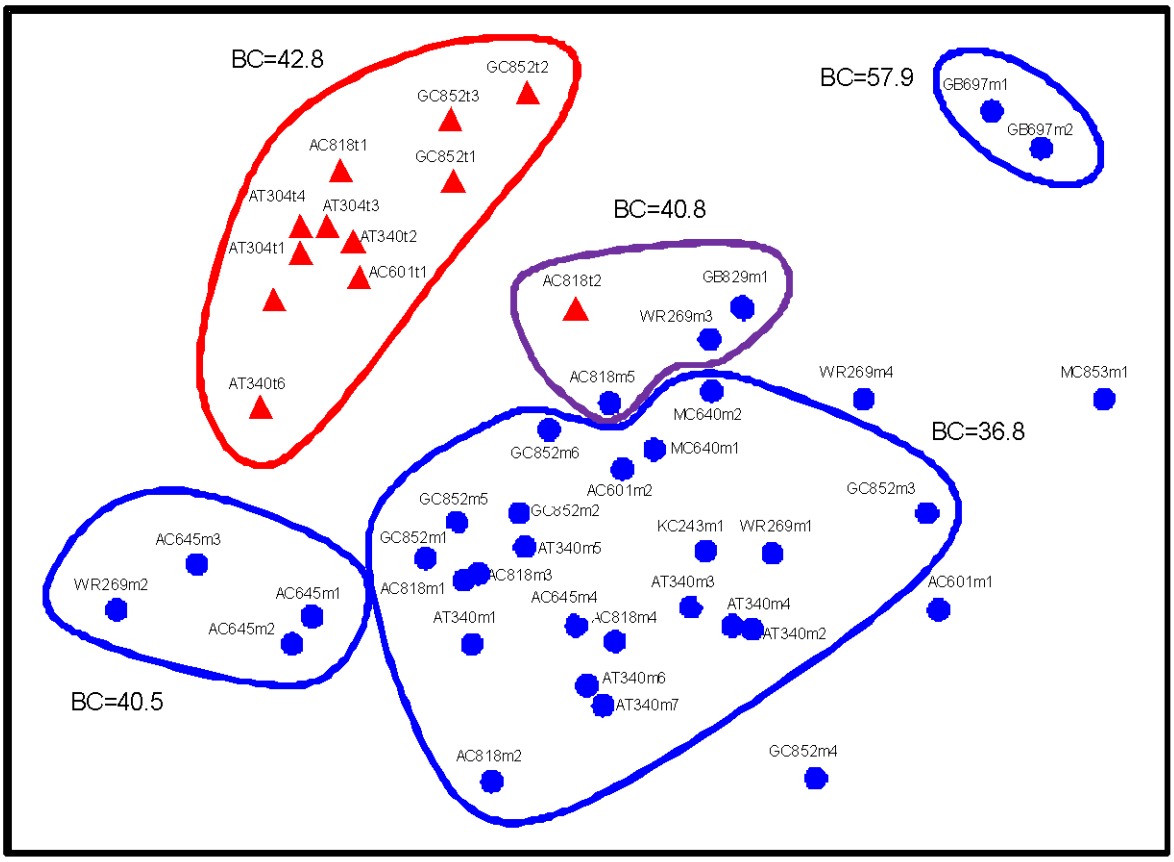

Figure 14-4a. Multidimensional scaling plot of community similarity among tube worm (red triangles) and mussel (blue circles) associated communities. Similarity is estimated by the Bray-Curtis (BC) similarity index based on fourth-root transformed species densities. Outlines represent clusters of samples exhibiting the BC similarity value listed. A: Including symbiotic species living within the mussel shells (*Branchipolynoe seepensis*) or tube worm tubes (*Protomystides* sp. and *Heteromastus* sp.).

The polychaete *Branchipolynoe seepensis* inhabits the mantle cavity of a variety of *Bathymodiolus* species (*B. heckerae* and *B. brooksi* in this study) and its occurrence has been correlated with damage of the host tissues of *B. puteoserpentis* and *B. azorcus* (Britayev et al. 2007). Although the mussel and tube worm associated communities did not separate as cleanly in the MDS ordination following the removal of these symbiotic species from the data set,

differences between the communities associated with the two foundation species were still significant (ANOSIM, R = 0.307, p = 0.001). These differences are likely due to a combination of factors including foundation species habitat preferences, the nature of the biogenic habitat provided, and other overlooked inter-specific interactions among the foundation species and associated fauna.

Overall, similarity among communities was most strongly correlated to the depth of collection. For mussel associated communities (Figure 14-5), similarity in depth (r = 0.245, P < 0.0001, n = 595) followed by similarity in the proportion of *B. brooksi* in the collections (r = 0.146, P = 0.0002, n = 595) were most highly correlated to Bray-Curtis community similarity. For the similarity among tube worm-hosted communities (Figure 14-6), the best explanatory variables were the average size of *E. laminata* in the collections (r = 0.284, P = 0.0059, n = 78), followed by the depth of collection (r = 0.184, P = 0.0534, n = 78). Even when samples came from sites at the eastern and western ends of the sampled area (Atwater Valley and Alaminos Canyon), the communities were similar if they were from similar depths (~2,200 m, AT340 and AC645).

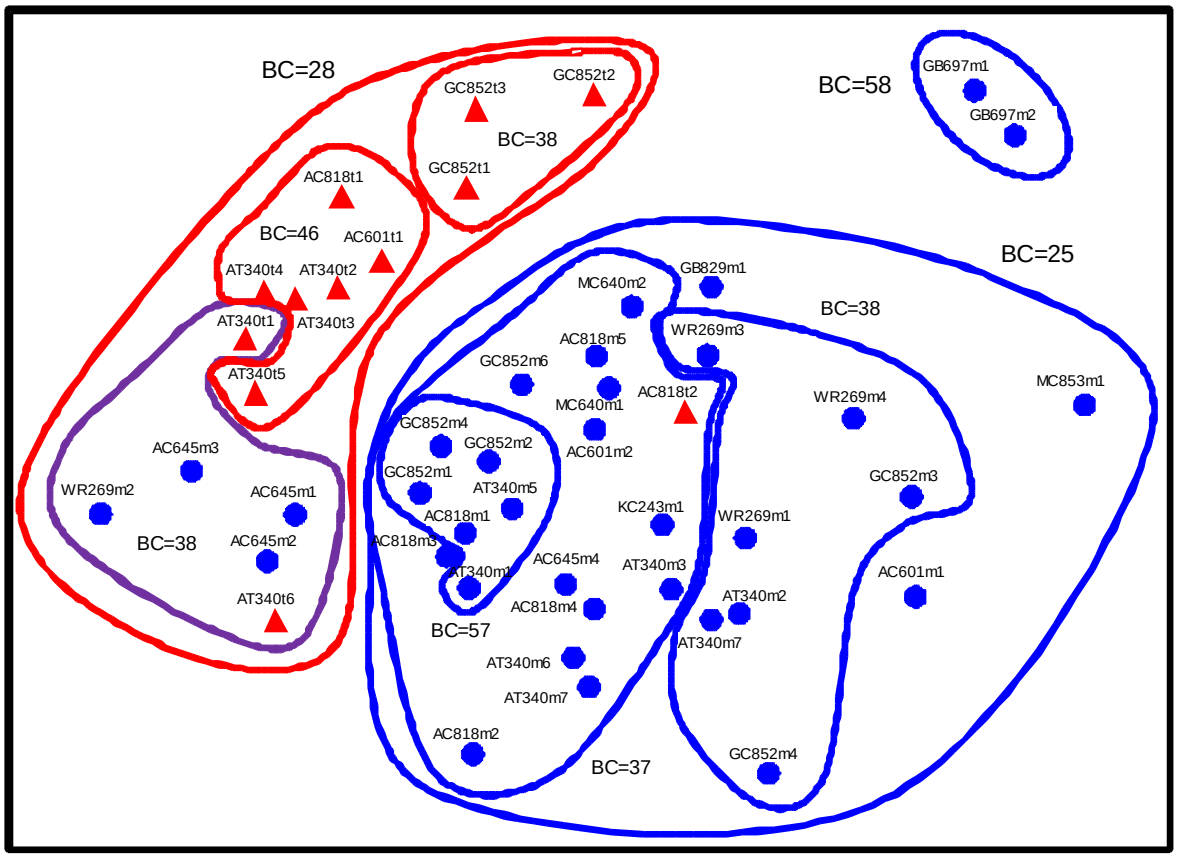

Fig. 14-4b. Excluding the symbiotic species. Despite the increased overlap of the communities inhabiting the two foundation species structures, the differences between tube worm and mussel communities are still significant (ANOSIM, R = 0.307, p = 0.001).

Patterns in community structure were best described by changes in distribution of five indicator taxa: *O. acies*, *A. muricola*, *Amphipoda* spp., *Prionospio* sp., and *Harmothoe* sp. These taxa each accounted for over 5% of the pairwise differences among communities in the SIMPER analysis. The relative abundance of *O. acies* consistently increased over the depth range sampled and *A. muricola* was also more abundant at the deeper sites (Figure 14-7a). The polychaete species *Harmothoe* sp. and *Prionospio* sp. were more abundant at the shallower sites, while amphipods were more common at the intermediate depths of the study. Horizontal gradients in the abundance of these indicator taxa were less apparent, further emphasizing the greater significance of depth over geographic location (Figure 14-7b). *O. acies* appears to be more common in the eastern-most and western-most sites and the polychaete species were more common at the central sites. However, this result is somewhat confounded with depth since the central sites were all in the 1,000 to 1,900 m depth range and the eastern and western sites included the Atwater Valley and Alaminos Canyon sites that exceed 2,000 m water depth.

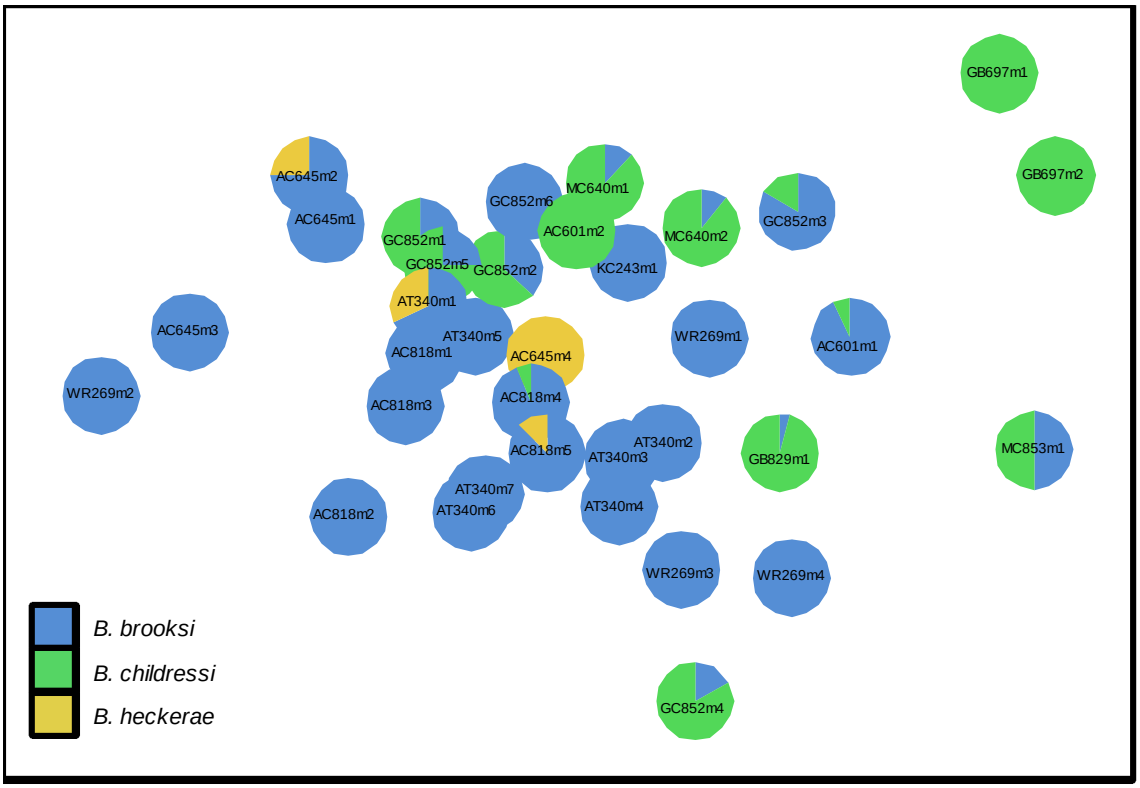

Figure 14-5. Multidimensional scaling plot of mussel-associated communities. Similarity among mussel bed samples is most highly correlated to the depth of the collection, with the shallowest site (GB697) shown in the upper right corner of the ordination and the deepest site (AC818) towards the lower left corner. The next most significant variable was the proportion of *Bathymodiolus brooksi* in the mussel bed, with species relative abundance represented in the pie charts at each sample position in the ordination.

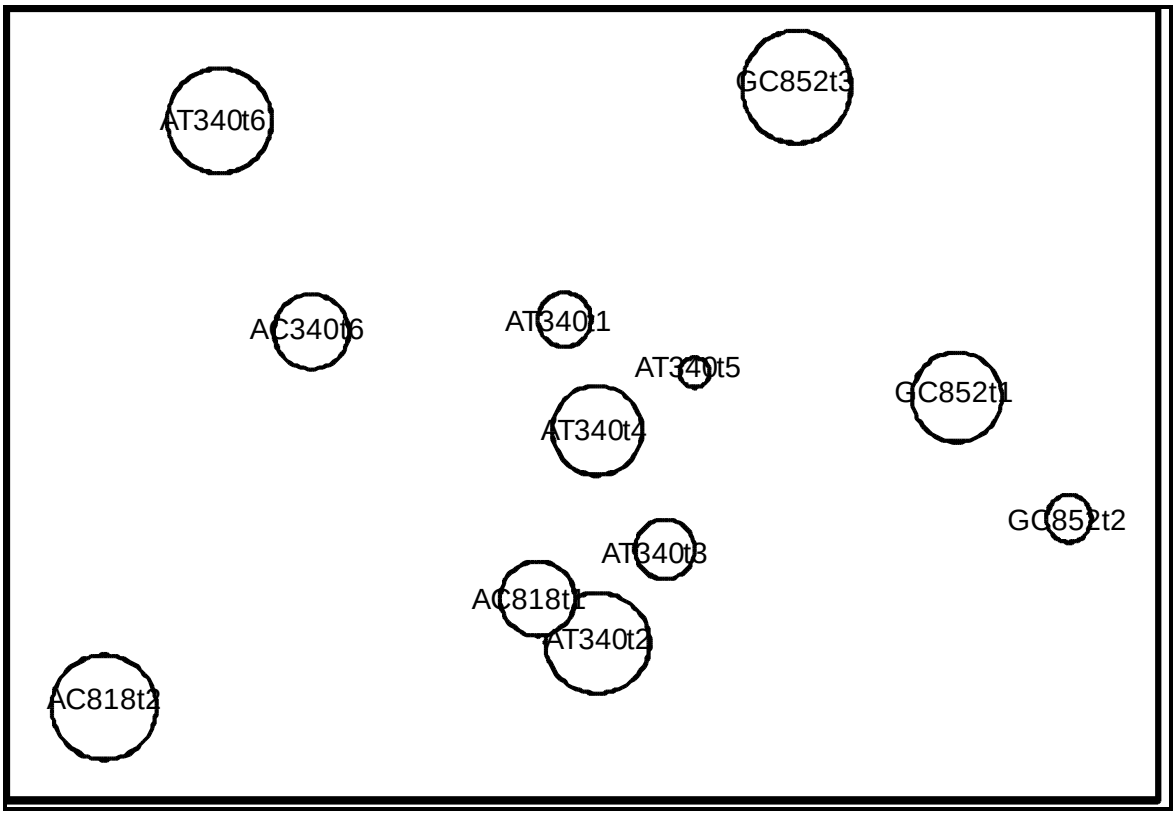

Figure 14-6. Multidimensional scaling plot of tube worm-associated communities. Similarity among tube worm communities was significantly correlated to average length of tube worms in the aggregation. The diameter of the circles corresponds to ranked average tube worm length.

The significance of these bathymetric patterns was further emphasized in the low degree of overlap with the communities of the upper slope, only 35% of the species in this study having been found in depths shallower than 1,000 m, despite the close proximity of the shallow sites, often within 40–50 nautical miles of the deep sites examined in this study. Four of the 23 species collected as part of this study with distributions extending to the upper slope were found in the communities sampled from Garden Banks 697 at 1,010 m depth and Mississippi Canyon 853 at 1,076 m depth, which were composed of a mixture of upper and lower slope species, giving rise to a distinct community.

The significant differences between the upper slope communities and those sampled as part of this study, and the overlap of upper and lower slope communities at the 1,000–1,100 m sites (GB697 and MC853), provides evidence that there is a zone of transition around 1,000 m in the seep communities of the GoM, similar to that found in the surrounding soft benthic habitats (Pequegnat et al. 1990). These findings suggest that the general features of deep-sea communities may be extended to the specialized habitat of cold seeps. Because of their reliance on local productivity (MacAvoy et al. 2003), these ecological patterns are likely not directly linked to factors such as the import of surface productivity, but rather the connectivity provided by different water masses (Howell et al. 2002) or bathymetric changes in inter-specific interactions such as predation and competition within seep communities (Carney 2005).

In addition to depth, when the foundation species were analyzed separately, community composition was influenced by the average size of the tube worms in an aggregation and the species of mussels that made up the mussel bed.

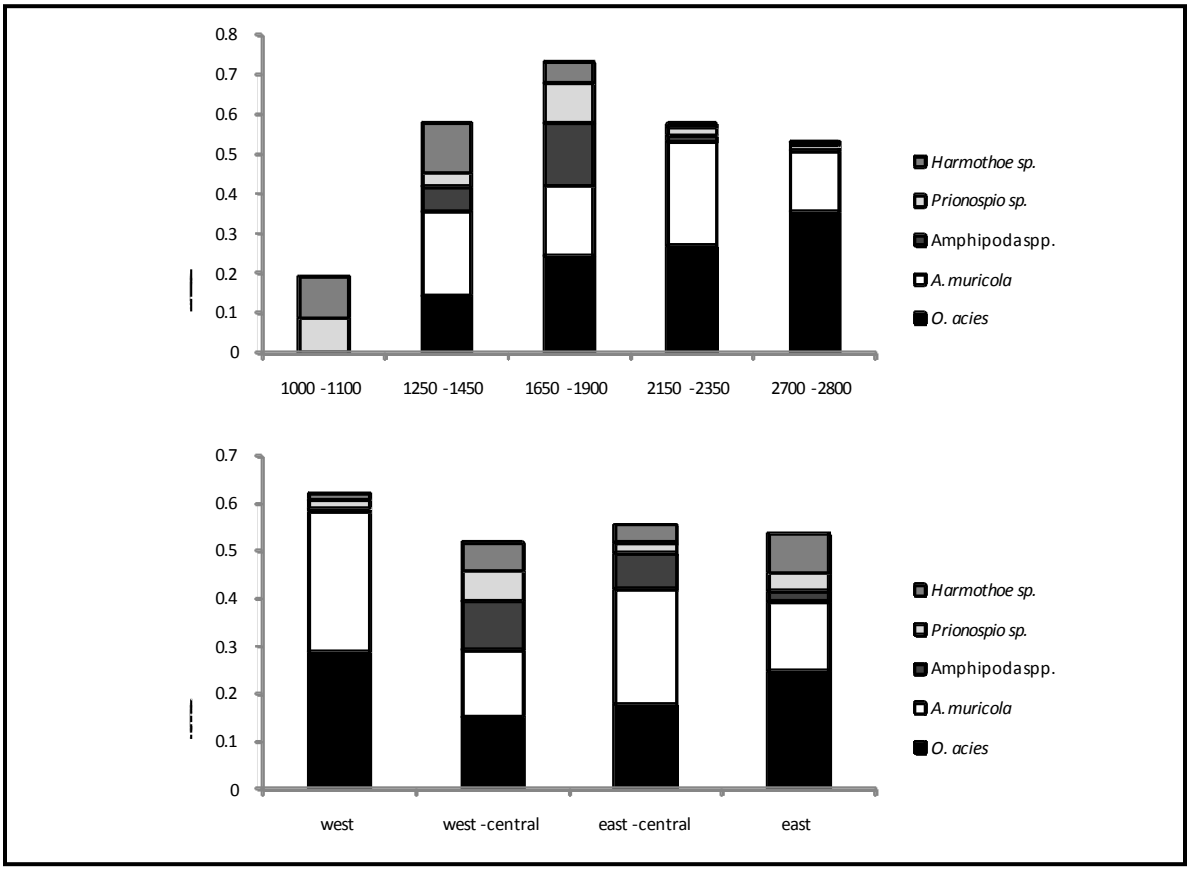

Figure 14-7. Relative abundance of the five indicator species.
These species account for the majority of the bathymetric and biogeographic differentiation among communities in this study. Collections of tube worm and mussel-hosted communities were combined within depth range (a top) or by longitude (b bottom) to examine broad trends in community composition in the northern GoM.

The significance of the average size of tube worms, the only statistically significant factor in the analysis of tube worm aggregations, suggests that there may be a successional shift in the composition of the communities, similar to that shown on the upper slope (Bergquist et al. 2003). On the upper slope, these successional trends in species abundance and biomass were directly linked to the amount of sulfide present in the epibenthic habitat surrounding the tube worm aggregations (Cordes et al. 2005). More detailed investigations of the growth rates and population dynamics of the lower slope tube worm species as well as trends in the concentration of sulfide in the habitat are necessary for this successional model to be evaluated in these communities. In addition to the broad differences between tube worm and mussel communities, the differences among beds of different mussel species composition may also be linked to differences in habitat chemistry. *B. childressi* contains methanotrophic symbionts only, and

therefore the sulfide levels in its habitat may be lower than in mussel beds composed of *B. brooksi* and/or *B. heckerae* since they both also contain symbionts that utilize reduced sulfur compounds. There may also be additional inter-specific interactions driving these differences, but more detailed ecological and behavioral investigations are required to evaluate this hypothesis.

The communities of the lower slope seeps are shaped by the type of foundation species they contain. This was shown in the broad differences between tube worm and mussel associated communities and also in the differences in community structure among beds composed of different mussel species. These differences are likely attributable to a combination of factors including habitat requirements of the tube worms and mussels, differences in the biogenic habitats produced, and inter-specific interactions, both conspicuous symbiotic interactions as well as less apparent relationships. Mussel beds harbor a diverse community at the beta level, while individual tube worm aggregations appear to contain higher diversity in a more predictable community. Some of the successional patterns demonstrated on the upper slope may be present in the tube worm aggregations of the lower slope, but additional information is required to fully evaluate this model. Despite these similarities, the low degree of overlap with the upper slope communities and the high number of species discovered here for the first time suggests that the seep communities of the deep slope are quite unique and ongoing efforts to preserve them should be supported.

Table 14-1

Collection and Diversity Information for Each Community Sample Obtained in this Study

Sample types are Bushmaster (bm), mussel pot (mp), or mussel scoop (ms). Dive numbers are from DSV *Alvin* (41##) or ROV *Jason II* (J2-##). Species richness, abundance, and diversity indices do not include the foundation species of tube worms or mussels. S (number of species), N (number of individuals), H' (Shannon-Weiner diversity as a natural log), J' (Pielou's index of evenness), ES(50) (expected number of species in a sample of 50 individuals).

Name	Sample	Dive	Latitude	Longitude	Depth	S	N	H'(loge)	J'	ES(50)
AC601m1	mpb	J2-283	26:22.1	94:31.1	2284	10	58	1.78	0.773	9.3
AC601m2	mpd	J2-283	26:22.1	94:31.1	2284	7	50	1.41	0.722	7.0
AC601t1	bm	4196	26:23.4	94:30.8	2323	11	403	0.74	0.308	4.0
AC645m1	mpA	4197	26:21.2	94:29.7	2195	3	14	0.66	0.597	3.0
AC645m2	mpB	4197	26:21.2	94:29.7	2195	3	15	0.63	0.571	3.0
AC645m3	ms	4197	26:21.2	94:29.7	2195	2	19	0.21	0.298	2.0
AC645m4	mpb	J2-281	26:21.2	94:29.8	2197	12	107	1.43	0.577	7.2
AC818m1	mp	4192	26:10.8	94:37.3	2744	8	131	1.01	0.486	5.8
AC818m2	ms	4195	26:10.8	94:37.3	2745	11	347	1.17	0.488	5.8
AC818m3	mpb	J2-282	26:10.8	94:37.4	2745	10	163	1.13	0.489	6.7
AC818m4	mpd	J2-282	26:10.8	94:37.4	2744	18	220	2.12	0.732	11.3
AC818m5	mpd	J2-284	26:10.8	94:37.3	2745	12	88	1.22	0.492	8.9
AC818t1	bm	4195	26:10.8	94:37.3	2745	11	466	0.56	0.234	4.6
AC818t2	bm	J2-282	26:10.7	94:37.2	2746	9	39	1.73	0.789	9.0
AT340m1	ms	4180	27:38.6	88:21.8	2183	8	188	1.38	0.663	6.0
AT340m2	mp	4181	27:38.8	88:22.2	2199	15	319	1.05	0.387	6.8
AT340m3	ms1	4181	27:38.8	88:22.4	2170	11	265	1.36	0.569	5.9
AT340m4	ms2	4181	27:38.8	88:22.2	2199	17	326	1.52	0.537	8.5
AT340m5	mp	J2-276	27:25.1	88:21.8	2190	5	88	0.91	0.565	4.1
AT340m6	mpa	J2-277	27:38.6	88:21.8	2190	13	737	0.69	0.269	5.4
AT340m7	mpf	J2-277	27:38.7	88:21.8	2190	9	163	1.00	0.455	5.4
AT340t1	bm	4179	27:38.6	88:21.8	2185	5	119	0.57	0.355	3.5
AT340t2	bm	4180	27:38.6	88:21.8	2184	8	417	1.30	0.625	6.3
AT340t3	bm	4183	27:38.8	88:22.4	2179	6	330	0.90	0.500	4.2
AT340t4	bm	J2-270	27:38.6	88:21.8	2192	6	145	1.19	0.666	4.3
AT340t5	bm	J2-276	27:25.1	88:21.8	2188	8	262	0.57	0.276	3.6
AT340t6	bm	J2-277	27:38.8	88:22.4	2175	10	1006	1.47	0.637	6.0

Table 14-1.

Collection and Diversity Information for Each Community Sample Obtained in This Study (continued)

Sample types are Bushmaster (bm), mussel pot (mp), or mussel scoop (ms). Dive numbers are from DSV *Alvin* or ROV *Jason II* . Species richness, abundance, and diversity indices do not include the foundation species of tube worms or mussels. S (number of species), N (number of individuals), H' (Shannon-Weiner diversity as a natural log), J' (Pielou's index of evenness), ES(50) (expected number of species in a sample of 50 individuals).

Name	**Sample**	**Dive**	**Latitude**	**Longitude**	**Depth**	**S**	**N**	**H'(loge)**	**J'**	**ES(50)**
GB697m1	mp	J2-274	27:18.7	92:06.3	1005	9	374	1.15	0.521	5.4
GB697m2	ms	J2-274	27:19.2	92:06.6	1015	8	28	1.84	0.883	8.0
GB829m1	mpa	J2-279	27:11.1	92:07.5	1258	14	75	1.78	0.675	10.9
GC852m1	mp	4186	27:06.3	91:09.9	1410	10	54	1.71	0.744	9.8
GC852m2	mp	4187	27:06.6	91:09.9	1406	8	24	1.47	0.705	8.0
GC852m3	msb	J2-273	27:07.0	91:09.9	1407	6	31	1.52	0.848	6.0
GC852m4	msw	J2-273	27:06.6	91:09.9	1407	10	62	1.55	0.675	9.2
GC852m5	mpa	J2-278	27:06.6	91:09.9	1407	8	31	1.73	0.833	8.0
GC852m6	mpf	J2-278	27:06.3	91:09.9	1408	10	45	1.94	0.842	10.0
GC852t1	bm	4186	27:06.3	91:09.9	1409	6	39	1.43	0.798	6.0
GC852t2	bm	4187	27:06.6	91:09.9	1406	5	72	1.02	0.633	4.6
GC852t3	bm	J2-278	27:06.3	91:09.9	1412	7	65	1.24	0.639	6.5
KC243m1	mp	4176	26:43.8	92:49.8	1651	5	171	0.28	0.171	3.1
MC640m1	mp	4182	28:21.4	88:47.5	1399	7	26	1.49	0.764	7.0
MC640m2	ms	4182	28:21.3	88:47.5	1398	8	37	1.26	0.604	8.0
MC853m1	mp	4178	28:07.6	89:08.5	1076	9	19	1.92	0.876	9.0
WR269m1	mp	4191	26:41.1	91:39.7	1908	10	33	1.91	0.831	10.0
WR269m2	mpb	J2-275	26:41.1	91:39.7	1909	3	12	0.92	0.836	3.0
WR269m3	mpf	J2-275	26:41.1	91:39.7	1910	10	96	1.24	0.537	7.9
WR269m4	ms	J2-275	26:41.1	91:39.7	1910	16	232	1.87	0.675	10.1

Table 14-2

Taxa Collected with Tube Worm Aggregation and Mussel Bed Samples in This Study

sample	AC601m1	AC601m2	AC601t1	AC645m1	AC645m2	AC645m3	AC645m4	AC818m1	AC818m2	AC818m3	AC818m4	AC818m5	AC818t1	AC818t2	AT340m1	AT340m2	AT340m3	AT340m4	AT340m5	AT340m6	AT340m7
Cnidaria																					
Actinaria spp.							1	1	4		2	4	7	3		240	61				
Nematoda																					
Nematoda spp.																			125		
Nemertea																					
Nemertea sp.									1		2		1					1		2	
Sipunculida																					
Phascolosoma sp.	5		2				1							1					15		
Annelida																					
Polychaeta																					
Ampharetidae sp. nov.																		1			
Branchinotogluma sp.			2				1	2				2	2	3		8		1			
Branchipolynoe seepensis				1			1							1		6					
Capitella sp.	2												5					27		58	
Cirratulid sp.																					
Dorvelleid sp.																					
Escarpia laminata					2																
Eurythoe sp.																					
Flabelliderma sp.																		2		2	
Flabelligerid sp.		1										1	7	1							
Glycera tesselata	2												1					2	2	4	
Glycera sp.																					

Table 14-2

Taxa Collected with Tube Worm Aggregation and Mussel Bed Samples in This Study (continued)

	sample	AC601m1	AC601m2	AC601t1	AC645m1	AC645m2	AC645m3	AC645m4	AC818m1	AC818m2	AC818m3	AC818m4	AC818m5	AC818t1	AC818t2	AT340m1	AT340m2	AT340m3	AT340m4	AT340m5	AT340m6	AT340m7
	Harmothoe sp.		8	1										3	1	1			3	1	2	
	Hesciocaeca methanicola		1					1					3		2		4		1		1	
	Hesionides sp.																				3	
	Heteromystides sp.										117					2		10				9
	Lumbinereis sp.	1													1					1		
	Maldanid sp.																					
	Methanoaricia sp.																					
	Micronephtys sp.																					
	Nautillinellid sp.																33					
	Nicomache sp.		9					1					1						4	2	17	
	Nereis sp.																		2			
	Notomastus sp.									1											1	
	Oligobrachia sp.													2								
	Phyllodocid sp.																					
	Pogonophoran sp.									3												
	Prionospio sp.		1					22					6	1					23	1	29	
	Protomystides sp.	311									188			73		99		83				235
	Spiochaetopteris sp.	1								3												
	Syllides sp.																					
	Terebellides sp.																					
	unid polychaete spp																					1
Mollusca																						

Table 14-2

Taxa Collected with Tube Worm Aggregation and Mussel Bed Samples in This Study (continued)

sample	AC601m1	AC601m2	AC601t1	AC645m1	AC645m2	AC645m3	AC645m4	AC818m1	AC818m2	AC818m3	AC818m4	AC818m5	AC818t1	AC818t2	AT340m1	AT340m2	AT340m3	AT340m4	AT340m5	AT340m6	AT340m7
Aplacophora																					
Aplacophora sp.																					
Polyplacophora																					
Ischnochiton sp.																					
Gastropoda																					
Cataegis meroglypta																					
Cocculinidae gen nov							1														
Fucaria sp.		11																			
Paraleptopsis sp.										1							1				2
Phymorhynchus sp.		1									1									2	
Provanna sculpta																					
Puncturella sp.																					
Pyropelta sp.		4																			
Bivalvia																					
Calyptogena sp.							1		5												
Cuspidaria sp.		1						4	5				19							1	
Lucinid sp.																					
Tamu fisheri																					
Arthropoda																					
Crustacea																					
Alvinocaris muricola	74		3	11	12	18	29	28	7	14	15	33	21	11	16	28	22	8	76	10	55
Amphipoda spp.	1							3		9	1		2	1		10	7		2	3	28

Table 14-2

Taxa Collected with Tube Worm Aggregation and Mussel Bed Samples in This Study (continued)

	sample	AC601m1	AC601m2	AC601t1	AC645m1	AC645m2	AC645m3	AC645m4	AC818m1	AC818m2	AC818m3	AC818m4	AC818m5	AC818t1	AC818t2	AT340m1	AT340m2	AT340m3	AT340m4	AT340m5	AT340m6	AT340m7
	Chaceon sp.																					
	Isopoda spp.			7					1		8			38				3				
	Munidopsis spp.	4									1	1		2				1				
	Munidopsis sp. nov.													1								
	Munidopsis sp.1																					
	unid. brachyuran																					
	unid. shrimp										1											
Echinodermata																						
Asteroidea																						
	unid. sea star										4											
Ophiuroidea																						
	Amphiura sp.																					
	Ophioctenella acies		21	27	2	1		47	89	413		10	108				88		239	38	184	
	Ophienigma spinilimbatum	1		8						23	2	3	2	27	61				4		5	
Holothuroidea																						
	Chirodota sp.	1					1	1	3	1	2	4	3	8	2	1			1	2	2	
Chordata																						
	unid fish																					

Table 14-2

Taxa Collected with Tube Worm Aggregation and Mussel Bed Samples in This Study (continued)

sample	AT340t1	AT340t2	AT340t3	AT340t4	AT340t5	AT340t6	GB697m1	GB697m2	GB829m1	GC852m1	GC852m2	GC852m3	GC852m4	GC852m5	GC852m6	GC852t1	GC852t2	GC852t3	KC243m1	MC640m1	MC640m2	MC853m1	WR269m1	WR269m2	WR269m3	WR269m4
Cnidaria																										
Actinaria spp.		1		4	24																					
Nematoda																										
Nematoda spp.				100	21				1																	
Nemertea																										
Nemertea sp.																										3
Sipunculida																										
Phascolosoma sp.				3			7	7			1		2	14				3					2			6
Annelida																										
Polychaeta																										
Ampharetidae sp. nov.								1	1													5				
Branchinotogluma sp.		3			5		2		1	4						1		1		5		1				
Branchipolynoe seepensis												2				2										
Capitella sp.									1						4								3		1	
Cirratulid sp.									1						1	1	2								4	18
Dorvelleid sp.									1																	
Escarpia laminata																										
Eurythoe sp.				242	21													1						5		
Flabelliderma sp.																							1			
Flabelligerid sp.					2																				3	11
Glycera tesselata						1									2							1			1	4
Glycera sp.																	1									1

Table 14-2

Taxa Collected with Tube Worm Aggregation and Mussel Bed Samples in This Study (continued)

	sample	AT340t1	AT340t2	AT340t3	AT340t4	AT340t5	AT340t6	GB697m1	GB697m2	GB829m1	GC852m1	GC852m2	GC852m3	GC852m4	GC852m5	GC852m6	GC852t1	GC852t2	GC852t3	KC243m1	MC640m1	MC640m2	MC853m1	WR269m1	WR269m2	WR269m3	WR269m4
	Harmothoe sp.		1		2			18	3	3		2	4	1	3			2	2	2	13	23	3	5		6	10
	Hesciocaeca methanicola					10		2	2	13							3				1	1					
	Hesionides sp.																										
	Heteromystides sp.	49		5								24		14					13								
	Lumbinereis sp.								4							8											
	Maldanid sp.																							1			
	Methanoaricia sp.							139																			
	Micronephtys sp.																						1				
	Nautillinellid sp.																										
	Nicomache sp.					1	1									5								1			38
	Nereis sp.																										
	Notomastus sp.																								1		
	Oligobrachia sp.																										
	Phyllodocid sp.																	1									
	Pogonophoran sp.																										
	Prionospio sp.					2				1					4	5				3		7	5	1		1	102
	Protomystides sp.	60		56			38					5		1					7								
	Spiochaetopteris sp.						4																				
	Syllides sp.																					1					
	Terebellides sp.														1	?											
	unid polychaete spp							4	1														1				
Mollusca																											

Table 14-2

Taxa Collected with Tube Worm Aggregation and Mussel Bed Samples in This Study (continued)

sample	AT340t1	AT340t2	AT340t3	AT340t4	AT340t5	AT340t6	GB697m1	GB697m2	GB829m1	GC852m1	GC852m2	GC852m3	GC852m4	GC852m5	GC852m6	GC852t1	GC852t2	GC852t3	KC243m1	MC640m1	MC640m2	MC853m1	WR269m1	WR269m2	WR269m3	WR269m4
Aplacophora																										
Aplacophora sp.															1											
Polyplacophora																										
Ischnochiton sp.									1						1			1				1				
Gastropoda																										
Cataegis meroglypta										1																
Cocculinidae gen nov																										
Fucaria sp.																										
Paraleptopsis sp.							8				2		1										1			
Phymorhynchus sp.																										
Provanna sculpta							192	8																		
Puncturella sp.		2									2							5								
Pyropelta sp.									30													1				
Bivalvia																										
Calyptogena sp.						1																				3
Cuspidaria sp.																										1
Lucinid sp.						2																				
Tamu fisheri											1															
Arthropoda																										
Crustacea																										
Alvinocaris muricola	32	32	25	39	13	109			17	7	5	26			34	39	5	10	1	3	1		9	6	10	1
Amphipoda spp.	2	1	1	148	2				3	9	11	1	1			8	2				1				65	26

Table 14-2

Taxa Collected with Tube Worm Aggregation and Mussel Bed Samples in This Study (continued)

sample	AT340t1	AT340t2	AT340t3	AT340t4	AT340t5	AT340t6	GB697m1	GB697m2	GB829m1	GC852m1	GC852m2	GC852m3	GC852m4	GC852m5	GC852m6	GC852t1	GC852t2	GC852t3	KC243m1	MC640m1	MC640m2	MC853m1	WR269m1	WR269m2	WR269m3	WR269m4
Chaceon sp.																				1						
Isopoda spp.													2						3							6
Munidopsis spp.	1					6			1									2			1					
Munidopsis sp. nov.																										
Munidopsis sp.1							2	2																		
unid. brachyuran																									1	
unid. shrimp																										
Echinodermata																										
Asteroidea																										
unid. sea star																										
Ophiuroidea																										
Amphiura sp.										1																1
Ophioctenella acies		221	1	452	633	1				17	1	39	2	5		11	6		162	2	2		9			
Ophienigma spinilimbatum	1			10										4			12			1					4	1
Holothuroidea																										
Chirodota sp.		1		6	2																					
Chordata																										
unid fish					1																					

15. TEMPORAL CHANGE IN SEEP COMMUNITY COMPOSITION AND STRUCTURE

Photomosaics of three discrete cold seep megafaunal communities were obtained in 2006 and repeated in 2007 to examine community-level changes over a single year. Two of the photomosaic sites were located approximately 100 m from one another in the Atwater Valley lease Block 340 (AT340) at approximately 2,200 m depth. On mosaic included a very large mussel bed, the Big Mussel Bed site (AT340 BMB) and the other was a linear feature over an apparent shallow fault, lined with mussel patches, the Mussel Brick Road site (AT340 MBR). The third was of a mixed assemblage of tube worms, mussels and urchins near a Chevron wellhead (Wellhead) at AC818 (Table 15-1). A mixed tube worm and mussel community in Alaminos Canyon lease Block 645 which was visited in 1992 (and included in a video mosaic constructed at that time) was re-imaged and photomosaicked in 2007 to examine longer-term changes. These mosaics were used to characterize the community compositions, identify associations among species, and document temporal change in the occurrence and distribution of the dominant habitat-creating organisms (including mussels and tube worms). The patterns of temporal change detected between years at all sites were examined to determine if these deep-seep communities follow successional patterns similar to those documented at shallow seeps.

15.1. Methods

15.1.1. Image Collection and GIS Analysis

All imagery from 2006 and 2007 was collected using a Nikon E995 camera encased in a pressure-safe housing and mounted on the submersible (DSV *Alvin* in 2006, ROV *Jason II* in 2007) perpendicular to the sea floor. Illumination was from a pair of 300 watt/sec strobe lamps. The submersible was maneuvered over the selected areas to collect a series of adjacent strips of images. The images within each line and the lines within the photomosaic overlapped one another by at least 20%. Parallel lasers were spaced 25 cm apart and used to provide a scale reference. The images were optimized using Photoshop CS2 auto level, auto color and auto contrast settings to maximize image clarity and minimize contrast and exposure differences among images. Optimized images were then assembled into photomosaics using a MATLAB application that seamlessly blends the overlapping edges of the images together to produce a composite image of the entire community (Pizarro and Singh 2003).

Each image was associated with geographic coordinates that were collected by the submersible in one-second intervals. These coordinates were used to georeference the photomosaic in a geographic information system (GIS) using ArcGIS v 9.1 with a projected coordinate system in WGS 1984. Each of the individual high-resolution images was hyperlinked to the photomosaic. The original images have resolution sufficient to identify organisms and objects greater than 2 cm in size and were referenced to identify and digitize fauna and abiotic substrata. Sediment, bacterial mats, small (<3 cm) and large (>3 cm) mussels, crushed shells, tube worms, mixed substrate, anthropogenic debris and carbonate rock and rubble were digitized as polygons in ArcGIS and were analyzed as potential habitat sources (substrata) for solitary organisms (Table 15-2). Solitary or mobile fauna, including arthropods, fishes, anemones, gastropods, and echinoderms were digitized as points. All fauna were identified to the lowest possible taxonomic level. The area covered by each of the substrata was obtained from the GIS and location-based queries were used to determine the distribution of the solitary fauna across each of the substrata.

To examine changes in these communities between years, the feature classes that had been digitized onto the photomosaics in 2007 were superimposed onto the digitized polygons from 2006 (or 1992, in the case of AC645). The amount of overlap from one feature class to another was determined using the Intersect tool in ArcGIS.

Table 15-1

Photomosaic Designations, Locations and Areal Extents

Site	**Area (m^2)**	**Depth**	**Latitude**	**Longitude**
AT340b (MBR)	93.9	2175	27° 38' 46.8378"	-88° 22' 13.3458"
AT340a (BMB)	109.5	2200	27° 38' 42.252"	-88° 21' 50.3208"
AC818	104.0	2740	26° 10' 49.0872"	-94° 37' 23.1024"
AC645	23.4	2240	26° 21' 16.1418"	-94° 29' 48.1338"

.

Table 15-2

Description of Substrata Classifications

Nine different classes were defined.

Substrata Classifications	**Description**
Large mussels	Large (>3 cm) *Bathymodiolus* sp. mussels
Small mussels	Small (<3 cm) *Bathymodiolus* sp. mussels
Disarticulated or crushed shells	Open, empty mussel shells or white shell hash
Tube worms	*Lamellibrachia* spp. or *Escarpia laminata*. tube worms
Carbonate rock and rubble	Bare, hard authigenic carbonate rocks or boulders, or isolated pieces of carbonate rock surrounded by sediment
Sediment	Includes undisturbed, bare sediment, animal trails, and black stained sediment
Bacterial mat	White and red *Beggiatoa*-like spp. mats
Mixed substrata	Difficult to differentiate clusters of tube worms, large, small and dead mussels, carbonate rock and rubble
Anthropogenic debris	Including fishing line, bags, nets, and wire

AC645 was the site of earlier explorations in 1992, during which several markers were placed on the seafloor at a mixed mussel and tube worm community. A video mosaic was obtained in 1992 that included several of these markers. This same area of the site was relocated in 2006 and photomosaicked in 2007 to enable a long-term analysis of temporal change in the community. Because the 1992 video mosaic lacked sufficient resolution to identify individual organisms, only the substrata were digitized in this data set.

15.1.2. Physical Collections and Biomass Density Determinations

Three mussel collections from the AT340 Big Mussel Bed site and three from the AC818 site were obtained using a modified "mussel pot" device (Van Dover, 2002, Cordes et al., this issue) to ground truth the images, to provide data on abundance and biomass of smaller and cryptic species, and to allow estimates of biomass in these communities. The mussel pots collected a 26 cm-diameter portion of the community and released a ring that allowed visual confirmation that the collection was complete within the device's footprint. One tube worm aggregation was also collected from each of these sites after the photomosaics were obtained during the June 2007 cruise. These community collections were obtained using the Bushmaster Jr. collection device, which is a hydraulically actuated net lined with 63 μm mesh capable of enclosing and collecting entire aggregations without loss of fauna (Bergquist et al., 2003, Cordes et al., 2005). The spatial footprint of these collections was determined from photomosaic images of the collected aggregations, obtained shortly before the collections. All collections were videotaped, and mussels and tube worms were counted, identified and weighed on board the ship.

First-order estimates of biomass for the portion of the photomosaic sites dominated by tube worms and mussels were calculated from the biomass per unit area from the mussel pot and Bushmaster collections and the amount of area occupied by mussels and tube worms at that site.

15.1.3. Statistics

Similarity in community composition between photomosaic sites and between years were calculated using the Bray-Curtis similarity index in PRIMER v5 with presence-absence transformations in order to permit analysis of both solitary and aggregated fauna (Cordes et al., 2006 and references therein). Analyses of nMDS ordination and average linkage clusters were used to examine similarities among community compositions of the photomosaic sites. ANOSIM tests using the Bray-Curtis similarity index data with presence/absence transformations were used to test for significant differences in community composition between the same photomosaic site during two consecutive years, among different photomosaic sites, and among different substrata within photomosaic sites. A BIO-ENV analysis was used to further examine the data to determine which species contributed most to differences in community compositions. Chi-square analyses tested whether there were significant associations between point fauna and substrata within photomosaic sites.

15.2. Results and discussion

15.2.1. Community Compositions across Sites

Collections from the AT340 and AC818 sites contained both *Bathymodiolus brooksi* and *Bathymodiolus heckerae*. *B. brooksi* was the only mussel present in the 3 mussel pots taken within the BMB site in AT340 but other collections in the general region at AT340 also included

B. heckerae. The mussel pot collections taken within the mosaicked area in AC818 contained primarily *B. brooksi* with a single individual of *B. heckerae*, and two other collections from the same site contained two more individuals of *B. heckerae*. At AC645, there were no collections made from within the photomosaic; however, collections made from other locations within the site contained both *B. brooksi* and *Bathymodiolus childressi*.

Tube worm aggregations were present at each site except for the Mussel Brick Road site at Atwater Valley 340. The identity of the tube worm species could not be resolved in the images. Although *Escarpia laminata* and *Lamellibrachia spp*. are known from AT340 and AC645, only *E. laminata* was present in the collection from the photomosaic site in AT340 (no tube worms were collected from the area mosaicked in AC645) (Table 15-3).

Every photomosaic site hosted *Munidopsis spp.* crabs, the sea cucumber *Chirodota heheva*, and a small white anemone (Table 15-4). *C. heheva* was more abundant at the Alaminos Canyon sites than in the Atwater Valley sites, while the small white anemone was much more abundant at Atwater Valley than at Alaminos Canyon. The spatangid urchin *Sarsiaster griegii* and the sea star *Ampheraster alaminos* were both abundant at the photomosaic sites at Alaminos Canyon, but were not observed at the photomosaic sites at Atwater Valley. In addition, a large flytrap anemone was observed at both Alaminos Canyon sites, but was missing from the Atwater Valley photomosaics (Table 15-4).

Analyses using nMDS ordination and average linkage cluster showed a separation of community compositions by photomosaic site (Figure 15-1), which was confirmed with an ANOSIM analysis that found significant differences in community compositions (global $R = 0.297$, $p = 0.001$). Specifically, there were significant differences between the Big Mussel Bed site at AT340 and every other site (Mussel Brick Road $r = 0.326$, $p = 0.001$; AC645 site $r = 0.537$, $p = 0.002$; AC818 site $r = 0.431$, $p = 0.001$), as well as significant differences between AC818 and the Mussel Brick Road site ($r = 0.168$, $p = 0.009$). Although depth may play a role in the differences between AC818 and some of the other sites, this is unlikely as there was no significant difference between the two Alaminos Canyon sites ($r = 0.161$, $p = 0.157$) and the others are at a similar depth to AC645. BIO-ENV analyses indicated that this separation was primarily due to the presence of *Munidopsis* spp. crabs, the sea cucumber *C. heheva*, and the large number of anemones present at the Atwater Valley 340 sites.

The communities associated with different substrata within photomosaics were more similar to each other than to communities on the same substrata across all photomosaic sites. Substrate type, however, did have a significant influence on community composition (ANOSIM, Global $R = 0.227$, $p = 0.001$). Pairwise tests indicated that significant differences in community compositions existed only between large mussels and sediment after Bonferroni corrections of significance levels ($r = 0.392$, $p = 0.006$). However, there were also strong trends supporting differences between the faunal assemblages on small mussels and large mussels ($r = 0.446$, $p = 0.009$) and small mussels and dead mussels, ($r = 0.372$, $p = 0.01$), between bacterial mats and large mussels ($r = 0.792$, $p = 0.008$), and between bacterial mat and carbonate rock or rubble ($r = 0.211$, $p = 0.008$).

Table 15-3

Abundance (in numbers of individuals) and Biomass of Foundation and Associated Fauna Collected within Each Mussel Pot (mp) and Bushmaster (bm) at the AT340 Big Mussel Bed Site and the AC818 Site

The designation "p" indicates a taxa was present but not enumerated, and the designation "AF biomass" indicates ash-free dry weight biomass.

	site	**AT340**	**AT340**	**AT340**	**AT340**	**AC818**	**AC818**	**AC818**	**AC818**
	sample	**mp**	**bm**	**mp1**	**mp2**	**mp1**	**mp2**	**bm**	**mp**
	dive	**J2-276**	**J2-276**	**J2-277**	**J2-277**	**J2-282**	**J2-282**	**J2-282**	**J2-284**
Cnidaria									
	Anemone spp.	1		4	24	2	4	7	3
	Hydroidea spp.		p						
	Stolonifera spp.		p						
Nematodes									
	nematode spp.			100	21				
Nemertea									
	nemertean sp.					2		1	
Sipunculida									
	Phascolosoma sp.			3					1
Annelida									
Polychaetea									
	Ampharetidae sp.								
	Ampeliscidae sp.			1					
	Branchinotogluma sp.	3			5		2	2	3
	Branchipolynoe seepensis								1
	Capitella sp.							5	
	Escarpia laminata	9	118					158	
	Eurythoe sp.			242	21				
	Flabelligeridae sp.				2		1	7	1
	Glycera sp.							1	
	Harmothoe sp.	1		2				3	1
	Heteromastus sp.		5						
	Hesciocaeca methanicola				10		3		2
	Lumbinereis sp.								1
	Nicomache sp.				1		1		
	Oligobrachia sp.							2	
	Protomystides sp.		56					73	
	Prionospio sp.				2		6	1	
Mollusca									
Gastropoda									
	Emarginula sp.								
	Phymorhynchus sp.					1			
	Puncturella sp.	2							
Bivalvia									
	Bathymodiolus brooksi	30		8	7	9	15		7
	Bathymodiolus heckerae						1		1
	Bathymodiolus sp.	2							
	Cuspidaria sp.							19	
Arthropoda									
Crustacea									
	Alvinocaris muricola	32	25	39	13	15	33	21	11

Table 15-3

Abundance (in numbers of individuals) and Biomass of Foundation and Associated Fauna Collected within Each Mussel Pot (mp) and Bushmaster (bm) at the AT340 Big Mussel Bed Site and the AC818 Site

"p" indicates a taxa was present but not enumerated, and the designation "AF biomass" indicates ash-free dry weight biomass.

	site	**AT340**	**AT340**	**AT340**	**AT340**	**AC818**	**AC818**	**AC818**	**AC818**
	sample	**mp**	**bm**	**mp1**	**mp2**	**mp1**	**mp2**	**bm**	**mp**
	dive	**J2-276**	**J2-276**	**J2-277**	**J2-277**	**J2-282**	**J2-282**	**J2-282**	**J2-284**
	Amphipoda spp.	1	1	148	2	1		2	1
	Isopoda spp.							38	
	Munidopsis sp.					1		3	
Echinodermata									
Ophiuroidea									
	Ophioctenella acies	221	1	452	633	10	108		
	Ophienigma spinilimbatum			10		3	2	27	61
Holothuroidea									
	Chirodota sp.	1		6	2	4	3	8	2
Chordata									
	Unid fish				1				
AF biomass of associated fauna		2.1	9.3	29.9	6.8	5	4	8.3	2.7
AF biomass of foundation fauna		189.1	203.9	213.3	223.8	196.7	270.9	141.7	185.2
Total Biomass (g)		191.2	213.2	243.2	230.6	201.7	274.9	150	187.9
Percent biomass foundation fauna		98.9	95.6	87.7	97	97.5	98.6	94.5	98.6
Area covered by mussels/tube worms (m)		32.6	4.4	32.6	32.6	3.7	3.7	7.5	3.7
Foundation fauna biomass per meter (g/m2)		3562.7	522.4	4019.8	4216.2	3706	5104.6	442	3489.3
Total estimated biomass at site (g)		116060.1	2321.8	130948.5	137347.7	13852	19079.2	3322.5	13041.7

Table 15-4

Abundance of the Taxa Observed in the Photomosaics over Different Years

"p" indicates that a taxa was present but not enumerated

		AT340 MBR 2006	**AT340 MBR 2007**	**AT340 BMB 2006**	**AT340 BMB 2007**	**AC818 2006**	**AC818 2007**	**AC645 1992**	**AC645 2007**
AREA		93.9	93.9	109.2	109.2	104	104	23.4	23.4
Arthopoda: Crustacea									
	Alvinocaris muricola	10	11	165	67				34
	Munidopsis sp. rge)	15				21	28		8
	Munidopsis sp. mall)	31	27	255	140	30	37		59
Annelida									
	Sabellidae spp.				5				
	Siboglinidae spp.			p	p	p	p	p	p
Chordata									
	Macrouridae sp.	2	3	3		1			
	Fish 2		5						
Cnidaria									
	White anemone	9	26	2828	2435	30	46		16
	Flytrap anemone					2	8		1
	Red anemone	37		10	3		10		
Echinodermata									
	Chirodota heheva	129	133	76	10	231	237		12
	Sarsiaster griegi					110	67		
	Amperaster alaminos					35	42		
Mollusca: Bivalvia									
	Bathymodiolus spp.							p	p
	Bathymodiolus ooksi	p	p	p	p	p	p		
	Bathymodiolus ckerae	p	p	p	p	p	p		

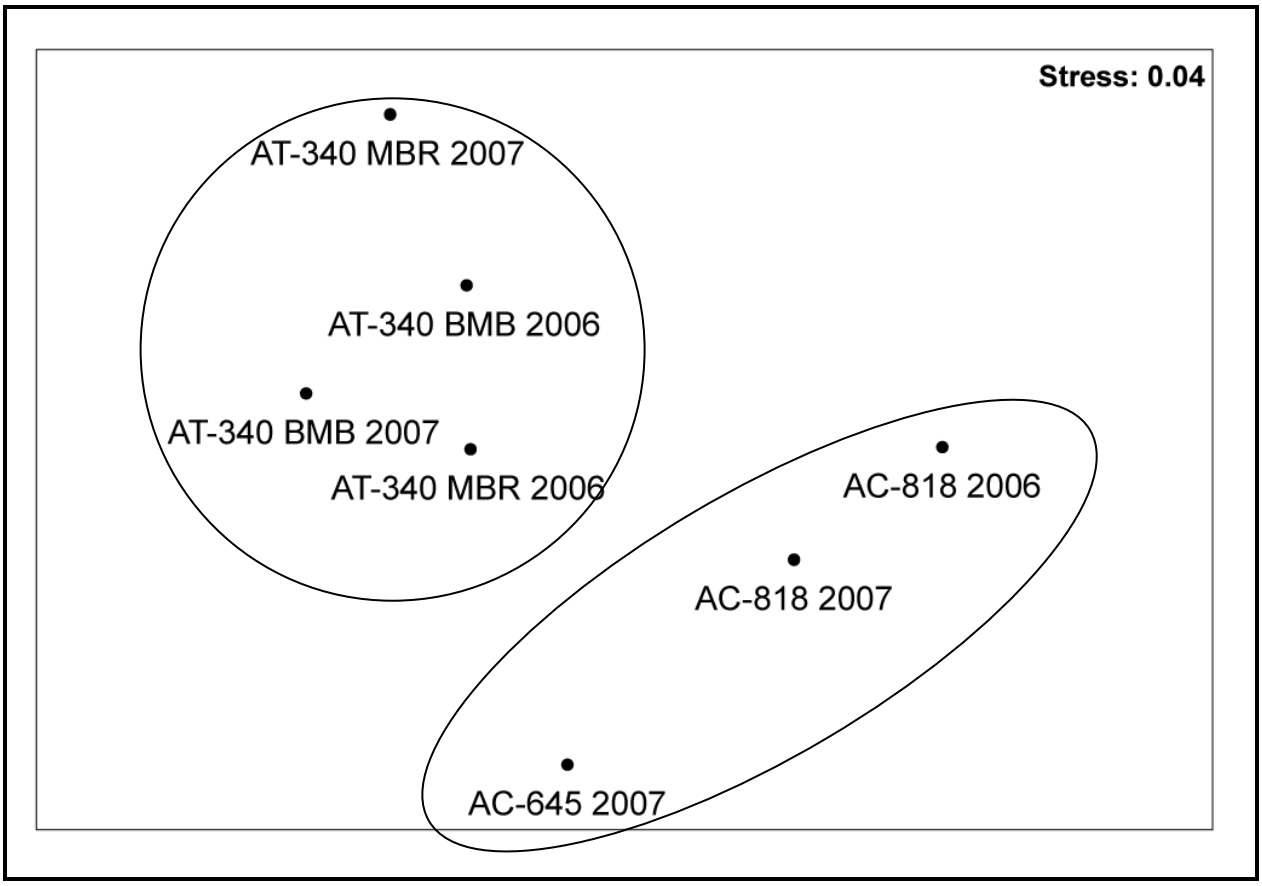

Figure 15-1. nMDS plot of the photomosaic sites, based on Bray-Curtis similarity with a presence or absence transformation of all of the organisms found within that site, including the foundation fauna. Circles represent sites that have greater than 75% similarity based on an average linkage cluster analysis of the same data.

Chi-square analyses indicated that many of the fauna associated with these seeps were non-randomly distributed across the available substrata and that there were positive associations between certain organisms and particular foundation fauna and substrata (Figure 15-2 and 15-3). In particular, *A. muricola* shrimp had a significant association with large mussels ($p < 0.001$), *C. heheva* was usually found associated with either live or dead mussels ($p < 0.001$), white anemones were found strongly associated with living mussels ($p < 0.001$), and *S. griegii* and *A. alaminos* were both found associated with the sediment surrounding the hard substrata ($p < 0.001$).

Both the large-scale differences between sites and regions and the small-scales patterns in animal distributions within a site could in part reflect differences in abiotic factors such as reduced chemicals in the water column or substrate availability, or ecological and biotic interactions such the availability of food sources, facilitation or chemical cues from other species (Vanreusel et al., 2009, Dattagupta et al., 2008), or successional trends. The presence of abundant small mussels at both the AT340 sites (but not at the AC818 or AC645 sites) indicates an early successional stage

at sites of active seepage, where access by many taxa may be limited by exposure to seep fluid in the epibenthic water (Bergquist et al., 2003; Cordes et al., 2005).

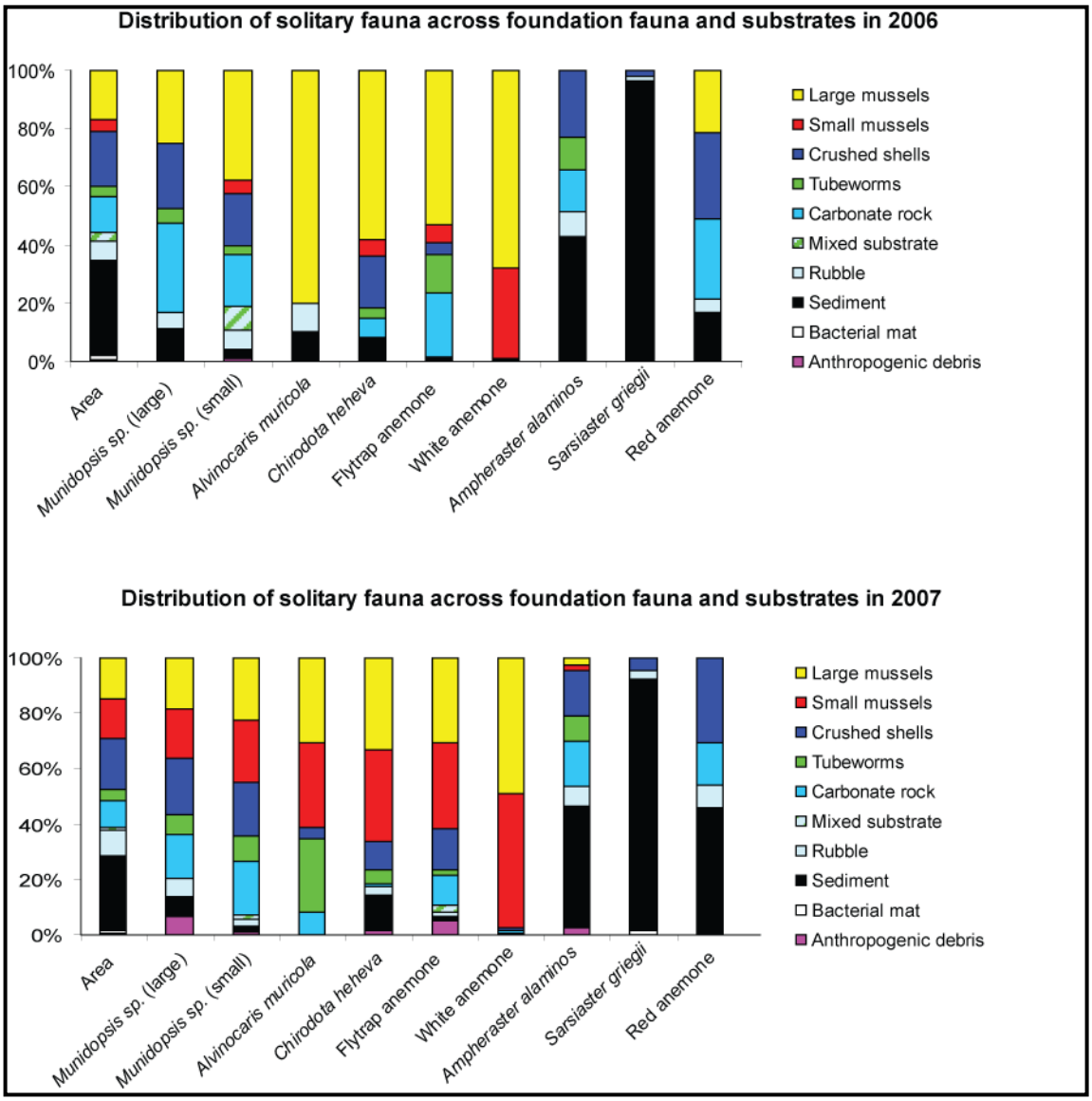

Figure 15-2. Distribution of solitary fauna across each substratum. Two additional solitary fauna, not seen in 2006, were observed in 2007.

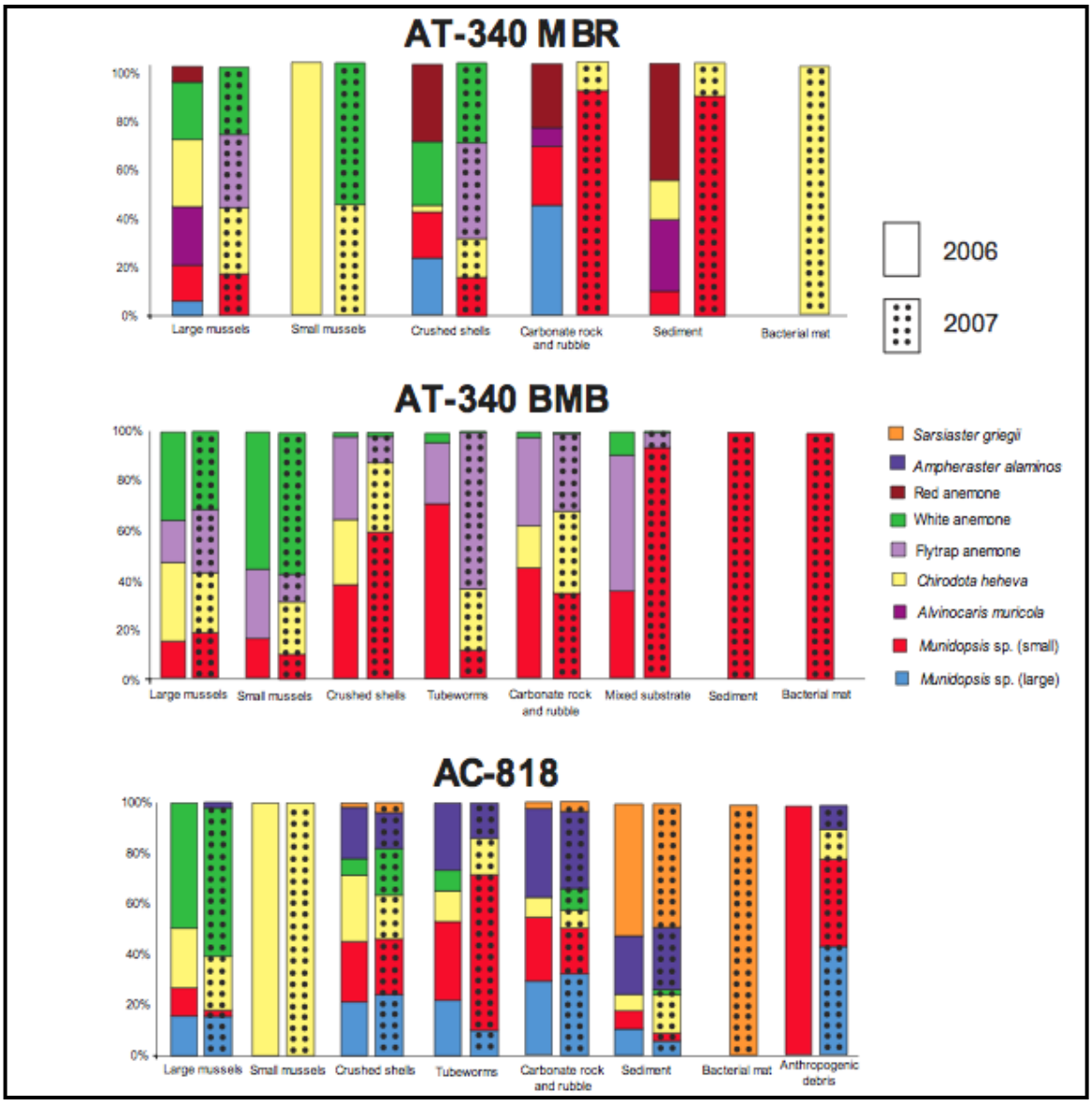

Figure 15-3. Percent distribution of solitary fauna (in numbers greater than 6) and its distribution across various substrata at AC818 and the two AT340 sites for both years. Any substrata without any solitary fauna were not included in the figure.

15.2.2. Physical Collections

Physical collections revealed the presence of many species that were not visible in the images. Some of these species include those that nestle underneath mussels, such as ophiuroids, polychaetes and gastropods, commensal species such as the polychaete *Branchipolynoe seepensis*, or *Protomystides* sp., and small or cryptic organisms, such as nematodes, amphipods and hydroids (Table 15-3). Species not present in physical collections but documented in the photomosaics included rare or large megafauna, such as fishes and large anemones, and organisms that are found near but not in the mussel beds and tube worm aggregations, such as the heart urchins *Sarsiaster griegi*, and the sea star *Ampheraster alaminos*.

Tube worm aggregations and associated communities collected on the Upper Louisiana Slope using the same equipment had higher biomass (when standardized to their areal footprint) than the tube worm communities collected within these photomosaics (Bergquist et al., 2003a). Tube worm communities collected for this study had ash-free dry weight (AFDW) biomasses of 0.44 and 0.52 $kg \cdot m^{-2}$, while communities on the upper slope ranged from 1.73 to 13.1 $kg \cdot m^{-2}$ kg. However, the fauna associated with the tube worms collected for this study accounted for similar proportions of the total community biomass reported from the collections on the upper slope (Bergquist et al., 2003a). The associated fauna accounted for between 4.4 and 5.5 % of the total community biomass at these sites, while these values ranged from 0.06 to 15% of the total community biomass in the upper slope collections. This suggests that, despite the fact that the vestimentiferan assemblages on the lower slope appear less dense and were composed of largely different species (Cordes et al., this issue), the general biomass relations between the foundation fauna and their associates remains approximately the same.

The community biomass calculated from the mussel pot collections was substantially higher than the tube worm community biomass from the same sites. The mussel community biomass in the photomosaic sites ranged from 0.87 $kg \cdot m^{-2}$ to 1.5 $kg \cdot m^{2}$, within the range reported for mussel beds on the upper Louisiana slope (0.83 $kg \cdot m^{-2}$ to 3.06 $kg \cdot m^{-2}$) (Bergquist et al., 2005). The AFDW biomass of the associated community was also within the range of other lower slope GoM cold seep communities (2-201 $g/AFDW/m^2$) (Cordes et al., 2007a) and upper slope GoM cold seep communities (2-206 $g/AFDW/m^2$). Cordes et al. (2007a) suggests that the deep and shallow seep communities provides a food supply that does not decrease with depth, which explains why there is the biomass associated with mussel beds does not decline with depth as has been observed in background communities (Pequegnat et al., 1990).

Physical collections were also used to determine a first-order estimate of the AFDW biomass of the mussels, tube worms, and associated fauna at the scale of a seep community. This estimate ignores other seep fauna not directly associated with the tube worms and mussel beds, and the larger mobile megafauna not physically collected, and will vary widely depending on the composition and density of seep megafauna and the boundaries used for a working definition of a seep community. The two communities for which we have physical collections that enable us to make this calculation represent reasonable examples of deep slope mussel and tube worm communities, as the AT340 BMB site is densely covered with mussels and tube worms, while the AC818 photomosaic site covers an area with more dispersed tube worm and mussel aggregations. In the area covered by the AT340 BMB site, the megafaunal biomass is about 1.28 kg $AFDW \cdot m^{-2}$ and in the area covered by the AC818 photomosaic it is approximately 0.18 kg $AFDW \cdot m^{-2}$. These values are 4-5 orders of magnitude higher than typical deep sea sediment benthos (Hashimoto et al., 1989, Thurston et al., 1994, Lavaleye et al., 2002) and 2-3 times higher than deepwater coral community biomass (Theroux and Wigley, 1998).

15.2.3. Temporal change

An ANOSIM based on the presence/absence transformed Bray-Curtis similarity of community composition across sites indicated no change over the course of one year at the site in AC818 (Global $R = -0.068$, $p = 0.824$) or at the AT340 BMB site (Global $R = 0.101$, $p = 0.174$). There were, however, significant changes at the MBR site in AT340 (Global $R = 0.349$, $p = 0.035$). There were also changes in the extent of the areal coverage and the locations of the different foundation fauna and other substrata over time at each site (Figures 15-4 and 15-5).

15.2.3.1. AT340 BMB Photomosaic Site

At the AT340 BMB site, there were large, live aggregations of both mussels and tube worms interspersed with exposed carbonate hard substrate (Figure 15-6a-f). Many of the mussels and tube worms at this site hosted encrusting organisms on their shells or tubes, including large numbers of anemones on the mussel shells and hydroids and stoloniferans on tube worms. Over the course of one year, there was a slight decrease in the area covered by live mussels, and a corresponding increase in the area covered by dead mussel. Tube worm areal coverage remained stable, and the area covered by hard substrata such as carbonate rock and rubble also showed little change (Figures 4 and 5). The increase in the area of surrounding sediment suggests that seepage was decreasing and that mussels were aggregating towards sources of optimum habitat, leaving behind dead shells and scattered rubble. The few bacterial mats present in 2006 were not present in 2007. This is also consistent with a decrease in seepage, but alternatively could reflect the ephemeral nature of visible bacterial mats at active seep sites (Vardaro et al., 2006). Nonetheless, the composition of this community and the changes observed over a single year are consistent with a seep community at a mid-level successional stage with thriving tube worm and mussel aggregations and a mix of seep colonists and vagrants (Bergquist et al., 2003; Cordes et al., 2005).

15.2.3.2. AT340 MBR Photomosaic Site

The AT340 MBR photomosaic site covered an area with numerous patches of mussels aligned in a roughly linear array associated with apparently active brine seepage originating from a fault in the underlying authigenic carbonate pavements (Figure 15-7a-h). There were several patchy bacterial mats in the photomosaic, and there were no tube worms. Over the course of one year, the area occupied by both small and large mussels increased, suggesting that recruitment and mussel growth was in progress at this site (Figures 15-4 and 15-5). The amount of area covered by hard substrata including carbonate rock and rubble also increased over the course of one year, while the area covered by sediment decreased, suggesting that authigenic carbonate precipitation was also ongoing and may provide additional suitable habitat for organisms that require hard substrate on which to settle (Figures 15-4 and 15-5), or that a light layer of sediment covered the existing underlying carbonate in 2006. There were also dramatic changes in the distribution of animals, suggesting that the animals at this site were moving to seek optimal habitat in this actively seeping area within AT340 (Figure 15-5). The composition of this community and these changes are all consistent with a seep community in an early successional stage as described by Bergquist et al. (2003b) and Cordes et al. (2005) for seep sites on the upper Louisiana slope.

15.2.3.3. AC818 Photomosaic Site

The seep megafaunal community at AC818 is, like the MBR at AT340, located over a shallow subsurface fault. The presence of bacterial mats, mussels and *Sarsiaster griegi* heart urchins nearby in highly reduced sediments all indicate active seepage at this site (Figure 15-8). However, unlike the MBR at AT340, there were also several medium-sized tube worm aggregations present in this area. At AC818, there was little change in areal coverage of foundation fauna, with none of the substrate types changing in area by more than 2% over the course of one year (Figure 15-4). There was easily detectable movement of the mussels and between 30 and 40% of the area covered by large and small mussels were replaced by dead mussel shells (Figure 15-5).

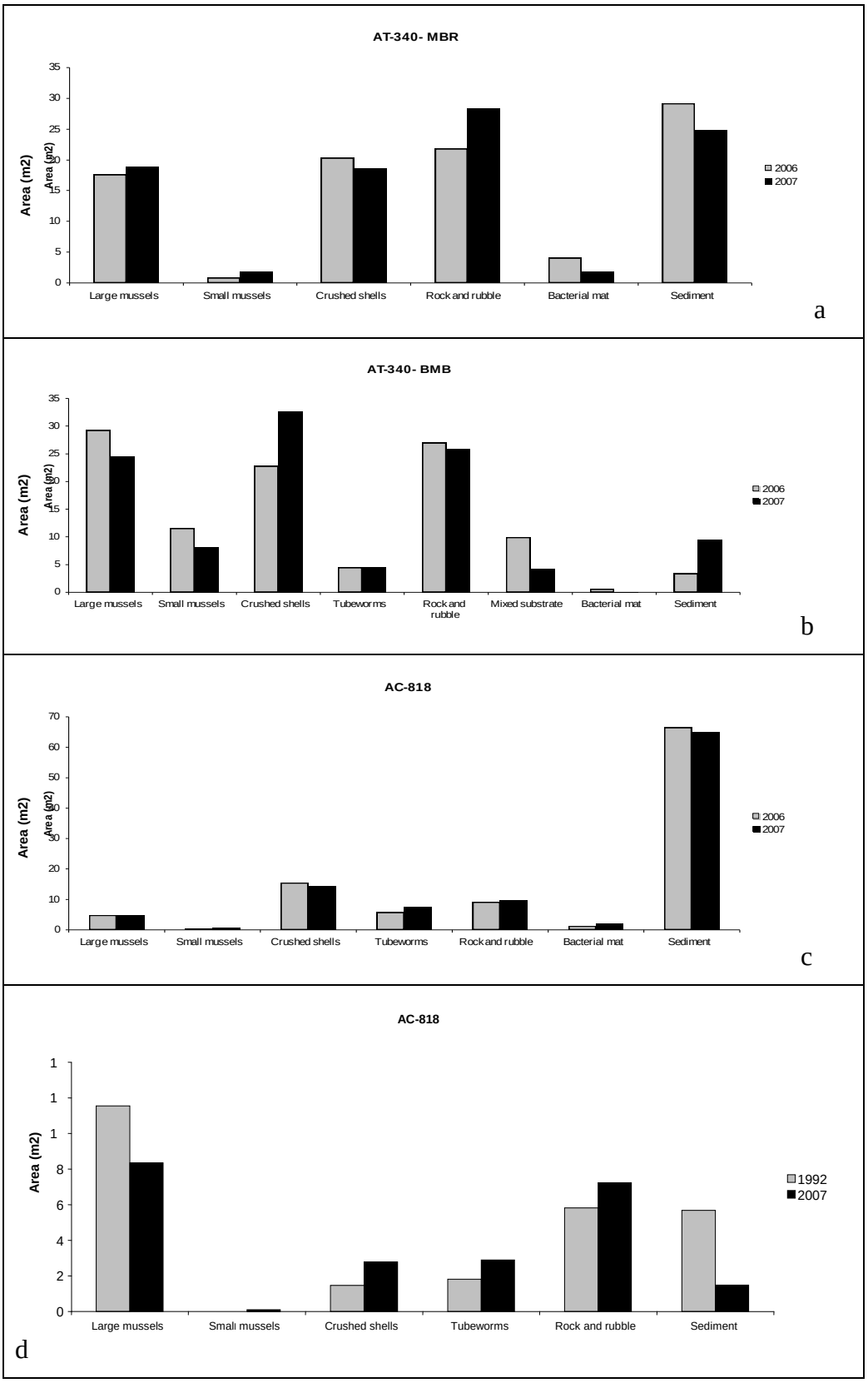

Figure 15-4. Area of substrata cover for each photomosaic site in 2006 and 2007.

Approximately 40% of the area covered by dead mussels in 2006 remained dead mussels, while the rest was replaced by sediment or rubble in 2007 (Figure 15-5). Bacterial mats were transient, and abundant bacterial mats that had been present in 2006 had disappeared and new mats had appeared on the sediment surrounding the seep site, a process which has been shown to occur over the span of hours, and is influenced by currents and the ability of mats to grow and retreat (Sassen et al., 1993, Vardaro et al.. 2006). Assuming similar rates of growth and successional processes in these communities and those of the upper slope, the community composition and the movement of mussels and bacterial mats suggest that seep megafauna have been established in this area for at least several decades and that there is still quite active localized seepage here. This community is likely intermediate in age to the two communities studied in AT340.

15.2.3.4. AC645 Photomosaic Site

The seep site in AC645 was first discovered using the DSRV *Alvin* in 1990 (Brooks et al., 1990) and CRF was present during a dive to the site. It was revisited in 1992 and again in 2003 (Cordes et al., 2009), 2006 (Roberts et al., 2007), and 2007, and some of the authors were present during each of these research expeditions. Abundant large carbonate slabs and boulders, large tube worm aggregations, extensive live mussel beds and areas with disarticulated shells were noted during each visit, and large gorgonian colonies were noted in the peripheral area during the visits after 2000 (and may have been present but were not noted in earlier visits). During one of the last dives of the 2006 series, several markers originally placed to aid a video mosaic effort in 1992 (Figure 15-9a) were found and this area was imaged for the photomosaic in 2007 (Figure 15-9b). Only 37% of the total area of the 2007 photomosaic consisted of the same substrata that were present in 1992. Live mussels covered approximately 9% less area in 2007 than they did in 1992, and tube worms covered twice the area in 2007 compared to 1992, increasing from 6% of the total to 12% of the total (Figure 15-4). The spatial distribution of the mussels had also changed (Figure 15-5). After 15 years, 50% of the original area covered by mussels still consisted of large mussels, and the remainder of the area originally covered by live mussels was covered by dead mussels or had been colonized by tube worms (Figure 15-5). Much of the area covered by small mussels was replaced by large mussels, while some large mussels had died or moved away, leaving behind bare patches of carbonate rock (Figure 15-5). All of these changes are consistent with the predictions of the upper slope successional model for a site with declining expression of seepage on the seafloor.

However, some areas that had been covered by dead mussels had new populations of small mussels, or isolated large mussels. While approximately 40% of the area covered by tube worms in 1992 remained tube worms, most of the remaining area had become colonized by both large and small mussels (Figure 15-5). Also, by 2007 new tube worm aggregations had developed in areas that had been covered by sediment, carbonate rock or rubble in 1992. These changes suggest renewed or redirected active seepage in some areas covered by the mosaic that allowed small mussels and tube worms to recruit to areas that were previously uninhabitable for these species that are reliant on exposure to significant concentrations of reduced chemicals. Clearly, this remains a dynamic site, and these observations emphasize both the small-scale variability that characterizes seep habitats and the potential longevity of both seep sites and seep megafauna.

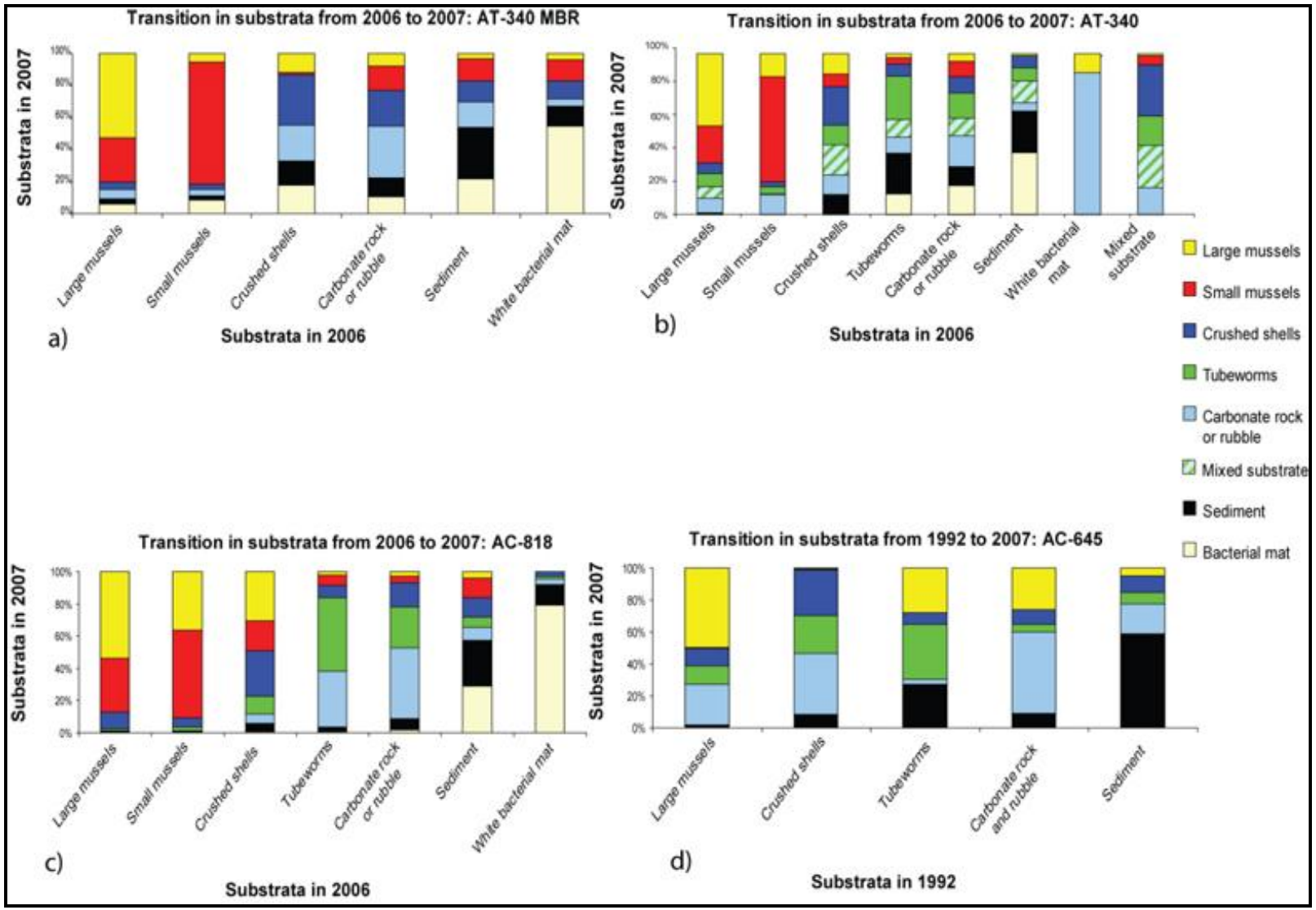

Figure 15-5. Transition from substrate cover in 2006 to substrate cover in 2007.

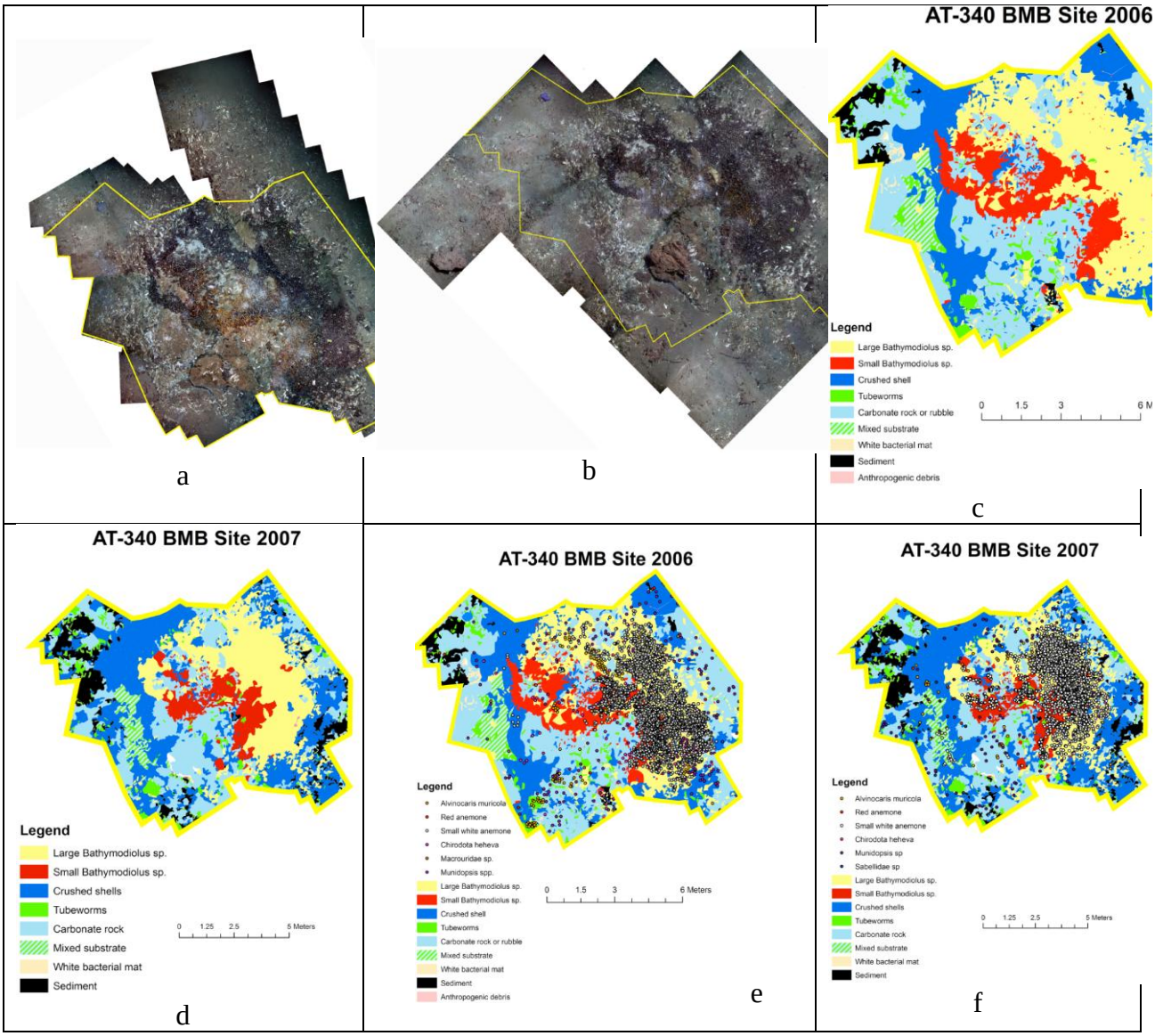

Figures 15-6a–e. Photomosaic of the Big Mussel Bed site in lease block AT340**.**

The area mosaicked in both years is indicated by the outline drawn on the images, where a) photomosaic obtained in 2006, b) 2007, c) 2006 photomosaic digitized for substrate type, d) 2007, e) 2006 mosaic digitized with substrate type and mobile fauna, and f) 2007.

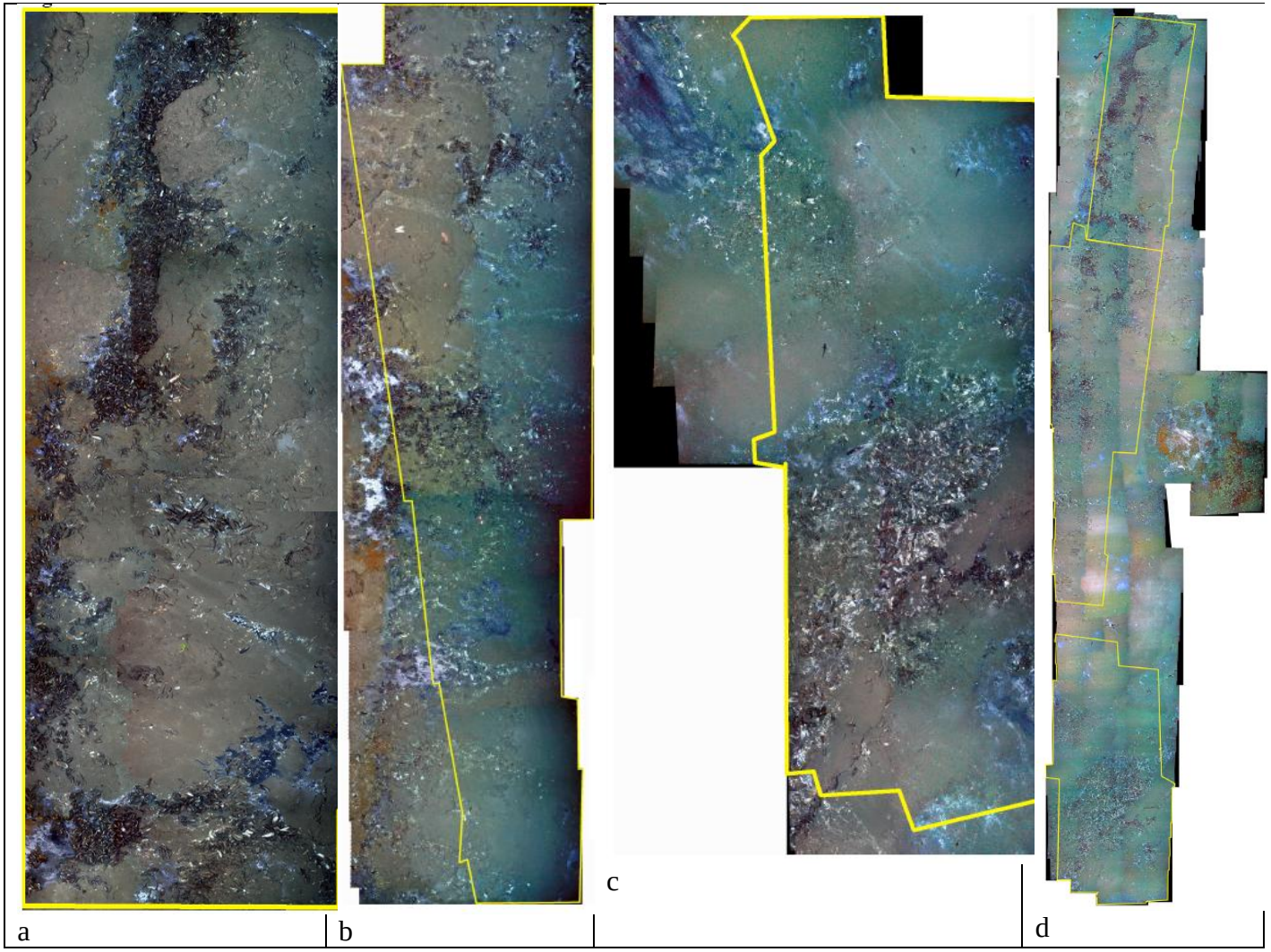

Figures 15-7a–d. Photomosaic of the Mussel Brick Road site in lease block AT340.
The area mosaicked in both years is indicated by the outline drawn on the images, where a, b, and c) are the three parts of the photomosaic obtained in 2006, d) was obtained in 2007, e) is the 2006 photomosaic digitized for substrate type, f) is the 2007 mosaic digitized for substrate type, g) is the 2006 mosaic digitized with substrate type and mobile fauna, and h) is the 2007 mosaic digitized with substrate type and mobile fauna.

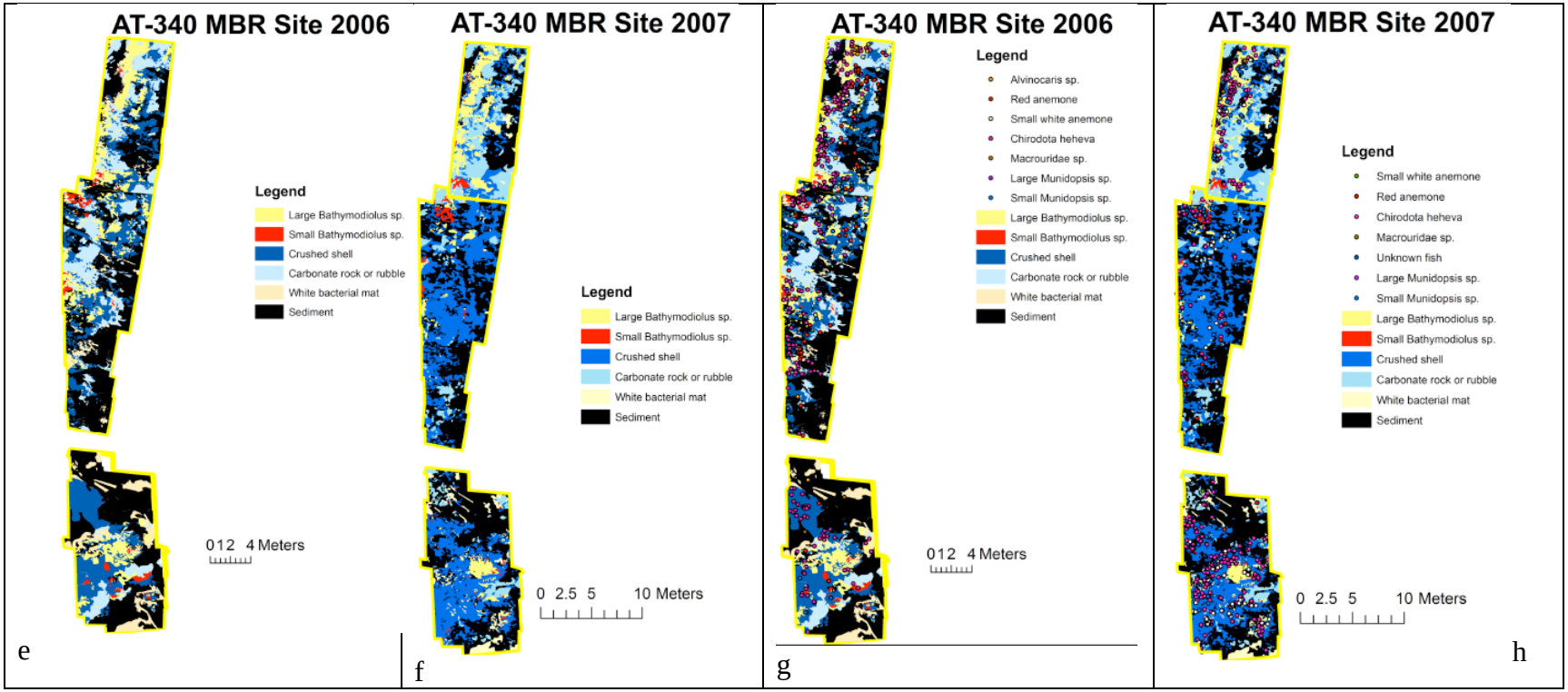

Figures 15-7e–h. Photomosaic of the Mussel Brick Road site in lease block AT340.
The area mosaicked in both years indicated by the outline drawn on the images, where a, b, and c) are the three parts of the photomosaic obtained in 2006, d) is the mosaic obtained in 2007, e) is the 2006 photomosaic digitized for substrate type, f) is the 2007 mosaic digitized for substrate type, g) is the 2006 mosaic digitized with substrate type and mobile fauna, and h) is the 2007 mosaic digitized with substrate type and mobile fauna.

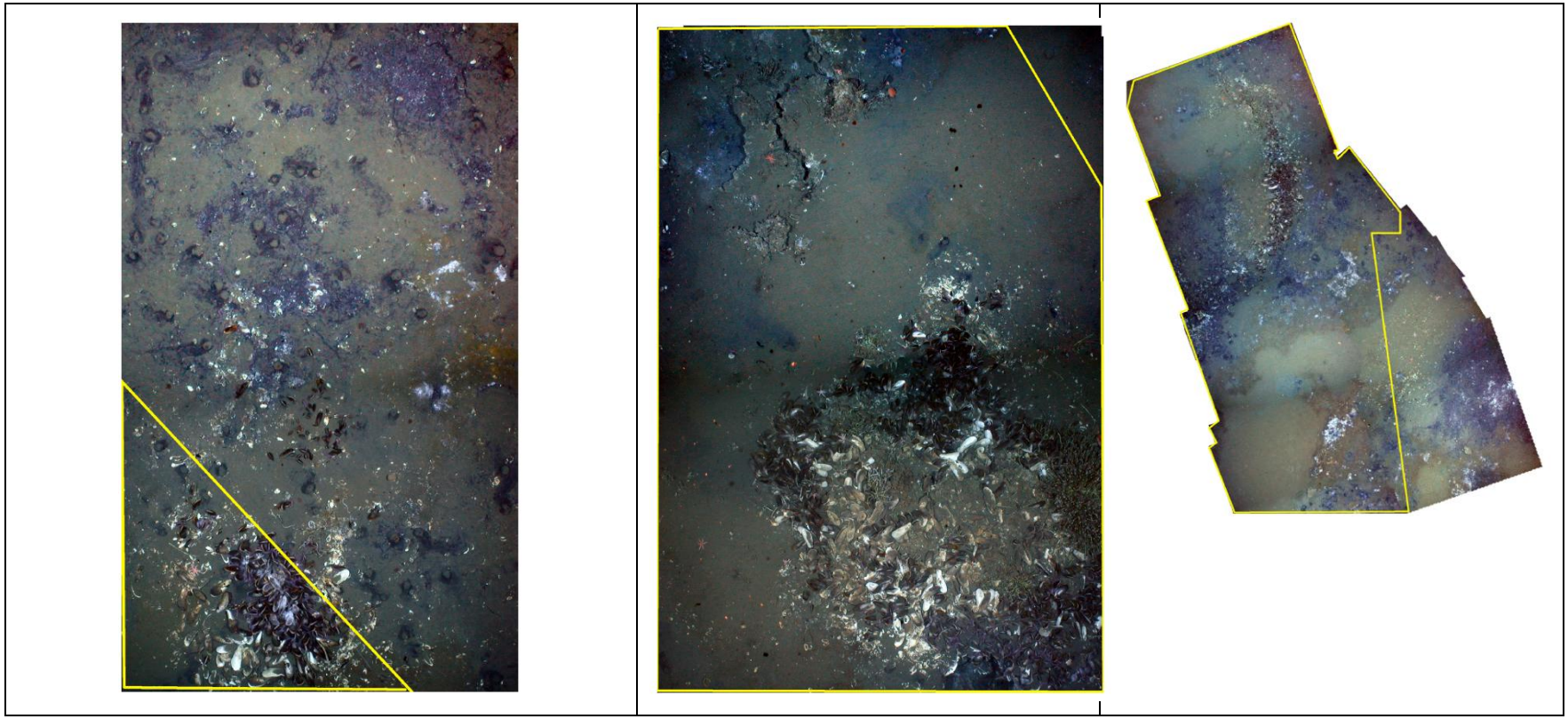

Figures 15-8 a–c. Photomosaic of a chemosynthetic community along a crack in the carbonate rock at AC818.
The area mosaicked in both years indicated by the outline drawn on the images, where a, b, c and d) are the four parts of the photomosaic obtained in 2006, e) is the mosaic obtained in 2007, f) is the 2006 photomosaic digitized for substrate type, g) is the 2007 mosaic digitized for substrate type, h) is the 2006 mosaic digitized with substrate type and mobile fauna, and i) is the 2007 mosaic digitized with substrate type and mobile fauna.

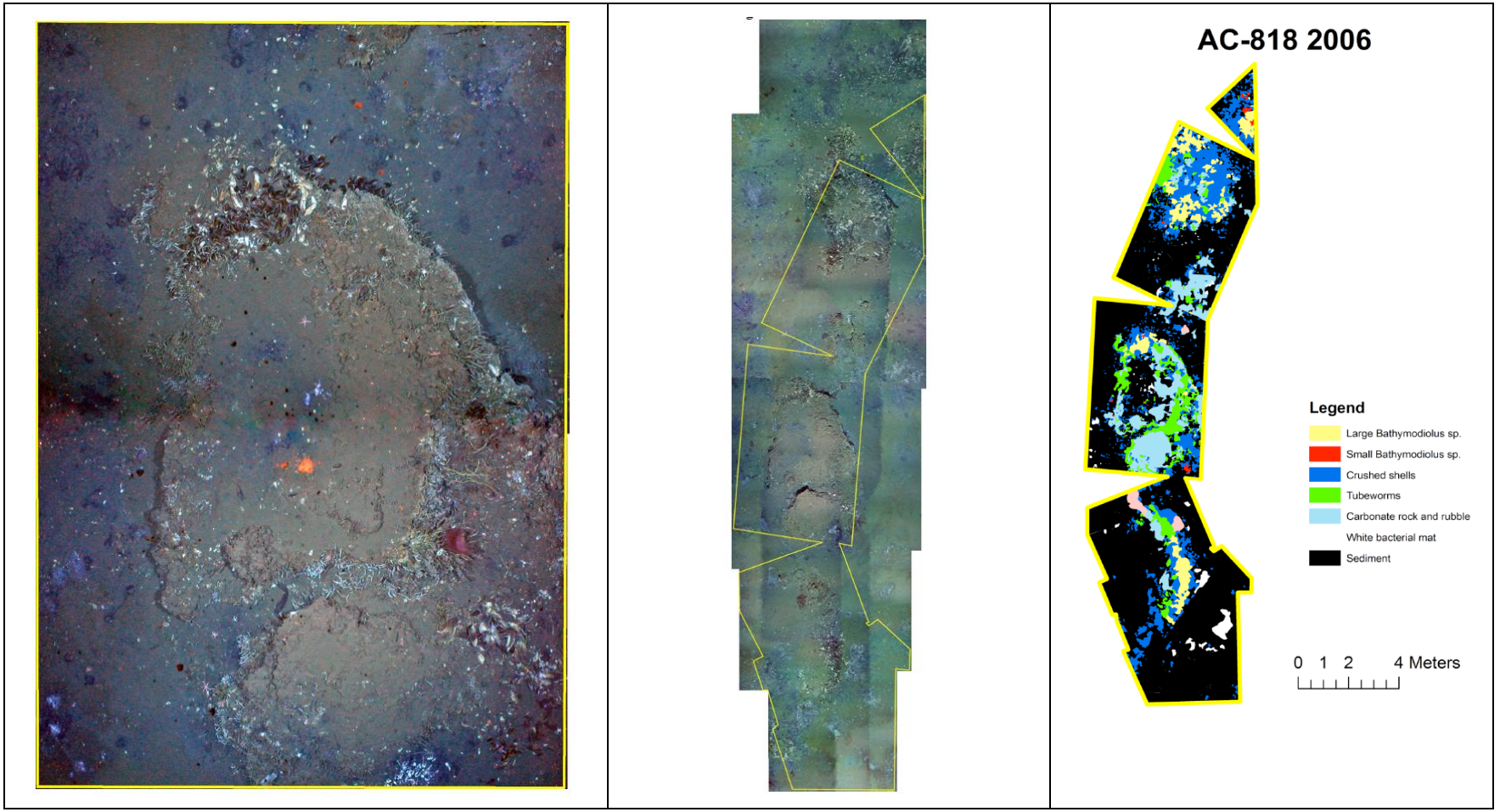

Figures 15-8 d–f. Photomosaic of a chemosynthetic community along a crack in the carbonate rock at AC818. The area mosaicked in both years indicated by the outline drawn on the images, where a, b, c and d) are the four parts of the photomosaic obtained in 2006, e) is the mosaic obtained in 2007, f) is the 2006 photomosaic digitized for substrate type, g) is the 2007 mosaic digitized for substrate type, h) is the 2006 mosaic digitized with substrate type and mobile fauna, and i) is the 2007 mosaic digitized with substrate type and mobile fauna.

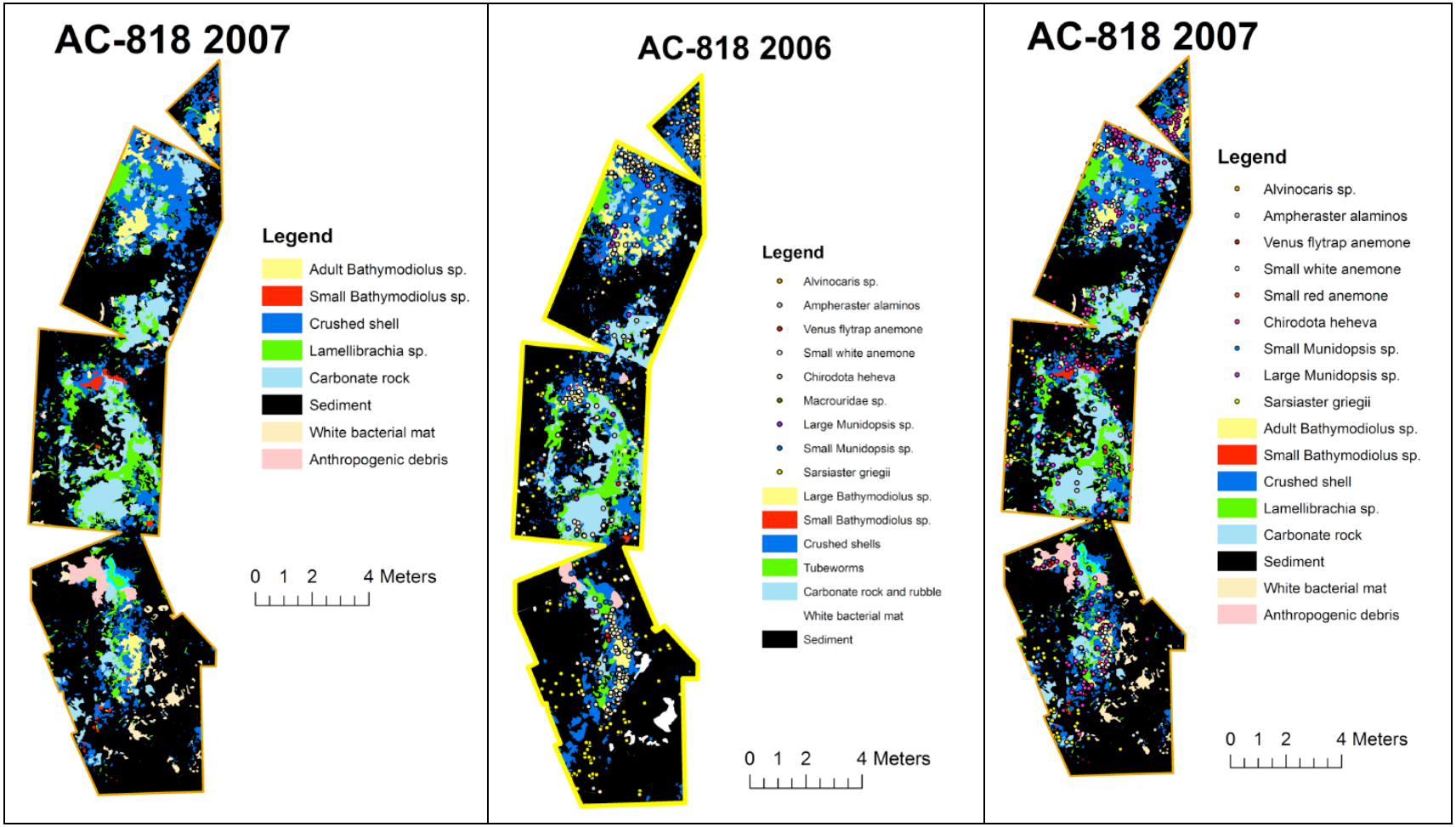

Figures 15-8 g–i. Photomosaic of a chemosynthetic community along a crack in the carbonate rock at AC818. The area mosaicked in both years indicated by the outline drawn on the images, where a, b, c and d) are the four parts of the photomosaic obtained in 2006, e) is the mosaic obtained in 2007, f) is the 2006 photomosaic digitized for substrate type, g) is the 2007 mosaic digitized for substrate type, h) is the 2006 mosaic digitized with substrate type and mobile fauna, and i) is the 2007 mosaic digitized with substrate type and mobile fauna.

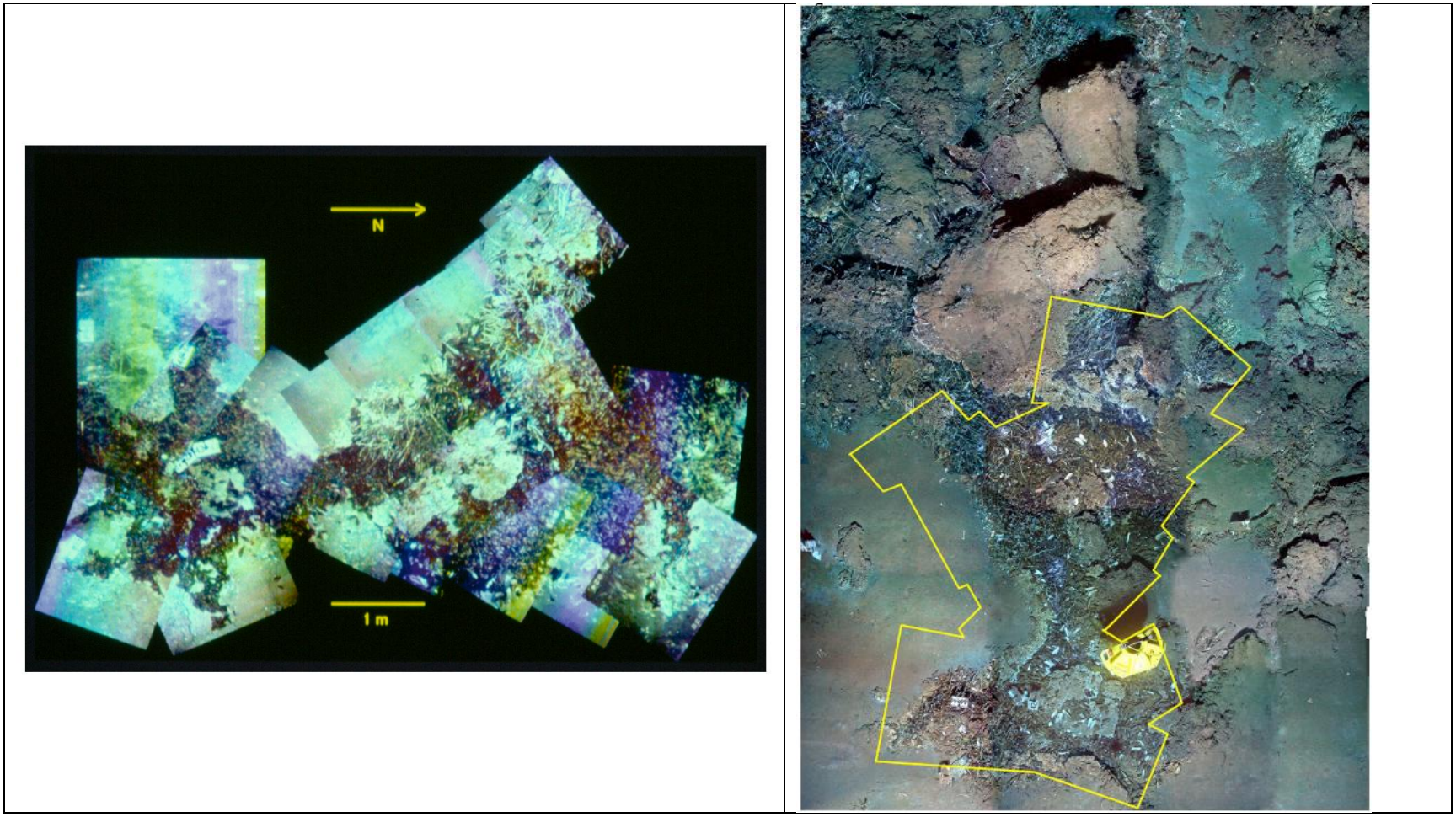

Figures 15-9 a, b. Photomosaic of a chemosynthetic community in AC645.
The area mosaicked in both years indicated by the outline drawn on the images, where a) is the video mosaic obtained in 1992, b) is the mosaic obtained in 2007, c) is the 1992 video mosaic digitized for substrate type, d) is the 2007 mosaic digitized for substrate type, and e) is the 2007 mosaic digitized with substrate type and mobile fauna.

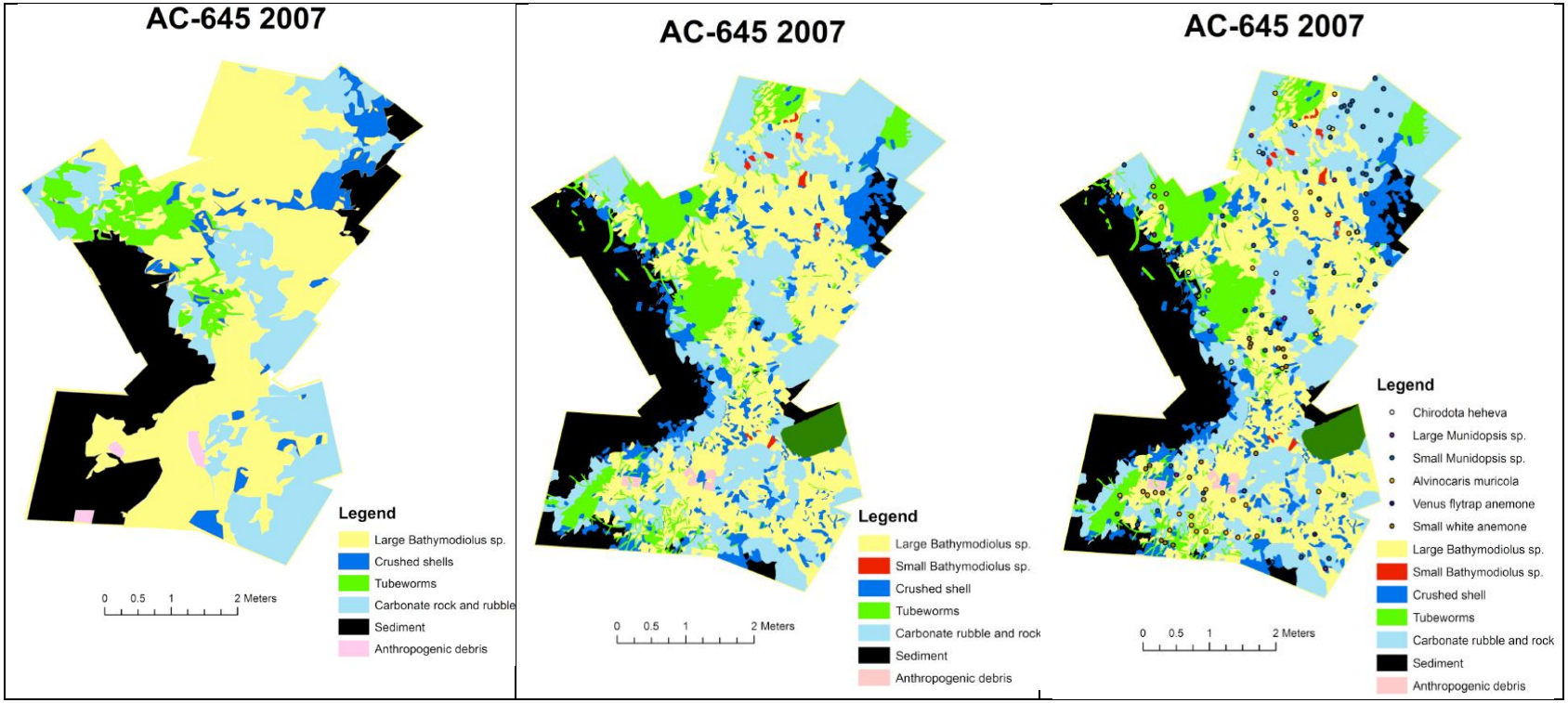

Figures 15-9 c–e. Photomosaic of a chemosynthetic community in AC645.
The area mosaicked in both years indicated by the outline drawn on the images, where a) is the video mosaic obtained in 1992, b) is the mosaic obtained in 2007, c) is the 1992 video mosaic digitized for substrate type, d) is the 2007 mosaic digitized for substrate type, and e) is the 2007 mosaic digitized with substrate type and mobile fauna.

15.2.4. Overall Trends

Changes in the areal coverage of each of the substrate types from one year to the next were apparent in the mosaic analysis (Figure 15-4). These changes are especially notable in the position of live mussels and the recruitment of small mussels to locations where they were not observed the previous year. Replacement by other substrates in 2007 where there were live mussels in 2006 could be a result of mussel mortality, particularly in the sites with evidence of decreasing seepage (i.e., the AT340 BMB site). Mussel movement or mortality could reflect a change in the chemistry at different locations in the site, or changes in seepage flow (Roberts, 1990). The presence of seep chemicals are patchy, both within and among tube worm and mussel aggregations (Nix et al. 1995, Bergquist et al. 2003b, Cordes et al., 2006), which may influence the patchy distribution of small mussels observed at these sites. The movement of the mussels from one year to another suggests that the mussels are adjusting to a dynamic environment as the seepage patterns change on over small spatial scales from year to year.

Most of the apparent changes in the area covered by tube worms over one-year periods are an artifact of the use of photomosaics as a sampling tool. Tube worms are digitized onto the two-dimensional map according to their apparent position over a substrate, and these animals are over 0.5 m long. The position of individual tube worms in the images can appear different between years as a result of slight changes in its orientation or as a result of currents or other factors or even slight changes in camera elevation and camera angle between years. As a result, the analysis may indicate replacement by whatever was underneath the tube worm, usually by sediment or carbonate rock or rubble, even though the tube worms have not really moved, died or grown. This was not the case for the tube worm aggregations at the AC645 site, where entirely new aggregations of tube worms have developed and others have disappeared over the course of fifteen years.

Seep community succession as modeled by Bergquist et al. (2003b) and tested by Cordes et al. (2005) suggests that there is a general trend from bacterial mats on newly emerging seep sites, to authigenic rock formation that allows for mussel colonization, to declining sulfide seepage, increasing dominance of tube worms, and eventually to senescent tube worm colonies and death. At these deeper sites, as at the shallower seeps, it appears as though these general trends hold true over long time scales at sites where there is authigenic carbonate precipitation. However, over shorter time scales, our analyses suggest that these communities undergo fluctuating phases of foundation fauna recruitment, substrate availability, and colonization by mobile fauna. In addition, some seep sites never progress through this general trend because of the lack of authigenic carbonate rock formation for larval settlement and growth. For example, the Brine Pool (NR1), which is a brine-filled pockmark surrounded by between 3 to 7 m of dense mussels, has been postulated to be at least several hundred years old (Smith et al., 2000) and consists only of live and dead mussels with no tube worms or carbonate. Bergquist et al. (2003b) suggested that due to the extremely long life span of the major foundation fauna at these sites, succession or temporal changes cannot be directly observed from these communities. At these sites, the replacement of one major substrate type with another suggests that small scale changes within seeps occur more quickly than we anticipated.

The frequency of these changes suggests that the strongest influences on community structure and composition are the abiotic influences of chemical seepage and the provision of habitat and hard substrate by the mussels and tube worms for mobile fauna. To fully understand the dynamics of seep community composition and succession, it may be necessary to revisit sites more frequently or to establish continuous observatories to resolve these rapid smaller-scale changes.

16. TUBE WORM GROWTH RATES

16.1. Methods

Tube worms were stained with a small dome staining device with *Alvin* in 2006. The stain is a non-toxic chitin stain (Acid Blue #158) and was mixed to super-saturation in fresh water so it remained buoyant in the staining device. The device was placed over the anterior ends of a small group of tube worms, the stain pumped into the dome and left on the tube worms for 5–10 minutes per application (Figure 16-1).

Following collection, the length and anterior diameter of the tube worms were measured. The anterior diameter was measured as the internal diameter of the tube opening with a pair of calipers. The length of the tube worms was measured from the anterior end to a constant posterior diameter of 2 mm for *E. laminata* and 4 mm for *Lamellibrachia* spp. Growth was measured as the distance from the anterior end of the tube worm to the beginning of the blue stained portion of the tube using a pair of calipers. The amount of growth was standardized to an annual growth rate by dividing it by the number of days between the staining and collection dives.

As a supplement to these data, a series of tube worms that had been marked with a banding device were fortuitously re-located in 2006 and fully imaged in 2007. In 1992, thirteen tube worms were successfully banded using a hydraulically powered tube worm bander at AC645 (Figure 16-2). Video and still images of these tube worms show the position of the bands at that point in time. Using markers left on the seafloor and the previous images, seven of these worms were located using the *Jason II* during the June 2007 cruise. Five of the worms were confirmed to be alive in 2007 and two of the banded worms appeared to be dead. The banded tube worms were imaged using a digital camera held perpendicular to the banded worms. These images were compared to the video and still images from 1992 to determine the amount of growth by these worms.

Growth was modeled using two different models (Cordes et al. 2007b). The standard model is based on a least-squares regression fit of an exponential function:

$$g = ae^{-bL}$$

where g is the growth rate in $cm \cdot y^{-1}$ and L is length in cm. This model was used previously for *L. luymesi* on the upper slope. In the second model, the size-specific probability of growth is determined from the equation:

$$p_g = e^{-cL_s}$$

where p_g is the probability of growth and L_s is the 10 cm size class of the tube worm. The data for this model were obtained by binning tube worms into 10 cm size classes and determining the proportion of individuals with non-zero growth. This model previously provided the best fit for *Seepiophila jonesi* on the upper slope. For both models, simulations were run for 1000 individuals for 500 years. In the first model, growth was determined by the regression function and the error determined using a normally distributed random number with average of zero and a standard deviation determined from the square root of the size-specific residuals of the regression function. In the second model, an evenly distributed random number between zero and one was generated and compared to the size-specific growth probability. If the number was

smaller than the probability score, then the individual was allowed to grow according to the average positive growth recorded for that species.

Figure 16-1. Staining and growth of tube worms. a. *Escarpia laminata* immediately after staining at AC818. b. Lamellibrachia sp. 1 in 2007 following approximately one year of growth.

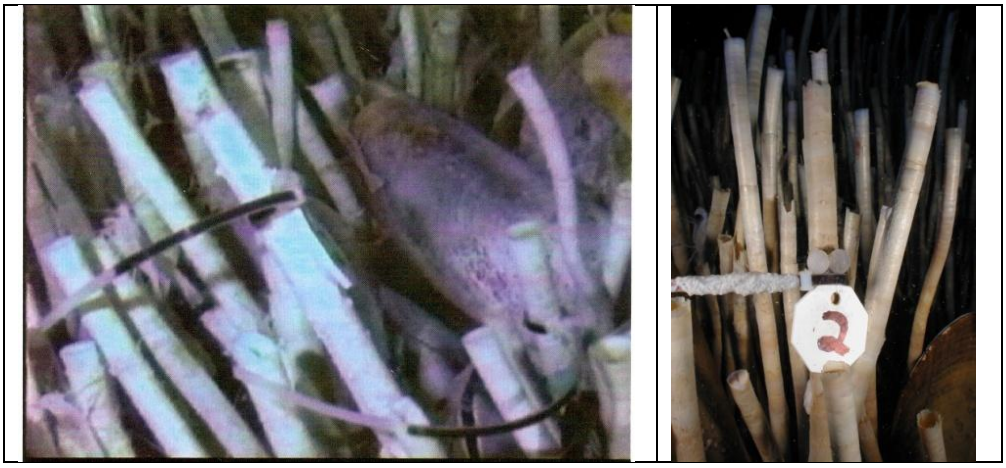

Figure 16-2. (A) A video capture from 1992 video showing a tube worm immediately after being banded. (B) The same tube worm imaged in 2007 using a high-resolution camera.

16.2. Results

A total of 391 tube worms were successfully stained and collected the following year in 12 collections on 7 dives at 3 different sites (Table 16-1). Overall growth rates were extremely slow, varying between zero growth and a maximum of 4.5 cm for *E. laminata*, 0.87 cm for *Lamellibrachia* sp 1, and 0.75 cm for *Lamellibrachia* sp 2.

Table 16-1

Tube Worms Successfully Stained and Collected

site	dive	collection	Escarpia	Lamellibrachia	L. sp #2
AT340	J2-270	Bushmaster	31		
AT340	J2-270	grab	4		
GC852	J2-273	Bushmaster	3	29	3
GC852	J2-273	grab #1		4	
GC852	J2-273	grab #2	6	19	
AT340	J2-276	Bushmaster	36		
AT340	J2-277	Bushmaster	22		
AT340	J2-277	grab	92	1	
GC852	J2-278	grab	3	5	
AC818	J2-282	Bushmaster	49		
AC818	J2-284	grab #1	63		
AC818	J2-284	grab #2	21		
			330	58	3

The majority of the available growth data were for *E. laminata*, and this species best fits the standard tube worm model for declining growth rate with increasing size (Figure 16-3). This is in contrast to the growth form of the other modeled escarpid species in the Gulf of Mexico, *Seepiophila jonesi*, which exhibited no decline in growth rate with size (Cordes et al. 2007a). When growth is simulated, this species shows a growth rate far slower than the previously examined upper slope species. Growth was higher at the deeper sites, AT340 and AC818, than it was at the shallower GC852 site (Figure 16-3). The average size of all of the *E. laminata* measured in this study (n = 1382) was 42.4 cm, corresponding to an age of 58 y (99.9 percentile growth = 38 years, 0.1 percentile growth = 87 years) (Figure 16-4). Based on the size of the largest tube worm collected (148.8 cm), this species may attain ages in excess of 1,000 years (avg = 1,809 year, 99.9 percentile growth = 1,680 years, 0.1 percentile growth = 2,127 years). However, it is possible (probable) that this individual underwent fairly rapid growth compared to the average. Based on the maximum measured growth rate of 4 $cm \cdot year^{-1}$ this individual could have attained this size in only 36 years, but this should be considered an extreme estimate since few individuals are likely to maintain the maximum measured growth for their entire existence. Assuming this individual exhibited positive growth every year, and using the average value for

positive growth of *E. laminata* (0.725 cm·year^{-1}), this individual would be 205 years old. Again, this is a highly conservative estimate, but may be more realistic than an age of 1.680 years based on the average modeled value.

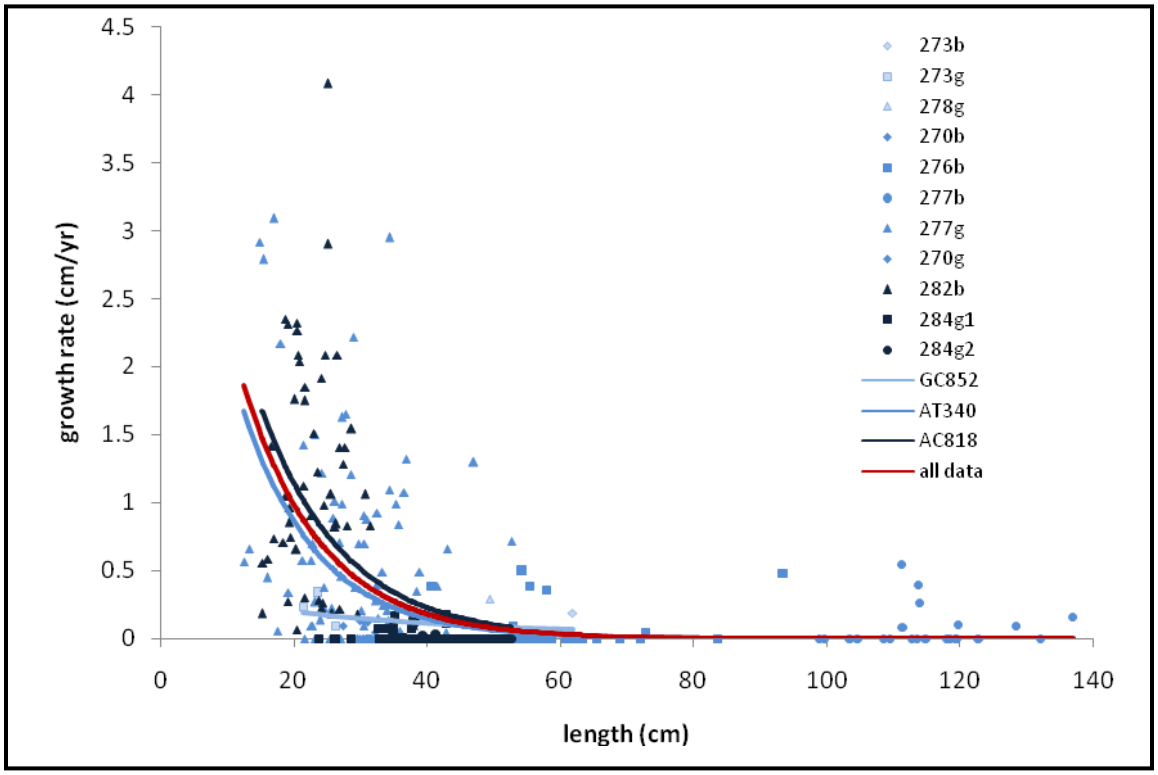

Figure 16-3. Non-linear regression of size specific growth rate for *Escarpia laminata*. Data are coded by color within site and by shape within aggregation. Numbers correspond to *Jason II* dive numbers and letter correspond to collection where b = bushmaster and g = grab. Regressions are presented for each site and for all data together.

These estimates are corroborated by the growth rates found in individuals that had been banded in 1992 (Table 16-2). These individuals were all estimated to be between 60 cm and 1 m in total length above the substrate from the video taken in 2007. Growth of the five living worms over that last 15 years ranged from 1 to 4 cm. Although growth was only recorded in a small number of animals, the fact that the banded animals were approximately the same length as nearby animals in 1992 and 2007 (Figure 16-2) suggests their growth was typical of tube worms in these aggregations. The average annual growth rate for these individuals was 0.138 cm·year^{-1} (sd = 0.078 cm·year^{-1}). This corresponds to the predicted growth rate of a 43 cm individual from the growth model, suggesting that the model may be slightly underestimating growth of larger individuals. At this longer-term integrated rate of growth, an average-sized (42 cm) individual would be 304 y old, and the largest collected individual (150 cm) is estimated to be 1,087 years old.

Table 16-2

Growth Rates in Individuals Banded in 1992

Band name	Date banded	1992 Status	2007 Status	Tag-to-tip distance in 1992 (cm)	Tag-to-tip distance in 2007 (cm)	Total growth (cm)	Annual growth (cm/y)
B23WS	5/23/1992	Large animal	found-live	5.6	6.6	1.0	0.067
G57WT	5/23/1992	Small animal	found-dead	3.4	3.3	-0.1	N.A.
W3WR	5/23/1992	Medium animal	found- live	2.0	2.8	1.6	0.107
G58WP	5/24/1992	Animal withdrawn	not found	2.7			
R47TS	5/24/1992		found- live	1.5	5.5	4.0	0.267
W5WT	5/24/1992		not found	1.2			
G29SG	5/24/1992		tag found on ground	1.2			
R8WS	5/24/1992		found- live band slid, no measurement	1.0			
W4WS	5/24/1992		found-live (cap)	2.0	3.5	1.5	0.100
G27TG	5/25/1992	near black bubbles	not found	1.4			
W2WP	5/26/1992	near bacteria-covered mussels	found-live	2.8	5.1	2.3	0.151
B20WG	5/26/1992	near bacteria-covered mussels	found-dead	2.0	1.3	-0.7	N.A.
G56WR	5/26/1992	near brown mussels	not found	1.8			
R7WG	5/26/1992	near brown mussels	not found	2.0			

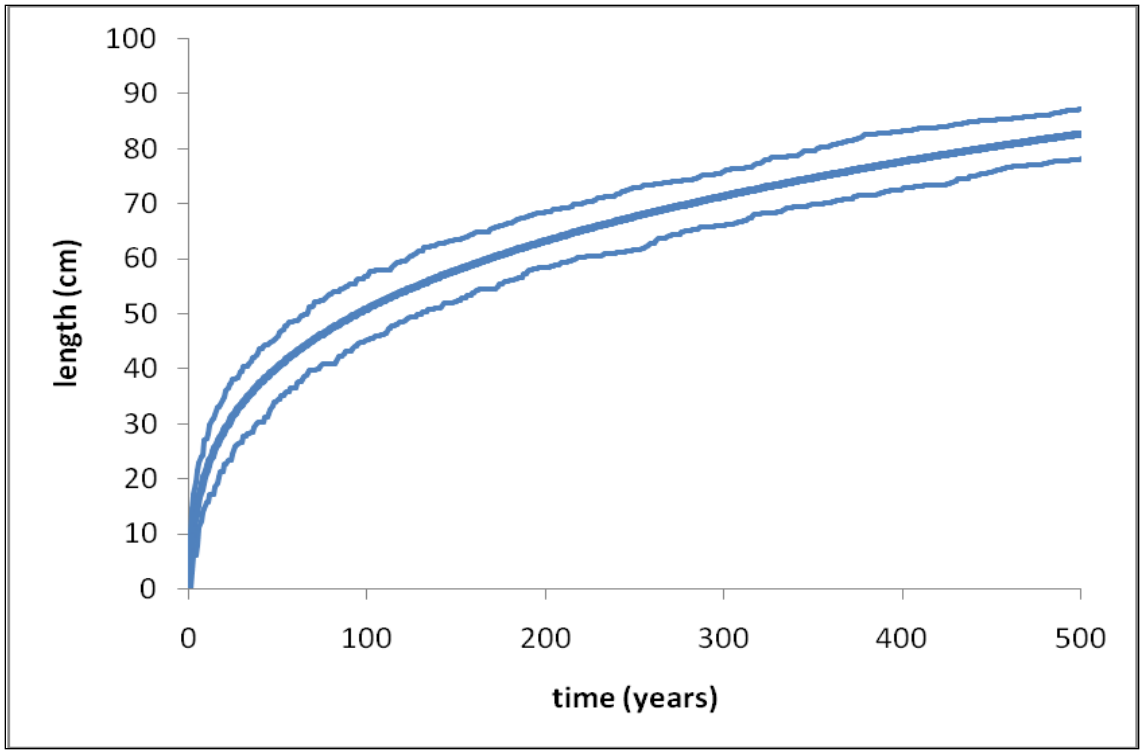

Figure 16-4. Modeled growth of *Escarpia laminata*. Results presented are the average, maximum, and minimum size of 1,000 iterations of the growth model.

The other two species of tube worms had far fewer available data to fit the models. *Lamellibrachia* sp. 1 did not exhibit a declining growth rate with size (Figure 16-5). There was also no significant decline in the frequency of growth with size in this species (Figure. 16-6). Growth was simply modeled as a constant probability of growth (pg = 0.621) and an average growth rate (0.27 ± 0.19 cm·year^{-1}) derived from all individuals who exhibited non-zero growth. Simulations of this simplified model resulted in age estimates for the largest collected individual (106 cm) of between 535 y and 682 y, and ages for a 50 cm individual estimated to be between 225 and 327 years (Figure. 16-7). Using the maximum growth rate measured (0.81 cm·year^{-1}) and assuming positive growth every year, these large and average-sized individuals would be 130 y and 62 years old, respectively. Only three *Lamellibrachia* sp. 2 individuals were stained and collected during the course of this study. They all exhibited some growth with annual growth rates of 0.30, 0.38, and 0.69 cm·year^{-1}. Based on these growth rates, a 60 cm long individual would be between 87 years and 200 years old. Without additional data for these species, it is difficult to determine the accuracy of these age estimates, but the existing data suggest that these species are generally slow growing and long-lived, just as the other seep tube worms of the GoM studied to date.

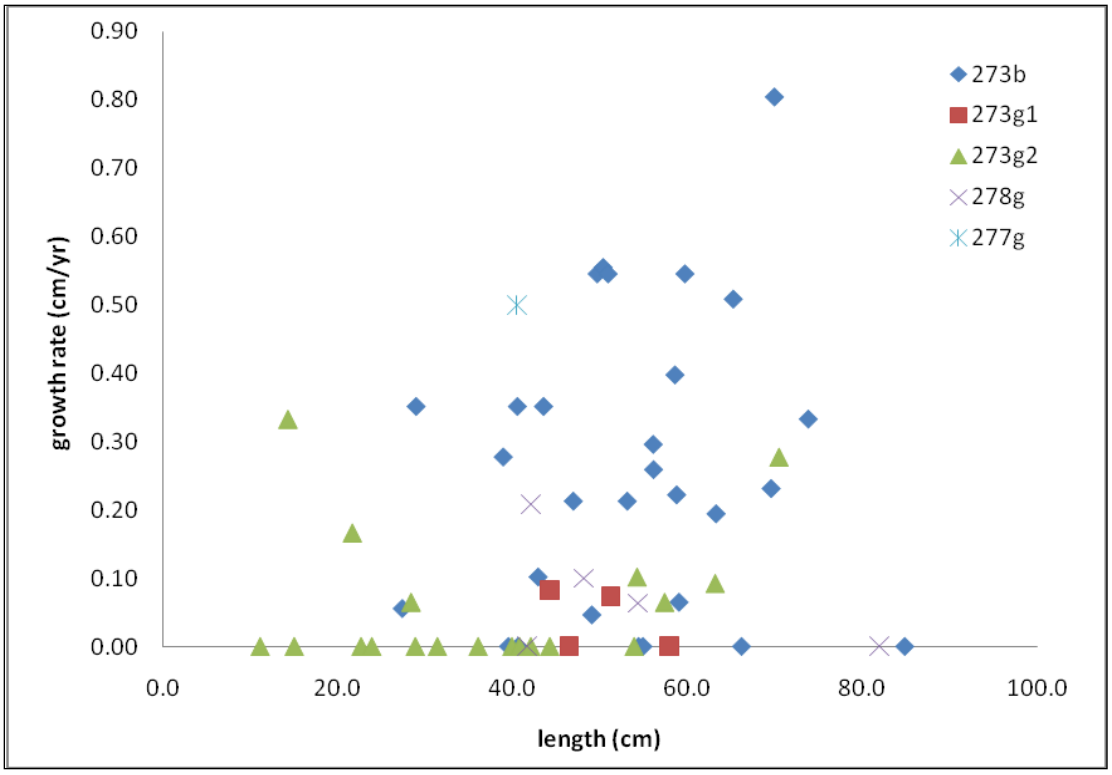

Figure 16-5. Growth rates of *Lamellibrachia* sp. 1 from 5 different collections. B = Bushmaster, g = grab

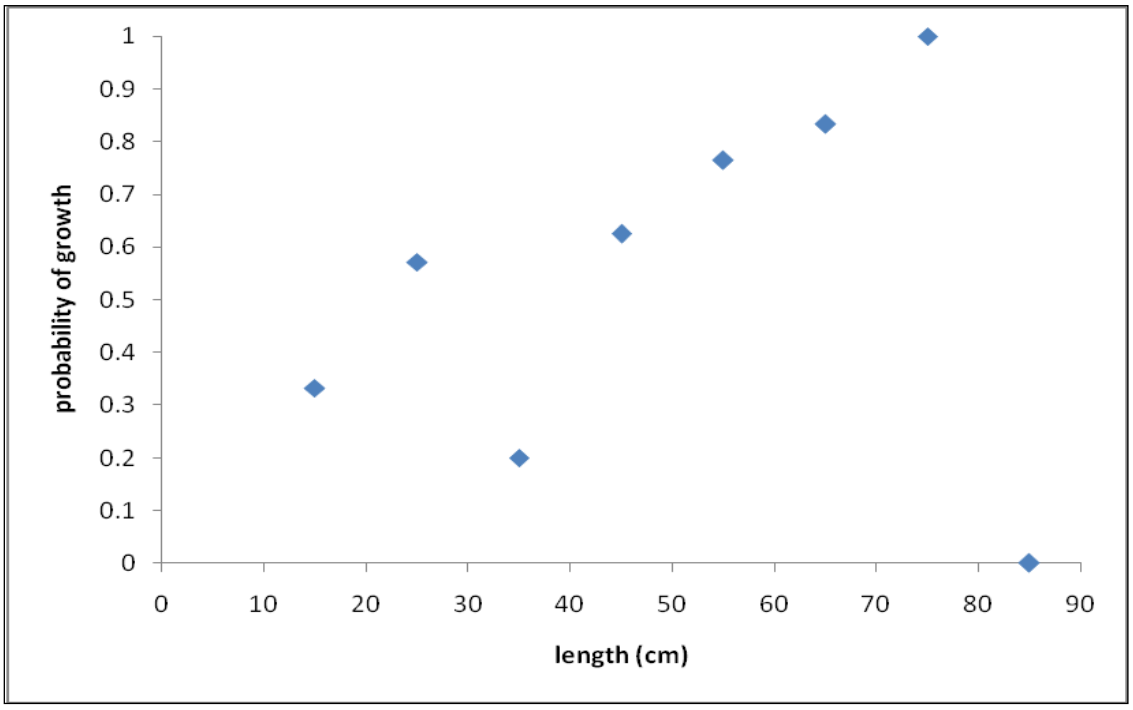

Figure 16-6. Proportion of *Lamellibrachia* sp. 1 individuals in each 10 cm size class that exhibited positive growth.

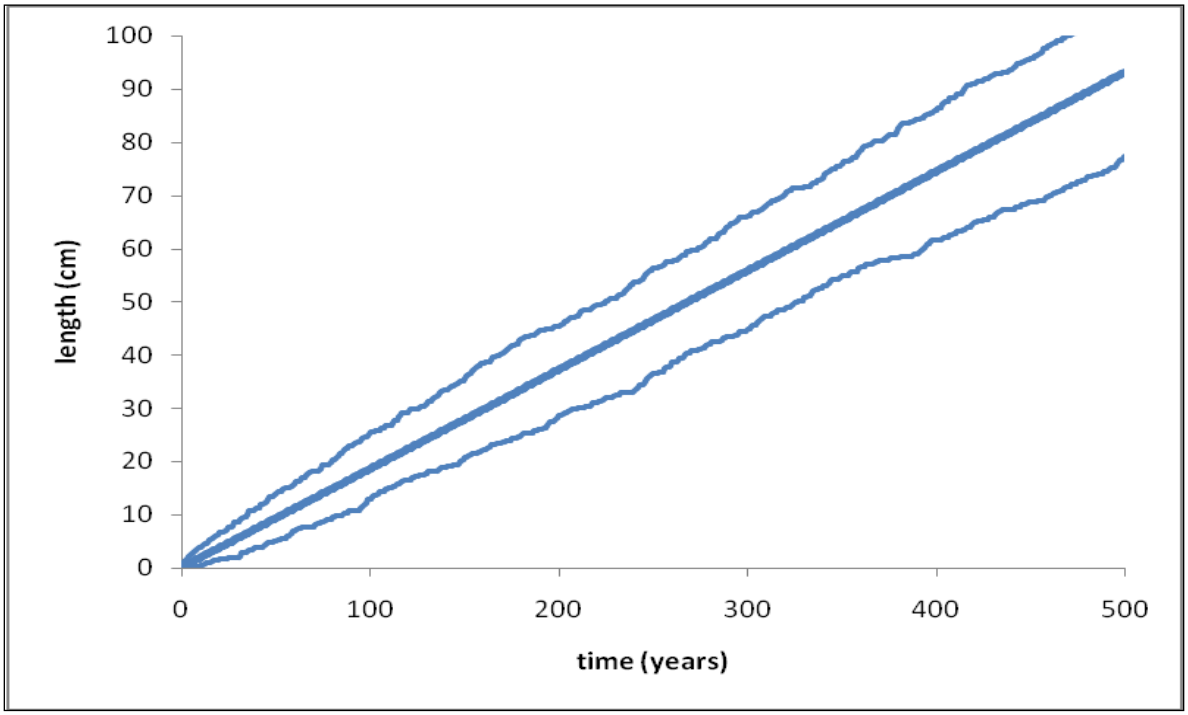

Figure 16-7. Modeled growth of *Lamellibrachia* sp. 1 using an average probability of growth and an average positive growth rate from all collected individuals.

17. TISSUE STABLE ISOTOPE ANALYSES

17.1. Introduction

Analyses of the stable carbon, nitrogen, and sulfur content of tissues from the seep fauna was used to address a number of different questions. By comparing the carbon (C), nitrogen (N), and sulfur (S) delta values among collections of mussels and tube worms from different collections, we can gain insight into site-specific differences in endmember seep fluid composition, identify the most likely inorganic chemical species utilized by different taxa, and assess possible resource partitioning between co-occurring species. By analyzing the C, N, and S delta values of non-symbiont containing seep fauna we can determine the degree to which these heterotrophic fauna depend nutritionally upon seeps, whether their isotope values seep to reflect those of their symbiont-containing foundation species, and, in some cases, we can assess specific predator-prey relationships between taxa. By analyzing the C, N, and S delta values of more mobile background fauna we can evaluate the degree of export of seep primary production through these species.

17.2. Methods

17.2.1. Sampling

Tissue samples were analyzed for stable isotopes from both quantitative and non-quantitative mussel, vestimentiferan, and monoliferan/frenulate (hereafter referred to as "monoliferan") community collections, as well as from samples of background fauna collected by trawls, traps, and opportunistically. Details on the collection methods are given in the in situ methods section of this report. Up to six individuals of each foundation faunal species per collection site were sampled for stable isotope analysis by dissecting a piece of mantle tissue (mussels and clams) or vestimentum (vestimentiferans). Monoliferans and frenulates were sampled whole, including the tube, as these individuals were very small and differences in isotope values between tubes and tissue were previously found to be very small (CRF, unpublished data). Up to three individuals of each species of associated fauna were sampled for stable isotope analysis. When possible, associated fauna were sampled by dissecting a piece of muscle tissue, and whole individuals were sampled for species that were too small to obtain adequate muscle tissue. The samples were rinsed with deionized water to remove any residual seawater and frozen at -70°C. Figure 17-1 shows the sites from which we made mussel and clam collections and Figure 17-2 shows the sites from which we made tube worm and monoliferan collections. The site names are based on BOEM lease block designations and consist of a two-letter abbreviation, which stands for the region (AC=Alaminos Canyon, for example), followed by a three-digit number. Usually, three of these six samples were processed and analyzed for carbon and nitrogen isotopic content, but in some cases more were analyzed.

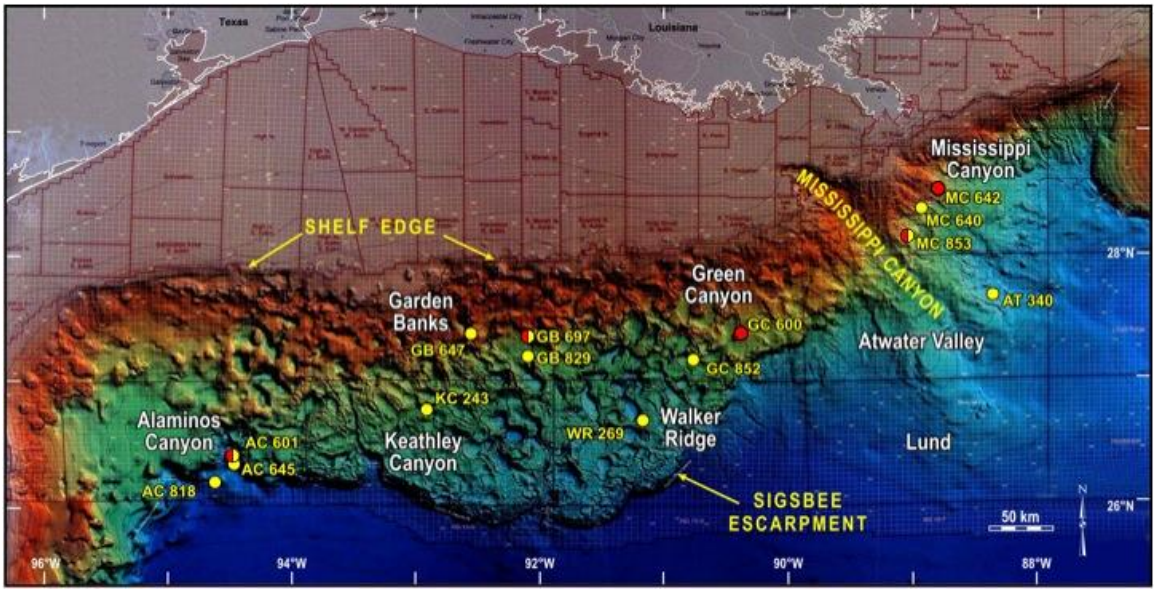

Figure 17-1. Map of study sites from which mussels and clams were collected.
Yellow site markers signify sites where mussels were collected, red signifies sites were clams were collected, and markers that are half yellow and half red signify sites where both clams and mussels were collected.

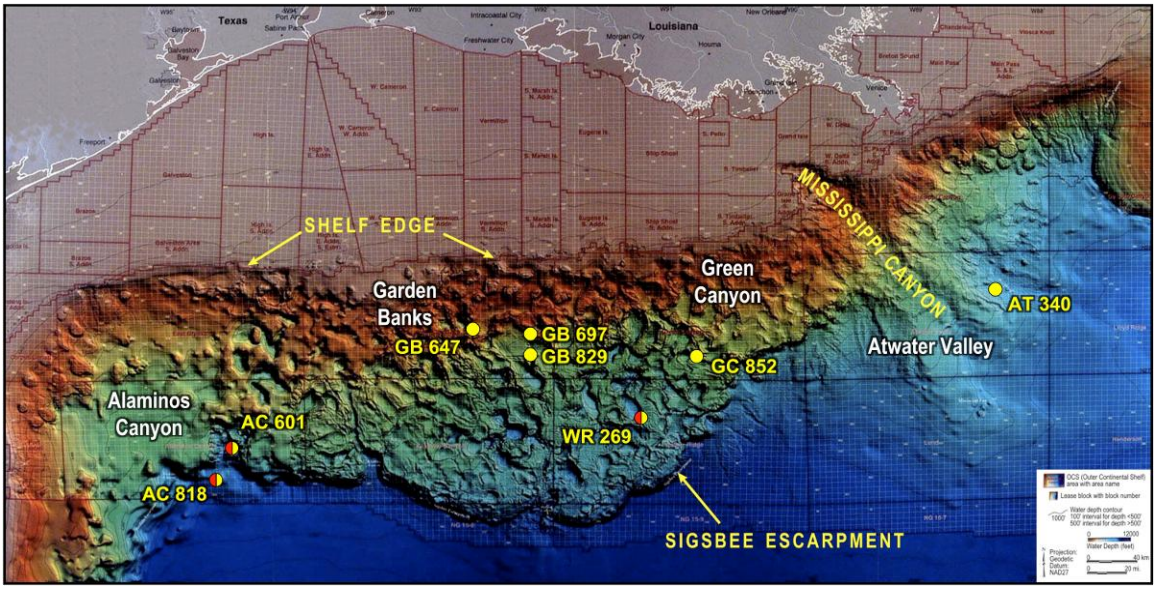

Figure 17-2. Map of study sites from which vestimentiferan, monoliferan, and frenulate siboglinid tube worms were collected.
Yellow site markers signify sites where vestimentiferan tube worms were collected, and markers that are half yellow and half red signify sites where both vestimentiferans and monoliferans were collected.

17.2.2. Stable Isotope Analysis

In the laboratory, all samples were dried at 60°C, homogenized, and acidified to remove any inorganic carbonate. Samples were redried and most subsamples were analyzed for stable carbon and nitrogen isotope composition at the Stable Isotope Facility at the University of California, Davis using an Integra elemental analyzer coupled with a PDZ Europa 20-20 isotope ratio mass spectrometer (Sercon Ltd., Cheshire, United Kingdom). Fourteen samples were analyzed by Raymond W. Lee (School of Biological Sciences, Washington State University) using a Costech (Valencia, CA United States) elemental analyzer. The resulting N_2 and CO_2 gases were separated by gas chromatography and admitted into the inlet of a GV Instruments (Manchester, United Kingdom) Isoprime isotope ratio mass spectrometer (IRMS) for determination of $^{15}N/^{14}N$ and $^{13}C/^{12}C$ ratios. Fourteen samples were analyzed by Stephen A. Macko (University of Virginia Stable Isotope Laboratory) using continuous-flow isotope ratio mass spectrometry involving a Carlo Erba elemental analyzer coupled to a Micromass Optima IRMS. The different analytical laboratories are calibrated to National Institute of Standards and Technology (NIST) reference materials and no one laboratory analyzed a data set that is compared with the data set from the other laboratory. We also avoided drawing broad conclusions based on small differences in isotope values.

Values are expressed using δ (delta) notation and reported in units of permil (‰), where

$$\delta X = [(R_{sample}/R_{standard}) - 1] \times 10^3,$$

$X = {}^{13}C$, ^{15}N, or ^{34}S and $R = {}^{13}C/{}^{12}C$, $^{15}N/^{14}N$, or $^{34}S/^{32}S$.

PDB was used as the standard for carbon, air N_2 for nitrogen, and Canyon Diablo triolite for sulfur.

17.2.3. Statistical Analyses

To assess the significance of differences among isotope values among collections, sites, or habitat types (i.e. foundation fauna type) we used one-way ANOVA and Tukey's honestly significant differences where assumptions for parametric tests were met. When these assumptions where not met, we used a nonparametric Kruskal-Wallis test. Tests were carried out only for collections that had three or more individuals. Where only two groups were being tested (two species within a collection, two collections within a site, etc.) we used a two-sample t-test when parametric assumptions where met and a Mann-Whitney test when they were not. All statistical analyses were carried out using Minitab 15® statistical software.

17.3. Implications of the Symbiont-Containing Bivalve Tissue Stable Isotope Signatures

17.3.1. Bathymodiolin Mussel $\delta^{13}C$ Results

Bathymodiolin mussel tissue $\delta^{13}C$ values ranged from about -72 to -40‰. This range is comparable to ranges previously reported for seep mussels elsewhere in the GoM (Cary et al., 1989; Kennicutt et al., 1992) (Table 17-1). Even within each species, the range in $\delta^{13}C$ values was at least 26‰ (Table 17-1). The majority of collection mean $\delta^{13}C$ values were between -70.8 and -58.8‰, although there were several more enriched outliers (Figure 17-3a): the GB647 and AC645 study sites each had single collections of *B. childressi* and *B. heckerae*, respectively, and

the respective means for these collections were -48.7 ± 1.4‰ and -40.4 ± 0.2‰, and 5 collections from AC818 ranged from -54.9 to -44.1‰. Within sites, collection means typically had a range of no more than 12‰ (Figure 17-3a); however, the three collections at AC601 had a large range in mean $\delta^{13}C$ values from -65.6 to -46.0‰ (Figure 17-3a).

Table 17-1

Means and Standard Deviations for Tissue $\delta^{13}C$, $\delta^{15}N$, and $\delta^{34}S$ Compositions of Seep Mussels (*Bathymodiolus* spp.) and Clams (*Calyptogena* spp.) on the Lower Louisiana lope

species	N_{CN}	N_S	$\delta^{13}C$ (‰) mean ± sd	min	max	$\delta^{15}N$ (‰) mean ± sd	min	max	$\delta^{34}S$ (‰) mean ± sd	min	max
Bathymodiolus brooksi	63	60	-60.9 ± 6.9	-72.3	-44.6	-4.4 ± 2.9	-14.8	2.2	11.1 ± 5.9	-10.9	18.5
B. childressi	30	18	-61.9 ± 8.1	-72.2	-45.8	-5.9 ± 8.3	-23.5	2.9	13.2 ± 4.9	0.5	20.5
B. heckerae	15	7	-57.6 ± 10.4	-67.6	-40.2	-2.3 ± 2.5	-6.3	1.9	8.1 ± 5.6	2.3	16.2
Calyptogena ponderosa	9	9	-35.8 ± 0.8	-37.0	-34.4	-1.0 ± 4.4	-9.2	4.4	4.0 ± 4.5	-1.2	12.8
Calyptogena sp. nov.	3	3	-34.7 ± 0.6	-35.4	-34.4	1.2 ± 1.2	-0.1	2.2	-8.2 ± 5.7	-14.1	-2.9

Within each *Bathymodiolus* species, Kruskal-Wallis tests revealed significant difference in tissue $\delta^{13}C$ values among sites ($p \leq 0.02$). The largest differences in $\delta^{13}C$ between sites were between AT340 (median -67.2‰) and AC818 (median -52.2‰) for *B. brooksi*, GC852 (median -68.6‰) and AC601 (median -45.9) for *B. childressi*, and AT340 (median -64.0‰) and AC645 (median -40.4‰) for *B. heckerae*.

There were also significant differences in tissue $\delta^{13}C$ values within mussel species among some collections within sites. *B. brooksi* at AT340 and GC852 showed significant pairwise differences between all collections containing three or more samples (3 collections at AT340 and 5 collections at GC852; $p<0.001$ for all comparisons) and significant differences among collections within the AC601 and AC818 study sites ($p=0.05$ and 0.02, respectively). *B. childressi* tissue $\delta^{13}C$ was significantly different among collections at one of the two sites containing large enough samples for analysis (GB697 $p=0.03$; GC852 $p=0.10$). The only site that contained two collections of *B. heckerae* was AC818, but these contained one and two samples, respectively. The two individuals from the same collection had tissue $\delta^{13}C$ values of -44.1 and -44.2‰ and the one from the other collection had a $\delta^{13}C$ value of -52.5‰.

17.3.2. Bathymodiolin Mussel $\delta^{15}N$ Results

The overall ranges in tissue $\delta^{15}N$ in *B. brooksi* and *B. childressi* were quite large (16 and 27‰, respectively) (Table 17-1); however, the majority of collection mean tissue $\delta^{15}N$ values were between -6.8 and 2.3‰ (Figure 17-3b), similar to the ranges of these species from the upper Louisiana slope and Florida Escarpment (Cary et al., 1989; Kennicutt et al., 1992).

All of the collections with outlying mean $\delta^{15}N$ values were the only collections made at their respective sites, and all contained the mussel *B. childressi*, although when *B. brooksi* co-

occurred, it had similar $\delta^{15}N$ values (Figure 17-3b). The tissue $\delta^{15}N$ values in *B. childressi* collected from GB 647 ranging from -23.7 to -21.7‰ were the most depleted values yet reported for seep invertebrates (Figure 17-3b). The next most depleted $\delta^{15}N$ values in this study were found in *B. brooksi* and *B. childressi* from MC853 and MC640 (-15.6 to -10.9‰) (Figure 17-3b). Values in this range have previously been reported for *B. childressi* (Dattagupta et al., 2004; Kennicutt et al., 1992).

Kruskal-Wallis tests revealed that tissue $\delta^{15}N$ values were significantly different among sites for all three *Bathymodiolus* species ($p \leq 0.02$). The largest pairwise differences in $\delta^{15}N$ between sites were between MC853 (median -11.7‰) and WR269 (median 0.3‰) for *B. brooksi*, GB647 (median -23.2‰) and GB697 (median 1.7‰) for *B. childressi*, and GB697 (median -6.2‰) and AT340 (median -4.5‰) for *B. heckerae*.

Two-sample t-tests showed significant differences in *B. childressi* tissue $\delta^{15}N$ between collections within the GB697 and GC852 study sites ($p=0.04$ and $p=0.02$, respectively). The samples at GB697 were about 1 km apart and the two at GC852 were about 0.5 km apart. The only significant difference in *B. brooksi* $\delta^{15}N$ among collections within a site was at AT340; one-way ANOVA revealed significant differences among collections ($p=0.001$) and that one sample was different from the other two, but the other two are not significantly different from each other. The different collection was much farther away from the other two collections than they were from each other (1 km vs. 18 m). One-way ANOVA revealed no significant differences in *B. brooksi* tissue $\delta^{15}N$ between collections within sites at AC601 ($p=0.07$), AC818 ($p=0.21$), and GC852 ($p=0.06$). Again the two collections of *B. heckerae* at the AC818 study site did not contain enough samples for statistical analysis, but qualitatively, the difference in $\delta^{15}N$ was about 2‰, which is no greater than the difference between two *B. heckerae* individuals within a single collection at AT340.

17.3.3. Bathymodiolin Mussel $\delta^{34}S$ Results

The overall range in $\delta^{34}S$ for bathymodiolin mussels was large, ranging from -10.9 to 20.5‰. The range within species was also quite large, ranging from -10.9 to 16.2‰ in *B. heckerae*, 0.5 to 20.5‰ in *B. childressi*, and 0.9 to 18.5 in *B. brooksi*. The majority (about 92%) are at least 3‰ more depleted than seawater sulfate ($\delta^{34}S = 20.3$‰). The mussels with the most enriched tissue $\delta^{34}S$ values were *B. childressi* from the MC640 collection ($\delta^{34}S = 15.3$ to 20.5‰) and the most depleted tissue $\delta^{34}S$ values were in *B. heckerae* from the AC645 collection (-10.9 to -2.8‰).

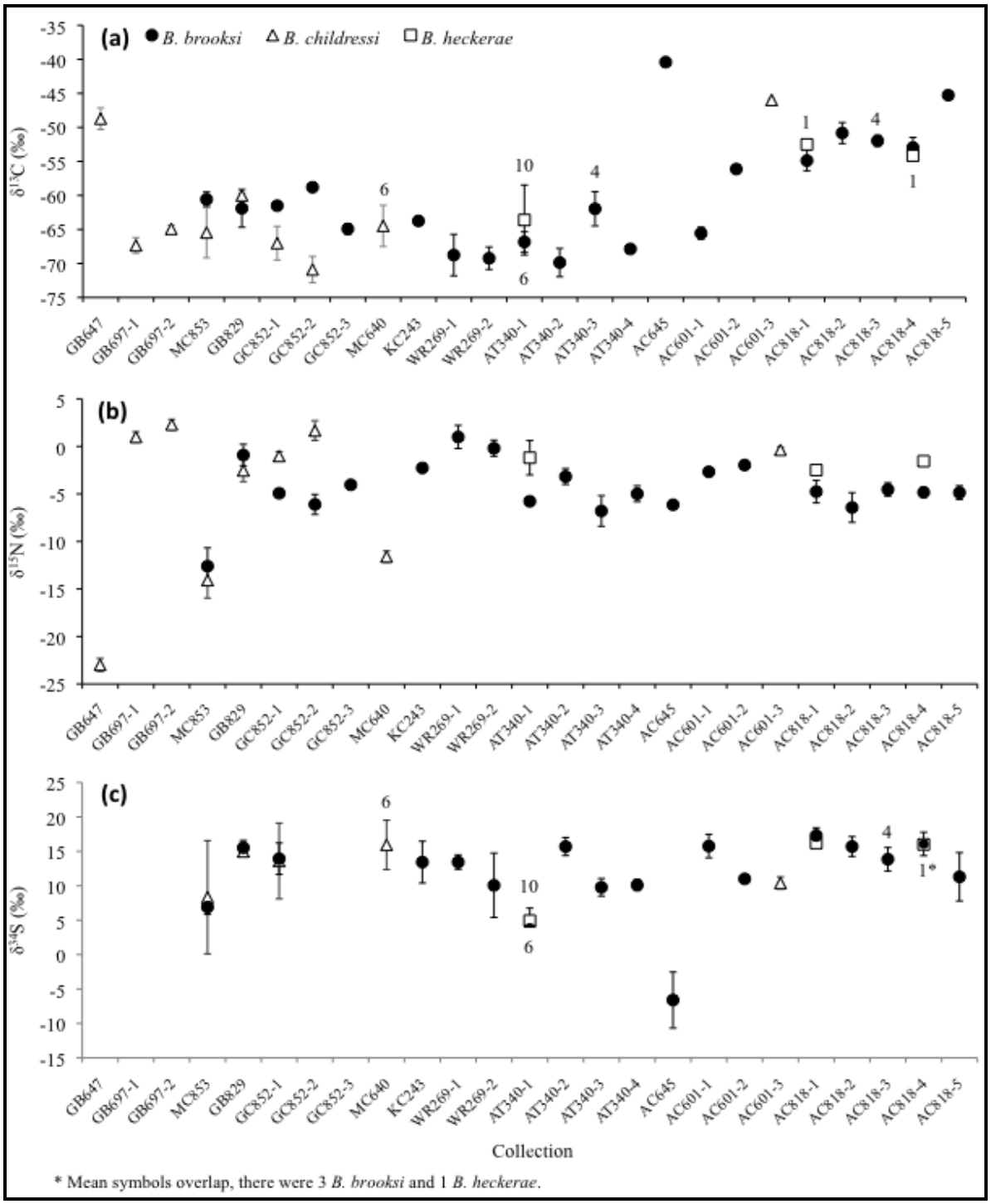

Figure 17-3. Average and standard deviation of tissue (a) $\delta^{13}C$, (b) $\delta^{15}N$, and (c) for all mussel collections.

Mean symbols represent the mean for three individuals unless otherwise indicated by a number above or below the symbol. The sample sizes for carbon and nitrogen are the same.

17.3.4. $\delta^{13}C$, $\delta^{15}N$ and $\delta^{34}S$ in Co-Occurring Mussel Species

In all collections containing both *B. brooksi* and *B. heckerae*, $\delta^{15}N$ was more enriched in *B. heckerae*, although not always significantly so (Figure 3b). *B. brooksi* and *B. heckerae* tissue $\delta^{13}C$ and $\delta^{15}N$ values were significantly different from each other in one of the two collections that contained three or more individuals of both species (AT340 $\delta^{13}C$ p=0.04; $\delta^{15}N$ p=0.01) and not significant in the other (AC818 $\delta^{13}C$ p=0.07; $\delta^{15}N$ p=0.77). *B. brooksi* and *B. childressi* tissue $\delta^{13}C$ were not significantly different within collections at GB829 (p=0.36), GC852 (two collections: p=0.06 and p=0.08), and MC853 (p=0.09). Qualitatively, tissue $\delta^{13}C$ in *B. childressi* tends to be more depleted than *B. brooksi* where they co-occur, which is the opposite of what has previously been seen for these species (Figure 17-3b) (Fisher et al., 1993). Tissue $\delta^{15}N$ for these two species was not significantly different within collections at GB829 (p=0.16) and MC853 (p=0.40) but was significantly different in the two collections from GC852 (p<0.001 and p=0.001). Where significant differences in $\delta^{15}N$ did occur, in two collections at the GC852 study site, *B. brooksi* was more depleted than *B. childressi* (Figure 17-3b). Co-occurring mussel species did not have any notable difference in $\delta^{34}S$ values, even in collections that contained both *B. childressi* (only methanotrophic endosymbionts) and *B. brooksi* (both methanotrophic and chemoautotrophic endosymbionts).

17.3.5. Discussion of Mussel Tissue Stable Isotope Signatures

Bathymodiolin mussels on the lower continental slope had a wide range of $\delta^{13}C$ values both overall and within species (Table 17-1). Significant and sometimes very large differences among sites and collections indicate that a large component of the overall range is likely due to differences in the isotopic composition of the endmember carbon sources. However, a portion of the variability in tissue $\delta^{13}C$ values will also be a function of different animal and symbiont activities among species and microhabitats. Tissue $\delta^{13}C$ values in *B. childressi* largely reflect the isotopic composition of methane in the local environment (Brooks et al., 1987). In a previous study, Fisher et al. (1993) found that *B. brooksi* that co-occurred with *B. childressi* had more depleted tissue $\delta^{13}C$ values. Since *B. brooksi* harbors both methanotrophic and chemoautotrophic endosymbionts, this finding contradicted the expectation that the tissue $\delta^{13}C$ values of the mussels would reflect a mixture of organic carbon derived from methane (<-50‰) and seawater CO_2 fixed via sulfide oxidation (-47 to -23‰; Fisher, 1990). The authors concluded that the chemoautotrophic symbionts that can co-occur in the same host cells as the methanotrophic symbionts might be fixing, and further fractionating, isotopically light respired carbon derived from methane. In the present study, with a much larger data set, we found either no difference or the opposite trend for co-occurring *B. brooksi* and *B. childressi*, with *B. childressi* having very similar or more depleted $\delta^{13}C$ values than *B. brooksi* (Fig. 2). Authigenic carbonates that formed as a result of microbial methane oxidation and SR reflect the $\delta^{13}C$ composition of pore water DIC (Roberts and Aharon, 1994). Carbonates collected with mussels in this study ranged in $\delta^{13}C$ from -51.7 to -28.7‰ (Roberts et al. this issue), indicating that significant fixation of pore water DIC by chemoautotrophic endosymbionts could also produce highly depleted tissue $\delta^{13}C$ values. Thus, incorporation of varying amounts of pore water DIC, methane, and seawater CO_2 and differences in $\delta^{13}C$ composition of the DIC pool could potentially produce tissue $\delta^{13}C$ values in *B. brooksi* that are the same as, more depleted than, or more enriched than co-occurring *B. childressi*. These findings caution against interpretations based on small data sets and suggest

that metabolic activities of the two symbiont types and interactions between them are likely different under different environmental conditions.

Another unexpected finding was a relatively large range in tissue $\delta^{13}C$ values in *B. childressi* within some collections. *B. childressi* tissue $\delta^{13}C$ values spanned 7 and 9‰ in the MC853 and MC640 collections, respectively. This was unexpected since *B. childressi* obtains the bulk of its nutritional carbon from methane, and previous studies found very little variation among individuals within a collection and virtually no fractionation during assimilation (Dattagupta et al., 2004). The variability suggests either that there is very small-scale spatial variability in the isotopic composition of the methane in a single mussel bed, or that individuals are deriving varying degrees of input from a different source, such as filter-feeding. Neither possibility can be discounted because near-surface biogenic methane production could shift the isotopic composition of methane on small spatial scales, and alternatively these mussels can supplement their nutrition by filter feeding (Page et al., 1990).

The two mussel species *B. brooksi* and *B. heckerae* both contain dual symbioses with methanotrophic and chemoautotrophic bacteria and can potentially utilize different inorganic carbon sources. However, when *B. brooksi* co-occurred with *B. childressi* their tissue $\delta^{13}C$ values differed by no more than 5.5‰. In fact, in the collections discussed above, with the large range in tissue $\delta^{13}C$ values in *B. childressi*, the co-occurring *B. brooksi* had a range of only 2‰ (n=3 for both species in both collections). Since the variation in tissue $\delta^{13}C$ values of individuals of all species is much smaller within a collection than among collections and there is no consistent substantial difference among species within collections, we assume that the tissue $\delta^{13}C$ values of all species generally reflects the composition of the local methane source when making comparisons between sites with large differences in the tissue $\delta^{13}C$ values.

The methane in GoM seep fluids originates from both geological processes deep within the crust (thermogenic) and from microbial degradation of seeping crude oil, which occurs closer to the sediment surface (biogenic). Each of these processes produces methane with distinctive $\delta^{13}C$ composition. On the upper Louisiana slope, the salt tectonics are characterized by vertical migration of the underlying salt, forming salt domes and pillars. Due to this variability in depth of the salt, some sites have methane of mostly thermogenic origin while others have methane that is largely biogenic. At sites on the upper slope where methane release is mostly of thermogenic origin, seep mussels have tissue $\delta^{13}C$ values around -40‰ (Brooks et al., 1987; Dattagupta et al., 2004), while at sites on the upper slope where methane has a biogenic component, seep mussels have tissue $\delta^{13}C$ values between -63 and -57‰ (MacAvoy et al., 2008). On the Florida Escarpment, where most of the methane is of biogenic origin (Martens et al., 1991), mussels have tissue $\delta^{13}C$ values around -74‰ (Paull et al., 1985).

The average $\delta^{13}C$ values of collections at AC818 (-54.8 to -44.1‰), AC645 (-40.4‰), and GB647 (-48.7‰) indicate that the methane at these sites is of primarily thermogenic origin (Fig. 2). The majority of mussel collections in this study, however, had average $\delta^{13}C$ compositions between -70.8 and -58.8‰, indicating that biogenic methane comprised a varying but significant portion of the methane at these sites (Bernard et al., 1977; Joye et al., 2010; Schoell, 1983). At the GB647 and GB697 study sites (the shallowest in this study at 1000m), the underlying salt tectonics are characterized by isolated salt masses (pillars) as is seen on the rest of the upper Louisiana slope. Whereas GB647 had mussels with tissue $\delta^{13}C$ values indicating methane of thermogenic origin, mussels at GB697 had tissue $\delta^{13}C$ values more indicative of a significant

biogenic component (mean $\delta^{13}C$ = -67.3 to -64.9‰). This variability between two sites in the same region at the same depth is typical of the upper slope and is likely caused by differences in depth of the salt layer at the different sites. Unlike the upper slope, the lower slope landward of the Sigsbee Escarpment is characterized by lateral migration of a shallow, solid salt sheet toward the Escarpment (Peel et al., 1995). Alaminos Canyon is a reentrant into the Sigsbee Escarpment (Figure 17-1) and as such has access to deeper thermogenic methane. The AC818 and AC645 study sites are within the canyon, and thus mussels at these sites reflect the use of thermogenic methane.

The AC601 study site was the only site at which the range of mean $\delta^{13}C$ values (-65.6 to -45.0‰) was indicative of methane that is of highly thermogenic origin and of highly biogenic origin in different collection locations within the same study site. The northernmost collection at AC601 (AC601-1) had $\delta^{13}C$ values (mean -65.5‰) more closely resembling the $\delta^{13}C$ values of mussels at most other sites on the lower slope, likely because this collection sits atop the shallow laterally migrating salt sheet. Conversely, the two southern collections are inside the canyon and have $\delta^{13}C$ values that more closely resemble the values of mussels at AC645 and AC818, which are located seaward of the Sigsbee Escarpment and express methane of thermogenic origin. Smaller-scale differences in the local environment can also have substantial effects on the microbial alteration of methane before it is released from the sediment surface, where it is available for uptake by mussels. The AC601-2 (mean $\delta^{13}C$=-56.1‰) and AC601-3 (mean $\delta^{13}C$=-45.0‰) collections (Fig. 2) were obtained on the same dive 25.8 m from each other in the southern area of the site. The AC601-2 collection consisted of *B. brooksi* in an isolated patch close to the shore of a large brine lake, while the AC601-3 consisted of *B. childressi* collected from the middle of a large contiguous mussel bed. The AC601-1 collected ~2.5km north of the other two also consisted of *B. brooksi* partially buried in mud near a brine pool. Briny sediments have been shown to contain more isotopically depleted methane than non-brine sediments at the same site (Joye et al., 2010).

In general, there was less variability among individuals within sites than overall and still less variability among individuals within collections (Figures 17-4, 17-5), reflecting differences in the composition of local methane pool across different spatial scales. Within sites overall, there is no apparent correlation between the distance separating collections and similarity in their tissue $\delta^{13}C$ values. Thus, methane isotopic compositions could be very different across a small distance (like 30 m) or very similar over a large distance (like 0.7 km) within a site. Mussels were often collected from visually very distinctive environments within a site—dense mussel beds vs. partially buried in briny sediment supporting bacterial mats, for example. Substantial alteration of the isotopic composition of methane may occur relatively close to the sediment surface as a result of microbial activity. The specific composition, relative abundance, and level of activity of a sediment microbial community depends on a suite of local conditions including supply of organic matter (oil), amount of mixing with seawater, rate of fluid flow, and composition of the seeping end-member fluid. Thus, differences in mussel tissue $\delta^{13}C$ values may reflect environmental parameters such as density and community composition of sediment microbes, which can vary substantially over short distances (Joye et al., 2010).

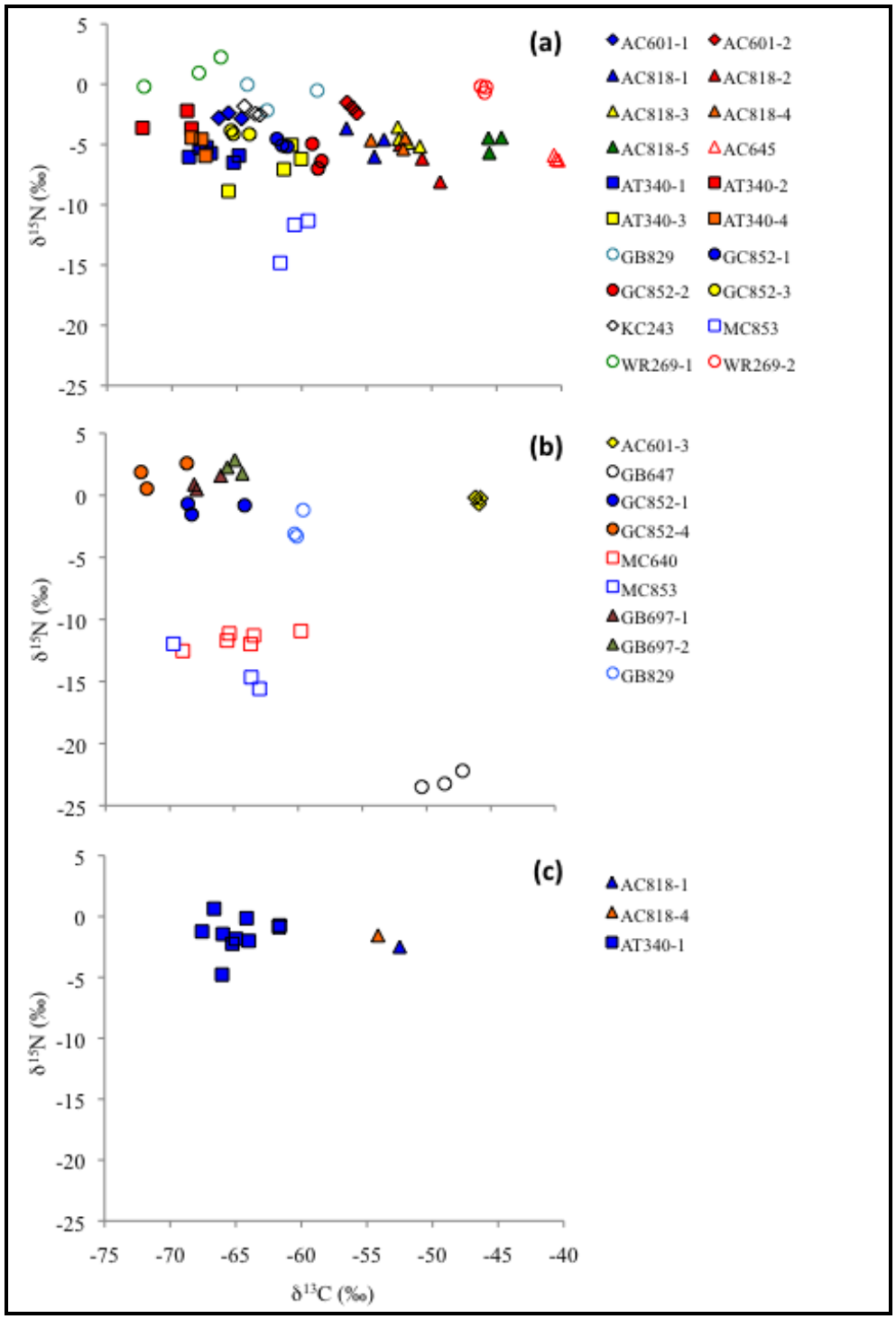

Figure 17-4. $\delta^{15}N$ vs. $\delta^{13}C$ for (a) *B. brooksi*, (b) *B. childressi*, and (c) *B. heckerae*.
Different symbols represent different study sites and different colors represent different collections.

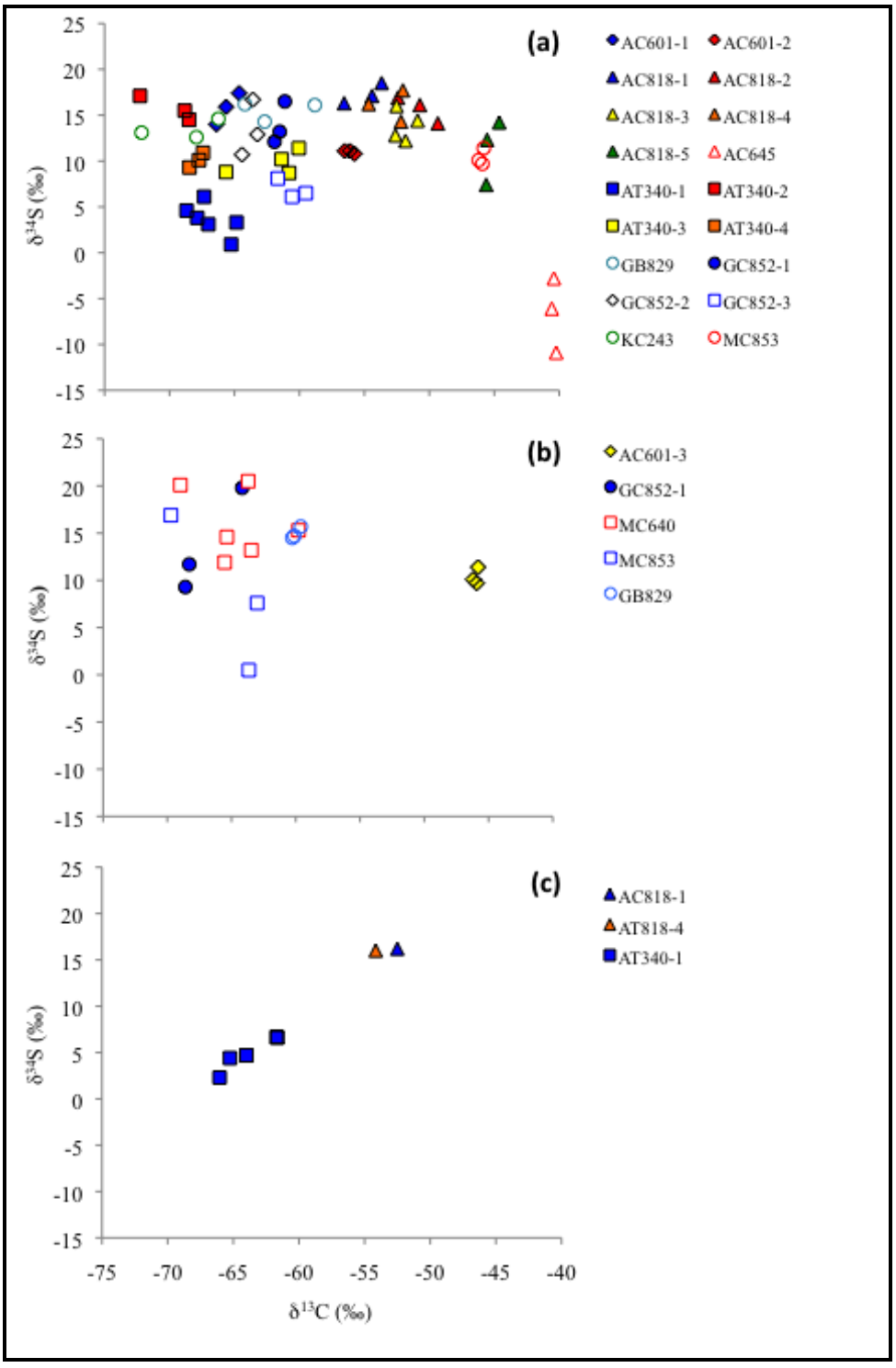

Figure 17-5. $\delta^{34}S$ vs. $\delta^{13}C$ for (a) *B. brooksi*, (b) *B. childressi*, and (c) *B. heckerae*.
Different symbols represent different study sites and different colors represent different collections.

Co-occurring *B. brooksi* and *B. childressi* often had very similar $\delta^{15}N$ compositions; however, in the two collections where the difference in mean tissue $\delta^{15}N$ values between the two species was greater than 6‰, *B. childressi* had more enriched $\delta^{15}N$ values. Both of these collections were from GC852 and could indicate resource partitioning at this site, although our sample size was too small to obtain statistical significance between the two species ($p=0.06$ and 0.08, $n=3$ individuals for each group). Where *B. brooksi* and *B. heckerae* co-occurred, *B. heckerae* had either very similar $\delta^{15}N$ compositions or was more enriched than *B. brooksi*, and this difference was significant for one collection. Again, our sample size is too small to conclude whether nitrogen resource partitioning is occurring between these two species, but these data suggest this is a distinct possibility for all three species.

The most remarkable isotope values in mussels in this study were the highly depleted $\delta^{15}N$ values in *B. childressi* from the GB647 study site. Ranging from -23.7 to -21.7‰, these are the most depleted $\delta^{15}N$ values yet reported in any modern animal, although tropical mangroves and lichens have values as low as -22‰ (Fogel et al., 2008). The next most depleted $\delta^{15}N$ values were found in *B. brooksi* and *B. childressi* from MC853 and MC640 (-15.6 to -10.9‰), which is in the range of the lowest values previously reported for *B. childressi* (Dattagupta et al., 2004; Kennicutt et al., 1992; MacAvoy et al., 2008). *B. childressi* has been shown to take up and assimilate environmental ammonium and free amino acids (Lee and Childress, 1994; Lee et al., 1992). In one study, freshly collected *B. childressi* was also shown to take up and incorporate nitrate (Lee and Childress, 1996). Very low $\delta^{15}N$ values could at least in part reflect very high abundance of one or more of these source compounds in the environment, allowing for high isotopic discrimination during incorporation into organic material. Isotopic fractionation of ammonia can be as high as 27‰ in marine bacteria (Hoch et al., 1994) and 20‰ in marine algae (Waser et al., 1998). Millimolar levels of ammonium have been measured in active seep environments such as the GC233 brine pool on the upper Louisiana slope (Joye et al., 2005; Lee et al., 1992), where *B. childressi* had tissue $\delta^{15}N$ values around -15‰ (Dattagupta et al., 2004). The most isotopically light mussels in this study were collected from a bacterial mat with brine staining. Thus, it is plausible that seeping of hypersaline effluent resulted in elevated concentrations of ammonium, allowing for a high degree of isotopic fractionation (Joye et al., 2010). It is also possible that the nitrogen source pool itself was ^{15}N-depleted. Ammonia can be produced via denitrification to ammonia, which can occur when nitrate is limiting and the concentration of electron acceptors such as DOC is high. The fractionation associated with dissimilatory nitrate reductase is generally in the range of 20 to 30‰ (Granger et al., 2008). If the resulting nitrate is reduced to ammonia, this would result in ammonia that is 20 to 30‰ lighter than the source nitrate. No isotopic data are available for nitrogen in seeping fluids, but the pattern of variability in mussel $\delta^{15}N$ at different spatial scales suggests that increased levels of ammonium are a more likely cause of depleted mussel $\delta^{15}N$ values than sediment microbial alteration of dissolved inorganic nitrogen.

There were significant differences in mussel tissue $\delta^{15}N$ among sites and generally no significant differences within sites. Differences in mussel $\delta^{15}N$ values within a site appear to be related to distance between collections to a greater degree than was seen with $\delta^{13}C$; where within-site differences in $\delta^{15}N$ values were significant, the collections were 0.5 to 1 km away from each other. Thus, the nitrogen pool utilized by mussels is more constant over moderate-to-small scales. This suggests a deep pool of nitrogen, which is not significantly altered by sediment microbes in the shallow subsurface as is the case with methane. Although explanation of the high NH_3 content in seep brines is lacking, Joye et al. (2004; 2010) hypothesized that ammonium

attached to sediment particles is desorbed by the hypersaline brine. In this scenario, ammonia concentration and the consequent level of isotopic discrimination during assimilation by mussel endosymbionts is related to salinity of upward-migration of fluid and sediment particle size, both of which do not vary on as small a spatial scale as microbial community composition and activity.

The fact that about 92% of mussels in this study are at least 3‰ more depleted than seawater sulfate ($\delta^{34}S$ = 20.3‰) indicates that mussels are using reduced sulfur compounds, in particular hydrogen sulfide, for a significant portion of their sulfur needs. This is not surprising for mussels containing both methanotrophic and chemoautotrophic endosymbionts, because the chemoautotrophic symbionts use reduced sulfur compounds and an energy source. However, even mussels containing only methanotrophic symbionts had notably depleted tissue $\delta^{34}S$ compositions. Several *B. childressi* individuals from three different sites had tissue $\delta^{34}S$ values between 0.5 and 11.7‰. This again highlights the problem with using stable isotopes alone to determine whether methanotrophy or chemoautotrophy is an animal's primary nutritional source.

17.3.6. Vesicomyid Clam Stable Isotope Signatures

The $\delta^{13}C$ ranges for both *C. ponderosa* (-37.0 to -34.4‰) and the undescribed *Calyptogena* species (*Calyptogena* sp. nov.) that was collected from AC601 (-35.4 to -34.4‰) were within of the previously reported range of *C. ponderosa* from the upper Louisiana slope (Table 17-1) (Kennicutt et al., 1992). The vesicomyid clam *C. ponderosa* from the same collection as the MC853 mussels (*B. brooksi* and *B. childressi* with $\delta^{15}N$ values around -15‰) had $\delta^{15}N$ values ranging from -9.2 to -3.9‰. These were the most depleted $\delta^{15}N$ values yet reported for seep clams (Table 17-1). The remaining clam tissue $\delta^{15}N$ samples ranged from -1.0 to 4.4‰, which is typical of values reported for *C. ponderosa* on the upper slope (Kennicutt et al., 1992). Tissue $\delta^{34}S$ in *C. ponderosa* ranged from -1.2 to 12.8‰, which is within the range of ca. -10 to 10‰ previously reported for *C. ponderosa* on the upper slope (Kennicutt et al., 1992). Tissue $\delta^{34}S$ for *Calyptogena* sp. nov. was -14.1 to -2.9‰.

The vesicomyid clams had narrower overall tissue $\delta^{13}C$ and $\delta^{15}N$ ranges than the mussels (Table 17-1). The narrow $\delta^{13}C$ ranges of both *C. ponderosa* and *Calyptogena* sp. nov. (-37 to -34‰) were similar to *C. ponderosa* on the upper Louisiana slope (Kennicutt et al., 1992) and to other *Calyptogena* species found at seeps near Japan (Fiala-Médioni et al., 1993) and at hydrothermal vents (Childress et al., 1993a; Fisher et al., 1988), indicating that this genus probably uses the same inorganic carbon substrate at different locations and that this substrate has little isotopic variation. *Calyptogena* species harbor chemoautotrophic endosymbionts, and therefore utilize DIC rather than isotopically variable methane as a carbon source. This carbon source is likely DIC in epibenthic bottom water taken up by the clams' incurrent siphon and pumped across their gills. DIC in seawater has a consistent $\delta^{13}C$ composition around 0‰ (Peterson and Fry, 1987) and use of this carbon source is also reflected in the $\delta^{13}C$ values of vesicomyid shells (reviewed in Childress and Fisher, 1992). On the other hand, the $\delta^{13}C$ values of DIC in pore fluids at seeps can be quite low and this is often reflected in the $\delta^{13}C$ values of authigenic carbonates at seeps (Roberts and Aharon, 1994). The carbonates collected from the clam beds in this study had $\delta^{13}C$ values between -25 and -15 ‰ (Roberts and Feng, 2010). The narrow range of tissue $\delta^{13}C$ values in seep vesicomyid clams suggests that any depleted DIC in seawater at the sediment water

interface is effectively diluted by the pumping of overlying seawater through the clam's mantle cavity.

The majority of clams of both species, *C. ponderosa* and *Calyptogena* sp. nov. had tissue $\delta^{15}N$ values between -1.0 and 4.4‰, which is within the range of isotope values of *C. ponderosa* on the upper Louisiana slope (Kennicutt et al., 1992). The one exception was *C. ponderosa* collected near the mussels at MC853, which had tissue $\delta^{15}N$ values ranging from -9.2 to -3.9‰. While these clams were enriched in tissue $\delta^{15}N$ relative to the mussels, they were the most depleted $\delta^{15}N$ values for clams in this study, and the individual with $\delta^{15}N$=-9.2‰ is the most depleted value yet reported for seep clams. In general, vesicomyid clam $\delta^{15}N$ values are depleted compared with non-seep animals, indicating that they utilize a local nitrogen source rather than PON. Very little is known about nitrogen uptake and utilization by this chemoautotrophic symbiosis, although ammonium assimilation enzyme activity has been found in the hydrothermal vent clam *Calyptogena magnifica* (Lee et al., 1999). Vesicomyids are known to take up sulfide from interstitial pools in the sediment, using sulfide-binding components present in their blood and their well-vascularized foot, which they can extend several body lengths into the sediment (reviewed by Childress and Fisher, 1992). The very depleted tissue $\delta^{15}N$ values in the collections from MC853 suggest that these clams are also capable of acquiring nitrogen from depleted or abundant interstitial nitrogen sources in the sediment beneath them.

17.4. Vestimentiferan Siboglinid Tube Worm Stable Isotope Signatures

17.4.1. Vestimentiferan $\delta^{13}C$ Results

The vestimentiferans analyzed in this study displayed a large range of $\delta^{13}C$ values within species (Table 17-2). Among the most enriched samples were three small (<15 cm) *E. laminata* individuals that were sampled from mussel community collections. The $\delta^{13}C$ values of these individuals were -26.8 and -25.2‰ at AT340 and -20.5‰ at AC818. One *E. laminata* collection from AC818 had $\delta^{13}C$ values ranging from -26 to -22‰. Three *S. jonesi* individuals had $\delta^{13}C$ values between -24.3 and -22.8‰ and one *Lamellibrachia* sp. 1 individual had a $\delta^{13}C$ value of -25.0‰. A common characteristic among these individuals is that they were all relatively small. The AC818 *E. laminata* collection had an average length of 22 cm, the three isotopically enriched *S. jonesi* individuals were 20.6 to 23.5 cm, and the *Lamellibrachia* sp. 1 individual was broken. In comparison, the typical length of individuals analyzed was 32 to 111 cm for *E. laminata*, 46 to 64 cm for *Lamellibrachia* sp. 1, and 44 to 80 cm for *S. jonesi*.

The $\delta^{13}C$ compositions for typical adult vestimentiferans in this study were much more depleted. In fact, we measured some of the lowest tissue $\delta^{13}C$ values yet reported for seep vestimentiferans, particularly in *E. laminata* (Table 17-2). The eleven most depleted $\delta^{13}C$ values for *E. laminata* were between -65 and -55‰ and were from individuals collected from the AT340 and GC852 study sites. The three most depleted $\delta^{13}C$ values for *Lamellibrachia* sp. 1 were around -55 to -50‰, also collected from AT340 and GC852. Only two individuals of the rare *Lamellibrachia* species (sp. 2) were analyzed for stable isotopes: one from GB697 with a $\delta^{13}C$ value of -23.0‰ and the other from GC852 with a $\delta^{13}C$ value of -42.5‰. The three small, isotopically enriched *S. jonesi* individuals mentioned above were all collected from GB647.

Other *S. jonesi* samples collected from the same site ranging in length from 29.6 to 87.4 cm had $\delta^{13}C$ values between -40.8 and -30.7‰.

Table 17-2

Means and Standard Deviations for $\delta^{13}C$, $\delta^{15}N$, and $\delta^{34}S$ Compositions of Siboglinids on the Lower Continental Slope, GoM

species	N_{CN}	N_S	$\delta^{13}C$ (‰) mean ± sd	min	max	$\delta^{15}N$ (‰) mean ± sd	min	max	$\delta^{34}S$ (‰) mean ± sd	min	max
Escarpia laminata	61	53	-40.4 ± 12.2	-65.6	-19.5	4.3 ± 1.1	0.2	6.2	-6.1 ± 9.9	-23.1	18.4
Lamellibrachia sp. 1	32	32	-38.5 ± 7.9	-55.2	-25.0	1.5 ± 1.9	-3.5	3.8	-8.4 ± 7.6	-22.3	5.7
Lamellibrachia sp. 2	2	2	-32.8 ± 13.7	-42.5	-23.0	2.7 ± 1.3	1.8	3.6	-14.1 ± 2.0	-15.5	-12.7
Seepiophila jonesi	5	3	-27.8 ± 5.8	-35.5	-22.8	3.3 ± 1.4	1.4	4.7	-6.9 ± 9.1	-12.2	3.6
Oligobrachia sp.	5	1	-45.4 ± 9.5	-55.7	-31.7	2.1 ± 1.1	0.2	2.9	-0.3		
Sclerolinum sp.	23	0	-35.4 ± 7.6	-50.6	-27.0	2.0 ± 1.5	-2.2	4.1			

In general, vestimentiferans showed significant differences in $\delta^{13}C$ composition among study sites. A Kruskal-Wallis test revealed significant differences in *Lamellibrachia* sp. 1 tissue $\delta^{13}C$ among sites ($p=0.001$), with the largest difference being between the GB697 and GC852 study sites ($p=0.0018$), representing the highest (-27.6‰) and lowest (-42.5‰) median values, respectively. *E. laminata* tissue $\delta^{13}C$ values were also significantly different among sites ($p<0.001$), with the largest difference being between AT340 (median $\delta^{13}C$ -48.8‰) and GB647 (median $\delta^{13}C$ -26.7‰) (p-value=0.018). *S. jonesi* was collected only from the two shallow sites in the Garden Banks region-GB647 and GB697. The latter site had only two individuals in the collection, but mean $\delta^{13}C$ values at the two sites were only separated by 4‰ (-30.3 and -34.1‰ for GB647 and GB697, respectively).

There were also differences in vestimentiferan $\delta^{13}C$ among collections within study sites. *E. laminata* $\delta^{13}C$ is significantly different among the collections at AT340. None of the collections that were close to one another (<7 m) were significantly different in $\delta^{13}C$. The shortest distance separating two collections that were significantly different from each other at this site was 50 m. At GC852, both *E. laminata* and *Lamellibrachia* sp. 1 in one collection were significantly different from the other two collections. This collection was 0.6 km away from one of the collections but only 26 m away from the other. At GB697, the two *Lamellibrachia* sp. 1 collections, separated by 3 km, were not significantly different from each other. *E. laminata* and *Lamellibrachia* sp. 1 $\delta^{13}C$ values were not significantly different from each other within collections except for one Bushmaster collection at the GC852 study site. In this collection, both

E. laminata and *Lamellibrachia* sp. 1 had markedly depleted $\delta^{13}C$ compositions (averaging -57.7‰ and -49.9‰, respectively, compared with the other collections which averaged -42.1 and -43.7‰ for *E. laminata* and -39.5 and -43.3‰ for *Lamellibrachia* sp. 1).

17.4.2. Vestimentiferan $\delta^{15}N$ Results

Vestimentiferan $\delta^{15}N$ values were less variable overall than $\delta^{13}C$ values with a maximum range of ca. 7‰ (Table 17-1). For both *Lamellibrachia* sp. 1 and *E. laminata*, $\delta^{15}N$ values are notably lower at WR269 compared with samples of the same species from other sites (Figure 5). *Lamellibrachia* sp. 1 from WR269, in particular, had the most depleted $\delta^{15}N$ of all vestimentiferans collected, ranging from -3.5 to -2.5‰. The next most depleted $\delta^{15}N$ value was -0.2‰, a full 2.3‰ more enriched than the samples at WR269. There were significant differences in both *E. laminata* and *Lamellibrachia* sp. 1 $\delta^{15}N$ among sites ($p=0.001$ and $p<0.001$, respectively). Vestimentiferan tissue $\delta^{15}N$ at WR269 was significantly different from all other sites (*see* Figure 17-6). Tissue $\delta^{15}N$ for both species at GC852 was also significantly different from AT340. GB829 and GC852 $\delta^{15}N$ values are not significantly different from each other but both were different from AC601 and GB697. There was no significant difference between *S. jonesi* tissue $\delta^{15}N$ values between the two Garden Banks sites. Again, there were only two samples for one collection, but qualitatively, the means are less than 1‰ different.

Unlike for $\delta^{13}C$, there was relatively little variation in $\delta^{15}N$ among collections within a site. The only significant difference was among median *E. laminata* $\delta^{15}N$ values in different collections at AT340, with the largest difference (3.5 vs. 5.6‰) being between two collections separated by 0.7 km ($p=0.037$).

E. laminata was consistently enriched in $\delta^{15}N$ relative to *Lamellibrachia* sp. 1 from the same collections by about 2.7 ± 0.5‰, except for WR269 in which *E. laminata* was about 4.3‰ heavier (Figure 17-6). At GC852, in contrast to $\delta^{13}C$, tissue $\delta^{15}N$ in *Lamellibrachia* sp. 1 was consistently lower that $\delta^{15}N$ in *E. laminata*, and the difference was significant ($p<0.05$) for all but two collections, which had p-values near 0.08 from Mann-Whitney tests.

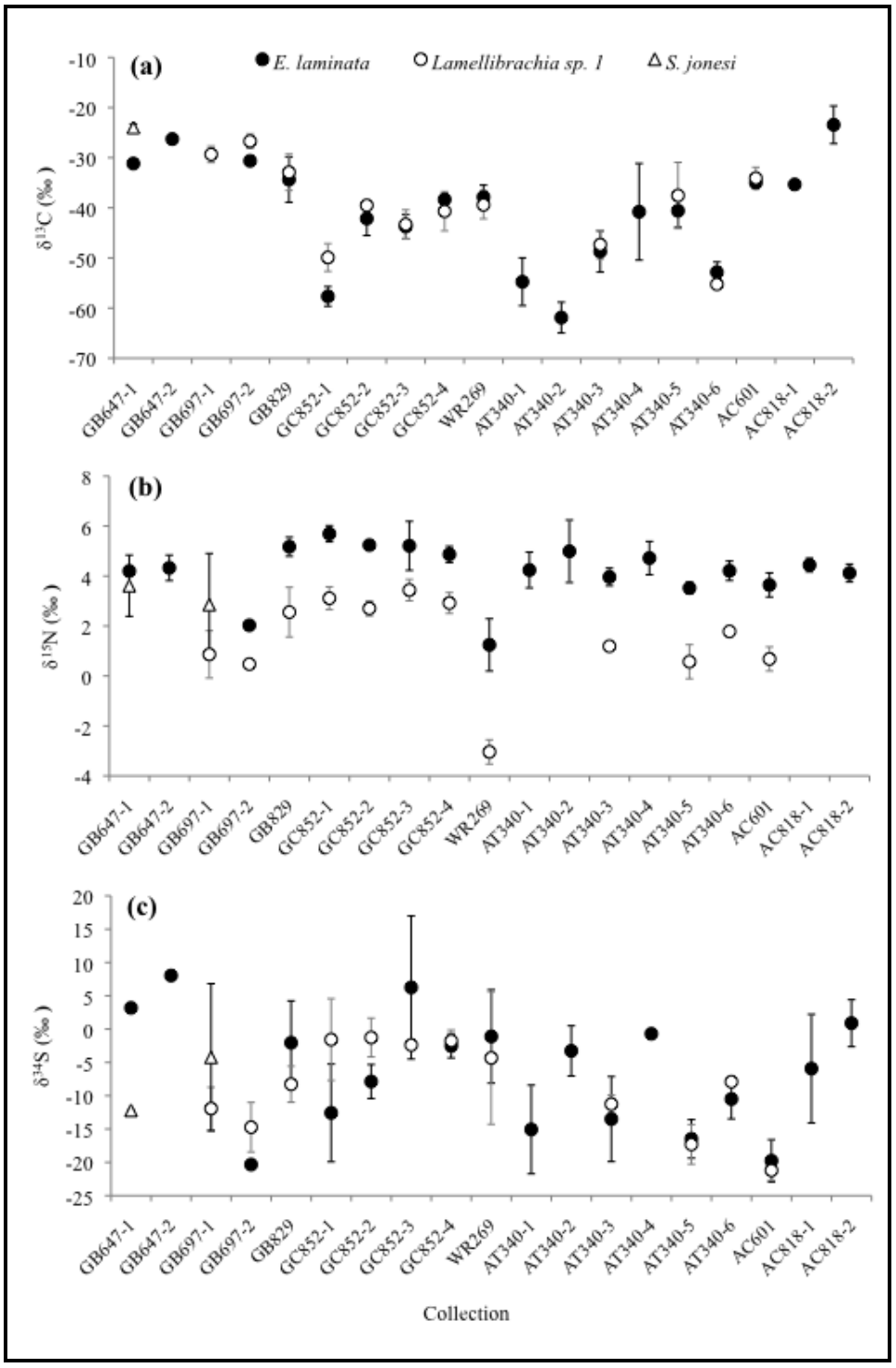

Figure 17-6. Average and standard deviation of tissue (a) $\delta^{13}C$, (b) $\delta^{15}N$, and $\delta^{34}S$ for all vestimentiferan collections.

17.4.3. Vestimentiferan $\delta^{34}S$ Results

Tissue $\delta^{34}S$ values in vestimentiferan tube worms ranged from -23.1 to 16.8‰. The three small *E. laminata* collected with mussels occupied the more enriched end of this range with tissue $\delta^{34}S$ values of 4.6, 10.1, and 16.8‰. There were, however, several larger individuals of both *E. laminata* and *Lamellibrachia* sp. 1 that had tissue $\delta^{34}S$ values in this range. There was considerable variation in $\delta^{34}S$ values within single collections. Eight out of twelve *E. laminata* collections had standard deviations in tissue $\delta^{34}S$ of 5 to 7‰ and two of the six *Lamellibrachia* sp. 1 collections had standard deviations of approx. 10‰.

17.4.4. Discussion of Vestimentiferan Tissue Stable Isotope Signatures

The pattern of tissue $\delta^{13}C$ and $\delta^{15}N$ in the vestimentiferans provides strong evidence supporting previous hypotheses concerning DIC uptake and new insights into potential resource partitioning between co-occurring species. A large range of $\delta^{13}C$ values within a species of vestimentiferan tube worm, such as that found in this study, is not atypical and has been attributed to differences in the isotopic signature of the DIC pool utilized by the worms (Kennicutt et al., 1992). The large variation in tissue $\delta^{13}C$ in vestimentiferans among sites indicates high variability in source pools and/or sediment microbial activities, while the large variation in $\delta^{13}C$ within sites indicates a high degree of spatial variability over relatively small distances. The variability in tissue $\delta^{13}C$ within sites does not seem to be affected by distance between collections, since collections separated by 0.5 km or more were often not significantly different while collections separated by <40 m were occasionally significantly different. This was also the case with tissue $\delta^{13}C$ values in bathymodiolin mussels on the lower slope (*see* Section 4.1). The most depleted tissue $\delta^{13}C$ values in vestimentiferans were found in one collection of *E. laminata* at the AT340 study site. With one collection having an average tissue $\delta^{13}C$ value of -62.4 ± 3.5‰, these are the most depleted $\delta^{13}C$ values yet reported for vestimentiferan tube worms. Values in this range are typically attributed to methanotrophy, since methane around seeps, particularly biogenic methane, can be very isotopically depleted. Like all vestimentiferan tube worms, however, *E. laminata* relies on sulfur-oxidizing chemoautotrophic symbionts for provision of fixed carbon.

Vent vestimentiferans utilize dissolved carbon dioxide that the worms acquire across their plume (Childress et al., 1993b; Goffredi et al., 1997). Seep tube worms can also acquire dissolved CO_2 across their plumes (Freytag et al., 2001), but recent studies indicate that they may also have the ability to access pore water DIC. Due to the relatively stable seep environment, seep vestimentiferans are able to live a very long time (200+ years) and extend the posterior portion of their bodies (or "roots") deep into the sediment. This adaptation allows them to mine for sulfide after surface expression has become undetectable (Freytag et al., 2001). More recently, it has been shown in the seep vestimentiferan *Lamellibrachia luymesi* that the worms also release sulfate and hydrogen ions (waste products of sulfide oxidation/carbon fixation) through their roots via a passive transport system (Dattagupta et al., 2006). Moreover, the mechanism for sulfate elimination is via an anion exchanger that is likely a sulfate-bicarbonate exchanger (Dattagupta et al., 2006). Since bicarbonate in seep sediments is the product of microbial SR and hydrocarbon oxidation, the isotopic composition of pore water bicarbonate can have quite depleted $\delta^{13}C$ values, reflecting its isotopically light source material: hydrocarbons. The highly depleted $\delta^{13}C$ values in our *E. laminata* samples further support the hypothesis of root DIC uptake.

This hypothesis is also supported by the most enriched vestimentiferan tissue $\delta^{13}C$ values in this study, which were from juvenile *E. laminata* individuals collected with bathymodiolin mussels. The most abundant mussel species in all collections that contained these small *E. laminata* was *Bathymodiolus brooksi*, although *B. heckerae* was also present in the AC 818 collection. Both of these mussel species contain both sulfur-oxidizing and methane-oxidizing endosymbionts (Cavanaugh et al., 1987; Duperron et al., 2007; Fisher et al., 1993). Although the presence of these mussels alone does not guarantee a high level of methane above the sediment surface, the depleted tissue $\delta^{13}C$ values of these mussels (ca. -65 to -55‰) indicates that they are using an isotopically depleted DIC source. The juvenile vestimentiferans, however, are apparently utilizing a different, more ^{13}C-rich source. The $\delta^{13}C$ values in the juvenile *E. laminata*, between -25 and -20‰, are consistent with chemoautotrophic fixation of dissolved CO_2 (seawater CO_2 $\delta^{13}C$ is around 0‰ (Peterson and Fry, 1987) and carbon fixation via sulfide oxidation produces a fractionation of about -25‰ (Ruby et al., 1987)). In contrast with the adult *E. laminata* discussed above, these juvenile worms may not have yet developed roots that are able to utilize pore water bicarbonate. Also, the isotopically light carbon source utilized by the mussels is likely methane, which is biologically inaccessible to vestimentiferans. *S. jonesi* and *Lamellibrachia* sp. 1 showed a similar trend with smaller worms having heavier $\delta^{13}C$ values, and so may have similar differences in carbon sources at different life stages.

Comparison of tissue $\delta^{13}C$ between species within a collection did not support resource partitioning of carbon sources between the two dominant vestimentiferan species, *E. laminata* and *Lamellibrachia* sp. 1 (Figure 17-6). For nitrogen, however, $\delta^{15}N$ values in *E. laminata* were consistently more enriched than *Lamellibrachia* sp. 1 from the same collections (Figure 17-6). This is the first known evidence of resource partitioning between co-occurring species of vestimentiferan. The consistent significant difference between tissue $\delta^{15}N$ values could indicate that the worms are either using different nitrogen sources (nitrate vs. ammonium, for example), the same chemical species from different locations (with different $\delta^{15}N$ values), or there is a difference in the degree of fractionation during nitrogen uptake and/or assimilation from the same source pool. The consistent difference in $\delta^{15}N$ values (2.6 ± 0.7‰) lends support to the latter of these possibilities. Uptake and utilization of environmental inorganic nitrogen has been shown in the seep mussel *B. childressi* and the vent vestimentiferan *Riftia pachyptila*, and this uptake and fixation is mediated through the bacterial symbionts (Lee and Childress, 1994; Lee et al., 1992). While mussel symbionts inhabit the gills where different molecules from the environment need only to diffuse across a few cell layers, vestimentiferan symbionts reside deep inside the bodies of their hosts, such that any inorganic molecules would have to be transported to the bacteria via the worms' blood. Also, unlike *Bathymodiolus* species, which can have different types of symbionts (methanotrophic and chemoautotrophic), *E. laminata* and *Lamellibrachia* sp. 1 both harbor the same phylotype of sulfur-oxidizing endosymbionts. This suggests that the consistent difference in $\delta^{15}N$ values reflects a difference in the uptake of inorganic nitrogen as mediated by the host vestimentiferan. The lack of a consistent difference in tissue $\delta^{13}C$ between the species (Figure 17-6) suggests that they likely share both physical rhizosphere and plume niche space, so should have access to the same nitrogen source pools. If there is spatial separation of inorganic nitrogen uptake, it would have to be a difference in the uptake site within the worm itself i.e. using the plume or the root to uptake nitrogen. To test this in a rigorous fashion would require exposing the vestimentiferans to different isotopically labeled inorganic nitrogen compounds to test for uptake and split-animal experiments (as in Dattagupta et al., 2006) to ascertain the site at which uptake occurs.

The $\delta^{15}N$ in vestimentiferans is relatively constant overall (Figure 17-6). Individuals of both vestimentiferan species and the common moniliferan *Sclerolinum* sp. had notably lower $\delta^{15}N$ values at the WR269 study site relative to individuals of the same species collected from other sites. The difference between *E. laminata* and *Lamellibrachia* sp. 1 tissue $\delta^{15}N$ was larger than at other sites, with *E. laminata* being 4.3‰ more enriched in $\delta^{15}N$ than *Lamellibrachia* sp. 1. The more depleted $\delta^{15}N$ values in the animals could be due to either a more depleted nitrogen source, or a very abundant nitrogen source, such as ammonium, that allows for a higher degree of fractionation. In the case of a very abundant nitrogen source, both species would show higher isotopic discrimination than usual, but *E. laminata* may be closer to reaching its full fractionation potential than *Lamellibrachia* sp. 1, causing the larger difference in tissue $\delta^{15}N$ values. These observations provide a fertile area for the further study of vestimentiferan physiology and environmental nitrogen sources at seeps.

Sulfur stable isotope values in vestimentiferans were highly variable, which is typical of sulfur isotopes in seep environments (Kennicutt et al., 1992). There was no consistent difference in tissue $\delta^{34}S$ compositions between *E. laminata* and *Lamellibrachia* sp. 1 (Figure 17-6c), and these two species contain the same phylotype of bacterial endosymbionts. Thus, the variability in $\delta^{34}S$ composition is not likely to be due to differences in metabolic or assimilatory pathways of the symbionts, but rather differences in the isotopic compositions of the endmember sulfur sources. Sulfide is the primary source of nutritional sulfur for vestimentiferans. The vast majority of sulfide available at seeps is formed by sediment microbes, which oxidize seeping hydrocarbons and concurrently reduce sulfate to sulfide. Isotopic fractionation during SR can lead to a sulfide product that is as much as 50‰ more depleted in ^{34}S relative to seawater sulfate ($\delta^{34}S \approx 20‰$) (Chambers and Trudinger, 1970; Harrison and Thode, 1958; Rees, 1973). The $\delta^{34}S$ compositions of sulfide collected from seep sediments can be highly variable (Aharon and Fu, 2000; Dattagupta et al., 2008). Aharon and Fu (2000) found that fractionation factor associated with SR decreases with increasing rate of SR. Fractionation was highest in non-seep sediments, became lower in oil seep sediments, and was lowest in gas seep sediments (Aharon and Fu, 2000). Also, $\delta^{34}S$ values of sulfide tend to increase with sediment depth, which has been attributed to deep-sea sediments acting as a closed or semi-closed system in which the isotopically light sulfate is rapidly depleted in the upper portion of the sediment leaving only isotopically heavy sulfate to be converted to sulfide (Aharon and Fu, 2000; Dattagupta et al., 2008). Thus, the variation we see in vestimentiferan tissue $\delta^{34}S$ could be attributable to very high SR rates leading to sulfate limitation within the sediment. This is a likely explanation for the enriched $\delta^{34}S$ values we found in small tube worms collected with mussels; this is a gas seep environment with plenty of methane to drive SR. It is also possible that the depth at which the worms acquire their sulfide could differ between individuals within a collection, giving rise to high within-collection variability in aggregations of larger vestimentiferans. A third contributing factor could be the upward migration of isotopically heavy sulfide from deeper sediment layers due to the general upward migration of seeping fluids.

17.5. Other Siboglinid Tube Worm Stable Isotope Signatures

The moniliferan *Sclerolinum* sp. had $\delta^{13}C$ values ranging from -50.6 to -27.0‰. There was an apparent site-specific trend in $\delta^{13}C$ values. WR269 samples were most depleted ranging from -50.6 to -44.8‰. Samples from AC818 ranged from -36.5 to -29.8 and samples from AC601 ranged from -34.2 to -27.1‰. Tissue $\delta^{15}N$ values ranged from 0.6 to 4.1‰ (Table 17-2) and also

showed some site-specific trends. As with the vestimentiferans, the lowest values were found in samples from WR269 ranging from -2.2 to 1.8‰, while other values ranged from 1.6 to 4.1‰. The majority of the more enriched samples (between 3.1 and 4.1‰) were collected from AC818. The frenulate *Oligobrachia* sp. always co-occurred with *Sclerolinum* sp. but was far less abundant than *Sclerolinum* sp. where the monoliferan occurred in large "fields." *Oligobrachia* sp. also occurred occasionally with vestimentiferan tube worms (3 of the 4 *Oligobrachia* sp. samples are from Bushmaster collections). *Oligobrachia* sp. had $\delta^{13}C$ that ranged from -55.7 to -31.7‰ in all collections and $\delta^{15}N$ that ranged from 2.2 to 2.9‰.

17.6. Stable Isotopes of Heterotrophic Seep Fauna Closely Associated with Seep Foundation Fauna

17.6.1. Overall Trends

The most depleted $\delta^{13}C$ values of all species in all collections were found in the deposit-feeding bristle worms *Notomastus* sp. (-80.3‰) and *Eurythoe* sp. (several individuals ranged from -77.3 to -75.4‰) from mussel collections at WR269 and AT340. Among the most enriched $\delta^{13}C$ values in heterotrophic fauna were amphipods (two indiv. -20 to -17‰), *A. muricola* (two indiv. -21 to -20‰), *O. spinilimbatum* (6 indiv. -25 to -22‰), and the anemone and hydroid from the clam scoop at MC462 (-22.6 and -22.7‰, respectively).

The majority of heterotrophic animals collected with clams (*Calyptogena ponderosa* and *Calyptogena* sp.) ranged in $\delta^{13}C$ from -42.6‰ (*Phymorrynchus* sp.) to -31.2‰ (*G. tesselata*) and from 0.0‰ (Nautilliniellidae sp.) to 6.3‰ (*Chirodota*) for $\delta^{15}N$. The anemone and hydroid collected with clams from MC462 were outside of this range with notably enriched $\delta^{13}C$ compositions of -22.6 and -22.8‰, respectively, and the anemone was also quite enriched in tissue $\delta^{15}N$ with a value of 10.5‰.

Most vestimentiferan associated fauna ranged in $\delta^{13}C$ composition from -62.4 (*A. muricola*) to -23.3‰ (*O. spinilimbatum*). The ampharetid amphipod sample with a $\delta^{13}C$ composition of -17.2‰ lay outside of this range. Vestimentiferan associated fauna $\delta^{15}N$ compositions ranged from -2.13 (*A. muricola*) to 11.3‰ (capitellid polychaete).

The overall $\delta^{13}C$ range of heterotrophic animals collected with mussels was -80.3 (*Notomastus* sp.) to -20.8‰ (*A. muricola*). The small *E. laminata* individuals were also at the enriched end of this range, as discussed above in section 3.2.1. The mussels themselves were usually the most depleted in $\delta^{13}C$ within their collections, but occasionally samples of heterotrophic associated fauna were more depleted. These included the deposit-feeding polychaetes *Notomastus* sp., *Nicomache* sp., and *Eurythoe* sp. Mussel associated fauna $\delta^{15}N$ compositions ranged from -6.1‰ (*Hesiocaeca mathanicola*) to 8.4‰ (*G. tesselata*), the majority (about 94%) of which were more depleted than typical particulate organic nitrogen (>6‰; Saino and Hattori 1987) and about 30% of which had negative $\delta^{15}N$ values. In almost all mussel collections, the mussels themselves have the most depleted $\delta^{15}N$. The one exception to this is one collection at GB829 in which the methane ice worm *Hesiocaeca methanicola* has a substantially more depleted $\delta^{15}N$ composition of -6.1‰ relative to the mussels in this collection (most depleted tissue $\delta^{15}N$ in mussel was -3.3‰). In the four collections for which we have $\delta^{34}S$ data for both the mussels and *H. methanicola*, *H. methanicola* had more depleted tissue $\delta^{34}S$ values relative to the co-occurring mussels. We do not yet have enough data to determine whether this is a significant trend.

There were several taxa of heterotrophic fauna that were found across two or more habitat types as defined by their foundation fauna (vestimentiferans, mussels, clams, and monoliferan-frenulates), which allowed for within-taxon analysis of variation across habitats and sites. Quite often, overall differences within taxon between different habitat types were significant; however, significant differences in isotope values within taxa from the same habitat among sites and among collections within a site were also different, so it was not possible to separate environmental differences among foundation fauna that might cause different isotopic compositions from spatial variability.

17.6.2. Implications for Individual Species and Trophic Interactions

A few potential trophic relationships were of interest before performing the stable isotope analyses. One of these was the phyllodocid polychaete *Protomystides* sp. that is commonly found on top of *E. laminata* prostomia, but is also frequently found inhabiting the outsides of vestimentiferan tubes and the insides of dead vestimentiferan tubes. The guts of these worms often contained a red substance assumed to be tube worm blood, possibly pointing toward a parasitic relationship between *Protomystides* sp. and *E. laminata*. When paired *Protomystides* sp. and *E. laminata* were regressed, there was a strong linear relationship between $\delta^{13}C$ of *Protomystides* sp. and their paired *E. laminata* ($p<0.001$; $R^2=0.8$), but this relationship was not significant between *Protomystides* sp. and *E. laminata* $\delta^{15}N$ ($p=0.7$; $R^2=0.08$) (Figure 17-7). The lack of a strong correlation in $\delta^{15}N$ could be due to the small total variation in $\delta^{15}N$ (about 2‰) compared with $\delta^{13}C$ (about 28‰), making it difficult to show a relationship with the nine paired samples collected in this study. There was a weak liner relationship between tissue $\delta^{34}S$ of *Protomystides* sp. and their paired *E. laminata* hosts ($p=0.07$; $R^2=0.35$). In general, within collections, *Protomystides* sp. that were found in locations other than atop *E. laminata* prostomia (such as inside dead vestimentiferan tubes or on the outsides of tubes) had isotopic compositions within the same range as those found on top of the live tube worms. A species of capitellid polychaete *Heteromystides* sp. also found inhabiting dead vestimentiferan tubes had isotopic compositions similar to those of *Protomystides* sp. within collections.

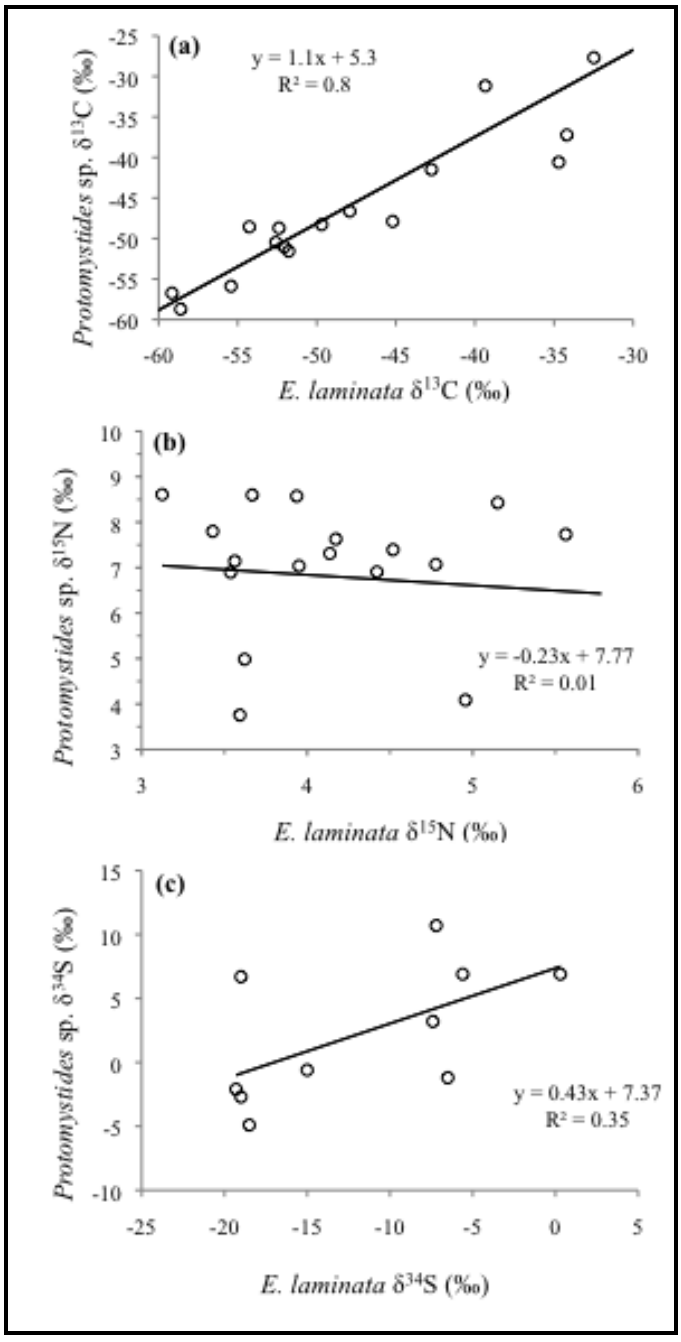

Figure 17-7. (a) $\delta^{13}C$, (b) $\delta^{15}N$ and (c) $\delta^{34}S$ in the small polychaete *Protomystides* sp. vs. the paired *E. laminata* individual upon which the Protomystides sp. was found.

The isotope data for paired *E. laminata* and *Protomystides* sp. did not clearly support or refute the hypothesis that *Protomystides* sp. is a parasite of *E. laminata*. The strong correlation between paired *Protomystides* and *E. laminata* tissue $\delta^{13}C$ may only indicate a strong reflection in both animals of the environmental carbon source. There was no strong correlation between the tissue $\delta^{15}N$ values of the *Protomystides* sp. and their host *E. laminata*, but a clear correlation may require a very large sample size since there is such a small range of tissue $\delta^{15}N$ values in these animals overall. There was a weak correlation ($R^2 = 0.35$) between tissue $\delta^{34}S$ in *Protomystides* sp. and their host *E. laminata* tissue $\delta^{34}S$. The sample size for $\delta^{34}S$ is smaller since several samples were not large enough to run sulfur isotopic analysis in addition to the carbon and nitrogen analyses, and this small sample size may partly account for the weaker correlation in comparison with the $\delta^{13}C$ correlation.

Protomystides sp. individuals that inhabit the outsides of tubes or the insides of dead vestimentiferan tubes do not appear to occupy a different ecological niche and their isotope values are similar to co-occurring *Protomystides* sp. from atop *E. laminata* prostomia. Also, the capitellid polychaete *Heteromystides* sp. may also inhabit a similar ecological niche as *Protomystides* sp. or feed upon a food source (such as free-living chemoautotrophic bacteria) that has similar isotope values to the food source of *Protomystides* sp. The two suspension-feeding cnidarian taxa that inhabit the outsides of tubes, hydroids and stoloniferans, have similar isotope values and thus feed on isotopically similar food sources, but this food source is different from that consumed by *Protomystides* sp. and *Heteromystides* sp (Figure 17-10). These cnidarians most likely feed on both suspended particulate organic matter (POM) and any small animals that come in contact with their nematocysts.

Another relationship that was of *a priori* interest was that between polychaetes living commensally within the gills of mussel and clam hosts. In a study of hydrothermal vent mussels *Bathymodiolus thermophilus* and the commensal polychaete *Branchipolynoe symmytilida*, which lives inside the mussel's body cavity, there was a strong correlation between the tissue isotopic compositions of polychaetes and hosts for both $\delta^{13}C$ and $\delta^{15}N$ (Fisher et al., 1994). Furthermore, the average enrichment in *B. symmytilida* tissue $\delta^{15}N$ relative to the host mussel tissue was 3.2‰, which is what is expected for a predator-prey relationship ($\delta^{15}N$ enrichment of 3.0 to 3.4‰ in the predator relative to the prey (Minagawa and Wada, 1984)). In the present study, there was a strong correlation (R^2=0.69) only in tissue $\delta^{13}C$ between commensal polynoids *Branchipolynoe seepensis* and Nautlliniellidae sp. and their bivalve hosts (*B. childressi*, *B. heckerae* or *Calyptogena* spp.) (Figure 17-8). This may reflect some sort of trophic relationship, but the lack of a strong linear relationship between tissue $\delta^{15}N$ in bivalve hosts and their commensal polynoids suggests that it is not a predator-prey relationship. It is possible that the polychaetes utilize a food source with a similar $\delta^{13}C$ composition to that of the mussels or clams (local free-living methanotrophic or chemoautotrophic bacteria) or some product of the bivalve, such as mucous, gametes or pseudofeces.

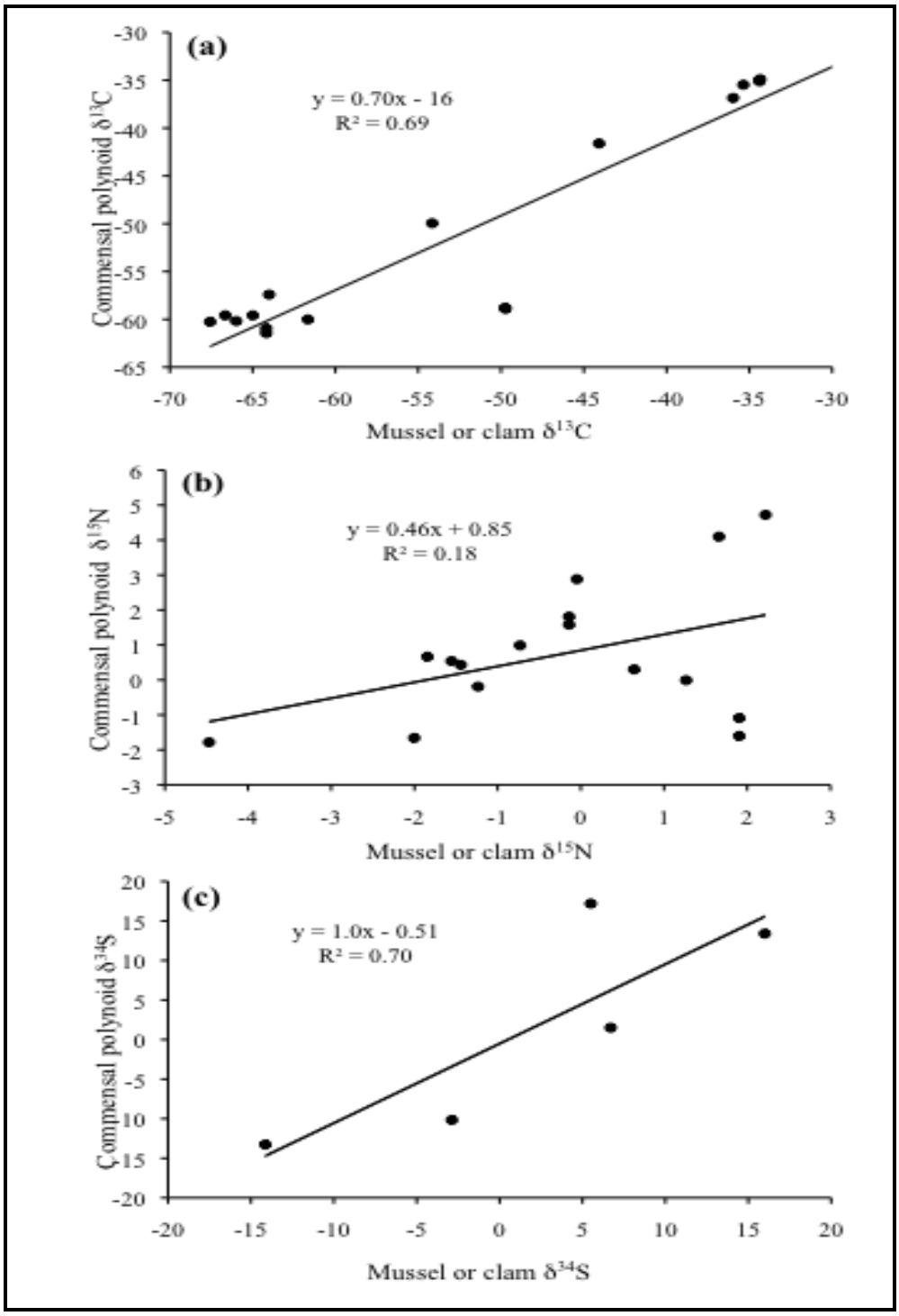

Figure 17-8. (a) $\delta^{13}C$, (b) $\delta^{15}N$, and (c) $\delta^{34}S$ in the commensal polynoid *Branchipolynoe seepensis* or *Nautilliniellidae* sp. vs the paired *B. heckerae, B. childressi,* or *C. ponderosa* individual in whose gills the polynoid was found.

In monoliferan communities, the notably abundant tiny white gastropods (Figure 17-9) did not show a clear predator-prey relationship with any other species sampled in these collections. The range of their values relative to the monoliferans was not consistent between collections at different sites and the snails were quite variable in both $\delta^{13}C$ and $\delta^{15}N$ within monoliferan patches (i.e., sometimes values were more depleted, more enriched, or overlapped the monoliferans). Also visually conspicuous in these communities was the purple sea cucumber *C. heheva* (Figure 17-9). Only a few individuals of this species were collected from two study sites, but in both cases the $\delta^{15}N$ compositions were about 4‰ higher than the $\delta^{15}N$ composition of the monoliferans, and they occupied the same $\delta^{15}N$ range as the top predators in these communities, such as *Harmothoe* sp., *Nicomache* sp., and the nemertean. The sipunculid *P. turnerae* showed a similar trend. *C. heheva* tissue $\delta^{13}C$ was sometimes more enriched, more depleted, or within the range of the monoliferans (Figure 7-12). There were very few individuals of *P. turnerae* in our collections, but this species always had tissue $\delta^{13}C$ values within the range of the co-occurring monoliferans (Figure 7-12).

Figure 17-9. The seep-associated sea cucumber *Chirodota heheva* burrows through a clump of the monoliferan tube worms *Sclerolinum* sp.; tiny white snails inhabit the monoliferan tubes; and many swimming amphipods.

In vestimentiferan tube worm collections, *A. muricola* are often among the most depleted in $\delta^{15}N$ relative to other animals within collections, including vestimentiferan tube worms (Figure 17-10). In mussel collections *A. muricola* are sometimes enriched and sometimes depleted in $\delta^{15}N$ relative to other animals, but are always enriched relative to the mussels (Figure 17-11). The variable $\delta^{15}N$ values relative to other animals in their collections may indicate that the shrimp has multiple food sources from more than one trophic level. The depleted values may reflect the shrimp grazing upon free-living bacteria that are fixing a local inorganic nitrogen source and the enriched values may reflect some feeding upon animals at higher trophic levels or possibly some incorporation of surface-derived nutrition. Some *A. muricola* individuals even had $\delta^{15}N$ compositions >6‰, which is similar to the values found in surface-derived POM (Peterson and Fry, 1987), although these same individuals still had relatively depleted $\delta^{13}C$ and $\delta^{34}S$ compositions. The overall ranges for $\delta^{13}C$ (-63.7 to -20.8‰) and $\delta^{34}S$ (-18.5 to 19.1‰) in *A. muricola* also reflect a combination of seep- and surface-derived nutrition.

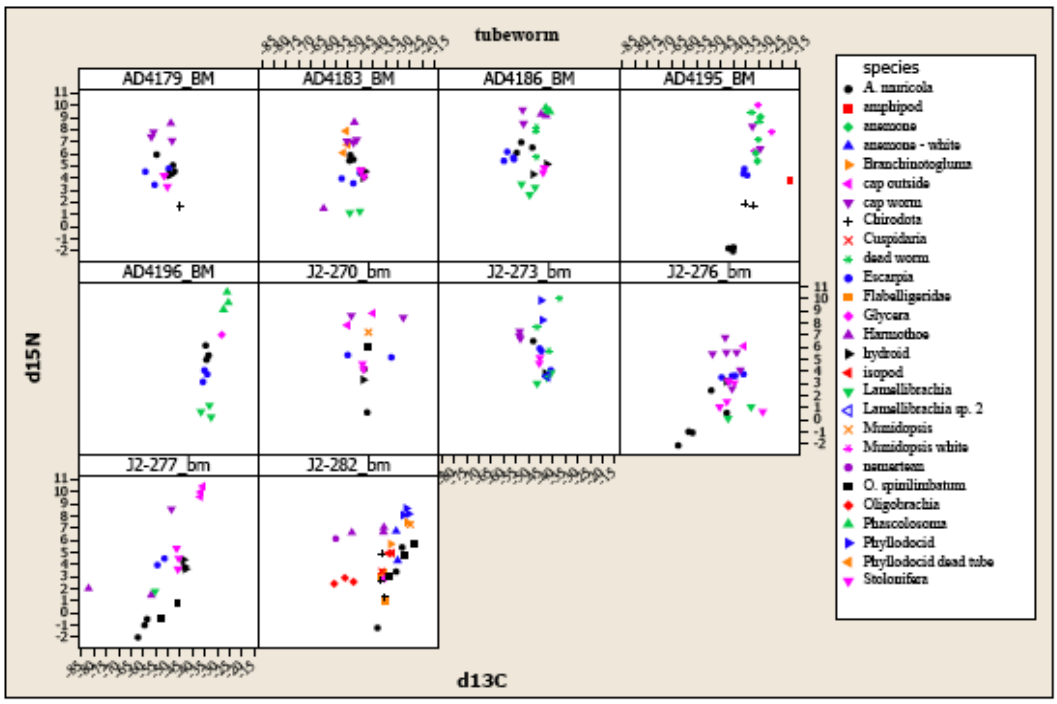

Figure 17-10. $\delta^{15}N$ vs. $\delta^{13}C$ for individual Bushmaster collections of vestimentiferan tube worms and their associated communities.

Phascolosoma turnerae was enriched in $\delta^{15}N$ relative to other animals when collected with any of the three foundation fauna (Figures 17-10, 17-11, and 17-12). However, *P. turnerae* has $\delta^{13}C$ values that are quite depleted ($\delta^{13}C$ = -58 to -30‰) and $\delta^{34}S$ values that are depleted relative to seawater sulfate ($\delta^{34}S$ = -18.2 to 14.3‰). Since this animal is sediment-dwelling and is often observed with a gut full of mud, it is not a predator in the usual sense, but filter out sediment-dwelling meiofauna that would have the trophic enrichment in $\delta^{15}N$ relative to their food source. It is also possible that *P. turnerae* derives a significant portion of its nutrition from a $\delta^{15}N$-enriched source such as surface PON. *P. turnerae* appears to be obtaining its carbon from a local source since its $\delta^{13}C$ values are often quite depleted. The depleted $\delta^{34}S$ values also indicate a mostly seep-derived sulfur source, likely microbially produced sulfide.

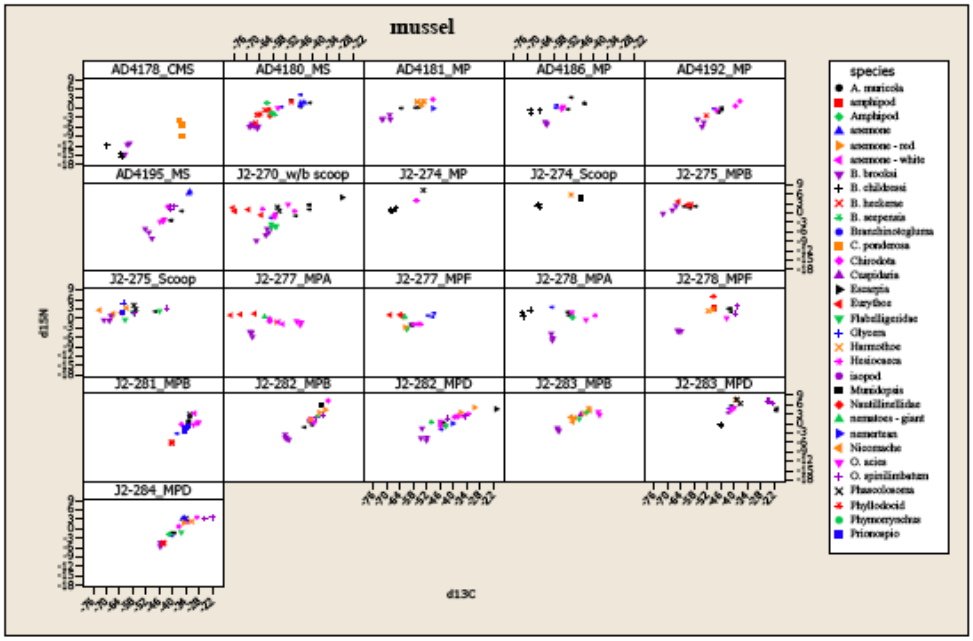

Figure 17-11. $\delta^{15}N$ vs. $\delta^{13}C$ for individual collections of mussels and their associated communities.

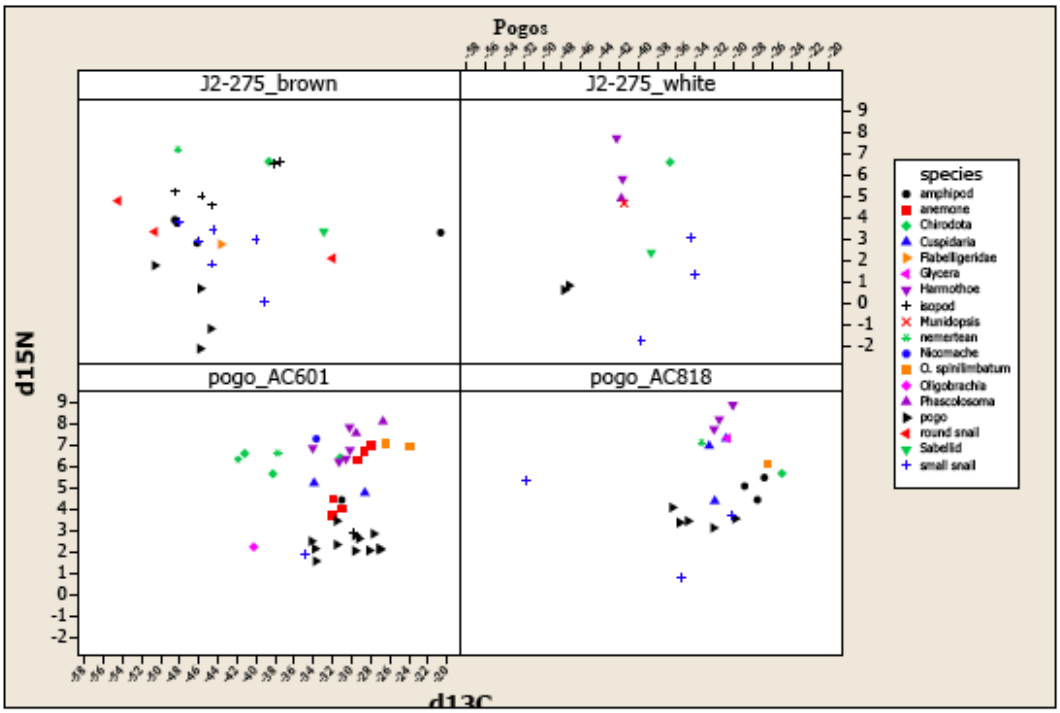

Figure 17-12. $\delta^{15}N$ vs. $\delta^{13}C$ for individual collections of monoliferans and their associated communities.
In this instance, a collection may be several push cores and/or suction samples from the same general area.

The most depleted $\delta^{13}C$ values of all species in all collections were found in the deposit-feeding bristle worms *Notomastus* sp. (-80.3‰) and *Eurythoe* sp. (several individuals ranged from -77.3 to -75.4‰) from mussel collections at WR269 and AT340. These values are more depleted than those of the mussels with which they were collected, indicating that these animals may directly graze upon free-living bacteria that use biogenic methane as a carbon source or methane that has been fractionated several times.

A previous study suggested that free-living chemoautotrophic bacteria are the main food source for *H. methanicola* (Fisher et al., 2000). Our data do not contradict this hypothesis; however, there are some considerations to keep in mind. Although the *H. methanicola* has a $\delta^{34}S$ value about 5‰ more depleted than *B. childressi*, the mussel containing only methanotrophic endosymbionts, *B. childressi* still has a tissue $\delta^{34}S$ composition that suggests it obtains some of its sulfur from an isotopically depleted source despite the fact that the bulk of the mussel's nutrition is obtained from methanotrophy. Indeed, we measured several *B. childressi* individuals with tissue $\delta^{34}S$ values between 0.5 and 11.7‰ from three different sites. Also, the $\delta^{13}C$ values of *H. methanicola* were consistently more enriched than the mussels with which they were collected but in general seemed to track the mussel tissue $\delta^{13}C$ values, an indication of the environmental carbon isotope signature. In fact, the majority of *H. methanicola* individuals in this study had $\delta^{13}C$ compositions between -63 and -40‰. As discussed above for vestimentiferan tube worms, which contain only chemoautotrophic endosymbionts, very

negative $\delta^{13}C$ compositions do not necessarily indicate methanotrophy as the primary nutritional source. Also, as discussed in section 4.1 for *B. childressi*, depleted tissue $\delta^{34}S$ values relative to seawater sulfate do not necessarily indicate chemoautotrophy as a primary nutritional source. Thus, it is possible that *H. methanicola* grazes upon free-living chemoautotrophic or methanotrophic bacteria or both.

18. STABLE ISOTOPE TROPHIC PATTERNS IN MEGAFAUNA IN CLOSE PROXIMITY AND REMOTE FROM SEEPS

18.1. Introduction

Chemosynthetic systems on continental margins are embedded in an extensive soft-bottom ecosystem that undergoes major bathymetric changes in species composition and faunal biomass. Therefore, the nature of and the extent to which seep systems interact with the background can be expected to change with depth. The work reported herein examines the possibility that the relative contribution of chemosynthetic production to heterotrophic species within and in close proximity to seeps increases with depth coinciding with a decrease in the biomass of the surrounding photosynthesis-supported benthos. Since the microbial symbionts of seep foundation species depend upon geologically derived reduced chemicals, the primary production of these systems is uncoupled from the carbon flux supporting the background biota.

18.2. Background: Depth Gradient of Organic Detritus Influx to Bottom

The supposition that lower-slope benthos experiences less food availability than on the upper slope is based upon patterns of biomass and flux. Fortunately, an interest in global-scale carbon flux has led to a substantial increase in understanding of the interplay of flux, benthic biomass, and depth across the full depth range of the ocean (Table 18-1). The starting points for this advancement were the initial empirical models for biomass (Rowe 1983) and particulate organic carbon (Suess 1980, Betzer 1984). Both shared basically similar exponential decreases with depth, strongly supporting the contention that deep biomass feeds upon the labile flux. Globally, the extent of biomass decline can be seen from an extensive compilation of microbial, meiofaunal, macrofaunal, and megafaunal biomass (Rex and Etter 2010). In that analysis the relationship with depth was determined after removal of geographic effects. Macrofauna and megafauna biomass decline 33% and 30% between 1,000–3,000 m depth respectively with notably smaller declines in microbes (6%) and meiofauna (17%).

Rowe et al. (2009) provide biomass information specifically for the continental slope of the northern GoM. With the dramatic exception of microbes, benthic biomass in the GoM is dramatically lower than that found for the global ocean consistent with the longstanding view that the GoM is oligotrophic. Faunal biomass at any given depth is from one to two orders of magnitude lower in the GoM. Rates of biomass decline with depth, however, are roughly similar. Accepting that the low metazoan biomasses are indicators of limited food for the background fauna, these biomass patterns support the proposition that seep-background contrast increases with depth in the GoM. If, however, microbial biomass is considered reflective of food supply, changes with depth become much harder to determine. For the global ocean there was no statistically significant decrease in biomass with depth (Rex 2006, Rex and Etter 2010). For the GoM the decrease with depth was modest, but statistically significant (Deming and Carpenter 2008).

Another method of assessing depth decreases of food input to bottom is the estimation of vertical carbon flux over a depth range. Actual particle traps were used in the initial studies of Suess (1980) and Betzer (1984). Such trap measurements have now been largely replaced by models

that allow flux calculation from satellite-determined sea surface cholorphyll standing stock and ocean depth. There has been insufficient confirmation at the seafloor of these estimated fluxes to determine their accuracy. They do, however, provide an easily obtained value. The rate of productivity is first calculated from apparent chlorophyll concentration using the Vertically Generalized Production Model (Behrenfeld and Falkowski 1997). Then flux to bottom is calculated assuming a globally constant exponential decay with depth (Pace et al. 1987). Such an estimation of flux has been carried out for the northern GoM by Biggs et al. (2008). Based on depth decay alone, the influx to bottom at 3000 m will only be 45% of that at 1000 m depth.

Table 18-1

Biomass Decline with Depth of the Phytodetritus Food Web

GLOBAL BENTHIC BIOMASS (Rex & Etter 2010)	**Log(gC/m^2), Z= m depth**	**mgC/m^2 at 1000m**	**Percent decline 1000–3000m**
Microbe	-0.423 - 0.00006Z	617	6%
Meiofauna	-0.559 - 0.00018Z	478	17%
Macrofauna	0.281 - 0.00045Z	845	33%
Megafauna	-0.843 - 0.00036Z	300	30%
NORTHERN GoM BENTHIC BIOMASS (Rowe et al 2009)	**mgC/m^2**		
Microbe	2043.30 -284.13Z	1,759	16%
Meiofauna	$72.^{)}\ 10e^{(-0.70Z)}$	36	41%
Macrofauna	$187.12e^{(-.53Z)}$	110	50%
Megafauna	$12.12e^{(-.2.36Z)}$	8	24%
NORTHERN GoM CARBON FLUX (Biggs et al. 2008)	**Estimated C flux to bottom, log(mgC/m2/day)**		
POC Flux Rate	NPP x 3.526 x $Z^{(0.734)}$	NPP x .0221	45%

18.3. Methods

The intent of sampling was to obtain an adequate number of background specimens from as many species as possible in close proximity to seeps as well as several km off the site. Specimen collecting was carried out by trawling at distances of 1–5 km remote from seep sites depending on bottom conditions. An otter trawl was used during the Recon cruise of the R/V *Gyre* and a beam trawl during the R/V *Atlantis* cruise. The R/V *Ronald Brown* could not carry out deep trawling. A Gomex-style box corer was used on the recon cruise at GC852 but failed to provide an sufficient number of species and specimens for analysis. Collection within and in close proximity (<10 m) to seeps was dependent upon and manipulator and slurp collecting using the HOV *Alvin* and the ROV *Jason* II. Since trapping had been successfully applied at upper slope seep sites in previous studies, it was again attempted. Small wire traps deployed by *Alvin*

yielded few specimens. The same negative result was obtained using baited minnow traps attached to elevators during *Jason II* operations. A larger free return trap was deployed during *Jason II* operations but malfunctioned and was lost.

At sea specimens were sorted to species level on the basis of morphology. Muscle tissue samples were removed from larger specimens and frozen at -20°C. Small specimens were frozen whole. In the laboratory tissues were thawed and examination at 25X magnification between crossed Nichol Prisms while wet to reveal the presence of any carbonates. When carbonates were present, powders were washed in 1N HCl followed with a rinse with de-ionized water, re-dried and re-powdered. This was particularly applicable to all echinoderm tissues. Vacuum drying was carried out at room temperature for 48 hrs followed by oven drying for 24 hrs at 60˚C. Dry samples were powdered with a steel mortar and pestle. Powders were stored in vacuum desiccators to assure dryness. In preparation for analysis, a 1 mg subsample of powder was weighed with 5-place precision and crimped in a tin foil boat. Crimped boats were stored in a vacuum desiccator until shipment to the Stable Isotope Laboratory at the University of California at Davis for analysis. Stable isotope data are expressed in parts per thousand (‰) deviation from international standards using the following equation:

$$\delta X = (R_{sample} / R_{standard} - 1) \times 1000$$

Where X = ^{13}C or ^{15}N, and R = ratio of heavy/light isotope content ($^{13}C/^{12}C$ or $^{15}N/^{14}N$). Working standards, sucrose for carbon and ammonium sulfate for nitrogen, are ($\delta^{13}C$ = –23.83‰ vs. VPDB, $\delta^{15}N$ = +1.33‰ vs. air N_2).

18.4. Results

18.4.1. Sample Collection Results

The most important samples for the purpose of this study were those collected in close proximity of seeps which had also be collected in the remote trawl samples. Only two groups were collected with a wide enough distribution and in sufficient numbers to support meaningful comparisons (Table 18-2). A total of five species of holothuroids were collected and identified by Dr. Robert Carney. Two species of the large conspicuous holothurian genus *Benthodytes* were easily sampled, *B. typica* and *B. lingua* along with the related *Psychropotes depressa* were collected both in close proximity and remote from seeps. Twelve species of asteroids and ophiuroids were collected and identified by Dr. Chris Mah. Three species were found both near and remote from seeps. Three were collected exclusively within close proximity to seeps. An additional five species were restricted to the background and only collected in trawls.

Table 18-2

Collections from Close Proximity Suitable for Isotope Analysis

Location	Lowerings	Holothuroids	Asteroids	Crustaceans
AC-601	J-283	3 spp 6 spec		
AC818	J-282,284	3 spp 12 spec	3 spp 7 spec	
AT340	J-270,276,277	2 spp 10 spec	1 spp 1 spec	
GC852	J-273, 278		1 spp 1 spec	3 spp 7 spec
GB-645	J-281	1 spp 4 spec	1 spp 1 spec	
WR-269	J-275	3 spp 8 spec		
6 Sites	10 lowerings	3 spp 40 spec	5 spp 10 spec	3 spp 7 spec

18.4.2. Isotopic Patterns Among Sites

Sixty-two megafauna samples consisting primarily of holothuroids and asteroids were collected in the close proximity of seeps and not within seep community mussel pot or Bushmaster samples. Simple average and standard deviation of both $\delta^{13}C$ and $\delta^{15}N$ showed overlapping ranges of values (Table 18-3). The averages clearly reflected a preponderance of photosynthetic carbon. It was notable, however, that the standard deviation at GC852, AC818, and AT340 was two to three times greater than at the other seep sites. In the case of GC852 where these megafauna were seldom encountered near seeps, only three specimens were examined. Of these, the crab *Chaceon quinquedens* had a $\delta^{13}C$ value of -32.68‰, which is low enough to indicate substantial seep trophic input. At AC818 values for holothuroids indicated photosynthetic carbon, but five specimens of the asteroid *Ampheraster* sp., a single asteroid *Plinthaster dentatus* and a crangonid shrimp had similarly low seep-influenced values (-31.63 to -41.30‰). Again at AT340, obvious departures from photosynthetic carbon were limited to asteroids, *Benthopectin simplex* and a brisingid (-31.52‰ to 37.80‰). At AC601 the more numerous holothuroids obscured the more seep-like value of -27.70‰ of the photogenic *Benthoctopus* sp. GB647 had both holothuroids and asteroids of the peculiar soft-bodied *Hymenaster* sp. The carbon values, however, reflected only photosynthetic carbon. Background megafauna collected > 1km from seeps contained a very narrow range of $\delta^{13}C$ and $\delta^{15}N$ values for the 107 specimens from five sites analyzed. Consisting primarily of the same species of holothuroids collected in close proximity of seeps, there was no indication of seep input.

$\delta^{15}N$ values can be reflective of seep input in those systems with highly depleted values, but are often used to assess trophic level (Post, 2002). With the exception of MC548, the average and standard deviation of $\delta^{15}N$ indicates a general lack of trophic complexity in the proximity of seeps and the background. The much higher average at MC548 is due entirely to background specimens of the holothuroid *Mesothuria lactea* (15.51 to 16.56‰). Normally, these high values would be taken as an indicator of a high trophic level. However, *M. lactea* is a mud-ingesting species that must be selecting for highly enriched food in the detritus. The utility of trophic-level assessment in these deposit feeders remains problematic.

Table 18-3

Summary of Site Statistics for Near Seep and Background Megafauna

Block	Type	N	$\delta^{13}C$		$\delta^{15}N$	
			Avg	StDev	Avg	StDev
GC852	SEEP	3	-24.47	7.22	9.80	1.38
AC818	SEEP	23	-22.65	7.68	10.26	2.30
AT340	SEEP	16	-20.75	7.56	10.72	2.12
AC601	SEEP	8	-19.14	3.31	10.86	1.02
WR269	SEEP	7	-17.96	1.39	11.25	0.61
GB647	SEEP	5	-17.63	1.03	11.47	1.88
Combined Seeps		**62**	**-20.86**	**6.66**	**10.57**	**2.31**
GC852	BKG	12	-18.05	1.87	10.12	2.31
AC818	BKG	13	-17.96	0.75	10.19	1.11
AT340	BKG	23	-17.65	1.73	11.04	1.78
AT209	BKG	43	-16.94	0.57	11.77	0.92
MC548	BKG	16	-16.75	1.37	14.88	2.34
Combined Background		**107**	**-17.31**	**1.30**	**11.70**	**2.16**

18.4.3. Isotopic Patterns in Common Echinoderms

Echinoderms were one of the few taxa collected both in close proximity to seeps as well as trawled from more remote locations in sufficient number to allow comparison. Stable isotope values and comparison between seep and background for asteroids and ophiuroids are displayed in Table 18-4. The low number of specimens of any given species limits the utility of significance testing, but the values suggest certain relationships. For the purpose of a more complete comparison the ophiuroid *Ophioctenella acies* (Tyler et al 1995), has been added to the data. These specimens were collected coincidental with foundation fauna sampling and appear to be a true seep endemic not found in the background Six species of asteroids were collected in close proximity to seeps. *Benthopectin simplex*, *Dytaster grandis* and *Plinthaster dentatus* are common in the background as well as within seep sites. They share similar continental slope distributions in the western Atlantic with a few eastern Atlantic reports. Average $\delta^{13}C$ for *B. simplex* suggest utilization of seep biomass when in close proximity to those systems. Background values are in the phytodetritus range. The seep versus background differences for

D. grandis and P. dentatus are less distinct. $\delta^{13}C$ is more depleted in close proximity to seeps, but only slightly so. Statistical testing of significance would require many additional specimens.

Brisingidae and *Hymenaster* sp. were also sampled in close proximity to seeps. There are relatively common in the background but were not sampled during the trawling of this project. *Hymenaster* showed no indication of feeding on seep biomass. The actual feeding mechanism for this gelatinous taxon is not known. The average $\delta^{13}C$ of the two brisingids is suggestive of some seep influence. These long-armed animals are thought to be suspension feeders.

Ampheraster alaminos was common in and near seep sites. Its six arms made it easy to recognize in video and photographic records. It was not collected by trawling during this study, but has been reported 46 times from the GoM and at a single location in the western Atlantic. Its $\delta^{13}C$ values indicate utilization of seep carbon. Based on morphology it is probably a predator.

Table 18-4

Asteroid and Ophiuroid Seep **Versus** Background Comparisons

			SEEP				BACKGROUND				
			$\delta^{13}C$		$\delta^{15}N$			$\delta^{13}C$		$\delta^{15}N$	
Taxon	ID	N	Avg	Stdev	Avg	Stdev	N	Avg	Stdev	Avg	Stdev
Asteroidea	*Benthopecten simplex*	2	-37.46	0.48	6.71	1.76	2	-20.10	1.18	8.84	1.76
Ophiuroidea	*Ophioctenella acies*	27	-35.88	9.091	2.31	2.621	0				
Asteroidea	*Ampheraster* sp	5	-33.78	1.32	9.95	0.25	0				
Asteroidea	Brisingidae	2	-26.58	6.98	10.26	1.57	0				
Asteroidea	*Dytaster grandis*	2	-23.08	4.16	9.23	1.08	5	-17.58	0.29	10.88	0.85
Asteroidea	*Plinthaster dentatus*	2	-20.21	0.83	14.70	0.97	3	-17.24	3.31	10.82	3.29
Asteroidea	*Hymenaster* sp	2	-17.37	0.78	13.04	1.01	0				
Asteroidea	*Litonaster* sp.	0					1	-19.86		13.91	
Asteroidea	*Nyphaster areanatus*	0					1	-19.31		11.83	
Ophiuroidea	*Ophiomusium* sp	0					1	-20.57		8.05	
Asteroidea	*Plutonaster agassisi*	0					2	-19.70	0.50	10.26	0.47
Asteroidea	*Zoraster fulgens*	0					4	-18.01	0.32	12.76	0.93

Examination of the full data sets for asteroids and ophiuroids shows a range of trophic complexity for these animals (Figure 18-1). Animals restricted to the background show a narrow range of $\delta^{13}C$ values. The spread of $\delta^{15}N$ values is consistent with trophic-level enrichment. Most species that enter the seep areas show the influence of seep biomass in their tissues stable isotope values. Since the actual prey of these species is unknown, the extent of seep utilization cannot be calculated.

Holothuroids were the second echinoderm group that occurred both within proximity of seep areas and were trawled from more distant locations. They represent a deposit-feeding contrast to starfish predation. Five species were collected and analyzed. *Benthodytes typica*, *B. lingua*, *Psychropotes* (*Euphronites*) *depressa* are sediment feeders that range over the background and enter the mud-covered portions of seeps. *B. typica* has been reported from the Pacific but seems to be primarily a common species on the Atlantic lower slope. *B. lingua* and *P. depressa* share a similar Atlantic distribution.

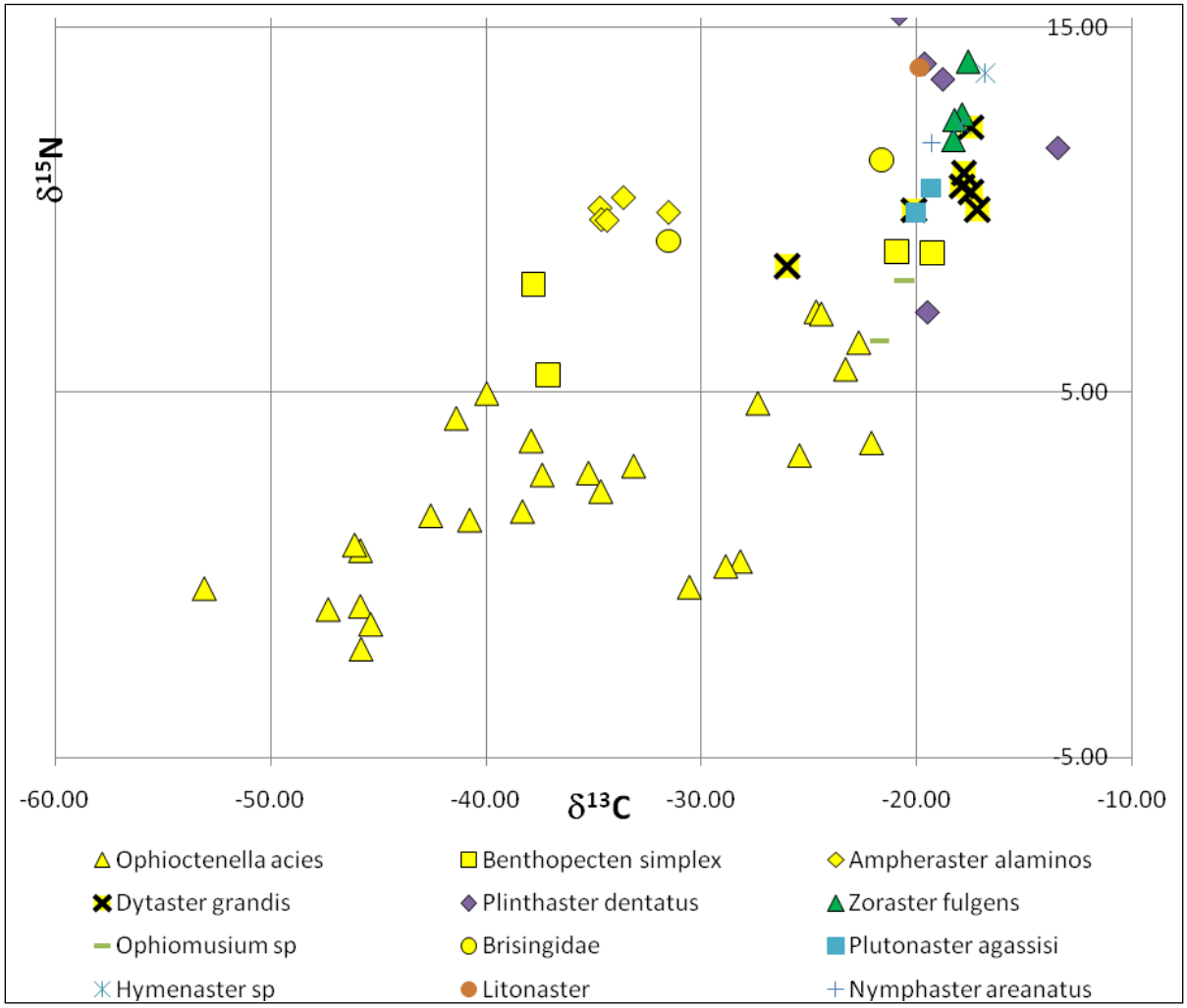

Figure 18-1. Stable isotope values for asteroids and Ophiuroids.

Additional background species *Mesothuria lactea* and *Benthothuria* sp. were trawled. These have been observed in seep systems in image surveys. For comparison the worm-like *Chiridota heheva* was included in the analyses. *C. heheva* like *O. acies* was collected in conjunction with foundation species sampling. It is restricted to natural seeps and manmade deep sulfidic environments (Pawson and Vance, 2004).

Average stable isotope values for $\delta^{13}C$ and $\delta^{15}N$ show *Chiridota heheva* to be distinctly different. It also displays the wide variability of $\delta^{13}C$ values typical of seep-associated feeding (Table 18-5). On first inspection, the background holothuroids collected in close proximity to seeps reflect only photodetritus feeding (Figure 18-2). When values within seeps are compared via simple T tests (unequal sample sizes and unequal variances) an interesting pattern is found. Average $\delta^{13}C$ is always slightly higher in seeps and $\delta^{13}C$ standard deviation is always greater. Employing the common criteria of $\alpha = 0.05$, average $\delta^{13}C$ in *Benthodytes lingua* and *Psychropotes depressa* are significantly different (two-tailed test) between the seep and background. *Benthodytes typica* just barely fails the test for a difference in means.

Table 18-5

Holothuroid Seep Versus Background Comparison

	SEEP					BACKGROUND					$\delta^{13}C$
		$\delta^{13}C$		$\delta^{15}N$			$\delta^{13}C$		$\delta^{15}N$		Prob. 1-Tail
ID	N	Avg	Stdev	Avg	Stdev	N	Avg	Stdev	Avg	Stdev	P(T<=t)
Chiridota heheva	15	-41.55	9.60	1.67	2.18	0					
Benthodytes typica	21	-17.70	1.10	10.85	0.90	23	-17.24	0.71	10.77	0.48	0.05863
Psychropotes depressa.	5	-17.43	0.58	10.90	0.41	17	-16.83	0.38	12.20	0.72	0.04127
Benthodytes lingua	16	-17.28	1.45	11.40	1.13	8	-15.99	0.52	11.92	1.17	0.00228
Mesothuria lactea	0					12	-16.12	0.75	16.09	0.31	
Benthothuria sp.	0					12	-16.96	0.49	12.22	0.57	

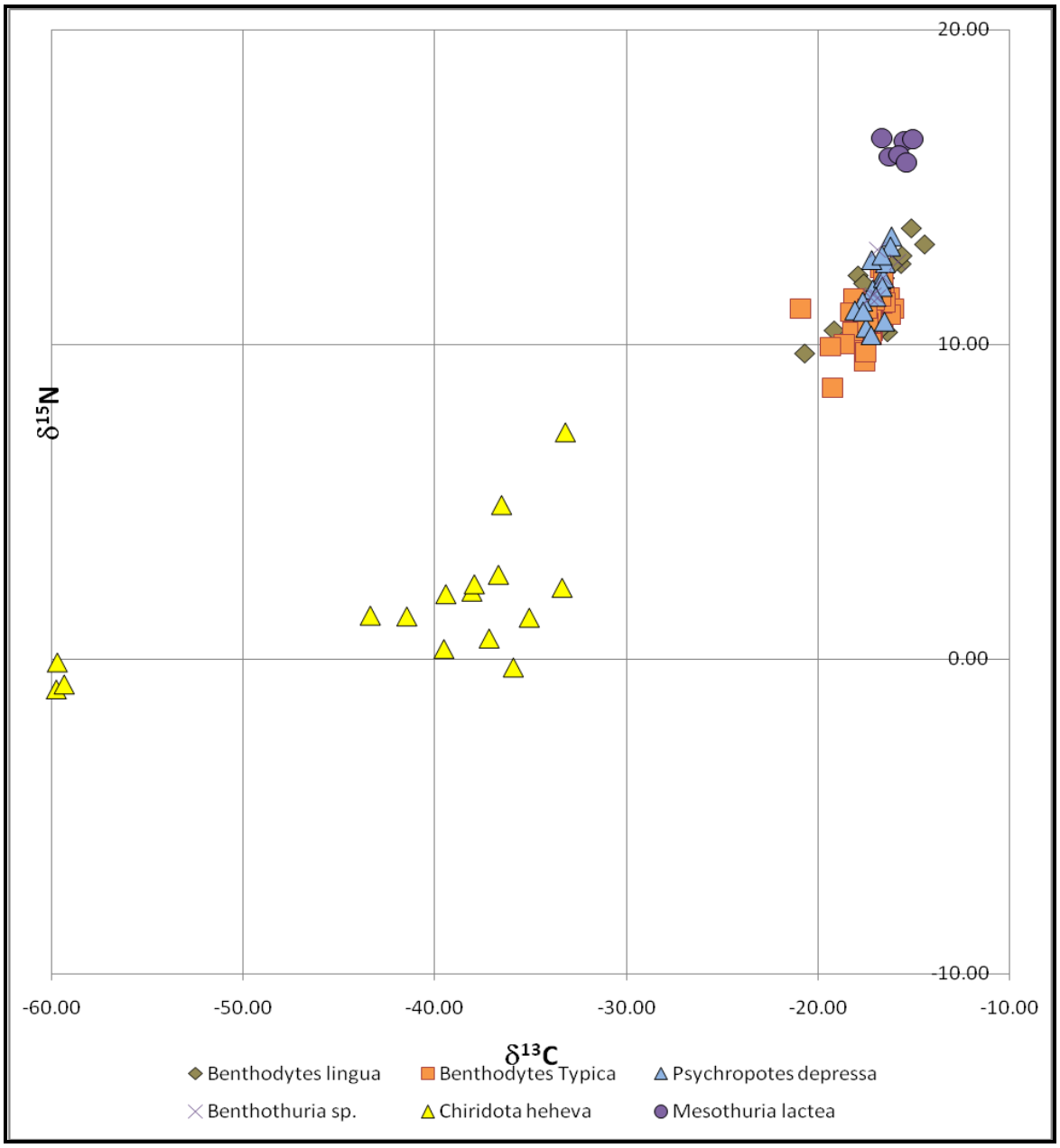

Figure 18-2. Stable isotope values for holothuroids.

18.5. Discussion

The intended direct comparison of upper and lower-slope utilization of seep biomass could not be completed due to differences in fauna and low sample sizes at the deeper sites. The lower-slope sites lacked the abundant and easily caught crabs, hagfish, and giant isopods that were the basis of the upper-slope studies. No convincing evidence, however, of greater seep utilization at the deeper sites was found. Background species acting as vagrants in seep communities were not notably more numerous at deeper sites. Isotopic values suggest somewhat similar utilization by

vagrants at shallow sites. MacAvoy et al., (2002) found that relatively few large benthic consumers derive food from the upper-slope seeps. Of the fishes, rat tails (*Nezumia* sp) and eels (*Synaphobranchus* sp., *Ophicthus cruentifer* and *Dysomma rugosa*) have similar $\delta^{13}C$ values (-32.7 and -42.5‰, respectively), reflecting chemoautotrophic carbon. Most specimens of predators/scavengers such as isopods *Bathynomus giganteus*, hagfish (*Eptatretus* sp.) and spider crabs (*Rochina crassa)*, had isotope values closer to phytoplankton ranges ($\delta^{13}C$: -20 to -18‰). Some individual *Eptatretus* sp. and *R. crassa*, however, did show a chemosynthetic component. Predatory invertebrates collected within seeps, such as the sea star (*Sclerasterias tanneri*) and snail *Buccinum canetae*, had greatly depleted $\delta^{13}C$ values, indicating an almost 100% reliance on seep production.

It is only possible to speculate on the cause of an apparent absence of increased seep utilization with depth. If we accept the traditional dogma that benthic fauna becomes increasingly more food limited with depth, then there may be avoidance of seep biomass. It is conceivable that the foundation species and the closely associated macro- and mega fauna are toxic or gain protection from the same chemical gradients that support them. Similarly, seep sediments may be toxic to some deposit feeders. Alternately, it could be argued that the trophic contrast between seep production and phytodetritus influx does not actually increase with depth. The estimated flux decrease of 45% between 1,000 and 3,000 m is small versus orders of magnitude that might be experienced across the abyssal plain of the Pacific. And, if the relatively constant microbial biomass is the primary source of food, then no change in contrast will be expected.

The slight shifts in $\delta^{13}C$ values for holothuoids in and out of seeps raises the possibility that there is a seep-detritus trophic pathway. This could be via free-living methanotrophic microbes in the water column. It is, however, a very small part of the diet of the megafauna. Confirmation of such a link will require collection of a substantial number of single species within and without of the seep systems.

The abundance of *Ampheaster alaminos* at the deeper seeps is similar to that of *Sclerasterias tanneri* shallower. This may be a simple background species replacement with depth. Both are similar to other asteroidea (seastars) which are a conspicuous component of deep-sea benthos exhibiting a wide range of feeding types (Carey 1972). Of the species included in this analysis four have a morphology often associated with predation or scavenging: *Ampheaster alaminos, Benthopectin simplex, Dytaster grandis, and Zoraster fulgens*. All have legs that are long relative to the central portion of the body. Three have morphologies associated with other feeding modes: the cushion-shaped *Plinthaster dentatus*, the very long-legged suspension feeder Brisingidae, and the gelatinous *Hymenaster*. The genus *Ophioctenella* contains a single species *O. acies* that is broadly distributed at Atlantic seep, vent, and deep corals sites but appears to be absent from non-seep bottoms (Stohr and Segonzac 2005). *Ophiomusium* sp. is a deep cosmopolitan species with over 60 nominal species. Ophiuroids are similar to asteroids in the breadth of feeding types.

The absence of a deep population analogous to hagfish at the shallow seeps is hard to explain. The genus *Eptatretus* is globally distributed with the possible exception of polar seas with 46 recognized species occupying a range of habitats including hydrothermal vents and hydrocarbon seeps (Moeller and Jones 2007). They have been found from inshore waters to greater than

2,400 m, but the reported depth range of most species extends from the mid shelf (~100 m) to the mid slope (~1,500 m). Normally inconspicuous due to burrowing, they can be very numerous at upper-slope seep sites when sampling damages mussel populations and the hagfish emerge to scavenge on damaged individuals. Similarly, on the upper slope hagfish can completely pack small baited traps. Hagfish were neither seen nor trapped at any of the lower-slope seep sites.

The paucity of large crabs at the deep sites is also hard to explain. Large decapod crabs in the family Majidae and related taxa are a common component of outer shelf and upper slope fauna both globally and in the GoM (Felder et al. 2009, Wiksten and Packard 2005). At upper-slope sites the species *Rochina crassa* were common over a wide size-age range and were often collected in traps both within and remote from seeps. As noted above, some specimens clearly had assimilated chemosynthetic carbon although most depended on a photosynthetic diet. Only two large crabs were encountered on the lower slope, *Chaceon quinquedens* and *Paralomis* sp. Smaller *Chaceon* were observed within seeps and on a single occasion fed upon damaged mussels. A single specimen of *Paralomis* was collected by the *Jason II* within a seep site but showed no isotopic evidence of feeding upon a seep source.

18.6. Conclusions

Lower-slope seeps provide a food resource to a few background species. This was most obvious in predatory seastars. There is no strong evidence of a large-scale export of seep carbon into the surrounding benthos. With respect to seep-background interactions, upper and lower-slope seep systems appear to be similar although the participating species change with depth.

19. SEEP MEIOFAUNA

19.1. Introduction

The size class of meiofauna is generally defined as the portion of the community passing through a 1 mm sieve and being retained on a 32 µm sieve. This community comprises protists and metazoan animals that remain small even when adult (permanent meiofauna), and animals which temporarily belong to this size class during their larval/juvenile development (temporary meiofauna). As a part of the sediment infauna, meiobenthos has been studied extensively worldwide from many different habitats, but less attention has been paid to the hard substrate epibenthic or epizooic, and epiphytal meiobenthos (Giere, 2009).

Previous meiobenthic community studies at cold seeps are scarce and mainly restricted to assessments of abundance, biomass, and composition of higher taxa. They cover a wide geographical and depth range from shallow-water sands between 10 m down to deep-sea muds at 5,000 m. They comprise various types of hydrocarbon gas and oil seep (Montagna and Spies, 1985; Palmer et al., 1988; Shirayama and Ohta, 1990; Olu et al., 1997; Robinson et al., 2004; Soltwedel et al., 2005; VanGaever et al., 2006; Sergeeva and Gulin, 2007; Sommer et al., 2007), gas, oil and asphalt seeps (Montagna et al., 1987), gas hydrates (Sommer et al., 2007), and brine seeps (Powell et al., 1983, 1986), but exclusively describe the infaunal meiobenthos from sediments. Previous seep meiofauna studies in the GoM were conducted for the shallow brine seep sand communities at East Flower Garden (Powell et al., 1983, 1986; Jensen, 1986) and the hydrocarbon seep bacterial mat communities in Alaminos Canyon (2,200 m), Green Canyon (about 700 m), and Atwater Valley (about 2000 m) (Robinson et al., 2004). The epifaunal foraminiferan communities associated with tube worm bushes on the upper slope was also studied in detail (Sen Gupta et al., 2007), but no study on the metazoan meiobenthos associated with tube worms or mussels has been conducted previously.

This study examines the abundance and higher taxonomic composition of epizooic, permanent, metazoan meiobenthos associated with aggregations of tube worms and mussels on the lower Louisiana Slope. The following questions were addressed: 1) Do abundance and higher taxonomic composition differ between geographical regions? 2) Do abundance and higher taxonomic composition differ between mussel and tube worm aggregations? 3) Is the seep epizooic metazoan meiobenthic abundance similar to seep infauna or non-seep sediments? 4) Are there similarities in abundance and higher taxonomic composition of seep and hydrothermal vent communities associated with mussels and tube worms? In addition, we studied in detail the genera composition of selected tube worm and mussel aggregations of Atwater Valley to address the following questions: 5) Do the diversity and genera composition differ between mussel and tube worm aggregations? 6) Is the seep epizooic metazoan meiobenthic community similar to seep infauna or vent epifauna?

19.2. Methods

19.2.1. Collection and Processing

Meiofauna were collected from three hydrocarbon seep sites: Green Canyon 852 (GC, depth 1,400 m), Alaminos Canyon 818 (AC, depth 2,800 m), and Atwater Valley 340 (AT, depth 2,200

m). During two cruises in 2006 and 2007, a total of 13 samples were taken with the submersible DSV *Alvin* (2006) or ROV *Jason II* (2007). Meiofauna from of each foundation group were collected at two different seep habitats: seven mussel samples M-GC1, M-GC2, M-GC3, M-AT1, M-AT2, M-AT3, M-AC1; six tube worm samples T-GC1, T-GC2, T-GC3, T-AT1, T-AT2, T-AT3 and three samples of non-seep sediments were taken as controls (S-GC1, S-GC2, S-GC3) in close vicinity (< 3 m distance) to seep megafauna communities (Table 19-1).

Epifauna collections were obtained from samples taken with the quantitative mussel pot sampling device for mussel aggregations and the Bushmaster Jr. for tube worm aggregations. Infauna of non-seep sediment was collected with push corers (6.3 cm diameter, 30 cm length). Samples were separately put into isolated, previously cleaned plastic boxes on the basket of DSV *Alvin* or ROV *Jason II*, transported to the surface, and recovered on deck of the research vessels RV *Atlantis* in 2006 or NOAA *Ronald Brown* in 2007. On board, the macro and megafauna of Bushmaster and mussel pot samples was carefully rinsed with cold 32 µm filtered seawater before we removed them from the samples in order to avoid loss of smaller fauna. Mussels and tube worms of each collection were identified and counted (Table 19-1). The samples were sieved through a 1 mm mesh size to separate macro- from meiofauna. Before sieving the samples through a 32 µm sieve, we measured the volume of sediment of the entire sample < 1 mm. The meiofauna fraction was fixed in 4% buffered formalin. The larger size fractions were retained for the megafaunal community composition and structure analyses.

To estimate the sediment depth distribution of meiobenthos in the push corer samples, we checked the fraction deeper than 5 cm carefully on board of the ship. Since one sample lacked any specimens, and two samples only contained a single nematode, we took only the upper 5 cm of all samples, and fixed them in 4% buffered formalin without sieving. The push core sample S-GC1 was split into 3 parts along the entire length, and 1 part (52 ml) was used for the present study. The other two samples S-GC2 and S-GC3 were split into half and these parts (78 ml) were used for the present analyses.

To extract meiofauna from the sediment, we used a density centrifugation technique with a medium consisting of a Silicapolymer (Fa. Levasil®) mixed with Kaolin (McIntyre and Warwick, 1984; Veit-Koehler et al., 2008). Except for sample T-AT1, all other samples were totally processed and the entire meiofauna community was counted and identified to higher taxon level. Sample T-AT1 was extremely large (7.5 l sediment including meiofauna after sieving through a 1 mm net), therefore we mixed the entire sample in a bucket, let it settle, randomly took a subsample of 217 ml and estimated the total abundance from this subsample.

All taxa belonging to the permanent metazoan meiobenthos were considered in this study. We noticed the presence of crustacean nauplii but did not include them in further analyses due to the fact that they could not be assigned to a specific higher crustacean taxon. We also recorded the protist meiobenthos, but did not include them in this study of permanent, metazoan meiobenthos.

Three mussel samples M-AT1, M-AT2, M-AT3 and three tube worm samples T-AT1, T-AT2, T-AT3 from Atwater Valley were identified to genus level. If present, 300 individuals (ind.) per taxon were randomly picked from each sample while the remaining organisms were counted. Nematodes were mounted on glycerine slides and identified to genus level according to Platt and

Warwick (1988). Copepoda, Ostracoda, Tanaidacea, Halacaridaewere sent to specialists for further identification and Kinorhyncha were identified to genus level at the University of Vienna.

Table 19-1

Sample Information Is Given on Geographical Location, Site, Dive Number (AD *Alvin* dive, JD *Jason II* dive), Latitude, Longitude, Depth, Sample Area ("footprint" of sediment surface, above which the mussel pot or the Bushmaster sampling device was placed; is equal to diameter of mussel pot and maximal diameter of Bushmaster), Surface Area (total area of tube worm tubes or mussel shells surfaces calculated per sample), Surface Area per Sample Area, Volume of Sediment (collected between mussels or tube worms), and Megafauna Listed per Species (% contributing to total megafauna)

Mussels

Sample	location	site	dive number	Latitude	longitude	Depth (m)	sample area (cm^{-2})	surface area (cm^{-2})	surface area per	sediment (ml)
M-GC1	Green Canyon	GC852								
M-GC2	Green Canyon	GC852	AD 4187	27º06.656	91º09.937	1406	531	1630	3.07	no info
M-GC3	Green Canyon	GC852	JD 278	27º06.380	91º09.953	1408	531	2140	4.03	41.21
M-AV1	Atwater Valley	AT340	D 276	27º25.197	88º21.853	2190	531	2190	4.12	21
M-AV2	Atwater Valley	AT340	JD 277	27°38.697	88°21.851	2190	531	1770	3.33	3600
M-AV3	Atwater Valley	AT340	JD 277	27:38.700	88°21.859	2190	531	1620	3.05	390
M-AC1	Alaminos Canyon	AC 818	AD 4192	26º10.819	94º37.380	2744	531	2900	5.46	42

Tube worms

Sample	Location	Site	Dive number	Latitude	Longitude	Depth (m)	Sample area (cm^{-2})	Surface area (cm^{-2})	Surface area per sample area	Sediment (ml)
T-GC1	Green Canyon	GC852	AD 4186	27º06.371	91º09.968	1409	2800	15060	5.38	no info
T-GC2	Green Canyon	GC852	AD 4187	27º06.676	91º09.932	1406	2800	4980	1.78	no info
T-GC3	Green Canyon	GC852	JD 273	27º06.370	91º09.967	1410	2800	8050	2.88	5.89
T-AV1	Atwater Valley	AT340	JD 277	27º38.839	88º22.429	2175	2800	12750	4.55	7500
T-AV2	Atwater Valley	AT340	JD 270	27º38.694	88º21.843	2192	2800	16870	6.03	16
T-AV3	Atwater Valley	AT340	AD 4179	27°38.677	88°21.879	2185	2800	8590	3.07	302

Sediment

Sample	Location	Site	Dive number	Latitude	Longitude	Depth (m)	Sample area (cm^{-2})	Surface area (cm^{-2})	Surface area per sample area	Sediment (ml)
S-GC1	Green Canyon	GC852	AD 4177	27º10.633	91º16.608	1450	10.33	10.33	1.00	41
S-GC2	Green Canyon	GC852	AD 4177	27º10.633	91º16.608	1450	15.50	15.50	1.00	107
S-GC3	Green Canyon	GC852	AD 4177	27º10.633	91º16.608	1450	15.50	15.50	1.00	88.5

19.2.2. Data Analyses

Total abundance of meiobenthos was standardized to 10 cm^2 sample area and additionally to 10 cm^2 surface area of mussel shells and tube worm tubes. The surfaces of mussels and tube worms were estimated for the main foundation species *Bathymodolus brooksi, B. childressi, B. heckerae*, *Esparpia laminata*, and *Lamellibrachia* spp. from measurements of lengths and widths for each individual in the collection. To test for significant differences in abundances among habitat types in the Green Canyon samples, data were square-root transformed and bootstrapping was used as this is a well proven method when working with a relatively low number of samples and high variances (10,000 resamplings each, t-test, 2-sided test, routine "FTBOOT" from the package "computer intensive statistics" [Nemeschkal, 1999]). Results were classical Bonferroni-corrected (p = alpha/n; alpha = 0.05). To evaluate similarity and dissimilarity among all samples, a Bray-Curtis similarity matrix was generated (abundance data from 10 cm^2 sample area were square-root transformed, but were not standardized in order to better recognize differences caused by total abundances), and similarity percentage (SIMPER) analysis, ANOSIM, and MDS ordination were performed using PRIMER v5 (Clarke 2001).

For the Atwater Valley samples, genera richness (G'), the diversity indices Pielou's evenness (J'), Shannon-Wiener diversity (H' log e) and estimated genus richness (EGn) were calculated from genera abundance data using PRIMER v6 package (Clarke and Gorley 2006.). The PRIMER 6.1 software was used to generate k-dominance curves to establish dominance patterns and genus heterogeneity within the two different habitats. The relative abundance of each genus was ranked from highest to lowest and plotted against the cumulative percent abundance. Student's t- tests were performed to assess significance in genera richness and sediment volume, tube worm- and mussel surface area. For this, data were square-root transformed for genera richness, ln transformed for sediment volume and surface area. Bootstrapping was also used to test for significant differences between the habitats for each parameter, due to the small number of samples and high variances (10,000 resamplings each, t-test, 2-sided test, routine "FTBOOT" from the package "computer intensive statistics" (Nemeschkal, 1999). Hierarchical clustering and non-metric MDS ordination using PRIMER v6 was performed to establish similarity and dissimilarity between and within tube worms- and mussels- aggregations using a Bray-Curtis similarity matrix generated from standardized and square-root transformed abundance data to facilitate the contribution of the less common genera by down- weighting the highly abundant genera. One-way ANOSIM was performed to test for significant differences in the community structure between the two habitats. To determine which genera have the greatest contribution and therefore are responsible for similarities within a habitat and dissimilarities between habitats, SIMPER analyses were carried out.

19.3. Results and Discussion

19.3.1. Abundance

The total abundance of the permanent, metazoan meiobenthos associated with mussel and tube worm aggregations of most samples from three different locations at the Northern GoM ranged from <1 to 1,839 ind. 10 cm^{-2} sample area. Most mussel bed samples revealed abundances higher than 10 ind. 10 cm^{-2}, with the exception of M-GC1 and M-GC2 from Green Canyon 852. Most

tube worm aggregation samples showed extremely low abundances less than 10 ind. 10 cm^{-2}. However, one tube worm aggregation sample (T-AV1) from Atwater Valley 340 revealed a total abundance between one and two orders of magnitude higher (447 ind. 10 cm^{-2}) than the five other seep samples from tube worm bushes. Non-seep sediment control samples showed abundance values from 870 to 1,523 ind. 10 cm^{-2} sample area (Table 19-2).

Table 19-2

Meiobenthic Abundance is Shown as Total Abundance, Individuals 10 cm–2 Sample Area, and Ind. 10 cm–2 Surface Area for All 13 Samples (five mussel community samples, five tube worm community samples, three non-seep sediment samples); Additionally Total Abundances of foraminifera and Nauplii Are Listed (not included in analyses)

Sample	**Nematoda**	**Copepoda**	**Halacaridae**	**Ostracoda**	**Tanaidacea**	**Kinorhyncha**	**Isopoda**	**total**
mussels								
M-GC1	<1	5	0	0	0	0	0	5
M-GC2	<1	3	<1	<1	0	0	0	4
M-GC3	14	6	<1	<1	0	0	0	21
M-AV1	47	10	<1	<1	<1	0	0	73
M-AV2	1650	162	1	5	0	0	0	1839
M-AV3	301	43	<1	5	0	0	0	373
M-AC1	58	23	<1	0	0	0	0	81
tubeworms								
T-GC1	4	3	<1	<1	0	0	0	7
T-GC2	<1	<1	0	0	0	0	0	<1
T-GC3	5	<1	0	0	0	0	0	<1
T-AV1	370	73	0	4	1	0	0	451
T-AV2	6	3	<1	<1	<1	0	<1	9
T-AV3	4	3	<1	<1	<1	<1	<1	7
sediment								
S-GC1	711	162	0	5	0	0	0	879
S-GC2	703	163	0	4	0	<1	0	870
S-GC3	1267	250	<1	3	<1	1	0	1523

Green Canyon 852 was the only site where the number of samples was sufficient to statistically compare the abundances between mussel and tube worm associated communities, and between the seep communities and adjacent non-seep sediments. We found no significant difference between mussel and tube worm meiobenthos abundance ($p = 0.190$), but significantly lower abundances at both seep communities than in non-seep sediments (both: $p = 0.003$) (Table 19-3). Also at Atwater Valley 340 we compared the meiobenthic abundances between tube worm and mussel aggregations and found no significant differences ($p = 0.125$).

The mussel beds at AT340 and AC818, and one sample from GC852 (M-GC3) were exclusively composed of *Bathymodiolus brooksi*. *B. childressi* co-occurred in the other two GC samples, contributing 50% and 63.2% to the total mussel abundance. All of the tube worm aggregations analyzed contained mixed populations of *Escarpia laminata* and *Lamellibrachia* spp.. As foundation species forming biogenic habitat, tube worms and mussels considerably increase the surface area and thus the potential living space for meiobenthos. By estimating the actual surface of the foundation species, we found an increase of surface in both types of aggregations between 1.78- to 6.03-fold. The ratio of sample area to the surface area of tubes-shells was similar

between the two biogenic habitat types, but was more variable in tube worm bushes (1.78 to 6.03), than mussel beds (3.05 – 5.46) (Table 19-1).

Table 19-3

Dissimilarity Results (Diss. %) Calculated by SIMPER, and ANOSIM Results (R-statistics and possible significance level p) Are Shown for Mussel Compared to Tube Worm communities, and mussel and tube worm communities to non-seep sediment communities. Seep Sites at Different Depths (1400 m, 2200 m, 2800 m) Are Compared with Each Other

	Diss%	R-Stat	p
mussel - tubeworms	54	0,15	0,13
mussel - sediment	**74**	**0,81**	**0,02**
tubeworm - sediment	**74**	**0,64**	**0,04**
seep: 1400 m - 2200 m	55	0,25	0,13
seep: 1400 m - 2800 m	62	0,56	0,14
seep: 2200 m - 2800 m	35	0,56	1

By assuming that the surface of foundation species was the actual living space of associated meiobenthos, we standardized the total abundance of this community to the surface area and calculated even lower densities; between 1 and 3 ind. 10 cm^2. Again, one tube worm sample (T-AT1) contained much greater densities of meiobenthos (20 ind.10 cm^{-2}) (Table 19-2). T-tests on abundance per surface area of the GC852 samples revealed similar results as calculations per sample area, with similarly low abundances found in the seep habitat types (mussel and tube worm: $p = 0.150$; seep and non-seep: both $p = 0.003$).

19.3.2. Higher Taxon Diversity

The seep metazoan meiobenthic communities were composed of the higher taxa Nematoda, Copepoda, Ostracoda, Halacarida, Tanaidacea, Isopoda, and Kinorhyncha. In addition, nauplii larvae were found in most samples with variable abundances but were excluded from analyses due to the impossibility of assignment to a specific crustacean taxon. The protist phylum Foraminifera was also represented in all seep samples.

In all six tube worm samples from three different locations, the most prominent taxa were the nematodes followed by the copepods. Ostracods, halacarids, kinorhynchs, and isopods were relatively rare and were not found in all samples (Figure 19-1).

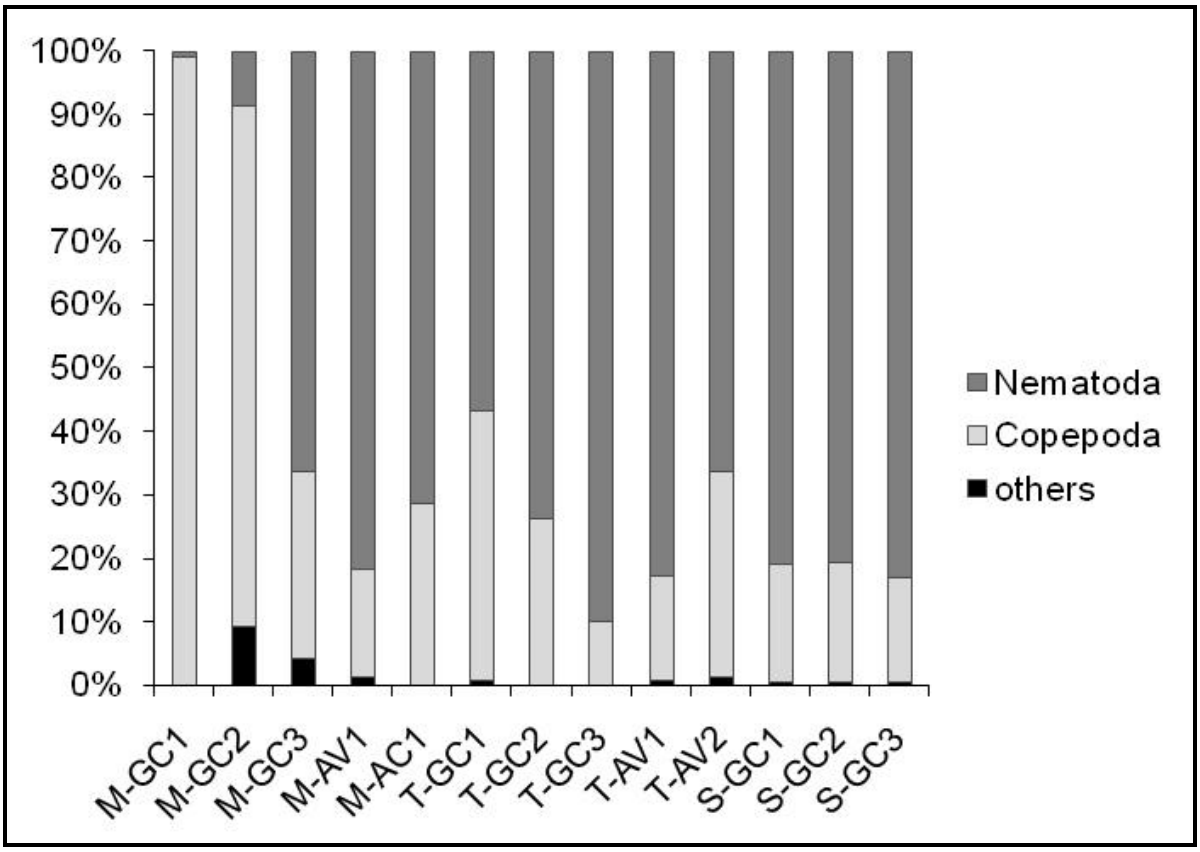

Figure 19-1. Relative abundance (%) of taxa for meiobenthos (five mussel community samples, five tube worm community samples, three non-seep sediment samples).
Nematoda, Copepoda and others (including Ostracoda, Halacarida, and Kinorhyncha) were present.

The relative distribution of higher taxa was more variable in mussel bed samples. In five samples (M-GC3, M-AV1, M-AV2, M-AV3, M-AC1), nematodes dominated followed by copepods, while in two samples (M-GC1, M-GC2) copepods were most abundant (82 and 99%). Ostracods were found in five, halacarids in six out of seven samples. Tanaids were only detected in one sample (M-AV1). Kinorhynchs and isopods lacked.

The non-seep control sediments collected in close vicinity to mussel and tube worms aggregations at GC was primarily composed of nematodes (80–81%), followed by copepods M(16–19%), ostracods, halacarids, and kinorhynchs (all < 1%). Isopods were not found. It was remarkable that nauplii were absent from these samples.

19.3.3. Higher Taxon Community Patterns

SIMPER and ANOSIM analyses did not demonstrate significant differences between mussel bed and tube worm aggregation meiobenthic communities at the taxonomic level examined. There were also no significant differences among sites, despite the differences in depth (GC 1,400 m, AT 2,200 m, AC 2,800 m) (Table 19-3). However, there were strong differences detected between non-seep sediment communities and tube worm and mussel associated communities (>

74% Bray-Curtis dissimilarity), and these differences were significant in the ANOSIM (R = 0.64; p = 0.040 for tube worm/sediment; R = 0.81; p = 0.020 for mussel/sediment). MDS ordination revealed that metazoan meiobenthos from seep habitats and from adjacent non-seep sediments formed distinct groups, with the exception of sample T-AT1 which exhibited relatively high similarity to non-seep communities (Figure 19-2).

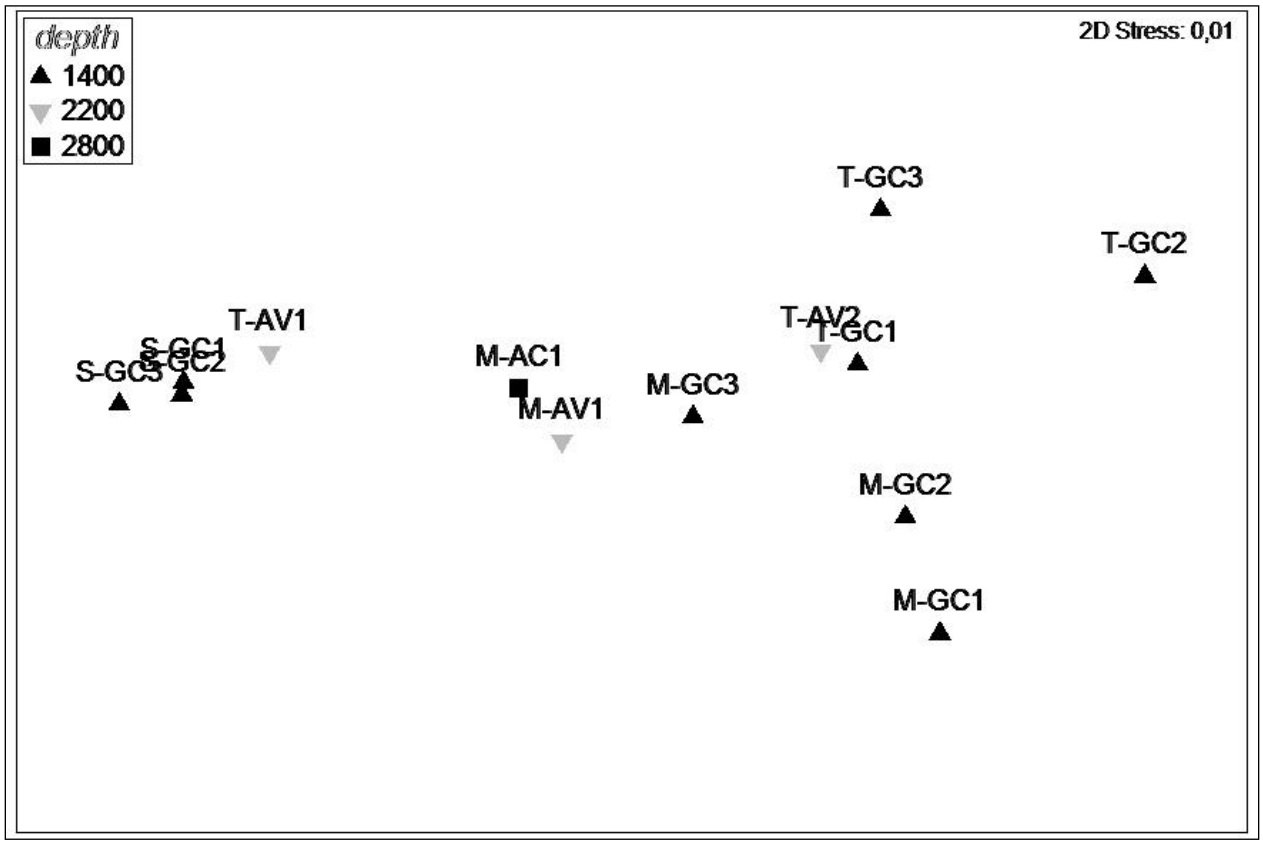

Figure 19-2. 2-D MDS configuration plot for 13 samples from five mussel community samples (M-GC1, M-GC2, M-GC3, M-AT1, M-AC1), five tube worm community samples (T-GC1, T-GC2, T-GC3, T-AT1, T-AT2), and three non-seep sediment samples (S-GC1, S-GC2, S-GC3) from three different depths.

19.3.4. Diversity at Atwater Valley

From the six samples at Atwater Valley we studied in detail, we identified a total of 113 genera (belonging to 53 families), 56 genera occurred in mussel beds and 104 in tube worm bushes (Table 19-3). Genera richness (G) and the values of Pielou' evenness (J), Shannon- Wiener (H'_{log}), EG (400) indexes and number of individuals are listed in Table 19-4.

Genera richness was neither positively correlated with surface area of the tube worm tubes and mussel shells ($r^2 = 0.72$, p =. 0.29), nor with the sediment volume. It ranged between 44 and 75 genera in tube worm bushes and was significantly higher than in mussel beds (G 22 to 48). Pielou's eveness exhibited the larges variation in tube worm aggregations from relatively uneven

distributed genera (0.85) to relatively even distributed genera (0.59). In mussel beds, Pielou's eveness values were between the lowest and highest values of tube worm bushes (0.67 to 0.77). Shannon-Wiener index was high at both sites (H'_{log} 2.11 to 3.65).

Table 19-4

Genera Richness (G), Pielou's Evenness Index (J') and Shannon-Wiener Diversity Index (H'log) for Total Meiobenthos, Nematoda, and Copepoda Calculated for All Six Samples Estimated Species Richness (ESn) Is Shown for Total Meiobenthos**.** T-AV1, T-AV2, T-AV3: tube worm habitat; M-AV1, M-AV2, M-AV3: mussel habitat

Total	**G**	**J'**	**H'_{log}**	**ES(400)**
T-AV1	63	0,59	2,46	59,02
T-AV2	44	0,75	2,84	40,07
T-AV3	77	0,84	3,66	72,12
M-AV1	50	0,76	2,97	45,7
M-AV2	26	0,67	2,20	24,32
M-AV3	22	0,68	2,11	21,9
Nematoda				
T-AV1	27	0,62	2,03	
T-AV2	28	0,74	2,45	
T-AV3	43	0,88	3,30	
M-AV1	30	0,79	2,67	
M-AV2	16	0,73	2,02	
M-AV3	16	0,70	1,94	
Copepoda				
T-AV1	30	0,86	2,94	
T-AV2	13	0,64	1,63	
T-AV3	26	0,69	2,26	
M-AV1	15	0,64	1,74	
M-AV2	7	0,35	0,68	
M-AV3	5	0,26	0,42	

The tube worm bushes were characterized by a genus-rich nematode community. Representing 3 to 33% of total meiobenthic genera, *Desmodora* was the most abundant meiobenthic genus. *Leptolaimus* had a relative abundance of 1 to 7%. *Comesa* was only high in abundance in one sample (18% of total meiobenthic genera in T-AV1). Further, the nematode community in tube worm aggregations consisted of *Odontanticoma* (3–9%), *Calyptronema* (6–9%), and *Daptonema* (1–8%). No other genus contributed to more than 5% of the total abundance in any sample from this habitat (Table 19-3). The mussel beds were inhabited by a slightly different nematode community with three genera exhibiting higher dominance: *Paracanthonchus* (3–27%), *Thalassomonhystera* (12–21%), *Linhomoeus* (2–22%). However, the two habitats shared two abundant genera *Leptolaimus* and *Desmodora* (Table 19-3).

Overall 48 copepod genera were identified, where the harpacticoids was the dominant copepod taxon with a contribution of 40 genera. The genus *Amphiascella* dominated at T-AV2 (15%) and T-AV3 (8%), while at T-AV-1 the relative abundance is low (<1). At the mussel bed the most

abundant harpacticoid genus was *Ameira* (5–8%). The other copepods belonged to the cyclopoids (4 genera), calanoids (1 genus), and poecilostomatids with the parasitic genus *Enalcyonium* and had a relative abundance of 9 to 19% in tube worm samples and 2 to 6% mussel samples. The relative abundance of the copepodites of the total meiobenthos was 7–19% in tube worm and 2 to 6% in mussel samples.

Halacarids as well as tanaidacaeas were represented by a single genus each in both habitats, *Copidognathus* and *Pseudotanais*, contributed less than 1% to the total meiobenthic abundance, but were not found in each sample. *Xylocythere* was the most dominant ostracod genus occurring at all six samples but with low abundances (<1%). The other ostracod genera were rare. Further, one individual of kinorhynch, *Echinoderes*, and one individual of isopod, which was unidentifiable due to insufficient fixation were found at T-AV3.

19.3.5. General Community Patterns at Atwater Valley

An MDS plot based on the abundances of meiobenthic genera (stress value = 0) revealed a cluster of two mussel bed samples (M-AV2 and M-AV3), while the other mussel bed sample and the three tube worm samples formed a distinct cluster (Figure 19-3). However, SIMPER analyses separated the two habitats from each other with an average dissimilarity of 64.9%. The nematode genera *Paracanthonchus* and *Desmodora* contributed with 5.4%, 4.2% respectively, the most to the dissimilarity of the two habitats, followed by the copepod genus *Amphiascella* with 3.9%. The similarity of the samples from tube worm bushes was 40.4%. The nematode genus *Desmodora* contributed on average 10.6% to the similarity of the three samples. The mussel bed samples showed a higher average similarity of 57.11% where the nematode genus *Thalassomonhystera* contributed with 15.3% to the similarity of the three mussel samples. Furthermore, hierarchical cluster analyses were generated to demonstrate the degree of similarity (Fig.6). The abundances of meiobenthos were compared by a one-way, crossed ANOSIM but the analyses did not point out any significant difference (global $R = 0.63$, $p = 0.1$) between the two habitats, which is possibly due to the limit number of samples.

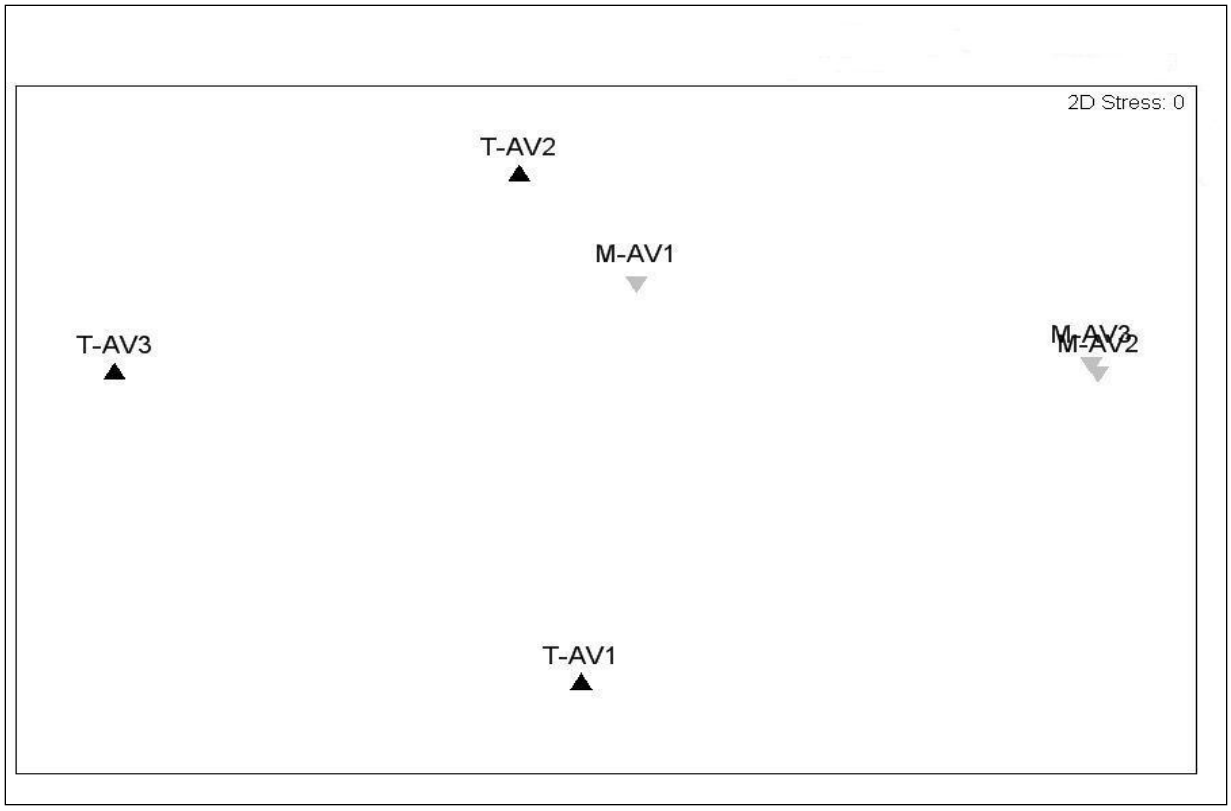

Figure 19-3. Multidimensional scaling analyses performed using genera composition for all six samples.
Tube worm habitat: T-AV1, T-AV2, T-AV3; mussel habitat: M-AV1, M-AV2, M-AV3.

19.4. Overall Trends

The epizooic metazoan meiobenthic communities associated with tube worm bushes and mussel beds at cold seeps in the GoM can be characterized as a community composed of seven higher taxa including Nematoda, Copepoda, Ostracoda, Halacarida, Tanaidacea, Kinorhyncha, and Isopoda occurring in remarkably low abundances, but relatively high diversity. As such, these seep communities are similar in abundance and higher taxa composition to epizooic meiobenthic vent communities associated with the bathymodiolin mussels or vestimentiferan tube worms, but exhibit much greater genera diversity similar to patterns found in deep-sea clays and oozes. However, these communities associated with biogenic habitats differ from the infaunal communities studied from sands of shallow-water seeps and clays of deep-water seeps, which show much higher abundances but lower diversity compared to the epizooic meiobenthos from our studied sites.

Tube worm aggregations and mussel beds are not only colonized by meiobenthos but also by a diverse and abundant macrobenthic community at the GoM cold seeps. In these same samples, mussel associated macrofauna were present in densities between 235.5 and 1196.3 ind. m^{-2} (0.2 and 1.2 ind. 10 cm^{-2}) and tube worm associated macrofauna were between 35.9 and 127.9 ind. m^{-2} (0.04 and 1.3 ind. 10 cm^{-2}). In other samples from the upper slope, macrobenthic abundances

calculated per sample area ranged from 209 to 9590 ind. m^2 (0.2 to 9 ind. 10 cm^{-2}) (Bergquist et al., 2003), and abundances standardized to the tube surface vary from 4–233 ind. m^{-2} on the upper slope (Cordes et al., 2005), and 134– 607 ind. m^{-2} on the lower slope (Cordes et al., 2007b). Abundances per mussel shell surface from the Florida Escarpment, a different site in Atwater Valley, and Alaminos Canyon were between 160 and 4,458 ind. m^{-2} (Cordes et al., 2007b). It appears that the macro- and megafauna are relatively well represented in such aggregations fueled by *in situ* primary production, while small meiobenthic animals are relatively scarce. Some shallow water studies indicate that the interaction between macrofauna and meiofauna are negative for the smaller size class, as adult large animals are potentially predators and/or dislocate meiofauna by movements. In addition, the juvenile macrofauna, temporarily in the meiofauna size class while growing up, can act as predators or competitors (Bell, 1980; Ólafsson, 2003). Also a recent study at seeps on the Norwegian margin revealed a negative correlation between meio- and macrofaunal abundance and predation pressure was speculated to be underlying cause for this pattern (VanGaever et al., 2009). However, whether the seep meiofauna community is regulated by such top-down or by bottom-up processes remains to be tested.

Overall, the abundances and higher taxonomic composition of meiobenthos associated with tube worm and mussel habitats from cold seeps in this study are quite similar to those at hydrothermal vents (Table 19-5). The epizooic communities of both environments are low in abundance (usually below 100 ind. 10 cm^{-2}) and are mostly dominated by nematodes. In addition, communities with equal nematode-to-copepod distribution (EPR, 9º50'N region, tube worm aggregations, Gollner et al, 2007), copepod-dominated communities (this study; Juan de Fuca Ridge, *ParAlvinella* aggregations, Tsurumi et al., 2003; EPR 11ºN region, mussel aggregation Zekely et al., 2006; EPR, 9º50'N region, tube worm aggregations, Gollner et al., 2007), or foraminiferan-dominated communities (EPR, 9º50'N region, tube worm aggregations Gollner et al., 2007) have also been found. Similar to varying higher taxa proportions in mussel aggregations at GC of this study, the tube worm aggregation at the EPR vent site Riftia Field also exhibited a high variability (Gollner et al., 2007), which points to a patchy distribution.

While the present study describes the epizooic meiobenthos from cold seeps, all other meiobenthic seep studies concern the infauna inhabiting seep sediments (Table 19-4). They range from very shallow sites down to 5,000 m depth, come from different geographic regions and a variety of seep types, mostly hydrocarbon gas or gas-oil seeps, but also gas-oil-asphalt seeps, gas hydrates or brine seeps. Most samples were taken from sites covered by bacterial mats or colonized by siboglinid tube worms, or were taken from underneath clam beds, but sometimes also from sites devoid of any microbial or megafaunal community. In addition to different approaches in extraction techniques and size classes included in the meiofauna fraction, there are also large variations in which part of the meiobenthic community was analyzed. Some include the entire permanent (metazoan and protist) and temporary meiobenthos, and some only parts. Overall, no trends in abundance according to depth, geographic regions, seep types, or habitat types are apparent. However, the available data set is currently rather limited.

Associated epizooic metazoan meiobenthos from seeps (1–81 ind. 10 cm^{-2}) and vents (1–976 ind. 10 cm^{-2}), as well as vent infauna from sediments (1–1,075 ind. 10 cm^{-2}), seem overall to be lower in abundance than infaunal meiobenthos from seeps (1–11,292 ind. 10 cm^{-2}) (Table 19-4). Low

abundances of seep infauna were only detected in anoxic sediments of the Black Sea and in some samples from a brine seep at East Flower Garden Banks and at the Norwegian Margin (Sergeeva and Gulin, 2007; Powell et al. 1983; VanGaever et al., 2009). All other infaunal abundances are at least above 100 ind. 10 cm^{-2} and most exceed 1,000 ind. 10 cm^{-2} (Table 19-4). The vast majority of epizooic and infaunal vent and seep meiobenthic samples are dominated by nematodes, usually followed by copepods. Other dominant taxa include gnathostomulids and plathelminths in highly sulfidic brine seep samples (Powell et al., 1983), and rotifers in gas hydrate samples (Sommer et al., 2007).

Although in several meiobenthic studies of seeps the nearby non-seep deep-sea samples were found to be lower in abundance than the seep sediment samples (Olu et al., 1997; Robinson et al., 2004; Soltwedel et al., 2005; VanGaever et al., 2006), this study did not confirm this trend. In general, the abundance of meiobenthos in the deep sea has been found to decrease with depth due to a decrease in POM flux in addition to sedimentary factors such as calcium carbonate content and sorting (see Soltwedel, 2000). Ranges between 100 and 1,000 ind. 10 cm^{-2} at shallower depths and between 10 and 100 ind. 10 cm^{-2} at deep sites are considered quite typical (see Giere, 2009). Based on a very large data set from the GoM deep-sea meiobenthos carried out between 200 and 3,000 m depth, a range between 600 to 9,500 ind. 10 cm^{-2} was found (Baguley et al., 2006). Calculated from the correlation between abundance and depth, approximately 2,500 ind. 10 cm^{-2} are expected in about 1,500 m depth (Baguley et al., 2006). This estimation is much higher than the actual abundances (870–1,523 ind. 10 cm^{-2}) in our comparable non-seep sediments at a similar depth of 1,450 m. The more puzzling result, however, of this study was the remarkably low abundances at the seep sites. The fact that meiobenthos associated with similar foundation species at vents is also low in abundance, points to a shared commonality between seeps and vents, and is in sharp contrast to the high abundance of associated seep and vent macrobenthos. Since *in situ* primary production obviously fuels the large-sized community, it seems unlikely that meiobenthos is bottom-up controlled. Rather the interactions with the macrobenthos, may it be high predation pressure and/or competition, are more likely underlying causes.

The meiobenthic epizooic diversity at seeps is much greater than the infaunal seep diversity. Looking at infaunal nematodes only, usually the most abundant meiobenthic taxon for which the data set is quite extensive, genera richness in reduced sediments, underneath bacterial mats, bivalves, and siboglinid tubewomrs ranges between 8 and 29 and $H'_{\log e}$ is between 0.03 and 2.39 (Vanreusel et al., 2010). In contrast, genera richess among mussel and tube worm aggregations ranges between 16 and 43 and $H'_{\log e}$ is between 1.94 and 3.30. Whether the overall higher diversity within foundation species is due to more benign environmental conditions compared to considerable stress due to hypoxic and sulfidic conditions within the sediment needs to be tested in future.

Table 19-5

List of Meiobenthic Infaunal and Epifaunal Studies from Vents and Seeps, Listed According to Type of Seep or Vent, Depth, Sampling Device, Extraction/Sieving Technique, Components of Meiobenthos Included in Study, Habitat, Abundance 10 cm^{-2}, and Reference

m metazoan permanent, p protist permanent, t temporary meiobenthos

location	type	depth (m)	sampling	extraction/sieving	fauna	habitat	abundance (1
seep infauna							
Kattegat, North Sea	gas	10 -12	corer	sieving 45 -500 µm	m + t	reduced sediments	650
East Flower Garden Gulf of Mexico	brine seep	72	grab	sieving >63 µm	m + t	bac mats	1 - 240
Isla Vista, Santa Barbara Channel	oil/gas	15	corer	decantation	m(+p?)+t	bac mats	1360
Isla Vista, Santa Barbara Channel	oil/gas	18	corer	decantation + sieving >63 µm	m+p+t	fine sand sediment	3550
	oil/asphalt	18	corer	decantation + sieving >63 µm	m+p+t	fines sand sediment	2661
	oil/gas	19	corer	decantation	m(+p?)+t	bac mats	2500
Hatsushima, Sagami Bay	gas	1100 - 1200	corer	sieving >63 µm	m+p+t	underneath calms	371 -414
Barbados prism	gas	5000	corer	no data	m(+p?)+t	sediment center	116
	gas	5000	corer	no data	m(+p?)+t	underneath clams	6541 - 8438
	gas	5000	corer	no data	m(+p?)+t	near clams	845 - 1893
Dnieper Canyon, Black Sea	gas	182 - 252	corer	sieving 64 µm - 1 mm	m+p+t	bac mats	2.39 - 52.50
Hydrate Ridge, off Oregon	gas hydrate	800	corer	centrifugation >32 µm	m+t	bac mats	623 - 965
	gas hydrate	800	corer	centrifugation >32 µm	m+t	underneath clams	1021 - 1566
Håkon Mosby, SW Barents Sea slope	gas	1280	corer	sieving 32 -500 µm	m+p+t	sediment center	4471
	gas	1280	corer	sieving 32 -500 µm	m+p+t	in Pogonophora	2878 - 3899
	gas	1280	corer	sieving 32 -500 µm	m+p+t	bac mats	3475
Håkon Mosby, SW Barents Sea slope	gas	1286 - 1288	corer	centrifugation >32 µm	m+t	sediment center	513.2 ± 38.4
	gas	1286 - 1288	corer	centrifugation >32 µm	m+t	in Pogonophora	1741.3 ± 577.
	gas	1286 - 1288	corer	centrifugation >32 µm	m+t	bac mats	11292.1 ± 225
Håkon Mosby, SW Barents Sea slope	gas	1250	corer	centrifugation >32 µm	m+t	grey mats	1198 ± 717
Nyegga Area, Mid – Norwegian Margin	gas	730	corer	centrifugation >32 µm	m+t	reduced sediments	333 ± 69
	gas	730	corer	centrifugation >32 µm	m+t	in Siboglinidae	7028 ± 1279
Storegga Slide, Mid – Norwegian Margin	gas	740	corer	centrifugation >32 µm	m+t	in Siboglinidae	41 ± 22
seep epifauna							
AC, AV, GC, Gulf of Mexico	gas	1400 - 2800	bushmaster	centrifugation 32 µm - 1 mm	m	ass. Vestimentifera	0.88 - 447
	gas	1400 - 2800	mussel pot	centrifugation 32 µm - 1 mm	m	ass. mussels	4.11 - 81.34
vent infauna							
Guaymas, East Pacific Rise	vent	2000	corer (?)	centrifugation >63 µm	m+t	bac mats	1 to 81
Bay of Plenty, New Zealand	vent	4 to 12	corer	sieving >50 µm	m+p	bac mats	1 to 241
Matupi Harbour, Papua New Guinea	vent	0 to 27	corer	sieving >500 µm	m+p	bac mats	2 to 131
Aegean Sea, Mediterranean Sea	vent	10	corer	elutriation >63 µm	m+p	bac mats	0 to 1075
Sulawesi, Indonesia	vent	3	corer	centrifugation >30 µm	m+t	sediments 10 cm off vent	49 ± 8
	vent	3	corer	centrifugation >30 µm	m+t	sediments 1 m off vent	652 ± 3
vent epifauna							
Juan de Fuca Ridge	vent	2300	grab	sieving >63 µm	m+p	ass. *Paralvinella*	14 - 87
Mid Atlantic Ridge	vent	3492	mussel pot	centrifugation >63 µm	m+p	mussel	36 - 46
N East Pacific Rise	vent	2480	mussel pot	centrifugation >63 µm	m+p	mussel	25 - 32
N and S East Pacific Rise	vent	2491 - 2690	mussel pot	centrifugation >62 µm	m+p	mussel	22 - 116
N East Pacific Rise	vent	2500	bushmaster	centrifugation >63 µm	m+p	ass. Vestimentifera	1 - 976

Interestingly, epizooic vent communities (Zekely et al. 2006, Gollner et al. 2007, Gollner et al., 2010) are also much lower in diversity than those at seeps. Both tube worm and mussel associated communities exhibited a total of 113 meiobenthic genera at seeps, identified from six samples only. In contrast, at tube worm and mussel aggregations of the EPR vents, a total of only 38 genera was found (Zekely et al. 2006, Gollner et al. 2007). Again, the differences in environmental conditions possibly creating stress in addition to much higher overall disturbances at vents compared to the seeps might explain these patterns.

As this was the first study of meiofauna directly associated with the foundation fauna of cold seeps, we expected to discover new species over the course of our analyses. However, the high diversity and number of undescribed animals in the collections was even greater than expected. Even though the final detailed taxonomic identification of all groups is not complete, we have already confirmed the presence of 107 new species including 24 undescribed species that do not fit into any described genera. This includes 18 new genera and 77 new species of copepod, 1 new genera and 17 new species of ostracod, 4 new species of tanaidacea and 3 new species of halacarids. And 5 new genera of nematodes (the total new nematode species count will be higher, but we have not finalized our species level separations of this very abundant and species-rich group).

20. HEART URCHIN COMMUNITIES

20.1. Introduction

A new hydrocarbon seep community type dominated by dense aggregations of heart urchins was discovered in 2006 in sediments with signs of active seepage, including brine and oil-stained sediment, and large bacterial mats. The urchins have been identified as *Sarsiaster griegii*, which have also been observed at seeps on Blake Ridge off the southeastern U.S. In some areas, aggregations of these urchins burrow across the sea floor, leaving trails that disturb the sediment. Three different sea urchin communities were studied, including two within lease block AT340, where urchins left visible trails of varying lengths and one within lease block AC818 that consisted of immobile urchins.

20.2. Methods

To better quantify the abundance of megafauna in the urchin communities and determine the rate of urchin movement in the mobile urchin aggregations, images for a photomosaic were collected from an undisturbed sea urchin community, repeated after 10 days and again after two additional days. These images were compiled into photomosaics and georeferenced into ArcMap (as described for the temporal change studies) to ease spatial analyses and species counts.

Tissue samples from six urchins from AC818 and five from AT340 were frozen at sea and then analyzed for stable carbon, nitrogen and sulfur isotope content as described in the tissue stable isotope section. The remainder of these urchins were preserved in 70% EtOH and sent to Dr. Dave Pawson (Smithsonian Institute) for taxonomic confirmation. We used a two-sample t-test to assess differences in isotope composition between sites, as the delta values met parametric assumptions (Anderson-Darling test, $p = 0.8$ for nitrogen, $p = 0.519$ for carbon and $p = 0.332$ for sulfur).

To investigate the meiofauna communities associated with the urchins and the possible impacts of the urchins on the meiofauna, sediment push cores from mobile urchin trails, in front of urchins, and underneath urchins were obtained at one of the AT340 communities, and also from underneath and beside still urchins at AC818. Urchins both bioturbate the surrounding sediment and potentially predate on meiofauna in their community, so to test if an effect of urchins on meiofauna is a result of bioturbation or predation, an artificial urchin was maneuvered through the sediment at a mobile urchin field at AT340. Sediment cores were obtained from within the urchin trail and in background sediments 9 days after the disturbance. Cores were sliced into the first two and the second three cm of sediment and mixed with $MgCl_2$ to narcotize the animals. The sediment samples were then fixed in 8% formalin. At Penn State, the animals were separated from the sediment through a density centrifugation technique using a silicapolymer (Fa. Levasil®) mixed with kaolin (McIntyre and Warwick, 1984; Veit-Koehler et al., 2008). Animals were then sorted into higher taxonomic categories of nematodes, copepods and "others," which include more rare taxa such as ostracods, tanaids and kinorynchs. Nematode samples were taken to the University of Vienna and further identified with the help of taxonomic experts there, while other fauna were sent to taxonomic experts for identification.

20.3. Results and Discussion

Besides the *Sarsiaster griegii* sea urchins, there were isolated bacterial mats, an isolated *Ampheraster alaminos* asteroid (1 per 60 m^2), and hermit crabs with anemones on their shells in the urchin field (1 per 10 m^2). There was an average of 2 urchins per square meter (m^2) within the urchin field, but this number ranged from between 0 and 8 urchins per square meter. These aggregations were found occasionally near typical cold-seep communities dominated by tube worms and mussels as well as in more isolated sediments.

From the changes in the urchin trails (Figure 20-1) we calculated that the average distance that an urchin travels per day is approximately 18 cm. The distances traveled ranged from between 2 to 60 cm per day, depending on the individual animals (Table 20-1). This is much faster than previously reported estimates of heart urchin movement, which are approximately 3 cm per day.

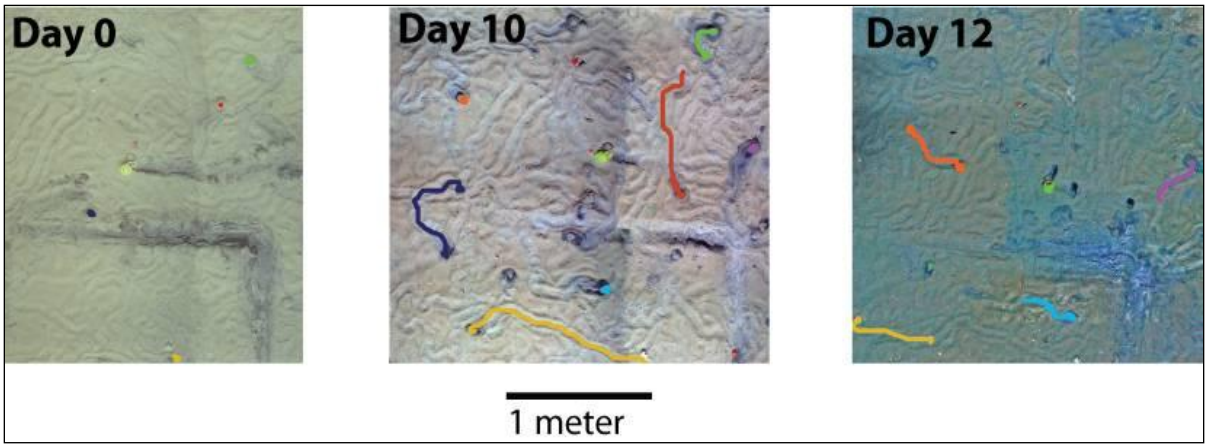

Figure 20-1. The site where the urchin experiment took place at AT340 was photomosaicked three times to determine urchin movement rate.
Shown is a small portion of the mosaics analyzed to determine the potential for tracking individual urchins. Urchins are indicated with colored points, and the trails are drawn with colored lines.

Table 20-1

Distances Urchins Traveled Based on Consecutive Photomosaics of the Same Region Determined by Tracing Urchin Trail Lengths Over Known Periods of Time

Distance 1 (D1) is the distance traveled over the first nine days; D2 is the distance traveled over the next two days

Urchin ID	D1 (cm)	Distance per hour (cm)	Distance per day (cm)	D2 (cm)	Distance per hour (cm)	Distance per day (cm)
1	41	0.19	4.45	70	0.05	1.32
2	138	0.62	14.99	125	0.19	4.44
3	177	0.80	19.22	40	0.24	5.70
4	202	0.91	21.94	76	0.27	6.50
5	122	0.55	13.25	74	0.16	3.93
7	157	0.71	17.05	81	0.21	5.05
8	138	0.62	14.99	8	0.19	4.44
9	186	0.84	20.20	34	0.25	5.98
12	191	0.86	20.74	105	0.26	6.15
13	244	1.10	26.50	77	0.33	7.85
14	120	0.54	13.03	123	0.16	3.86
16	132	0.60	14.33	47	0.18	4.25
17	204	0.92	22.15	36	0.27	6.56
18	94	0.43	10.21	99	0.13	3.02
19	114	0.52	12.38	41	0.15	3.67
20	128	0.58	13.90	53	0.17	4.12
21	132	0.60	14.33	66	0.18	4.25
22	41	0.19	4.45	87	0.05	1.32
23	104	0.47	11.29	49	0.14	3.35
24	89	0.40	9.67	17	0.12	2.86
25	100	0.45	10.86	69	0.13	3.22
26	374	1.69	40.62	89	0.50	12.03
28	297	1.34	32.25	205	0.40	9.56
29	266	1.20	28.89	18	0.36	8.56
Average	157.96	0.71	17.15	70.38	0.21	5.08
Range	41-374			17-205		

Carbon samples ranged from -40.972 to -32.868%, nitrogen samples ranged from 3.287 to 9.172%, and sulfur ranged from 10.03 to 16.41% (Table 20-20, Figure 20-2). There was no significant correlation between any delta values and the collection site (AT340 and AC818) ($p = 0.09$ for carbon, $p = 0.17$ for nitrogen and $p = 0.19$ for sulfur). However, the carbon isotope values indicate that urchins are obtaining their carbon from non-photosynthetic sources.

Nitrogen values suggest they are feeding near the base of the seep food chain. Sulfur isotope values are much lower than seawater sulfate, which also indicate reliance on local organic sulfur sources. The rather large range in all delta values among individuals suggests a range of diets for individuals and does not suggest a tight nutritional dependence on a particular symbiont. However, these urchins are clearly reliant on seep primary production for at least the bulk of their nutrition.

Table 20-2

Carbon, Nitrogen and Sulfur Stable Isotope Values (%) for the Eleven Urchins Collected

The first six are from Alaminos Canyon 818; the next five are from Atwater Valley 340.

	C^{13}	N^{15}	S^{34}
AC818-1	-39.72	5.67	13.55
AC818-2	-34.06	6.37	16.41
AC818-3	-37.37	3.29	10.03
AC818-4	-32.87	3.80	12.23
AC818-5	-34.20	4.68	13.46
AC818-6	-34.79	4.59	13.11
AT340-1	-37.65	9.18	11.81
AT340-2	-40.97	7.44	11.82
AT340-3	-37.10	5.37	11.05
AT340-4	-37.24	6.78	11.62
AT340-5	-36.70	3.41	12.59
Average	**-36.61**	**5.51**	**12.52**
STDEV	**2.35**	**1.74**	**1.59**
Max	**-32.87**	**9.18**	**16.41**
Min	**-40.97**	**3.29**	**10.03**

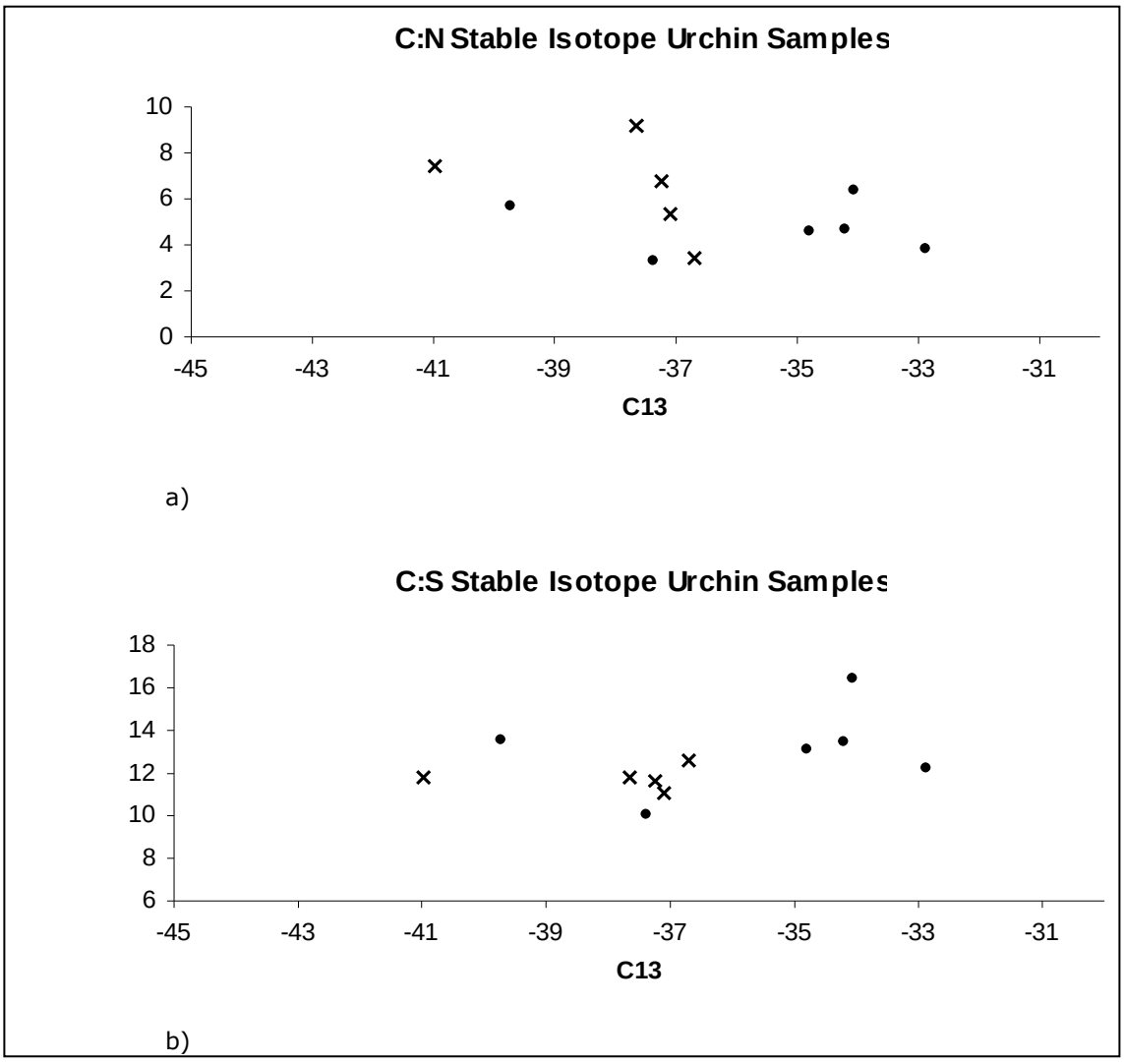

Figure 20-2. a) $\delta^{15}N$ vs δ13C for *Sarsiaster griegi* heart urchins; b) $\delta^{34}S$ vs δ13C for the same animals.
Circles represent animals from AC818, and Xs represent animals from AT340. Each point represents a different individual.

Permanent meiofauna infauna was dominated by nematodes (between 75 and 99% of individuals). Harpacticoid copepods formed the second largest group of higher-order taxa (between 0.5 to 20% of individuals). Occasional crustaceans such as ostracods, cumaceans, and tanaids were found in low abundance, and there were also occasional kinorynchs. Temporary meiofauna included occasional polychaetes and amphipods (Table 20-3).

Table 20-3

Higher Taxon Abundance Found in Sediment Cores

All abundances are standardized to 10 $cm^{3.}$

Site	Dive	Core	Core depth	Where	Urchin	Ostracod	Polychaete	Hydrozoan	Amphipod	Tanaidecea	Kinorynch	Oligochaete	Halacarid	Unknown	Nematode	Copepod
AT340	J2-269	Y2	0-2	B	2a	0.57	0.11	0.23	0.00	0.00	0.00	0.00	0.00	0.45	71.08	11.20
AT340	J2-269	Y2	2-5			0.17	0.00	0.52	0.00	0.00	0.00	0.00	0.00	0.61	208.31	2.60
AT340	J2-269	Y3	0-2	U	1a	0.34	0.00	0.34	0.00	0.00	0.00	0.00	0.00	0.34	456.10	3.06
AT340	J2-269	Y3	2-5			0.43	0.00	0.00	0.00	0.00	0.00	0.00	0.00	0.17	234.03	0.26
AT340	J2-269	Y5	0-2	B	1a	0.68	0.00	0.34	0.00	0.00	0.00	0.00	0.00	0.34	289.28	1.47
AT340	J2-269	Y5	2-5			0.00	0.00	1.04	0.00	0.00	0.00	0.00	0.00	1.21	27.11	0.26
AT340	J2-269	Y6	0-2	U	2a	0.00	0.00	0.00	0.00	0.00	0.00	0.00	0.00	0.00	3.96	0.00
AT340	J2-269	Y6	2-5			0.00	0.00	0.00	0.00	0.00	0.00	0.00	0.00	0.00	5.37	0.00
AT340	J2-269	Y7	0-2	T	2a	1.92	0.00	0.45	0.00	0.00	0.00	0.00	0.00	0.91	292.22	5.21
AT340	J2-269	Y7	2-5			0.09	0.00	0.17	0.00	0.00	0.00	0.00	0.00	0.17	377.12	1.21
AT340	J2-269	Y8	0-2	T	1a	0.45	0.11	0.68	0.00	0.00	0.00	0.00	0.00	1.24	416.72	2.38
AT340	J2-269	Y8	2-5			0.78	0.00	0.35	0.00	0.00	0.00	0.00	0.00	0.78	228.92	0.87
AT340	J2-270	G1	0-2	U	2b	0.45	0.23	0.34	0.00	0.00	0.00	0.00	0.00	0.34	236.99	15.73
AT340	J2-270	G1	2-5			0.09	0.09	0.09	0.00	0.09	0.00	0.00	0.00	0.17	86.79	1.47
AT340	J2-270	G3	0-2	B	1b	0.00	0.11	0.68	0.00	0.00	0.00	0.00	0.00	0.79	3.85	0.23
AT340	J2-270	G3	2-5			0.09	0.00	0.69	0.00	0.00	0.00	0.00	0.00	0.69	141.18	7.28
AT340	J2-270	G4	0-2	T	2b	0.68	0.00	0.79	0.00	0.00	0.00	0.00	0.00	1.24	137.85	5.77
AT340	J2-270	G4	2-5			0.00	0.00	0.52	0.00	0.00	0.00	0.00	0.00	0.61	145.86	1.56
AT340	J2-270	G6	0-2	B	2b	0.45	0.00	0.34	0.11	0.45	0.00	0.00	0.00	0.57	67.23	20.26
AT340	J2-270	G6	2-5			0.17	0.00	0.09	0.09	0.35	0.00	0.00	0.00	0.17	321.34	8.75
AT340	J2-270	G7	0-2	U	1b	0.34	0.11	0.00	0.00	0.00	0.00	0.00	0.00	0.00	338.17	9.28
AT340	J2-270	G7	2-5			0.00	0.00	0.00	0.00	0.00	0.00	0.00	0.00	0.00	333.47	2.69
AT340	J2-270	G8	0-2	T	1b	0.23	0.11	1.36	0.00	0.00	0.00	0.00	0.00	2.04	263.59	2.15
AT340	J2-270	G8	2-5			0.61	0.00	0.43	0.00	0.00	0.00	0.00	0.00	0.43	36.72	0.09
AT340	J2-276	R1	0-2	B	4	0.00	0.00	0.00	0.00	0.00	0.00	0.00	0.00	0.91	16.86	0.57
AT340	J2-276	R1	2-5			0.00	0.00	0.69	0.00	0.00	0.00	0.00	0.00	1.04	46.77	0.09
AT340	J2-276	R6	0-2	AT	4	0.11	0.11	0.34	0.00	0.11	0.11	0.23	0.00	0.45	177.01	3.28

Table 20-3

Higher Taxon Abundance Found in Sediment Cores (continued)

All abundances are standardized to 10 $cm^{3.}$

Site	Dive	Core	Core depth	Where	Urchin	Ostracod	Polychaete	Hydrozoan	Amphipod	Tanaidecea	Kinorynch	Oligochaete	Halacarid	Unknown	Nematode	Copepod
AT340	J2-276	R6	2-5			0.09	0.09	0.17	0.00	0.00	0.09	0.00	0.00	0.17	37.07	2.17
AT340	J2-276	R7	0-2	AT	4	0.11	0.11	0.11	0.00	0.11	0.23	0.57	0.00	0.45	213.68	2.49
AT340	J2-276	R7	2-5			0.09	0.00	0.00	0.00	0.09	0.09	0.00	0.00	0.09	56.99	0.35
AT340	J2-276	W1	0-2	B	2	0.23	0.79	0.34	0.00	0.23	0.11	0.00	0.00	0.34	318.48	12.56
AT340	J2-276	W1	2-5			0.09	0.00	0.09	0.00	0.00	0.00	0.00	0.00	0.26	82.46	2.60
AT340	J2-276	W2	0-2	AT	2	0.34	0.00	0.79	0.11	0.00	0.11	0.00	0.00	0.79	82.85	3.85
AT340	J2-276	W2	2-5			0.00	0.00	0.43	0.00	0.00	0.35	0.00	0.00	0.43	35.17	1.13
AT340	J2-276	W3	0-2	AT	2	1.47	1.24	3.96	0.00	0.00	0.91	0.00	0.00	3.96	149.39	18.90
AT340	J2-276	W3	2-5			0.00	0.17	0.17	0.00	0.00	0.00	0.00	0.00	0.17	138.93	1.39
AT340	J2-276	W4	0-2	AT	3	0.00	0.23	0.11	0.00	0.00	0.11	0.00	0.00	0.11	76.73	4.07
AT340	J2-276	W4	2-5			0.26	0.26	0.17	0.00	0.00	0.00	0.00	0.00	0.35	84.02	2.86
AT340	J2-276	W5	0-2	AT	3	0.23	0.68	0.79	0.00	0.23	0.23	0.00	0.00	1.24	65.87	3.62
AT340	J2-276	W5	2-5			0.09	0.09	0.26	0.00	0.09	0.09	0.00	0.00	0.26	71.02	1.65
AT340	J2-276	W6	0-2	B	3	0.34	0.68	0.34	0.11	0.34	0.57	0.11	0.00	0.57	184.48	11.88
AT340	J2-276	W6	2-5			0.00	0.00	0.17	0.00	0.09	0.00	0.00	0.00	0.17	89.21	1.99
AC818	J2-282	B2	0-2	B	1c	0.00	0.11	0.57	0.11	0.00	0.00	0.00	0.00	0.91	8.71	2.72
AC818	J2-282	B2	2-5			0.35	0.09	0.09	0.09	0.00	0.00	0.00	0.00	0.26	7.97	1.82
AC818	J2-282	B3	0-2	U	1c	0.00	0.00	0.23	0.00	0.11	0.00	0.00	0.00	0.45	18.45	2.83
AC818	J2-282	B3	2-5			0.43	0.00	0.00	0.00	0.00	0.00	0.00	0.00	0.00	9.18	3.46
AC818	J2-282	B4	0-2	B	2c	0.23	0.00	0.00	0.11	0.23	0.00	0.00	0.00	0.00	9.51	5.43
AC818	J2-282	B4	2-5			0.17	0.09	0.00	0.00	0.00	0.00	0.00	0.00	0.00	45.13	1.56
AC818	J2-282	B7	0-2	U	2c	0.00	0.00	0.00	0.11	0.00	0.00	0.00	0.00	0.00	19.35	0.91
AC818	J2-282	B7	2-5			0.00	0.00	0.00	0.00	0.00	0.00	0.00	0.00	0.00	10.05	0.35
AC818	J2-284	Y1	0-2	B	4d	1.36	0.68	0.11	0.00	0.57	0.00	0.00	0.00	0.45	94.84	11.66
AC818	J2-284	Y1	2-5			0.09	0.00	0.00	0.09	0.00	0.00	0.00	0.00	0.09	55.09	0.87
AC818	J2-284	Y2	0-2	U	1d	0.11	0.00	0.00	0.00	0.00	0.11	0.00	0.11	0.11	82.17	1.92
AC818	J2-284	Y2	2-5			0.00	0.09	0.09	0.00	0.00	0.00	0.00	0.00	0.26	13.86	1.82
AC818	J2-284	Y3	0-2	B	1d	1.13	0.11	0.00	0.00	0.11	0.45	0.00	0.11	0.34	59.19	30.11
AC818	J2-284	Y3	2-5			0.09	0.09	0.17	0.00	0.09	0.00	0.00	0.00	0.43	44.61	3.12

Nematode-to-copepod ratios ranged dramatically from 900 x higher abundance of nematodes to copepods to 3x higher abundance of nematodes to copepods (Table 20-4, Figure 20-3).

Table 20-4

Nematode and Copepod Average Abundance and Standard Error per 10 cm^3 of Sediment from Different Sites and Cores

	AT340					
	Nematodes		Copepods		Others	
	Average	Std. Error	Average	Std. Error	Average	Std. Error
Depth	*Background*		*Background*		*Background*	
0–2	107.9	62.4	8.3	4.7	1.6	0.1
2–5	174.5	61.6	4.7	2.0	1.5	0.3
	Trail		*Trail*		*Trail*	
0–2	277.6	57.2	3.9	0.9	3.1	0.3
2–5	197.2	71.7	0.9	0.3	1.2	0.3
	Under		*Under*		*Under*	
0–2	258.8	96.0	7.0	3.5	0.7	0.3
2–5	164.9	73.5	1.1	0.6	0.3	0.1

	AC818					
	Nematodes		Copepods		Others	
	Average	Std. Error	Average	Std. Error	Average	Std. Error
Depth	*Background*		*Background*		*Background*	
0–2	43.1	20.9	12.5	6.2	1.9	0.5
2–5	38.2	10.4	1.8	0.4	0.6	0.2
	Under		*Under*		*Under*	
0–2	40.0	21.1	1.9	0.6	0.5	0.2
2–5	11.0	1.4	1.9	0.9	0.3	0.1

	Experiment AT340					
	Nematodes		Copepods		Others	
	Average	Std. Error	Average	Std. Error	Average	Std. Error
Depth	*Background*		*Background*		*Background*	
0–2	183.3	87.3	8.3	3.9	2.0	0.6
2–5	72.9	13.2	1.6	0.8	0.9	0.4
	Artificial Trail		*Artificial Trail*		*Artificial Trail*	
0–2	127.6	25.0	6.0	2.6	3.5	1.7
2–5	70.5	15.7	1.6	0.4	0.8	0.1

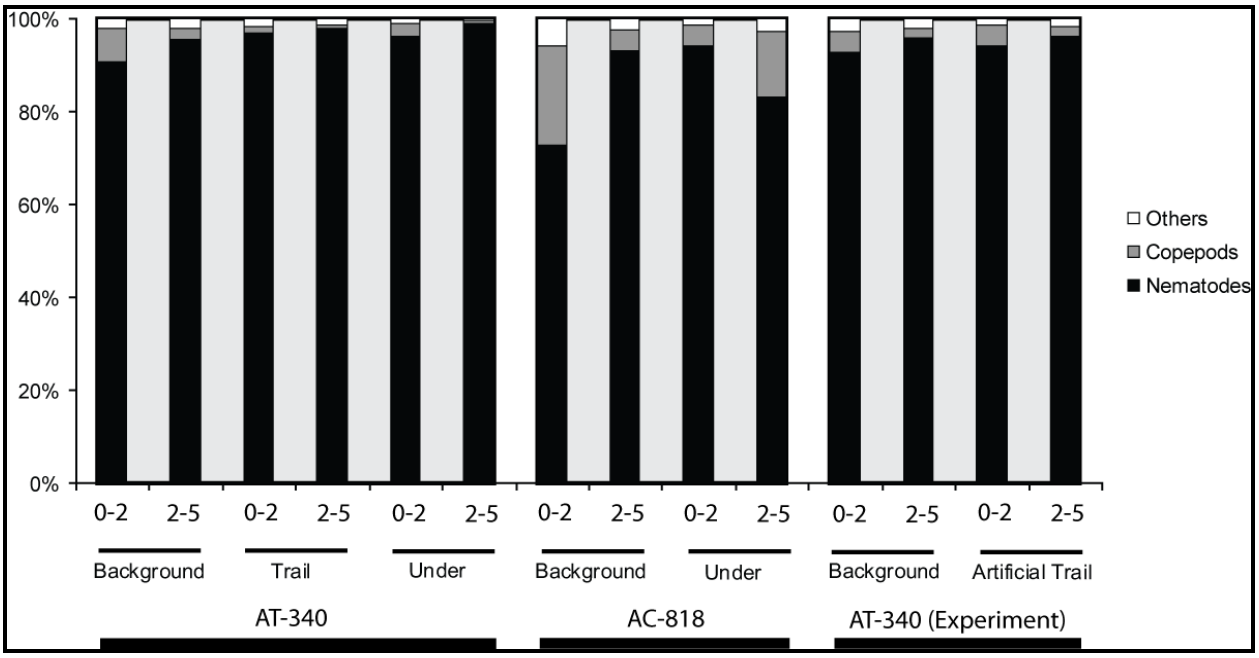

Figure 20-3. Percent abundance of nematodes, copepods, and aggregated other fauna.

A Kruskal-Wallis test found a trend towards higher abundance of nematodes underneath urchins than in background sediment at shallow sediment depths (0-2 cm) at AC818 ($p = 0.07$), and higher abundance in disturbed trails than in background sediments at AT340 at shallow depths ($p = 0.005$). At AT340, we also found higher copepod abundance underneath urchins than in background cores at deeper sediment depths (2–5 cm, $p = 0.05$) and also higher abundance in trails than in background cores at both depths ($p = 0.05$, $p = 0.02$). There was also a trend towards higher nematode abundance within real urchin trails than experimental urchin trails at the 0–2 cm sediment depths (Kruskal-Wallis test, $p = 0.07$).

Analyses to obtain diversity data at lower taxonomic levels are extremely time-consuming. However, preliminary results of nematode diversity have found 38 genera of nematodes at the urchin sites, including 28 at AT340 and 16 at AC818 (Table 20-5). Genera richness and the Shannon diversity index is highest in artificially disturbed sediments (28 taxa). Bioturbated sediments had a higher Shannon diversity index than background sediments, but both background and bioturbated sediments had higher nematode diversity and richness than the sediments underneath the urchins. There were also differences in dominant fauna among regions. At AT340, the dominant nematode genera is *Desmodora* sp., while at AC818, the dominant nematode genera is *Molgolaimus* sp..

Table 20-5

Nematode Genera, Listed per Site and Habitat

Dive J2-276 consists of experimentally disturbed sediment cores and background cores, while the others consist of urchin-disturbed habitats and background sediments.

Region	AT340																AC818							
Dive	J2-269						J2-270						J2-276				J2-282				J2-284			
Where	Background		Trail		Under		Background		Trail		Under		Background		Disturbed		Under		Background		Under		Background	
Depth	0-2	2-5	0-2	2-5	0-2	2-5	0-2	2-5	0-2	2-5	0-2	2-5	0-2	2-5	0-2	2-5	0-2	2-5	0-2	2-5	0-2	2-5	0-2	2-5
Acanthopharyx	0	0	0	0	0	0	0	0	0	0	0	0	0	0	0	0	0	0	0	0	0	0	1	0
Actinonema	0	0	0	0	0	0	0	0	0	0	0	0	0	0	1	0	0	0	0	0	0	0	0	0
Chromadora	1	0	0	0	0	0	0	0	1	0	0	0	0	0	2	0	0	0	0	0	0	0	0	0
Chromadorella	0	0	0	0	0	0	0	0	0	0	0	0	0	0	0	0	0	1	0	0	0	0	0	0
Daptonema	8	0	8	0	0	7	4	0	2	5	10	0	0	10	10	7	1	14	9	0	2	0	20	1
Desmodora	51	42	30	0	0	21	54	0	87	30	91	0	41	16	46	17	1	11	6		0	0	3	4
Desmolaimus	0	0	0	0	0	0	0	0	0	0	0	0	0	0	1	0	0	0	0	0	0	0	0	0
Dichromadora	0	0	0	0	0	0	0	0	0	0	0	0	0	2	1	0	0	0	0	0	0	0	0	0
Diplolaimella	0	0	0	0	0	0	0	0	0	0	0	0	0	0	0	1	0	0	0	0	0	0	0	0
Halamonhystera	0	0	0	0	0	0	0	0	0	0	0	0	0	0	0	1	0	0	0	0	0	0	0	0
Halaphanolaimus	0	0	0	0	0	0	0	0	0	0	0	0	0	0	2	0	0	0	0	0	0	0	0	0
Leptolaimus	2	1	1	0	0	0	0	0	0	0	0	0	15	1	4	5	0	0	0	0	0	0	4	0
Linhomeous	0	0	0	0	0	0	0	0	0	0	0	0	0	0	2	0	0	0	0	0	0	0	0	0
Linhystera	0	0	0	0	0	0	0	0	0	0	0	0	0	0	1	0	0	0	0	0	0	0	0	0
Metachromadora	0	0	0	0	0	1	0	0	0	0	0	0	0	0	0	0	0	0	0	0	0	0	0	0
Metacyatholaimus	0	0	0	0	0	0	0	0	0	1	0	0	0	21	13	37	0	1	0	0	0	0	0	0
Metalinhomeous	0	0	0	0	0	0	0	0	0	0	0	0	0	0	2	2	0	0	0	0	0	0	0	0
Microlaimus	0	0	0	0	0	0	0	0	0	0	0	0	0	2	4	6	0	0	0	0	0	0	0	0
Molgolaimus	4	1	0	0	0	0	0	0	1	0	1	0	1	3	5	1	76	54	59	0	37	0	5	30
Nannolaimoides	0	0	0	0	0	0	0	0	0	0	0	0	0	0	0	1	0	0	0	0	0	0	0	0
Neochromadora	0	0	0	0	0	0	0	0	0	0	0	0	0	0	1	0	0	0	0	0	0	0	0	0
Neotonchus	0	0	0	0	0	0	0	0	1	0	0	0	0	0	0	0	0	0	0	0	0	0	0	0
Parachanthonchus	0	0	0	0	0	0	0	0	0	0	0	0	0	0	1	0	0	0	0	0	0	0	0	0
Paralinhomeous	1	0	0	0	0	0	0	0	0	0	0	0	0	0	3	2	0	1	0	0	0	0	0	1
Paralongicyatholaimus	0	0	0	0	0	0	0	0	0	0	0	0	0	2	1	1	0	0	0	0	1	0	0	0

Table 20-5

Nematode Genera, Listed per Site and Habitat

Dive J2-276 consists of experimentally disturbed sediment cores and background cores, while the others consist of urchin-disturbed habitats and background sediments

Region	AT340																AC818							
Dive	J2-269						J2-270						J2-276				J2-282				J2-284			
Where	Background		Trail		Under		Background		Trail		Under		Background		Disturbed		Under		Background		Under		Background	
Depth	0-2	2-5	0-2	2-5	0-2	2-5	0-2	2-5	0-2	2-5	0-2	2-5	0-2	2-5	0-2	2-5	0-2	2-5	0-2	2-5	0-2	2-5	0-2	2-5
Paramonhystera	0	0	0	0	0	0	0	0	0	0	0	0	0	0	2	1	0	0	0	0	1	0	6	2
Polysigma	0	0	0	0	0	0	0	0	0	0	0	0	0	0	0	0	1	0	0	0	0	0	0	0
Prochromadora	0	0	0	0	0	0	0	0	0	0	0	0	0	0	1	0	0	0	0	0	0	0	0	0
Psammonema	0	0	0	0	0	0	0	0	0	0	0	0	0	0	29	3	0	0	0	0	0	0	0	0
Pseudochromadora	17	0	7	0	0	10	0	0	0	0	0	0	0	0	3	0	0	0	0	0	4	0	22	4
Pseudodesmodora	0	0	0	0	0	0	0	0	0	0	0	0	0	1	7	0	0	0	0	0	0	0	1	0
Retrotheristus	0	0	0	0	0	0	0	0	0	0	0	0	0	0	3	0	0	0	0	0	0	0	0	0
Sabatieria	5	3	0	0	0	6	0	0	4	27	0	0	0	11	4	5	0	4	0	0	1	0	3	0
Southerniella	0	0	0	0	0	0	0	0	0	0	0	0	0	0	4	1	0	0	0	0	0	0	0	0
Sphaerolaimus	2	1	1	0	0	1	0	0	0	2	0	0	1	1	3	1	0	2	1	0	0	0	0	2
Stylotheristus	0	0	0	0	0	0	0	0	0	0	0	0	0	0	0	1	0	0	0	0	0	0	0	0
Thalassomonhystera	0	0	0	0	0	0	0	0	0	0	0	0	0	0	2	0	0	0	0	0	0	0	0	0
Theristus	0	0	0	0	0	0	0	0	0	0	0	0	0	0	0	0	0	0	0	0	0	0	1	0

These results indicate that the urchins are altering their environment by disturbing the sediment to produce conditions that are amenable to higher meiofauna abundances. Urchins have been shown to have important effects on immediate surroundings through bioturbation because their movements mix sediment layers, oxygenating deeper sediment layers and perhaps providing habitat for organisms that would otherwise be unable to survive. At these sites, both bioturbated and artificially disturbed sediments have higher diversity than background sediments, but while bioturbated trails had higher abundance than artificially disturbed trails, the artificially disturbed trails had higher genera richness. Decreased richness underneath the urchins suggests that the urchins may either be consuming specific taxa, specific taxa are responding to the presence of a resource provided by the urchin, such as mucus or feces, or that these processes are occurring concurrently. The higher genera richness in the artificially disturbed trails than in the bioturbated trails suggest there is also a response to sediment disturbance, but the urchins also have an effect that is separate from a merely physical disturbance of the sediment.

21. CORAL COMMUNITIES

Although the emphasis of this program was on the chemosynthetic communities, investigation of other hardground communities on the lower slope was also part of the project mandate. The BOEM *Lophelia* I project focused on the coral communities of the upper slope, from approximately 350 to 600 m water depth. This study found a specialized fauna associated with the hardgrounds and corals on the upper slope with a lack of nutritional ties between the coral and seep communities. The hypothesis was that there would be similar groups of organisms occupying the hardgrounds of the lower slope, but that there may be some reliance on seep productivity due to the reductions in nutritional input from shallow waters. However, little information was available on the coral communities below approximately 600 m, beyond a series of species descriptions and biogeographic studies of the scleractinian and gorgonian fauna (Cairns et al. 1993), largely based on trawl specimens.

There were few large colonial cnidarians found at the majority of the sites examined. Isolated gorgonians (including bamboo corals) and antipatharians were, however, occasionally encountered. There were at least nine different species of gorgonians sampled at four different sites (Appendix 8). The most remarkable of the gorgonian observations was a colony of *Iridogorgia pourtalessi* (identified by Dr. Steve Cairns), which had previously only been known from a single, poorly preserved trawl specimen that served as the type for the species description. Beyond these isolated collections, the most significant hardground finding of this study was the high-density scleractinian community at a site in Green Canyon 852. This community became the focus of our investigations of the non-seep hardground communities of the lower slope for this project.

21.1. Green Canyon 852

Images for a photomosaic of a large boulder field with isolated colonies of scleractinians, anemones and octocorals (the Coral Garden site) were obtained in 2007 (Figure 21-1) after discovering the site in 2006.

Corals were observed on the tops of the boulders, presumably as a result of the availability of high currents, which carry food particles for the corals, and remove sediment. Coral species included the scleractinian reef-building corals *Madrepora oculata, Enallopsammia rostrata* and *Solenosmilia variabilis*, as well as several octocorals, including *Paramuricea* sp., *Acanthogorgia* sp., and the bamboo coral *Keratoisis sp.*, as well as several unidentified species. Isolated tube worms were present at the base of the boulders, but there were not large tube worm aggregations within the boulder field, and there were no large megafauna that appeared to be specifically associated with the presence of the worms. Demospongiae sponges were also observed on carbonate boulders, and were not associated with any large megafauna.

Chirostylid crabs were observed perched on the branches of gorgonians, but were not observed on the boulders or on the soft corals. Other crab species, including *Munidopsis* sp. and shrimp were abundant on dead corals and the surrounding carbonate boulders and rubble, which could indicate that these animals are less specialized than the chirostylids, and are attracted to the

habitat provided by the boulders and the high-current areas rather than the corals themselves. This was also found for the galatheoid crabs at the shallower *Lophelia pertusa* coral structures of the upper slope. Venus flytrap and large actinostolid anemones were usually found near hard corals and gorgonians, but were not associated with soft corals and only rarely observed on carbonate rock. Small *Caryophyllia* solitary corals were found near the reef-building corals on boulders, but did not appear to be associated with the presence of the coral itself, suggesting that these animals prefer similar habitats to the corals but are not dependent on the presence of corals. Ophiuroids were found associated with gorgonians, and were not observed on other types of corals or on boulders (Table 21-1), suggesting that there is a potential obligate relationship that merits further investigation.

Table 21-1

Fauna Observed within the GC852 Photomosaic

Colonial fauna or those that were partially obscured by boulders are described as "present," while all other fauna were enumerated.

Green Canyon 852 Coral Mosaic					
Annelida					
	Polychaeta				
				Lamellibrachia sp.	present
Arthropoa					
	Crustacea				
		Decapoda			
				Alvinocaris sp.	22
				Brachyura sp.	4
				Chyrostylidae sp.	27
				Munidopsis sp.	35
Chordata					
				Unidentified fish	2
Cnidaria					
	Anthozoa				
		Hexacorallia			
			Actinaria		
				Actinoschyphia sp.	7
				Actinostolidae sp.	43
			Scleractinia		
				Madrepora oculata	present
				Solenosmilia variabilis	present
				Caryophyllia sp.	15
		Octocorallia			
			Alcyonacea		
				Acanthogorgia sp.	12
				Keratoisis sp.	25
				Paramuricea sp.	11
				Octocorallia sp. 1	present
				Octocorallia sp. 2	present
			Pennatulacea		
				Iridogorgia pourtalesis	4
	Medusazoa				
		Hydrozoa			
			Hydroida		
				Hydroidea spp.	present
Echinodermata sp.					
				Ophiuroidea sp.	16
Porifera					
	Demospongiae				
				Demospongiae sp.	7

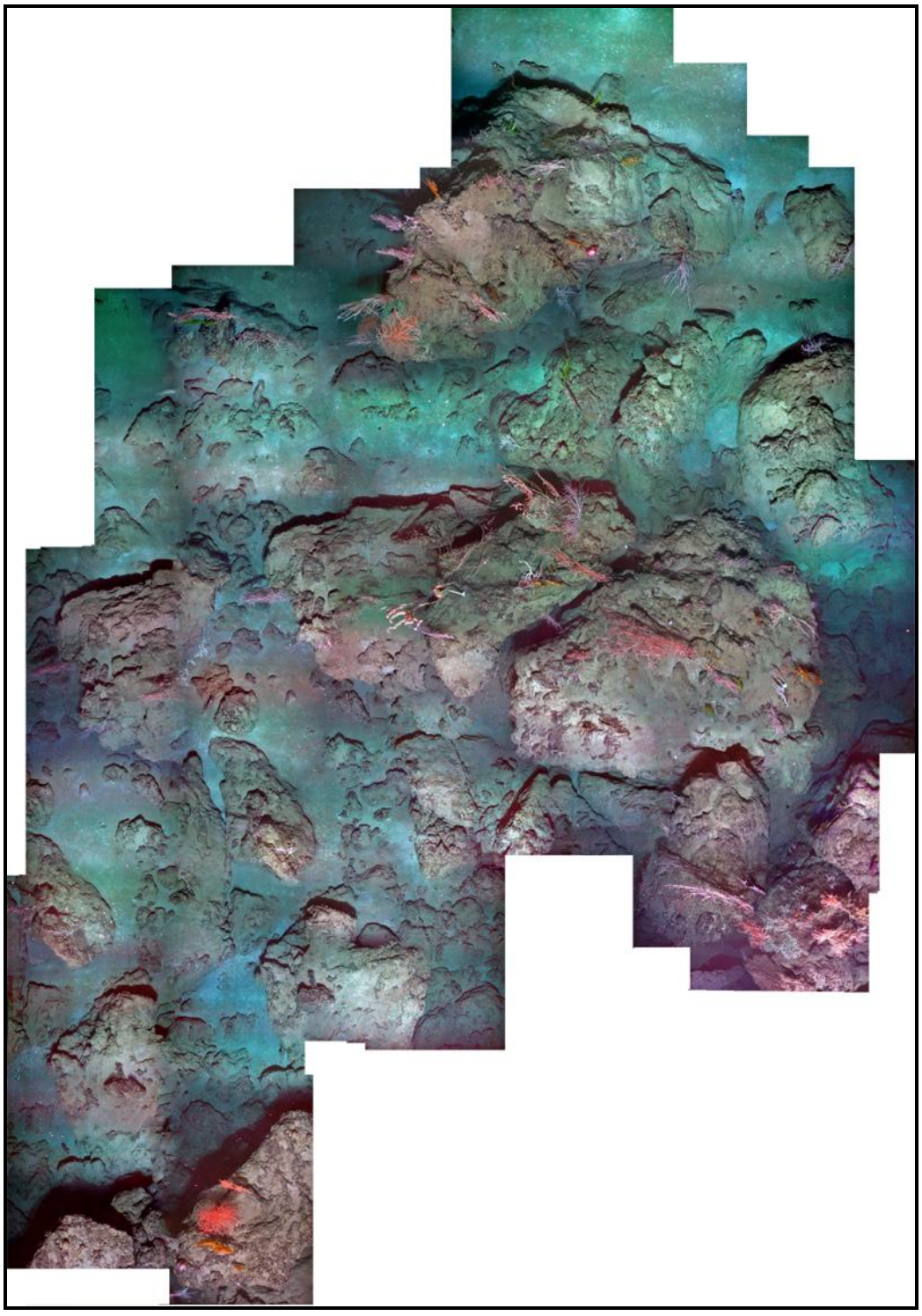

Figure 21-1. Photomosaic of the Coral Garden within GC852. This photomosaic comprises an area of 40 m^2.

22. SEEP CARBONATE

During the *Alvin* and *Jason II* cruises, a total of 99 samples of seep carbonate were collected. These samples were initially photographed in the laboratory, slabbed, and rephotographed resulting in a total of 712 photographs (Appendix 9a- Rock Sample Photos). Subsamples of the carbonate slabs were selected for thin sections (Figure 22-1). To determine the mineralogy of the samples, X-ray diffraction (XRD) analyses were conducted. Analyses for trace elements and rare earth elements were conducted as was AMS dating of samples. A critical geochemical analysis for characterization of seep carbonates is stable isotopes of carbon and oxygen. A summary of the analyses performed on these samples is shown in Table 22-1. The following address details of the analysis techniques.

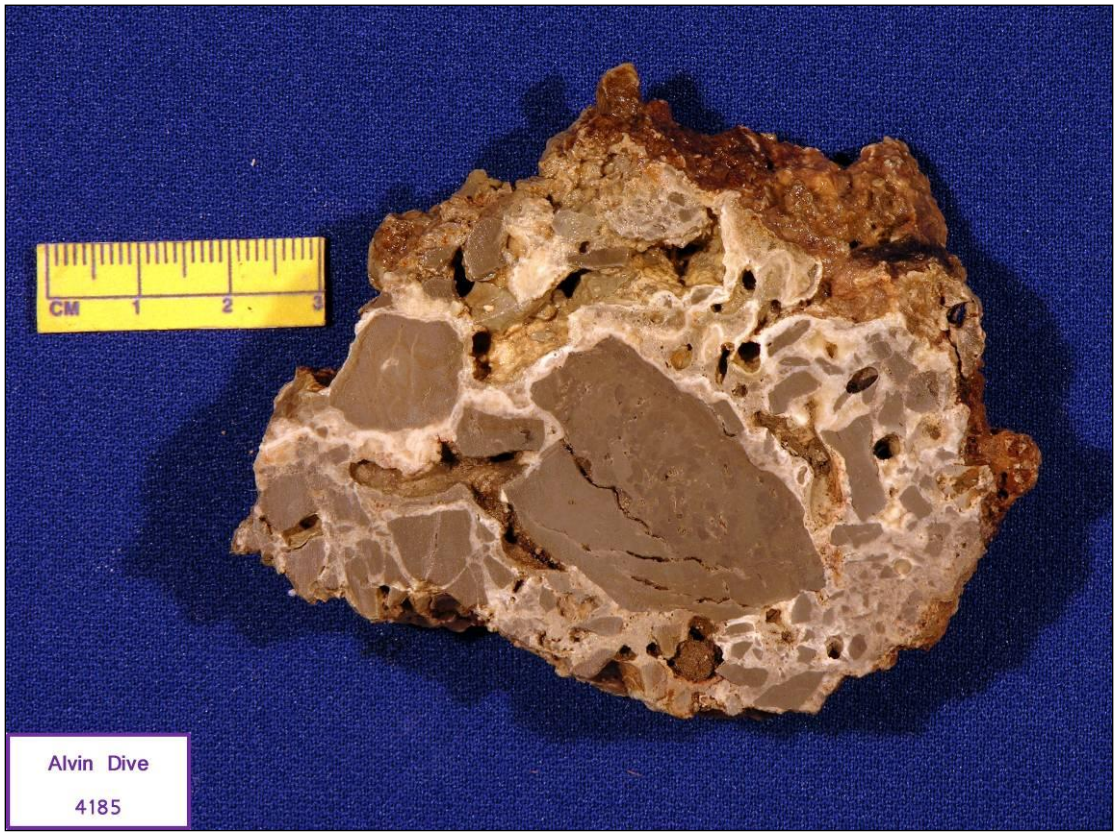

Figure 22-1. Example of slab sample from *Alvin* Dive 4185.

Petrographic observation of thin sections of the samples was made using a LEICA-DMRX optical microscope with Leica Qwin Program (Appendix 9b-Thin Sections). The microstructure of the seep carbonate on the fresh surfaces of fractured samples was examined with a scanning electron microscope (SEM). The samples were prepared by gold coating to a thickness of ~200 Angstroms for the SEM observations. Photographs were taken using a Sirion 200 FE-SEM equipped with EDAX GENESIS (Appendix 9c - SEM).

Table 22-1

Analyses Summary (853)

Location	Site	Rock sample	Thin section	SEM	XRD	ICP-MS	C-O Isotopes	^{14}C dating	U/Th dating
AT	AT340	21	6	8	21	21	145	5	2
GC	GC415	4		2	4	4	11	2	
	GC600	7	1	1	7	7	17	2	
	GC852	24	5	5	35	35	108	4	2
WR	WR269	1	1	1	1	1	5		
MC	MC 462	2			2	2	7	3	
	MC640	2			2	2	6		
	MC853	2			3	3	7		
KC	KC243	3			3	3	2		
AC	AC601	6	2	2	5	5	18	5	
	AC645	7	2	2	9	9	53	5	2
	AC 818	9	2	1	9	9	31	3	
GB	GB 647	7		1	8	8	20	2	
	GB697	3			3	3	9	2	
	GB829	1			1	1	5	3	
Total	**15**	**99**	**19**	**23**	**113**	**113**	**444**	**36**	**6**

For XRD, the samples were crushed into powder less than 200 mesh using an agate mortar and pestle. The XRD analyses (Appendix 9d) were performed using a Rigaku DXR 3000 computer-automated diffractometer utilizing Bragg-Brentano geometry. The X-ray source was a Cu anode operated at 40 kV and 40 mA using CuKα radiation equipped with a diffracted beam graphite monochromator. The orientated samples were scanned at an interval of 5−65° (2θ) with a step size of 0.02° and count time of five seconds per step. Divergence, scattering, and receiving slits were 0.5°, 0.5° and 0.15 mm, respectively. Relative abundance of the minerals was semi-quantified by Rietveld analysis of the diffractograms with the program SIROQUANT.

The powdered samples were processed with 100% phosphoric acid to release CO_2 for stable carbon and oxygen isotope analysis. Carbonate carbon and oxygen isotopic compositions in permil (‰) relative to the PDB standard were measured by using the GV Isoprime II stable isotopic mass spectrometry with deviations less than 0.01‰ (2σ) for both $\delta^{18}O$ and $\delta^{13}C$ values.

The seep carbonate powder (0.1−0.5 g) was treated with 50 ml of 5% HNO_3 in a centrifuge tube for two to three hours to separate the carbonate mineral phase and residue phase. Then, 2500 ng of Rhodium was added as an internal standard for calculating the element concentration of dissolved carbonate mineral phase. Five milliliters of this solution was further diluted 10 times to be used for the Rare Earth Element and trace elements analysis by using Finnigan MAT ELEMENT high-resolution Inductively Coupled Plasma Mass Spectrometer (ICP-MS). Precision of the Rare Earth Element and trace element analysis was checked by multiple analyses of international carbonate standard samples CAL-S. The average standard deviations are less than 10%, and average relative standard deviations are better than 5% (Appendix 9e I- 14C, C-OIsotpes, U Th Dating).

23. PHOTO SURVEYS

23.1. Introduction

Findings from the upper continental slope (depths < 1000 m) of the GoM demonstrated that chemosynthetic communities occupy discrete regions affected by persistent and protracted flux of hydrocarbons; the fauna occur in dense patches amid a surface geology heavily altered by biogeochemcial alteration of seep carbon (Roberts and Carney, 1997). In a region where possible community sites are very wide-spread (Frye, 2008), cost-effective methods for documenting the occurrences of chemosynthetic communities can address scientific questions (e.g., population connectivity) and can serve conservation interests where there is a potential for human impact. The geological traces of hydrocarbon seepage appear to persist much longer than the living components (Bergquist et al., 2003a; MacDonald and Peccini, 2009; MacDonald et al., 2003). Geological indicators include carbonate hard grounds, shell beds, and fluid flows caused by brine or mud discharge. Fauna tend to be prominent and to function as ecosystem engineers by altering the environment in ways that produce habitat for characteristic communities (Bergquist et al., 2003b; Cordes et al., 2007a): bush-like aggregations of siboglinid tube worms stand above the bottom with a relief of 1 m or more and can extend for tens of m; mussels beds (*Bathymodilous* sp.) often comprise thousands of individuals in contiguous assemblages covering 10s of square meters, and mats of bacteria (*Beggiatoa*) create large areas of distinctive patterning in the seafloor. These characters all offer highly visible targets that were often detected by visual surveys (MacDonald et al., 2007).

Photographic surveys have been used to detect and assess benthic communities in the deep sea for decades and have provided crucial insights regarding chemosynthetic animals and processes. For example, a photographic survey of enormous bivalves on the eastern Pacific Ocean spreading center (Lonsdale, 1977) was a direct line of evidence that led to discovery of the Rose Garden vent field and the eventual descriptions of chemosynthetic life (Corliss et al., 1979). Photographic surveys of sites provisionally targeted by geological or geochemical evidence in the GoM (Kennicutt et al., 1985) were subsequently confirmed by findings of siboglinid tube worms (Boland, 1986) and vesicomyid clams (Rosman et al., 1987). Combining remote sensing data with targeted photographic survey led to discovery and delineation of asphalt-based hydrocarbon seep communities in the southern GoM (Brüning et al., 2010; MacDonald et al., 2004c. Photographic surveys of seeps continue to inform mission planning for science and industry (Le Guilloux et al., 2009) and as a means for extending insights from time-intensive sample collection (Olu-Le Roy et al., 2004). A recurring challenge for photographic surveys is the sparse occurrence of chemosynthetic fauna in randomized samples of the benthos. Because chemosynthetic fauna tend to be sparse and patchily distributed, sampling design often resorts to pre-targeting of known communities (Brüning et al., 2010; Olu et al., 2009).

In this project, the targeted photographic sampling was completed with use of high-resolution mosaics (Lessard-Pilon et al., this volume) in which areas up to 10s of sq m are completely imaged for faunal census and possible detection of temporal change. A principal objective of image-based investigations in this project was to extend the efficacy for detecting and discriminating among different types of chemosynthetic communities using photographic survey techniques. Many of the sites were selected by interpretation of seismic data, in particular, patterns in the surface reflectance that are characteristic of hard grounds, gas hydrates, and

hydrocarbon seeps (Fisher et al., 2007). The photographic surveys provided a means to test whether chemosynthetic communities show a preference for relative levels of seismic reflectance. Secondary objectives were to document the visual characteristics of seep communities as an aid to species identification and as a benchmark for future studies.

In the preliminary phases of this project, reconnaissance surveys conducted with a surface ship using a passive drift camera system successfully verified the locations of suspected chemosynthetic communities identified from geophysical data, including the sites WR269, GC852, GC600, MC462, and AT340. These sites were subsequently occupied during sampling dives with submersibles. Also useful was the elimination or down-grading of sites where reconnaissance did not indicate presence of a lush community. The nested approach to site selection and sampling effort included evaluation of satellite remote sensing indicators as well as geophysical data. The design of photo-surveys will be discussed in this section.

23.2. Materials and Methods

23.2.1. Analytical Methods

23.2.1.1. Image Processing

Digital images were sorted by time to identify transect series, i.e., photographs taken along the randomized transects within each of the ten-transect site surveys. The images were oriented in landscape format, with the top of the image being the leading edge recorded as the ROV transited along the transect lines. Prior to review, each image was reviewed to determine the area sampled by the photograph. The scale of each image was normalized to the calculated size of the image pixels. When the laser dots were visible within the image, the dot-to-dot distance was measured in pixels; dimension of the pixels was then adjusted to the known distance between the parallel laser beams (28 cm). When the scale of the image was obtained, the total number of pixels in the image or within any sub-area within the image was the estimate for the area covered by the image or portion of image. If the lasers were not visible, the scale of the image was estimated from the target altitude that was specified for each transect. Although the interval between images was adjusted to avoid overlap between images, this did not always succeed. When overlap was detected, the bottom-, or trailing overlap was excluded from analysis to avoid double counting of subjects.

Subjects in the photos were identified and classified as either habitat or fauna. Table 23-1 gives a description of the habitats and fauna groups that were quantified for analysis. The taxonomic resolution was truncated at a high group level to avoid over-specifying identifications. For example, although several species of tube worms (Polychaeta: Siboglinidae) are known to occur at GoM seeps, identification from morphological characters is challenging and would not be supported by characters that could be consistently resolved in photographs, so all siboglinids were assigned to a single practical designation, i.e., “tube worms.” Similar designations were adopted for the seep mussels (Modiolinae: *Bathymodiolus*), which also includes several species that co-occur in mixed aggregations. Habitats were classified based on a series of descriptive characteristics, carefully compiled and frequently cross-checked for consistency among the sites and image series.

Habitats were quantified as the area covered by the feature in question, outlined in the digital images and scaled as described above. Fauna were counted when this was practical, such as when an individual or a group was visible in the image. However, for dense and complex aggregations of fauna, such as aggregations of tube worms, the number of individuals was estimated to the nearest factor of ten. The final data set produced by the image analyses comprised a list of 2791 images, grouped by site and transect. For each image, the location (navigated position within photographic survey) and coverage area (m^2) is known and the area or count of habitat and or fauna is appended. Depth was recorded for every image. However, the depth range within survey sites was much smaller than between sites.

The surface amplitude of seismic survey data, which was a crucial factor in selection of the sites during the early stages of the project (Fisher et al., 2007), was appended to each image as an environmental factor. These data were obtained from BOEM (W. Shedd, personal communication) as geo-rectified images generated from surveys conducted by separate survey operators, using instruments tuned for specific exploration objectives. As such, the minimum spatial resolution varied from approximately 10 m to over 50 m in pixel dimension; not all surveys presented square pixels. The amplitude range also varied markedly for the displays at different sites, from a minimum range of 8 levels to a maximum of over 5000 levels. To facilitate global comparisons, the amplitude data for all sites were categorized to an 8-level range. The locations of images were matched to the underlying surface amplitude map using co-located GIS layers and the resulting values were appended to the habitat and fauna results for each image.

23.2.1.2. Data Analysis

The data were treated by site-survey and subset by transect where appropriate. Two broad objectives were pursued for analysis: 1) description of the similarities and differences between sites and 2) hypothesis testing with regard to paired comparisons and power testing. For similarity descriptions, the data were examined with principal component analysis (PCA) and MDS using PRIMER-6 software (Clarke and Gorley, 2006). Prior to analysis, the fauna (count) data were square-root transformed and the habitat (area) data were normalized across their range. Paired samples were then contrasted in a diagonal resemblance matrix based on a Bray-Curtiss similarity measure (for fauna) or Euclidian distance (for habitats). Similarity measures were compared with “site""as a design factor using the PRIMER-6 ANOSIM procedure, which compares observed distributions with random groupings. The cluster routine was used to establish a hierarchy of sites or transects based on the Euclidean distance. These distance thresholds provide grouping contours for comparisons of site similarity based on fauna density and diversity. Principal component analysis was used to show how the habitat variables contribute to the similarity among sites.

For hypothesis testing regarding comparisons among sites, estimates for the area covered by a habitat of interest (*H*) or for the count of a particular fauna (*F*), estimates and standard errors were obtained for the transects *(T)* sampled in each survey area. Consider the total area (A_i) sampled by photographs in the ith transect. Let Y_i be the total area of the photographs covered by habitat *H* or the total count of fauna *F* observed in the photographs. The data for each site consists of $A_1, A_2, \ldots, A_T$ and $Y_1, Y_2, \ldots, Y_T$. Given that the photographs cover roughly equal areas

and are spaced at approximately distances along the transects, the assumption is that $Y_1, Y_2, \ldots, Y_T$ are independent with means $EY_t = \beta A_t$ and variances $Var\ (Y) = \sigma^2 A_t$. The goal in the surveyed area is to estimate the true proportion (β) of habitat H or the true mean density (count per unit area) of fauna F. Estimates of σ^2 are required for standard error. The usual generalized least square estimates of β and σ^2 are as follows:

$$\hat{\beta} = \frac{\sum_{i=1}^{T} Y_i}{\sum_{i=1}^{T} A_i} \text{ and } \hat{\sigma}^2 = \frac{1}{T-1} \sum_{i=1}^{T} \frac{(Y_i - \hat{\beta} A_i)^2}{A_i}$$

In situations where substantial proportions of Y_i are zero, the distribution is very different from a normal Gaussian. This was the case in the photo-surveys, so the estimate $\hat{\beta}$ will not be approximately normal. The variance of the estimate $\hat{\beta}$ is given as follows:

$$Var\left(\hat{\beta}\right) = \frac{\sigma^2}{\sum_{i=1}^{T} A_i}$$

The estimated standard error of $\hat{\beta}$ is obtained by substituting $\hat{\sigma}^2$ for σ^2 as follows:

$$standard\ error\left(\hat{\beta}\right) = \sqrt{\frac{\hat{\sigma}^2}{\sum_{i=1}^{T} A_i}}$$

These estimates become less valid where the transects are very close together (not usually the case) or where $Y_i = 0$ for most of the transects, as was the case in several of the photo-surveys. These estimates should be interpreted with due caution.

23.3. Results

Usable photographic surveys were obtained at nine locations at seven of the program study sites (Table 23-1). In all cases, the survey followed an array of ten, randomly placed transects at randomly selected altitudes inside designated regions of interest found in the sites (Figure 4-4). The proportion of photographed area was on the average about 4% of bottom area in the regions of interest. The smallest survey area was sampled at GB697 (19600 m^2), the largest at AT340 (AT340.3, 142500 m^2). In total, the photo transects covered about 3% of a total survey area of about 7000 hectare. Within this area, a large majority of the photographs at all sites were blanks i.e., contained no classifiable feature.

Despite the large proportion of blanks, descriptive differences among the sites were clear for area covered by habitat associated with hydrocarbon seepage presented as proportions of the surveyed area (Figure 23-1) and for relative densities of fauna, presented as counts per m^2 (Figure 23-2 and 23-3). "Habitat," as the term is used here, includes the abiotic bottom types characteristic of hydrocarbon seeps (MacDonald et al., 2003; Roberts and Carney, 1997a) and the habitat formed by dense or extensive aggregations of so-called ecosystem engineers, e.g., clusters of tube worms (Bergquist et al., 2003b). Carbonate rubble was the predominant habitat among most of the sites. This habitat included low pavement and broken or jointed sections as well as loose or scattered rocks. Carbonate boulders, which were common at four of the sites, designated free-standing edifices with exposed faces over 50 cm in height. Bacteria mat (*c.f. Beggiatoa*) were common at

four of the sites, but are elevated in overall abundance because of very extensive areas seen at a single site, GC852.2. Tube worm clusters represent the largest subset of living habitat at six of the survey sites. Tube worms clusters were associated with a variety of fauna groups including epifauna such small octocorals attached to the outside of the tubes. This group was too small and too numerous for accurate counts, so it was classified as present or absent. Mussel beds also represent an important living habitat at seeps. However, among the photo-surveys, mussel beds were relatively isolated features and comprised a small fraction of the total habitat area. Only one of the sites (AC601) featured a brine pool. Other distinctive habitats turned out to be relatively rare among the surveys. Fields (extensive, continuous regions) of small pogonophora, which were commonly observed during submersible operations, were relatively rare among the survey photographs. Brine channels were observed at six of the sites, but represented a very minor proportion of the survey area.

Groups supported by chemosynthetic symbiosis were observed at eight of the nine sites (none observed at MC462). Tube worms were the most abundant group overall and exceeded the abundance of methanotrophic mussels in all cases where both groups were seen. Groups primarily associated with tube worms and mussels (Bergquist et al., 2003b) included the carid shrimp (e.g., *Alvinocaris sp*.) and galatheid crabs (e.g., *Munidopsis sp*.) were also relatively abundant. The most abundant non-symbiotic group were echinoids, particularly heart urchins (e.g., *Sarsiaster griegi*), which were the second most abundant fauna after tube worms. Heart urchins were always associated with extensive bioturbation of surface sediments.

The second tier of abundance (Figure 23-4) included mobile heterotrophs, dominated by holothuroids, and sessile fauna, which were predominantly anemones (Actiniaria) and soft corals (Gorgonacea). The gorgonians were always attached to carbonate or similar hard substrata; no scleractinians were seen. The anemones were seen on visible hard substrata and also on open ground without a visible hard attachment surface.

Table 23-1

Design Table and Summary Results for Photo-survey Efforts during 2007

All images collected with down-looking camera along random transects (nominally 10) within sub-areas of study sites. Photo-survey sites are arranged by depth, habitat area and fauna counts by abundance. *Octocorallia were classified according to presence or absence

	SITE NAME									
Site Statistics	**MC462**	**GB697**	**GC852.1**	**GC852.2**	**WR269**	**AT340.3**	**AT340.2**	**AC645**	**AC601**	**ALL**
Mean Depth (m)	956	1005	1399	1408	1915	2180	2189	2208	2330	1732
Survey site size (m^2)	62500	19600	90000	30000	60000	142500	135000	62500	95200	697300
Total Images	176	216	178	286	235	432	375	512	381	2791
Total Image Area (m^2)	1219	1142	1319	2854	1548	3623	3309	3922	3523	22459
Habitat Area (m^2)										
Carbonate Rubble	0.0	7.0	17.2	61.5	0.0	384.8	304.8	214.5	13.8	1003.7
Bacteria Mat	0.0	1.5	0.0	204.9	0.0	3.3	26.0	0.0	97.9	333.6
Tube Worm Cluster	0.0	0.0	0.2	25.7	0.0	92.4	24.6	158.6	0.0	301.6
Carbonate Boulder	0.0	0.0	68.8	34.1	0.0	31.8	35.5	0.0	0.0	170.2
Brine Pool	0.0	0.0	0.0	0.0	0.0	0.0	0.0	0.0	88.7	88.7
Mussel Bed	0.0	0.0	0.0	1.7	0.0	1.0	16.5	14.0	1.3	34.5
Pogonophoran Field	0.0	0.0	0.0	0.0	0.0	0.0	0.6	20.7	1.9	23.2
Brine Channel	0.0	0.0	2.5	6.4	0.0	0.2	0.0	1.8	0.0	10.9
Fauna Counts										
Tube Worms	0	2	7	519	0	2826	1121	5046	0	9521
Caridea	2	0	65	17	10	363	13	791	30	1291
Echinoidea	0	2	0	0	0	800	58	4	338	1202
Mussels	0	0	2	44	0	108	300	447	51	952
Galatheid	0	0	74	31	17	316	87	180	1	706
Holothurian	2	1	0	0	4	28	26	18	60	139
Actiniaria	0	0	9	0	1	29	12	38	1	90
Octocorallia*	0	0	1	0	0	33	0	23	0	57
Gorgonacea	0	0	18	0	0	2	0	0	0	20
Fish	5	0	2	0	0	2	0	7	0	16
Asteroidea	0	3	0	0	2	0	8	0	1	14
Brachyura	0	6	0	1	0	0	0	2	0	9
Ophiuroidea	0	1	0	0	0	4	0	1	0	6
Alcyonacea	0	0	0	0	0	2	2	1	0	5

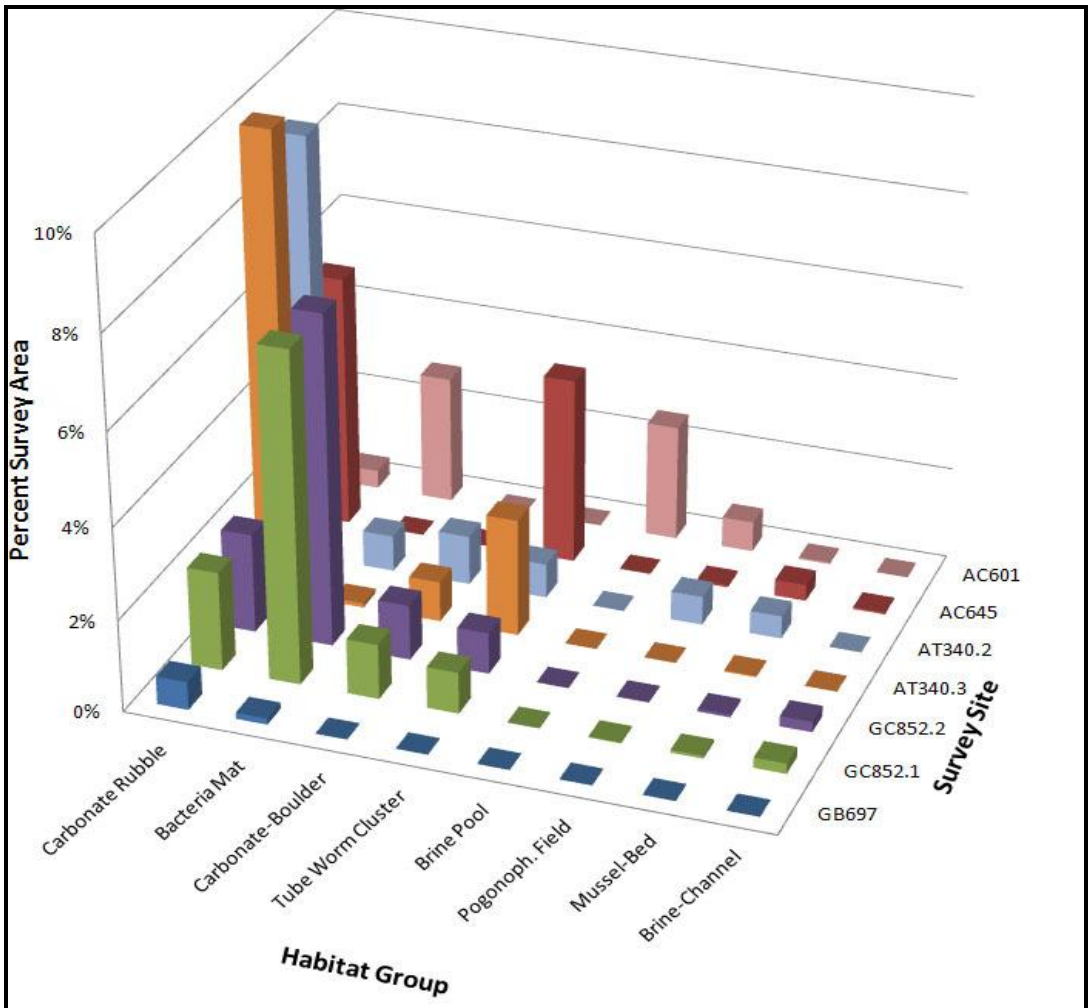

	Carbonate Rubble	Bacteria Mat	Carbonate-Boulder	Tube Worm Cluster	Brine Pool	Pogonoph. Field	Mussel-Bed	Brine-Channel
GB697	0.61%	0.13%	0.00%	0.00%	0.00%	0.00%	0.00%	0.00%
GC852.1	2.15%	7.18%	1.20%	0.90%	0.00%	0.02%	0.06%	0.22%
GC852.2	2.15%	7.18%	1.20%	0.90%	0.00%	0.02%	0.06%	0.22%
AT340.3	10.62%	0.09%	0.88%	2.55%	0.00%	0.00%	0.03%	0.01%
AT340.2	9.21%	0.78%	1.07%	0.74%	0.00%	0.63%	0.50%	0.00%
AC645	5.47%	0.00%	0.00%	4.05%	0.00%	0.05%	0.36%	0.05%
AC601	0.39%	2.78%	0.00%	0.00%	2.52%	0.66%	0.04%	0.00%

Figure 23-1. Proportional occurrences abundances of habitat associated with hydrocarbon seepage.
Sites are sorted by depth, fauna by abundance. No seep-related habitat was observed at two of the survey sites, MC462 and WR269, which are not plotted.

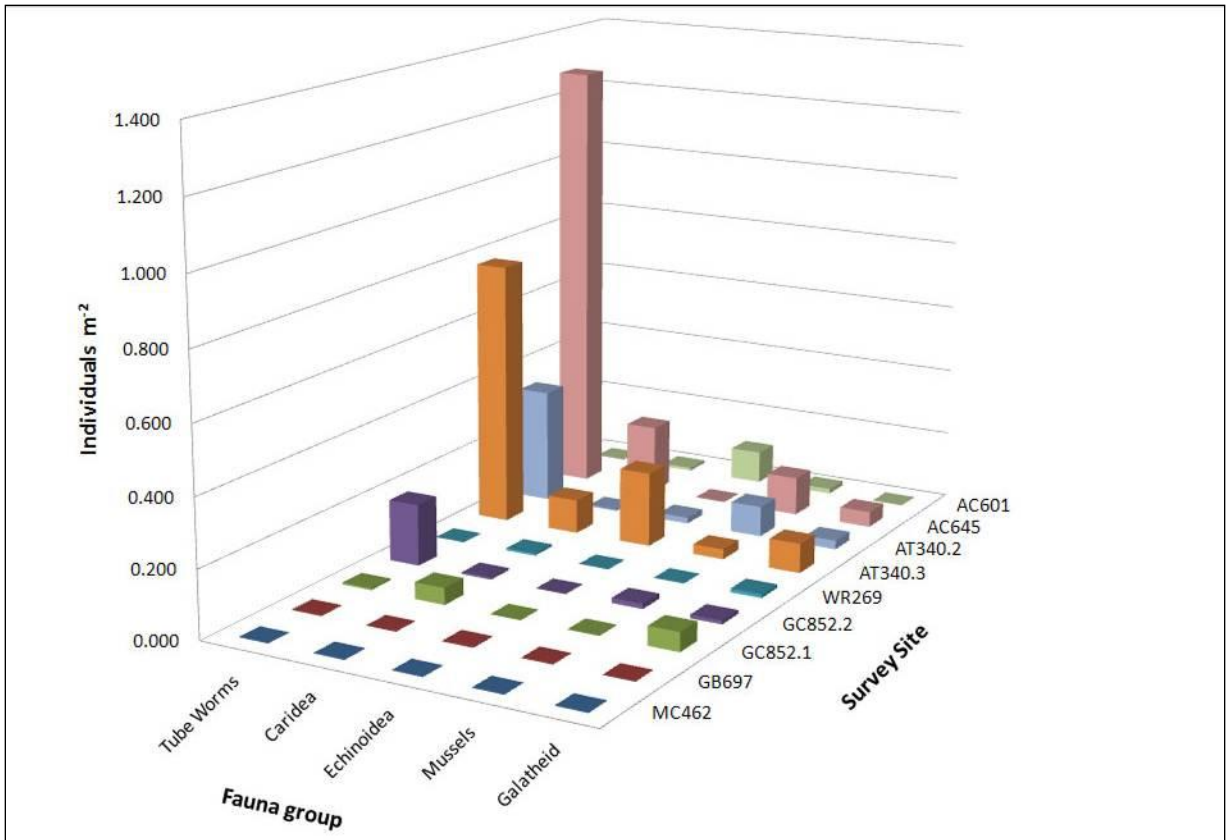

	Tube Worms	Caridea	Echinoidea	Mussels	Galatheid
MC462	0.000	0.002	0.000	0.000	0.000
GB697	0.002	0.000	0.002	0.000	0.000
GC852.1	0.005	0.049	0.000	0.002	0.056
GC852.2	0.182	0.006	0.000	0.015	0.011
WR269	0.000	0.006	0.000	0.000	0.011
AT340.3	0.780	0.100	0.221	0.030	0.087
AT340.2	0.339	0.004	0.018	0.091	0.026
AC645	1.287	0.202	0.001	0.114	0.046
AC601	0.000	0.009	0.096	0.014	0.000

Figure 23-2. Relative densities of chemosynthetic fauna and associated groups. Sites are sorted by depth, fauna by abundance.

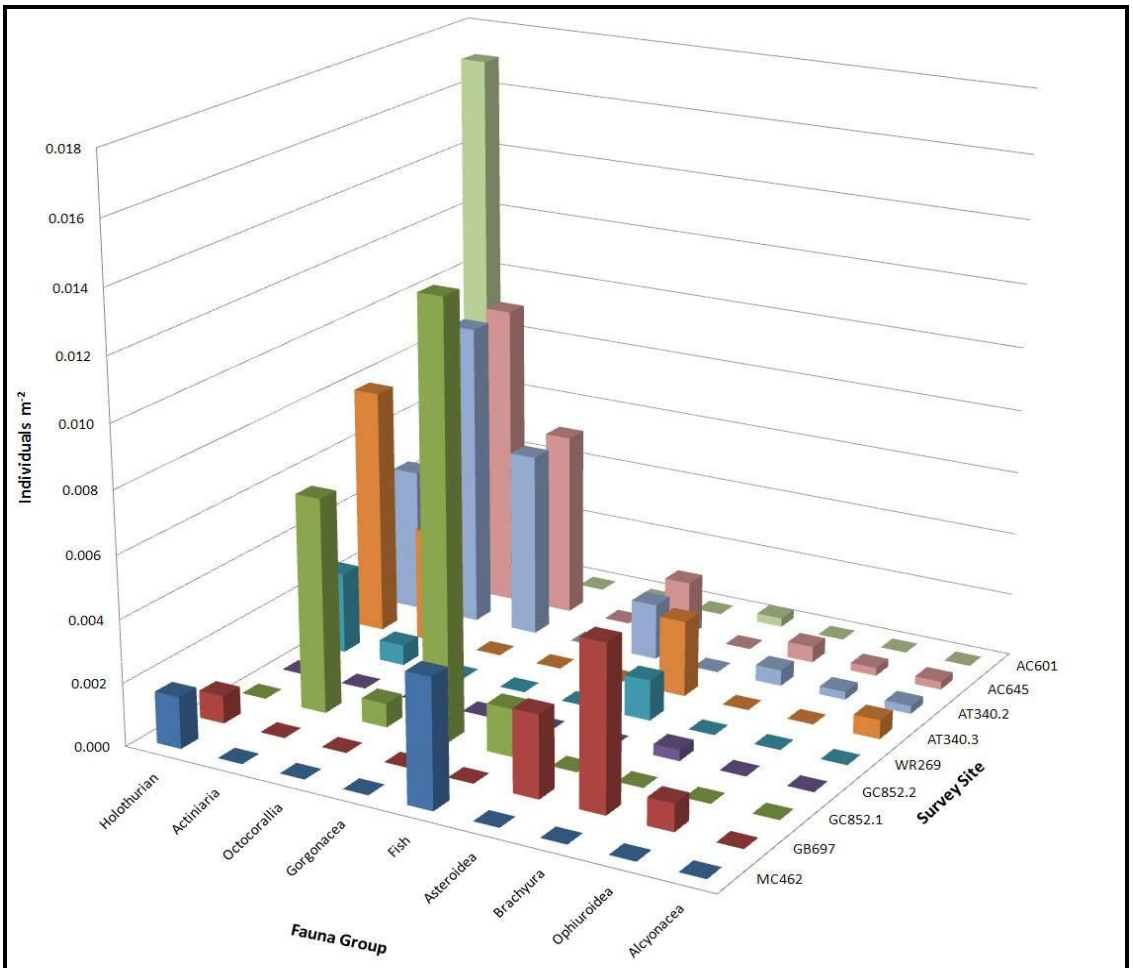

	Holothurian	Actiniaria	Octocorallia	Gorgonacea	Fish	Asteroidea	Brachyura	Ophiuroidea	Alcyonacea
MC462	0.002	0.000	0.000	0.000	0.004	0.000	0.000	0.000	0.000
GB697	0.001	0.000	0.000	0.000	0.000	0.003	0.005	0.001	0.000
GC852.1	0.000	0.007	0.001	0.014	0.002	0.000	0.000	0.000	0.000
GC852.2	0.000	0.000	0.000	0.000	0.000	0.000	0.000	0.000	0.000
WR269	0.003	0.001	0.000	0.000	0.000	0.001	0.000	0.000	0.000
AT340.3	0.008	0.004	0.000	0.000	0.000	0.002	0.000	0.000	0.001
AT340.2	0.005	0.010	0.006	0.000	0.002	0.000	0.001	0.000	0.000
AC645	0.005	0.010	0.006	0.000	0.002	0.000	0.001	0.000	0.000
AC601	0.017	0.000	0.000	0.000	0.000	0.000	0.000	0.000	0.000

Figure 23-3. Relative densities of non-chemosynthetic fauna, normalized. Sites are sorted by depth, fauna by overall abundance. Octocorallia abundance indicates presence among individual photographs.

A more detailed descriptive comparison of the survey sites was provided by output from the PRIMER-6 analytical routines (Figure 23-4). Overall, the large proportion of blank photographs tended to mask real differences among the sites, so the results show relatively low discrimination. PCA separates transects (at all sites) according to loadings of normalized habitat area, including the surface amplitude data (Figure 23-4A). The major axis of the plot shows a clear (and expected) distinction between transects exhibiting habitat associated with hydrocarbon seepage and those where no such evidence was observed.

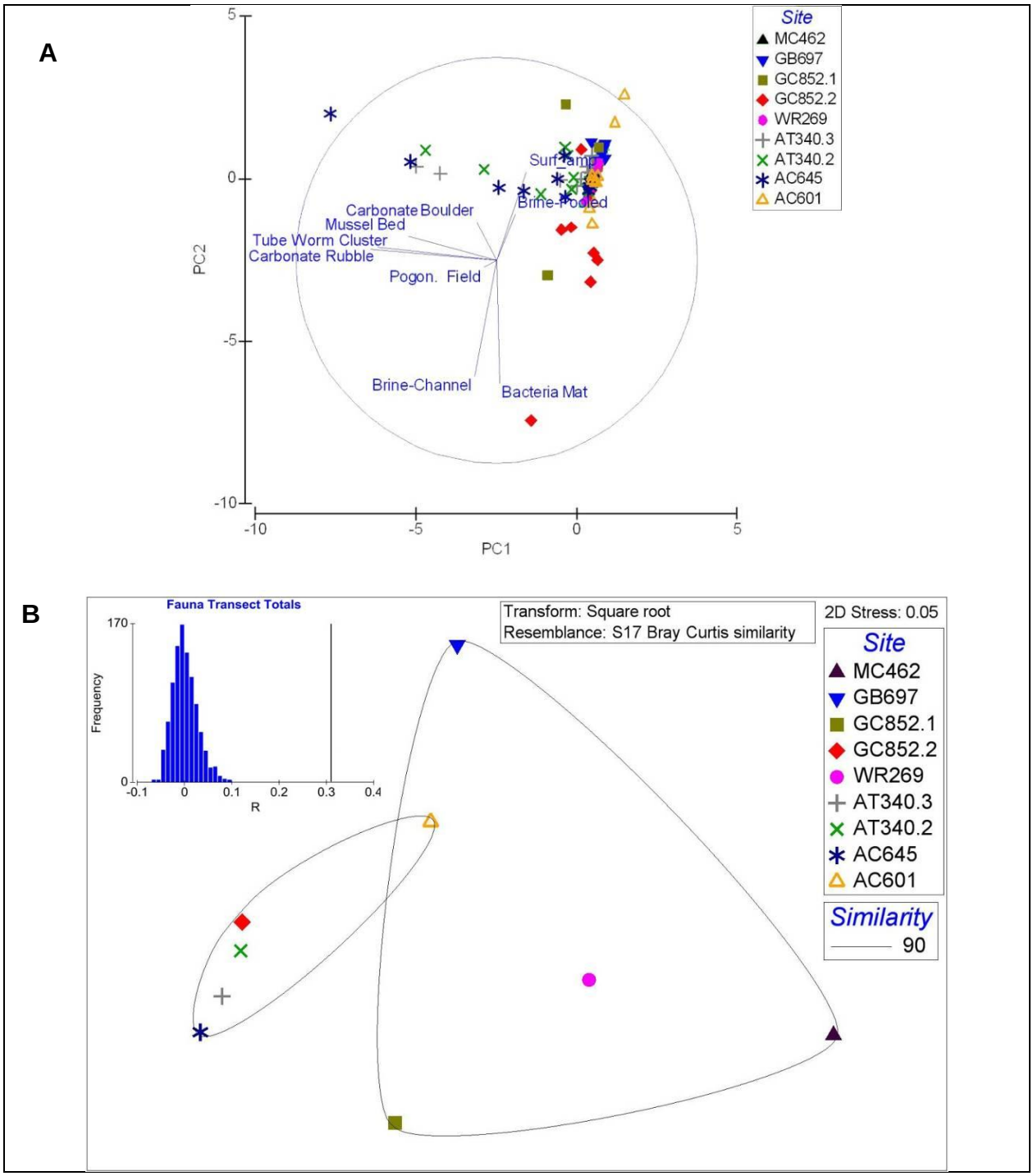

Figure 23-4. Non-parametric comparisons of photo-survey results.
A. Principal component classification of sites by habitat (normalized Euclidian distance). B. Multi-dimensional scaling classification of similarity (Bray-Curtis) according to abundance of fauna, by site. Inset shows ANOSIM test of transect similarities by site (histogram) compared with random groupings (vertical line).

The minor (vertical) axis of the plot shows separation predominated by difference between higher values of surface reflectance and the prevalence of bacterial mats and brine channels. In general, the habitat values indicate that transects can be classified into reasonable categories that could be consistent with different types of chemosynthetic communities. It should be noted that the inclusion of depth and longitude among the habitat characteristics contribute very minimal loading to the principal component loading. These variables were not explicitly included in the analysis. However, the sites are sorted by depth (least to greatest) in all the plots.

Comparison of the transects according to the relative abundance of fauna using a Bray-Curtis similarity measure examines whether the community composition differs to a degree distinguishable in a photographic survey. Compared to random groupings compiled by the PRIMER-6 ANOSIM routine, transects grouped by the factor "site" were strongly different from random (Figure 23-4B-inset). The PRIMER-6 BEST routine suggests that the highest correlation (Spearman's rank, $p = 0.905$) between groups of transects is obtained using five of the fauna: Tube Worm Clusters, Caridia, Echinoidea, Holothuroids, and Actiniaria.

The results for all site-wise similarities of all transects were plotted using axes chosen and scaled by the PRIMER-6 MDS routine (Figure 23-4B). This output gives two groups, one relatively tight and the other relatively dispersed. The clustering of sites according to their habitat characteristic can then be overlaid on the differences among the fauna at the sites to see whether habitat differences are consistent with fauna differences.

The contours of habitat groupings separate the tight and dispersed groupings of the sites according to fauna, so there is some support for the interpretation that differing habitat among the sites contributes to communities that are statistically distinct. Two caveats should be applied, however. First, there is an automatic correlation between the abundance of tube worms and the prevalence of the tube worm cluster habitat type. Second, the relative differences between transects remain low. The habitats only separate into clusters at the 90th percentile. This means that the PRIMER-6 results discriminate among transects that only differ in about 10% of their overall variation.

Although the non-parametric comparisons should be interpreted with caution, the approach for further analysis is to examine the survey results using other means and consider whether the results are consistent with the insights suggested by the PCA and MDS. Figures 23-5 and 23-6 show, respectively, the estimates of habitat area and faunal abundances (normalized to unit area) obtained from the photographic results pooled by transect. These plots allow comparison among sites according to individual variables. Differences greater that plus or minus one standard error provide a significance level approximately $p=0.95$. As before, sites are sorted by water depth.

Carbonate rubble was found seven of the surveys. Three of the surveyed areas (AT340.2, AT340.3m, and AC645) were strongly distinguished by this habitat variable. Tube worm clusters also occurred at most of the survey sites, but with more variable prevalence. Two of the sites with prevalent carbonate rubble were different when compared according to tube worm habitat (AT340.2 versus AT340.3). Two habitats were less common overall, but important at certain sites. Bacteria mat was common at GC852.2 and AC601, but not elsewhere; these sites were significantly different from the others and from each other with respect to this variable.

Carbonate boulders likewise distinguish GC852.1, but the variance was too high to estimate whether these are significant differences. Mussel beds were everywhere too sparse in occurrence to provide a means for comparing sites. For all habitat area combined, results show six of the sites strongly influenced by seep habitat, which is a grouping similar to MDS results.

Comparing the sites according to the abundance of fauna groups picks out individual sites in ways that sometime contrast with the seep-habitat result. Holothurians, for example, were relatively abundant at two of the sites (MC482 and WR269) where seep habitat was lacking. Overall there is weak trend of increasing abundance with depth for this group. The Echinoidea were abundant at only two of the sites (AT340.3 and AC645), but the very high variances created by dense clustering of these species obscure possible differences between these sites. Actiniaria closely track the prevalence of hard substrate, i.e. carbonate rubble or boulders. Groups associated with tube worms seem to track their relative abundance well for the caridians, but less well for galatheids. Interestingly, the octocorals, which were mainly the epifaunal colonies on tube worm tubes, were abundant at the two deeper tube worm sites (AT340.3 and AC645), but largely absent among the abundant tube worms at the shallower GC852.2 site. Differences at the species level are not resolved by these data, but broad area comparisons can suggest differences that could be checked in the detailed photographic mosaics or sample collections.

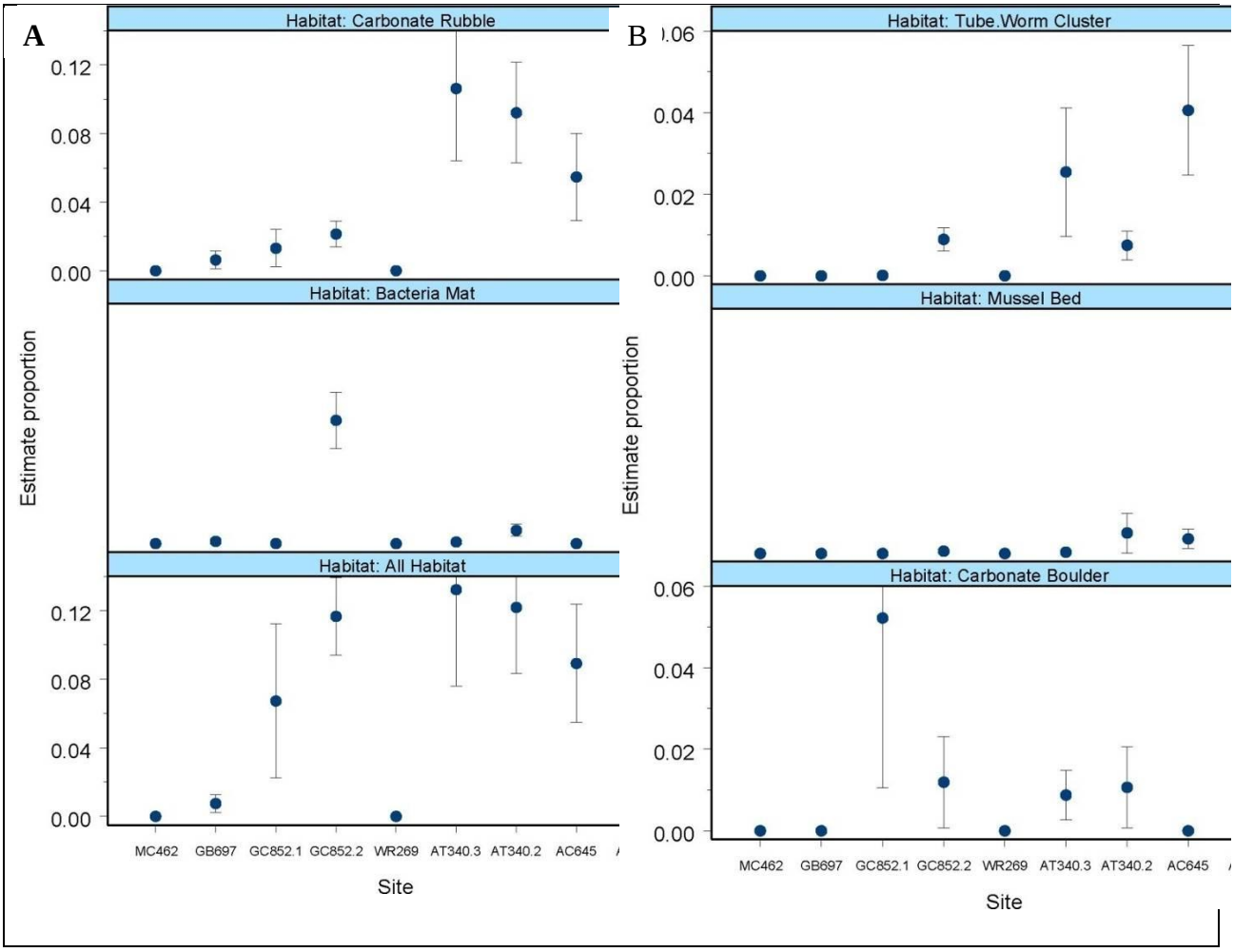

Figure 23-5. Comparison of habitat area estimates (solid circles) from transects at the nine survey sites expressed as proportion of survey area. A. Two most abundant habitats and all habitat areas combined for each site. B. Habitats created by chemosynthetic fauna and large boulders.
Error bars shown with the range of plus or minus one standard error.

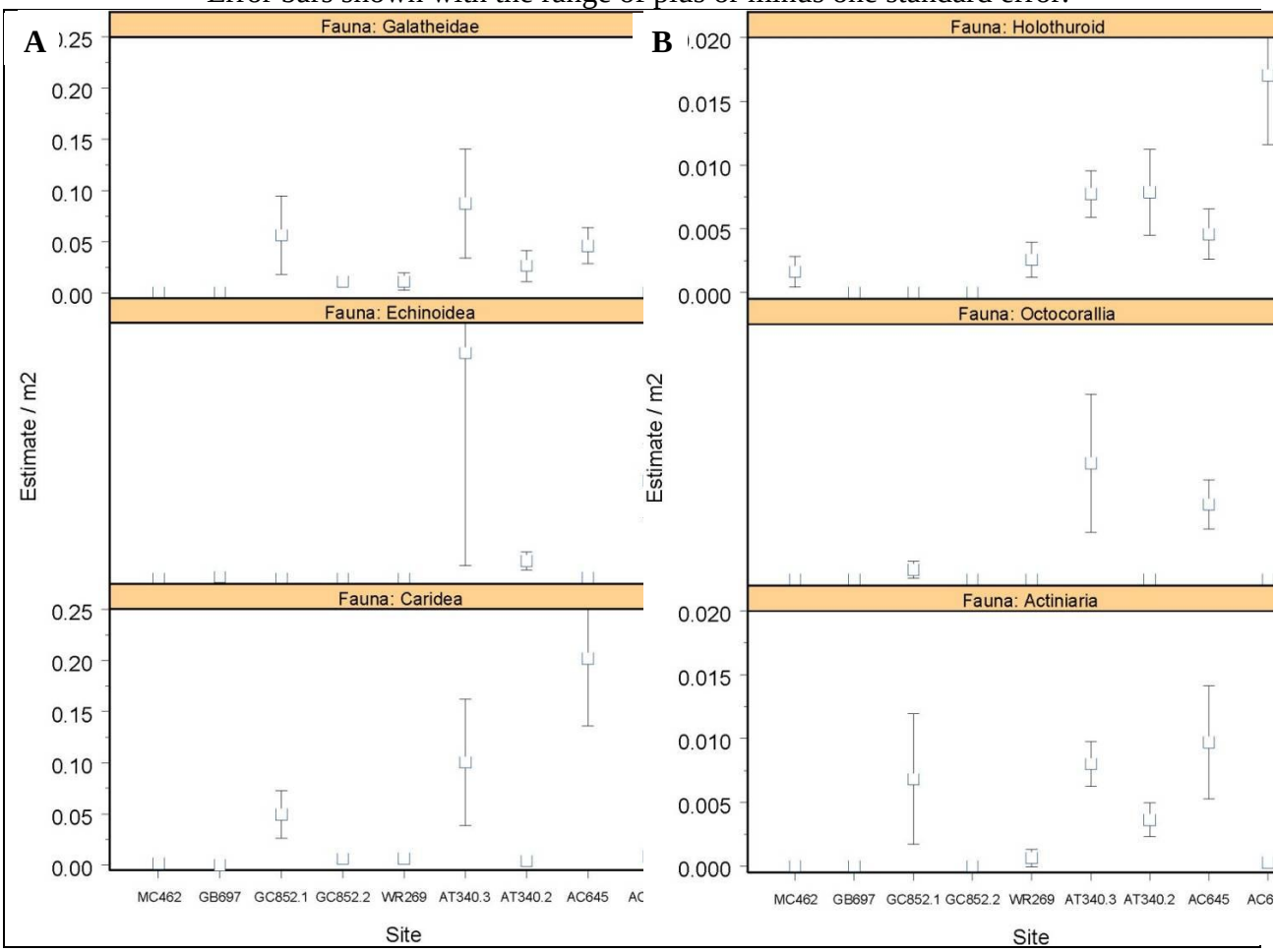

Figure 23-6. Comparison of fauna abundance estimates (hollow squares) from transects at the nine survey sites, expressed as number of individuals per m^2. A. Three most abundant faunal groups for all sites combined. B. Three less abundant faunal groups.
Error bars shown with the range of plus or minus one standard error.

23.4. Discussion and Conclusions

The results of the Recon Cruise show that photographic surveys provide a cost-effective complement to detailed sampling with submersibles. The documentary photographic material that are offered in digital appendices provide a means for comparing future results with the community structure observed in the 2006–2007 timeframe. This section has been concerned chiefly with examining the inferences that can be made based on carefully randomized surveys of sub-areas within sites where chemosynthetic communities are known or suspected to occur. Generally the results show that a modest sampling effort, i.e. two to four hours of bottom time, can yield useful results despite relatively low taxonomic resolution. Differences among sites are consistent with the general observations of the submersible work during the larger project (Fisher et al. 2007) and with previous work in shallower GoM seeps. Some cautions apply, however. At the WR269 site, the random transect array missed several mussels beds, including a bed of over 100 m^2. Although other chemosynthetic indicators were observed, in general, the site was probably under-classified or miss-classified as a result of the photo-survey. The results also provide a means for testing the predictive power of potential environmental factors such as surface reflectance.

The result at WR269 can be used to understand the hypothesis testing that could be conducted with photographic surveys. If we test the null hypothesis that the occurrence of fauna or habitat within a new survey is equal to some target or example level:

$$H_0: \beta = \beta_0 \text{ versus } H_1: \beta < \beta_0$$

versus the alternative that the fauna or habitat area occurs below some threshold abundance, there are two types of error that can be made. One might fail to reject H_0 when it is false, i.e., conclude that chemosynthetic fauna are present when they are not. Or, one might reject H_0 when it is true, i.e., conclude that there are no chemosynthetic fauna present at a site when in fact they exist. Of these two errors, the former seems more likely, given the results described from this work. The existing surveys can be provisionally used to prospectively evaluate the power of future photographic surveys to detect chemosynthetic indicators that occur in the same abundance as those seen at the study sites, e.g., AT340.2, AT340.3, AC645, etc.

A prospective survey would deploy n transects with total photographed areas A_1, $A_2, \ldots A_n$. The computations require the cumulative distribution function for the non-central t-distribution which will be written as $F_m(x; \xi)$, where x is the argument, m is the number of degrees of freedom, and ξ is the non-centrality parameter, which is available in most statistical packages (e.g., R, S-plus). Setting $\xi=0$ gives the usual t-distribution. Critical values for t-tests are obtained using the inverse function: $F_m^{-1}(\alpha; 0)$. A typical value for α would be 0.95. The non-centrality parameter is the number of standard errors difference between β and β_0, given by:

$$\delta = \frac{\beta - \beta_0}{\sqrt{\frac{\sigma^2}{\sum_{i=1}^{n} A_i}}} \qquad t^* = F_{n-1}^{-1}(\alpha; 0)$$

Power is computed by specifying the parameters for the statistical function

$$Power = F^{-1}_{n-1}(t^*; \delta)$$

The results can be shown for different multiples (k) of standard error for the separation between the abundance of an indicator, e.g., tube worm clusters, in the new survey versus the example site. Figure 23-7 shows likelihood of rejecting the null hypothesis, that is deciding that there are no chemosynthetic fauna at the site for multiples of k of 0.5 to 3.0. By comparing these curves with the estimates and errors in the surveys done for this project (Figure 23-5), it appears that with a photographic sampling effort equivalent to between 10 and 15 transects, one would have a reasonable chance of detecting that a newly surveyed community had two standard errors less carbonate rubble or tube worm clusters, for example, than one of the example sites. If the new site had none of the indicator, a survey with this level of effort would be very likely to reject the null hypothesis and conclude that the site was not a chemosynthetic community.

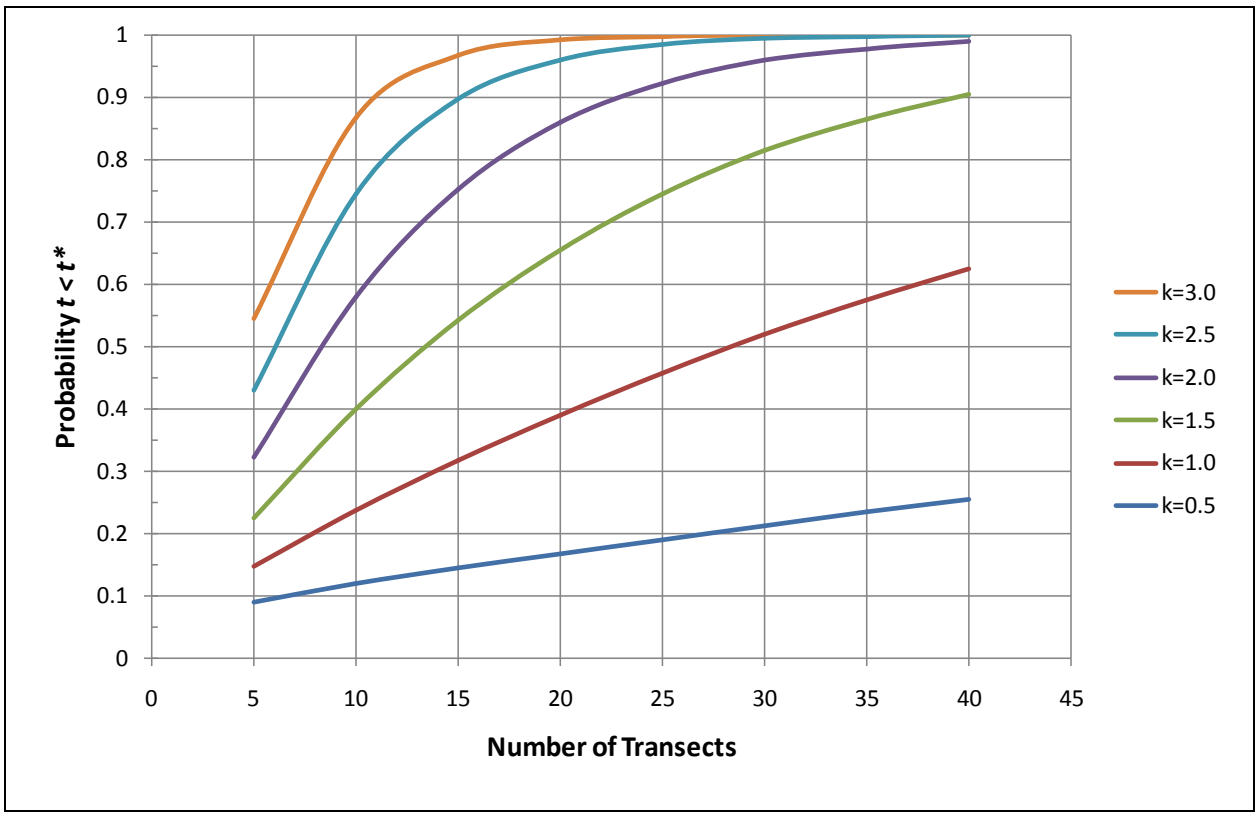

Figure 23-7. Hypothetical power curves for prospective surveys.
Values of k are the multiples of standard errors that abundance of an indicator in the new survey differs from example sites. The x-axis shows the number of transects of sampling effort and the y-axis shows the probability of correctly rejecting the null hypothesis.

Future effort should include designing hybrid survey methods, whereby random transecting could be concentrated in an area of interest from a surface ship to allow cost-effective comparisons with higher resolution than was obtained during the Recon Cruise .

A robust test of whether surface reflectance is a significant factor in determining chemosynthetic habitats is to compare the prevalence of habitats of interest with the overall frequency of surface reflectance. If the habitat shows a non-random preference for a particular level of reflectance, one would expect its distribution to differ from the overall distribution among the transects. Previous work has suggested that this might be the case in upper slope tube worm habitats (MacDonald et al. 2003).

Figure 23-8 makes this comparison for prominent habitats among the more active seep sites. The results for carbonate rubble at the AT340.2 and AT340.3 survey sites (Figure 23-8A-B) show that the distribution of surface reflectance was different between the two surveys, but the prevalence of carbonate rubble tracks the distribution of reflectance classes at each site, rather than showing a preference for a particular level or range of levels. This same lack of independent pattern is shown for tube worm clusters at AT340.2, AT340.3, and AC645 (Figure 23-8C-E), despite very evident differences between the reflectance frequencies. In the case of bacteria mats at GC852.2, there is some indication that medium reflectance values are preferred, but this is not a strongly persuasive result. Overall, the surface reflectance can be interpreted for pattern recognition, but not as a determining factor in habitat formation. Additional environmental variables could be tested from this data or similar surveys if appropriate measurements could be made.

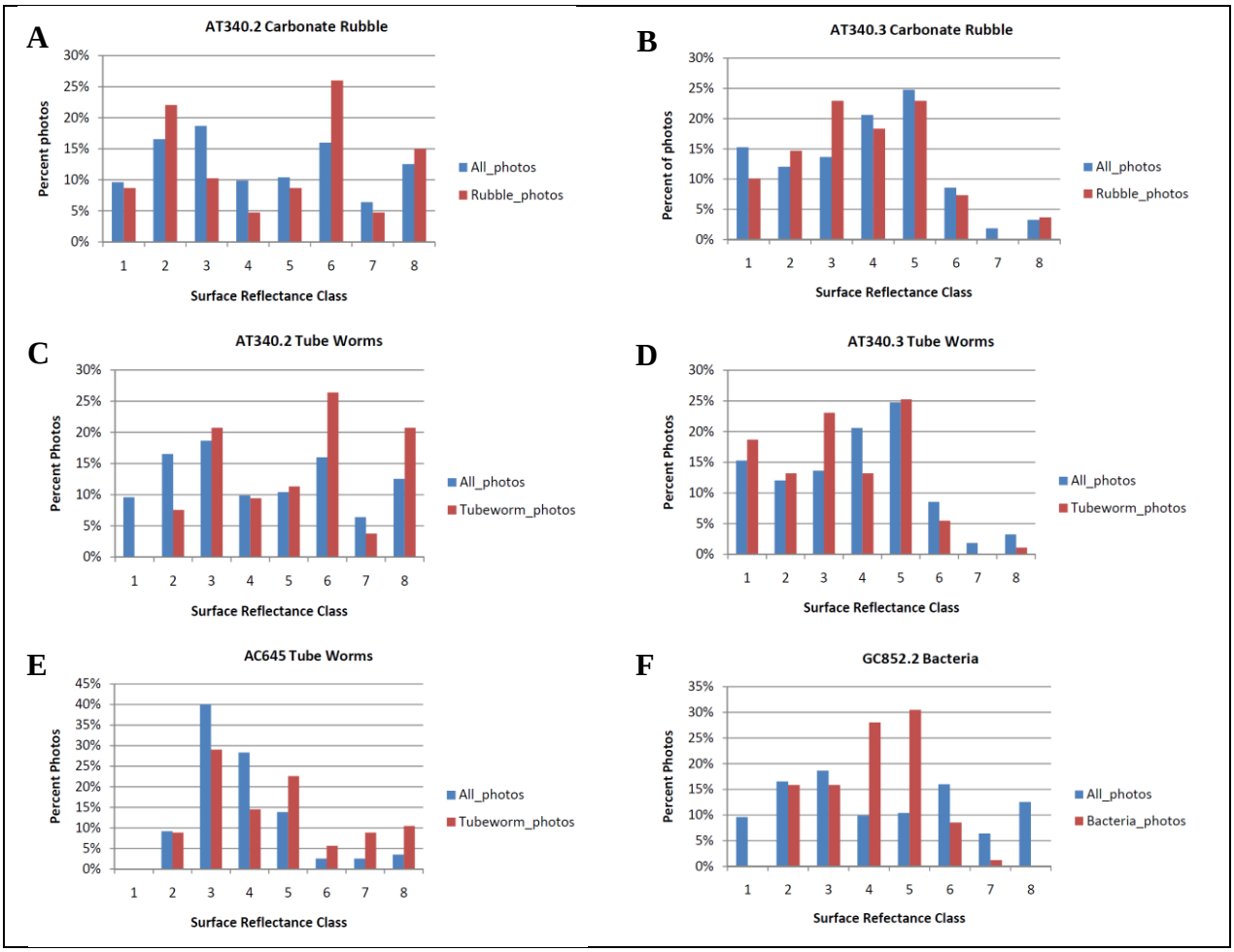

Figure 23-8. Comparison of chemosynthetic habitat with levels of surface reflectance obtained from seismic surveys of the sites.

The frequency of reflectance levels in all photographs are compared with frequency in photographs containing specific indicators. Selected portions of the results are shown for comparison: A-B Carbonate rubble at AT340.2 and AT340.3, C-D Tube worms at AT340.2 and AT340.3, E Tube worms at AT645, F Bacteria mats at GC852.2.

24. BACKGROUND FAUNA DENSITY AROUND SEEPS

24.1. Summary

The question as to whether background mud-bottom fauna increase in abundance near seep communities was examined through faunal counting along georeferenced video transects carried out by the HOV *Alvin*. This study was devised and carried out post-cruise to take advantage of the video archive. As such, it was not an optimal study, but it provided useful information. There was no simple pattern of near-seep aggregation found in the observed megafauna. Faunal counts/distance, however, varied greatly among blocks. This could be due to site-specific differences in seep-background linkage. Insufficient data prevent a definitive conclusion.

24.2. Expectations of Seep-Background Interactions

When hydrocarbon seep systems are considered in the context of the larger continental slope ecosystem, a series of questions can be posed about the existence and nature of interactions between the two. Since BOEM affords protection to seep systems by means of distance standoff requirements specified in Notice to Lessees 2009-G40, a management-relevant question is "What is the actual spatial structure and size of seep systems?" Are they constrained to the proximal areas of seepage, carbonates and foundation biota or do larger distal areas exist that are dependent on the seeps for existence?

Trophic export whereby background species depend to some degree on chemosynthetic production is one likely process that could give rise to a spatially extended system. On a large scale, a decrease in benthic fauna measured as either biomass or abundance is such a prevalent aspect of continental margin ecology (Rowe 1983; Rex and Etter 2010) that it has been widely assumed that food limitation is an increasingly important ecological factor with depth. Therefore, the existing fauna should show metabolic, anatomical, and behavioral adaptation which compensate for the lack of food (Jumars et al. 1990). If true, aggregation of consumers in the vicinity of increased food availability would be expected. Hydrocarbon seeps appear to be sources of increased food in the form of foundation species (tube worms, mussels, etc.) biomass, associated species (seep crustaceans, snails, etc.) biomass, exudates (mucus, gametes, etc. from these species), and free-living chemosynthetic, as well as hydrocarbon-consuming, microbes.

Research to date has been so narrowly focused upon within-seep ecology that the question of background species population increases nearby remains unresolved. Certainly there are megafauna consumers found in both cold seeps and hot vents which have been given the term vagrants (Tunnicliffe and and Jensen 1987; Carney 1994). These are often large crabs (Martin and Haney 2005) and occur both within and away from the chemosynthetic system but show no elevated populations in the proximity of seeps other than what might be considered a reef effect (attraction to the complex topography of seep-associated carbonates).

The work reported herein asks the simple question as to whether there is increased abundance of background consumers on mud bottoms adjacent to seeps as compared with seafloor remote from seeps. To an observer executing transects towards and away from seeps, this increase might be manifested as observing more animals within the field of view or as encountering animals more frequently as the seep is approached. Ideally, the question would be examined within a

formally-designed study employing some variant of advanced distance sampling as developed by Buckland and his associates (Buckland et al. 2004; Buckland et al. 2010). In addition to appropriate transect layout and analysis of statistical power, such an undertaking would require the dedicated use of submersible imaging systems and was not feasible within the broad missions of the current study. As a preliminary investigation of the question, however, it was possible to use bottom video made when transiting from seep site to seep site in place of formal transects. As will be shown below, this provided useful information.

24.3. Methods

Seafloor imaging has been an integral part of ocean studies since the advent of water-tight housings for cameras. Imaging became an important tool in the study of unseen deep-sea habitats with the advent of the Edgerton strobe and pressure housed 35mm camera (Thorndike 1958). The scientific values of imaging at all depths increased in the 1960s with design of underwater lens systems (Hopkins and Edgerton 1961). Replacement of film by digital cameras has greatly increased the ease at which surveys are carried out and images processed. Rapid advancements in digital imaging quickly find their way into scientific application such that manuals for surveying undergo frequent revision (Roelfsema and Phinn 2009). Relatively recent reviews such as that focusing on video by (Smith and Ruhmohr 2005) quickly become outdated. Both the HOV *Alvin* and ROV *Jason II* can provide a variety of imaging systems suitable for executing and analyzing bottom transects. For this preliminary study *Alvin* video was used due to the fairly consistent camera elevation and angle of view. The usual procedure for compiling linear image mosaics from *Alvin* video requires use of a three-chip camera mounted on the starboard manipulator aimed normal to bottom (Rzhanov and Beaulieu 2007). During the 2006 *Alvin* Cruise the video recordings from the sponson cameras (also called brow cameras) provided a more consistent record and were selected as the data source. These are single chip digital cameras producing a National Television System Committee (video standard) image measuring 720 x 480 pixels. Optically the vertical field of view is 40^0 and the horizontal view is 60^0. The cameras must be angled forward ~30^0 from vertical to prevent the *Alvin* working deck from obscuring the bottom. This angle produces a useful forward perspective but introduces too much distortion to allow for good quality mosaics to be assembled. When *Alvin* maintains two m altitude above bottom, the sponson cameras are approximately four m high and provide an image of the seafloor that is six m wide at the center of the vertical field of view.

Data are generated by an observer playing the video and recording fauna and bottom condition (i.e., mud, rocks, seep, mats, burrows, etc.). Fauna included had to move across the field of view and cross an inclusion line coincident to the camera's angular center of vertical view (Figure 24-1). Even though observed, objects leaving the field of view prior to crossing the line were excluded in order to maintain a reasonably consistent geometry of observation. An advantage to working with video rather that extracted stills is that the brain can develop a better impression of a moving object even though the resolution is poor. To facilitate both data generation and analyses, observations are collected then entered at 30 second internals. Thus the data are binned. This interval length was selected as a practical matter. The *Alvin* Frame Grabber data logger provides a convenient record of position, depth, and other parameters at that interval. The linear distance covered in each 30-second bin was calculated from the logged coordinates. Data analyses were kept very simple and limited to calculation of fauna count along 100-m transect sections, calculation of the coefficient of dispersion to examine aggregation, and visual

inspection of plots. It was considered preferable to deal with linear occurrence rather than density/area. A first approximation of area surveyed, however, can be obtained by multiplying transect length by the 6 m typical of the field of view.

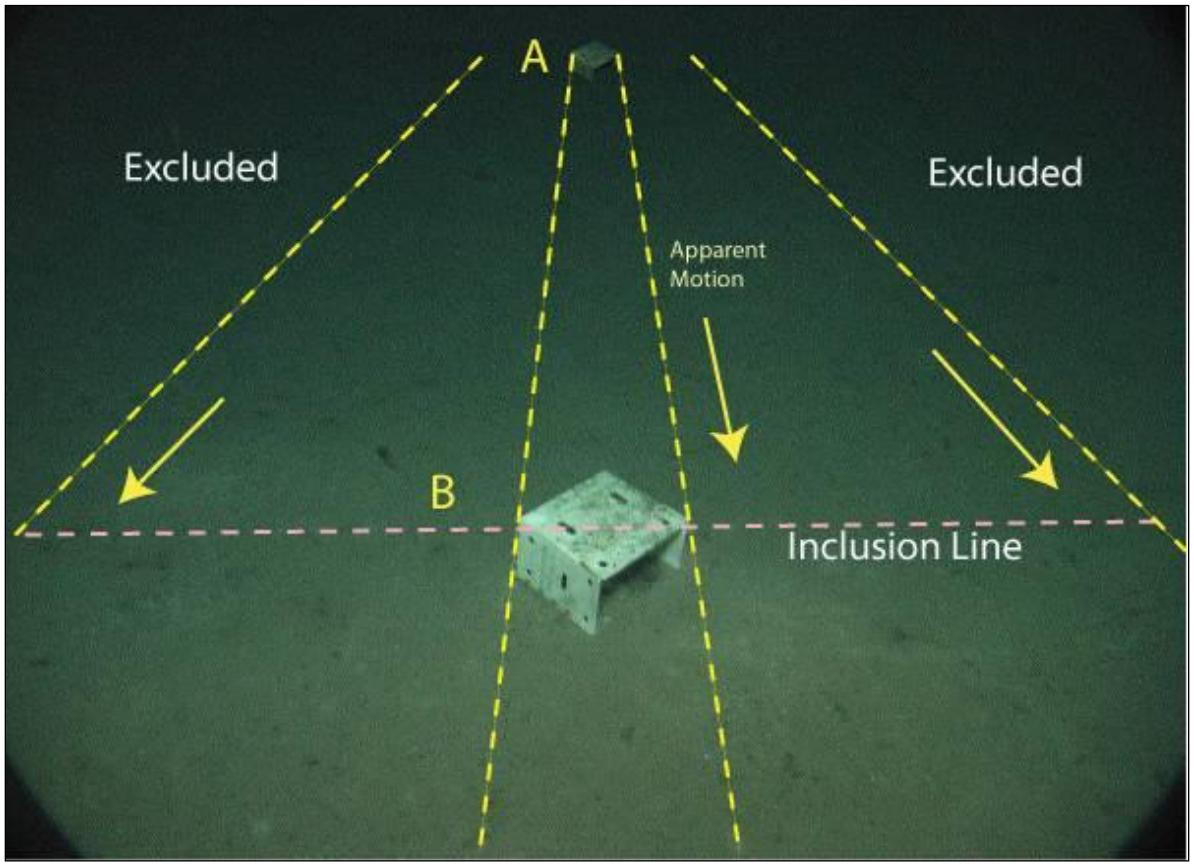

Figure 24-1. Once observed (A) objects are only counted only when they cross an inclusion line (B) which corresponds with the center of the angular center of the vertical field of view.

A major factor that limited data to occurrences of fauna >10cm in cross section was the use of Moving Picture Experts Group (MPEG) format video object files. Management of the image datasets which may be stored across 100s of 4.7 gigabyte optical disks is a serious task in itself. The procedures used by the National Deep Submergence Facility at WHOI for digital image storage were undergoing a transition during the course of this investigation. Initially SONY DVCAM tape format was employed using 124-minute tape cartridges. The relatively short ~4 four hours of bottom time of the HOV *Alvin* with two recorders running made it practical but somewhat inconvenient and expensive to use this high-quality format. The much longer deployments of the ROV *Jason II* recording three cameras made tape impractical as an archive of continuously-recorded video.

While MPEG format video produces a compact and easily viewed data archive, this comes with a considerable loss of image information. An image is initially compressed within a digital camera when the digitized scene is stored in Digital Video format. During production, this format may be converted into intermediate forms or directly converted to MPEG format. MPEG

encoded video in full color and standard resolution of 720x480 pixels is just a bit more that 1/100th of the data if the video had been stored as a series of uncompressed snapshot images. The actual appearance of the MPEG-compressed image versus the original scene is dependent on scene content and scene-scene change. If the original scene contains few elements and there is little scene-scene change, the displayed MPEG video can be a very good replica of the original. The more complex and detailed the scene and the more scene-to-scene changes, the poorer the replication. Video surveys of the bottom, unfortunately, contain a considerable degree of movement frame-to-frame and therefore are relatively poor duplicates of the original moving scene.

24.4. Results

24.4.1. Transect Statistics

All video from the 2006 *Alvin* operations were initially reviewed using the frames grabbed and logged in the Frame Grabber system. Useful transects had to exceed 150 m over non-seep mud bottom in length, be carried out at ~2 m altitude, have a constant camera vertical angle, forward direction and zoom factor, and position data had to be consistent for the duration of the transect. On the basis of these criteria, nine dives were selected for full video analysis (See Table 24-1). Four lease blocks were included: Atwater Valley 340, Garden Banks 852, Alaminos Canyon 645, and Alaminos Canyon 818. The seafloor distance traversed was 8,682 m. This distance was divided into 20 transects ranging in length from a maximum of 601 m to a minimum of 150 m. An additional transect over a seep at AC818 was included for comparison. That seep lacked high relief and contained large muddy areas where fauna were clearly visible. Speed over bottom ranged widely from 30 m/min to 10 m/min. Although a constant rate would have been preferred, variable rate video playback and freeze framing reduced biases associated with speed and the 10 cm size cutoff for fauna was easily observed even at the faster rates. Altitude could not be fully evaluated due to sensor or logging failures. At altitudes above 2 m, however, the bottom became indistinct and such high video segments were not used. Therefore, altitude is considered to have been fairly uniform within and across transects.

24.4.2. Fauna Encountered

The count of animals observed was 573 (Table 24-2). The distinctive holothuroid *Benthodytes typica* represent 38% of this number. Two other large holothuroids, *B. lingua* and *Benthothuria* sp. amounted to 5% and 8% respectively. Less common holothuroids such as *Psychropotes* sp., *Mesothuria*, sp., and *Psuedostichopus* sp. combined for 3%. Asteroids at 17%, fish at 8%, shrimp 1%, and large crustaceans at 1% were the total inventory of mobile organisms. Sessile animals were dominated (18%) by an elongated, single-shaft gorgonian probably of the genus *Lepidicis*. Mud-dwelling cerianthid anemones added an additional 1%. The paucity of large crustaceans and the prevalence of holothurians is a common bathymetric pattern on lower continental slopes.

24.4.3. Patterns Along Transects

The most obvious result is that very few epibenthic megafauna were encountered along most of the transects between seeps (Figure 24-2). The highest values of ~16 animals/100 m was encountered along with other high values at AC645 and along a single transect at AT640. The

high counts/distance at AC645 were caused by relatively high densities of mobile holothuroids and well as sessile cnidarians.

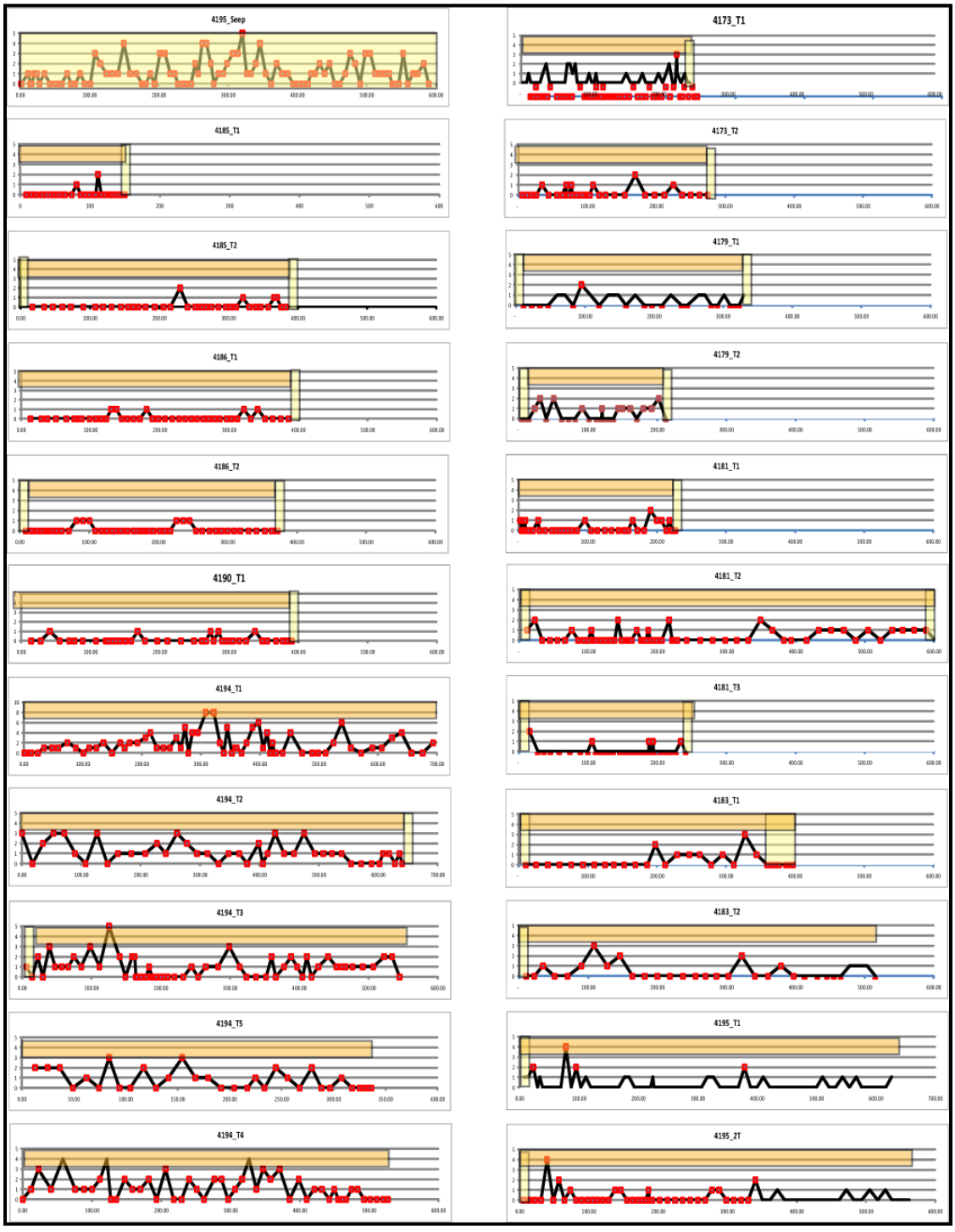

Figure 24-2. Occurrence of megafauna along ROV transit. Counts are indicated on y axis. Brown barsindicates mud bottom. Yellow bars indicate seep bottom.

Aggregation of counts at transect ends near seep communities was not consistently observed in the 20 transects. Thus, acknowledging the limitation of these methods, there appears to be no simple aggregation of consumers in the proximity of lower slope seep communities.

Table 24-1

Transect Performance Statistics Based on Frame Grabber Dive Logs

BLOCK	DIVE	DEPTH	TRANSECT	LENGTH M	DURATION MINUTES	AVERAGE 30 SEC SEGMENT METERS	STDEV SEGMENT M
AT340	4173	2216	T1	245	33	3.71	1.56
			T2	275	16.5	8.34	4.44
	4179	2200	T1	330	14.5	12.61	2.57
			T2	212	13.5	7.72	3.11
	4181	2200	T1	227	20	5.67	3.37
			T2	601	30.5	9.86	6.11
			T3	241	22.5	5.35	4.19
	4183	2200	T1	397	15	12.88	5.41
			T2	515	16	16.10	3.22
Subtotals				**3043**	**181.5**	**8.38**	
GB852	4185	1410	T1	150	13.5	5.55	1.69
			T2	383	14	10.06	3.89
	4186	1410	T1	386	21	9.19	2.52
			T2	372	24.5	7.58	2.75
	4190	1410	T1	391	20.5	9.53	4.8
Subtotals				**1682**	**93.5**	**8.99**	
AC645	4194	2240	T1	694	32	10.8	4.47
			T2	640	21.5	15.72	4.24
			T3	545	29	9.39	3.55
			T4	525	25.5	10.52	3.05
			T5	336	16	10.51	2.73
AC818	4195	2747	T1	627	35	8.95	2.27
			Seep	590	45	6.55	1.79
Subtotals				**3957**	**204**	**9.70**	
TOTALS				**8682**	**479**	**9.06**	

Table 24-2

Megafauna Statistics along Transects

BLOCK	DIVE	TRANSECT	Fauna	Count/100m	MEAN OBS/SEGMENT	COEFF DISPERSION	*Benthodytes typica*	*Benthothuria sp.*	*Benthodytes lingua*	Misc. Holothuroids	Asteroids	Fish	Sessile Cnidarians	Cerianthid	Shrimp	Large Crustaceans
AT340	4173	T1	24	9.7959	0.364	1.323	12	3	2	1	1	1	2	1	1	0
		T2	7	2.5455	0.212	1.107	5	2	0	0	0	0	0	0	0	0
	4179	T1	13	3.9394	0.448	0.731	8	0	0	0	2	2	1	0	0	0
		T2	14	6.6038	0.519	0.945	6	0	1	1	0	4	0	2	0	0
	4181	T1	11	4.8458	0.275	0.93	1	4	0	2	1	1	0	0	0	2
		T2	22	3.6606	0.361	1.02	3	4	2	3	5	2	1	1	1	0
		T3	6	2.4896	0.133	1.227	0	0	0	0	1	5	0	0	0	0
	4183	T1	10	2.5189	0.323	1.527	3	1	0	2	2	0	0	1	0	1
		T2	14	2.7184	0.438	1.318	9	0	0	0	2	3	0	0	0	0
Sub			**121**	**1.4937**			**47**	**14**	**5**	**9**	**14**	**18**	**4**	**5**	**2**	**3**
GB852	4185	T1	3	2	0.111	1.615	0	0	0	0	0	2	0	1	0	0
		T2	5	1.3055	0.132	1.303	0	0	0	2	0	1	0	1	0	1
	4186	T1	5	1.2953	0.119	0.902	0	0	0	0	0	2	0	1	1	1
		T2	6	1.6129	0.123	0.896	0	0	0	0	0	4	1	0	0	1
	4190	T1	5	1.2788	0.122	0.9	0	0	0	1	1	3	0	0	0	0
Sub			**24**	**1.4269**			**0**	**0**	**0**	**3**	**1**	**12**	**1**	**3**	**1**	**3**
AC645	4194	T1	113	16.282	1.766	2.297	54	2	1	1	0	1	53	0	0	1
		T2	52	7.9688	1.86	0.934	18	10	3	1	0	5	14	0	1	1
		T3	56	10.275	1.018	1.221	29	7	5	1	0	1	12	0	0	1
		T4	57	10.634	1.118	1.276	25	8	3	0	0	3	17	0	1	0
		T5	25	7.4405	0.781	1.217	17	1	6	1	0	0	0	0	0	0
AC818	4195	T1	24	3.8278	0.343	1.428	15	1	2	1	1	3	1	0	0	0
		Seep	101	17.119	1.111	1.324	11	1	3	0	81	5	0	0	0	0
Sub			**428**	**10.761**			**169**	**30**	**23**	**5**	**82**	**18**	**97**	**0**	**2**	**3**
			573				**216**	**44**	**28**	**17**	**97**	**48**	**102**	**8**	**5**	**9**
							0.4	**0.1**	**0.1**	**0**	**0.2**	**0.1**	**0.2**	**0**	**0**	**0**

24.4.4. Patterns among Transects and Blocks

When lease blocks are compared, each is distinct. GB852 consistently had the lowest faunal densities. The usually dominant holothuroids were almost absent. Fish dominated but were not more abundant than elsewhere. The bottom along all five GB852 transects was heavily burrowed, indicating an unobserved fauna component. At the other extreme were the transects at AC645 where holothuroids and sessile organisms were relatively abundant. The prevalence of a gorgonian (cf. *Lepidicis*) on soft bottom was unusual, as well as an apparent aggregation within transects. Faunal densities at AT340 and the non-seep transect at AC818 all have similarly low faunal densities. With the exception of two higher values at AT340 associated with relatively short transects and clusters of holothuroids. The single seep transect at AC818 had the highest count/distance observed. While it contained a fauna similar to the surrounding mud bottom, asteroids were dramatically more abundant. Most clearly had six arms and were later identified as *Ampheraster alaminos*.

The coefficient of dispersion (variance/mean) should have a value of 1.0 is the distribution of animals across transect segments follows a random Poisson distribution. Lower values reflect over dispersion and higher values reflect clumping. The range of observations per transect ranges so widely (5 to 113 counts) that significance testing has limited utility. An examination of values is, however, useful. Only at AC645, dive 4,194, transect 1 is there strong indication of aggregation. The mud-dwelling gorgonian definitely occurs as a patch of several tens of m in length.

24.5. Discussion

While this study provides no support for the contention that background consumers aggregate in the vicinity of seep foundation species, it is important to review the method-imposed biases that could influence the final conclusion. First is the necessary focus upon megafauna larger that 10cm. This eliminates from consideration the vast majority of deep-sea species. Abundant taxa such as ophiuroids might show increased abundance in the proximity of seeps and completely escape video detection. Second is the necessity of omitting infauna which also may be more abundant near seeps. Analysis of lebenspurren might be attempted, but this is problematic in the sense that traces are easily erased. In addition their features are obscured by the video compression. Lastly is the snapshot nature of the transect sampling. The actual amount of time spent at the intersection of seeps and mud bottoms is just a few seconds, even when 20 transects have been executed. For highly mobile consumers that enter and leave the seeps quickly, there is a low probability of successful imaging.

Having considered that the limited study may have missed aggregation of various omitted fauna, the finding of no simple aggregation needs to be considered versus more complex seep-associated aggregations. Over all of the 20 mud transects, counts/distance ranged from consistently low at GB852 to consistently high at AC645. This inter-block difference might reflect a different seep-background linkage operating in the two areas. Unfortunately, there is insufficient comparable information on the distribution of benthic megafauna from non-seep areas in the GoM to make the judgment as to whether this falls within the range of typical variation or is influenced by seeps.

The higher density fauna encountered at AC645 is especially interesting in that only two components showed an elevated presence, *B. typica* and the sessile *Lepidicis.* The former feeds on detritus using small oral tentacles and a narrow gut. The latter is a suspension feeder. The other holothurians which have large tentacles and large sediment packed guts did not increase in number. Similarly, predatory/scavenging fishes did not show an increase. This would suggest the existence of an enhanced detrital influx to bottom, but an influx to which only a few species respond.

25. SITE SUMMARIES

25.1. Atwater Valley 340

Latitude/Longitude: 27.645°N, 88.364°W
Depth: 2200 m

This site (AT340) was one of the prime study sites for the project. It was originally surveyed during the Recon Cruise and also by the Hugin AUV. There were five *Alvin* dives and four *Jason II* lowerings at this site. *Alvin* dives included AD4173, AD4179, AD4180, AD4181 and AD4183. *Jason II* dives included J2-269, J2-270, J2-276, and J2-277.

25.1.1. Site Overview

The bathymetry maps generated from the AT340 seismic data highlighted areas in the GoM with distinct highs and lows that were likely formed by hydrocarbon seeps (Figure 25-1). These same areas showed anomalous variation in the amplitude (or, the strength of the returning signal of the seismic data) that had earlier been shown to be caused by carbonates in the sediments formed by the chemosynthetic bacteria consuming hydrocarbons. Those areas appear "hard" (as red, yellow, and dark green on seismic amplitude maps).

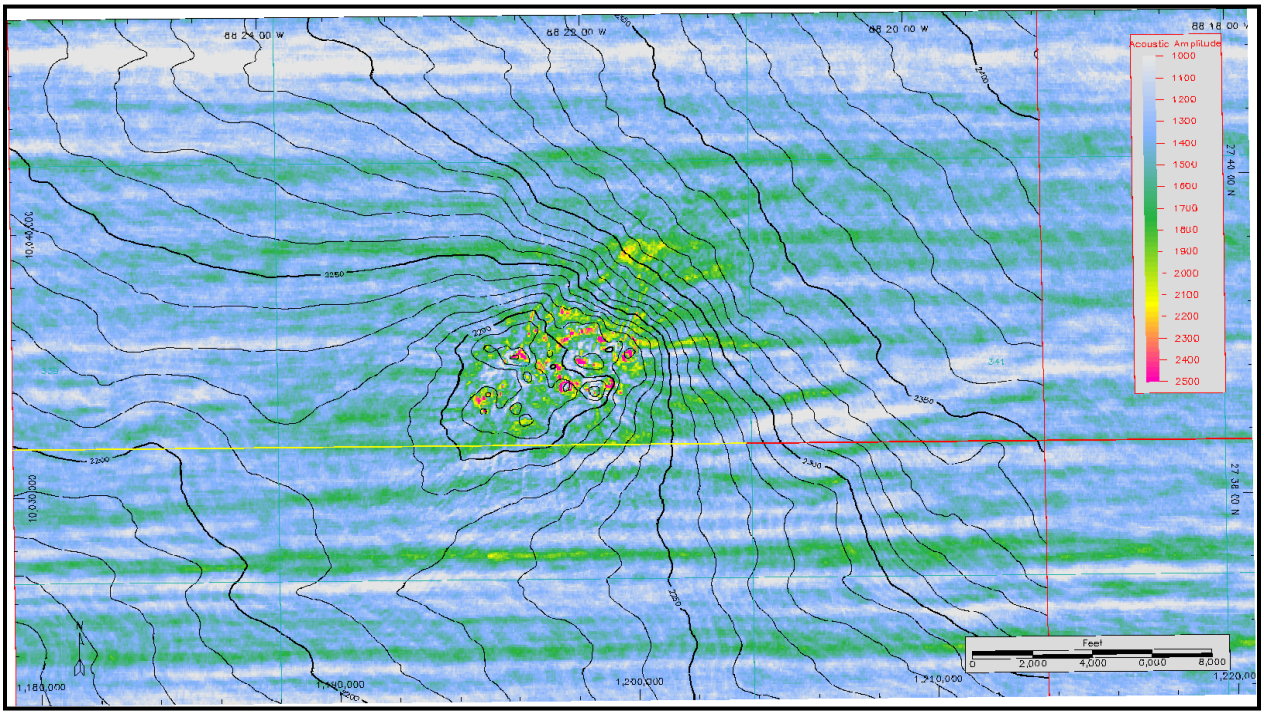

Figure 25-1. 3-D seismically derived bathymetric map (contour interval, 10 m) with amplitude overlay at site AT340; seismic data and derivative interpretations used by permission.

There are also spots on the amplitude maps that appear to be softer than the typical soft-bottom mud, that have been shown by previous research (Roberts et al., 2001) to be seeps with very high, episodic flow rates and void of chemosynthetic communities. These "soft" spots are usually surrounded by carbonates, where the flow is slower and steady (where there is a steady source of food for these communities).

This is the easternmost site intensively studied as part of this program. This site is highly variable in terms of its seafloor morphology, bottom types, and distribution of benthic communities. Large areas of seafloor are lithified. Authigenic carbonate slabs and blocks are common in the key sampling areas. Well-developed mussel beds and tube worm communities are distributed throughout this type of terrain. The normal deep-sea fauna in the vicinity of the seeps was dominated by elasipod holothuroids typical of lower slope and abyssal plain environments: *Benthodytes typica, Benthodytes lingua,* and a synallactid *Benthothuria sp.*

The site is geologically characterized as a bathymetric high along the eastern extension of Mississippi Canyon where it transitions from a canyon to a submarine fan. The site consists of three mounded areas on top of the overall bathymetric high. Geophysical data indicate that the feature is supported by salt in the shallow subsurface. Seismic profiles identify a clear vertical migration pathway for the flux of fluids and gases to the modern seafloor. This pathway is defined by acoustic blanking of the seismic record, suggesting both reflection of acoustic energy by hard bottom conditions at the surface and perhaps gas in the subsurface along the migration route. The surface reflectivity maps, created by analyzing the first return from the seafloor from 3-D seismic data, indicate high reflectivity in the areas localized around the three mounded features. Five *Alvin* dives were made at the site. Three dives concentrated on the local mounded area in the southeast quadrant. On the 3-D seismic surface reflectivity maps, this area displayed a complex pattern of high-to-moderate reflectivity. Observations from *Alvin* confirm extensive hard bottom conditions that result from authigenic carbonate precipitation, a by-product of microbial utilization of seeping hydrocarbons. Inspection of these carbonates reveals that they contain abundant mussel shells. In addition, carbonate precipitation occurs around the bases of tube worm bushes. Scattered among the blocks and pavements of authigenic carbonate are living mussel beds and tube worm colonies. One site named the "Mussel Brick Road" represents an elongate (about 75 m long) and densely packed bed of living mussels forming in a joint or separation in the underlying authigenic carbonate pavement. Between the blocks of carbonates, clumps of tube worms, and beds of mussels are patches of sediment colonized by urchins (Figure 25-2), a few soft corals, and other sparsely distributed organisms.

Figure 25-2. Urchins were abundant in portions of the AT340 site.

In the northwest quadrant of the AT340 study area, a distinct mound occurs. On surface reflectivity maps derived from 3-D seismic data, this mound stands out as a very high amplitude feature. Two dives on this feature confirm the fact that it is composed almost entirely of hard bottom. Inspection of the areas of lithified seafloor shows that the carbonate block and pavements (Figure 25-3) are composed almost entirely of mussel shells, one layer on top of another.

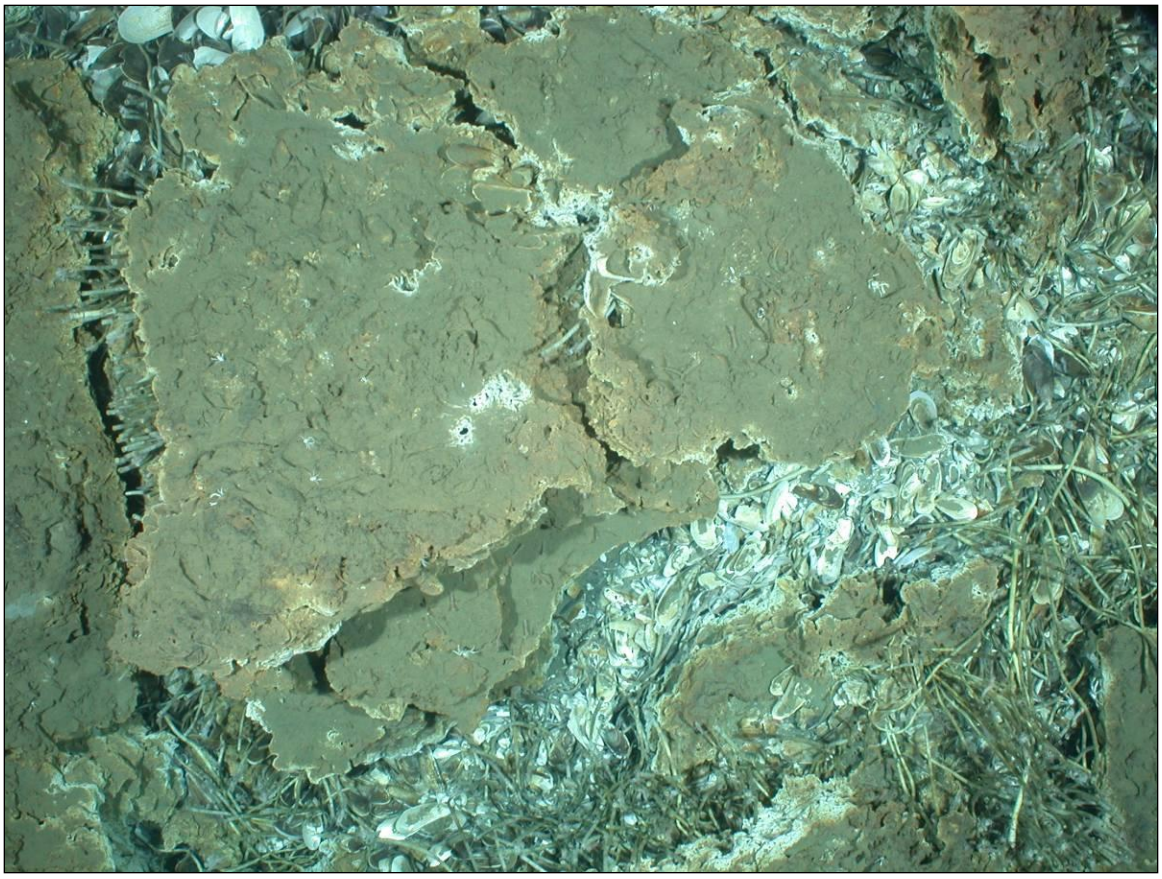

Figure 25-3. Extensive carbonate pavements indicate protracted seepage.

Because of this unique construction we named the site “mussel mound.” Many blocks seemed to have very little sediment matrix, just mussel shells and binding carbonate cements. Although most of the mussel shells did not house live mussels, several patches of live mussels were observed at the apex of the mound. Both the crest areas and flanks of the mound were covered with tube worms. Many tube worm colonies occurred beneath and at the edges of carbonate blocks, but free-standing colonies were also present. To the east and off the flank of the mound a brine vent is present. Fluidized sediment, brine, and hydrocarbons are being vented at this site (Figure 25-4).

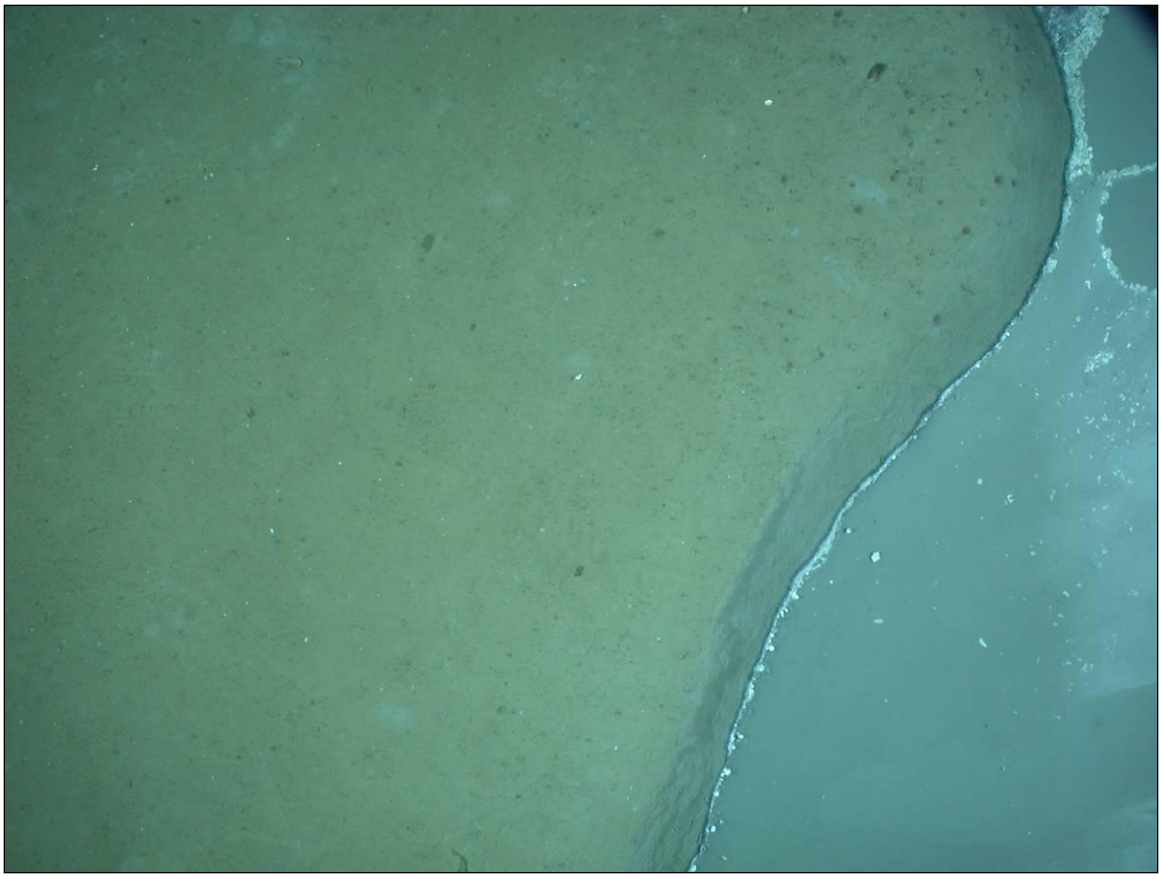

Figure 25-4. Surface brine flows generate extensive pools and channels that support mussel aggregations at AT340.

Around the vent site and along the flow field there are extensive mussel beds. Seismic profiles across the AT340 feature indicate the presence of salt in the relatively shallow subsurface. The brine is likely coming from the dissolution of this salt body.

Atwater Valley 340 is a large and complex site with abundant and varied chemosynthetic communities spread over a relatively large area. It has the largest mussel beds of any site yet visited. Two of these were especially spectacular. One is a solid bed of mixed species and sizes of live mussels that we estimate is over 10 m wide and 20 m long, and we nicknamed "Big Mussel Bed" (Figure 25-5). The other was a relatively continuous linear bed over 70 m in length that was nicknamed the "Mussel Brick Road." Both of these were imaged intensively enough to allow almost complete photographic reconstruction of the entire features during both *Alvin* and *Jason II* cruises.

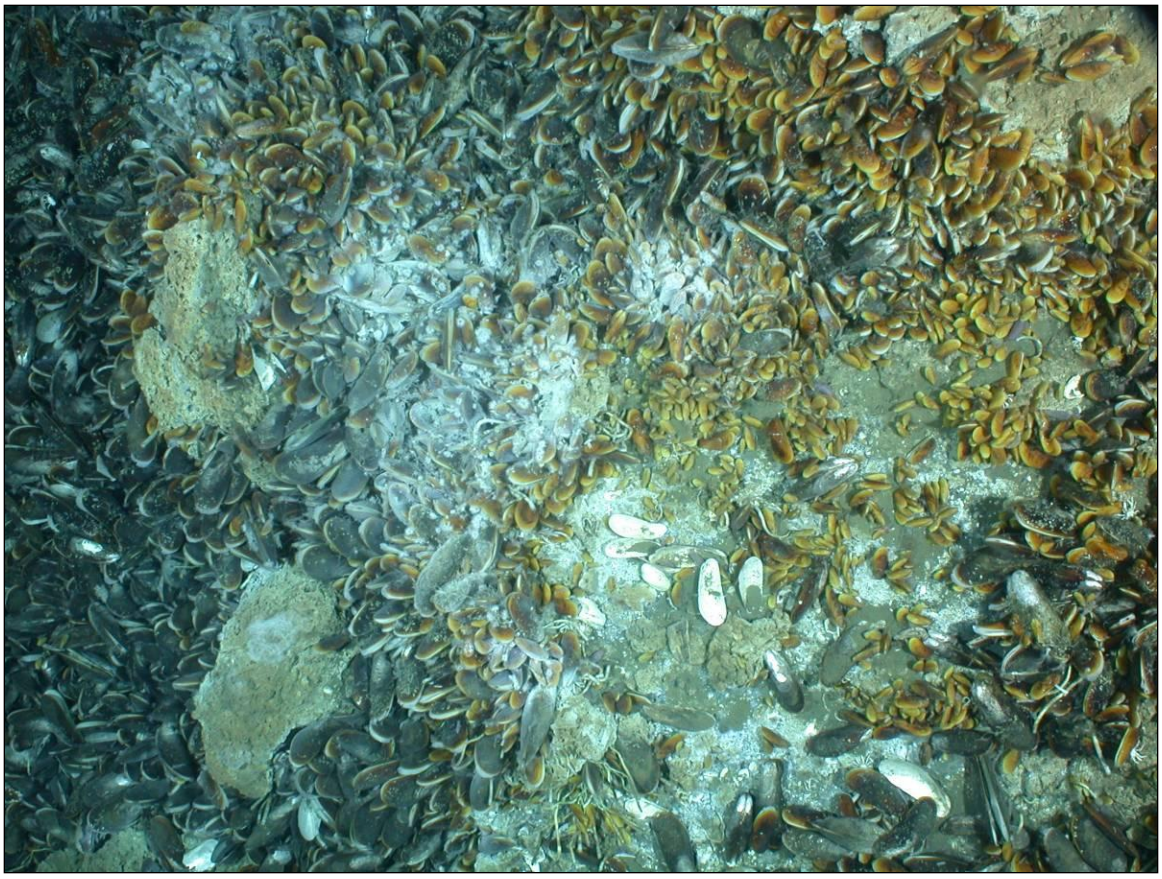

Figure 25-5. This down-cam image shows two species of seep mussels in a dense bed.

We collected both *B. heckerae* and *B. brooksi*, the two bathymodioline mussels that harbor both methanotrophic and chemoautotrophic symbionts from both of these features. Both of these features are in the southeast quadrant of the site. There are patchy small mussel aggregations (of large individuals) in the northeast quadrant, and scattered intermediate-sized mussel beds near the topographic high in the far western edge of the site and in the bottom of what appears to be 2 m diameter blowout craters in that area.

Tube worms are also very abundant at this site. They occur in large numbers among the large carbonate slabs in the southeastern and western portions of the site. *Escarpia laminata* is the dominant species in the aggregations ("bushes") sampled and appears to be dominant in most of the aggregations seen. However, *Lamellibrachia* sp is also quite abundant; found as large individuals and in small groups protruding from underneath and between carbonate slabs and in mixed aggregations with *E. laminata*. In addition to two large areas with abundant tube worms, several smaller ridges with carbonates were also colonized by both species.

The most dominant megafauna species associated with the tube worm aggregations was the shrimp *Alvinocaris muricola*. This shrimp species was also abundant in the mussel collections, co-occurring with the abundant brittle star *Ophioctenella acies* in this habitat. The *B. heckerae* that were collected also contained the commensal polychaetes *Branchipolynoe seepensis* and a

nautillinellid. A large proportion of the *E. laminata* collected contained a phyllodocid polychaete that is likely a blood-sucking parasite.

Another animal that was abundant (and dominant) in some areas of soft sediment with visual evidence of seep impact was a spatangid heart urchin. Several (at least five) beds of these were found over the course of the original five *Alvin* dives to this site. None of these beds were associated with carbonates, but some were close to the other sites or isolated mussel clumps. In areas where the sediments around the urchins were stained black and white, the urchins did not appear to be moving much. In areas where seepage was less apparent, there were often long trails associated with the urchins. Urchins in both types of areas were imaged for density and movement calculations and cores were taken in association with a manipulative experiment to examine the effects of the urchins on meiofauna communities in one area.

Few colonial cnidarians were seen at this site. However, small gorgonian colonies were present near the scattered mussel beds in the northeast quadrant of the site and noted on the carbonates in the western edge. Isolated whip corals were present in many areas. In some areas a small colonial anemone was abundant on tube worm tubes and dead mussel shells. Individual anemones were often noted over non-seep affected sediments and a small crab with an orange anemone was a regular site in the vicinity of the active seep areas as was anthropogenic debris (Figure 25-6).

Figure 25-6. Anthropogenic debris like this monofilament line was common at AT340.

25.2. Green Canyon 600

Latitude/Longitude: 27.370°N, 90.569°W
Depth: 1,250 m

This site (GC600) was surveyed during the Recon Cruise and during *Alvin* Dives 4174 and on 4184. There were no *Jason II* dives at this site.

The GC600 site was selected for submersible dives based on several lines of evidence, including characteristics determined from seismic data, the presence of persistent oil slicks on RADARSAT data, and photo reconnaissance. The site is located in a water depth of approximately 1,180 m on the upper-middle continental slope. The overall geometry of the area of interest is an elongate northwest-to-southeast trending ridge that separates two intraslope basins. The 3-D seismic surface reflectivity maps and accompanying seismic profiles suggest that this is an area of very active expulsion of fluids and gases from the deep subsurface. Clear migration pathways are visible on the seismic profiles and RADARSAT images of this part of the Gulf show persistent oil slicks originating from the GC600 site. Two areas of high surface reflectivity occur at this site, and these were the objective of the *Alvin* dives. The area of complex surface reflectivity anomalies to the northwest center around a localized bathymetric high, the apex of which occurs at a water depth of approximately 1,177 m. The second area of high-amplitude surface reflectivity anomalies occur to the southeast and is also a localized mound, but with very subtle bathymetric relief.

25.2.1. Site Overview

This site extends along a northwest-southeast axis, with about 1 km between the tube worm area (northwest) and the clams and mussel pockmarks (SE), Bench Marker 2 (X-264 m, Y-912 m) in the tube worm area and Ian marker 5 (X-1426 m, Y-167 m) in the southeast pockmark area with clams and mussels.

Direct observational data from both photo reconnaissance work using a drift camera system and the *Alvin* confirms the geologic and biologic complexity of the area. In the areas of high surface reflectivity mapped from seismic data, massive hydrocarbon seep-related carbonate hardground pavements and isolated blocks occur (Figure 25-7).

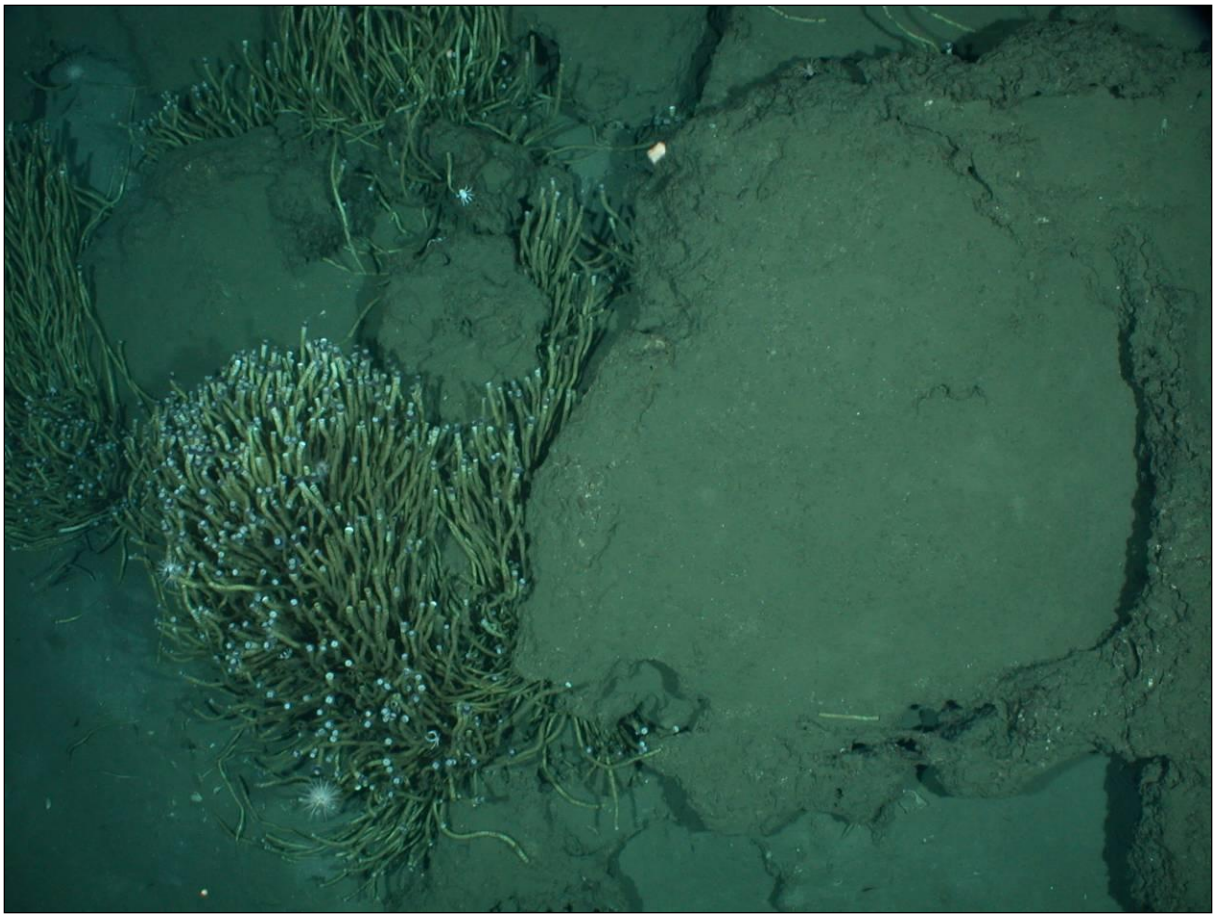

Figure 25-7. Massive carbonates and sparse tube worms are characteristic of GC600.

Gas was observed bubbling through cracks in the carbonates on *Alvin* Dive 4174. Patches of tube worms and mussels were observed growing out of fissures in the carbonate pavements. *Beggiatoa* mats and small coverings around open burrows, both white and orange, occurred throughout the area where pockets of sediment occurred between areas of hardground. Pockmarks were observed, some with crude oil bubbling out. Although there were few living communities found, mussel and clam shells littered the area of both mound-like anomalies. Cnidarians (sea pens, sea feathers, and anemones) were observed on the hard substrates.

This site corresponds to a low ridge, with carbonate outcrops at the northwest corner, and pockmarks over most of the area. Some small carbonate outcrops were sometimes present on the rims of the pockmarks. Due to time limitations, we did not explore the topographic high point. Target 10 (Geo10) had a mud bottom only, target 9 had bacterial mats.
The tube worm area was covered extensively during Dive 4184 while searching for a suitable tube worm bush for collection. It corresponds to a topographic high, with tube worms as isolated individuals or small groups in cracks. A few bushes were also found. The only species observed on the bottom was *Lamellibrachia* sp. nov. Patches of tube worms and mussels were observed growing out of fissures in the carbonate pavements (Dive 4174).

Two extensive areas with pockmarks and clams were also covered. Target 11 was chosen from the Recon Cruise as a mussel area, but none were seen. At the end of the dive (near Target 12, originally described as clams), large mussels were seen at the bottom of a pockmark. Gorgonians and other cnidarians (anemones) were common close to tube worms (especially on the northwest corner of the tube worm area) and on some carbonate pieces around pockmarks (Figure 25-8).

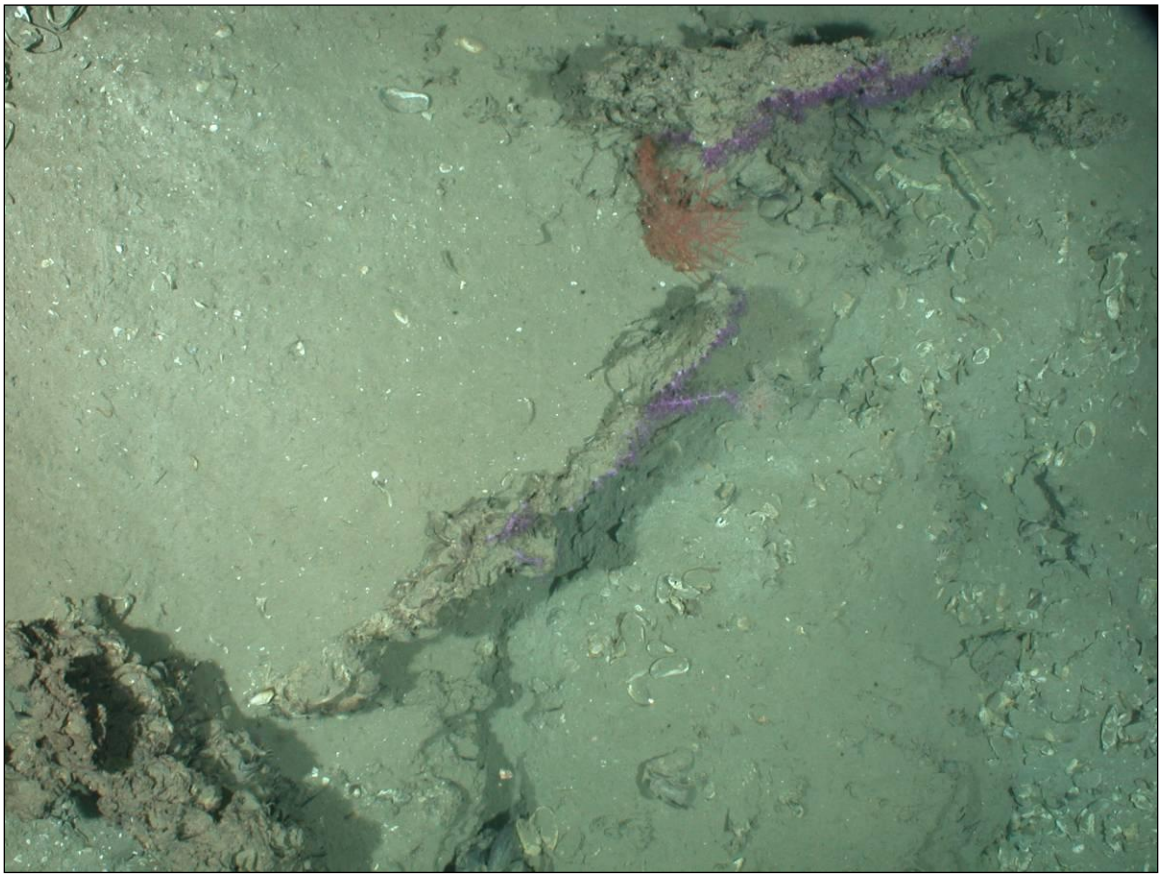

Figure 25-8. Varieties of soft corals were seen on some of the carbonate boulders, but no significant aggregations were observed during the two dives at the site.

Most of the area surveyed during the dive showed bacterial mats of various sizes. No *Alvinocaris* shrimp were associated with them. The mussel appears to be *B. brooksi*. The clams were *Calyptogena ponderosa*.

25.3. Walker Ridge 269

Latitude/Longitude: 26.686°N, 91.661°W
Depth: 1,950 m
There were two *Alvin* dives at Walker Ridge 269, AD4175 and AD4191 and one *Jason II* dive, JII 275.

25.3.1. Site Overview

WR269 is near the southern extent of the vertical salt diapiric province and north of the area of the GoM where the salt bodies are primarily tabular, or in the form of horizontal sheets that block vertical hydrocarbon migration to the seafloor. Therefore, seismic seafloor amplitude anomalies (hydrocarbon seeps) are rare south of WR269/270 to the Sigsbee Escarpment, where the salt canopy terminates. This site is 1,910 – 2,000 m of water and is approximately 3,000 m long by 1,000 m wide. Moderate-to-high positive amplitude covers the entire feature except at a discrete, circular high that appears to be a mud volcano with distinctly lower positive amplitude (either due to steeper slopes and attenuated return signal or less lithification). Subsurface active gas migration is clear from the blanking of sedimentary bedding below the entire feature. The site is mounded with features that trend toward the west and are interpreted as old mudflows that originated from the mound-like area to the east into WR270. These mounded features are on a ridge that separates two very distinct intraslope basins that are floored by salt or salt welds.

Previous studies, using high quality 3-D seismic data, indicate the presence of a well-defined bottom simulating reflector that cuts across stratigraphic reflectors of the basin fill to the south of the area of interest. This feature, which is interpreted to indicate the base of the gas hydrate stability zone, appears to have free gas trapped beneath the bottom simulating reflector . The mounds on the modern seafloor are updips of the interpreted gas hydrates and associated free gas. It appears that gas is bypassing the gas hydrate stability zone along permeable beds that are upturned along the basin margin. The topographic buildups that are the focal points of our investigation are interpreted as being several large expulsion features that have built mounds through the extrusion of fluidized sediment along with other products such as hydrocarbons.

Surface reflectivity maps of the area derived from 3-D seismic data suggest the location of several active vents (circular low-amplitude zones) and associated flows that have localized areas of high reflectivity. The areas of high reflectivity were interpreted as regions of local seafloor lithification and perhaps fields of clam shells.

The particular area selected for investigation is characterized by rather subtle topography except for a localized mound that rises some 30 m above the surrounding seafloor. The area was selected on the basis of its characteristics on geophysical records. The mound-like feature was interpreted as a sediment extrusion site and the surrounding areas as overlapping mud flows. The surface reflectivity maps suggest that there are some highly reflective zones that surround and are located to the west of this central vent feature. These highly reflective zones are usually lithified seafloor areas or fields of clam shells in this setting. The fact that the surface reflectivity maps showed a low-amplitude response in the vent area suggests the presence of gas or soft bottom condition. Small islands of slightly higher reflectivity suggested variable bottom conditions in the area of the vent and a reasonable probability of finding tube worm, mussels, and carbonate rocks.

There is an extensive monoliferan “field” in the eastern part of the site where we took several push cores of monoliferans and frenulates. About 300 m to the west, there were tube worm and mussel communities and carbonate rocks. We collected vestimentiferans (*E. laminata* and *Lamellibrachia* sp. 1) from this location. More extensive communities, including dense aggregations of tube worms and thriving mussel communities were found on the flanks of the central crater (Figures 25-9 and 25-10).

Figure 25-9. Although there were extensive areas of seep-affected sediments at the WR269 site, development of tube worm or mussels aggregations was very restricted.

Figure 25-10. Surface sediment in the regions of seepage featured a rich assortment of pogonophorans, holothurians, and crustaceans.

25.4. Keathley Canyon 243

Latitude/Longitude: 26.731°N, 91.166°W
Depth: 1610 m

This site (KC 243) was visited during the Recon Cruise and one *Alvin* dive was made at this site (AD4176). There were no *Jason II* dives at this site.

25.4.1. Site Overview

This site occurs on a ridge separating a large intraslope basin to the south from three smaller intraslope basins to the north. Surface reflectivity mapping of 3-D seismic data indicates two areas of scattered seafloor anomalies along the southeastern and eastern upper flanks of the ridge. Seismic profiles across the ridge indicate well-defined and vertically oriented "chimneys" that have no internal acoustic character, acoustic "wipe-out zones." These features are interpreted as gas-rich migration pathways for fluids and gases to be transported from the deep subsurface to the ocean floor. Photo reconnaissance work prior to the *Alvin* cruise confirmed the presence of chemosynthetic organisms in the vicinity of the southern anomaly identified from 3-D seismic data. The site is mainly covered by soft sediment. It shows some steep features, with drop-offs and pronounced slopes. Exposed carbonate is frequent, sometimes located at the top of drop offs. The carbonate was mostly forming large slabs, which were cracked and fissured (Figure 25-11).

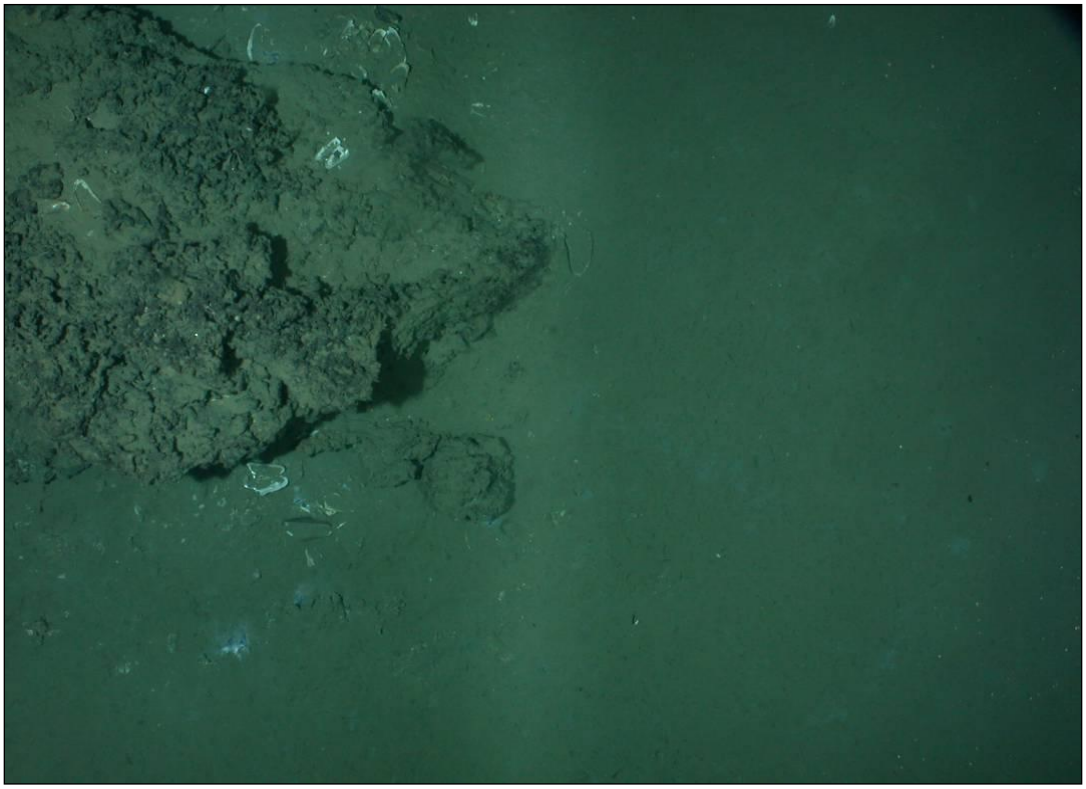

Figure 25-11. Relatively few carbonate structures were observed, indicating little flux of hydrocarbons.

The carbonates were mainly rubble at the beginning of the dive. No exposed methane hydrate was observed. Small depressions filled with brine were common near mussels and a few other places, including near Target 3. No rocks were collected.

Scattered mussel shells were found almost everywhere on the dive track. They were denser in some areas. Briny areas were common, with bacterial mats and a restricted area with live mussels stretching northwest to southeast halfway between the targets. These mussels were most often found in small patches, with a few larger beds (Figure 25-12).

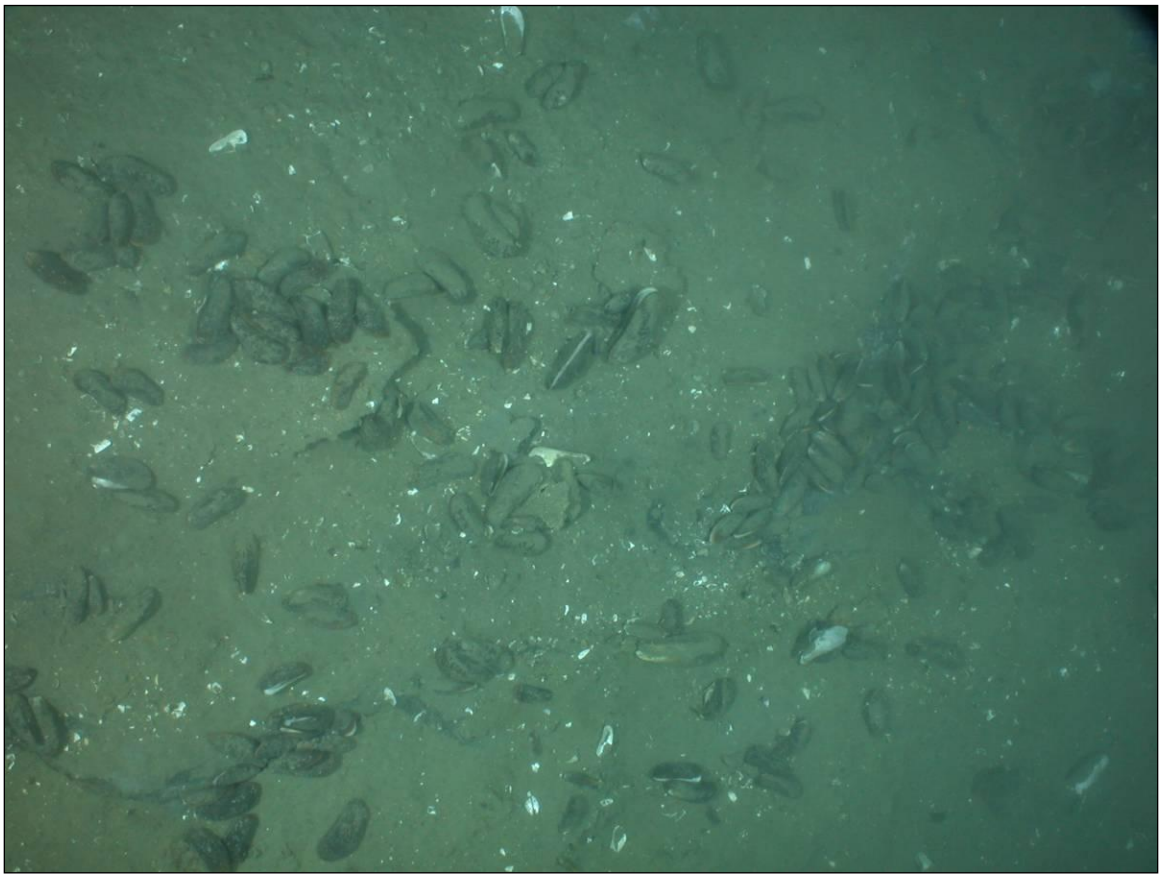

Figure 25-12. KC243 site had relatively little development of chemosynthetic communities, comprising sparse mussel beds for the most part.

Tube worms were seen on a hand-held camera photo after the dive but none were collected. A mussel pot and a mussel scoop in the mussel bed (right next to each other) were collected. The only species of *Bathymodiolus* was *B. brooksi*. Other species found were: *Ophioctenella acies*, *Harmothoe* sp., *Prionospio* sp., *Capitella* sp., and *Nereis* sp. Other fauna found were: large round sponge, *Chaceon affinis*, *Nematocarcinus*, and *Paralomis sp*.

25.5. Green Canyon 852

Latitude/Longitude: 27.110°N, 91.166°W
Depth: 1410 m

This site (GC852) was visited during the Recon Cruise and also mapped with the Hugin AUV. There were six *Alvin* dives at GC852, including AD4177, AD4185, AD4186, AD4187, AD4189 and AD4190. There were also two *Jason II* dives, J2-273 and J2-278.

25.5.1. Site Overview

The bathymetry maps generated from the GC852 seismic data highlighted areas with distinct highs and lows that were likely formed by salt diapirism (Figure 25-13). These same areas showed subtle anomalous variation in the amplitude.

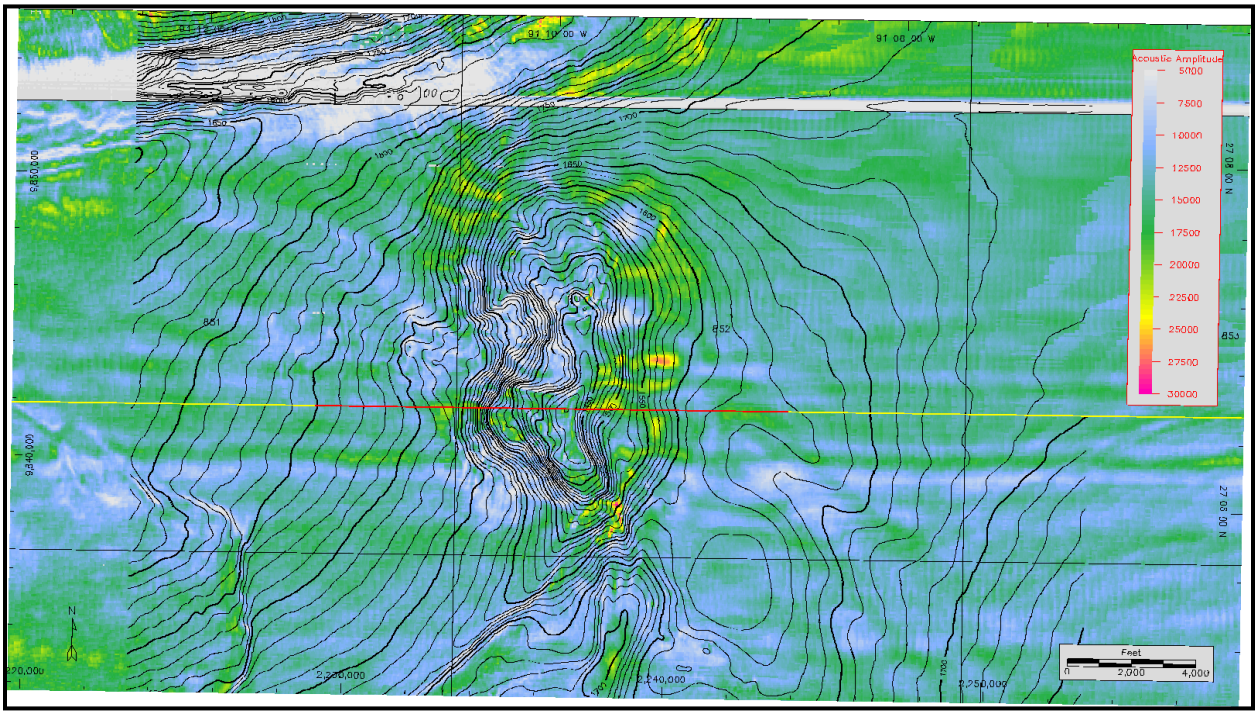

Figure 25-13. 3-D seismically derived bathymetric map with amplitude overlay (C.I.=10 m) used for selecting targets at site GC852; used by permission.

The GC852 site was one of the most diverse in the study. The primary area of interest was the north-south-oriented elongate mound that rises from the seafloor at the southeastern edge of a middle-to-lower slope suprasalt sedimentary basin. The top of this mounded region is at a water depth of approximately 1,435 m. The overall elongate-mounded area is approximately 2 km long, the highest elevation on this feature is at the southern end. This southern area is characterized by a localized mound that rises more than 20 m above the northern crest of the overall feature. The 3-D seismic surface reflectivity data indicate that the entire crest of this feature exhibits a high-amplitude response, suggesting the presence of hard-bottom conditions. Scattered highly reflective targets are also present around the upper flanks of the ridge-like feature. Profiles of the subsurface configuration of this feature indicate acoustically turbid

migration pathways to the modern seafloor. These vertically oriented acoustic "wipeout zones" are migration routes for fluids and gases to the modern seafloor. The structural and stratigraphic framework of the subsurfaces focuses these products (including hydrocarbons) to the GC852 mounded area.

This site lies on the southern extent of a steep-sided north-south trending elongated mound rising from over 1,500 to 1,395 m depth. This feature occurs at the southeastern edge of a well-defined sedimentary basin. The overall mounded area is approximately 2 km long with the highest elevation at the southern end. This area of primary interest is characterized by a localized mound that rises more than 20 m above the rest of this overall feature. The 3-D seismic surface reflectivity data from this area indicate that the entire crest of the elongated feature exhibits a high amplitude response relative to surrounding seafloor, suggesting the presence of hard bottom conditions. Scattered highly reflective targets are concentrated in the vicinity of the southern mound. Profiles of the southern end of the elongated mound indicate acoustically turbid migration pathways to the modern seafloor. These "wipeout zones" are interpreted as routes for upward transport of fluids and gases from the deep subsurface. Submersible operations confirmed the indicators of hydrocarbon seepage in this area. These operations were conducted on the crest of this feature in an area approximately 650 m north-south and 300 m east-west. The crest of the feature has extensive carbonate that appears to have been scoured by currents removing sediment from between 2–3 m high carbonate pillars.

Photo reconnaissance work in March 2006, as well as direct observations made later confirmed the presence of numerous chemosynthetic communities around the mounded area in the southern half of the study area. Tube worms, mussel beds, and carbonate outcrops are common around the flanks of the southern mound. Although the *Alvin* did not travel to the extreme northern end of the north-south trending overall feature, the photo reconnaissance indicated brine seeps and carbonates, but no chemosynthetic communities. At the apex of the southern mound, carbonate blocks and hardgrounds are common, and soft corals are taking advantage of the hard substrates as a place to attach and grow. Bacterial mats seem to be few and far between.

At the tops of the pillars are numerous types of corals: gorgonians, antipatharians, bamboo coral, and scleractinians (Figure 25-14), as well as numerous individuals of a globose soft-ball sized hexactinilid sponge, a few anemones, and a yellow zoanthid sp encrusting dead bamboo corals.

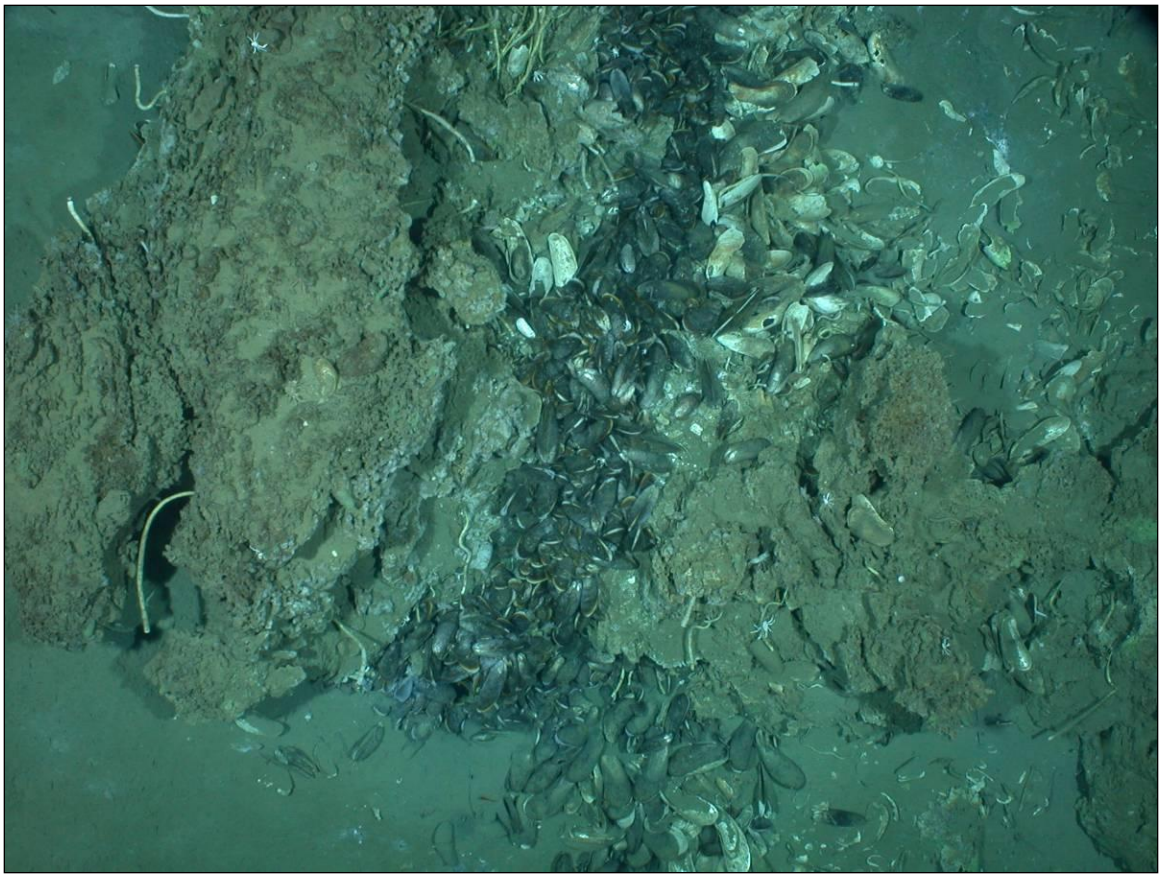

Figure 25-14. Chemosynthetic communities at theGC852 site comprised a series of features situated along a 1.5 km ridge line.

Numerous plumate polychates and hydroids were visible in macrophotos of the carbonates. The hard corals *Solenosmilia variablis* and *Madrepora oculata* was collected. A potential identification of *Lophelia pertusa* was also made from the photographic record, but this was never confirmed despite numerous collections. There was an unidentified species of chirostylid crab commonly associated with the soft corals and a species of ophionerid brittle star on the gorgonians (Figures 25-15 and 25-16).

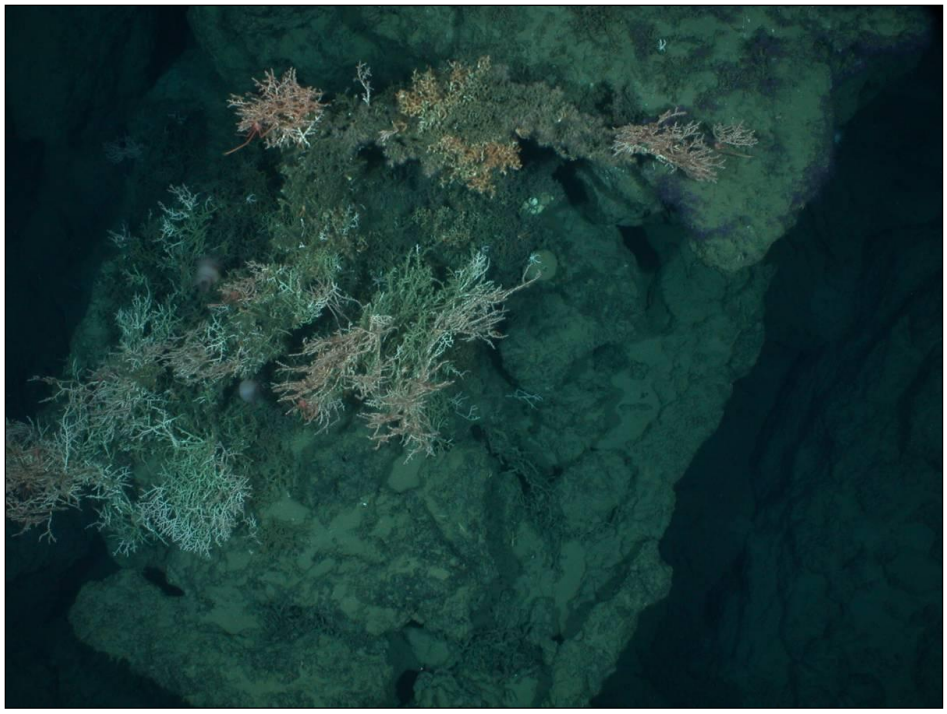

Figure 25-15. Northern portion of GC852 with massive carbonates colonized by scleractinian corals.

Figure 25-16. Soft corals included living octocoral polyps and dead skeletons colonized by zooanthids at GC852.

Also on top of the mound are some scattered tube worms and smaller carbonates and an area of active oil seepage. On the flanks of the mound were two areas of active seepage and authigentic carbonate. One feature is about 80 m to the northeast of the corals and consisted of low-lying cracked carbonate blocks, occasional methane bubble streams, and oily sediments. Aggregations of both species of tube worms, *Escarpia laminata* and *Lamellibrachia* sp., were collected here. Small mussel beds nested in carbonate (Figure 25-17) were comprised of *Bathymodiolus brooksi* and *B. childressi*.

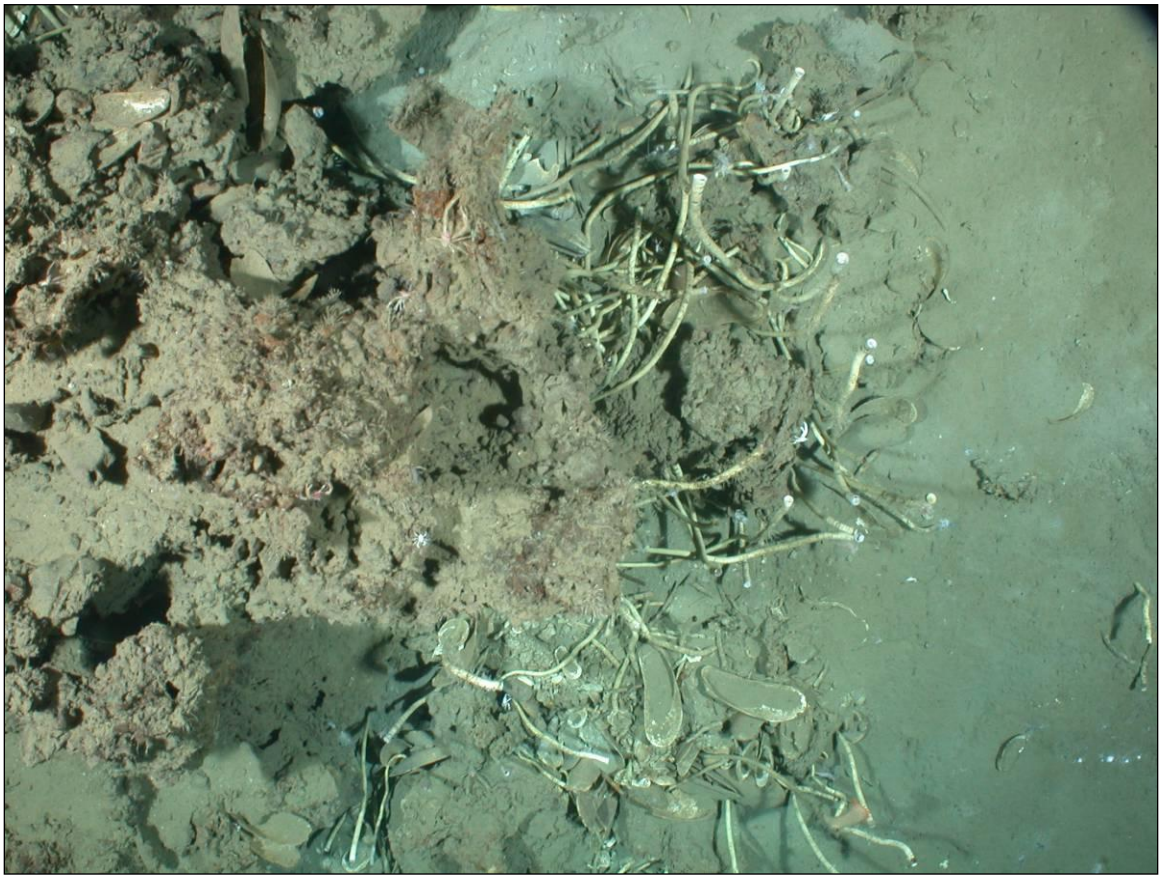

Figure 25-17. Tube worm colonies at GC852 were generally sparse assemblages attached to carbonate and cemented shells.

The most common seep-associated fauna were *A. muricola* and *O. acies*. Many of the *E. laminata* collected contained a species of phyllodocid polychaete, which is an apparent blood-sucking parasite. Dead tube worm tubes often contained this species and another polychaete filling their tubes. A second area of active seepage was found approximately 400 m to the south of the corals near the top of a ridge extending down from the other sites. The substrate in this area consisted of numerous small-to-medium-sized carbonate slabs and boulders and areas of carbonate rubble. Numerous transits between the two areas found only mud between the sites.

The same species noted above were present in the second area. The tube worms were present as scattered individuals as well as small aggregations associated with the carbonates and mussels were present in beds among the carbonates and in small groups apparently nestled in the

sediment. Vesicomyid clams were also present in this area, although none were collected. These collections extend the depth range of the common upper slope gastropod *Cataegis meroglypta*, the mussel *Tamu fisheri*, and the methane ice-worm *Hesiocaeca methanicola* to 1,400 m, and extends the geographic range of *S. variables* to the northeast from previous GoM records in the Straits of Florida.

Oil slicks were visible on the sea surface during much of the time *Atlantis* occupied this site. Streams of bubbles, probably lined with oil, were observed escaping through beds of mussels at several positions on the bottom. Gas hydrate was inferred from hard layers encountered while collecting push cores and was photographed in an exposed patch with the macro camera.

The background fauna at GC852 was generally rather sparse on mud bottom. On a transect from the southern to northern end only 3 possible holothuroids were observed. Mobile animals were largely restricted to rocky areas.

25.6. Mississippi Canyon 853

Latitude/Longitude: 28.125°N, 89.141°W
Depth: 1,070 m

This site (MC853) was not visited during the Recon Cruise, however it had been visited previously by *Alvin* in 2000 by Ian MacDonald. One *Alvin* dive, AD4178 was made at this site as part of this program. There were no *Jason II* dives at this site.

25.6.1. Site Overview

The MC853 site consists of an oblong northwest-to-southeast trending mound that rises over 100 m above the surrounding seafloor. It is located along the eastern margin of the Mississippi Canyon and the mound rises above the levee deposits that are a part of this regional geologic feature. The top of the mound has a water depth of approximately 1,065 m. The 3-D seismic surface reflectivity data over the mound area describe a pattern of highly reflective seafloor in the middle of the mound and scattered high reflectivity targets around the northwest and southeast parts of the mound top and upper flanks. Seismic profiles across the mound indicate a subsurface stratigraphic and structural configuration highly influenced by the presence of a large salt mass in the shallow subsurface. When viewed from the optimal perspective, it is apparent that the high-amplitude surface reflectivity zone in the middle of the mound is salt at or extremely close to the seafloor. Even though the salt blocks the migration of fluid and gas to the central part of the mound, there are numerous leak points along the edges of the salt mass. The center of the mound was characterized by hummocky bottom topography with brine seeps and associated gullies. Small slumps of mussels and areas of hard bottom with scattered bacterial mats are common to this region of the mound. Tube worms were generally absent from this area, although a few isolated tubes were spotted.

The dominant fauna at this site were mussels, clams, microbial mats and various fish. A few gorgonians (several of which were quite large) were also observed. One of the most interesting creatures we observed during the dive was a large, colorful siphonophore. Live clam tracks and empty clam shells were common. Microbial mats of the sulfide-oxidizing bacteria *Beggiatoa*

were observed on sediments characterized by intense seepage-derived staining (sediments beneath were black and reducing). Mainly, white mats were observed, but small patches of cantaloupe orange *Beggiatoa* was also observed (these were photo-documented during the dive). The light (cantaloupe) orange color of these *Beggiatoa* is interestingly different from the bright orange color that typifies *Beggiatoa* of the shallow slope. *Beggiatoa* mats occupied areas varying in size between tens of cm to m in diameter and mat localities were often co-inhabited by mussels. Numerous small fish were observed in the mat areas as well. Many of these fish were sitting in the sediment surface directly on top of *Beggiatoa*. In the laboratory, the *Beggiatoa* filaments were observed to be quite small (about 5–10 µm in diameter) compared to the giant *Beggiatoa* (>100 µm in diameter) commonly observed at shallow slope sites. During the dive, black streams from topographic highs were assumed to be brine flows, but geochemical examination of sediment cores back in the lab showed no evidence of brine (the pore water salinity at all sites was ~35). The microbial mats at this site are the most extensive and prolific of all the sites.

Numerous dense accumulations of mussels and clams were observed during most of the dive to this site. Several enormous specimens of *B. brooksi* were recovered. Clams (and mussels) were particularly abundant at the topographic highs. These huge pockmarks and carbonate banks seems to be areas of intense seepage, which supports dense accumulations of chemosynthetic fauna.

No tube worms were observed during this dive though tube worms have been noted previously at the site.

25.7. Mississippi Canyon 640

Latitude/Longitude: 28.357°N, 88.973°W
Depth: 1,410 m
This site (MC640) was visited during the Recon Cruise and on *Alvin* dive, AD 4182, took place at MC640. There were no *Jason II* dives at this site.

25.7.1. Site Overview

The Mississippi Canyon 640 (MC640) dive site is located on the upper continental slope, east of Mississippi Canyon and south of the modern Mississippi "birdfoot" delta. The overall feature is roughly circular in plan-view outline. At the top of this larger feature is a mound that rises roughly 15 m above the surrounding seafloor, which is at a water depth of 1,420 m. The 3-D seismic surface reflectivity data indicate variable patches of high- and low-amplitude responses over the area of the mound. This pattern suggests that the bottom will be covered with soft mud alternating with areas of seafloor hardgrounds, pavements, and other hydrocarbon seep-related carbonate blocks. Additional patterns of moderate seabed reflectivity describe linear patterns that originate from the mound and radiate from that point to deeper water areas surrounding the mound. These features are interpreted as fluidized sediment flows that originate from highly productive vents at the top of the circular mound-like feature. This type of geologic feature is usually indicative of rapid and episodic expulsion of fluids and gases. These rapid flux systems frequently are the sites of oil slicks on the sea surface. These slicks are usually visible in calm seas and from RADARSAT satellite images. Inspection of the seismic profiles across this feature

reveals a highly focused migration pathway from the deep subsurface. This subsurface configuration generally leads to rapid venting and the construction of mud mounds on the seafloor.

Drift camera reconnaissance tracks and direct observations from *Alvin* confirmed the variability of seafloor types at this site, reflecting the variations in patterns observed on the surface reflectivity maps. The surface of the mound displays scattered pockmarks and craters of varying sizes. The pockmarks and craters ranged considerably in size and content. Small depressions a m or two across and less than a m deep were usually filled with oxidized brown sediments no different than the surrounding bottom and contained no color or faunal evidence of seepage. Large depressions had sharp edges and were at least 10 m across (exact size hard to determine) and >2 m deep. *Alvin* could fit within these and still have limited room to maneuver. Large depressions usually had brine or bacterial staining to some extent at the bottom and on the flanks. This ranged from small irregular patches up to brine, bacteria, and mussels covering the entire floor.

Seep fauna seemed limited to mussel beds. Scattered articulated and disarticulated shells could be seen on almost all areas of the mound top and flanks. A smaller number of isolated live mussels were also observed away from chemically discolored sediments. Exposed carbonates on the flanks had scattered live mussels in clumps of a few specimens. Dense beds were found and sampled in two depressions. The mussel beds consisted of two species, *Bathymodiolus childressi* and *B. brooksi*. Size ranged from very large to a few mm. Both beds were associated with brine and stained sediments. Obvious mussel associated fauna was limited to white galatheids (not sampled) and a few small bracyuran crabs (sampled). No shrimp, gastropods, large polychaetes, or chirodotids were observed associated with the mussels. What appeared to be tube worms were reported from the Recon Cruise but were not encountered during the single *Alvin* dive to this site.

An unusual aspect of the brines at MC640 was the presence of a white “fog” layer about half a meter thick drifting above the brine surface. Niskin bottles were tripped, but the high mounting point on the sub may have precluded obtaining definitive samples. The fog may be a chemical precipitate or bacteria forming or growing in the seeping fluids. The walls of the depressions may be limiting advection and making the phenomena more easily observed (Figure 25-18).

The seafloor surrounding the mound and on non-seeping portions of the top was unusual in the high number of 2–3cm tubes scattered on the surface. These are probably amphipod tubes previously reported as abundant in the Mississippi Canyon area and interpreted by G. Rowe and reflective of Mississippi River high sediment influx. Megafauna consisted of species typical for the depth such as the white holothuroid *Mesothuria lactea*, *Chaceon* crabs, and a variety of eels and other fish.

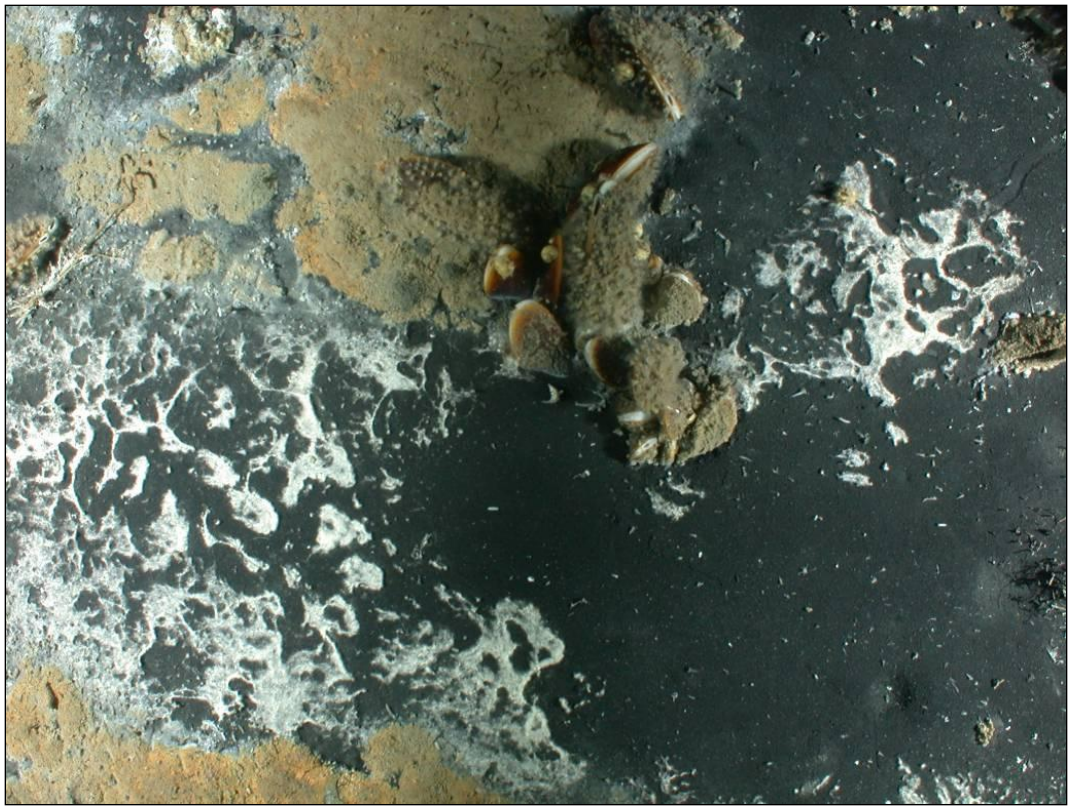

Figure 25-18. Extensive brine pools and flow channels supported bacterial mats and mussel colonies at the MC460 site.

25.8. Alaminos Canyon 818

Latitude/Longitude: 26.180°N, 94.623°W
Depth: 2,740 m

This site (AC818) was not visited during the Recon Cruise. This site was discovered during an industry ROV survey in connection with exploratory drilling at the site. There were two *Alvin* dives at AC818, AD4192 and AD4195, and two *Jason II* lowerings, J2-282 and J2-284. This site is about 50 m north of an exploratory drill site (wellhead left in place X555, Y 892).

25.8.1. Site Overview

The AC818 site is located seaward of the Sigsbee Escarpment and slightly to the west of Alaminos Canyon. The site is associated with the ChevronTexaco Tiger Prospect in a water depth of approximately 2,750 m. A wellhead is present in the vicinity of a well-developed chemosynthetic community discovered on an ROV survey of the immediate wellhead area. The regional geology of this region is that of a rather flat area of relatively low reflectivity on 3-D seismic surface reflectivity data. Immediately to the southwest is a highly reflective area of seafloor that corresponds to a submarine fan extending seaward and to the southeast from Perdido Canyon. This fan has very high surface reflectivity on 3-D seismic reflectivity data and is interpreted to be composed largely of sand. The chemosynthetic community site is located on a

regional fault that trends north-northeast to south-southwest. This fault is clearly defined in seismic profile data, but the location of the known chemosynthetic community, and perhaps others along the fault, are not well defined on surface reflectivity data. However, there are small and very localized reflective anomalies along the fault like beads on a necklace. The lack of seismic response is probably due to the small sizes of the chemosynthetic community sites. Direct observation from our first *Alvin* dive at the AC818 community site near the wellhead confirmed the localized nature of this assemblage of chemosynthetic organisms. The seismic data suggest that there should be a number of these small communities distributed along the fault.

Along a north-south fault, there is an area of diffuse seepage, as evidenced by sediment stains, pogonophorans, sea urchins, and a relatively small area with tube worms and mussels. It starts about 50 m north of the wellhead and stretches for about 50 m. After a short break, there is a second active smaller area north with two small mussel beds and one tube worm patch. Dive 4195 explored about 350 m north of the area covered during Dive 4192 and also south of the wellhead.

Sediment stain and some oil bubbling out were observed. This site has quite active seepage colonized by tube worms and mussels and is close to exposed carbonate. Carbonate sometimes forms overhangs and pits, with obvious bacterial stain.

Sea urchins were very common in the area where the sediment was stained (Figure 25-19). The snail *Phymorhynchus* was abundant on the stained areas. Beds of dead clam shells were also common. No live clams were observed, but five small live individuals were found in a mussel scoop sample collected during Dive 4195. The clams that were collected were a different species from *Calyptogena ponderosa* and appear to be the same as observed in the clam beds on the sea-floor. Tube worms (*Escarpia laminata*) are common in the central area (Figure 25-20), found close to mussels (mainly *Bathymodiolus brooksi* and a few *B. heckerae*) and spatangoid sea urchins. No *Lamellibrachia* sp. were observed on either dive. The sea-cucumber *Chiridota* sp. is very abundant in mussel beds. The shrimp collected were *Alvinocaris muricola* and a single specimen of a possibly new *Alvinocaris* species. Two species of brittle star were collected (*Ophioctenella acies* and *Ophienigma spinilimbata*).

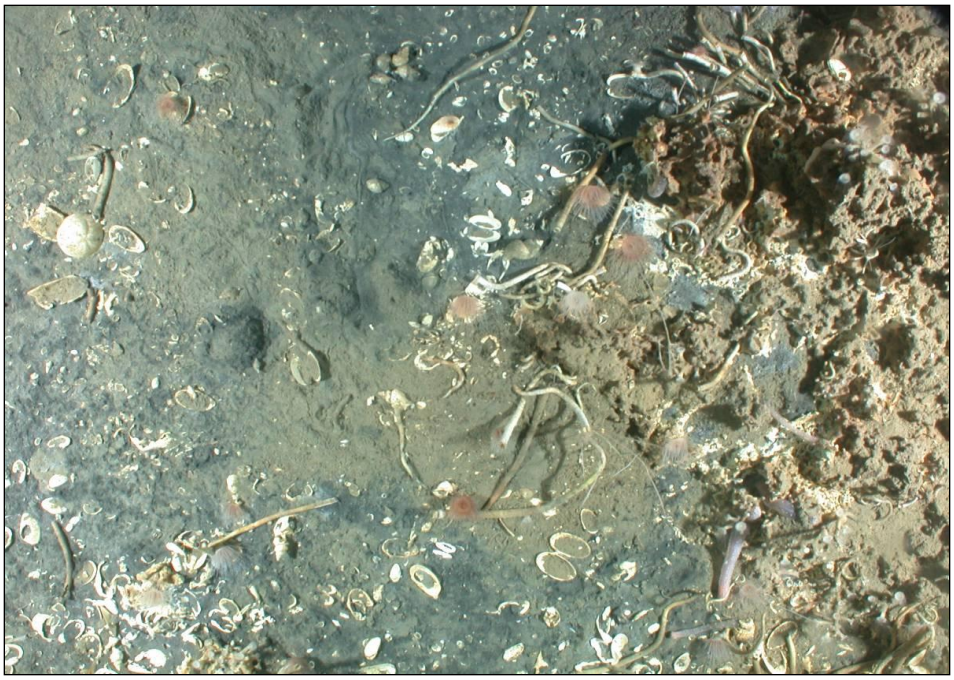

Figure 25-19. AC818 site featured extensive bacterial mats and hard urchin aggregations, but relatively few and isolated tube worm clusters.

Figure 25-20. Tube worms at the AC818 site were stained to study their growth rate.

25.9. Alaminos Canyon 601

Latitude/Longitude: 26.292°N, 94.514°W
Depth: 2,340 m

This site (AC601) was not visited during the Recon Cruise, but one of the brine lakes was discovered during ROV operations in the area by H. Roberts in 2005. There were two *Alvin* dives at AC601, AD4193 and AD4196 and one *Jason II* lowering, J2-283. The area was also mapped with the Hugin AUV.

25.9.1. Site Overview

Alaminos Canyon is a reentrant into the Sigsbee Escarpment at the base of the continental slope off western Louisiana-eastern Texas, slightly west of the longitude of the Sabine River. From the edge of the Sigsbee Escarpment, the Alaminos Canyon extends landward a distance equivalent to 6–7 lease blocks. Our dive sites in AC601 are located in approximately the middle of the canyon and toward the eastern side. Geologically, the sites are located on the top of a breached anticline that generally trends east-west. The base of the continental slope is a compressional environment forced by the sedimentary loading upslope. Compressional folding characterizes the strata underlying the Louann salt sheet that is being thrust out over the basin floor. The AC601 area of interest is stratigraphically above one of these compressional features that has been fractured and faulted. The fractures and faults that breach the crestal area of the anticlinal structure provide the migration pathways for transporting fluids and gases to the modern seafloor. The AC601 block is situated directly over the breached anticline crest and, consequently, there are a number of well-defined expulsion features in this block. The locations of these features are easily identified on 3-D seismic surface reflectivity maps. On subsurface profiles, clear migration pathways to the seafloor can be identified. There are four major reflectivity targets and a number of smaller targets in AC601. The primary anomaly of interest for this project is in the northwest corner of the block. It was mapped with deep tow side-scan sonar and subbottom data in the 1990s. It became clear from analysis of these data that the feature in the northwest quadrant of the block was a mounded fluid and gas expulsion feature with some evidence of mudflow activity radiating from the crestal area of the mound. More recent analysis with 3D seismic data indicates high reflectivity targets associated with the mound top and a low amplitude zone to the north of the mound. The high amplitude targets at the crest and on the upper flanks of the mound suggested lithification of the seafloor which usually indicates inactivity of fluidized sediment venting, an old feature. In 2005, an MMS-sponsored ROV survey confirmed the presence of chemosynthetic communities at this site. This survey also found that the low-amplitude zone to the north of the mound represented a sizeable brine lake. The brine lake was confirmed to be about 160 m in diameter with a salinity of about 90 practical salinity units.

There were several unique impressions of the biology of the brine lake and environs. The first thing noticed after crossing the shoreline and moving over the lake, was an abundance of pelagic sea cucumbers. However, many of these were swimming very slowly (even for a sea cucumber) and many others were not swimming at all. After poking a few, it was confirmed that many were simply drifting through the "fog." Occasional fish were seen in a similar state. An apparently drunk octopus was easily collected from the perimeter of this lake, apparently under the same influence as the other megafauna. The photo of this red octopus in the manipulator of the *Alvin* has been widely distributed, and is included on the cover of this report.

The first impression of the brine lake was that there was a clear interface and shoreline of brine, with flock aggregations of various sizes floating at this interface. Over that is a more amorphous layer that was refered to as fog. It looks almost smokey. In places, it is thick; in others, especially near some shorelines, it is almost non-existent. The brine below the visible interface is quite clear in some areas, and very cloudy in others. It is easily disturbed, as our "bow wave" is clearly disturbing the interface, even while moving slowly. After stopping to sample, *Alvin* got just heavy enough to settle on the interface, where it rested on the denser layer. From here the smokey layer could reach the level of the camera bar, but was sometimes below it (about 1.5 m thick). Looking out the port view-port, the interface normally could be seen, but it was sometimes in the murk. Divers noted no signs of hypersaline macrofauna living in the brine.

The shoreline, intertidal, and "beach" are shown in Figure 25-21. It is very similar in appearance to a beach, with areas of shell deposition, areas of what looks like sand and rocks, and areas of relatively clean beach. There are carbonates in the shallows that are only partially submerged in the brine. The brine on the "shorelines" is so clear that it is sometimes hard to see. The bathymetry of the shoreline is quite variable on different areas of the lake. On the east edge a "sand spit" was observed and the shallows extended for quite a distance. On the northwest edge, it was a relatively steep dropoff. In areas along the shoreline 10 m away from the pool (the north to northeast edges), an old shoreline (resembling a high tide mark) was clearly visible. Urchins could be seen and, what appeared to be pogonophorans, occasionally small mussel clumps, and very occasionally a few tube worms on the shoreline 5–10 m from the pool were also observed.

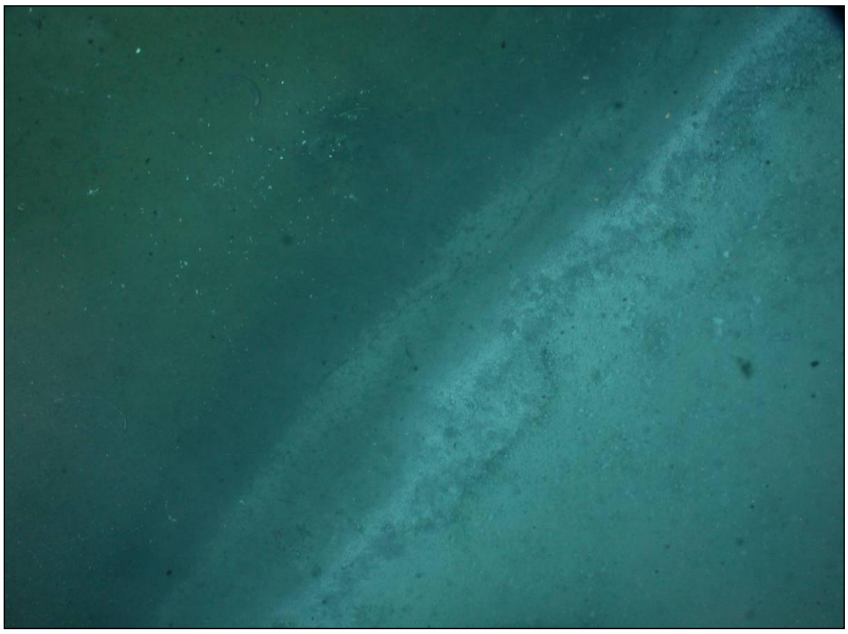

Figure 25-21. Shoreline of a brine pool, at AC601, which was approximately 150 m in diameter.

Upslope to the south, mud prevailed. The common pelagic sea cucumber was very abundant, feeding on the mud; 8–10 were often in view. Near the top of the ridge, the bigger species was moderately abundant with scattered smaller ones (3–4 in the field of view at a time). Near the

tops of the ridges, usually on the flanks, scattered exposed carbonates and tube worm clumps were observed. Many were isolated clumps without visible carbonates (one of these was collected, along with pieces of the buried carbonate it was attached to.) Many of the clumps were heavily colonized with attached fauna. They generally appeared quite old, but occasional smaller, non-encrusted aggregations were seen. No live mussels were seen on any carbonates outcrops in this area. The small area of "ridge" to the south did not seem to circle the pool, but it is a minor feature and the "ridge" was not very distinct. Quite a few scattered areas with a few nice tube worm clumps and associated communities and moderate sized carbonate outcroppings were observed (Figures 25-22 and 25-23).

Figure 25-22. Two species of shrimp and epifaunal octocorals on an *Escarpia* tube worm at AC601.

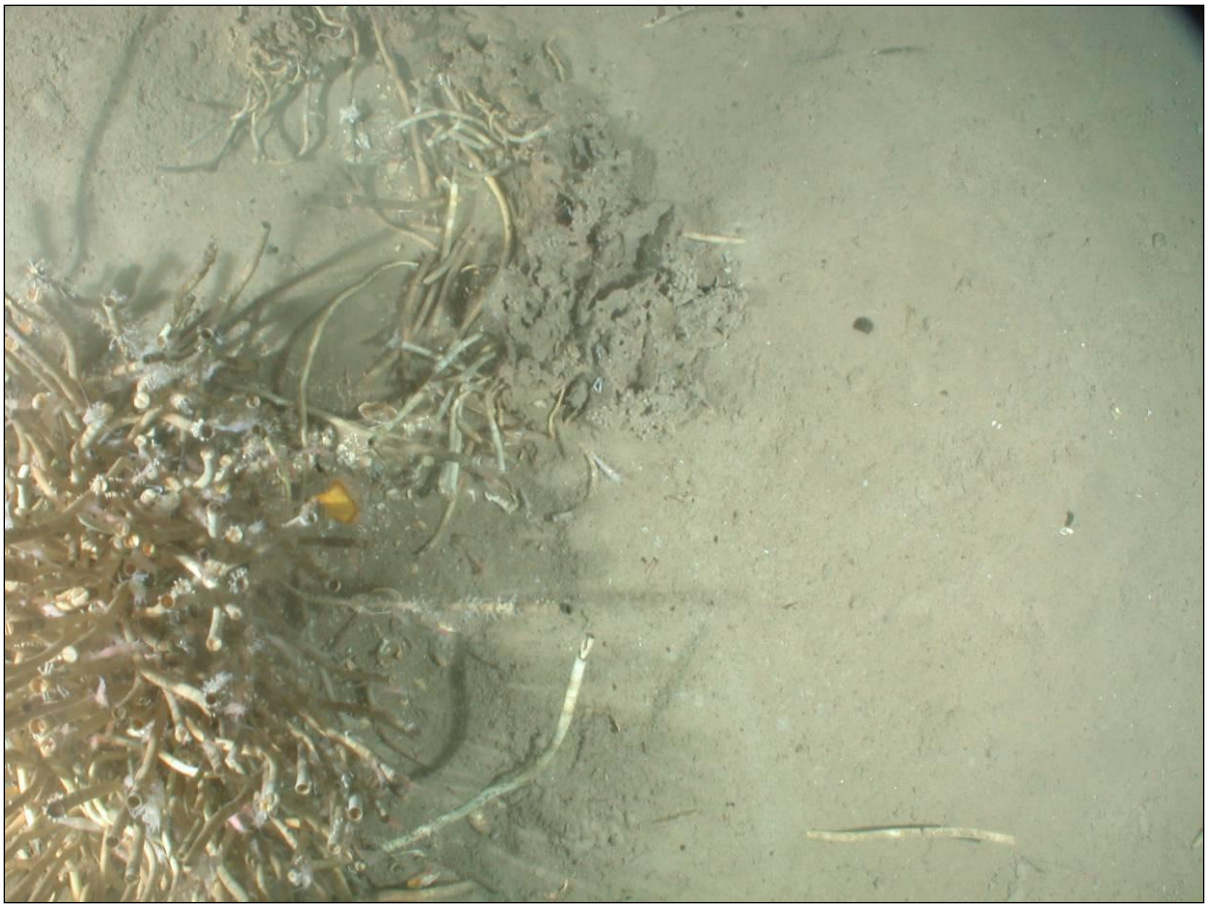

Figure 25-23. Typical chemosynthetic fauna at AC601 included isolated aggregations of tube worms and mussels.

During *Jason II* operations at this site, another large brine lake was discovered approximately 1.5 km to the south. This was nicknamed Lake Eerie by *Jason II* pilots. There were areas of extensive red stains in the area defined by the crater enclosing this brine lake. On one edge, the largest continuous bed of mussels yet encountered in the GoM was discovered. Non-seep fauna at this site was typical for the depth and dominated by elasipod holothurians. Ten specimens were collected. Fish were limited in numbers and crabs were not observed.

25.10. Alaminos Canyon 645

Latitude/Longitude: 26.354°N, 94.498°W
Depth: 2,200 m

This site was discovered in 1990 during an *Alvin* dive series led by James Brooks. It was again visited in 1992 during an expedition led by Ian MacDonald. Additional dives at this site were made here in 2003 during an expedition led by Robert Carney. In 2006, we made two *Alvin* dives at AC645, AD4194 and AD4197. In 2007 one *Jason II* lowering (J2-281) was made at this site.

25.10.1. Site Overview

This previously surveyed, well-documented location is a low, east-west trending ridge with topographic highs at the eastern and western ends (see Figure 25-24). It is in the same geological setting as its northern adjacent block AC601, which is described above. The AC645 site does not show evidence of flows or low amplitudes suggestive of high-flux, gas-saturated mud at the surface, just hard grounds and active subsurface migration on the seismic cross sections.

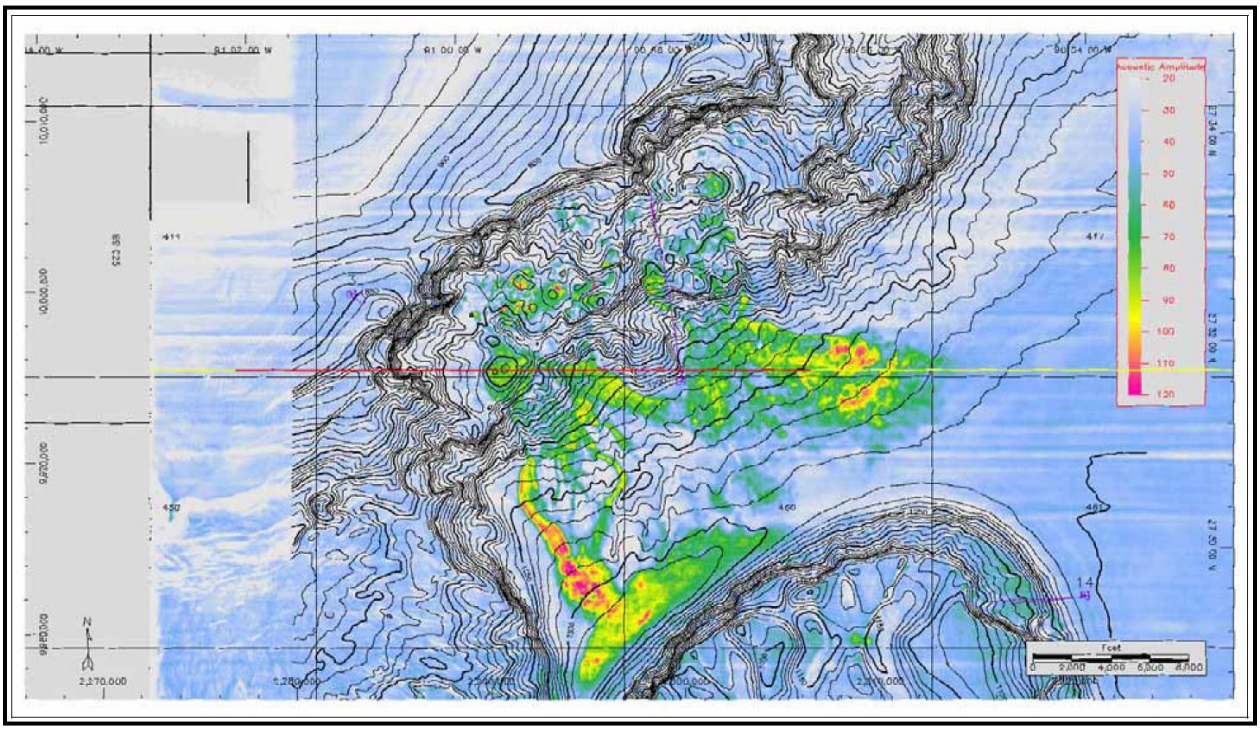

Figure 25-24. 3-D seismically derived bathymetric map with amplitude overlay (C.I.=10m); used by permission, Veritas.

The western mound identified on the seismic maps turned out to be typical deep-sea floor covered with light brown oxidized hemipelagic sediments and deep sea megafauna typical for this depth. Conspicuous megafauna included four holothurians (*Benthodytes typica, Benthodytes lingua, Euphronites* sp., and *Benthothurian* sp.) and a whip-like cnidarian. To the east of this mound is a western-facing slope with fractured carbonate pavement. Tube worms and mussels were abundant in this area among and adjacent to the carbonates, and sediments here were stained. Northeast of this area are additional carbonate fields and seep fauna. This area was the site of the 1992 dives and markers deployed during those dives in association with banded tube worms, other collections, and video mosaics are present here. Immediately downslope from this location, large expanses of normal deep sea sediments and fauna were encountered; however, in an area further downslope (identified as "Target 2" for AD4194), another area of carbonate with tube worms, live and dead mussels and dead vesicomyid clams was found. Limited exploration south, west, east, and north of this location did not detect any additional seep communities.

Areas with extensive coverage of pogonophorans were discovered near the carbonate hosted seep communities. There was a notable development of soft corals associated with many of the carbonate pavements and boulders. No hard corals were seen at this site.

25.11. Mississippi Canyon 462

Latitude/Longitude: 28.492°N, 88.883°W
Depth: 970 m

This site (MC462) was not visited during the Recon Cruise and there were no *Alvin* dives at MC462. There was one *Jason II* lowering (J2-271) at this site.

25.11.1. Site Overview

The Mississippi Canyon Block 462 (MC462) site is a relatively small potential seep site (~700 m by 3,000m) in 950 m to 970 m water depth, located just east of the Mississippi Fan complex. Compared to other areas of the deepwater Gulf of Mexico, there are relatively few sites in this immediate area that appear on seismic data to be actively seeping hydrocarbons to the seafloor and potentially supporting chemosynthetic communities.

The site has two distinct bathymetric features: a small, but prominent, mound and an adjacent crater (Figure 25-25). The mound has one small area of high positive acoustic amplitude response that suggested the presence of carbonate hard-grounds and/or gas hydrates. The crater has a larger and stronger positive response indicating thicker and more widespread hard-grounds/hydrates. The seafloor reflector on the flank and in the crater weakens and changes phase from a peak (hard spot) to a trough (very soft spot) in a couple of places, suggesting an active, high-flux vent site with soft, gas saturated mud.

The site was selected for investigation because of its depth and location and because the hard-grounds, if present, could provide a substrate for chemosynthetic organisms, as well as corals. The gas hydrates would indicate a steady supply of hydrocarbon to the surface sediments as a source of food for the organisms. The two features are different on seismic cross-sections. The high does not show active vertical gas migration (or, a gas chimney), whereas the subsurface expression below the crater does.

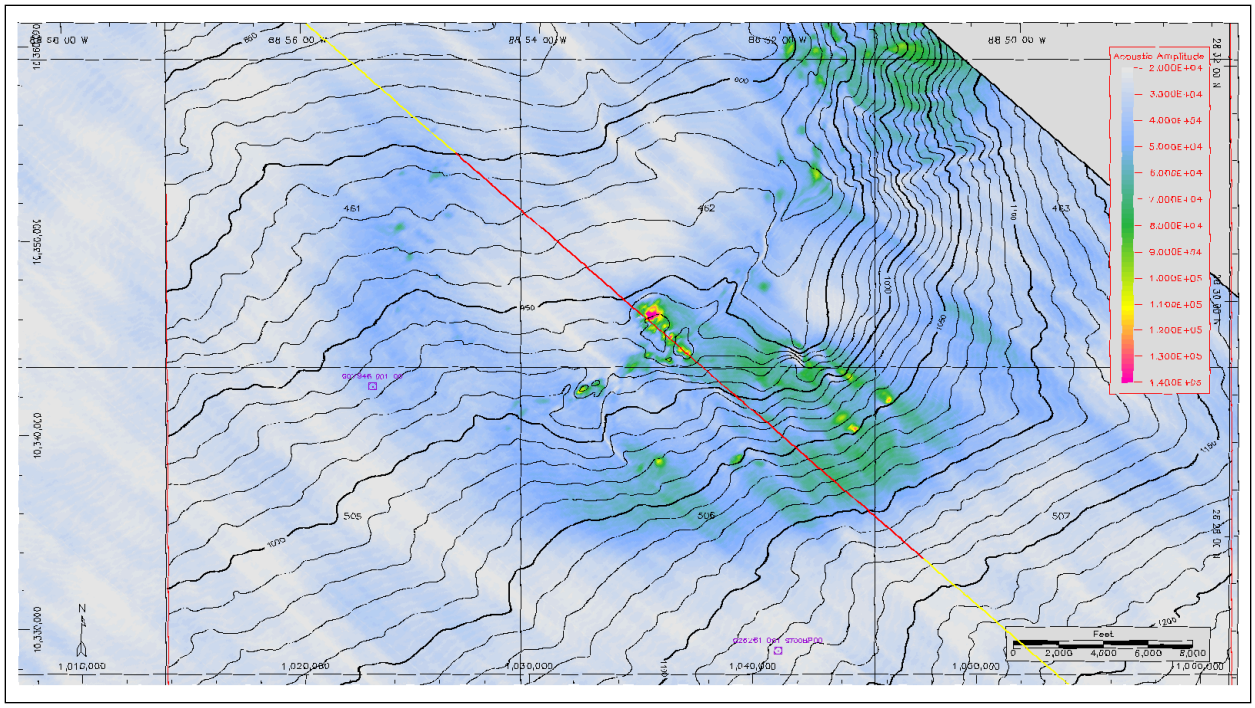

Figure 25-25. 3-D seismically derived bathymetric map (C.I.=10 m) with amplitude overlay used for target selection at site MC462; used by permission, TGS.

The surface character of the mound top and flanks appeared to be primarily burrowed hemipelagic mud. En route to Geo 3, we observed and logged a brine seep with a bacterial mat. Heading to Geo 6, we noticed a few outcropping carbonates with gorgonians on them. The bacterial mats (Figure 25-26) occurred at the base of a low-relief mound. The mound had a smooth surface with thin bacterial mats and evidence of small slope failures derived by fluid expulsion. When we disturbed the sediment, hundreds of gas bubbles, hydrate fragments, and oil droplets floated up into the water. We also saw yellow hydrate floating out of the disturbed coring area and layered gas hydrate in the areas we had cored. During coring, we noticed a few shells on the periphery of the bacterial mat. These were collected and turned out to be *Calyptogena ponderosa*, the same species of chemosynthetic clam that is on the upper slope. We did not find carbonates, mussel beds, or colonies of tube worms in the area. It is likely that the high reflectivity is from shallow gas hydrate under the sizeable areas of high surface amplitude.

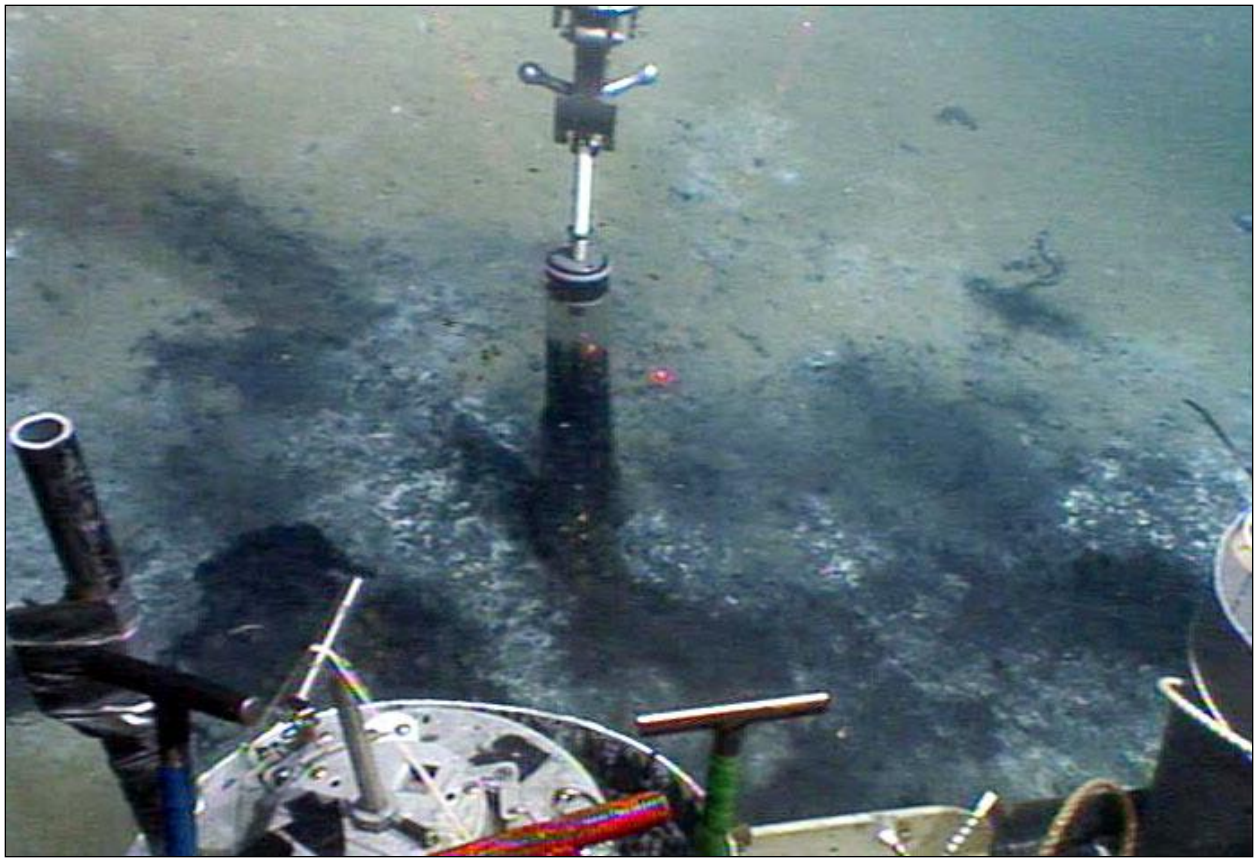

Figure 25-26. Collecting push-core samples in bacterial mat.

We collected several coral specimens in this area, including the colonial hard coral *Madrepora oculata*, a purple gorgonian, and a yellow octocoral. We also collected a piece of carbonate that contained two *Caryophila* sp. individuals, a solitary hard coral. Logged soft-sediment megafauna can be considered typical for this depth in the northern GoM. Rattails and eels were quite common, followed by the large white holothurian *Mesothuria lactea*. Less common were Geryoind crabs (red or golden crabs) and Lithodid crabs (cf. *Paralomis*).

25.12. Green Canyon 415

Latitude/Longitude: 27.528°N, 90.997°W
Depth: 1,000 m

This site was not visited during the Recon Cruise and the only submersible work was accomplished during a single *Jason II* lowering, J2-272.

25.12.1. Site Overview

Green Canyon Block 415 (GC415) is in an area of the GoM with extensive diapiric salt movement resulting in extreme bathymetric variation and common seepage of hydrocarbons to

the seafloor near the flanks of the salt. Extrusion of sediment along with the hydrocarbons from the subsurface out of many of these high-flux vents either builds mud volcanoes on areas of low slope or forms flows in areas of high slope. Oil slicks are very common, as are outcrops of gas hydrates and chemosynthetic communities around low- and moderate-flux sites. GC415 displays the geophysical signature of all these types of seep sites.

There are two separate areas with distinct geophysical characteristics at the GC415 dive site. The southern area is a large mound with moderately high positive amplitude response on top of a northeast-southwest trending bathymetric ridge supported by diapiric salt. Sediment flows extend down-slope for over 3 km and pond in the adjacent intersalt basin. The amplitude response is quite consistent across the mound. The northern area is broken up into smaller, discrete highs and lows with highly variable amplitude response. The small highs have the strong positive amplitude response of low- to moderate-flux seep sites and the intervening lows have the low positive background response of typical, non-seep hemipelagic mud. No flows are associated with the northern amplitude anomalies.

Before diving on this site, several members of the scientific party observed an oil slick over the dive site. This observation was considered a good indication that we would find chemosynthetic communities at the surface reflectivity targets established by analyzing 3-D seismic data from the area.

In the south area of the site, bacterial mats were the only notable seepage indicators. Since the area north of the initial dive site had many highly reflective, but small, targets, as determined from the 3-D seismic data, we expected these areas and their features to be much more productive in terms of hydrocarbon seep features and associated chemosynthetic fauna. We observed fish, bacterial mat, crabs, clams, and holothurians. A field of numerous pockmarks was present in the vicinity of Geo 5. They were impressively displayed on the forward-looking sonar.

There was a large bacterial mat at Geo 9. When cores were taken in the mat, they only penetrated about four inches and gas bubbles were released from the sea floor. Underlying hydrate was suspected. During the coring operations, a small area of about 50 cm^2 of brown fine grain “sediment” with “blue fuzz” around its perimeter was seen in the video. These resembled, and were later confirmed to be, a colonial ciliate in the family Folliculinidae, that is thought to have chemoautotrophic symbionts. The hand-held Cool Pix camera was used to take about 80 close-up images of these colonies, the bacterial mat, and the push core holes. It became apparent that this area was actually a thin carbonate crust, over four inches of sediment, overlying a buried hydrate.

Logged soft-bottom fauna were typical for this depth in the northern GoM. Rattails and eels were common but not notably abundant. Holothurians were dominated by the large white *Mesothuria lactea* although the purple *Paelopatides* was also present. Crabs were dominated by Geryonids.

25.13. Garden Banks 697

Latitude/Longitude: 27.282°N, 92.113°W
Depth: 1,010 to 1,280 m

This site (GB697) was not visited during the Recon Cruise and there were no *Alvin* lowerings at this site. It was selected for a study during the *Jason II* cruise because its geographic location represented a relatively unstudied area and the depths of the potential seep sites spanned a critical range of interest to explore the depth ranges of key faunal groups. There was one *Jason II* lowering, at this site, J2-274.

25.13.1. Site Overview

Garden Banks Block 697 (GB697) is in an area of active salt tectonism and oil and gas seepage along the flanks of salt diapirs and oil slicks on the sea surface. There are two main areas separated by about 3 km: the southern area is in ~1,280 m of water, and the northern site is ~1,010 m. The southern site is small and discrete and is just off the flank of a large salt-supported high. The northern site has several small, but bright, high-positive-amplitude anomalies along the top of the salt high that show, in seismic cross-section, clear hydrocarbon migration pathways to the seafloor (Figure 25-27).

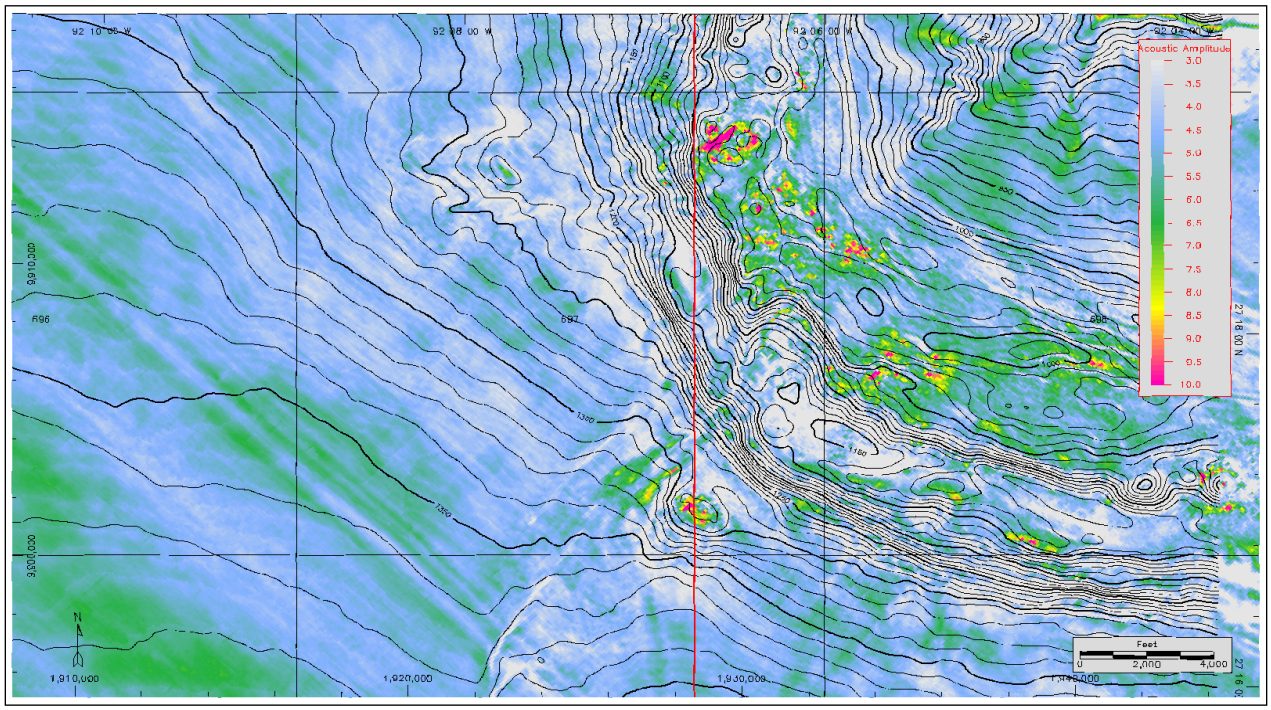

Figure 25-27. 3-D seismically-derived bathymetric map with amplitude overlay (C.I.=10m) used for selecting targets at site GB697; used by permission.

The primary dive site appears to be younger and more active than the sites on the large high. It has a clear gas chimney (a vertical migration pathway where all sedimentary bedding has been acoustically wiped out by vertical gas migration) emanating off the deep flank of salt that created

a small mound at the seafloor between the flank of salt and the adjacent mini-basin. The small mound has a strong positive amplitude anomaly on top and does not have seismic indications of sediment flows on its flank; the lack of flows suggests a moderate-flux site with just hydrocarbons seeping and possibly more conducive to chemosynthetic community development. The individual high positive amplitude anomalies at the second site are smaller than the first site, and are separated by areas of very low positive amplitude response, suggesting the presence of very soft, gas saturated muds (fresh flows?) or hemipelagic mud.

This site contained various indicators of active seepage including bacterial mats (Figure 25-28), a "Brine River" (Figure 25-29), carbonates, tube worms (*E. laminata* and *Lamellibrachia* sp. 1 and 2), mussels (*B. childressi*), and vesicomyid clams. The southern area, where we made one tube worm collection, was at about 1,270 m depth and one area with lush tube worm aggregations and a mussel bed was found and sampled. The more northern section contained a very active mud volcano with tube worms nearby. Tube worms and mussels associated with carbonates were collected from the same area about 1 km south of the mud volcano at 1,000 m depth. Vesicomyid clams and a species of soft coral we had not previously encountered were also collected from this area

Non-seep mobile fauna was typical for the depth. Holothuroids were dominated by the white *Mesothuria lactea*. Fish were common and diverse. Crabs included both Geryonids and lithodids.

Figure 25-28. Bacterial mat and chimney.

.

Figure 25-29. "Brine River."

25.14. Garden Banks 829

Latitude/Longitude: 27.178°N, 92.130°W
Depth: 1,300 m

This site was not visited during the Recon Cruise and there were no *Alvin* dives at this site. It was chosen primarily because of its depth at the transition zone between the shallow and deep seep foundation fauna and there was one *Jason II* lowering, J2-279 during our last cruise of the project

25.14.1. Site Overview

Garden Banks Block 829 (GB829) is located in the middle slope of the Central GoM (Figure 25-30). The target block is located along the southeast margin of a large minibasin that was formed from recent deepwater sedimentation (Miocene, Pliocene, and Pleistocene) and salt withdrawal. A series of seafloor amplitude anomalies are aligned along the eastern margin of the basin and are coincident with locally positive bathymetric features on the seafloor. The features are interpreted to be high-flux vents capable of extruding sediment and hydrocarbons, often resulting in the construction of mud volcanoes. The Magnolia Field (GB783), located approximately four

miles northwest of GB829, contains oil accumulations in Pliocene and Pleistocene turbidite sand reservoirs ponded near the southern margin of the basin.

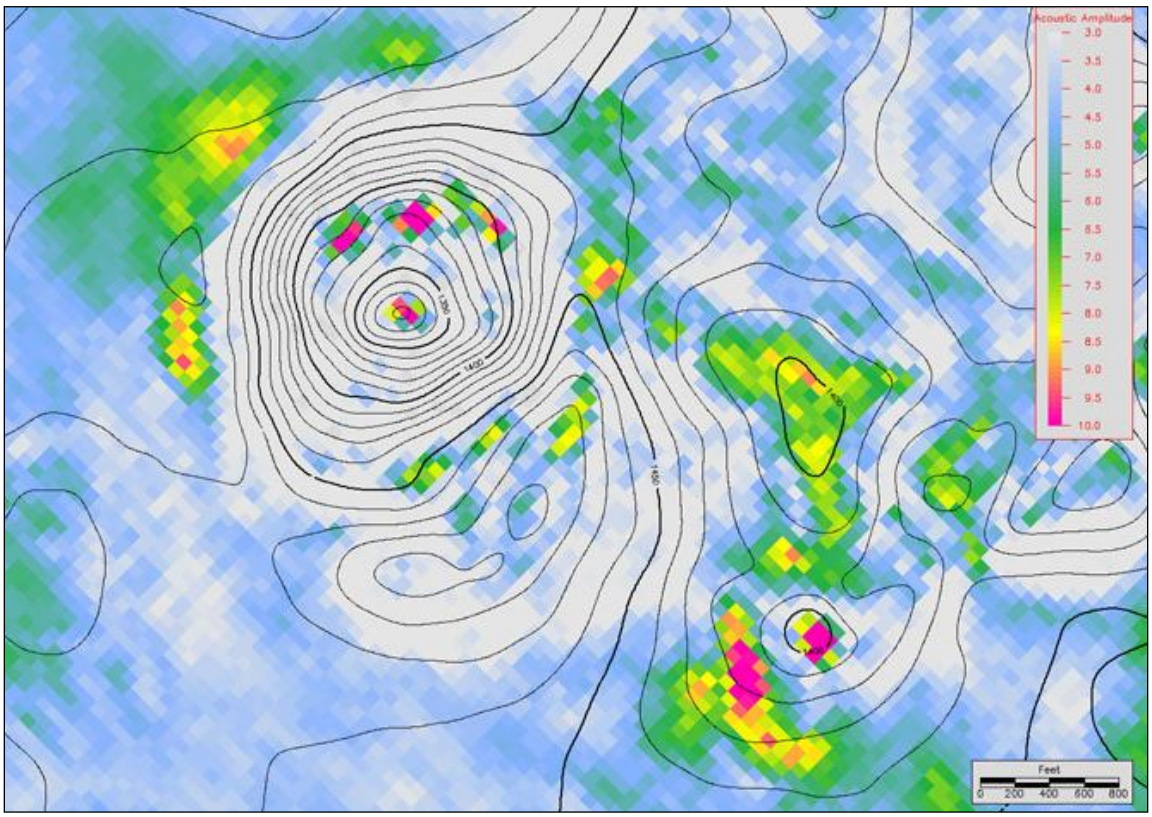

Figure 25-30. 3-D seismically derived bathymetric map with amplitude overlay showing the high relief mound, referred to as the "Christmas Tree," located on GB829; used by permission.

The northeast corner of GB829 contains several distinct mounds on the seafloor with a corresponding positive acoustic amplitude response. Three low-relief mounds on the southeast margin of the complex contain fairly widespread accumulations of positive amplitude returns. The high-relief mound (Figure 25-31) on the western margin of the complex (referred to as the "Christmas Tree") is the primary zone of interest, largely due to the unusually steep gradient (>40 degrees) and high vertical relief (130 m). A very small strong positive amplitude response is noted on the crest of the feature, and a few associated strong anomalies are noted on the north slope at the vertical midpoint. A weak positive response at the toe of the slope on the northwest side could represent a recent flow. The conventional seismic data beneath the Christmas Tree is wiped out, indicating an abundance of gas in the shallow

A dense mussel bed extending over approximately 3.5 m west to east and 2 m south to north was located on a slope near the expected location of the high reflector at a depth of approximately 1,260 m. The bed was also surrounded by briney sediments. About 140 m to the west-southwest, there is an area with abundant carbonate outcrops and associated tube worm aggregations and mussel beds. Additional tube worms and mussels were found at additional locations associated with carbonates on the sides but near the top of this feature.

25.15. Garden Banks 647

Latitude/Longitude: 27.333°N, 92.433°W
Depth: 1,000 m

This site was not visited during the Recon Cruise and there were no *Alvin* dives at this site. There was one *Jason II* lowering at this site (J2-280).

25.15.1. Site Overview

The Garden Banks Block 647 (GB647) site is in an area of Garden Banks where most of the subsurface production is more likely to be gas than oil and oil slicks are less common than to the east; therefore, seeps in this area are more likely to be gas than oil. Many of the salt diapirs in the area are relatively shallow, as is the case with GB467; salt comes within as close as 15 m to the seafloor, but averages ~250 m of sediment thickness above salt. Brine flows are, therefore, possible at this site.

The study area is the crestal portion of a northeast-southwest trending salt ridge that connects two large salt highs. It is in 950-980 m of water and is ~700 m wide by ~2000 m long; the entire ridge is 1,500 m by ~6,000 m. There are many small, discrete, and bright high-amplitude anomalies scattered across the top of the ridge; the ones chosen for exploration (Targets "Geo1 through Geo6") appear in seismic cross-section to have the best migration conduits below them, thus, are probably the most active (see Figure 25-32). Lithified flows on the flanks of the ridge are not apparent on the amplitude map. The CRP was located on an apparent local topographic highpoint slightly north of Geo Targets 1–6.

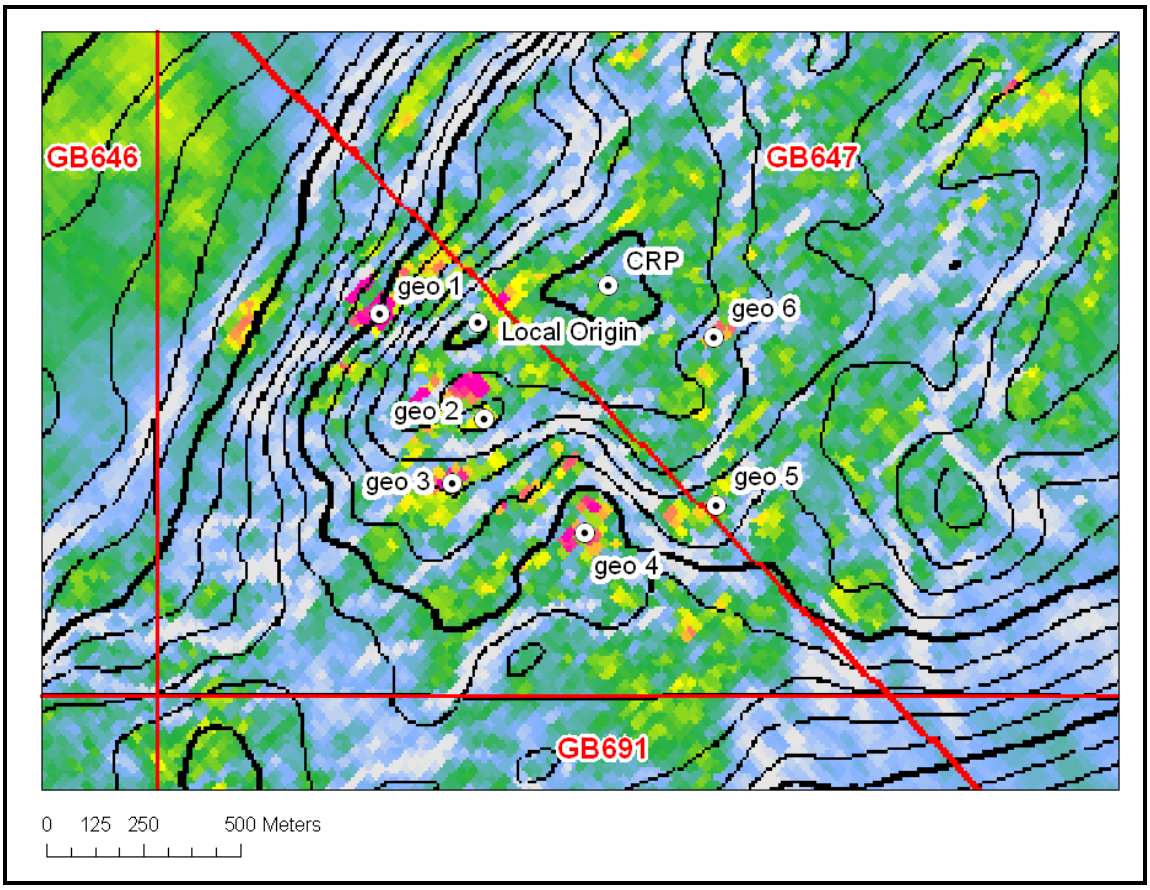

Figure 25-32. Target locations for site GB647 on 3-D seismically derived bathymetric map with amplitude overlay (C.I.=10 m); used by permission.

This area has characteristics in common with both GC852 and AT340. Like GC852, it is a prominent ridge exposed on two sides by open water and currents from the east or the west that could carry larvae and plankton for filter feeders like corals. Like AT340, there are a number of discrete sites with good indication in the subsurface of active hydrocarbon migration.

GB647 contained outcrops of both carbonate and asphalt and small mostly isolated tube worms (*E. laminata* and *S. jonesi*) in oily sediment. Gorgonians and sponges were observed attached to these outcrops and one was collected. When tube worms were collected from here, an oily tar/asphalt substance was dripping from the roots and the same substance floated up from the disturbed sediment. Bacterial mats were occasionally encountered and indications of briney flows were observed. The only *B. childressi* seen at this site were almost completely buried in the sediment at the base of one of the flows. Although present, both tube worms and mussels were quite rare at this asphaltic site.

26. EDUCATION AND OUTREACH

26.1. Summary: From SEAS to FLEXE and GLOBE

Outreach associated with the CHEMO III grant centered on developing and disseminating educational materials associated with grant research topics. Original educational deliverables for this project included the development (Phase I) of Classroom to Sea comparative labs delivered to secondary school students through the Student Experiments at Sea (SEAS) program with dissemination (Phase II) through teacher workshops offered through the COSEE-CGoM. Although support for the SEAS program ended in 2006, the concepts of SEAS were incorporated into a larger project, From Local to EXtreme Environments (FLEXE), a Global Learning and Observations to Benefit the Environment (GLOBE) project with an extensive dissemination network. GLOBE is an established web-based science education program with an international audience that includes over 17,000 schools and 1,000,000 students in 110 countries. FLEXE is one of four National Science Foundation-funded Earth System Science Projects of the GLOBE program and is developed in partnership with GLOBE personnel and The Pennsylvania State University College of Education faculty. FLEXE materials are pilot tested and disseminated through the extensive GLOBE network of Partners, Trainers, Teachers and Students worldwide. The educational philosophy of FLEXE is based on the same comparative approach of SEAS - to help students understand remote deep-sea "extreme" environments through comparison with analogous local systems. Materials initially developed under the CHEMO III grant for SEAS have been repurposed for use in the FLEXE program. Original timeframes for development and dissemination of these materials anticipated under the CHEMO III grant have been extended to fit within FLEXE timeframes and its development-evaluation cycle. Although work associated with the CHEMO III grant is complete, because of its incorporation into FLEXE, evaluation and dissemination of the materials continues as part of the FLEXE grant.

26.2. Background: FLEXE Overview

FLEXE is a web-based science education program for middle and high school students. As part of the worldwide GLOBE program, FLEXE engages students in learning activities and protocol-based investigations around a particular topic. Additionally, FLEXE features structured interactions between students engaged in scientific report-writing and peer review, as well as facilitated interactions with scientists around topic-related deep-sea datasets—a two pedagogical components of particular interest to GLOBE as part of their efforts to engage students in authentic science activities. Evaluation of the efficacy of these components (i.e., in terms of student learning, student understanding of the nature of science, and student interest in science) is central to the FLEXE grant.

26.2.1. Instructional Units (Energy and Ecology)

Two instructional units have been developed as part of the FLEXE project: an Energy Unit and an Ecology Unit. Both units have been designed around key Earth System Science concepts and are aligned with National Science Education Standards to ensure the widest possible applicability to classrooms. The Energy Unit focuses on the processes of energy transfer between components of the Earth system, a topic taught in most U.S. middle school curricula, and features the hydrothermal vent environment. The Ecology Unit features the ecology of deep-sea

chemosynthetic-based ecosystems–cold seeps and hydrothermal vents. Materials developed under the CHEMO III grant have been incorporated into this unit.

The FLEXE Ecology Unit topic include:

- Animal distribution patterns, and biotic-abiotic interactions in a deep-sea ecosystem
- Primary productivity, chemosynthesis and the importance of microbes in deep-sea ecosystems, featuring the discovery of the tube worm-microbe symbiosis
- Feeding adaptations in marine mussels and the importance of symbiosis
- Food web, trophic structure and succession in seafloor communities
- Biodiversity patterns in seafloor communities

Additionally, students learn important nature-of-science concepts, including understanding the difference between correlation and causation, that scientific discoveries build on previous research, the importance of protocols in data collection, and how to develop research questions and hypothesis testing.

26.2.2. Testing and Evaluation

Testing of the FLEXE Energy Unit is complete. Evaluation of this unit focused on understanding the effects of class-to-class partnering and student-to-student peer review. Formal evaluation of student learning outcomes (through argumentative discourse analysis of student writing samples and embedded surveys) is on-going, although preliminary results have been reported by Steve Kerlin in a poster on Design of an Online Global Learning Community presented at the 8th International Conference on Computer Supported Collaborative Learning in June 2009. The Ecology Unit was tested with teachers and students. Evaluation emphasis of this unit will be on the effect of the FLEXE Forum on student learning and attitudes towards science. Evaluation results will be presented in the final report.

26.3. CHEMO III Education Outreach Phase I: Development

Three comparative lab and learning activities were developed as part of the CHEMO III project.

26.3.1. The FLEXE Mussel Lab: Adaptation and Symbiosis

Deep-sea mussels are a foundation species in the cold seep environment and are one of the key study organisms of this project. As described in previous reports, a Classroom to Sea Mussel Lab has been developed to engage students in a comparison of shallow-water mussels to deep-sea mussels, in particular focusing on adaptations in feeding strategies in both environments. The intention of the lab is to guide students to a better understanding of the mechanism of symbiosis and the significance of this adaptation in the deep-sea environment. The lab has been incorporated into the FLEXE Ecology Unit and serves as the basis for a FLEXE Forum. Beginning with a basic lesson on mussel taxonomy and anatomy, students follow a scientific protocol to measure mussel gill size in shallow-water mussel species, and then compare their data to deep-sea mussel data obtained using the same protocol. Data from dissections of vent mussels (*Bathymodiolus thermophilus*) and cold seep mussels (*B. brooksi*) are provided to students along with Field Notes describing at-sea dissections, collection techniques (e.g., Mussel

Pot vs. Scoop) and the broader research questions associated with the CHEMO III project. At the completion of the Mussel Lab, students engage in a FLEXE Forum with Dr. Nicole Dubilier, responding to questions about the lab and receiving feedback on their analyses and on the possible evolution of this feeding adaptation. Dr. Dubilier will also emphasize the significance of multiple symbionts in seep mussel species. This FLEXE Forum is scheduled for March 2010 as part of the FLEXE Ecology Unit pilot.

26.3.2. Biodiversity in the GoM Cold Seep Environment

Understanding biodiversity patterns is an important objective of this grant, as well as most ecological research. As described in previous reports, a Classroom to Sea Biodiversity lab was envisioned to provide students with techniques for determining biodiversity in their local environment and then challenging them to compare their results with deep-sea biodiversity data. Because of difficulties inherent in comparing diversity in widely differing environments, we have instead developed a FLEXE learning activity that teaches students about the challenges of sampling and determining true diversity, and invites them to interpret deep-sea biodiversity data (i.e., rarefaction curves from the GoM environment) as part of a FLEXE Forum Exchange. To give students some hands-on experience, we have developed a class simulation exercise using GoM Cold Seep Community Cards (see Appendix 10 for full description). The Cold Seep Community card simulation was developed to 1) introduce species within the GoM seep ecosystem, and 2) give students experience developing species accumulation curves based on sampling from the deck of organism cards. Following the simulation exercise, a FLEXE Forum with Dr. Erik Cordes engages students in analysis of seep biodiversity data and features sampling (e.g., Bushmaster collections) and sorting techniques used to measure biodiversity. The rarefaction curves reveal patterns of low biodiversity in seep tube worm and mussel communities compared with background communities, but high biomass in these communities relative to the sediment community. Through the FLEXE Forum, students learn that these patterns are likely due to the rich (but toxic) energy source (i.e., chemicals for chemosynthesis). This FLEXE Forum is scheduled for testing in April 2010 as part of the FLEXE Ecology Unit pilot.

26.3.3. Trophic Structure and Cold Seep Community Succession

Another central question of the CHEMO III research involves understanding successional patterns in the GoM cold seep environment. To help students understand this topic and feature research associated with this grant, we developed a multipart FLEXE Learning Activity in which students first explore local and deep-sea food webs, and then examine trophic structure changes in cold seep communities of different successional stages. The activity uses the GoM Cold Seep Community cards and community succession data from Dr. Cordes.

After creating local food webs, students explore hydrothermal vent food webs using the NOAA Ocean Explorer Multimedia Discovery Mission http://oceanexplorer.noaa.gov/edu/learning/welcome.html. Next, to understand seep community successional patterns, students again use the GoM Cold Seep Community cards, sorting their subset of cards by trophic level and then comparing the proportion of each trophic level to data from the cold seep environment. In general, students see changes in the community of organisms associated with tube worms. They observe that primary production (excluding tube worms) declines and the proportion of higher order consumers increases as tube worms age and the

associated community undergoes succession. This FLEXE Learning Activity is part of the FLEXE Ecology Unit pilot and will be tested with students in spring 2010.

26.3.4. The Rust Lab

As described in earlier reports, a third Classroom to Sea lab, The Rust Lab, was designed to feature the concept of oxidation and its importance in the deep-sea environment. CHEMO III Teacher-At-Sea Cynthia Petersen helped develop the lab while at sea in 2006 and then tested the protocol with her students at St. Hubert's Catholic School in Chanhassen, MN. The lab protocol instructs students to test oxidation patterns on various metals and to explore various techniques to measure rust. At this time, the Rust Lab is not planned to be incorporated within a FLEXE unit, primarily because it does not fit within an instructional unit. It is possible that the lab may be adapted for dissemination through another venue.

26.4. CHEMO III Education Outreach Phase II: Dissemination

Phase II of the project involves dissemination of the materials, primarily through teacher professional development. Originally, dissemination of materials would be accomplished through a teacher workshop for 20 teachers, offered through the Centers for Ocean Science Education Excellence: Central Gulf of Mexico (COSEE-CGoM). By incorporating this project into the FLEXE project and timeframe, we have enjoyed a much wider dissemination through the GLOBE network and have conducted two teacher workshops through the COSEE-CGoM.

As described in previous reports, we worked with COSEE-CGoM personnel (Dr. Sharon Walker and Dr. Shelia Brown) to recruit teachers from the GoM region and to help arrange workshop logistics (i.e., meeting facilities, lab space, food and lodging for teachers). Because the Ecology Unit was not yet available in 2008 and we had initiated plans for a COSEE-CGoM workshop that summer, our first workshop introduced FLEXE to teachers in the GoM area and focused on the FLEXE Energy Unit featuring the hydrothermal vent environment. Dr. Ian MacDonald was the guest scientist, giving presentations on the deep-sea environment and helping with learning activities. NOAA Ocean Explorer activities on hydrothermal vents and related topics were also presented at the workshop to the 22 participating teachers.

We held a second workshop in July 2009 with 20 teachers and introduced the FLEXE Ecology Unit, with Dr. Erik Cordes as guest scientist. This workshop introduced teachers to the GoM cold seep environment and the work of this CHEMO III project. NOAA Ocean Explorer activities and multimedia discovery modules were also introduced and explored during the workshop. Costs for both workshops were shared by the FLEXE and CHEMO III grants. Both workshops were very well received (in 2008: 73% rated course Very Valuable, 22% Valuable; in 2009: 68% rated course Very Valuable, 31% as Valuable). Additionally, six teachers from each workshop participated in that year's pilot. Workshop objectives, agendas, participant lists, and evaluation results are in Appendix 11

In addition to recruiting teachers through the COSEE-CGoM workshops, we have used the existing GLOBE network to disseminate the FLEXE project. This includes presenting during GLOBE Partner and Trainer Trainings (August 2008), and GLOBE HelpDesk support to distribute project announcements and pilot invitations through their extensive Internet network. For the current FLEXE Ecology Unit pilot, 28 teachers in the U.S., 1 teacher in Canada, 1

teacher in England, 1 teacher in Costa Rica, and 15 teachers in Thailand will be participating, with a total of approximately 1,600 students.

26.5. Supporting J.L. Scott Marine Education Center

The J.L. Scott Marine Education Center suffered tremendous loss due to Hurricane Katrina, including the loss of all teaching specimens collected over the years. In addition to supplying workshop teachers with educational resources (e.g., books, DVDs) and specimens, such as tube worm tubes and mussel shells, we have given extra specimens and resource books to the J.L. Scott Marine Education Center whenever possible. Dr. Cordes also arranged to meet personnel from the J.L. Scott Marine Education Center at the ship to transfer recently collected extra specimens to the center for educational purposes.

27. SYNTHESIS AND FUTURE DIRECTIONS

27.1. Remote Detection of Chemosynthetic and Other Significant Hard-Bottom Communities

The site selection methodology used in this project has proved to be extremely successful in finding areas in deepwater that are potential habitats for deep-water chemosynthetic communities, as well as for other hard-bottom fauna such as corals. The success of our site-selection process was directly linked to the enormous database of 3-D-seismic data held by BOEM in their New Orleans office. Working directly with BOEM geoscientists and using this database to select potential study sites based on seabed reflectivity and sub-bottom profiles proved extremely efficient for choosing cross-slope and along-slope sites for investigation. Many more potential sites were identified than it was possible to investigate directly using deep submergence assets. Combing this primary information with the large geochemical coring database at TDI Brooks allowed further refinement of our site selection, as this database provides direct information on presence of hydrocarbons in the seafloor sediments. A third piece of important data for identification of especially actively seeping sites was the use of Satellite SAR data to identify persistent natural oil slicks on the sea surface and narrow down source areas for these slicks to a few square km (see Section 7). By using all of these remote data, we were able to select a subset of about 100 potential sites for consideration. We narrowed these down based on the need to sample over a wide geographic and bathymetric range. We then added additional information to our site selection process using a very cost-effective approach of photographic imaging of the sea floor with a drift camera (see Section 8). From these data, six new sites were identified as harboring chemosynthetic or coral communities and targeted for more intensive submersible investigations. We ultimately used a combination of the images from the drift camera and the 3-D seismic data sets to plan our first set of dives which were 100% effective in locating at least some chemosynthetic megafauna on the sea floor (see Section 10).

Prior to our second submersible cruise, it became evident that investigation and sampling of additional sites in the 900–1,200 m depth range would be critical to understanding the bathymetric distribution of the foundation fauna species (tube worms and mussels) and their associated communities. We returned to the 3-D-seismic database and, without additional sea-floor imaging but based on what we had learned from our ground-truthing of the original site selection process, selected five sites in this depth range for *Jason II* survey dives. Of these sites, three proved to harbor chemosynthetic tube worm and/or mussel communities; vesicomyid clams only were found in the 4th and at the 5th sites. The only biological expression of seepage found on the sea floor were bacterial mats and a presumptive symbiont-containing colonial ciliate (Section 10). In short, it is possible to predict with high confidence the occurrence of chemosynthetic communities using the extant high-quality datasets available for the GoM. With additional reconnaissance drift camera or other remote imaging of the seafloor, one can predict with even greater certainty the occurrence of lush and potentially significant chemosynthetic communities. We continue to work towards refining identification of significant coral communities from remote data.

27.2. Seep Macrofauna

The project used a variety of different approaches to characterize the communities on the sea floor after the site selection process had identified the dive sites. Although one of the primary goals was a quantitative comparison among sites, this proved to be unrealistic because of the time constraints for appropriate sea floor activities. Our primary approach for quantitative site comparisons was photographic sampling from randomized transects. We tested the use of 10 randomized transects of 100 m length per site to collect the data for quantitative comparisons among sites. Although we developed very efficient methodology for this approach, especially using *Jason* II, even when transect areas were constrained to boxes 1–300 m on a side with the highest local abundance of chemosynthetic or coral communities, this approach was reliable only for abundant features, such as carbonate rubble and bacterial mats. Statistical evaluation of the power of this approach indicated that it is reliable for such abundant features, its power for detection and quantification of very patchy and less abundant community types (such as mussels, corals, and tube worms at most sites), is low. However, this general approach remains a valuable potential tool for site verification purposes, such as the detection of bacterial mats or even a single sighting of chemosynthetic megafauna that represents critical information for site selection. Nonetheless, we were very successful in qualitative characterization of the sites as is clear in the site summary sections of this report.

Quantitative data on community composition, which allowed statistical examination of variation on large geographic and bathymetric scales, was efficiently obtained using the Bushmaster, mussel pot, and lined scoop-net collection devices (see Section 14). The use of high-resolution imagery collected at high density over marked areas of the sea floor allowed description of megafaunal patterns at an intermediate scale. More important, the assembly of mosaics established study sites that can continue to be revisited to examine natural temporal change in the communities and also effects of human perturbations to the water column or sea floor (see Section 15).

The use of molecular tools to identify the foundation tube worm and mussel fauna proved more valuable than expected. Analysis of what originally appeared to be three easily distinguishable morphospecies of *Lamellibrachia* has initiated a Ph.D. thesis to further examine the very high level of genetic similarity between the shallow dwelling *Lamelllibrachia luymesi* and the deep dwelling *Lamellibrachia* sp nov 1 (while confirming another new species, *L.* sp. nov. 2) (see Section 12). Similarly, the three previously-known species of *Bathymodiolus* from the GoM proved to be quite difficult to distinguish based on morphology alone and both site occurrence and the depth distribution of these species were altered after the results of molecular analysis of over 100 samples (see Section 13). Completely unexpected and exciting was the very recent discovery of a new cryptic species of *Bathymodiolus* at a site visited as part of the *Lophelia* II project in 2009.

Although the primary goals of this project necessitated extensive exploration and visitation of numerous sites, we were also able to conduct a number of process-oriented studies and analyses and have made excellent progress towards a holistic understanding of the ecology of cold seep communities in the deep GoM. The community collections acquired as part of this study have nearly doubled the total number of quantitative samples of seep communities of the GoM (see Section 14). This sampling effort has provided the opportunity to examine whether some of the

trends that were well established in the upper slope communities were more broadly applicable to the full depth range of seeps in the GoM. Our analyses of the mosaics are consistent with successional community changes predicted from upper slope studies; however, the time spans of 1 to 17 years between analyses is not sufficient to directly confirm these trends in these very long-lived communities. From our community collections of mussels and tube worm aggregations, the clear pathway of succession documented for the upper slope communities was not as evident in the seeps of the lower slope. This is likely in part a reflection of the paucity of collections of clearly young tube worm aggregations, and in fact their rarity at the sites we visited on the lower slope was among the more surprising findings of the study. The lack of a consistent pattern of community change with age in the tube worm aggregations may also reflect the fact that our lower slope data set is partially confounded by its great spatial and bathymetric coverage and we have not intensively sampled individual sites in the way that we did to elucidate these patterns on the upper slope. What is clear from our data is that the tube worms are very slow growing and live at least as long as they do on the upper slope (centuries, Section 16), and the mussel communities appear to be long lived as well (although this observation for mussels is not well constrained and based largely on revisitation of AC645, originally surveyed in 1989). Identification of deep-water sites analogous to the Bush Hill, GC234 and GC232 sites on the upper slope, where tube worm aggregations and mussel beds of a range of ages are abundant, would facilitate a more rigorous examination of the applicability of the upper slope succession hypotheses to the lower slope.

The collection of a comparable number of communities from the lower slope in this single study also afforded the opportunity to examine bathymetric trends in community composition, abundance, biomass, and diversity (see Section 14). Previously, the limited number of samples from the communities below 1000 m prevented a rigorous examination of these trends. If the general patterns of the deep sea were reflected in the seep communities, a decline in abundance and biomass, along with a mid-slope diversity maximum, were expected. Instead, there was no decline in abundance or biomass in the communities, and a more complicated picture of diversity appeared. In the tube worm communities, the highest diversity appears at upper slope depths due to the colonization by background species of the benign habitats of the later-stage tube worm aggregations. This level of colonization is not apparent in the deeper tube worm aggregations, either because the habitat chemistry does not change as dramatically over time as it does on the upper slope, or because there are simply fewer background species to colonize the seep habitat. In mussel communities, the trend is the opposite, with the lowest diversity measured in the upper slope communities. This is likely due to the high levels of methane and low oxygen generally found in upper slope mussel beds, which would limit community composition to seep endemic species. Diversity in the lower slope mussel beds is comparable to or higher than the tube worm communities in the same depth ranges, with a slight mid-slope diversity maximum observed in the mussel-associated communities. The diverse metabolic capacities of the mussels of the lower slope, which often include multiple strains of symbiont within a single individual, combined with the diversity of mussel species on the lower slope, may explain this elevated diversity in the associated community. This study allowed clear demonstration of the patterns of biomass and diversity of the chemosynthetic communities on the lower slope as well as description of the fauna. However, teasing apart the confounding variables that are behind the patterns documented will require additional study of the lower slope.

Another question addressed by several components of the study was the impact of seep primary production on the local non-chemosynthetic fauna and surrounding deep-sea communities (Section 17). This was addressed primarily by the analysis of tissue stable isotopes. On the first order, this is facilitated for chemosynthetic communities by the very different carbon, nitrogen, and sulfur signatures of seep primary production (compared to surface production). However, analyses of the data sets collected for this project turned out to be unexpectedly complex on the lower slope because of the very wide range in primary producer values evidenced in the symbiont-containing species of tube worms and mussels. Detailed analyses and interpretation of the tube worm and mussel stable isotope values are given in the relevant portions of Section 17 and are not repeated here. Despite this variability, the bulk tissue stable isotope data provided significant information on the overall nutritional patterns within the benthic communities studied, and exchange with the general background fauna. Like on the upper slope, the gross majority of the macrofauna and megafauna closely associated with mussel beds and tube worm aggregations derive the overwhelming bulk of their nutrition from seep primary production. Only a few of the larger mobile fauna found in proximity to the seeps exhibited evidence for high levels of incorporation of seep organics in their tissues (Section 18). Significant in this regard were predatory asteroids, which may exert considerable predation pressure on mussel beds of the deep slope. The lack of a clear signal in holothuroids collected in the vicinity of seeps was surprising, considering the overall low levels of phytodetritus input to the lower-slope benthos. Similarly, analysis of video archives did not find evidence of aggregation of this taxa in the immediate vicinity of seeps (Section 24). These data are very similar to what we have found for the upper slope communities and stand in opposition to our original expectation of a higher degree of utilization of seep primary production on the lower slope.

We knew that we would find tube worm and mussel-based communities as well as at least scattered vesicomyid clams in the deep GoM but a surprise was the discovery of dense aggregations of heart urchins, *Sarsiaster griegii*, at several of the deeper sites (Section 20). These echinoderm aggregations were found over large areas (100s of square meters) of sites at both ends of the east-west geographic range covered by this study. In some areas they do not appear to be moving (other than disturbing the sediment in contact with their bodies), in others their trails literally covered the sea floor. They move through the sediment at speeds up to 60 cm per day and occur at densities as high as 8 per m^2. They appear restricted to sites greater than 2,200 m deep, and have never been documented during the extensive exploration of the upper slope. Their tissue stable isotope signature clearly indicates that they obtain the bulk of their nutrition from seep primary production and microbiological studies indicated that these habitats hosted the highest activities of sulfate-reducing bacteria of any sampled in this study. However, we did not find any evidence of chemoautotrophic symbionts like those that characterize the other seep community foundation fauna. The preliminary results of a comprehensive study to document the meiofauna communities in these habitats and the urchins' impacts on these communities is presented in Section 20 of this report and is being finalized for publication as part of a Ph.D. dissertation. Surprisingly, the impact of urchin activity is not a reduction in the meiofauna abundance (as we hypothesized would result from predation), but rather to increase abundance and diversity of the meiofauna communities.

27.3. Seep Meiofauna

An especially productive aspect of this study was the coupled investigation of meiofauna communities in collections tube worms and mussels from three of the most intensively studied sites (Section 19). This is the first study of seep meiofauna associated with seep megafauna ever conducted. A total of seven samples from mussel habitats and six from tube worm aggregations were analyzed along with three control cores taken approximately 3 m from any megafaunal communities. The overall abundance and higher taxa composition of these communities were similar to what we have found associated with mussel and tube worm communities at hydrothermal vents on the EPR. However, the diversity at seeps was much higher, with a total 113 meiobenthic genera found in the seep collections compared to a total of 38 genera found with similar sampling effort at vents. The very high diversity and abundance of undescribed species in the collections required a large effort in this analysis. The final taxonomic identification of all groups is not complete; however 107 new species, including 24 undescribed species that do not fit into any described genera, have been confirmed. These include 18 new genera and 77 new species of copepod, one new genera and 17 new species of ostracod, four new species of tanaidacea, and three new species of halacarids. There are at least five new genera of nematodes and the total new nematode species count will be higher when the species level identification of this very abundant and species-rich group is complete.

27.4. Microbial Ecology

The microbial ecology component (Section 11) was similarly successful in qualitative description of deep slope seep microbiology, but the very time-consuming laboratory analyses necessary for high quality microbial studies required that this work be largely constrained to a few of the most interesting sites. Nonetheless, the work detailed in Section 11 clearly documented very significant variability in microbial community activity and community composition between and within sites. Despite this variability, striking differences in the rates of microbial activity were documented between the previously studied upper slope sites and the sites studied on the lower slope. The direct analysis of the stable isotopic composition of methane was consistent with analysis of the tissue values for methanotrophic symbiont-containing species and demonstrated the much more widespread occurrence of biogenic methane in the lower slope communities than on the upper slope. Rates of methanogenesis measured at some of the most spectacular lower slope brine influenced sites (such as AC601), were among the highest ever measured and created a very significant methane signal that could be followed all the way to the sea surface. Analysis of this data set further demonstrated that water column methane oxidation is a very poor sink for methane flux arising from the sea floor. These studies also proved very complementary to the macrofaunal work, demonstrating for example that the newly discovered heart urchin communities are inhabiting sediments with the highest rates of SR found in any macrofaunal habitat currently known in the GoM.

27.5. Corals

Although a focus of this project was exploration of hard grounds associated with seeps, only a single significant coral community was discovered over the course of this project. There were at least a few large colonial cnidarians observed at most of the sites surveyed, and small cnidarian

colonies were often present on carbonates associated with almost every site. At GC852, a significant and diverse coral assemblage was found on a local topographic high in close proximity to both tube worm and mussel aggregations (Section 21). This included three species of the scleractinian reef-building corals *Madrepora oculata, Enallopsammia rostrata*, and *Solenosmilia variabilis,* several octocorals, including *Paramuricea* sp., *Acanthogorgia* sp., *Iridogorgia* sp., and the bamboo coral *Keratoisis sp.*, and several other unidentified colony-forming cnidarians. We hypothesized that the proximity to seeps would result in a significant input of seep primary production to these deep-living corals, but this was not detected using stable carbon and nitrogen isotope analyses (Becker et al., 2009). A photomosaic of the community was compiled to quantify the megafauna associated with the corals and also to allow revisitation and quantitative assessment of changes over time or as a result of anthropogenic influence.

27.6. Future Directions

The future research support from BOEM and NOAA Office of Exploration and Research is especially important in several general areas. The first is in further exploration and site characterization. Most of our observations of hard-bottom areas have been in the <1,000 m water depth range since the first hard-bottom areas and chemosynthetic communities were discovered in the mid-1980s. During this project and the ongoing *Lophelia* II Project, numerous sites of the middle and lower slope have been (will be) explored and sampled; however, because of the vastness of the northern GoM continental slope, our sampling of these deepwater areas is still inadequate for a comprehensive characterization of deepwater hard-bottom communities to fully understand the distribution, biodiversity, and connectivity of communities in the deep GoM. In addition to further exploration and sampling at key areas in the central northern GoM, understanding the biogeography of the deep GoM will require considerably more work in the undersampled surrounding regions of the GoM. This was made especially evident during the *Lophelia* II project in 2009 by the fortuitous discovery of a new species of bathymodiolid mussel dominating the communities at a site in De Soto Canyon. Why is this species found here and nowhere else? Why are the other bathymodiolids not found here? Is this apparent isolation reflected in the rest of the community?

Additional studies of connectivity among the populations must be coupled with more exploration and study. We have made a lot of progress in this regard and the expectation is that more will be made with respect to colonial cnidarians, as part of the United States Geological Survey and BOEM components of the *Lophelia* II project. However, the technology and theory for these studies is advancing at an amazing rate. Continued studies in this area, linked with additional oceanographic studies to better understand the larval highways of the deep GoM below the 1,000 m depth limit of the loop current will continue to significantly advance our predictive capability for occurrence of a wide variety of fauna in the deep GoM.

Another key area where investment of BOEM resources is important, if not critical, has been made especially evident by the recent disaster at the *Deepwater Horizon* platform. This is investment in the establishment and maintenance of long-term observatories and monitoring stations. Not only will these temporal studies provide information on how animals grow and sites and communities evolve over time, they will also provide important data on changes that may

occur as the result of both acute and prolonged anthropogenic impacts to the deep GoM. These stations should include the deployment of instruments to monitor a wide range of physical, chemical and biological parameters, and sufficiently detailed and replicated community characterization to allow quantitative documentation of any changes that may occur.

As is always the case with almost any area of research, new discoveries led to new questions and the discovery of patterns leads to questions about their causes. In this study, one of these key areas is investigation of the nature of the boundary between the upper and lower slope. The depth range between 800 and 1,200 m contains a very high rate of species turnover in the seep communities, but also in the background fauna. Because this feature is common to both the chemosynthetic and heterotrophic fauna, it is not necessarily food-related (although this is likely to be one of the factors influencing the background fauna). It may be related to other oceanographic variables, including dissolved oxygen concentration or the bathymetric distribution of water masses controlling larval dispersal. It may also be related to the effects of pressure on enzyme function, which would suggest that there would be a common difference between the physiology of upper and lower slope species irrespective of taxonomy.

To begin to answer this question, the boundaries in species distributions need to be better refined. Although species turnover appears rapid in this depth range, very few of our sites were in the 1,000–1,200 m depth range. Similarly, very few of the Chemo I and Chemo II sites were in the 700–1,000 m depth range. This is a big gap in our understanding of these communities. Additional work in this intermediate depth range is likely to result in refined species boundaries, and perhaps the addition of a number of new species due to the limited sampling in this range. Part of this question is obtaining a better understanding of vestimentiferan biogeography and population genetics. Over the course of this study, it has become increasingly apparent that these key members of cold seep communities have a very different rate of evolution of their mitochondrial genes than most other animals. Consider the close identity between the mitochondrial COI gene of *Escarpia* species in the GoM, the West Coast of the U.S. and Costa Rica, and the East Coast of Africa. In order to understand the nature of the connectivity among populations and species of the genus *Escarpia* and *Lamellibrachia* will require a continuing effort. Once we can cleanly and reliably tell the presumptive species apart, we can conduct more process-oriented studies that will shed light on the variables that allow the co-existence of at least five species of vestimentiferan in the GoM and up to three species at a given site and even in a single aggregation on both the upper and lower slope. The stable isotope studies clearly indicate that inorganic nitrogen uptake may be key to niche separation in the two most common co-occurring species on the lower slope, but many other variables impacting their interaction with the external environment, both internal and external symbionts, and presumptive parasites, such as the "capworm" *Protomystides* sp., are not well constrained.

A continuing impediment to a complete understanding of the relations between microbes, animals and the seep environment has been a lack of adequate *in situ* instrumentation to measure appropriate variables, especially methane and sulfide, but ideally oxygen, pH and temperature, as well. To understand the animals' physiological ecology and distribution in the seep habitats, these measurements need to be made simultaneously, in the places appropriate to the animals (by plumes, next to roots, within mussel beds, etc.) and on the correct spatial scales to understand their microhabitat distribution. Because of the very high degree of spatial variability and

resultant patchy distribution of animals, analysis of, as one example, push cores taken next to a tube worm aggregation or mussel bed really provides little insight into the conditions present in or below the aggregations. Over the course of this study, we worked with several different Principal Investigators and instruments that were unable to make the necessary measurements reliably and accurately or in sufficient numbers for the replication necessary for ecological studies. However, despite being incorporated into the program at the last minute, we were able to deploy and use an *in situ* mass spectrometer in a wide variety of environments and conduct some of the first *in situ* measurements of the most biologically important gasses in the deep GoM. This technology was used successfully on several dives and shows great promise for further measurements made from either a mobile deep submergence asset or in stand-alone mode for long term monitoring. There are other technologies that are reaching maturity for these types of studies, including Raman spectrometers and *in situ* flourometers. Regardless, the next generation of seep studies must include appropriate *in situ* instrumentation for the detailed characterization of the seep environment that will allow a real understanding of the physiological ecology of the seep and coral communities of the deep GoM.

Not only will use of this type of technology greatly increase our understanding of the macrofauna communities, it is also important to further our understanding of the microbial communities that are the ultimate drivers of seep primary production. When coupled with evolving molecular microbial technologies, such as quantitative polymerase chain reaction, microarrays, and community-level genomics and transcriptomics, investigators will be in a position to model and really understand the relations between microbial community composition, geochemical variables and the microbial activity driving such processes as sulfide and biogenic methane production.

28. BIBLIOGRAPHY

Aharon, P. and B.S. Fu. 2000. Microbial sulfate reduction rates and sulfur and oxygen isotope fractionations at oil and gas seeps in deepwater Gulf of Mexico. Geochimica et Cosmochimica Acta 64 (2): 233-246.

Alperin, M.J. and W.S. Reeburgh. 1988. Carbon and hydrogen isotope fractionation resulting from anaerobic methane oxidation. Global Biogeochemical Cycles 2: 279-288.

Alpers, W. and H. Espedal. 2004. Oils and Surfactants. In: Jackson, C. and J. Apel, Eds., Synthetic Aperture Radar Marine User's Manual. U.S. Dept. of Commerce, NOAA, 263-277.

Arellano, S. M. and C. M. Young. 2009. Spawning, development, and the duration of larval life in a deep-sea cold-seep mussel. Biological Bulletin 216(2):149-162.

Arvidson, R. S., J. W. Morse, and S.B. Joye. 2004. The sulfur biogeochemistry of chemosynthetic cold seep communities, Gulf of Mexico, USA. Marine Chemistry 87: 97-119.

Baguley, J.G., C.D. Montagna, L.J. Hyde, R.D. Kalke, and G.T. Rowe. 2006. Metazoan meiofauna abundance in relation to environmental variables in the northern Gulf of Mexico deep sea. Deep-Sea Research Part I 53: 1344–1362

Behrenfeld, M.J. and P.G. Falkowski. 1997. Photosynthetic rates derived from satellite-based chlorophyll concentration. Limnology and Oceanography 42:1-20.

Bell, S.S.. 1980. Meiofauna-macrofauna interactions in a high salt marsh habitat. Ecological Monographs 50(4): 487–505.

Bell, R.J., R.T. Short, F.H. van Amerom, R.H. Byrne. 2007. Calibration of an In Situ Membrane Inlet Mass Spectrometer for Measurements of Dissolved Gases and Volatile Organics in Seawater. Environmental Science & Technology 41 (23), 8123-8128.

Bernard, B., J.M. Brooks, and W.M. Sackett, 1977. A geocemical model for characterization of gas sources in marine sediments. Offshore Technology Conference, pp. 435-438.

Bergquist, D.C., F.M. Williams and C.R. Fisher. 2000. Longevity record for deep-sea invertebrate. Nature 403 (6769):499-500.

Bergquist, D.C., I.A Urcuyo and C.R.Fisher. 2002. Establishment and persistence of seep vestimentiferan aggregations on the upper Louisiana slope of the Gulf of Mexico. Marine Ecology-Progress Series 241:89-98.

Bergquist, D.C., T. Ward, E.E. Cordes, T. McNelis, S. Howlett, R. Kosoff, S. Hourdez, R. Carney, and C.R. Fisher. 2003a. Community structure of vestimentiferan-generated habitat islands from upper Louisiana slope cold seeps. Journal of Experimental Marine Biology and Ecology 289:197-222.

Bergquist, D.C., J.P. Andras, T. McNelis, S. Howlett, M.J. VanHorn, and C.R. Fisher. 2003b. Succession in Gulf of Mexico seep communities: the importance of spatial variability. P.S.Z.N. Marine Ecology 24:31-44.

Bergquist, D.C., C. Fleckenstein, E. Smith, J. Knisel, and C.R. Fisher. 2004. Environment drives physiological variability in the cold seep mussel *Bathymodiolus childressi*. Limnology and Oceanography 49: 706-715.

Bergquist, D.C., C. Fleckenstein, J. Knisel, B. Begley, I.R. MacDonald, and C.R. Fisher. 2005. Variations in seep mussel bed communities along physical and chemical environmental gradients. Marine Ecology Progress Series 293:99-103.

Betzer, P.R., W.J. Showers, E.A. Laws, C.D. Winn, G.R. Ditullio and P.M. Kroopnick. 1984. Primary productivity and particulate fluxes on a transect of the equator at 153°W in the Pacific Ocean. Deep-Sea Research 31:1–11.

Bielawski, J. P. and J. R Gold. 2002. Mutation patterns of mitochondrial H- and L-strand DNA in closely related cyprinid fishes. Genetics 161:1589-1597.

Biggs, D. C., C. Hu and F. Muller-Karger. (2008). Remotely sensed sea-surface chlorophyll and POC flux at Deep Gulf of Mexico Benthos sampling stations. Deep Sea Research Part II: Topical Studies in Oceanography **55**:2555-2562.

Bisol, P.M., R. Costa and M. Sibuet. 1984. Ecological and Genetic Survey on 2 Deep-Sea Holothurians - Benthogone-Rosea and Benthodytes-Typica. Marine Ecology-Progress Series 15 (3):275-281.

Black, M.B., A. Trivedi, P.A.Y. Maas, R.A. Lutz and R.C. Vrijenhoek. 1998. Population genetics and biogeography of vestimentiferan tube worms. Deep Sea Research Part II: Topical Studies in Oceanography 45:1-3.

Bleidorn, C., L. Podsiadlowski and T. Bartolomaeus. 2006. The complete mitochondrial genome of the orbiniid polychaete Orbinialatreillii (Annelida, Orbiniidae) – A novel gene order for Annelida andimplications for annelid phylogeny. Gene 370:96–103.

Boland, G.S. 1986. Discovery of co-occurring bivalve Acesta sp. and chemosynthetic tube worms Lamellibrachia. Nature (London) 323: 759.

Britayev, T.A., D. Martin, E. M. Krylova, R. von Cosel, and T. S. Aksiuk, 2007. Life-history traits of the symbiotic scale-worm *Branchipolynoe seepensis* and its relationships with host mussels of the genus *Bathymodiolus* from hydrothermal vents. Marine Ecology 28, 36-48.

Brooks, J.M., M.C. Kennicutt, C.R. Fisher, S.A. Macko, K. Cole, J.J. Childress, R. Bidigare, and R.D. Vetter. 1987. Deep-sea hydrocarbon seep communities: evidence for energy and nutritional carbon sources. Science 238 (4830): 1138-1142.

Brooks, J.M., D.A. Wiesenburg, H. Roberts, R.S. Carney, I.R. MacDonald, R.A. Burke, P. Ahron, and T.J. Bright. 1990. Salt, seeps, and symbiosis in the Gulf of Mexico: a preliminary report of deepwater discoveries using DSV *Alvin*. EOS, Transactions, American Geophysical Union 74:1772-1773.

Bruening, M., H. Sahling, I. R. MacDonald, F. Ding, and G. Bohrmann. 2010. Origin, distribution, and alteration of asphalts at Chapopote Knoll, Southern Gulf of Mexico, Mar Petrol Geol, 27(5), 1093-1106.

Buckland, S. T., D. R. Anderson, K. P. Burnham, J. L. Laake, D. L Borches, and L. J. Thomas, , Eds. 2004. Advanced Distance Sampling. Oxford: Oxford University Press. 434 pp.

Burton, K.W., H.F. Ling and R.K. Onions. 1997. Closure of the Central American Isthmus and its effect on deep-water formation in the North Atlantic. Nature 386 (6623):382-385.

Cairns, S.D., D.M. Opresko, T.S. Hopkins, and W.W. Schroeder. 1993. New records of deep-water Cnidaria (Scleractinia & Antipatharia) from the Gulf of Mexico. Northeast Gulf Sci. 13:1-11.

Carey, A.G., Jr. 1972. Food sources of sublittoral, bathyal and abyssal asteroids in the northeast Pacific Ocean. Ophelia 10:35-47.

Carney, R.S., 1994. Consideration of the oasis analogy for chemosynthetic communities at Gulf of Mexico hydrocarbon vents. Geo-Marine Letters 14, 149–159.

Carney, R.S., 2005. Zonation of deep-sea biota on continental margins. Oceanography and Marine Biology: An annual review. 43, 211-279.

Carney, S.L., M.I. Formica, H. Divatia, K. Nelson, C.R Fisher and S.W. Schaeffer. 2006. Population structure of the mussel "*Bathymodiolus*" *childressi* from Gulf of Mexico hydrocarbon seeps. Deep-Sea Research Part I-Oceanographic Research Papers 53 (6):1061-1072.

Cary, C., B. Fry, H. Felbeck, and R.D. Vetter. 1989. Multiple trophic resources for a chemoautotrophic community at a cold water brine seep at the base of the Florida Escarpment. Mar Biol 100 (3): 411-418.

Cavanaugh, C.M., P.R. Levering, J.S. Maki, R. Mitchell, and M.E. Lidstrom. 1987. Symbiosis of methylotrophic bacteria and deep-sea mussels. Nature 325: 346-348.

Chambers, L.A., and P.A. Trudinger. 1970. Microbiological fractionation of stable sulfur isotopes: A review and critique. Geomicrobiology Journal 1: 249-293.

Chase, M.R., R.J. Etter, M.A. Rex and J.M. Quattro. 1998. Bathymetric patterns of genetic variation in a deep-sea protobranch bivalve, Deminucula atacellana. Marine Biology 131 (2):301-308.

Childress, J.J., and C.R. Fisher. 1992. The biology of hydrothermal vent animals: physiology, biochemistry, and autotrophic symbioses. Oceanography and Marine Biology 30: 337-441.

Childress, J.J., C.R. Fisher, J.A. Favuzzi, A.J. Arp, and D.R. Oros. 1993a. The role of a zinc-based, serum-borne sulfide-binding component in the uptake and transport of dissolved sulfide by the chemoautotrophic symbiont-containing clam *Calyptogena elongata*. Journal of Experimental Biology 179: 131-158.

Childress, J.J., R.W. Lee, N.K. Sanders, H. Felbeck, D.R. Oros, A. Toulmond, D. Desbruyeres, M.C. Kennicutt, and J. Brooks. 1993b. Inorganic carbon uptake in hydrothermal vent tube worms facilitated by high environmental pCO_2. Nature 362 (6416): 147-149.

Clarke, M.E. and R.N. Gorley. 2006. PRIMER v6: User Manual/Tutorial. PRIMER-E Ltd., Plymouth, U.K.

Clarke, K.R. and R. M. Warwick. 2001. Change in Marine Communities: An Approach to Statistical Analysis. Primer-E Ltd.

Copley, J.T.P., H.C. Flint, R.J. Ferrero, and L. Van Dover. 2007. Diversity of meiofauna and free-living nematodes in hydrothermal vent mussel beds on the northern and southern East Pacific Rise. Journal Marine Biological Association U.K. 87: 1141–1152.

Cordes, E.E., S. Hourdez, B.L. Predmore, M.L. Redding, and C.R. Fisher. 2005. Succession of hydrocarbon seep communities associated with the long-lived foundation species *Lamellibrachia luymesi*. Marine Ecology Progress Series 305:17-29.

Cordes, E.E., D.C. Bergquist, B.L. Predmore, C. Jones, P. Deines, G. Telesnicki, and C.R. Fisher. 2006. Alternate unstable states: convergent paths of succession in hydrocarbon seep tube worm associated communities. Journal of Experimental Marine Biology and Ecology 339:159-176.

Cordes, E.E., D.C. Bergquist, M.L. Redding, and C.R. Fisher. 2007a. Growth of *Seepiophila jonesi*: a second species of long-lived tube worm. Marine Ecology 28: 160-168.

Cordes, E.E., S.L. Carney, S. Hourdez, R.S. Carney, J.M. Brooks, and C.R. Fisher. 2007b. Cold seeps of the deep Gulf of Mexico: Community structure and biogeographic comparisons to Atlantic equatorial belt seep communities. Deep-Sea Research I 54:637-653.

Cordes, E.E., D. C. Bergquist, and C. R. Fisher. 2009. Macro-ecology of Gulf of Mexico cold seeps. Annual Review of Marine Science 1, 143-168.

Cordes, E.E., E.L. Becker, S. Hourdez, C.R. Fisher. 2010. Influence of foundation species, depth, and location on biodiversity and community structure at Gulf of Mexico lower slope cold seeps. Deep-Sea Research II 57 (21-23), 1870-1881.

Corliss, J.B., J. Dymond, L. Gordon, J.M. Edmond, R.P. von Herzen, R.D. Ballard, K. Green, D. Williams, A. Bainbridge, K. Crane and T.H. VanAndel. 1979. Submarine thermal springs on the Galápagos Rift. Science 203: 1073-1083.

Craddock, C., W. R. Hoeh, R. G. Gustafson, R. A. Lutz, J. Hashimoto and R. J. Vrijenhoek (1995). Evolutionary relationships among deep-sea Mytilids (Bivalvia, Mytilidae) from hydrothermal vents and cold-water methane sulfide seeps. Marine Biology 121(3): 477-485.

Dattagupta, S., D.C. Bergquist, E.B. Szalai, S.A. Macko, and C.R. Fisher. 2004. Tissue carbon, nitrogen, and sulfur stable isotope turnover in transplanted *Bathymodiolus childressi* mussels: relation to growth and physiological condition. Limnology and Oceanography 49 (4): 1144-1151.

Dattagupta, S., L.L. Miles, M.S. Barnabei, and C.R. Fisher. 2006. The hydrocarbon seep tube worm *Lamellibrachia luymesi* primarily eliminates sulfate and hydrogen ions across its roots to conserve energy and ensure sulfide supply. Journal of Experimental Biology 209: 3795-3805.

Dattagupta, S., M.A. Arthur, and C.R. Fisher. 2008. Modification of sediment geochemistry by the hydrocarbon seep tube worm *Lamellibrachia luymesi*: A combined empirical and modeling approach. Geochimica et Cosmochimica Acta 72 (9): 2298-2315.

De Beer, D., E. Sauter, H. Niemann, N. Kaul, J.P. Foucher, U. Witte, M. Schluter, and A. Boetius. 2006. In situ fluxes and zonation of microbial activity in surface sediments of the Haakon Mosby mud volcano. Limnology Oceanography 51: 1315-1331.

De Beukelaer, S.M., I. MacDonald, N.L.J. Guinnasso and J.A. Murray. 2003. Distinct side-scan sonar, RADARSAT SAR, and acoustic profiler signatures of gas and oil seeps on the Gulf of Mexico slope. Geo-Mar Lett 23: 177-186.

Del Sontro, T.S., I. Leifer and B. Luyendyk. 2004. Factors Affecting the Temporal and Spatial Variability and Characteristics of Marine Hydrocarbon Seepage, Coal Oil Point, CA. American Geophysical Union.

Deming, J. W. and S. D. Carpenter, 2008. Factors influencing benthic bacterial abundance, biomass, and activity on the northern continental margin and deep basin of the Gulf of Mexico. Deep Sea Research Part II: Topical Studies in Oceanography **55**: 2597-2606.

Deonier, R., S. Tavare and M. Waterman. 2005. Similarity, Distance, and Clustering, Computational Genome Analysis. Springer New York, pp. 263-289.

Dinet, A., F. Grassle, and V. Tunnicliffe. 1988. Premières observations sur la meiofauna des sites hydrothermaux de la dorsale East-Pacifique (Guaymas, 21°N) et de l'Exlorer Ridge. Oceanologica Acta 85 : 7–14.

Doyle, J.J. and J.L. Doyle. 1987. A rapid DNA isolation procedure for small quantities of fresh leaf tissue. Phytochemical Bullettin 19:11-15.

Duan, Z., S. Mao. 2006. A thermodynamic model for calculating methane solubility, density and gas phase composition of methane-bearing aqueous fluids from 273 to 523K and from 1 to 2000 bar. Geochimica et Cosmochimica Acta 70 (13), 3369-3386.

Duperron, S., M. Sibuet, B.J. MacGregor, M.M.M. Kuypers, C.R. Fisher, and N. Dubilier. 2007. Diversity, relative abundance and metabolic potential of bacterial endosymbionts in three

Bathymodiolus mussel species from cold seeps in the Gulf of Mexico. Environmental Microbiology 9 (6): 1423-1438.

Duperron, S., J. Lorion, S. Samadi, O. Gros and F. Gaill (2009). Symbioses between deep-sea mussels (Mytilidae: Bathymodiolinae) and chemosynthetic bacteria: diversity, function and evolution. Comptes Rendus Biologies 332(2-3): 298-310.

Espedal, H. and T. Wahl. 1999. Satellite SAR oil spill detection using wind history information. International Journal of Remote Sensing 20: 49-65.

Excoffier, L., G. Laval and S. Schneider (2005). Arlequin ver. 3.0: An integrated software package for population genetics data analysis. Evolutionary Bioinformatics Online (1): 47-50.

Faure, B., D. Jollivet, A. Tanguy, F. Bonhomme and N. Bierne (2009). Speciation in the deep-sea: multi-locus analysis of divergence and gene flow between two hybridizing species of hydrothermal vent mussels. PlosOne 4 (8): e6485.

Felder, D.L., F. Alvarez, J.W. Goy, and R. Lemaitre. 2009. Decapoda (Crustacea) of the Gulf of Mexico with comments on the Aphionidacea. Chapter 59 In Gulf of Mexico Origins, Waters, and Biota, Vol. 1 Biodiversity . Tunnell, J.W. Jr., Felder, D.L., and Earle, Sylvia. Texas A&M University Press.

Felsenstein, J. 1985. Confidence limits on phylogenies: An approach using the bootstrap. Evolution 39 (4):783-791.

Feng, D. and H. H. Roberts. 2010. Initial results of comparing cold-seep carbonates from mussel- and tubeworm-associated environments at Atwater Valley lease block 340, northern Gulf of Mexico: Deep-Sea Research II, v. 57, p. 2030-2039.

Fernholm, B. 1998. Hagfish systematics. Chapter 3 In J.M. Jorgensen, J.P. Lomholt, R.E. Weber, and H. Malte. The Biology of Hagfish. Chapman and Hall London p 33-44.

Fiala-Médioni, A., J. Boulègue, S. Ohta, H. Felbeck, and A. Mariotti. 1993. Source of energy sustaining the *Calyptogena* populations from deep trenches in subduction zones off Japan. Deep-Sea Research Part I: Oceanographic Research Papers 40 (6): 1241-1258.

Fisher, C.R. 1990. Chemoautotrophic and methanotrophic symbioses in marine invertabrates. Aquatic Sciences 2 (3-4): 399-436.

Fisher, C.R., J.J. Childress, A.J. Arp, J.M. Brooks, D.L. Distel, J.A. Dugan, H. Felbeck, L.W. Fritz, R.R. Hessler, K.S. Johnson, M.C. Kennicutt, II, R.A. Lutz, S.A. Macko, A. Newton, M.A. Powell, G.N. Somero, and T. Soto. 1988. Variation in the hydrothermal vent clam, *Calyptogena magnifica*, at the Rose Garden vent on the Galapagos spreading center. Deep-Sea Research 35: 1811-1831.

Fisher, C.R., J.M. Brooks, J.S. Vodenichar, J.M. Zande, J.J. Childress, and R.A. Burke. 1993. The coocurance of methanotrophic and chemoautotrophic sulfur-oxidizing bacterial symbionts in a deep-sea mussel. Marine Ecology 14: 277-289.

Fisher, C.R., J.J. Childress, S.A. Macko, and J.M. Brooks. 1994. Nutritional interactions in Galapagos Rift hydrothermal vent communities: inference from stable caron and nitrogen isotope analyses. Marine Ecology Progress Series 103: 45-55.

Fisher, C.R., I.R. MacDonald, R. Sassen, C.M. Young, S.A. Macko, S. Hourdez, R.S. Carney, S. Joye, and E.R. McMullin. 2000. Methane ice worms: *Hesiocaeca methanicola* colonizing fossil fuel reserves. Naturwissenschaften 87: 184-187.

Fisher, C R., H. Roberts, E. Cordes, and B. Bernard. 2007. Cold seeps and associated communities of the Gulf of Mexico. Oceanography 20: 68 – 79.

Fogel, M.L., M.J. Wooller, J. Cheeseman, B.J. Smallwood, Q. Roberts, I. Romero, and M.J. Meyers. 2008. Unusually negative nitrogen isotopic compositions ($\delta^{15}N$) of mangroves and lichens in an oligotrophic, microbially-influenced ecosystem. Biogeosciences 5 (6): 1693-1704.

Folmer, O., M. Black, W. Hoeh, R. Lutz, and R. Vrijenhoek. 1994. DNA primers for amplification of mitochondrial cytochrome c oxidase subunit I from diverse metazoan invertebrates. Mol Mar Biol Biotechnology 3 (5):294-299.

Fortuny-Guasch, J. 2003. Improved Oil Slick Detection and Classification with Polarimetric SAR, in: Lacoste, H. (Ed.), Proceedings of the Workshop on POLinSAR - Applications of SAR Polarimetry and Polarimetric Interferometry (ESA SP-529), Frascati, Italy.

France, S.C. and L.L. Hoover. 2002. DNA sequences of the mitochondrial COI gene have low levels of divergence among deep-sea octocorals (Cnidaria : Anthozoa). Hydrobiologia 471:149-155.

France, S.C. and T.D.Kocher. 1996. Geographic and bathymetric patterns of mitochondrial 16S rRNA sequence divergence among deep sea amphipods, *Eurythenes gryllus*. Marine Biology 126 (4):633-643.

Freytag, J.K., P.R. Girguis, D.C. Bergquist, J.P. Andras, J.J. Childress, and C.R. Fisher. 2001. A paradox resolved: sulfide acquisition by roots of seep tube worms sustains net chemoautotrophy. Proceedings of the National Academy of Science, United States 98 (23): 13408–13413.

Frye, M. 2008. Preliminary Evaluation of In-Place Gas Hydrate Resources: Gulf of Mexico Outer Continental Shelf. U.S. Department of the Interior, M.M.S., Resource Evaluation Division. OCS Report, MMS 2008-04: 94p.

Garcia-Pineda, O., I.R. MacDonald and B. Zimmer. 2008. Synthetic Aperture Radar Image Processing Using The Supervised Textural-Neural Network Classification Algorithm. Proceedings of the IEEE 2008 International Geoscience and Remote Sensing Symposium (IGARSS'08), Boston, USA.

Gardiner, S.L., E. McMullin and C.R. Fisher. 2001. *Seepiophila jonesi*, a new genus and species of vestimentiferan tube worm (Annelida : Pogonophora) from hydrocarbon seep communities in the Gulf of Mexico. Proceedings of the Biological Society of Washington 114 (3):694-707.

Genio, L., S. B. Johnson, R. C. Vrijenhoek, M. R. Cunha, P. A. Tyler, S. Kiel and C. T. S. Little (2008). New record of "Bathymodiolus" mauritanicus Cosel 2002 from the Gulf of Cadiz (NE Atlantic) mud volcanoes. Journal of Shellfish Research 27(1): 53-61.

Gens, R. and T. Logan. 2003. Alaska Satellite Facility software tools.

Giere, O. 2009. Meiobenthology : The Microscopic Motile Fauna of Aquatic Sediments (2^{nd} Edition) Springer Verlag Berlin Heidelberg, pp. 527.

Goffredi, S.K., J.J. Childress, N.T. Desaulniers, R.W. Lee, F.H. Lallier, and D. Hammond. 1997. Inorganic carbon acquisition by the hydrothermal vent tube worm *Riftia pachyptila* depends upon high external pCO_2 and upon proton-equivalent ion transport by the worm. Journal of Experimental Biology 200 (5): 883-896.

Gollner, S., J. Zekely, B. Govenar, N. Le Bris, H.L. Nemeschkal, C.R. Fisher, and M. Bright. 2007. Tube worm-associated permanent meiobenthic communities from two chemically different hydrothermal vent sites on the East Pacific Rise. Marine Ecology Progress Series 337: 39–49.

Gollner S., B. Riemer, P. Martinez Arbizu, N. Le Bris, and M. Bright. 2010. Meiobenthos from the 9º50´N East Pacific Rise over the full range of hydrothermal vent flux in comparison to other chemosynthesis-based ecosystems. Plos One 5(8): e12321.

Gonzalez, R., R. Woods and S. Eddins. 2004. Digital Image Processing Using Matlab. Pearson Education, Inc., New Jersey.

Gotelli, N.J., and G. L. Entsminger. 2004. EcoSim: Null models software for ecology. Version 7. Acquired Intelligence Inc. & Kesey-Bear. Jericho, VT.

Granger, J., D.M. Sigman, M.F. Lehmann, and P.D. Tortell. 2008. Nitrogen and oxygen isotope fractionation during dissimilatory nitrate reduction by denitrifying bacteria. Limnology and Oceanography 53: 2533-2545.

Guindon, S. and O. Gascuel. 2003. A simple, fast, and accurate algorithm to estimate large phylogenies by maximum likelihood. Syst Biol 52 (5):696-704.

Gustafson, R. G., R. D. Turner, R. A. Lutz and R. C. Vrijenhoek (1998). A new genus and five new species of mussels (Bivalvia, Mytilidae) from deep-sea sulfide/hydrocarbon seeps in the Gulf of Mexico. Malacologia 40(1-2): 63-112.

Halanych, K.M., R.A. Feldman and R.C. Vrijenhoek. 2001. Molecular evidence that S*clerolinum brattstromi* is closely related to vestimentiferans, not to frenulate pogonophorans (Siboglinidae, Annelida). Biological Bulletin 201 (1):65-75.

Hall, T. A. (1999). BioEdit: a user-friendly biological sequence alignment editor and analysis program for Windows 95/98/NT. Nucleic Acids Symposium Series 41: 95-98.

Harrison, A.G., and H.G. Thode. 1958. Mechanism of the bacterial reduction of sulfate from isotopic fractionation studies. Transactions of the Faraday Society 54: 84-92.

Hashimoto, J., S. Ohta, T. Tanaka, H. Hotta, S. Masuzawa, and H. Sakai. 1989. Deep-sea communities dominated by the giant clam, *Calyptogena soyoae*, along the slope foot of Hatsushima Island, Sagami Bay, Central Japan. Paelogeography, Paleoclimatology, Paleoecology 71:179-192.

Hopkins, R. E. and H. E. Edgerton. 1961. Lenses for underwater photography. Deep Sea Research 8(3-4): 312-316.

Howell, K.L., D. S. M. Billett, and P. A. Tyler. 2002. Depth-related distribution and abundance of seastars (Echinodermata: Asteroidea) in the Porcupine Seabight and Porcupine Abyssal Plain, N. E. Atlantic. Deep-Sea Research I 49, 1901–1920.

Howell, K.L., A.D. Rogers, P.A. Tyler and D.S.M. Billett. 2004. Reproductive isolation among morphotypes of the Atlantic seastar species *Zoroaster fulgens* (Asteroidea : Echinodermata). Marine Biology 144 (5):977-984.

Hurtado, L.A., R.A. Lutz and R.C. Vrijenhoek. 2004. Distinct patterns of genetic differentiation among annelids of eastern Pacific hydrothermal vents. Mol Ecol 13 (9):2603-2615.

Iwasaki, H., A. Kyuno, M. Shintaku, Y. Fujita, Y. Fujiwara, K. Fujikura, J. Hashimoto, L. D. Martins, A. Gebruk and J. I. Miyazaki (2006). Evolutionary relationships of deep-sea mussels inferred by mitochondrial DNA sequences. Marine Biology 149(5): 1111-1122.

Jain, A. and R. Dubes. 1988. Algorithms for Clustering Data. Prentice-Hall, Upper Saddle River, NJ.

Jensen, P. 1986. Nematode fauna in the sulphide-rich brine seep and adjacent bottoms of the East Flower Garden, NW Gulf of Mexico: IV. Ecological aspects. Marine Biology 92: 489–503.

Jensen, P., I. Aagaard, R.A. Burke Jr, P.R. Dando, N.O. Jorgensen, A. Kuijpers, T. Laier, S.C.M. O'Hara, and R. Schmaljohann. 1992. "Bubbling reefs" in the Kattegat: submarine

landscapes of carbonate-cemented rocks support a diverse ecosystem at methane seep. Marine Ecology Progress Series 83: 103–112.

Jones, W. J., Y. J. Won, P. A. Y. Maas, P. J. Smith, R. A. Lutz and R. C. Vrijenhoek. 2006. Evolution of habitat use by deep-sea mussels. Marine Biology 148(4): 841-851.

Joye, S.B., T.M. Connell, L.G. Miller, R. Oremland. 1999. Oxidation of ammonia and methane in an alkaline, saline lake. Limnology and Oceanography. 44:178-188.

Joye, S.B., A. Boetius, B.N. Orcutt, J.P. Montoya, H.N. Schulz, M.J. Erickson, and S.K. Lugo. 2004. The anaerobic oxidation of methane and sulfate reduction in sediments from Gulf of Mexico cold seeps. Chemical Geology 205 (3-4): 219-238.

Joye, S.B., I.R. MacDonald, J.P. Montoya, and M.B. Peccini. 2005. Geophysical and geochemical signatures of Gulf of Mexico seafloor brines. Biogeosciences 2: 295-309.

Joye, S. B., V.A. Samarkin, B.N. Orcutt, I.R. MacDonald, K.-U. Hinrichs, M. Elvert, A.P. Teske, K.G. Lloyd, J.P. Montoya, and C.D. Meile. 2009. Surprising metabolic variability in seafloor brines revealed by carbon and sulfur cycling. Nature Geoscience. 2: 349-354.

Joye, S.B., M.W. Bowles, V.A. Samarkin, K.S. Hunter, and H. Niemann. 2010. Biogeochemical signatures and microbial activity of different cold seep habitats along the Gulf of Mexico lower slope. In Roberts, H. (ed.), Deep Sea Research Part II: Topical Studies in Oceanography, 2010. Gulf of Mexico Cold Seeps, Volume 57, Issues 21-23, pp 1990-2001.

Jumars, P. A., L. M. Mayer, J. W. Deming, J. A. Baross and R. A. Wheatcroft. 1990. Deep-Sea deposit-feeding strategies suggested by environmental and feeding constraints. Philosophical Transactions of the Royal Society of London Series A-Mathematical Physical and Engineering Sciences 331(1616): 85-101.

Kamenev, G.M., V.I. Fadeev, N.I. Selin, and V.G. Tarasov. 1993. Composition and distribution of macro- and meiobenthos around sublitoral hydrothermal vents in the Bay of Plenty. New Zealand. New Zealand Journal of Marine and Freshwater Research 27: 407–418.

Kennicutt, M.C., J.M. Brooks, R.R. Bidigare, R.R. Fay, T.L. Wade and T.J. McDonald. 1985. Vent-type taxa in a hydrocarbon seep region on the Louisiana Slope. Nature 317: 351-353.

Kennicutt, M.C., R.A. Burke, I.R. MacDonald, J.M. Brooks, G.J. Denoux, and S.A. Macko. 1992. Stable isotope partitioning in seep and vent organisms: chemical and ecological significance. Chemical Geology 101 (3-4): 293-310.

Kniemeyer, O., F. Musat, S.M. Sievert, K. Knittel, H. Wilkes, M. Blumenberg, W. Michaelis, A. Classen, C. Bolm, S.B. Joye, and F. Widdel. 2007. Anaerobic oxidation of propane and ethane by novel marine sulphate-reducing bacteria. Nature 449: 898-902.

Kojima, S., R. Segawa, T. Kobayashi, T. Hashimoto, K. Fujikura, J. Hashimoto and S. Ohta. 1995. Phylogenetic-Relationships among Species of *Calyptogena* (Bivalvia, Vesicomyidae) Collected around Japan Revealed by Nucleotide-Sequences of Mitochondrial Genes. Marine Biology 122 (3):401-407.

Kojima, S., R. Segawa, J. Hashimoto and S. Ohta. 1997. Molecular phylogeny of vestimentiferans collected around Japan, revealed by the nucleotide sequences of mitochondrial DNA. Marine Biology 127 (3):507-513.

Kornacki, A.S., J. Kendrick and J. Berry. 1994. The impact of oil and gas vents and slicks on petroleum exploration in the deepwater Gulf of Mexico. Geo-Marine Letters, 14(2/3): p. 160-169.

Kumar, S., K. Tamura and M. Nei (2004). MEGA3: Integrated software for Molecular Evolutionary Genetics Analysis and sequence alignment. Briefings in Bioinformatics 5(2): 150-163.

Lavaleye, M.S.S., G.C.A. Duineveld, E.M. Berghuis, A. Kok, and R. Witbaard. 2002. A comparison between the megafauna communities on the N.W. Iberian and Celtic continental margins- effects of coastal upwelling? Progress in Oceanography 52:459-476.

Le Guilloux, E., K. Olu, J.F. Bourillet, B. Savoye, S.P. Iglesias and M. Sibuet. 2009. First observations of deep-sea coral reefs along the Angola margin. Deep-Sea Research Part Ii-Topical Studies in Oceanography 56: 2394-2403.

Lee, R.W., and J.J. Childress. 1994. Assimilation of inorganic nitrogen by marine invertebrates and their chemoautotrophic and methanotrophic symbionts. Appl. Env. Microbiol. 60 (6): 1852-1858.

Lee, R.W., and J.J. Childress. 1996. Inorganic N assimilation and ammonium pools in a deep-sea mussel containing methanotrophic endosymbionts. Biological Bulletin (Woods Hole) 190 (3): 373-384.

Lee, R.W., E.V. Thuesen, J.J. Childress, and C.R. Fisher. 1992. Ammonium and free amino acid uptake by a deep-sea mussel (*Bathymodiolus* sp., undescribed) containing methanotrophic bacterial symbionts. Mar Biol 113: 99-106.

Lee, R.W., J.J. Robinson, and C.M. Cavanaugh. 1999. Pathways of inorganic nitrogen assimilation in chemoautotrophic bacteria-marine invertebrate symbioses: expression of host and symbiont glutamine synthetase. Journal of Experimental Biology 202 (3): 289-300.

Leifer, I. and I. MacDonald. 2003. Dynamics of the gas flux from shallow gas hydrate deposits: interaction between oily hydrate bubbles and the oceanic environment. Earth and Planetary Science Letters 210: 411-424.

Lessard-Pilon , S. A., E. L. Podowski, E. E. Cordes, C. R. Fisher. 2010. Megafauna community composition associated with Lophelia pertusa colonies in the Gulf of Mexico, In: Roberts, H. (ed.), Deep Sea Research Part II: Topical Studies in Oceanography, 2010. Gulf of Mexico Cold Seeps, Volume 57, Issues 21-23, pp 1882-1890.

Leung, T. and J. Malik. 2001. Representing and Recognizing the Visual Appearance of Materials using Three-dimensional Textons. International Journal of Computer Vision 43: 29–44.

Lonsdale, P. 1977. Clustering of suspension-feeding macrobenthos near abyssal hydrothermal vents at oceanic spreading centers. Deep-Sea Research 24: 857-863.

Lorion, J., S. Duperron, O. Gros, C. Cruaud and S. Samadi (2009). Several deep-sea mussels and their associated symbionts are able to live both on wood and on whale falls. Proceedings of the Royal Society B-Biological Sciences 276(1654): 177-185.

MacAvoy, S.E., R.S. Carney, E. Morgan, and S.A. Macko. 2008. Stable isotope variation among the mussel *Bathymodiolus childressi* and associated heterotrophic fauna at four cold-seep communities in the Gulf of Mexico. Journal of Shellfish Research 27 (1): 147-151.

MacDonald, I.R. and M.B. Peccini. 2009. Distinct activity phases during the recent geologic history of a Gulf of Mexico mud volcano. Marine and Petroleum Geology 26: 1824-1830.

MacDonald, I.R., J.F. Reilly, Jr., S.E. Best, R. Venkataramaiah, R. Sassen, N.L. Guinasso, Jr. and J. Amos. 1996. A remote-sensing inventory of active oil seeps and chemosynthetic communities in the northern Gulf of Mexico. In: D. Schumacher and Abrams, M.A. (eds.), Hydrocarbon migration and its near-surface expression. AAPG Memoir, 66:27-37.

MacDonald, I. R., D. Buthman, W.W. Sager, M.B. Peccini and N.R. Guinasso, Jr. 2000. Pulsed oil discharge from a mud volcano. Geology 28(10):907-910.

MacDonald, I., I. Leifer, R. Sassen and P. Stine. 2002. Transfer of hydrocarbons from natural seeps to the water column and atmosphere. Geofluids, Blackwell Science Ltd 2: 95-107.

MacDonald, I.R., W.W. Sager and M.B. Peccini. 2003. Association of Gas Hydrate and Chemosynthetic Fauna in Mounded Bathymetry at Mid-Slope Hydrocarbon Seeps: Northern Gulf of Mexico. Marine Geology 198: 133-158.

MacDonald, I.R., H. Roberts, W. Shedd, J. Hunt and B. Bernard. 2006.Exploring Lower Slope Chemosynthetic Communities in the Gulf of Mexico: A Nested Survey Approach. OS34A-07 AGU Fall Meeting, San Francisco.

MacDonald, I.R., H.H. Roberts, C.R. Fisher, B.B. Bernard, S. Joye, R. Carney, J. Hunt and W. Shedd. 2007. Reconnaissance Strategy for Seep Chemosynthetic Communities in the Gulf of Mexico, Ocean Sciences 2007. American Geophysical Union, Orlando FL, pp. abstract #OS51B-06.

Maddison, D.R. and W.P. Maddison. 2000. MacClade 4: Analysis of Phylogeny and Character Evolution. Sinauer Associates Inc, Sunderland, Massachusetts.

Marsh, A.G., L.S. Mullineaux, C.M. Young, and D.T. Manahan. 2001. Larval dispersal potential of the tube worm *Riftia pachyptila* at deep-sea hydrothermal vents. Nature 411 (6833):77-80.

Martens, C.S., J.P. Chanton, and C.K. Paull. 1991. Biogenic methane from abyssal brine seeps at the base of the Florida escarpment. Geology 19 (8): 851-854.

Martin, J. W. and T. A. Haney. 2005. Decapod crustaceans from hydrothermal vents and cold seeps: a review through 2005. Zoological Journal of the Linnean Society 145(4): 445-522.

Martini, F.H. The ecology of hagfishes. Chapter 5 In: J.M. Jorgensen, J.P. Lomholt, R.E. Weber, and H. Malte (eds.). The Biology of Hagfish. Chapman and Hall London 57-78.

McIntyre, A.D., and R.M. Warwick. 1984. Meiofauna techniques, In: Holme, N.A. and A.D. McIntyre (Eds.), Methods for the study of marine benthos, 2nd edn. Blackwell Scientific Publications, Oxford, pp. 217–244.

Minagawa, M., and E. Wada. 1984. Stepwise enrichment of ^{15}N along food chains: Further evidence for the relation between $d^{15}N$ and animal age. Geochimica et Cosmochimica Acta 48: 1135-1140.

Mitchell, R., I.R. MacDonald and K. Kvenvolden. 1999. Estimates of total hydrocarbon seepage into the Gulf of Mexico based on satellite remote sensing images. EOS Supplement 80: OS242.

Montagna, P.A., and R.B. Spies. 1985. Meiofauna and chlorophyll associated with *Beggiatoa* mats of a natural submarine petroleum seep. Marine Environmental Research 46: 231–242.

Montagna, P.A., J.E. Bauer, J. Toal, D. Hardin, and R.B. Spies. 1987. Temporal variability and the relationship between benthic and meiofaunal and microbial populations of a natural coastal petroleum seep. Journal of Marine Research 45: 761–789.

Nabholz, B., S. Glemin and N. Galtier. 2008. Strong variations of mitochondrial mutation rate across mammals--the longevity hypothesis. Mol Biol Evol 25 (1):120-130.

Nei, M. (1987). Molecular Evolutionary Genetics. New York, Columbia Univ. Press.

Nemeschkal, H.L. 1999. Morphometric correlation patterns of adult birds (Fringillidae: Passeriformes and Columbiformes) mirror the expression of developmental control genes. Evolution 53: 899–918.

Niemann, H., M. Elvert, M. Hovland, B. Orcutt, A.G. Judd, I. Suck, J. Gutt, S. Joye, E. Damm, K. Finster, and A. Boetius. 2005. Methane emission and consumption at a North Sea gas seep (Tommeliten area). Biogeosciences 2: 335-351.

Niemann, H., J. Duarte, C. Hensen, E. Omoregie, V.H. Magalhães, M. Elvert, L.M. Pinheiro, A. Kopf, and A. Boetius. 2006a. Microbial methane turnover at mud volcanoes of the Gulf of Cadiz. Geochimica et Cosmochimica Acta 70: 5336-5355.

Niemann, H., T. Lösekann, D. de Beer, M. Elvert, T. Nadalig, K. Knittel, R. Amann, E.J. Sauter, M. Schlüter, M. Klages, J.P. Foucher, and A. Boetius. 2006b. Novel microbial communities of the Haakon Mosby mud volcano and their role as a methane sink. Nature. 443: 854-858.

Ólafsson, E. 2003. Do macrofauna structure meiofauna assemblages in marine soft-bottoms? Vie Milieu 53: 249–265.

Olu, K., S. Lance, M. Sibuet, P. Henry, A. Fiala-Medioni, and A. Dinet. 1997. Cold seep communities as indicators of fluid expulsion patterns through mud volcanos seaward of the Barbados accretionary prism. Deep-Sea Research I 44: 881–841.

Olu, K., J.C. Caprais, J. Galéron, R. Causse, R. von Cosel, H. Budzinski, K.L. Ménach, C.L. Roux, D. Levaché, A. Khripounoff and M. Sibuet. 2009. Influence of seep emission on the non-symbiont-bearing fauna and vagrant species at an active giant pockmark in the Gulf of Guinea (Congo-Angola margin). Deep Sea Research Part II: Topical Studies in Oceanography 56: 2380-2393.

Olu-Le Roy, K., M. Sibuet, A. Fiala-Medioni, S. Gofas, C. Salas, A. Mariotti, J.-P. Foucher and J. Woodside. 2004. Cold seep communities in the deep eastern Mediterranean Sea: composition, symbiosis and spatial distribution on mud volcanoes. Deep Sea Research Part I: Oceanographic Research Papers 51: 1915-1936.

Olu-Le Roy, K., J. C. Caprais, A. Fifis, M.-C. Fabri, J. Galeron, H. Budzinsky, K. L. Menach, A. Khripounoff, H. Ondreas and M. Sibuet. 2007. Cold-seep assemblages on a giant pockmark off West Arica: spatial patterns and environmental control. Marine Ecology 28: 115-130.

Orcutt, B.N., V.A. Samarkin, A. Boetius, M. Elvert, and S.B. Joye. 2005. Molecular biogeochemistry of sulfate reduction, methanogenesis and the anaerobic oxidation of methane at Gulf of Mexico methane seeps. Geochimica et Cosmochimoca Acta 69: 4267-4281.

Pace, M., G. Knauer, D. Karl and J. Martin. 1987. Primary production, new production and vertical flux in the eastern. Pacific Ocean. Nature. 325:803-804

Page, H.M., C.R. Fisher, and J.J. Childress. 1990. The role of suspension-feeding in the nutritional biology of a deep-sea mussel with methanotrophic symbionts. Mar Biol 104: 251-557.

Palmer, M.A., P.A. Montagna, R.B. Spies, and D. Hardin. 1988. Meiofauna dispersal near natural petroleum seeps in the Santa Barbara Channel: a recolonization experiment. Chemical Pollution 4: 179–189.

Palumbi, S. R. 1992 .Marine speciation on a small planet. Trends in Ecology and Evolution 7: 114-118.

Paull, C.K., A.J.T. Jull, L.J. Toolin, and T. Linick. 1985. Stable isotope evidence for chemosynthesis in an abyssal seep community. Nature 317: 709-711.

Pawson, SD.L. and D.J. Vance. 2004. Chiridota heheva, new species, from Western Atlantic deep-sea cold seeps and anthropogenic habitats (Echionodermata: Holothuroidea: Apodida). Zootaxa 535:1-13.

Peel, F.J., C.J. Travis, and J.R. Hossack, 1995. Genetic structural provinces and salt tectonics of the Cenozoic offshore U.S. Gulf of Mexico: a preliminary analysis. In: Jackson, M.P.A., Roberts, D.G., Snelson, S. (Eds.), Salt Tectonics: A Global Perspective. American Association of Petroleum Geologists Memoir, pp. 153-175.

Pellon de Miranda, F., A.M. Quintero Marmol, E. Campos Pedroso, C. Henrique Beisl, P. Welgan and L. Medrano. 2004. Analysis of RADARSAT-1 data for offshor monitoring activities in the Cantarell Complex, Gulf of Mexico, using the unsupervised semivariogram textural clasifier (UTSC). Canadian Journal of Remote Sensing 30: 424-436.

Pequegnat, W., B. Gallaway, and L. Pequegnat. 1990. Aspects of the ecology of the deep-water fauna in the Gulf of Mexico. American Zoologist 30:45-64.

Peterson, B.J., and B. Fry. 1987. Stable isotopes in ecosystem studies. Annual Review of Ecology and Systematics 18: 293-320.

Pizarro, O. and H. Singh. 2003. Towards large-area mosaicking for underwater scientific applications. IEEE Journal of Ocean Engineering 28:651-672.

Plouviez, S., T. M. Shank, B. Faure, C. Daguin-Thiebaut, F. Viard, F. H. Lallier and D. Jollivet (2009). Comparative phylogeography among hydrothermal vent species along the East Pacific Rise reveals vicariant processes and population expansion in the South. Molecular Ecology 18(18): 3903-3917.

Pont-Kingdon, G., N.A. Okada, J.L. Macfarlane, C.T Beagley, C.D.Watkins-Sims, T. Cavalier-Smith, G.D. Clark-Walker and D.R.Wolstenholme. 1998. Mitochondrial DNA of the coral Sarcophyton glaucum contains a gene for a homologue of bacterial MutS: a possible case of gene transfer from the nucleus to the mitochondrion. J Mol Evol 46 (4):419-431.

Posada, D. 2003. Using MODELTEST and PAUP* to select a model of nucleotide substitution. Curr Protoc Bioinformatics Chapter 6, Unit 6 5.

Posada, D. and K.A. Crandall. 1998. MODELTEST: Testing the model of DNA substitution. Bioinformatics 14 (9):817-818.

Post, D. M. 2002. Using stable isotopes to estimate trophic position: models, methods, and assumptions. Ecology 83: 703–718.

Powell, E.N., T. J. Bright, A. Woods, and S. Gittings. 1983. Meiofauna and the Thiobios in the East Flower Garden Brine Seep. Marine Biology 73: 269–283.

Powell, E.N., T. J. Bright, and J.M. Brooks. 1986. The effect of sulfide and an increased food supply on the meiofauna and macrofauna at the East Flower Garden brine seep. Helgoländer Meeresuntersuchungen 40: 57–82.

Powers, D.A., T. Lauerman, D. Crawford and L. DiMichele. 1991. Genetic mechanisms for adapting to a changing environment. Annu Rev Genet 25:629-659.

Quattro, J.M., M.R. Chase, M.A. Rex, T.W. Greig, and R.J. Etter. 2001. Extreme mitochondrial DNA divergence within populations of the deep-sea gastropod *Frigidoalvania brychia*. Marine Biology 139 (6):1107-1113.

Rees, C.E. 1973. A steady-state model for sulfur isotope fractionation in bacterial reduction processes. Geochimica et Cosmochimica Acta 37: 648-649.

Rex, M.A. and RJ. Etter. 2010. Deep-Sea Biodiversity Pattern and Scale. Cambridge: Harvard University Press. 354 pp.

Ripley, B. 2005. Spatial Statistics. Wiley-IEEE.

Ritger, S., B. Carson, and E. Suess. 1987. Methane-derived authigenic carbonates formed by subduction-induced pore-water expulsion along the Oregon/Washington margin. Geological Society of America Bulletin 98: 147-156.

Roberts, H. 2001. Fluid and gas expulsion on the northern Gulf of Mexico continental slope: mud-prone to mineral-prone responses. In: Paull, C. K. and Dillon, W. P. (Eds.), Natural Gas Hydrates: Occurrence, Distribution, and Detection: American Geophysical Union, Washington, D.C., USA, p. 145-161.

Roberts, H. 2006. Seafloor reflectivity. An important seismic property for interpreting fluid/gas expulsion geology and the presence of gas hydrate. The leading Edge 25: 620-628

Roberts, H., and P. Aharon. 1994. Hydrocarbon-derived carbonate buildups of the northern Gulf of Mexico continental slope: a review of submersible investigations. Geo-Marine Letters 14 (2-3): 135-148.

Roberts, H.H., and R.C. Carney. 1997a. Evidence of episodic fluid, gas, and sediment venting on the northern Gulf of Mexico continental slope. Economic Geology 92: 863-879.

Roberts, H.H. and R.S. Carney. 1997b. Evidence of episodic fluid, gas, and sediment venting on the northern Gulf of Mexico continental slope. Econ. Geol. Bull. Soc. Econ. Geol. 92: 863-879.

Roberts, H.H., D. Feng. 2010. Cold seep carbonates of the middle and lower Continental Slope, Northern Gulf of Mexico. Deep-Sea Research II 57 (21-23), 2040-2054.

Roberts, H.H., D.J. Cook, and M.K. Sheedlo. 1992. Hydrocarbon seeps of the Louisiana continental slope: Seismic amplitude signature and sea floor response: Transactions 42nd Annual Gulf Coast Association of Geological Societies Convention, p. 349-362.

Roberts, H.H. and G. Boland. 2010. Preface, Gulf of Mexico Cold Seeps. Deep-Sea Research II 57 (21-23), 1835-1856.

Roberts, H.H., W. Shedd, J. Hunt, Jr. 2010. Geologic framework and seafloor impacts of fluid-gas expulsion sites on the middle and lower Continental Slope, Northern Gulf of Mexico. Deep-Sea Research II 57 (21-23), 1837-1858.

Roberts, H. H., W. Shedd, and J. Hunt, Jr., 2010, Dive site geology: DSV *Alvin* (2006) and ROV *Jason* II (2007) dives to the middle and lower continental slope, northern Gulf of Mexico: Deep Sea Research II, v. 57, p. 1837-1858.

Roberts, H. H., C. R. Fisher, B. Bernard, J. M. Brooks, M. Bright, R. S. Carney, E. E. Cordes, S. Hourdez, J. L. Hunt, Jr., S. B. Joye, I. R. MacDonald, C. Morrison, K. Nelson, V. Samarkin, W. Shedd, E. Becker, M. Bernier, G. Boland, M. Bowles, L. Goehring, M. Kupehik, S. Lessard-Pilon, H. Niemann, C. Petersen, J. Potter, and G. Telesnicki. 2007. *Alvin* Explores the Deep Northern Gulf of Mexico Slope. EOS, Trans. Am. Geophys. U. 88: 341-342.

Robinson, C.A., J. M. Bernard, L.A. Levin, G.F. Mendoza, and J.K. Blanks. 2004. Surficial hydrocarbon seep infauna from the Blake Ridge (Atlantic Ocean, 2150 m) and the Gulf of Mexico (690–2240 m). PSZN: Marine Ecology 25: 313–336.

Roelfsema, C. M. and S. R. Phinn. 2009. A Manual for Conducting Georeferenced Photo Transects Surveys to Assess the Benthos of Coral Reef and Seagrass Habitats version 3.0.. Brisbane: The University of Queensland. CSIRO Science.

Rosman, I., G.S. Boland and J.S. Baker. 1987. Epifaunal aggregations of Vesicomyidae on the continental slope off Louisiana. Deep-Sea Research 34: 1811-1820.

Rowe, G. T. 1983. Biomass and production of the deep-sea macrobenthos. Deep-Sea Biology. New York, Wiley InterScience. 8**:** 97-121.

Rozas, J., J. C. Sànchez-DelBarrio, X. Messeguer and R. Rozas (2003). DnaSP, DNA polymorphism analyses by the coalescent and other methods. Bioinformatics 19: 2496-2497.

Ruby, E.G., H.W. Jannasch, and W.G. Deuser. 1987. Fractionation of stable carbon isotopes during chemoautotrophic growth of sulfur-oxidizing bacteria. Appl. Env. Microbiol. 53 (8): 1940-1943 Saitou, N. and M. Nei. 1987. The neighbor-joining method: a new method for reconstructing phylogenetic trees. Mol Biol Evol 4:406-425.

Rzhanov, Y. and S. E. Beaulieu. 2007. *Alvin* Video Mosaicking Software Suite User Manual. Woods Hole, Woods Hole Oceanographic Institution**,** Wood Hole, MA. Internet website. www.whoi.edu/sites/*Alvin*VideoMosaic/. February 2010.

Saino, T. and A. Hattori. 1987. Geographical variation of the water column distribution of suspended particulate organic nitrogen and its 15N natural abundance in the Pacific and its marginal seas. Deep-Sea Research 34 (5-6) 807-827.

Saitou, N. and M. Nei. 1987. The neighbor-joining method: a new method for reconstructing phylogenetic trees. Mol Biol Evol 4:406-425.

Sassen, R. and I.R. MacDonald. 1997. Hydrocarbons of experimental and natural gas hydrates, Gulf of Mexico continental slope. Organic Geochemsitry 26(3-4):289-293.

Sassen, R., H.H. Roberts, P. Aharon, J. Larkin, E.W. Chinn, R. Carney. 1993. Chemosynthetic bacterial mats at cold hydrocarbon seeps, Gulf of Mexico continental slope. Organic Geochemistry 20, 77-89.

Sassen, R., S.L. Losh, L. Cathles, H.H. Roberts, J.K. Whelan, A.V. Milkov, S.T. Sweet and D.A. DeFreitas. 2001. Massive vein-filling gas hydrate: relation to ongoing gas migration from the deep subsurface in the Gulf of Mexico. Marine and Petroleum Geology 18: 551-560.

Schoell, M. 1983. Genetic classification of natural gas. American Association of Petrology and Geology Bulletin 67: 2225-2238.

Sen Gupta, B.K., L.E. Smith, and M.K. Lobegeier. 2007. Attachment of Foraminifera to vestimentiferan tube worms at cold seeps: Refuge from seafloor hypoxia and sulfide toxicity. Marine Micropaleontology 62: 1–6.

Sergeeva, N.G. and M.B. Gulin M.B. 2007. Meiobenthos from an active methane seepage area in the NW Black Sea. Marine Ecology – An Evolutionary Perspective 28: 152–159.

Sharp, J.H., R. Benner, L. Bennett, C.A. Carlson, R. Dow, S.E. Fitzwater 1993. A re-evaluation of high temperature combustion and chemical oxidation measurements of dissolved organic carbon in seawater. *Limnology and Oceanography*. 38:1774-1782.

Sheriff, R.E., 2002, Encyclopedic Dictionary of Applied Geophysics, Fourth Addition: Society of Exploration Geophysicists, Tulsa, Oklahoma, 429 p.

Shirayama, Y. and S. Ohta. 1990. Meiofauna in a cold-seep community off Hatsushima, Central Japan. Journal of the Oceanographic Society of Japan 46: 118-124.

Smith, C. J. and H. Ruhmohr. 2005. Imaging techniques. In: Eleftheriou, A. and McIntyre, A. eds. Methods for the Study of Marine Benthos. Oxford: Blackwell Science**.** Pp. 87-111.

Smith, E., K.M. Scott, E.R. Nix, C. Korte and C.R. Fisher. 2000. Growth and condition of seep mussels *(Bathymodiolus childressi)* at a Gulf of Mexico brine pool. Ecology 81:2392-2403.

Soltwedel, T. 2000. Metazoan meiobenthos along continental margins: a review. Progress in Oceanography 46: 59–84.

Solorzano, L. 1969. Determination of ammonia in natural waters by the phenol hypochlorite method. Limnology and Oceanography. 14:799-801.

Soltwedel, T., D. Portnova, I. Kolar, V. Mokievsky, and I. Schewe. 2005. The small-sized benthic biota of the Håkon Mosby Mud Volcano (SW Barents Sea slope). Journal of Marine Systems 55: 271–290.

Sommer, S., E. Gutzmann, and O. Pfannkuche. 2007. Sediments hosting gas hydrates: oasis for metazoan meiofauna. Marine Ecology Progress Series 337: 27–37.

Stohr, S. and M. Segonzac. 2005. Deep-sea ophiuroids (Echinodermata) from reducing and non-reducing environments in the North Atlantic Ocean Journal of the Marine Biological Association of the United Kingdom 85:383-402.

Suess, E. 1980. Particulate organic carbon flux in the ocean: surface productivity and oxygen utilization. Nature 288:260-263.

Suess, E., M.E. Torres, G. Bohrmann, R.W. Collier, J. Greinert, P. Linke, G. Rehder, A. Trehu, K. Walllman, E. Zuleger 1999. "Gas hydrate destabilization: Enhanced dewatering, benthic material turnover and large methane plumes at the Cascadia convergent margin." Earth Planet Science Letters. 170:1-15.

Tamura, K. and M. Nei (1993). Estimation of the number of nucleotide substitutions in the control region of mitochondrial-DNA in Humans and Chimpanzees. Molecular Biology and Evolution 10(3): 512-526.

Tamura, K., J. Dudley, M. Nei and S. Kumar. 2007. MEGA4: Molecular Evolutionary Genetics Analysis (MEGA) software version 4.0. Mol Biol Evol 24 (8):1596-1599.

Tarasov, V.G., A.V. Gebruk, V.M. Shulkin, G.M Kamenev, V.I. Fadeev, V.N. Koshmynin, V.V. Malakhov, D.A. Starynin, and A.I. Obzhirov. 1999. Effect of shallow-water hydrothermal venting on the biota of Matupi Harbour (Rabaul Caldera, New Britain Island, Papua New Guinea). Continental Shelf Research 19: 79–116.

TDI-Brooks. 2006. Deep Chemosynthetic Community Characterization Cruise Report. Technical Report No. 06-1745, 225 pp.

Theroux, R.B. and R.L. Wigley. 1998. Quantitative composition and distribution of the macrobenthic invertebrate fauna of the continental shelf ecosystems of the northeastern United States. U.S. Department of Commerce. NOAA Technical Report NMFS 140.

Thiermann, F., I. Akoumianaki, J.A. Hughes, and O. Giere. 1997. Benthic fauna of a shallow-water gaseohydrothermal vent area in the Aegean Sea (Milos, Greece). Marine Biology 128: 149–159.

Thompson, J. D., D. G. Higgins and T. J. Gibson (1994). CLUSTAL W: improving the sensitivity of progressive multiple sequence alignment through sequence weighting, positions-specific gap penalties and weight matrix choice. Nucleic Acids Research 22: 4673-4680.

Thompson, J.D., T.J. Gibson, D.G. Higgins. 2002. Multiple sequence alignment using ClustalW and ClustalX. Curr Protoc Bioinformatics Chapter 2, Unit 2 3.

Thurston, M.H., B.J. Bett, A.L. Rice, and P.A.B. Jackson. 1994. Variation in the invertebrate abyssal megafauna in the North-Atlantic Ocean. Deep-Sea Research I 41:1321-1348.

Thompson, J.D., T.J. Gibson, D.G. Higgins. 2002. Multiple sequence alignment using ClustalW and ClustalX. Curr Protoc Bioinformatics Chapter 2, Unit 2 3.

Treude, T., A. Boetius, K. Knittel, K. Wallmann, and B.B. Jorgensen. 2003. Anaerobic oxidation of methane above gas hydrates at Hydrate Ridge, NE Pacific Ocean. Marine Ecology Progress Series 264: 1-14.

Tsurumi, M., R. C. de Graaf, and V. Tunnicliffe. 2003. Distributional and biological aspects of copepods at hydrothermal vents on the Juan de Fuca Ridge, north-east Pacific ocean. Journal Marine Biological Association UK. 83: 469–477.

Turnipseed, M., C. D. Jenkins, and C. L. Van Dover. 2004. Community structure in Florida Escarpment seep and Snake Pit (Mid-Atlantic Ridge) vent mussel beds. Marine Biology 145, 121-132.

Tyler, P.A and C.M. Young. 1999. Reproduction and dispersal at vents and cold seeps. J Mar Biol Ass. UK 79:193-208.

Tyler, P.A., G.L.J. Paterson, M. Sibuet, A. Guille, B.J. Murton, M. Segonzac. 1995. A new genus of ophiuroid (Echinodermata:Ophiuroidea) from hydrothermal mounds along the Mid-Atlantic Ridge. Journal Marine Biological Association UK 75:977-986.

Vander Land, J. and A. Narrevang. 1975. The systematicposition of *Lamellibrachia* [sic] (Annelida,Vestimentifera). In: Norrevang, A. (Ed.), The phylogeny and systematic position of Pogonophora, pp. 86-101.

Van Dover, C.L. 2002. Community structure of mussel beds at deep-sea hydrothermal vents. Marine Ecology Progress Series 230, 137-158.

Van Dover, C.L., P. Aharon, J.M. Bernhard, E. Caylor, M. Doerries, W. Flickinger, W. Gilhooly, S.K. Goffred, K. Knick, S. Macko, S. Rapoport, E.C. Raulfs, C. Ruppel, J. Salerno, R.D. Seitz, B.K. Sen Gupt, T. Shank, M. Turnipseed, and R. Vrijenhoek. 2002. Blake Ridge methane seeps: characterization of a soft-sediment, chemosynthetically based ecosystem. Deep Sea Research I 50:281-300.

VanGaever, S., L. Moodley, D. De Beer, and A. Vanreussel. 2006. Meiobenthos at the Arctic Håkon Mosby Mud Volcano, with a parental-caring nematode thriving in sulphide-rich sediments. Marine Ecology Progress Series 321: 143–155.

VanGaever, S., K. Olu, S. Deryke, and A. Vanreusel. 2009. Metazoan meiofaunal communities at cold seeps along the Norwegian margin: Influence of habitat heterogeneity and evidence for connection with shallow-water habitats. Deep-Sea Research I 56: 772–785.

Van Hamme, J.D., A. Singh, O.P. Ward. 2003. Recent Advances in Petroleum Microbiology. Microbiology and Molecular Biology. vol. 67 no. 4503-549.

Vanreusel A., A.C. Andersen, A. Boetius, D. Connelly, M.R. Cunha, C. Decker, A. Hilario, K.A. Kormas, L. Maignien, K. Olu, M. Pachiadaki, B. Ritt, C. Rodrigues, J. Sarrazin, P. Tyler, S. VanGaever, and H. Vanneste. 2009. Biodiversity of Cold Seep Ecosystems along the European Margins. Oceanography 22:110-127.

Vanreusel A., A. De Groote, S. Gollner, and M. Bright. 2010c. Advances in ecology and biogeography of free-living nematodes associated with chemosynthetic environments in the deep sea: A Review. PLoS ONE 5(8): e12449.

Vardaro, M.F., I.R. MacDonald, L.C. Bender, N.L. Guinasso. 2006. Dynamic processes observed at a gas hydrate outcropping on the continental slope of the Gulf of Mexico. 26: 6-15.

Veit-Koehler G., J. Laudien, J. Knott, J. Velez, and R. Sahade. 2008. Meiobenthic colonization of soft sediments in artic glacial Kongsfjorden (Svalbard). Journal of Experimental Marine Biology and Ecology 363: 58–65.

Wankel, S. D., S. B. Joye, V. A. S. R. Shah, G. Friederich, J. Melas-Kyriazi, P. R. Girguis. 2010. New constraints on methane fluxes and rates of anaerobic methane oxidation in a Gulf of Mexico brine pool via in situ mass spectrometry. In: Roberts, H. (ed.), Deep Sea Research Part II: Topical Studies in Oceanography, 2010. Gulf of Mexico Cold Seeps, Volume 57, Issues 21-23, pp 2022-2029.

Waser, N.A.D., P.J. Harrison, B. Nielsen, S.E. Calvert, and D.H. Turpin. 1998. Nitrogen isotope fractionation during the uptake and assimilation of nitrate, nitrite, ammonium, and urea by a marine diatom. Limnology and Oceanography 43 (2): 215-224.

Wicksten, M. K. and J. M. Packard. 2005. A qualitative zoogeographic analysis of decapod crustaceans of the continental slopes and abyssal plain of the Gulf of Mexico. Deep Sea Research Part I: Oceanographic Research Papers 52:1745-1765.

Wilgenbusch, J.C. and D. Swofford. 2003. Inferring evolutionary trees with PAUP*. Curr Protoc Bioinformatics Chapter 6, Unit 6 4

Won, Y. J., P. A. Y. Maas, C. L. Van Dover and R. C. Vrijenhoek (2002). Habitat reversal in vent and seep mussels: seep species, Bathymodiolus heckerae, derived from vent ancestors. Cahiers De Biologie Marine 43(3-4): 387-390

Won, Y., C.R. Young, R.A. Lutz and R.C. Vrijenhoek. 2003. Dispersal barriers and isolation among deep-sea mussel populations (Mytilidae: *Bathymodiolus*) from eastern Pacific hydrothermal vents. Mol Ecol 12 (1):169-184.

Young, C.M., E. Vazquez, A. Metaxas and P.A. Tyler. 1996. Embryology of vestimentiferan tube worms from deep-sea methane/sulphide seeps. Nature 381 (6582):514-516.

Zahn, C.T. 1971. Graph-theoretical methods for detecting and describing Gestalt clusters. IEEE Transactions on Computers: 68-86.

Zardus, J.D., R.J. Etter, M.R. Chase, M.A. Rex and E.E. Boyle. 2006. Bathymetric and geographic population structure in the pan-Atlantic deep-sea bivalve *Deminucula atacellana* (Schenck, 1939). Molecular Ecology 15 (3):639-651.

Zatyagalova, V., A. Ivanov and B. Golubov. 2007. Application of ENVISAT SAR imagery for mapping and estimation of natural oil seeps in the South Caspian Sea. Envisat Symposium 2007. ESA SP-636, Montreaux, Switzerland.

Zekely, J., C.L. VanDover, H.L. Nemeschkal, and M. Bright. 2006. Hydrothermal vent meiobenthos associated with mytilid mussel aggregations from Mid-Atlantic Ridge and the East Pacific Rise. Deep-Sea Research I 53: 1363–1378.

Zeppilli, D. and D. Danovaro. 2009. Meiofaunal diversity and assemblage structure in a shallow-water hydrothermal vent in the Pacific Ocean. Aquatic Biology 5: 75–84.

Zwickl, D.J. 2006. Genetic algorithm approaches for the pylogenetic analysis of large biological sequence data sets under the maximum likelihood criterion. Ph.D. Dissertation, The University of Texas at Austin, TX, USA.

The Department of the Interior Mission

As the Nation's principal conservation agency, the Department of the Interior has responsibility for most of our nationally owned public lands and natural resources. This includes fostering the sound use of our land and water resources; protecting our fish, wildlife, and biological diversity; preserving the environmental and cultural values of our national parks and historical places; and providing for the enjoyment of life through outdoor recreation. The Department assesses our energy and mineral resources and works to ensure that their development is in the best interests of all our people by encouraging stewardship and citizen participation in their care. The Department also has a major responsibility for American Indian reservation communities and for people who live in island communities.

The Bureau of Ocean Energy Management Mission

The Bureau of Ocean Energy Management (BOEM) works to manage the exploration and development of the nation's offshore resources in a way that appropriately balances economic development, energy independence, and environmental protection through oil and gas leases, renewable energy development and environmental reviews and studies.